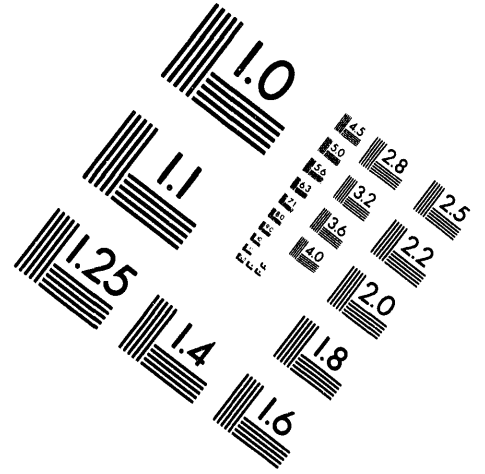
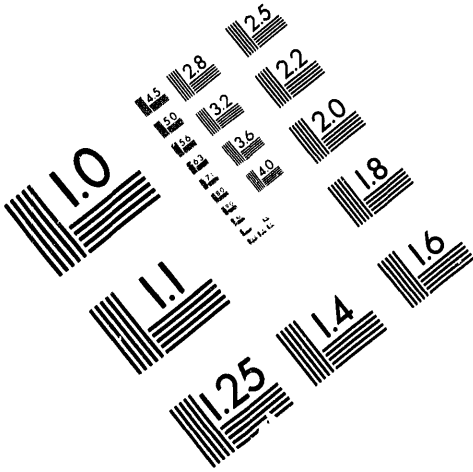




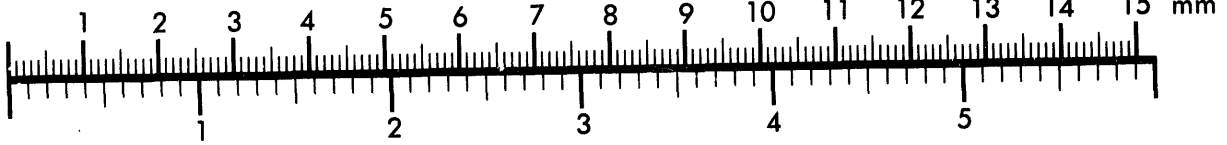
**AIM**

**Association for Information and Image Management**

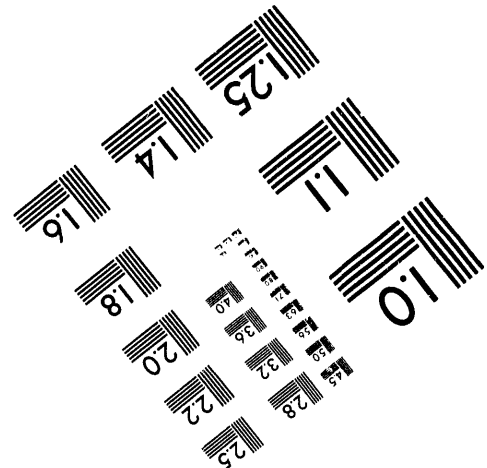
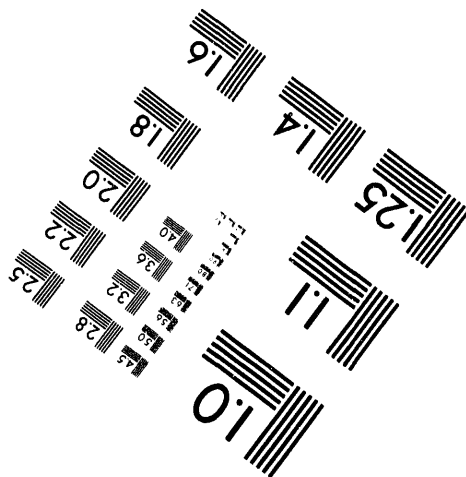
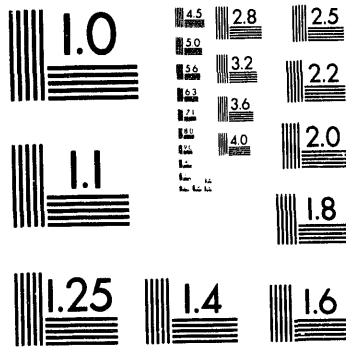
1100 Wayne Avenue, Suite 1100  
Silver Spring, Maryland 20910  
301/587-8202



Centimeter



Inches



MANUFACTURED TO AIM STANDARDS  
BY APPLIED IMAGE, INC.

**1 of 5**

**WBS: 1.2.5.4.1**  
**QA: N/A**

**Civilian Radioactive Waste Management System  
Management and Operating Contractor**

**TOTAL SYSTEM PERFORMANCE ASSESSMENT - 1993:**

**AN EVALUATION OF THE POTENTIAL  
YUCCA MOUNTAIN REPOSITORY**

**B00000000-01717-2200-00099-Rev. 01**

**March 1994**

**Prepared for:**

**U.S. Department of Energy  
Yucca Mountain Site Characterization Project  
P.O. Box 98608  
Las Vegas, Nevada 89193-8608**

**Prepared by:**

**Robert W. Andrews, Timothy F. Dale, and Jerry A. McNeish  
INTERA, Inc.  
101 Convention Center Drive  
Suite P-110  
Las Vegas, Nevada 89109-2006**

**Under Contract Number  
DE-AC01-91RW00134**

**DISCLAIMER**

This report was prepared as an account of work sponsored by an agency of the United States Government. Neither the United States Government nor any agency thereof, nor any of their employees, makes any warranty, express or implied, or assumes any legal liability or responsibility for the accuracy, completeness, or usefulness of any information, apparatus, product, or process disclosed, or represents that its use would not infringe privately owned rights. Reference herein to any specific commercial product, process, or service by trade name, trademark, manufacturer, or otherwise does not necessarily constitute or imply its endorsement, recommendation, or favoring by the United States Government or any agency thereof. The views and opinions of authors expressed herein do not necessarily state or reflect those of the United States Government or any agency thereof.

**MASTER**  
*as*

**DISTRIBUTION OF THIS DOCUMENT IS UNLIMITED**

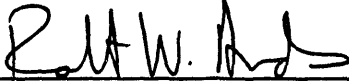
**Civilian Radioactive Waste Management System  
Management and Operating Contractor**

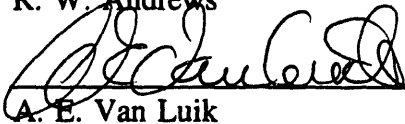
**TOTAL SYSTEM PERFORMANCE ASSESSMENT - 1993:**

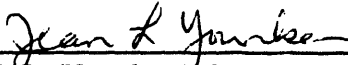
**AN EVALUATION OF THE POTENTIAL  
YUCCA MOUNTAIN REPOSITORY**

**B00000000-01717-2200-00099-Rev. 01**

**March 1994**

Prepared by:  Date: 3/18/94  
R. W. Andrews

Reviewed by:  Date: 3/18/94  
A. E. Van Luik

Approved by:  Date: 3/18/94  
J. L. Younker, Manager  
Regulatory and Technical Evaluation

Interdiscipline Review:

---

---

---

---

---

---

---

---

---

---

## ACKNOWLEDGEMENTS

Analyses of integrated total system performance assessment require input from numerous individuals familiar with the multiple disciplines affecting the behavior of the system. Such is certainly the case in this document. We would like to acknowledge the formal and informal contributions of several of our colleagues within the Civilian Radioactive Waste Management System Management and Operating Contractor who have augmented our understanding of some detailed process directly or indirectly imbedded in the total system performance analyses. These individuals include (in alphabetical order): John King, Suresh Lingineni, Srikanta Mishra, Mark Reeves, Anthony Smith, and David Stahl. In addition, we have had very fruitful discussions with several individuals outside our organization, including Thomas Buscheck, Alan Lamont, and William Halsey of Lawrence Livermore National Laboratory; Arend Meijer and Ines Triay of Los Alamos National Laboratory; Ralston Barnard, John Gauthier, and Michael Wilson of Sandia National Laboratories; Alan Flint, Lorraine Flint, and Dwight Hoxie of the U.S. Geological Survey; and Daniel Bullen of Iowa State University. When information from one of these individuals was used directly in our analyses, we have attached the relevant information provided in an Appendix to this document. We would also like to acknowledge the significant support provided to the early phases of the analyses by Carl Bruch who is presently pursuing a law career.

This document has benefitted significantly by reviews of earlier drafts conducted by Albin Brandstetter, Suresh Pahwa, and Abraham Van Luik. We were ably supported by Trina Herbst, Judy Long, Lin Wilson, Sandra Trillo, and Beverly Plumley in the final preparation of this manuscript.

The work reported in this document was funded under Work Breakdown Structure 1.2.5.4.1—Total System Performance Assessment by the U.S. Department of Energy Office of Civilian Radioactive Waste Management—Yucca Mountain Site Characterization Project Office under Contract #DE-AC01-91RW00134. The Branch Chief responsible for this work is Jeremy Boak; the Work Breakdown Structure Manager responsible for this work is Eric Smistad. The Management and Operating Contractor Office Manager responsible for this work is Jean Younker. The support of these individuals and organizations is gratefully acknowledged.

## EXECUTIVE SUMMARY

Total System Performance Assessments are an important component in the evaluation of the suitability of Yucca Mountain, Nevada as a potential site for a mined geologic repository for the permanent disposal of high-level radioactive wastes in the United States. The Total System Performance Assessments are conducted iteratively during site characterization to identify issues which should be addressed by the characterization and design activities as well as providing input to regulatory/licensing and programmatic decisions. During fiscal years 1991 and 1992, the first iteration of Total System Performance Assessment (hereafter referred to as TSPA 1991) was completed by Sandia National Laboratories and Pacific Northwest Laboratory. Beginning in fiscal year 1993, the Civilian Radioactive Waste Management System Management and Operating Contractor was assigned the responsibility to plan, coordinate, and contribute to the second iteration of Total System Performance Assessment (hereafter referred to as TSPA 1993). This document presents the objectives, approach, assumptions, input, results, conclusions, and recommendations associated with the Management and Operating Contractor contribution to TSPA 1993. A parallel effort was conducted by Sandia National Laboratories and is reported in Wilson et al. (1994, in press).

The principal objectives of the second iteration of Total System Performance Assessment are to (1) enhance the realism/representativeness of the analyses, (2) incorporate new information and designs that have become available since the completion of TSPA 1991, (3) test the significance (i.e., sensitivity) of various conceptual model and parameter uncertainties on the predicted performance, and (4) evaluate alternate measures of postclosure performance.

The representativeness of the analyses has been significantly enhanced over that presented in TSPA 1991 by (1) directly incorporating the thermohydrologic behavior in the near-field environment, (2) directly incorporating the possible corrosion processes and their thermohydrologic dependence in the determination of the degradation time of the waste package containers, and (3) the incorporation of a more complete radionuclide inventory that includes 39 radionuclides. The near-field environment used in TSPA 1993 is based on thermohydrologic analyses conducted at the panel scale in order to evaluate the potential edge effects associated with unheated portions of the repository due to the presence of main axis drift and associated side adits, the setback of waste packages from these drifts, and the existence of the lower thermal output from the defense high-level waste.

The new information incorporated in TSPA 1993 includes (1) revised estimates of radionuclide solubilities (and their thermal and geochemical dependency), (2) thermal and geochemical dependency of spent fuel waste alteration and glass dissolution rates, (3) new distribution coefficient ( $k_d$ ) estimates, (4) revised estimates of gas-phase velocities and travel times, and (5) revised hydrologic modeling of the saturated zone which provides updated estimates of the advective flux through the saturated zone. The new designs that have been proposed since the completion of TSPA 1991 (which focused on the Site Characterization Plan design) include (1) alternate thermal loads, (2) alternate waste package emplacement designs, and (3) the concept of multibarrier waste package containers consisting of an outer corrosion-allowance material and an inner corrosion-resistant material of various thicknesses.

The alternate conceptual models that have been evaluated in TSPA 1993 include the assumed criteria affecting the initiation of aqueous corrosion under the possible thermohydrologic environments in the vicinity of the repository as well as the conceptual model for corrosion itself.

Finally, the alternate postclosure total system performance measures that have been evaluated in this TSPA 1993 include (1) the normalized cumulative release of radionuclides to the accessible environment for 10,000 years and (2) the peak individual dose associated with possible releases for a 1,000,000-year time period. These later analyses were conducted in recognition of the role that the individual dose performance criterion may play in the National Academy of Science's evaluation of the reasonableness/appropriateness of alternate environmental standards that may be applied to Yucca Mountain (per Section 801 of the Energy Policy Act of 1992 [U.S. Congress, 1992]).

The general approach taken in the Management and Operating Contractor's contribution to TSPA 1993 is to (1) abstract primary functional relationships from either the results of detailed process models (for example, the thermohydrologic analyses) or directly from uncertain parameter distributions, (2) define the dependence of relevant waste package containment, radionuclide exposure, waste package release, engineered barrier system release, and geosphere transport properties on the primary thermohydrologic and geochemical variables, (3) incorporate the functional relationships and dependencies into the Repository Integration Program, and (4) predict the performance and the uncertainty associated with the uncertain conceptual models and parameter values. The Repository Integration Program, developed by Golder Associates Inc., has been chosen for this assessment because it allows the user to incorporate a sufficient specificity in the process or process interactions to ensure that potentially important correlations and dependencies are included in the analysis. The utility of the Repository Integration Program has been previously verified in an earlier comparison of it to the analyses conducted in TSPA 1991 (INTERA, 1993).

Numerous comparisons of the predicted results associated with alternate thermal loads, waste package designs, and conceptual representations of the initiation of aqueous corrosion plus the corresponding rates of corrosion, are documented in this report. The results may generally be grouped into those related to releases from the waste package, those related to releases to the accessible environment, and those associated with peak individual doses at the accessible environment. For the waste package, results are presented for (1) the expected value radionuclide releases for 10,000 and 100,000 years, (2) the expected value cumulative normalized release to the 40 CFR 191 Table 1 values for 10,000 and 100,000 years, (3) complementary cumulative distribution functions of normalized cumulative releases from the waste package for 10,000 and 100,000 years, and (4) scatter plots of cumulative normalized release vs. pH. For releases from the geosphere, results are presented for (1) the expected value radionuclide release for 10,000 and 100,000 years, (2) the expected value of the normalized cumulative release for 10,000 and 100,000 years, (3) complementary cumulative distribution functions of the cumulative normalized gaseous release for 10,000 years, (4) complementary cumulative distribution functions of the cumulative normalized aqueous release for 10,000 and 100,000 years, and (5) scatter plots illustrating the sensitivity of cumulative normalized release to the unsaturated zone percolation flux. For individual peak doses, results are presented for (1) the expected value doses for 1,000,000 years, (2) complementary cumulative distribution functions of the peak dose for 1,000,000 years, and (3) scatter plots of the sensitivity of peak individual dose to the unsaturated

zone flux, the saturated zone flux, and pH. For each result, comparisons are made to evaluate the sensitivity of waste package and geosphere releases to alternative thermal loads and waste package designs.

Based on the Total System Performance Assessment results presented, it is possible to conclude that, in general, when considering the integrated release from the waste package for 10,000 years (and the corresponding release to the accessible environment over this time period), the higher and lower thermal loads, represented by 282 kW/ha (114 kW/acre) and 70.4 kW/ha (28.5 kW/acre) respectively, yield slightly lower releases than does the 141 kW/ha (57 kW/acre) case. In the case of the 282 kW/ha (114 kW/acre) case, this reduction is due to the delay in the initiation of aqueous corrosion at the higher temperatures/lower water saturations. In the case of the 70.4 kW/ha (28.5 kW/acre) case, this reduction is due to the lower aqueous corrosion rates and waste form alteration rates at the lower temperatures. These conclusions are also germane to the 100,000- year time period, although the differences are not significant given the range of other uncertainties affecting the results.

As in previous Total System Performance Assessments, the normalized 10,000-year cumulative releases to the accessible environment are dominated by  $^{14}\text{C}$  releases. The  $^{14}\text{C}$  release is controlled by the time of "failure" of the waste package container and therefore is strongly dependent on the thermohydrologic near-field regime as well as the conceptual representation of aqueous corrosion and corrosion rates. The integrated aqueous releases to the accessible environment for 10,000 years are extremely small (less than a 10 percent probability of being greater than  $10^{-6}$  of the 40 CFR 191 Table 1 values), and are also controlled by the time at which the containment is breached as well as the percolation flux and dispersion in the unsaturated zone. The dominant aqueous radionuclide released over this time period is  $^{99}\text{Tc}$ .

The effect of alternative thermal loads on the peak individual dose over a 1,000,000-year time period is insignificant. This is a direct result of the fact that while the thermal load can cause differences in expected releases and the corresponding doses over the time period that the thermal regime is perturbed, at larger time these effects have no impact on the predicted consequences. However, this conclusion must be prefaced by noting that the long-term "dryout" of the geosphere expected at very high thermal loads was not evaluated in this study due to a lack of a sufficient suite of process-level thermohydrologic analyses over a wide range of uncertain hydrogeologic parameters and boundary conditions. This so-called "extended-dry" concept should be considered more explicitly in future Total System Performance Assessment iterations.

The result of varying the waste package container thicknesses indicate, as expected, that as the outer wall thickness is increased, the package lifetime also increased and the corresponding releases decreased. While the differences between a 10-cm and 20-cm outer mild steel container are not significant, there is virtually no release for 10,000 years when a 45-cm outer container is used. This conclusion also is relevant when comparing the releases for a 100,000-year time period. Again, however, as the time period is increased to 1,000,000 years, even the long-lived 45-cm waste package is predicted to yield equivalent peak doses to the other waste package designs.

It warrants noting that conclusions regarding the relative advantages or disadvantages of particular design options based on the present Total System Performance Assessment analyses

must be qualified by the confidence in the current conceptualization of the system and its components. As significant uncertainties remain in the understanding of the very-near-field environment and its effect on the initiation and rate of aqueous corrosion, some caution should be exercised prior to unconditionally accepting the conclusions presented above.

The Total System Performance Assessment analyses conducted as part of TSPA 1993 have significantly extended the analyses performed in TSPA 1991. However, uncertainties still remain. As performance assessment is an iterative process, it is important to identify those assumptions and uncertainties which contribute significantly to the predicted performance so they may be the focus of continued investigation and analysis. The primary sources of significant uncertainty are (1) panel- and drift-scale thermohydrologic analyses, (2) initiation and rates of aqueous corrosion processes, (3) the ambient unsaturated-zone percolation flux, and (4) the conceptual representation of fracture-matrix interactions.

Additional thermohydrologic analyses are required to evaluate the effect of uncertain and spatially variable thermohydrologic properties, uncertain fracture-matrix conceptual models, and uncertain ambient percolation fluxes on the expected far-field, near-field and very-near-field (waste package-scale) thermal and hydrologic regimes as a function of space and time. Considerable uncertainty remains regarding the processes affecting the initiation and rate of aqueous corrosion under the range of possible thermohydrologic environments likely to be encountered under various thermal loading scenarios at Yucca Mountain. Greater understanding is required of the cathodic protection of the inner container, the processes affecting the growth of pits, and even the definition of waste package "failure" in order to provide a more defensible argument for the range of likely waste package lifetimes.

The ambient unsaturated zone percolation flux remains a very significant parameter in this iteration of Total System Performance Assessment. Any direct or indirect observations to better quantify the expected flux value and its uncertainty should be employed. It is foreseen that the preliminary site-scale unsaturated-zone model, to be completed by the U.S. Geological Survey in fiscal year 1994, should be the basis for subsequent iterations of Total System Performance Assessments. In addition, the conceptual understanding of how water moves through the unsaturated zone at Yucca Mountain needs to be improved before initiating the next Total System Performance Assessment iteration. In the present iteration, the composite porosity model of fracture-matrix interaction is used, but additional "testing" is required to determine the relative significance of alternate conceptualizations.

## TABLE OF CONTENTS

	Page
1. INTRODUCTION .....	1-1
1.1 OBJECTIVES .....	1-2
1.2 APPROACH .....	1-5
1.3 GENERAL DESCRIPTION OF THE REPOSITORY INTEGRATION PROGRAM .....	1-6
1.3.1 Waste Package/Engineered Barrier System Radionuclide Release Module	1-6
1.3.2 Geosphere Radionuclide Transport Module .....	1-8
1.3.3 Biosphere Transport and Dose Module .....	1-9
1.4 RELATED TSPA 1993 ANALYSES .....	1-10
1.5 ORGANIZATION OF THIS REPORT .....	1-10
2. WASTE PACKAGE/ENGINEERED BARRIER SYSTEM .....	2-1
2.1 CONCEPTUAL AND PARAMETER DESCRIPTIONS .....	2-2
2.1.1 Radionuclide Inventory .....	2-3
2.1.2 Container Failure .....	2-4
2.1.2.1 TSPA 1991 Failure Distribution Description .....	2-4
2.1.2.2 Stahl Failure Distribution Description .....	2-5
2.1.2.3 Lamont Failure Distribution Description .....	2-6
2.1.2.4 Bullen Failure Distribution Description .....	2-6
2.1.2.5 Container Failure Implementation in TSPA 1993 .....	2-7
2.1.3 Waste Mobilization .....	2-12
2.1.3.1 Matrix Dissolution Rates—Spent Fuel .....	2-13
2.1.3.2 Matrix Dissolution Rates—Classified High-Level Waste .....	2-13
2.1.3.3 Additional Parameters Important to Waste Mobilization .....	2-15
2.1.4 Modes of Radionuclide Transport .....	2-15
2.1.4.1 Solubilities .....	2-16
2.1.4.2 Diffusion Coefficients .....	2-17
2.1.5 Engineered Barrier System Configuration .....	2-18
2.1.6 Comparison with Sandia National Laboratories' TSPA 1991 .....	2-18
2.2 WASTE PACKAGE RESULTS .....	2-19
2.2.1 Failure Distributions .....	2-19
2.2.1.1 Alternate Thermal Loads .....	2-20
2.2.1.2 Alternate Outer Container Thicknesses .....	2-20
2.2.1.3 Alternate Processes for Initiation of Aqueous Corrosion .....	2-20
2.2.2 Waste Package Release from Expected Value Case .....	2-21
2.2.2.1 Alternate Thermal Loads .....	2-21
2.2.2.2 Alternate Design .....	2-22
2.2.2.3 Alternate Initiation of Aqueous Corrosion .....	2-22

## TABLE OF CONTENTS (Continued)

	Page
2.2.3 Complementary Cumulative Distribution Functions of Waste Package Release . . . . .	2-22
2.2.3.1 Alternate Thermal Loads . . . . .	2-23
2.2.3.2 Alternate Design . . . . .	2-23
2.2.3.3 Alternate Initiation of Aqueous Corrosion . . . . .	2-23
2.2.4 Sensitivity Analysis Results . . . . .	2-23
2.3 CONCLUSIONS FROM WASTE PACKAGE ANALYSES . . . . .	2-24
3. GASEOUS AND AQUEOUS FLOW AND TRANSPORT . . . . .	3-1
3.1 UNSATURATED- AND SATURATED-ZONE AQUEOUS FLOW AND TRANSPORT . . . . .	3-1
3.1.1 Conceptual Description . . . . .	3-1
3.1.2 Parameter Values . . . . .	3-3
3.1.3 Aqueous Flow Regime . . . . .	3-5
3.2 UNSATURATED-ZONE GASEOUS FLOW AND TRANSPORT . . . . .	3-6
3.2.1 Conceptual Description . . . . .	3-6
3.2.2 Unsaturated-Zone Gaseous Flow Regime . . . . .	3-7
3.3 RESULTS . . . . .	3-8
3.3.1 Results of Releases to the Accessible Environment at 10,000 Years . . . . .	3-8
3.3.2 Results of Releases to the Accessible Environment at 100,000 Years . . . . .	3-10
3.3.3 Scatter Plots of Releases . . . . .	3-12
3.3.4 Radiation Dose Exposures from Aqueous Pathways . . . . .	3-13
3.3.5 Scatter Plots of Dose . . . . .	3-16
4. SUMMARY AND CONCLUSIONS . . . . .	4-1
4.1 SIGNIFICANCE OF KEY ASSUMPTIONS . . . . .	4-1
4.1.1 Waste Package/Engineered Barrier System Assumptions . . . . .	4-1
4.1.2 Geosphere Flow and Transport Assumptions . . . . .	4-6
4.1.3 Biosphere Assumptions . . . . .	4-8
4.2 SENSITIVITY AND SIGNIFICANCE OF RESULTS . . . . .	4-9
4.2.1 Significance of Results to Design . . . . .	4-9
4.2.2 Significance of Results to Site Characterization . . . . .	4-13
4.2.3 Significance of Results to Alternate Environmental Standards . . . . .	4-16
4.3 RECOMMENDATIONS FOR ADDITIONAL ANALYSES/INFORMATION . . . . .	4-17
5. REFERENCES . . . . .	5-1
6. ACRONYMS AND ABBREVIATIONS . . . . .	6-1

**TABLE OF CONTENTS (Continued)**

	<b>Page</b>
APPENDIX A FAR-FIELD THERMOHYDROLOGIC CALCULATIONS . . . . .	A-1
APPENDIX B NEAR-FIELD THERMAL CALCULATIONS . . . . .	B-1
APPENDIX C RADIONUCLIDE INVENTORY FOR TSPA 1993 . . . . .	C-1
APPENDIX D WASTE STREAM AND WASTE PACKAGE DESCRIPTIONS: YOUNGEST FUEL FIRST WITH MRS FLOW THROUGH EMPLACEMENT SCENARIO) . . . . .	D-1
APPENDIX E WASTE PACKAGE CORROSION RATES (STAHL) . . . . .	E-1
APPENDIX F WASTE PACKAGE CORROSION RATES (LAMONT) . . . . .	F-1
APPENDIX G SOLUBILITY DATA AND EXPERT ELICITATION RESULTS . . . . .	G-1
APPENDIX H DISTRIBUTION COEFFICIENT EXPERT ELICITATION RESULTS .	H-1
APPENDIX I THERMALLY INDUCED RETARDED <sup>14</sup> C TRAVEL TIME DISTRIBUTIONS . . . . .	I-1

## LIST OF TABLES

		<b>Page</b>
2-1.	Summary of Analysis Variations Evaluated in TSPA 1993 . . . . .	2-26
2-2.	Spent Fuel Waste Inventory . . . . .	2-27
2-3.	High-Level Waste Inventory . . . . .	2-29
2-4.	Elicited General Corrosion Rates for Overpack (After Lamont (1993)) . . . . .	2-30
2-5.	Pitting Corrosion Rates (After Lamont (1993)) . . . . .	2-31
2-6.	Failure Time and Fraction of Container Susceptible to Certain Temperature Zone (Bullen, 1993) . . . . .	2-32
2-7a.	Calculated Time to Failure (Years) Due to General Corrosion Using Stahl Corrosion Model - 28.5 kW/acre . . . . .	2-33
2-7b.	Calculated Time to Failure (Years) Due to Pitting Corrosion Using Stahl Corrosion Model - 28.5 kW/acre . . . . .	2-33
2-8a.	Calculated Time to Failure (Years) Due to General Corrosion Using Stahl Corrosion Model - 57 kW/acre . . . . .	2-34
2-8b.	Calculated Time to Failure (Years) Due to Pitting Corrosion Using Stahl Corrosion Model - 57 kW/acre . . . . .	2-34
2-9a.	Calculated Time to Failure (Years) Due to General Corrosion Using Stahl Corrosion Model - 114 kW/acre . . . . .	2-35
2-9b.	Calculated Time to Failure (Years) Due to Pitting Corrosion Using Stahl Corrosion Model - 114 kW/acre . . . . .	2-35
2-10.	Calculated Time to Failure (Years) Due to Pitting Corrosion Using Stahl Corrosion Model - 57 kW/acre and 114 kW/acre - 100°C switchpoint . . . . .	2-36
2-11a.	RIP Implementation of Failure Time for 28.5 kW/acre Using Stahl Corrosion Model (Pitting) . . . . .	2-37
2-11b.	RIP Implementation of Failure Time for 57 kW/acre Using Stahl Corrosion Model (Pitting) . . . . .	2-37
2-11c.	RIP Implementation of Failure Time for 114 kW/acre Using Stahl Corrosion Model (Pitting) . . . . .	2-38

## LIST OF TABLES (Continued)

		Page
2-12.	RIP Implementation of Failure Time for 57 kW/acre and 114 kW/acre Using Stahl Corrosion Model (Pitting) - 100°C switch to aqueous corrosion . . .	2-39
2-13.	Calculated Time to Failure for General Corrosion Using Lamont Corrosion Model - 57 kW/acre . . . . .	2-40
2-14.	Calculated Time to Failure for Pitting Corrosion Using Lamont Corrosion Model - 57 kW/acre (10 cm overpack) . . . . .	2-41
2-15a.	Calculated Time to Failure for Pitting Corrosion Using Lamont Corrosion Model and 57 kW/acre - 100°C switchpoint . . . . .	2-42
2-15b.	Calculated Time to Failure for Pitting Corrosion Using Lamont Corrosion Model and 114 kW/acre - 100°C switchpoint . . . . .	2-42
2-16.	RIP Implementation of Pitting Corrosion for Inner Container with 10 cm overpack for 57 kW/acre Using Lamont Corrosion Model - 8 percent saturation - Weibull distribution . . . . .	2-43
2-17a.	RIP Implementation of Pitting Corrosion for Inner Container with 10 cm overpack for 57 kW/acre Using Lamont Corrosion Model - 100°C switchpoint - Weibull distribution . . . . .	2-44
2-17b.	RIP Implementation of Pitting Corrosion for Inner Container with 10 cm overpack for 114 kW/acre Using Lamont Corrosion Model - 100° C switchpoint - Weibull distribution . . . . .	2-45
2-18.	Solubilities for TSPA 1993 . . . . .	2-46
2-19a.	Temperature- and pH-Dependent Solubilities for Americium . . . . .	2-48
2-19b.	Temperature- and pH-Dependent Solubilities for Neptunium . . . . .	2-48
2-19c.	Temperature- and pH-Dependent Solubilities for Plutonium . . . . .	2-48
2-20.	Comparison of TSPA 1991 Container Parameters With TSPA 1993 Container Parameters . . . . .	2-49
2-21a.	Comparison of TSPA 1991 Inventory Parameters With TSPA 1993 Parameters	2-50
2-21b.	Comparison of TSPA 1991 Inventory Parameters With TSPA 1993 Parameters	2-51
2-21c.	Comparison of TSPA 1991 Inventory Parameters With TSPA 1993 Parameters	2-52

**LIST OF TABLES (Continued)**

		<b>Page</b>
2-21d.	Comparison of TSPA 1991 Inventory Parameters With TSPA 1993 Parameters	2-53
2-22.	Comparison of TSPA 1991 Waste Package Failure Parameters With TSPA 1993 Parameters . . . . .	2-54
2-23.	Comparison of TSPA 1991 Exposure Parameters With TSPA 1993 Exposure Parameters . . . . .	2-55
2-24.	Comparison of TSPA 1991 Transport Parameters With TSPA 1993 Transport Parameters . . . . .	2-57
2-25.	Waste Package Configurations—57 kW/acre (Memory, 1992) . . . . .	2-58
2-26.	Normalized Cumulative Release from the Waste Package for Reference Case .	2-59
2-27.	Summary Results for 10,000 and 100,000 Year Normalized Cumulative Release from the Waste Package . . . . .	2-61
3-1.	Simulation Identifiers Based on Waste Package/Engineered Barrier System Configurations . . . . .	3-17
3-2.	Stratigraphic Thicknesses of the Nine Unsaturated-Zone Columns Used in the Aqueous Transport Simulations . . . . .	3-18
3-3.	Stratigraphic Column Correlations between the Thermomechanical (Ortiz et al., 1985) and the USGS (1993) Stratigraphies as used in TSPA 1993	3-19
3-4.	Reference Points for the Calculation of the Water-Table Elevation . . . . .	3-20
3-5.	TSPA 1993 Unsaturated- and Saturated-Zone Aqueous Flux Distributions (m/yr)	3-20
3-6.	Correlation of TSPA 1993 and TSPA 1991 (Barnard et al., 1992) Stratigraphic Designations . . . . .	3-21
3-7.	TSPA 1993 Beta Bulk Porosity Distributions (Barnard et al., 1992) . . . . .	3-21
3-8.	TSPA 1993 Ambient Unsaturated-Zone Liquid Saturations (Appendix A) . . . .	3-22
3-9.	TSPA 1993 Distribution Coefficient Distributions (mL/g) (Appendix H) . . . .	3-23
3-10.	TSPA 1993 Beta Bulk Density Distributions (g/mL) . . . . .	3-26

**LIST OF TABLES (Continued)**

	<b>Page</b>
3-11. Expected-Value Retardation Factors for Selected Radionuclides . . . . .	3-27
3-12. Step-Function Travel Times and Unit Average Linear Velocities for <sup>14</sup> C at 1,000 Years (modified from Ross, 1993) . . . . .	3-28
3-13. Time Frames for <sup>14</sup> C Travel-Time Designations . . . . .	3-29
3-14. Normalized Cumulative Release to the Accessible Environment for the Expected-Value Simulations at 10,000 and 100,000 Years . . . . .	3-30
3-15. TSPA 1993 Dose Conversion Factors . . . . .	3-31

## LIST OF FIGURES

		Page
2-1.	Repository Panel Conceptualization (Plan View) . . . . .	2-62
2-2.	Repository Panel Conceptualization (Cross-Section) . . . . .	2-63
2-3.	Waste Package/Engineered Barrier System Schematic . . . . .	2-64
2-4.	Dry Oxidation Penetration Depths (Stahl, 1993) . . . . .	2-65
2-5.	Pitting Corrosion Penetration Depths (Stahl, 1993) . . . . .	2-66
2-6.	Quadratic Fit of Penetration Rates for General Aqueous Corrosion (Lamont, 1993) . . . . .	2-67
2-7.	Dry Oxidation Rates (Bullen, 1993) . . . . .	2-68
2-8.	Aqueous Corrosion Penetration Rates (Bullen, 1993) . . . . .	2-69
2-9.	Method to Determine Failure Distribution . . . . .	2-70
2-10.	Penetration Depth due to Pitting Corrosion Using Stahl Corrosion Model - 28.5 kW/acre . . . . .	2-71
2-11.	Penetration Depth due to Pitting Corrosion Using Stahl Corrosion Model - 57 kW/acre . . . . .	2-72
2-12.	Penetration Depth due to Pitting Corrosion Using Stahl Corrosion Model - 114 kW/acre . . . . .	2-73
2-13.	Spent Fuel Dissolution as a Function of Temperature and Total Carbonate . . .	2-74
2-14.	Glass Dissolution as a Function of Temperature (pH = 7) . . . . .	2-75
2-15.	Neptunium Solubility as a Function of pH and Temperature . . . . .	2-76
2-16.	Americium Solubility as a Function of pH and Temperature . . . . .	2-77
2-17.	Plutonium Solubility as a Function of pH and Temperature . . . . .	2-78
2-18.	Conca Diffusion Coefficient Curve (Conca, 1990) . . . . .	2-79
2-19a.	Cumulative Waste Package Failure Distribution - APD Cases . . . . .	2-80
2-19b.	Actual Waste Package Failure Distribution - APD Cases . . . . .	2-81

## LIST OF FIGURES (Continued)

		Page
2-20.	Waste Package Failure Distribution - Outer Container Thickness Cases . . . . .	2-82
2-21.	Waste Package Failure Distribution - Saturation vs. Temperature Cases - Stahl Model . . . . .	2-83
2-22a.	Cumulative Waste Package Failure Distribution - Saturation vs. Temperature Cases - Lamont Model . . . . .	2-84
2-22b.	Actual Waste Package Failure Distribution - Saturation vs. Temperature Cases - Lamont Model . . . . .	2-85
2-23a.	Waste Package Release Rate: Reference Case - Expected Value Case - 10,000 Years . . . . .	2-86
2-23b.	Waste Package Release Rate: Reference Case - Expected Value Case - 100,000 Years . . . . .	2-87
2-24a.	Waste Package Release Rate: Thermal Loading Cases - 10,000 Years . . . . .	2-88
2-24b.	Waste Package Release Rate: Thermal Loading Cases - 100,000 Years . . . . .	2-89
2-25a.	Waste Package Release Rate: Thermal Loading Cases - 20 cm Overpack - 10,000 Years . . . . .	2-90
2-25b.	Waste Package Release Rate: Thermal Loading Cases - 20 cm Overpack - 100,000 Years . . . . .	2-91
2-26.	Waste Package Release Rate: Thermal Loading Cases - 45 cm Overpack - 100,000 years . . . . .	2-92
2-27a.	Waste Package Release Rate: Overpack Cases - 57 kW/acre - 10,000 Years . . . . .	2-93
2-27b.	Waste Package Release Rate: Overpack Cases - 57 kW/acre - 100,000 Years . . . . .	2-94
2-28a.	Waste Package Release Rate: Inner Container Cases - 10,000 Years . . . . .	2-95
2-28b.	Waste Package Release Rate: Inner Container Cases - 100,000 Years . . . . .	2-96
2-29a.	Waste Package Release Rate: Saturation vs. Temperature Dependent Corrosion Initiation - 10,000 Years (after Stahl, 1993) . . . . .	2-97
2-29b.	Waste Package Release Rate: Saturation vs. Temperature Dependent Corrosion Initiation - 100,000 Years (after Stahl, 1993) . . . . .	2-98

## LIST OF FIGURES (Continued)

		Page
2-30a.	Waste Package Release Rate: Saturation vs. Temperature Dependent Corrosion Initiation - 10,000 Years (after Lamont,1993) . . . . .	2-99
2-30b.	Waste Package Release Rate: Saturation vs. Temperature Dependent Corrosion Initiation - 100,000 Years (after Lamont,1993) . . . . .	2-100
2-31.	CCDF of Normalized Release from All Waste Packages: Reference Case at 10,000 Years . . . . .	2-101
2-32.	CCDF of Normalized Release from All Waste Packages: Reference Case at 100,000 Years . . . . .	2-102
2-33.	CCDF of Normalized Release from All Waste Packages: Thermal Load Cases at 10,000 Years . . . . .	2-103
2-34.	CCDF of Normalized Release from All Waste Packages: Thermal Load Cases at 100,000 Years . . . . .	2-104
2-35.	CCDF of Normalized Release from All Waste Packages: Outer Container Thickness Cases at 10,000 Years . . . . .	2-105
2-36.	CCDF of Normalized Release from All Waste Packages: Outer Container Thickness Cases at 100,000 Years . . . . .	2-106
2-37.	CCDF of Normalized Release from All Waste Packages: Corrosion Initiation Sensitivity Cases at 10,000 Years . . . . .	2-107
2-38.	CCDF of Normalized Release from All Waste Packages: Corrosion Initiation Sensitivity Cases at 100,000 Years . . . . .	2-108
2-39a.	Scatter Plot of pH vs. Total Normalized Release - Reference Case - 10,000 Years . . . . .	2-109
2-39b.	Scatter Plot of pH vs. Total Normalized Release - Reference Case - 100,000 Years . . . . .	2-110
2-40a.	Scatter Plot of pH vs. Total Normalized Release - 114 kW/acre - 10,000 Years . . . . .	2-111
2-40b.	Scatter Plot of pH vs. Total Normalized Release - 114 kW/acre - 100,000 Years . . . . .	2-112

**LIST OF FIGURES (Continued)**

		<b>Page</b>
2-41a.	Scatter Plot of pH vs. Total Normalized Release - 28.5 kW/acre - 10,000 Years .....	2-113
2-41b.	Scatter Plot of pH vs. Total Normalized Release - 28.5 kW/acre - 100,000 Years .....	2-114
2-42a.	Scatter Plot of pH vs. <sup>237</sup> Np Normalized Release - Reference Case - 10,000 Years .....	2-115
2-42b.	Scatter Plot of pH vs. <sup>237</sup> Np Normalized Release - Reference Case - 100,000 Years .....	2-116
2-43a.	Scatter Plot of pH vs. <sup>237</sup> Np Normalized Release - 114 kW/acre - 10,000 Years .....	2-117
2-43b.	Scatter Plot of pH vs. <sup>237</sup> Np Normalized Release - 114 kW/acre - 100,000 Years .....	2-118
2-44a.	Scatter Plot of pH vs. <sup>237</sup> Np Normalized Release - 28.5 kW/acre - 10,000 Years .....	2-119
2-44b.	Scatter Plot of pH vs. <sup>237</sup> Np Normalized Release - 28.5 kW/acre - 100,000 Years .....	2-120
2-45a.	Scatter Plot of pH vs. Total Normalized Release - Lamont Model Case - 10,000 Years .....	2-121
2-45b.	Scatter Plot of pH vs. Total Normalized Release - Lamont Model Case - 100,000 Years .....	2-122
2-46a.	Scatter Plot of pH vs. <sup>237</sup> Np Normalized Release - Lamont Model Case - 10,000 Years .....	2-123
2-46b.	Scatter Plot of pH vs. <sup>237</sup> Np Normalized Release - Lamont Model Case - 100,000 yrs .....	2-124
3-1.	Stratigraphic Cross-Section Through Yucca Mountain on a Line from the Topopah Spring South Portal, West to the Intersection with the Proposed Repository at BC-2 (modified from USGS, 1993) .....	3-32
3-2.	Areal Repository Conceptualization Showing Centroidal Locations of the Nine Unsaturated-Zone Columns (modified after Ryder (1993)) .....	3-33

## LIST OF FIGURES (Continued)

	<b>Page</b>
3-3. Percolation Flux Change Over One Million Years Due to the Expected Climate Changes . . . . .	3-34
3-4. Aqueous Transport Pathway Conceptualizations . . . . .	3-35
3-5. Ross (1993) Areal Repository Conceptualization Showing Cross-Sectional Lines N765000, N762500 and N760000 . . . . .	3-36
3-6. Cross-sectional View Through Yucca Mountain along the N762500 Line (taken from Ross et al., 1992) . . . . .	3-37
3-7. Probability Density Function of the Retarded <sup>14</sup> C Travel Times for Particles Released at 1,000 Years (Ross, 1993) . . . . .	3-38
3-8. Cumulative Density Function of <sup>14</sup> C Travel Times for Releases at 1,000 Years . . . . .	3-39
3-9. TSPA 1993 Step-function Fit of the Cumulative Density Function of <sup>14</sup> C Travel Times for Releases at 1,000 Years . . . . .	3-40
3-10. Partial Presentation of <sup>14</sup> C Travel Pathway Configurations within the RIP . . . . .	3-41
3-11. Expected-Value Releases to the Accessible Environment over 10,000 Years for 57/10/0.95/S1 . . . . .	3-42
3-12. CCDF of Normalized Cumulative Release to the Accessible Environment at 10,000 Years for 57/10/0.95/S1 . . . . .	3-43
3-13. Expected-Value Releases to the Accessible Environment over 10,000 Years for 28.5/10/0.95/S1, 57/10/0.95/S1, and 114/10/0.95/S1 . . . . .	3-44
3-14. CCDF of Normalized Cumulative Releases to the Accessible Environment at 10,000 Years for 28.5/10/0.95/S1, 57/10/0.95/S1, and 114/10/0.95/S1 . . . . .	3-45
3-15. Expected-Value Releases to the Accessible Environment over 10,000 Years for 57/10/0.95/S1, 57/20/0.95/S1, and 57/10/3.5/L1 . . . . .	3-46
3-16. CCDF of Normalized Cumulative Release to the Accessible Environment at 10,000 Years for 57/10/0.95/S1, 57/20/0.95/S1, and 57/10/3.5/L1 . . . . .	3-47
3-17. Expected-Value Releases to the Accessible Environment over 100,000 Years for 57/10/0.95/S1 . . . . .	3-48

## LIST OF FIGURES (Continued)

		<b>Page</b>
3-18.	Expected-Value Releases to the Accessible Environment over 100,000 Years for 28.5/10/0.95/S1, 57/10/0.95/S1, and 114/10/0.95/S1 . . . . .	3-49
3-19.	Expected-Value Releases to the Accessible Environment over 100,000 Years for 57/10/0.95/S1, 57/20/0.95/S1, 57/45/0.95/S1, and 57/10/3.5/L1 . . . . .	3-50
3-20.	CCDF of Normalized Cumulative Release to the Accessible Environment at 100,000 Years for 57/10/0.95/S1 . . . . .	3-51
3-21.	CCDF of Normalized Cumulative Release to the Accessible Environment at 100,000 Years for 28.5/10/0.95/S1, 57/10/0.95/S1, and 114/10/0.95/S1 . . . . .	3-52
3-22.	CCDF of Normalized Cumulative Release to the Accessible Environment at 100,000 Years for 57/10/0.95/S1, 57/20/0.95/S1, 57/45/0.95/S1, and 57/10/3.5/L1 . . . . .	3-53
3-23.	Scatter Plot of Unsaturated-Zone Flux vs. Normalized Release of <sup>99</sup> Tc to the Accessible Environment at 10,000 Years for 57/10/0.95/S1 . . . . .	3-54
3-24.	Scatter Plot of Saturated-Zone Flux vs. Normalized Release of <sup>99</sup> Tc to the Accessible Environment at 10,000 Years for 57/10/0.95/S1 . . . . .	3-55
3-25.	Scatter Plot of pH vs. Normalized Release of <sup>99</sup> Tc to the Accessible Environment at 10,000 Years for 57/10/0.95/S1 . . . . .	3-56
3-26.	Scatter Plot of Unsaturated-Zone Flux vs. Normalized Total Release to the Accessible Environment at 100,000 Years for 57/10/0.95/S1 . . . . .	3-57
3-27.	Scatter Plot of Saturated-Zone Flux vs. Normalized Total Release to the Accessible Environment at 100,000 Years for 57/10/0.95/S1 . . . . .	3-58
3-28.	Scatter Plot of pH vs. Normalized Total Release to the Accessible Environment at 100,000 Years for 57/10/0.95/S1 . . . . .	3-59
3-29.	Expected-Value Dose Exposures over 1,000,000 Years for 57/10/0.95/S1 . . . . .	3-60
3-30.	Expected-Value Dose Exposures over 1,000,000 Years for 28.5/10/0.95/S1 . . . . .	3-61
3-31.	Expected-Value Dose Exposures over 1,000,000 Years for 114/10/0.95/S1 . . . . .	3-62
3-32.	CCDF of Peak Dose Exposures over 1,000,000 Years for 28.5/10/0.95/S1, 57/10/0.95/S1, and 114/10/0.95/S1 . . . . .	3-63

**LIST OF FIGURES (Continued)**

	<b>Page</b>
3-33. Expected-Value Dose Exposures over 1,000,000 Years for 57/20/0.95/S1 . . . .	3-64
3-34. Expected-Value Dose Exposures over 1,000,000 Years for 57/45/0.95/S1 . . . .	3-65
3-35. Expected-Value Dose Exposures over 1,000,000 Years for 57/10/3.5/L1 . . . . .	3-66
3-36. CCDF of Peak Dose Exposures over 1,000,000 Years for 57/10/0.95/S1, 57/20/0.95/S1, 57/45/0.95/S1, and 57/10/3.5/L1 . . . . .	3-67
3-37. Scatter Plot of Unsaturated-Zone Flux vs. Peak Dose Exposure over 1,000,000 Years for 57/10/0.95/S1 . . . . .	3-68
3-38. Scatter Plot of Saturated-Zone Flux vs. Peak Dose Exposure over 1,000,000 Years for 57/10/0.95/S1 . . . . .	3-69
3-39. Scatter Plot of pH versus Peak Dose Exposure over 1,000,000 Years for 57/10/0.95/S1 . . . . .	3-70

## 1. INTRODUCTION

Yucca Mountain, Nevada, is currently being characterized by the U.S. Department of Energy (DOE) to determine its suitability as a potential site for a mined geologic repository for the permanent disposal of high-level radioactive waste. An important component in the determination of the suitability of the Yucca Mountain site is the ability of the natural and engineered barriers to contain and isolate the radioactive wastes from the biosphere. The method used to evaluate the ability of the site and engineered barriers to meet regulatory criteria is referred to as performance assessment. Although several different criteria may be used to determine the performance of the site and engineered barriers, generally the evaluations conducted to date have used the total cumulative radionuclide release for 10,000 years to the accessible environment normalized to the Table 1 limits specified in the U.S. Environmental Protection Agency (EPA) Standard (40 CFR Part 191).<sup>1</sup> Although the EPA standard is no longer directly applicable to Yucca Mountain, it is a useful measure of total system performance and can be used as a surrogate performance measure for judging the suitability of the potential geologic disposal system. In addition, because the NAS committee is evaluating the possibility of a dose-based standard, the performance of the site and engineered barriers using dose as the performance measure has also been evaluated.

Total system performance assessment (TSPA) combines the effects of the waste package and other engineered barriers and the site to determine the release of radionuclides to the accessible environment due to all significant processes and events. Several evaluations of total system performance of the Yucca Mountain site have been conducted by a number of different organizations. These earlier assessments have included the Sandia National Laboratories (SNL) preliminary evaluations reported in the Environmental Assessment (DOE, 1986), which reported the results of performance evaluations by Thompson et al. (1984) and Sinnock et al. (1984). Pacific Northwest Laboratory (PNL) performed a preliminary total system risk assessment in 1988 (Doctor et al., 1992). Independent of the DOE program, the NRC completed Phase 1 of their Iterative Performance Assessment in 1990 (NRC, 1990). The Electric Power Research Institute (EPRI) completed a Phase 1 performance assessment in 1990 (McGuire et al., 1990), and a Phase 2 evaluation in 1992 (McGuire et al., 1992). Recent assessments have been performed on behalf of the Yucca Mountain Site Characterization Project (YMP). These are reported in PNL (Eslinger et al., 1993) and SNL (Barnard et al., 1992) documents. These latter analyses constitute the first iteration of the TSPAs and are referred to as TSPA 1991. Each of the above analyses has used a different level of detail with which to represent the individual processes of relevance to the performance of the potential mined geologic disposal system.

---

<sup>1</sup>The EPA Standard promulgated under 40 CFR 191 does not currently apply to Yucca Mountain as per the language of Section 801 of the Energy Policy Act of 1992. This Act directs the EPA to contract with the National Academy of Sciences (NAS) to conduct a study to determine the reasonableness of different types of environmental standards (notably, individual dose) to protect human health. Based on the NAS recommendations, EPA is to promulgate a new standard explicitly for Yucca Mountain. The U.S. Nuclear Regulatory Commission (NRC) would then modify 10 CFR Part 60 to be consistent with the revised EPA Standard.

The TSPAs are conducted iteratively during the course of the investigations leading to the license application. The iterative assessments are used to identify the key issues which should be the focus of site characterization and design activities. The results of a performance assessment iteration provide input to regulatory/licensing and programmatic decisions as well as providing guidance to prioritize site characterization and design activities.

Beginning in fiscal year 1993, the Civilian Radioactive Waste Management System Management and Operating Contractor (CRWMS M&O) was given the responsibility to plan, coordinate, and manage the second iteration of TSPA (hereafter referred to as TSPA 1993) for the Yucca Mountain Site Characterization Project Office (YMPO) of the Office of Civilian Radioactive Waste Management. The M&O responsibility also includes conducting TSPAs which would complement the analyses being performed by other participants (principally SNL with support from Lawrence Livermore National Laboratory (LLNL) in the area of waste package performance). This document presents the objectives, approach, assumptions, input, results, conclusions, and recommendations associated with the M&O TSPA 1993.

## **1.1 OBJECTIVES**

The primary objectives of TSPA 1993 have been derived after a review of the programmatic needs for TSPA and the assumptions incorporated in TSPA 1991. The aim of any assessment of total system performance is to either (1) enhance the realism/representativeness of the analyses, (2) incorporate new information or designs into the analyses, (3) test the impact/importance (i.e., sensitivity) of certain assumptions on the behavior of the system, or (4) evaluate alternative measures of performance or safety. In the case of TSPA 1993, all of the above general objectives apply.

In TSPA 1991, while it was recognized that the thermohydrologic environment in the vicinity of the waste packages and repository would be perturbed following waste emplacement, the thermohydrologic regime was not incorporated into the analyses except as an assumed delay time related to the "rewetting" of the repository. This "rewetting" was assumed to start at 300 years following emplacement and continue with a uniform distribution for 1,000 years so that all those waste packages that were going to come in contact with liquid water were "rewet" at 1,300 years after emplacement. Similarly, the container lifetime incorporated in TSPA 1991 was an assumed log-uniform distribution between 500 and 10,000 years after the repository was "rewet". Both of these assumptions were required due to the paucity of thermohydrologic analyses and corrosion rate information.

The TSPA 1993 analyses presented in this document directly incorporate the expected dependency of several processes and parameters on the thermohydrologic regime. In particular, detailed thermohydrologic analyses are used to determine the temperature, aqueous flux, gaseous flux, and liquid saturation in the vicinity of the repository under a number of possible thermal loads. These primary results are then used to modify the radionuclide exposure, engineered barrier system (EBS) release, and geosphere transport properties that affect the radionuclide release to the accessible environment. In addition, TSPA 1993 directly incorporates the corrosion (both general and pitting) of the waste package's corrosion allowance outer barrier and corrosion resistant inner barrier in determining the expected time to "failure" of the waste package. The

direct inclusion of thermally-dependent processes and parameters, and the corrosion of the waste package, is a significant advancement over the simplifications required in TSPA 1991.

The analyses of aqueous releases presented in TSPA 1991 utilized a radionuclide inventory that was limited to the radionuclides believed to contribute most significantly to the normalized cumulative release over 10,000 years (with the normalization being to the Table 1 values in 40 CFR 191). The present TSPA 1993 greatly expands the inventory to include all radionuclides (and their parents) which may potentially contribute to the peak individual dose over a time period up to one million years. In addition, TSPA 1993 considers the inventory associated with spent fuel from commercial nuclear reactors as well as defense high-level radioactive waste. A defense waste inventory component was not considered in the SNL analyses in TSPA 1991, but was considered in the PNL analyses (Eslinger et al., 1993).

Since the completion of TSPA 1991, significant new information has been collected and new designs have been proposed which change some of the fundamental premises of the earlier analyses. In particular, laboratory measurements of radionuclide solubility and retardation over a range of likely environmental conditions (namely, temperature and geochemistry) have been generated by scientists at Los Alamos National Laboratory (Los Alamos). In addition, thermally dependent waste form alteration and glass dissolution rates are available from studies conducted at LLNL and PNL. The design of the repository (with special emphasis on the thermal load), the mode of waste package emplacement (vertical in borehole vs. horizontal in drift), and the waste package design (varying thicknesses of an outer corrosion-allowance material such as mild steel surrounding varying thicknesses of an inner corrosion-resistant material such as Alloy 825) have all undergone changes since the completion of TSPA 1991. The earlier analyses concentrated on the Site Characterization Plan (SCP) thermal load (nominally 141 kW/ha or 57 kW/acre), waste emplacement mode (vertical in borehole) and waste package design (thin corrosion resistant material). Although the proposed designs are not fixed, an important role of performance assessment in general and the TSPAs in particular is to assess the advantages/disadvantages of the different proposed designs from a postclosure performance perspective. As a result, TSPA 1993 incorporates alternate designs and investigates the sensitivity of the releases to the accessible environment to these alternate designs.

An important goal of any assessment of performance must be an evaluation of the impact of certain assumptions on the expected behavior of the system being modeled. The results may be sensitive to certain components, processes, or parameters used to describe the subsystem behavior. Identifying the important processes and parameters can be useful in assisting the project in focussing resources on those areas that contribute most significantly to the overall performance. As a result, analyses conducted as part of TSPA 1993 aim to identify the key assumptions and the sensitivity of the results to these assumptions.

Since the completion of TSPA 1991, the total system postclosure performance measure applicable to Yucca Mountain has been questioned by Section 801 of the Energy Policy Act of 1992. Previously, the principal postclosure performance measure was the cumulative normalized release integrated over 10,000 years (referred to as the EPA sum). Section 801 calls for the NAS to evaluate the reasonableness/appropriateness of alternate environmental standards to assure the protection of the public if a nuclear waste repository is located at Yucca Mountain. In particular, the NAS is to evaluate the potential use of a dose-based standard to protect the public from

future radiation exposure. Although it is impossible to prejudge the outcome of the NAS committee convened to address this issue (as well as how EPA may decide to implement the recommendations of the NAS committee), it does seem prudent to quantify the expected doses associated with a potential repository at Yucca Mountain. As a result, TSPA 1993 considers *both* the cumulative normalized radionuclide release at the accessible environment and the peak individual dose as relevant performance measures. The peak dose is the highest dose the maximally exposed individual may receive within one million years following repository closure. In addition, because the time period of regulatory concern is also uncertain, the analyses to incorporate the arrival of the most significant radionuclide peaks (which can occur several tens to hundreds of thousands of years after closure depending on the package lifetimes and water travel times) have been extended.

In summary, the major objectives of the current TSPA 1993 iteration are to:

1. Incorporate thermal dependency on individual processes and parameters,
2. Evaluate the effects of alternate thermal loads,
3. Evaluate the effects of alternate waste package designs,
4. Evaluate alternate measures of total system performance,
5. Incorporate new site and design information,
6. Incorporate a more representative inventory including high-level waste (HLW),
7. Conduct sensitivity analyses to identify the key processes and parameters affecting postclosure performance, and
8. Provide guidance to site characterization and design activities.

In addition to defining the enhancements/modifications in this M&O contribution to TSPA 1993, it is useful to identify those aspects that are different from either TSPA 1991 or the SNL contribution to TSPA 1993. Due to limited resources and the desire to minimize duplication, the TSPA 1993 analyses presented in this document do not consider the possible effects of disruptive events such as human intrusion, volcanic intrusion (whether direct release effects or indirect effects), and tectonism. These processes and their potential impact on postclosure performance are discussed in TSPA 1991 (Barnard et al., 1992; Eslinger et al., 1993). The SNL contribution to TSPA 1993 does incorporate analyses of some disruptive events (see Wilson et al., 1994, in press). While it is acknowledged that a complete TSPA must include all reasonable scenarios which could contribute to the release of radionuclides to the accessible environment, our attention is focused on the site- and design-related effects on the expected release rather than the externally initiated releases that are much more dependent on the assumptions regarding the probability of occurrence and geometric descriptions of the event. The reader interested in the direct releases associated with these disruptive scenarios is referred to Barnard et al. (1992), Eslinger et al. (1993), and Wilson et al. (1994, in press).

## 1.2 APPROACH

The general approach taken in this TSPA 1993 to evaluate the postclosure performance of a potential repository at Yucca Mountain, is to (1) abstract primary functional relationships either indirectly from results obtained from detailed process models, or directly from uncertain parameter distributions; (2) define the dependence of relevant radionuclide exposure, EBS release, and geosphere transport properties on the primary thermohydrologic regime; and (3) incorporate the functional relationships and dependencies into the Repository Integration Program (RIP). The RIP is a performance assessment and site characterization strategy evaluation program developed by Golder Associates Inc. (Golder Associates Inc., 1993). The RIP is a TSPA model that uses the Monte Carlo method to propagate uncertainty in parameters and processes to produce probabilistic predictions of the repository performance. The RIP is not a model in the normal sense of the word in that it does not *explain* the behavior of the system or its components, but instead attempts to *describe* the behavior by incorporating as many of the system dependencies as the user chooses to specify. To a certain extent, the RIP program is similar to a spreadsheet calculation which tracks the movement of mass from a source to a receptor. The theory and capability of RIP are described in Miller et al. (1993, in press). A user's guide for RIP has been published by Kossik and Hachey (1993). An example application of RIP to the Yucca Mountain potential repository site is presented in Golder Associates Inc. (1993). A comparative evaluation of RIP-generated results with those generated in TSPA 1991 has been documented in INTERA Inc. (1993).

The RIP has been chosen for this assessment because it allows the user to incorporate sufficient specificity in the process or process interactions to ensure that potentially important correlations and dependencies are included in the analysis. The user may specify the relevant parameters describing the behavior of each of the major components of the waste disposal system (i.e., the waste package, the EBS, the geosphere, the biosphere, and externally initiated events and processes). In Section 1.3 a brief description of how RIP was implemented in TSPA 1993 is presented.

Because RIP does not explicitly explain the behavior of any component or process incorporated in the representation of the total system, it requires significant abstraction from a variety of sources. In the present application of RIP in TSPA 1993, the following sources have been used to derive input values.

TOPIC	REFERENCE
Hydrothermal regime	
- Panel scale flux, temperature, water saturation	See Appendix A
- Waste package scale temperature	See Appendix B
Radionuclide inventory	See Appendix C
Waste stream	See Appendix D
Oxidation/aqueous corrosion rates	See Appendix E (Stahl, 1993) See Appendix F (Lamont, 1993)
Spent fuel alteration rates	Gray (1993)
HLW Glass dissolution rates	Bourcier (1993)

**TOPIC****REFERENCE**

---

Radionuclide solubilities	See Appendix G (Triay, 1993)
Diffusion coefficients	Conca (1990)
Radionuclide distribution coefficients	See Appendix H (Meijer, 1993)
Gaseous flux	See Appendix I (Ross, 1993)
Saturated Zone velocity	Barr, personal communication (1993) (see also Wilson et al., 1994, in press)
Percolation flux	Wilson, personal communication (1993) (see also Wilson et al., 1994, in press)

Because one of the primary objectives of this iteration of TSPA is to evaluate alternate designs, analyses at a range of thermal loads (70.4, 141, and 282 kW/ha, or 28.5, 57, and 114 kW/acre), with a range of outer corrosion-allowance material thicknesses (10, 20, and 45 cm), and a range of inner corrosion-resistant material thicknesses (0.95 and 3.5 cm) have been conducted. The results of both radionuclide release and dose calculations are presented.

### **1.3 GENERAL DESCRIPTION OF THE REPOSITORY INTEGRATION PROGRAM**

The general structure of RIP consists of a front-end, a back-end, and a post-processor. The front-end is where the user defines and samples the parameter values and functional relationships using a Monte-Carlo type sampling algorithm. Each sampling represents a realization, a description of a possible state of the system. The back-end is where the actual computation occurs. The back-end is run for each sampled realization created by the front-end. The RIP also has the capability to run only the expected value realization, in which case the expected value from each probabilistic distribution is used as input to the back-end. The post-processor is used to display the results and conduct simple sensitivity analyses. The results may be presented as time history plots in which the temporal response of the dependent variable (whether release or dose) is plotted, complementary cumulative distribution functions (CCDF), or sensitivity analyses consisting of either one- or two-dimensional scatter plots or simple parameter correlations.

The computational part of RIP consists of four primary components: the waste package/EBS radionuclide release module, the geosphere radionuclide transport module, the biosphere transport and dose module, and the disruptive events module. The first three modules are briefly described in the following sections. Because no disruptive events have been implemented in this TSPA 1993, the interested reader is referred to Miller et al. (1993, in press) for a discussion of how RIP may be used to treat scenarios.

#### **1.3.1 Waste Package/Engineered Barrier System Radionuclide Release Module**

The waste package/EBS component of RIP can be used to describe several processes which, if they occur, could lead to radionuclide release to the geosphere. These processes include container degradation and "failure", the exposure of the rapid-release fraction of the inventory, the alteration/dissolution of the waste form causing the exposure of the bound portion of the radionuclide inventory, and the mass transfer of radionuclides from the waste package through

the EBS to the host rock. Each of these processes may be dependent on the near-field environment; in particular the thermal, hydrologic, and geochemical conditions in the vicinity of the waste package. Many of these dependencies are incorporated in this iteration of TSPA 1993.

Container degradation or "failure" is a function of the time it takes for aqueous corrosion processes to be initiated as well as the corrosion rates (both general and pitting) once corrosion has started. [Note: For most temperatures, dry oxidation of the container walls is extremely slow (see Appendices E and F) and can reasonably be neglected. However, it is conceivable that certain backfill designs might result in extremely high temperatures which could necessitate the inclusion of dry oxidation degradation processes (Ryder, personal communication, 1993; see also Wilson et al., 1994, in press, and Appendix B).] The time at which aqueous corrosion is initiated is dependent on the thermal load, as a result of the "drying" effect of the thermal regime. The factors affecting the initiation of aqueous corrosion under varying humidity and temperature conditions are complex and uncertain (McCright, 1993). To address this uncertainty, two different criteria for the initiation of aqueous corrosion, based on either the degree of water saturation or temperature have been considered. The corrosion rates are also uncertain and variable. Two alternate conceptualizations of the corrosion rates based on the assumptions described by either Stahl (see Appendix E) or Lamont (see Appendix F) have been considered. In general the time to "failure" of the mild steel outer wall is a function of the corrosion rate and the thickness of the outer wall. The corrosion rate in turn is a function of temperature and time, with the temporal dependency reflecting the possible build-up of an external rind which tends to slow the corrosion process. The time to "failure" of the Alloy 825 inner wall is a function of the corrosion rate (which is uncertain and variable from waste package to waste package), temperature, and the thickness of the inner wall. For all analyses, it is conservatively assumed the cladding has "failed" congruently with the inner container wall.

Once the waste package and cladding have been breached, the radionuclide inventory is exposed. The RIP allows three inventories to be specified: a free inventory that is released instantaneously once the primary container fails, a gap inventory that is released instantaneously once the secondary container (i.e., cladding) fails, and a matrix or bound inventory that is released as the waste form is altered and dissolved. Because the inner wall of the waste package and the cladding are assumed to fail congruently in TSPA 1993, only a prompt release inventory (to represent the sum of the free and gap inventories) and the matrix inventory have been used.

The exposure of bound radionuclides in the spent fuel or glass matrix is a function of the alteration rate. In TSPA 1993, the alteration rate (represented by the fraction of the bound inventory available for release in a given time period) is a function of the normalized dissolution rate and the total normalized surface area of the spent fuel or glass matrix. The normalized dissolution rate (in gm/m<sup>2</sup>yr) is a function of temperature and dissolved carbonate content. The total normalized surface area (in m<sup>2</sup>/gm) is assumed to be a constant for each realization (i.e., the potential dependency of temperature on the effective surface area is not considered).

Once radionuclides have been dissolved, they may be transferred to the host rock by advective or diffusive transport. [Note: Gaseous radionuclides are released instantaneously once they are exposed, whether they are part of the prompt release or bound inventory.] Aqueous phase advective releases are a function of the dissolved radionuclide concentration in contact with the waste and the flux past each waste package. Aqueous phase diffusive releases are a function of

the effective diffusion coefficient, a geometric factor for steady-state diffusion (see Chambré et al., 1985), and the dissolved radionuclide concentration. The radionuclide concentration will be controlled by either the elemental solubility or the exposed but unreleased radionuclide mass divided by the water volume in contact with the waste matrix. The individual radionuclide solubility is determined by the mass fraction of each radionuclide of a particular element which varies with time due to ingrowth and decay. In TSPA 1993, elemental solubilities are a function of temperature and, in some cases, pH. In TSPA 1993, the aqueous flux is controlled by the applied thermal load, while the effective diffusion coefficient is a function of the water content (after Conca, 1990) which in turn is a function of the thermal load and the ambient water saturation and percolation flux.

### **1.3.2 Geosphere Radionuclide Transport Module**

The RIP incorporates a simplified description of radionuclide transport through the geosphere. The geosphere may be "discretized" into multiple legs or pathways that may be combined in parallel or in series. These pathways may be specified to represent different flow regimes (i.e., aqueous or gaseous flow), different flow domains (i.e., the saturated or unsaturated zone), or different cross sections of the repository. In TSPA 1993, both gaseous and aqueous flow and radionuclide transport are considered, with the aqueous phase being divided into the unsaturated and saturated zones. The unsaturated zone has been divided into nine columns corresponding to nine panels of the repository. Each column has been divided into five or six pathways based on the inferred hydrostratigraphy at the centroid of each column. The hydrostratigraphic unit thicknesses were based on U.S. Geological Survey (USGS) cross sections through Yucca Mountain (USGS, 1993).

The RIP allows for different flow modes to be assigned to each pathway. A single-flow mode may be used to represent an equivalent continuum porous medium and a multiple-mode pathway may be used to approximate varying degrees of fracture-matrix coupling in a dual-porosity, dual-permeability medium. For single-mode pathways, RIP uses an analytical solution to the one-dimensional advective-dispersion equation. For multiple-mode pathways, RIP uses a modified Markovian solution algorithm to predict the transition of mass between the modes. In TSPA 1993, the rate of water imbibition into the matrix and/or the rate of radionuclide diffusion into the matrix exceeds the rate of fracture transport has been assumed; therefore, radionuclide transport is matrix-dominated. As a result, only the single-mode equivalent continuum approximation to describe the transport in the geosphere has been used. The possible effect of assuming varying degrees of fracture-matrix coupling have been investigated in the earlier application of RIP to the TSPA 1991 data set (INTERA, 1993).

In TSPA 1993, the retarded travel time of  $^{14}\text{C}$  from the repository to the accessible environment (i.e., the surface) has been derived from analyses conducted by Ross (1993) (see Appendix I and Wilson et al., 1994, in press). These analyses are based on first predicting the gaseous phase temporal and spatial velocity at Yucca Mountain due to the application of a 141 kW/ha (57 kW/acre) thermal load. This velocity field is then used to predict the arrival times for retarded  $^{14}\text{C}$  particles released at 1,000 year time increments from 1,000 to 18,000 years following repository closure to reach the accessible environment (with the retardation being temperature dependent).

The unsaturated-zone aqueous transport employed in TSPA 1993 has used hydrologic and transport properties derived from either TSPA 1991 or more recent information. The ambient unsaturated zone aqueous flux used in TSPA 1993 is the same as that employed by SNL in their TSPA 1993 analyses (i.e., an exponential distribution with an expected value of 0.5 mm/yr), with the exception that (a) the percolation flux when the saturated matrix hydraulic conductivity is less than the percolation flux has not been reduced, and (b) a linearly increasing/decreasing flux to approximate the effects of possible climate changes has been considered, while the SNL contribution to TSPA 1993 uses a step-function change in flux when the climate change is inferred to occur. Possible thermal perturbations to the unsaturated-zone aqueous flux are not considered in this TSPA iteration. That is, it is assumed that once radionuclides are released from the EBS, they are transported through the geosphere at a rate proportional to the ambient percolation flux.

Radionuclide transport in the saturated zone is also assumed to be represented by an equivalent continuum in TSPA 1993. The interstitial velocity distribution has been based on recent process modeling reported by Barr (1993) (see Wilson et al., 1994, in press). Other transport properties (namely distribution coefficients), were obtained through expert elicitations of YMP scientists at Los Alamos (see Appendix H).

### **1.3.3 Biosphere Transport and Dose Module**

Recent modifications to RIP, since the release of Version 3.0, described in Kossik and Hachey (1993), allow for dose to be predicted. In general, RIP tracks the mass of each individual radionuclide through the system to the accessible environment. This mass is then converted to activity prior to post processing (such as determining the cumulative activity released over a certain time period and normalizing the cumulative activity released by the Table 1 values in 40 CFR 191 for comparison to the EPA limit). In the biosphere transport module of RIP, the radionuclide mass released in each time step is transferred to a mixing cell where it is diluted with the assumed lateral flow through the aquifer. The mixing cell is considered to be large enough to capture the entire radionuclide plume. Water from the mixing cell is assumed to be available for consumption as drinking water or for other household or farming uses. The radionuclide concentrations of the water extracted from the mixing cell are converted to doses using published dose conversion factors such as those presented by PNL in TSPA 1991 (Eslinger et al., 1993) or by the Waste Isolation Systems Panel (NAS, 1983).

The volumetric flux in the aquifer with which any radionuclides released from the unsaturated zone will be diluted is a function of the Darcy flux through the saturated zone as well as the cross-sectional area perpendicular to the flow. The cross-sectional area may be a function of the horizontal and vertical dispersion of the radionuclide plume and/or the capacity of the well used to pump the water to the surface. For TSPA 1993, the horizontal Darcy flux has been based on the results of Barr (1993) (see Wilson et al., 1994, in press). A cross-sectional area of  $2.0 \times 10^5 \text{ m}^2$  which is based on a plume width of 4000 m and thickness of 50 m has been assumed. The assumed thickness is the mid-point of the range analyzed by SNL in their contribution to TSPA 1993 (Wilson et al., 1994, in press).

## **1.4 RELATED TSPA 1993 ANALYSES**

Both the M&O and SNL have conducted TSPA analyses in the current iteration. The M&O approach, assumptions, results, conclusions, and recommendations are presented in this document. The SNL approach, assumptions, results, conclusions, and recommendations are presented in Wilson et al. (1994, in press). The aim is to combine the two organizations' documents into a single YMPO report that could then be reviewed by external organizations (such as the Performance Assessment Advisory Group of the Paris-based Organization for Economic Cooperation and Development's Nuclear Energy Agency [OECD/NEA]).

All analyses of total system performance are, by their very nature, abstractions or "roll-ups" from more detailed physically-based representations of the relevant processes and parameters affecting radionuclide release to the accessible environment and ultimately the biosphere. Both the work reported on in this document as well as that described in Wilson et al. (1994, in press) have relied on input from process-level understanding generated by data interpretation and detailed modeling conducted by other participants, including LLNL, Los Alamos, the USGS, SNL, and the M&O.

The TSPA software being used by the M&O and SNL are essentially shells into which varying levels of detail can be placed. The level of detail depends more on the overall objectives of the analyses, the desired computational efficiency, and the assumptions deemed relevant by the analysts, than on the software itself. In general, RIP simplifies the individual processes incorporated in the assessment so they can be represented by analytical expressions and relies on functionally-dependent relationships developed from more detailed models or information. As a result, RIP has a lot of flexibility to evaluate the effects of parameter dependencies and alternate parameter distributions on cumulative release or other performance measures. The Total System Analyzer/Yucca Mountain Integrating Model software used in the SNL analyses also uses simplified representations of individual processes. However, these representations differ from RIP in that they can use numerical solution techniques. This can allow an increased level of detail, if the analyst so desires, at the expense of increased computational time and decreased flexibility to address parameter dependencies and correlations.

Although the M&O and SNL are using two different computational tools for assessing the total system performance, the primary difference in the two approaches is the level of detail incorporated in the abstraction from the process models. This difference between the two sets of analyses is embodied in the assumptions made by both organizations as to what and how process-level understanding is abstracted. The assumptions made in the two sets of analyses are much more important to the results than is the computational scheme embodied in the codes being used. No decision has been made as to which approach (or both) will be used for future TSPAs.

## **1.5 ORGANIZATION OF THIS REPORT**

Following this introductory section in which the overall objectives and general approach followed in TSPA 1993 are described, the assumptions, input, and results of our TSPA 1993 analyses are presented. Our presentation has been divided into a discussion of the waste package/EBS

performance (i.e., the source term for geosphere transport) in Chapter 2 and the geosphere performance in Chapter 3.

Within the waste package/EBS chapter (Chapter 2) a conceptual description and input parameter values for the radionuclide inventory, the container "failure", the mobilization of the radionuclides, and the transport of radionuclides to the host rock are presented. For a number of different alternative designs and assumptions regarding the initiation and rate of aqueous corrosion, the following is presented (1) the expected value radionuclide release time history over 10,000 and 100,000 years, (2) the expected value cumulative release normalized to the 40 CFR 191 Table 1 values over 10,000 and 100,000 years, (3) CCDFs of normalized cumulative releases from the waste package over 10,000, and 100,000 years, and (4) scatter plots of cumulative normalized release vs. pH (due to the effect of pH on radionuclide solubility). The principal aim of these comparisons is to evaluate the sensitivity of the waste package releases to different thermal loads, waste package designs, and conceptual representations of corrosion initiation and rates in a spatially and temporally variable thermal regime.

Within the geosphere chapter (Chapter 3), conceptual descriptions and input parameter values for gaseous phase transport, aqueous phase transport in the unsaturated zone, and transport in the saturated zone and the biosphere are presented. For a number of different thermal loads and waste package designs the following are presented (1) the expected value time history of radionuclide release to the accessible environment over 10,000 and 100,000 years, (2) the expected value of the cumulative release to the accessible environment normalized to the 40 CFR 191 Table 1 values over 10,000 and 100,000 years, (3) CCDFs of the cumulative normalized gaseous release over 10,000 years, (4) CCDFs of the cumulative normalized aqueous release over 10,000 and 100,000 years, (5) the expected value time history of dose over 1,000,000 years, (6) CCDFs of the peak dose over 1,000,000 years, (7) scatter plots illustrating the sensitivity of cumulative normalized release to the unsaturated zone percolation flux, and (8) scatter plots of the sensitivity of peak individual dose to the unsaturated zone flux, the saturated zone flux, and pH. The principal aim of these comparisons is to evaluate the sensitivity of geosphere releases to alternative thermal loads and waste package designs as well as to evaluate alternate measures of postclosure total system performance.

Following the presentation of the materials and results in Chapters 2 and 3, the results are summarized and relevant conclusions and recommendations are made for additional analyses and/or information that should be acquired by the site characterization and design activities that would assist in increasing the certainty/robustness of the performance predictions (Chapter 4). To a limited extent, TSPA 1993 results are compared with those presented in TSPA 1991 to highlight the improvements in the conceptualizations employed in this iteration. Information needs that would be important prior to initiating the next total system performance iteration are also identified.

## 2. WASTE PACKAGE/ENGINEERED BARRIER SYSTEM

The waste package and EBS analyzed in TSPA 1993 is described in this section. The waste package is the waste form, either spent nuclear fuel or vitrified high-level waste, and the primary and secondary metallic barriers that contain it. The EBS is the waste package and the engineered setting into which it has been emplaced. The EBS may consist of the drifts or of vertical boreholes. The EBS may have an air gap between the waste package and the host rock, or may have a backfill engineered to have certain hydrologic and/or geochemical properties. When EBS is used herein, it may refer to an emplaced waste package, an ensemble of emplaced waste packages, or all emplaced waste packages.

The analysis of waste package and EBS covered several designs and included several different conceptualizations of container failure. A summary of the analysis variations (design and conceptualization) is presented in Table 2-1. Note the labeling convention established in Table 2-1 for each of the cases (right hand column). Three thermal loads were considered: 70.4, 141, and 282 kW/ha (28.5, 57, and 114 kW/acre). The waste packages were assumed to be located in the excavated drift with no backfill. Three different outer container or overpack thicknesses were considered: 10, 20, and 45 cm. For the 141 and 282 kW/ha (57 and 114 kW/acre) cases, two different inner container thicknesses were considered: 0.95 cm and 3.5 cm. For the 70.4 kW/ha (28.5 kW/acre), only the 0.95-cm case was analyzed.

Four distinct failure conceptualizations were also evaluated. The conceptualizations are different in two primary areas: (1) definition of when aqueous corrosion of the containers begins, and (2) overall waste package failure model (Stahl (1993, Appendix E) or Lamont (1993, Appendix F)). These differences are described in detail in Section 2.1.2. Briefly, the aqueous corrosion is assumed to begin or initiate either due to saturation in the repository being greater than residual saturation, or due to the repository temperatures dropping below 100°C. The threshold for saturation-dependent corrosion initiation is based on the irreducible saturation. At saturations greater than 8 percent (which corresponds to the residual rock matrix saturation), a continuous layer of water is assumed to form on the rock, allowing for aqueous waste package corrosion and diffusive transport of radionuclides from the waste package. The Stahl and Lamont models are different in the rates of corrosion assumed to occur at different temperatures. This leads to different failure distributions for each of the models.

The waste package/EBS conceptual representation employed in TSPA 1993 includes thermal effects on solubilities, saturations, flux distribution, and alteration rate. A two-dimensional hydrothermal analysis using VTOUGH (Nitao, 1989) was conducted in order to evaluate temperature, saturation, and flux distributions for three thermal loads, 70.4, 141, and 282 kW/ha (28.5, 57, and 114 kW/acre). The analysis used an equivalent continuum assumption, and the thermohydrologic stratigraphy and parameters of Klavetter and Peters (1986). The horizontal model geometry consisted of a central heated area surrounded by a nonheated area. Figure 2-1 shows the plan view of the repository, indicating the area with spent fuel (concentric, equal area Rings 1-6) and the area with defense HLW (Ring 7). The HLW was assumed not to contribute any heat, thus was placed in the outer unheated ring of the model. The temperature was calculated for a location of 5 m from the drift wall. The vertical discretization is shown in Figure 2-2. The base case initial condition was zero ambient infiltration with a geothermal

temperature distribution. The upper boundary was assumed to be at constant temperature (13°C) and pressure (0.86 atm). The lower boundary, located 1 km into the saturated zone, was assumed to be at constant temperature (53°C) and constant pressure (15 atm). The lateral boundaries were closed to fluid and heat flow. The fuel characteristics were similar to that used in the SNL contribution to TSPA 1993: (1) 40,750 metric tons heavy metal (MTHM) pressurized water reactor (PWR) fuel and 22,250 MTHM boiling water reactor (BWR) fuel, (2) 22.5 year out-of-reactor PWR and 23.5 year out-of-reactor BWR fuel, and (3) 42,200 MegaWatt-day per MTHM (MWd/MTHM) PWR burnup and 32,200 MWd/MTHM BWR burnup fuel.

The description of the waste package/EBS which was analyzed in TSPA 1993 includes: radionuclide inventory, container failure, waste mobilization, transport of radionuclides, and description of the EBS. A schematic of the waste package/EBS is presented in Figure 2-3. The inventory consists of both spent fuel and HLW in separate containers. The container failure description includes both the primary outer container failure as well as the secondary inner container failure. Three outer container thicknesses (10, 20, and 45 cm) are considered, and two inner container thicknesses (.95 and 3.5 cm) are evaluated. Corrosion leading to container failure is initiated according to two different conceptual models: saturation or temperature dependent. TSPA 1993 assumes there are three basic release modes: (1) no release, (2) advective release, and (3) advective plus diffusive release, with the ratio determined by advective and diffusive properties. Waste is mobilized for advective release by the water flux in the repository which will vary over time and space due to both thermal and hydrogeologic factors. Diffusive release may also occur. Transport from the containers depends on the flux, saturation, temperature, and characteristics of the engineered backfill.

The waste package section is divided into three subsections: Section 2.1 - Conceptual and Parameter Descriptions, Section 2.2 - Waste Package/EBS Results, and Section 2.3 - Conclusions. In Section 2.1, the radionuclide inventory, waste package design, waste package failure, alteration and mobilization of the waste inventory, and transport from the containers are defined both conceptually and with detailed values for each parameter. Comparison with the TSPA 1991 conceptualization is also included in this section. In Section 2.2, results of waste package analyses conducted for TSPA 1993 are provided. The container failure distributions developed for TSPA 1993 are presented. Expected value releases are then presented to compare different thermal loads, waste package designs, and initiation of corrosion models. The CCDFs for 100 realizations are presented followed by the selected sensitivity analyses for the uncertain parameters. Section 2.3 presents conclusions based on the waste package analyses conducted for TSPA 1993.

## **2.1 CONCEPTUAL AND PARAMETER DESCRIPTIONS**

The conceptual and parameter description of the waste package includes five subsections (radionuclide inventory, container failure, waste mobilization, radionuclide transport, and EBS configuration) as well as a comparison with SNL's TSPA 1991 (Barnard et al., 1992) conceptualization.

### 2.1.1 Radionuclide Inventory

The radionuclide inventory used in the TSPA 1993 analysis is divided into two basic components: spent fuel (PWR and BWR) and HLW. The inventory used in the analyses is based on inventories for the PWR, BWR and HLW in the Characteristics Database (CRWMS M&O, 1993). A weighted average spent fuel inventory was determined. Screening was conducted based on contribution of the radionuclide to (1) potential release normalized to 40 CFR 191 Table 1 values over time periods from 1,000 to 1,000,000 years, and (2) potential average annual whole body dose over time periods from 1,000 to 1,000,000 years. This screening is explained in more detail later in the section. Spent fuel (both PWR and BWR) and HLW are included in the inventory. The spent fuel is apportioned into the heated area of the repository conceptualization, and the HLW inventory is located in the unheated area. It is not expected that the HLW waste package temperatures will be significantly different from the host rock in the vicinity. The spent fuel is divided into the six equal area rings shown in Figure 2-1. Thirty-nine radionuclides for spent fuel and thirty two radionuclides for HLW are included in the analyses.

**Spent Fuel:** The spent fuel is composed of PWR and BWR fuel with tonnages of 40,747 MTHM and 22,253 MTHM respectively to reach a total of 63,000 MTHM. The average burnup rate for the TSPA 1993 analyses is based on a content of 64.68 percent PWR fuel and 35.32 percent BWR fuel with burnups of 42,300 MWd/MTHM and 32,250 MWd/MTHM respectively for an average burnup of 36,437 MWd/MTHM. Thirty-year-old fuel is assumed. The spent fuel inventory assumes the PWR and BWR fuel are mixed (Table 2-2). The metric tons of uranium (MTU) (for practical purposes the equivalent of MTHM) is calculated by the number of PWR spent fuel assemblies per container. The decay chains for the radionuclides are presented in Appendix C.

**High-Level Waste:** The HLW inventory presented in Table 2-3 is directly from DOE (1987). The thermal output of the HLW is small in comparison to the spent fuel. The burnup value for HLW is assumed to be 10,000 MWd/MTU after Golder Associates Inc. (1993). This is used only for purposes of normalization to the EPA standard. The assumption is 7,000 MTHM of HLW in 14,000 containers. The waste is assumed to be derived from West Valley, Idaho National Energy Laboratory, Savannah River Laboratory, and Hanford Facilities.

**Screening:** The screening of radionuclides for inclusion in the analyses was done using the ratio of the inventory to EPA Table 1 release limits. The screening process followed several steps. The ratio of the weighted average spent fuel inventories of specific radionuclides to corresponding EPA Table 1 values were determined for 1,000, 10,000, 100,000, and 1,000,000 years. The fractional contribution of each isotope to release at a time of 1,000, 10,000, 100,000, and 1,000,000 years was calculated assuming a combination of delay due to waste package lifetime and retarded transport of 1,000 to 1,000,000 years. Isotopes which contributed at least a fraction of the EPA limit at any of the selected times passed this screening. The entire decay chain for daughters which contributed greater than  $10^{-5}$  of the EPA limit at any time were also included.

The screening using dose was based on inventories from the Characteristics Database at the same time periods. The waste form was assumed to be altered at a rate of  $10^{-5}$  of the total inventory per year (Ci/yr). The isotopes were assumed to dissolve, as they were made available by the

assumed waste form alteration rate, at the maximum solubilities according to NAS (1983), EPRI (1992), and Barnard et al. (1992). The advective, downward flux in ground water moving through the unsaturated zone was assumed to occur at 0.1 mm/yr over a cross sectional area of 33,000 m<sup>2</sup>. On arrival at the saturated zone, the isotopes were assumed to mix in the saturated zone with a flow rate of 10,000 m<sup>3</sup>/yr. Ingestion of 700 liters/year by a person using this ground water was assumed. The ingested dose was calculated using the maximum effective (whole body) dose conversion factor from DOE (1988), NRC (1981), or EPA (1988). The fractional contribution of each isotope to total dose at times of 1,000, 10,000, 100,000, and 1,000,000 years was determined. For radionuclides with two or more isotopes present in the waste, the solubility limit was set for the element (i.e., all isotopes) and then proportioned between the individual isotopes by the mass fraction present at the corresponding time. All isotopes contributing less than 10<sup>-5</sup> of total dose at any time period were eliminated from the inventory unless they were in the decay chain for daughters which contributed 10<sup>-5</sup> of total dose at any time.

## **2.1.2 Container Failure**

The container failure conceptualization for TSPA 1993 is defined to include effects of temperature, saturation, and oxidation rates. The TSPA 1993 analyses consider container descriptions of several configurations approximating multibarrier waste package designs. The design consists of an inner and an outer container. The waste package designs analyzed in TSPA 1993 include:

- 0.95-cm inner container of Incaloy and a 10-cm outer container of mild steel
- 0.95-cm inner container and 20-cm outer container
- 0.95-cm inner container and 45-cm outer container
- 3.5-cm inner container and 10-cm outer container

A number of approaches have been taken to develop container failure rates. Barnard et al. (1992), Lamont (1993), Stahl (1993), and Bullen (personal communication) have all developed container degradation models. The following presents a description and a comparison of the various container degradation models. This is followed by a description of the TSPA 1993 method for developing container failure distributions.

### **2.1.2.1 TSPA 1991 Failure Distribution Description**

The TSPA 1991 container failure model (Barnard et al., 1992) was a distribution based on, but not directly dependent on temperature. An initial dry out period of 300 years during which no container failure occurred was followed by a "rewetting" period with a uniform distribution of 1,000 years, so that all packages were rewet at 1,300 years after emplacement. Container failure started following the rewetting period. A loguniform distribution from 500 to 10,000 years was sampled to provide a maximum failure time, prior to which all containers were to fail. The failure distribution did not explicitly account for different container oxidation modes or temperature effects on container failure.

### 2.1.2.2 Stahl Failure Distribution Description

Based on empirical data, Stahl (1993, Appendix E) developed equations for three penetration rates: (1) high temperature oxidation, (2) general aqueous corrosion, and (3) general corrosion with a pitting factor. The equations are temperature and time dependent. The primary documentation for the model is included in Appendix E. The equations are concerned with overpack penetration.

The equations, which give the total penetration, are summarized as follows:

- (1) High-temperature oxidation (dry oxidation):

$$P = 178,700 \times t^{0.33} \times e^{-6870/T}$$

where P = penetration in microns,  
t = time in years, and  
T = temperature in ° Kelvin.

This corrosion mode is only active when conditions are considered to be "dry". Such conditions are assumed to occur in some TSPA 1993 analyses when liquid saturation is below residual saturation and in other analyses when temperature is above 100°C. Figure 2-4 presents the penetration depth for arbitrary constant temperatures using the Stahl formulation. The penetration is relatively insignificant, even for high temperatures.

- (2) General aqueous corrosion:

$$P = 2,525,000 \times t^{0.47} \times e^{-2850/T}$$

This corrosion mode is active when conditions are "wet". This condition is assumed to occur in some TSPA 1993 analyses when liquid saturation is above residual saturation and in other analyses when temperature is below 100°C.

- (3) General corrosion with a pitting factor (aqueous pitting corrosion):

$$P = 10,100,000 \times t^{0.47} \times e^{-2850/T}$$

This corrosion mode is also active when conditions are "wet", and is four times more rapid than general aqueous corrosion. Figure 2-5 presents the penetration depth for the Stahl (1993, Appendix E) formulation for pitting corrosion at arbitrarily selected constant temperatures.

These equations can be used to determine the penetration depth given constant temperature. For variable temperatures (both spatially and temporally), the equations have been manipulated to

determine the penetration depth for a particular time period at a particular time-varying temperature distribution.

### **2.1.2.3 Lamont Failure Distribution Description**

Lamont (1993, Appendix F) developed a container failure model based on oxidation/corrosion rates at various temperatures. The oxidation rates for dry oxidation, general aqueous corrosion, and pitting corrosion were elicited from waste package corrosion experts at LLNL. These are the same three corrosion modes as Stahl (1993, Appendix E) described. The effect of dry air oxidation was determined to be negligible in most cases, but was included in the model (Lamont, 1993, Appendix F). The two other corrosion modules in the Lamont container failure conceptualization are general wet or aqueous oxidation and aqueous pitting corrosion. Draft documentation on the model is included in Appendix F.

For general wet oxidation, Lamont elicited information on the expected corrosion rates and temperatures. The model assumes this is only active for a mild steel outer wall of the multibarrier waste package. The expected corrosion rates, assuming a single pit per container, for the three multibarrier waste package overpack thicknesses are presented in Table 2-4. The highest corrosion rate is expected to occur when temperatures are near 80°C. If temperatures are greater or less, the corrosion rates are slower which leads to longer expected failure times.

A quadratic function was fit to the 20°C and 80°C corrosion rates. The 100°C rate was not used in the Lamont quadratic fit, but was evaluated in this study to see if the determined fit was close (Lamont, personal communication). To match the 80°C peak and fit the 100°C rate also, a fourth point was inserted (Figure 2-6). For temperatures greater than 96°C, the general wet oxidation process was assumed inactive (Lamont, 1993, Appendix F).

The Lamont model included another component, pitting corrosion, which is only active on the inner container, and only after failure of the outer container. Information was elicited from LLNL concerning the distribution of annual pitting rates at two different temperatures (70 and 100°C) for this model. This information was then implemented in a probabilistic pitting model (Lamont, 1993, Appendix F). LLNL elicited values for the median and 95 percentile of pitting rates, for a low, median and high growth rate scenario. The elicited container corrosion rates are presented in Table 2-5. The corrosion rates are given as a growth factor and a probability, and have been used to calculate a conservative time to failure (see Table 2-5). Lamont used the rates to develop distributions for the pit growth for all pits on a container. Lamont assumed many pits may exist on a particular container, and then implemented an extreme value distribution to determine the pit which was considered to grow during a particular time step. If a single pit penetrated the container, the container was assumed to have failed. The TSPA 1993 abstraction of the Lamont model is presented in Section 2.1.2.5.

### **2.1.2.4 Bullen Failure Distribution Description**

Bullen (personal communication) developed container failure curves showing the fraction of containers failed at a particular time for given environmental conditions. Similar cases have been

developed by Bullen for use by EPRI (see Shaw and McGuire, 1993). The failure modes included by Bullen (personal communication) were the same as Stahl and Lamont, with the addition of a defective construction mode. The failure distributions developed by Bullen have been generated for four different thermal regions in the repository for three thermal loading scenarios. Three different thermal redistribution mechanisms have also been evaluated by Bullen, namely conduction, convection, and heat-pipe. Table 2-6 includes the Weibull distribution parameter values for conduction for the three thermal loading scenarios for both the SCP design container and for a steel container like the multibarrier waste package outer container. The values in Table 2-6 are only given for two conditions: (1) a temperature zone with a time period above boiling and then some time below boiling (alpha), and (2) a temperature region with temperature always below boiling (beta). If one were to look only at these two temperature regimes, the additional waste packages not included in these two temperature regions would need to be reapportioned to these two regions. Figure 2-7 presents the dry oxidation rate information used by Bullen. Figure 2-8 presents Bullen's calculated penetration rates for the SCP design container. The Bullen results are presented only for comparison purposes and are not used in the development of container failure distributions for TSPA 1993.

#### **2.1.2.5 Container Failure Implementation in TSPA 1993**

The RIP allows the user to define several failure distributions for both a primary container option and a secondary container option. In TSPA 1993, for the primary container option the obvious choice is to simulate the overpack failure distribution. However, the secondary container option in RIP does not allow any dependency of the failure distribution based on environmental conditions. Thus, the primary container failure distribution option was used to include the combined effects of dry oxidation and general aqueous oxidation on the overpack as well as pitting corrosion on the inner container. The secondary container option in RIP was used to simulate degenerate or immediate failure of the cladding.

The development and implementation of container failure distributions in RIP for TSPA 1993 required several steps. Briefly, these steps are defined below. Figure 2-9 presents the steps in sequence.

1. Given a certain thermal load, the temperature, flux and saturation distributions were calculated for each of six spent fuel waste package groups and one HLW waste package group. (See Appendix A).
2. The corrosion rates for the abstraction of each of the failure models (Stahl (1993, Appendix E) and Lamont (1993, Appendix F)) were determined as a function of temperature and time.
3. For a particular analysis, a determination was made to use either temperature or residual saturation as the initiation process for corrosion. The time prior to the initiation of corrosion was determined based on the hydrothermal analyses presented in Appendix A.

4. The steel corrosion penetration depth as a function of temperature and time was plotted and the time required to breach the outer container was determined.
5. The inner container penetration depth as a function of temperature was determined for the 5th, 50th, and 95th percentile cases (for Lamont abstraction only).
6. The time required to penetrate the outer container was combined with the time required to penetrate the inner container to determine the time required to breach both of the barriers.

More detail on each of these steps is provided below.

### **STEP 1: Temperature, Saturation, and Flux**

The three previously defined areal power density (APD) scenarios were implemented in the TSPA 1993 analyses. These three scenarios each resulted in a unique temperature distribution for each ring for each loading. The temperature distributions for locations 5 m from the waste package center, developed using VTOUGH (Nitao, 1989) are presented in Appendix A. In RIP, these temperatures were implemented as a temperature distribution table for each ring.

The liquid saturations for the three APDs were also calculated using VTOUGH. The plots of liquid saturation as a function of time for each of the rings are presented in Appendix A. The saturations for each repository ring were implemented in RIP using an approximate fit to the VTOUGH saturation curve. For initial TSPA 1993 analyses, cases with a saturation of less than residual saturation assumed general aqueous corrosion and pitting corrosion were not active. Additional analyses used temperature as the dependent parameter for corrosion processes (i.e., when the temperature was greater than 100°C, no aqueous corrosion occurred). The liquid fluxes for the three APDs were also calculated using VTOUGH. The results of the VTOUGH analyses for repository level flux were implemented in RIP for each ring by approximating the flux at a given time with a simple function. The flux curves from VTOUGH are presented in Appendix A. These flux values were compared with results from a similar conceptualization by Buscheck and Nitao (1993), and the results compared favorably (see Appendix A).

### **STEP 2: Dry Oxidation**

Temperatures developed in VTOUGH were averaged for each time step, and a corrosion rate was determined for these averaged temperatures. This corrosion rate was then active for the length of the time step. This calculation was also conducted external to RIP. A plot showing the implementation of the Stahl (1993, Appendix E) dry oxidation penetration depth at various temperatures was presented in Figure 2-4. For the temperatures calculated both at the waste package surface and 5 m into the rock, the penetration depth is considered insignificant. Thus, dry oxidation was disregarded in the following analyses.

The Lamont model uses an Arrhenius relationship as follows:

$$P = k_1 \exp\left(-\frac{k_2}{T}\right)$$

where

P = penetration rate (mm/yr),  
 k<sub>1</sub>, k<sub>2</sub> = constants, and  
 T = temperature (°K)

and assumes dry oxidation is a temperature dependent process. The penetration rate due to dry oxidation of carbon steel is (Uhlig, 1948):

<u>Temp °C</u>	<u>Rate (mm/yr)</u>
25	6.35E-6
540	10.08

For temperatures similar to those obtained in Appendix A (i.e., 100° to 200°C), the penetration is insignificant. For greater temperatures (i.e., 300°C), similar to those achievable with a backfill (Appendix B), the oxidation penetration rate becomes quite significant. These dry oxidation results were not included in the following analyses because no backfill was assumed in the drift for the thermal calculations.

### STEP 3: Aqueous Corrosion Initiation

For the cases with corrosion initiation dependent on saturation, it was assumed that when the saturation dropped below residual saturation, corrosion was inactive; otherwise corrosion was active at the rate governed by the temperature in the particular ring. For the cases with corrosion initiation dependent on temperature it was assumed that when the temperature increased above 100°C, corrosion was assumed inactive; otherwise corrosion was active at the rate according to the temperature in the particular ring. Particularly for the 282 kW/ha (114 kW/acre) case, with both of these conceptual models, a period of time elapsed prior to the initiation of aqueous corrosion.

### STEP 4: Aqueous Corrosion of Outer Container

For general aqueous corrosion, TSPA 1993 uses four different conceptualizations for comparison; two each for both Stahl and Lamont. The conceptualizations use either saturation or temperature as a basis for corrosion initiation and are as follows.

**Stahl - Saturation Based (S1).** This conceptualization abstracts information from Stahl (1993). Dry oxidation is not included. Aqueous pitting corrosion is simulated to develop failure distributions for the outer containers. As long as liquid saturation is above residual saturation, corrosion is assumed to occur. The temperature distribution for each of the seven rings was developed in VTOUGH for each APD analyzed. A total penetration depth with time for each of the rings was determined using the temperature distributions presented in Appendix A and the

Stahl penetration equations. Figures 2-10, 2-11, and 2-12 depict the penetration depth vs. time for the innermost and outermost repository rings for the three thermal loads investigated: 70.4, 141, and 282 kW/ha (28.5, 57, and 114 kW/acre). The time at which the penetration depth was equal to a specified overpack thickness was determined. This failure time was used as the midpoint of a uniform distribution and a range extending an arbitrary value of +/-25 percent from the mean was determined. A similar distribution was calculated for each ring. Tables 2-7 to 2-9 present the calculated failure times for each of the APDs based on corrosion occurring when water saturation is greater than residual saturation. Tables 2-7a, 2-8a, and 2-9a present the time to failure assuming general corrosion occurs on the outer container. The time to failure for each of the three outer container thicknesses is presented. For the 20-cm and 45-cm outer containers, the time to failure is greater than 100,000 years for all seven rings. Tables 2-7b, 2-8b, and 2-9b show the time to failure assuming pitting corrosion (four times the general corrosion rate) occurs on the outer container. The time to failure is greatly decreased from the general corrosion time to failure. Tables 2-7b and 2-8b show a consistent increase in time to failure from the inner repository ring to the outer ring, due to generally decreasing temperatures (i.e., lower corrosion rates) as one moves away from the center of the repository. Tables 2-9a and 2-9b (282 kW/ha [114 kW/acre] case) indicate a complexity associated with a dryout period, or a time period in some of the rings in which the liquid saturation is below residual saturation. During this time period, no corrosion occurs. Thus, the time to failure for the waste packages in different rings shows an increase from Rings 1-4, but then drops for Rings 5-7. Ring 7, because it has no dryout time, has the shortest time to failure of any of the rings for the 282 kW/ha (114 kW/acre) case. Because the Stahl (1993) model causes relatively rapid (10s of years) failure of the inner container, this additional time was not added to the failure time.

**Stahl - Temperature Based (S2).** This conceptualization also abstracts information from Stahl (1993) and deals only with the overpack. Dry oxidation is not included. As an alternative to the saturation based corrosion initiation, temperature is used as the dependent parameter. When the temperature drops below 100°C, general aqueous corrosion is assumed to initiate. When temperature is above 100°C, no corrosion occurs. Table 2-10 presents the calculated time to failure when corrosion is assumed to occur at temperatures below 100°C. The 70.4 kW/ha (28.5 kW/acre) case is not included in Table 2-10 because temperatures are never greater than 100°C. Also, Table 2-10 only shows the time to failure for the pitting corrosion model with a 10 cm overpack. The trends in the time to failure in Table 2-10 can generally be attributed to the proximity of a ring to the center of the repository and the dryout period for a ring.

Table 2-11 presents the saturation based failure distribution as it was implemented in RIP. Table 2-12 presents the temperature based failure distribution as it was implemented in RIP. Table 2-11 values were calculated from the previously presented (Tables 2-7 to 2-9) times to failure caused by pitting corrosion on the different overpack thicknesses. The start time was calculated as 75 percent of the expected time to failure, and the duration of the failure time was calculated by adding 25 percent to the expected time to failure and then subtracting the start time from this value. Table 2-12 values were calculated with the same method as Table 2-11, but using Table 2-10 as the expected value for time to failure. Because Tables 2-11 and 2-12 are based on Tables 2-7 to 2-10, the times to failure follow the same trends.

**Lamont - Saturation Based (L1).** Abstracting the Lamont (1993) general aqueous corrosion rate information into RIP requires fitting a curve to the elicited thermally-dependent corrosion rates

(Figure 2-6) and using the temperature distribution defined in the hydrothermal analyses. The aqueous corrosion was assumed to occur when saturation was greater than residual saturation. The mean container failure times for general aqueous corrosion only at the 141 kW/ha (57 kW/acre) APD for the Lamont model are presented in Table 2-13. The times to failure presented in Table 2-13 indicate a general decrease in time to failure from the center of the repository outward. This trend occurs because the hotter central repository has lower corrosion rates (see Figure 2-6) than do the cooler outer rings. The trend is evident for each container thickness.

**Lamont - Temperature Based (L2).** The abstraction of the Lamont (1993) general aqueous corrosion model was also used for this failure distribution description. However, corrosion was assumed not to occur when simulated temperatures were above 100°C.

### **STEP 5: Pitting Corrosion of Inner Container**

Because Stahl (1993) assumes the inner container fails in only 10 years, this small time factor is not included in the Stahl failure distributions.

For pitting corrosion, failure distribution descriptions L1 and L2 were abstracted from Lamont (1993). The median growth rate (Table 2-5) was used. A single pit was tracked per container. This is different than the Lamont model which includes multiple pits per container, and three different growth rates—low, median and high. The information on the median corrosion rate (5th, 50th and 95th percentiles) was used to determine container failure distributions. Weibull distributions were developed to incorporate the potential variability in corrosion rates. The pitting corrosion rates active on the inner container are combined with general aqueous corrosion penetration of the outer container and the corresponding times to failure for saturation dependent corrosion initiation are presented in Table 2-14. The temperature dependent failure distributions are presented in Table 2-15. Table 2-14 shows the calculated time to failure for the cases with a 10-cm overpack and either a .95-cm or a 3.5-cm inner container thickness. The median, 5th, and 95th percentile time to failure is shown for each ring. The 5th percentile time to failure increases from Ring 1 to 7. The trends in the median and 95th percentile are less consistent because of the temperature effects on the time of failure of the outer container, which may contribute to rapid failure if the system temperature is near the peak corrosion temperature of 80°C. This defines why the hottest ring (Ring 1) does not fail the quickest.

Table 2-15 presents data similar to Table 2-14 for 141 and 282 kW/ha (57 and 114 kW/acre), except the assumption is that corrosion initiation doesn't occur unless temperature is below 100°C. Generally, time to failure is longer than those in Table 2-14 (saturation dependent corrosion initiation) for the hotter rings and about the same for the outer, cooler rings of the repository. The RIP implementation of the Lamont failure distributions is presented in Tables 2-16 to 2-17. These distributions were developed by taking the calculated data in Tables 2-14 and 2-15 and fitting a Weibull distribution to the data.

## **STEP 6: Total Time to Failure**

The time required for penetration of both the outer container and the inner container is assumed to be the time to failure of the waste package. This is conservative because it does not take any credit for the cladding and it assumes the whole waste package inventory is available for release when a single hole penetrates the waste package. The outer container penetration depth with time was calculated using the aforementioned general aqueous corrosion abstracted models. When the outer container was penetrated, the corrosion model was switched to the pitting corrosion model (in Lamont's case) and the total time to penetrate the outer container and the inner container was determined.

The reference case for TSPA 1993 takes no credit for the cladding. However, alternative approaches to incorporating the cladding are provided by Golder Associates Inc. (1993). Golder Associates Inc. uses two different scenarios for cladding failure. Scenario A assumes the cladding fails instantly as soon as the primary container fails. Scenario B assumes that all fuel rods experience pinhole failures instantly after emplacement, but only fuel rods in containers that fail at early times are additionally degraded due to oxidation of the fuel pellets. The area of the spent fuel is assumed to increase by 100 times in this case, due to increase in surface area caused by oxidation reaction. Containers whose fuel rods are split by the increase in spent fuel volume due to oxidation, release both aqueous and gaseous nuclides. Those which only experience pinhole failures release primarily gases. Golder Associates Inc. (1993) assumed each cladding scenario has a 50 percent likelihood of occurrence.

### **2.1.3 Waste Mobilization**

Previous TSPA analyses have included a factor identified as water contact mode, with certain waste release characteristics. This analysis does not use such a formulation. Instead, TSPA 1993 divides the waste packages into seven groups, each of which has a characteristic set of saturation, temperature and flux histories which define conditions at the waste package and thus the potential release mechanisms. Within each repository ring, all waste packages experience the same environmental conditions. For example, a repository ring may start off in the "nominal" or dry mode due to the high initial temperature and low saturation, but be modified to advective and/or diffusive release characteristics as the temperature decreases and flux increases. The seven repository rings are based on the VTOUGH analyses discussed previously. TSPA 1993 assumes there are three basic release modes: (1) no release, (2) advective release, and (3) advective plus diffusive release.

The TSPA 1993 conceptualization of waste mobilization is affected by temperature, saturation, and flux. For initial analyses, no release is allowed when saturation is less than residual saturation when it is assumed that aqueous waste package corrosion and diffusive transport of radionuclides from the waste package does not occur. The advective release condition occurs when the seepage in the repository is greater than the matrix hydraulic conductivity. For saturations greater than eight percent and zero background ambient percolation flux, there is only diffusive release. For nonzero downward fluxes, there is both advective and diffusive release.

Additional analyses were conducted using 100°C as the transition between dry oxidation and general aqueous corrosion. The failure distributions and, thus, waste mobilization, are somewhat different than for the saturation dependent failure distributions.

### 2.1.3.1 Matrix Dissolution Rates—Spent Fuel

Gray et al. (1992) experimentally analyzed the effects of pH, temperature, and total carbonate concentration on the dissolution rate of spent fuel. They provided three possible curve fits to their data: a theoretical Arrhenius-type fit, a mixed theoretical and empirical fit, and an empirical polynomial fit. The second was chosen for TSPA 1993 because it provided a reasonable fit and preserved much of the functional form expected by Gray et al. (1992):

$$R_{dis} = 1.65 + 1.41(\log[C]) + 0.0341(pH) + 0.160 T$$

where  $R_{dis}$  = matrix dissolution rate ( $\text{mg}/\text{m}^2 \cdot \text{day}$ ),  
C = total carbonate concentration (molarity),  
pH = nominal pH of the water contacting the matrix (assumed to be the same as the pH of the ground water), and  
T = temperature of the spent fuel ( $^{\circ}\text{C}$ ).

Converting the dissolution rate to  $\text{g}/\text{m}^2 \cdot \text{yr}$  yields:

$$R_{dis} = 0.602 + 0.515(\log[C]) + 0.01245(pH) + 0.0584 T$$

The graphic representation of the temperature and carbonate dependent spent fuel dissolution rate is shown in Figure 2-13.

In TSPA 1993, the carbonate concentration (C) was sampled over a uniform distribution from 0.002 to 0.02 (Gray, 1993), and pH was sampled from an arbitrarily selected uniform distribution from 6.0 to 9.0.

### 2.1.3.2 Matrix Dissolution Rates—Classified High-Level Waste

Bourcier (1993) outlines a conservative conceptualization for the dissolution of the glass waste form. The rate equation commonly used to describe the dissolution of glass is:

$$R_{gl} = A_{m,gl} k_{T,pH} (1 - Q/K)$$

where  $R_{gl}$  = dissolution rate of glass (g/day),  
 $A_{m,gl}$  = surface area of the glass exposed to solution (m<sup>2</sup>),  
 $k_{T,pH}$  = rate constant for glass dissolution which is primarily a function of temperature and pH (gm/m<sup>2</sup> day),  
 $Q$  = concentration of dissolved silica in water, and  
 $K$  = equilibrium constant for amorphous silica.

Bourcier estimates a "reasonable and conservative value" for the surface area to be  $A_{m,gl} = 125 \text{ m}^2/\text{canister}$ .

A functional form for the rate constant for glass dissolution,  $k$ , was derived from regression analysis of experimental data:

$$k = 10^{(-0.00172 - 0.0231T + 0.00149T^2 - 1.136 \times 10^{-5}T^3 - 1.155pH + 0.0813 pH^2 + 0.000138pH^3)}$$

where  $k$  has units of gm of glass/m<sup>2</sup> day, and  $T$  is in °C. This equation is valid from 10 to 100°C and pH values from 1 to 12.

From Bourcier's temperature-dependent estimates of  $Q$  and  $K$ , a reasonable linear dependence of  $Q/K$  on temperature was derived:

$$Q/K = 0.1425 + 0.001878 T$$

where  $T$  is in °C. Graphically, the glass dissolution with respect to temperature is presented in Figure 2-14.

The dissolution conceptualization presented here embodies several assumptions and limitations. The radionuclides are released as fast as the glass structure breaks down, which is conservative because it does not account for solubility-limited radionuclides. No credit is taken for the fact that "experiments have shown that the actinides more commonly are included in alteration phases at the surface of the glass either as minor components of other phases or as phases made up predominantly of actinides" (Bourcier, 1993). The model ignores all solution chemistry other than pH and silica concentration. However, a variety of experiments show that species such as dissolved Mg and Fe can change glass dissolution rates by up to several orders of magnitude, with Mg decreasing the rate and Fe increasing the rate (Bourcier, 1993). The model also ignores vapor phase alteration of the glass. In addition, "if a canister containing glass is breached and humid air reaches the glass, the glass will react and form a thick alteration rind composed of hydrated glass and secondary phases. The durability of this material with respect to later contact with liquid water may be much greater or much less than the unaltered glass" (Bourcier, 1993).

### 2.1.3.3 Additional Parameters Important to Waste Mobilization

**Spent Fuel Surface Area:** There is 5.0894 m<sup>2</sup> of surface per assembly of PWR and 1.9494 m<sup>2</sup> of surface area per assembly of BWR. For the case of waste packages containing 21 PWR fuel assemblies, this is equal to 21 x 5.0894 or 107 m<sup>2</sup> per waste package. This case is comparable to the 40 BWR case which is 40 x 1.9494 or 78 m<sup>2</sup> per waste package. The range for spent fuel surface area used in TSPA 1993 was 78 to 107 m<sup>2</sup> per waste package.

**Defense High-Level Waste:** For each canister, the surface area is 5 m<sup>2</sup> with a factor of 10 to 30 included to account for cracking (Bourcier, 1993) leading to 50 to 150 m<sup>2</sup> per canister. Since it is assumed that there are 4 canisters per waste package, for the case corresponding to the 21 PWR case, this suggests 200 to 600 m<sup>2</sup> of surface area per waste package.

The volume of water contacting the spent fuel and glass waste forms is equal to the surface area times an assumed 0.001-m thick water film. Thus, the volume of water contacting the spent fuel becomes 0.078 to 0.107 m<sup>3</sup>, and contacting HLW becomes 0.2 to 0.6 m<sup>3</sup>.

**Effective Catchment Area:** The effective catchment area is the total area over which vertical liquid flux is collected and thus available for a single waste package. The effective catchment area is assumed to be a uniform distribution from 8.5 to 46.5 m<sup>2</sup>. The range is from a minimum of the area of one waste package to the projected area for a waste package assuming a center to center distance of 3.75 m by 12.4 m.

**Geometric Factor for Diffusion:** The geometric factor for diffusion is defined as

$$\Omega = 4\pi R n f_s$$

where

- R = the equivalent spherical radius of the waste package which is 2.23 m for Rings 1 to 6 and 2.50 m for Ring 7,
- n = porosity = 0.1 to 0.3, uniform distribution (Golder Associates Inc., 1993), and
- f<sub>s</sub>(i) = 1 if saturation is greater than 8 percent; otherwise it is 0.

### 2.1.4 Modes of Radionuclide Transport

Once the radionuclides are released from the waste form and dissolved in the water film around the fuel matrix, they may be released from the waste package. The release rate is a function of mode of transport (advective and/or diffusive) and the concentration of the radionuclides in the water. This concentration may be limited by the solubility limit of the element. The mode of transport is dependent on the saturation and flux for the particular waste package group.

### 2.1.4.1 Solubilities

The solubilities for the radionuclides used in the TSPA 1993 analyses include the effects of temperature and pH where the data or theory exist to support the formulation of such dependencies. An expert elicitation at SNL (see Appendix G) noted that different isotopes of the same element have the same solubilities, although the actual solubility in a particular solution is dependent on the mass fraction of the isotope in the solution. The solubilities of some of the elements were also expected to have the same temperature and pH dependencies. The groups of elements whose solubilities behave similarly were taken to be:

- (1) Ra and Sr
- (2) Pa, Sn, Th, and Zr
- (3) Ni, Pb
- (4) Np, U
- (5) Ac, Am, and Sm.

For the first three groups, very little temperature-dependent data are available. Thus, the solubilities were assumed to be those elicited (which were valid for  $25^{\circ}\text{C} \leq T \leq 95^{\circ}\text{C}$ ,  $6 \leq \text{pH} \leq 9$ , and all ground-water compositions expected at the proposed repository). For the fourth and fifth groups, the most detailed and recent data (Nitsche et al., 1992a,b) were for Np and Am, respectively. As per the elicitation, the solubilities of the other members of the fourth and fifth groups were correlated directly to the solubilities of Np and Am. The solubilities of the elements within a particular group are thought to behave similarly, therefore, in RIP they were assumed to be exactly correlated. There is inevitably some error in this assumption. However, the data do not exist for a more accurate formulation. The ground-water composition is very important in determining the temperature and pH dependence of the solubilities (Appendix G). The solubilities corresponding to UE-25 J#13 water were selected for the following reasons: (1) The water from UE-25 J#13 (tuff aquifer) is probably more representative of the water that will be found at the proposed repository horizon than the water from UE-25 p#1 (carbonate aquifer); (2) most of the previous solubility work has assumed UE-25 J#13 water, and this is consistent with PNL's TSPA-91 (Eslinger et al., 1993) efforts; (3) more temperature-dependent data are available for UE-25 J#13 in the work by Nitsche et al. (1992a,b); and (4) the solubilities of Np and Pu do not vary more than an order of magnitude between the two waters. Table 2-18 presents the solubility values or functions used in TSPA 1993 analyses. Note that some of the solubilities do not have a defined pH and/or temperature dependency. The table lists the radionuclides, the solubility of the radionuclide, the function of any pH or temperature dependency for the solubility, and the source of the data. Table 2-19 presents solubilities for Am, Np, and Pu. These are both pH and temperature dependent.

Some of the solubilities that were elicited had log-beta distributions. These were approximated using log-normal distributions. The differences are negligible, except perhaps for Ni. For Ni, the log-normal distribution is broader, extends farther to the higher values, and has a slightly higher mean value. Thus, the log-normal distribution is nominally conservative with respect to the log-beta distribution.

For Cs, Wilson's (1993) measured solubilities (using UE-25 J#13 ground water) ( $1.2\text{E } 5 \text{ gm/m}^3$  at  $25^{\circ}\text{C}$ , and  $1.5\text{E}-9 \text{ gm/m}^3$  at  $85^{\circ}\text{C}$ ) were used. He did not have any estimate of the error, so

a log-triangular distribution was assumed that extended an order of magnitude in each direction from each data point. The temperature at which the solubility was switched from one distribution to the other was selected to be the mid-point, 55°C.

When incorporating the temperature-dependent solubility data into TSPA 1993, a functional form was assumed that was provided by Ines Triay of Los Alamos (Appendix G, personal communication to Carl Bruch, July 22, 1993):

$$\ln(S) = c_0 + \frac{c_1}{T} + \frac{c_2}{T^2} + c_3T + c_4 \ln(T)$$

where S is the solubility, T is the temperature in degrees Kelvin, and  $c_0 \dots c_4$  are the coefficients that are determined from curve fitting. The assumptions for this formulation are included in Appendix G. To incorporate the pH-dependence, a functional form was assumed similar to that described by Gray et al. (1990) for dissolution rates:

$$\ln(S) = c_0 + \frac{c_1}{T} + \frac{c_2}{T^2} + c_4T + c_3 \ln(T) + c_5 pH$$

Using the multiple linear regression component in SPSS software (SPSS, 1993), the following coefficients were calculated:

Element	$c_0$	$c_1$	$c_2$	$c_3$	$c_4$	$c_5$	$R^2$
Am	453.2986	0	-1.602404E7	-0.922433	0	-0.801841	0.73455
Np	134.7607	0	-4227824	-0.242123	0	-1.492653	0.85197
Pu	19.69678	0	-143002.9	-0.070033	0	0.067152	0.90185

The corresponding graphic representation is given in Figures 2-15 through 2-17.

For Np, the lower the pH, the higher the solubility. Temperature has a significant effect on the solubility when greater than 70°C. For Am, the same trends are evident but the change in solubility with temperature is relatively much smaller than it is for Np. The Pu solubility decreases constantly with increasing temperature, and is relatively unaffected by pH differences.

#### 2.1.4.2 Diffusion Coefficients

The diffusion coefficients used in TSPA 1993 are derived from the diffusion coefficient curves presented in Conca (1990). The diffusion coefficient is presented as a function of water content for tuff gravel. The 2nd order polynomial regression curve fitted to the data is:

$$D_{\text{eff}} = (-1.8773 \times 10^{-8}) + 6.2741 \times 10^{-9} WC + 4.1674 \times 10^{-9} WC^2$$

with an  $R^2 = 1.000$ , where  $D_{\text{eff}}$  = effective diffusion coefficient in  $\text{cm}^2/\text{sec}$ , and  $WC$  = water content. This relationship does not hold at extremely low water contents (Conca, 1990).

To implement the above equation in RIP, the volumetric water content values were converted to saturation by dividing by a porosity of 0.4. The diffusion coefficient was set to  $1.0 \times 10^{-6} \text{m}^2/\text{yr}$  when saturation was less than residual saturation. The equation implemented in RIP was:

$$D_{\text{eff}} = -5.9135 \times 10^{-5} + 7.9154 \times 10^{-4} S_w + 2.103041 \times 10^{-3} S_w^2$$

where  $S_w$  = liquid saturation and  $D_{\text{eff}}$  is in  $\text{m}^2/\text{yr}$ . The curve is presented in Figure 2-18.

### 2.1.5 Engineered Barrier System Configuration

The TSPA 1993 analyses evaluated an in-drift emplacement design. A design was assumed with the container placed on a layer of crushed tuff above the drift floor. The drift was assumed not to be backfilled. The repository may be sloped at an approximate three percent grade to promote drainage of any seepage away from the packages. In this case, so long as a continuous water film exists, the diffusive pathway will always be present, and any aqueous releases will be diffusive if the velocity of the repository flux is small. The diffusive velocity is calculated as:

$$vel = D_{\text{eff}}/L$$

where  $D_{\text{eff}}$  = effective diffusion coefficient ( $\text{m}^2/\text{yr}$ ), and  $L$  = path length (m).

The material under the in-drift waste package design will be simulated in RIP as a pathway. Material characteristics determined for the crushed tuff and implemented in the EBS pathway are described below. The thickness of the crushed tuff invert is expected to be 0.5 m. Porosity is 0.1 to 0.3. The diffusion coefficient is determined from Conca (1990).

### 2.1.6 Comparison with Sandia National Laboratories' TSPA 1991

The TSPA 1993 conceptualization contains numerous differences from the SNL TSPA 1991 conceptualization. The data input for TSPA 1993 is compared with TSPA 1991 (Barnard et al., 1992) in Tables 2-20 to 2-24. In particular, temperature dependencies were explicitly included in TSPA 1993 for such parameters as solubility, dissolution, repository flux and saturation, and container failure. The following highlights some of the differences between TSPA 1993 and TSPA 1991 and indicates the significance of such differences.

The inventory used in TSPA 1993 contains the same number of metric tons as in TSPA 1991, but the number of curies is slightly higher (Tables 2-20 and 2-21). Also, burnup values are significantly higher. Solubility values are substantially different for selected radionuclides, such as  $^{237}\text{Np}$ . The gap fraction is assumed to be the same percentage in TSPA 1993 as in SNL's TSPA 1991. TSPA 1993 contains 39 radionuclides, instead of just 9 as used in the aqueous releases in TSPA 1991.

The container failure distributions implemented in TSPA 1993 are developed dependent on saturation, temperature, and corrosion rates, unlike the relatively simple distribution developed for TSPA 1991. Table 2-22 shows the comparison of the parameters.

Table 2-23 presents the comparison of TSPA 1993 and TSPA 1991 parameters for waste alteration. Two of the major differences are: (1) TSPA 1993 uses the Conca diffusion curve explicitly, instead of segmenting the curve as was done in TSPA 1991; and (2) the TSPA 1993 alteration rate is temperature dependent.

Table 2-24 presents the TSPA 1993 and TSPA 1991 parameters for waste transport. Significant differences are evident in nearly all parameters. Some of the major differences between TSPA 1991 transport parameters and TSPA 1993 transport parameters are: (1) explicit representation of Conca diffusivity curve in TSPA 1993, (2) repository level spatially variable percolation rate calculated in hydrothermal analyses for TSPA 1993 with constant rate below repository using different percolation rate than TSPA 1991, (3) larger effective catchment area in TSPA 1993 than in TSPA 1991, (4) implementation of rubble zone, below waste packages in TSPA 1993 instead of air gap, and (5) in-drift emplacement in TSPA 1993 instead of in-borehole emplacement.

## **2.2 WASTE PACKAGE RESULTS**

The results of the analyses of the TSPA 1993 waste package are presented in this section. The various container failure distributions developed external to RIP and then implemented in RIP are presented. Simulated expected value case releases from the waste package are then presented for the three APDs, different container designs, and different corrosion initiation conceptualizations. A subsection showing the CCDFs, in terms of cumulative releases from the waste packages into the host rock, for the various cases is presented. The section closes with a presentation of several sensitivity analyses of selected input parameters.

### **2.2.1 Failure Distributions**

The failure distribution curves for the many configurations analyzed are compared to determine variations due to thermal loading, container design, and corrosion initiation models. The figures presented in this section are derived from simulations which are set up to show when individual waste packages fail. Each waste package in the simulation contains a single curie of a radionuclide which does not decay during the time period of interest (i.e., 100,000 years). The total number of waste packages is the same as the number of packages used in the 21 PWR cases.

### **2.2.1.1 Alternate Thermal Loads**

The cumulative container failure distributions for alternate thermal loads using the Stahl model with a 10-cm overpack are presented in Figure 2-19. Note the curve labels are the same as those used previously where the first number indicates the APD, the second is the outer container thickness, the third is the inner container thickness, and the last is the model and whether or not it is temperature or saturation dependent corrosion initiation. The failure distribution for 70.4 kW/ha (28.5 kW/acre) initiates later than both of the other APDs. The failure of containers in Ring 7 is evident in the failure distribution for all three APDs, though it is earlier than Rings 1-6 in the 282 kW/ha (114 kW/acre) case and later in the 70.4 and 141 kW/ha (28.5 and 57 kW/acre) cases. Ring 7 failure shows up as the distinct straight segment from over 6,000 to the peak of the 141 and 70.4 kW/ha (57 and 28.5 kW/acre) curves. For the 282 kW/ha (114 kW/acre) curve, the Ring 7 segment is the straight portion of the curve from 0 to almost 4,000. Generally, the waste packages fail earlier for 141 kW/ha (57 kW/acre), than for the 282 kW/ha (114 kW/acre), or 70.4 kW/ha (28.5 kW/acre) cases. The actual individual failure distribution for each of these cases is presented in Figure 2-19b.

### **2.2.1.2 Alternate Outer Container Thicknesses**

The container failure distributions for waste packages with different outer container thicknesses at the 141 kW/ha (57 kW/acre) thermal load are presented in Figure 2-20. The outer container thickness is 10, 20, or 45 cm. The failure distributions for the 10-cm and 20-cm case have the same shape, though the 20-cm distribution is pushed out in time by several thousand years. The 45-cm case starts significantly later in time and many of the containers have not failed by the end of the simulation period of 100,000 years. This is due to the overpack being thick enough to keep from failing during the high temperature early period, after which corrosion rates are significantly slower so failure requires much longer.

### **2.2.1.3 Alternate Processes for Initiation of Aqueous Corrosion**

The container failure distributions for alternate conceptualizations of the processes which may cause aqueous corrosion to become active have several important differences. For the Stahl (1993) case, 141 kW/ha (57 kW/acre), and 10-cm overpack, Figure 2-21 shows the distinction between saturation dependent and temperature dependent corrosion initiation. Saturation dependent corrosion initiation begins earlier, and correspondingly the packages fail more quickly than when the temperature dependent corrosion initiation is assumed. Thus, saturation dependent corrosion initiation is conservative. Using Lamont (1993), 141 kW/ha (57 kW/acre), and 10-cm overpack, the distinction between saturation dependent and temperature dependent corrosion initiation is similar (Figure 2-22a). The saturation dependent distribution begins earlier and fails the packages more quickly than the temperature dependent corrosion initiation case. The container failures in the individual rings are more obvious in the temperature dependent corrosion initiation case, than in the saturation dependent corrosion initiation case (Figure 2-22b).

## 2.2.2 Waste Package Release from Expected Value Case

The analyses conducted for TSPA 1993 included sensitivity on a number of important design aspects of the waste package and the surrounding engineered barriers as well as conceptual differences in the corrosion model. The primary design variants were APD (70.4, 141, and 282 kW/ha, or 28.5, 57, and 114 kW/acre), outer container thickness (10, 20, and 45 cm), and inner container thickness (.95, and 3.5 cm). The conceptual difference was whether corrosion initiation was dependent on saturation or temperature. A summary of the basic designs and conceptualizations which were analyzed is depicted in Tables 2-1 and 2-25. The discussion which follows begins with an initial design of 141 kW/ha (57 kW/acre), outer container thickness of 10 cm, inner container thickness of .95 cm, and the saturation dependent corrosion transition. For the purpose of this analysis, this case is selected as the Reference Case.

The 10,000- and 100,000-year expected value cumulative normalized release from the waste package for the 141 kW/ha (57 kW/acre), 10-cm overpack, .95-cm inner container, S1 failure distribution (Stahl model, saturation dependent corrosion initiation) and 39 radionuclide inventory are presented in Table 2-26. The radionuclides with the highest normalized release are  $^{227}\text{Ac}$ ,  $^{243}\text{Am}$ ,  $^{14}\text{C}$ ,  $^{59}\text{Ni}$ ,  $^{237}\text{Np}$ ,  $^{210}\text{Pb}$ ,  $^{239}\text{Pu}$ ,  $^{226}\text{Ra}$ , and  $^{99}\text{Tc}$ . The expected value release curves for Reference Case total release and selected radionuclides are presented in Figure 2-23. The highest normalized release over 10,000 years is provided by  $^{14}\text{C}$  and  $^{237}\text{Np}$ , while  $^{210}\text{Pb}$  and  $^{226}\text{Ra}$  provide the highest normalized release over 100,000 years.

Table 2-27 presents the 10,000- and 100,000-year normalized cumulative release for 17 design cases. Column 1 in Table 2-27 identifies the design according to APD (kW/acre), outer container thickness (cm), inner container thickness (cm), and failure distribution. The other columns present the total normalized cumulative release, as well as the normalized release for  $^{14}\text{C}$ ,  $^{237}\text{Np}$ ,  $^{99}\text{Tc}$ , and  $^{210}\text{Pb}$ , for both 10,000- and 100,000-year simulations.

### 2.2.2.1 Alternate Thermal Loads

The expected value case release for the alternate APDs are presented in Figure 2-24a for 10,000 years and Figure 2-24b for 100,000 years. These curves represent the case for the 10-cm overpack and the .95-cm inner container, Stahl failure distribution, and saturation dependent corrosion initiation. For the 10,000-year simulation, the 141 kW/ha (57 kW/acre) case expected release occurs sooner and appears to be larger than the other two cases. The normalized cumulative release shown in Table 2-27 for 141 kW/ha (57 kW/acre) is greater than for 282 kW/ha (114 kW/acre) which is greater than the 70.4 kW/ha (28.5 kW/acre) release. It is expected that this is due primarily to the corrosion rates being higher at the temperatures more prevalent to the 141 kW/ha (57 kW/acre) case. Figure 2-24b shows a greater release for the 70.4 kW/ha (28.5 kW/acre) than for the 282 kW/ha (114 kW/acre) case. However, the case of 70.4 kW/ha (28.5 kW/acre) has significantly more  $^{210}\text{Pb}$  than the 282 kW/ha (114 kW/acre) case, thus the normalized value for 282 kW/ha (114 kW/acre) is still higher than 70.4 kW/ha (28.5 kW/acre).

For the 20-cm overpack, the results are relatively similar (Figures 2-25a,b). For the 45-cm overpack, the results are provided in Figure 2-26. The 70.4 kW/ha (28.5 kW/acre) case does not

have any container failure during the 100,000-year simulation period. The 141 kW/ha (57 kW/acre) case produces earlier release and appears to level off, while the 282 kW/ha (114 kW/acre) case begins release around 70,000 years, and is steadily increasing at 100,000 years. The normalized cumulative release for the 282 kW/ha (114 kW/acre) case is significantly larger than for the 141 kW/ha (57 kW/acre) case. This may be due to the 45-cm overpack securing the 141 kW/ha (57 kW/acre) case canisters through the hot period so when the outer container fails, the system has cooled.

### **2.2.2.2 Alternate Design**

Comparison of the releases for designs with the same APD and different outer container thicknesses is shown in Figures 2-27a and 2-27b. As might be expected, when the outer container thickness is increased at a given APD, the release decreases. Especially, when the container size is increased to 45 cm, the release drops substantially. At late times, 70.4 and 141 kW/ha (28.5 and 57 kW/acre) case releases begin to look similar. The results in Table 2-27 allow this comparison to be made for the S1 failure distribution for all APDs.

Comparison of the effect of increasing the thickness of the inner container for the Lamont (1993) failure distribution shows increasing the thickness decreases the release (Figures 2-28a, 2-28b). The decrease in release is always approximately 10 percent, independent of the failure distribution type.

### **2.2.2.3 Alternate Initiation of Aqueous Corrosion**

A direct comparison of the release due to different failure distribution types is important in order to evaluate whether or not the difference in saturation or temperature has an effect on release. For the 141 kW/ha (57 kW/acre), 10-cm outer container thickness, and .95-cm inner container thickness, the saturation dependent failure distributions (S1: Stahl; L1: Lamont) provide greater release than the temperature dependent failure distributions (S2: Stahl; L2: Lamont) (S1>S2; L1>L2) (Figures 2-29a, b and 2-30a, b). The difference is primarily in the early time release when saturation dependent corrosion is active and temperature dependent corrosion is not active. For the 282 kW/ha (114 kW/acre) case, the same relationship is present (S1>S2). When comparing Stahl vs. Lamont for the same conditions (saturation or temperature corrosion transition), the Stahl distributions provide greater release (S1>L1; S2>L2) (Table 2-27). The difference between conceptualizations results is approximately a five percent difference in release, hardly significant given the other uncertainties in the simulations.

## **2.2.3 Complementary Cumulative Distribution Functions of Waste Package Release**

The waste package configurations presented in Section 2.2.2 were also simulated for multiple realizations. The results of normalized cumulative release for 100 realizations are combined into CCDFs for comparison purposes. Due to the minimal number of parameters with probability distributions in TSPA 1993 (as most parameters are now functionally dependent on the thermohydrologic environment), the CCDF results mimic the expected value results. The

parameters which were sampled included pH, effective catchment area,  $^{14}\text{C}$  gap fraction, many of the radionuclide solubilities and surface area of waste. The results are presented in the following subsections for alternate thermal loads, alternate designs, and alternate conceptualizations for corrosion initiation. The Reference Case CCDF is presented in Figure 2-31 for 10,000 years and in Figure 2-32 for 100,000 years. The total CCDF is primarily due to  $^{14}\text{C}$ ,  $^{237}\text{Np}$  and  $^{99}\text{Tc}$  releases. [Note: The 100,000-year CCDF is normalized using the same values as the 10,000-year CCDF.]

### **2.2.3.1 Alternate Thermal Loads**

The CCDFs for alternate APDs for 10,000-year simulations are presented in Figure 2-33 and CCDFs for 100,000 years are presented in Figure 2-34. As observed in the expected value cases, the CCDFs from greatest to lowest release were 141, 282, and 70.4 kW/ha (57, 114, and 28.5 kW/acre). The CCDF for 100,000 years does not include  $^{14}\text{C}$ , but the relationship between APDs still holds.

### **2.2.3.2 Alternate Design**

A comparison of normalized release from alternate designs of outer container thickness (10 and 20 cm) for 10,000 years is shown in Figure 2-35. The 45-cm case is not shown because there is no release at 10,000 years. The CCDFs for 100,000 years are presented in Figure 2-36. Again, the 100,000-year CCDF does not include  $^{14}\text{C}$ , but the relative difference is similar to the 10,000-year CCDF. As observed previously, the CCDF release decreases as the overpack thickness increases. A significant decrease in release is gained by simulating a 45-cm overpack.

### **2.2.3.3 Alternate Initiation of Aqueous Corrosion**

Cumulative releases associated with corrosion initiation differences are comparable in Figure 2-37. CCDFs for 100,000 years are presented in Figure 2-38. The saturation dependent corrosion initiation results in greater normalized release than the temperature dependent corrosion initiation. Again, this is similar to the expected value case.

### **2.2.4 Sensitivity Analysis Results**

While the uncertainty of the waste package parameters is recognized, the parameters as input to RIP did not generally contain large uncertainty ranges. The pH and radionuclide solubility (dependent on pH and temperature) are two parameters with significant uncertainty ranges actually input to RIP. Sensitivity analysis in the form of scatter plot analysis was conducted on these parameters to determine the overall impact of pH and solubility on radionuclide release. In particular, the solubility of Np as a function of pH was evaluated due to its significant contribution to the total release.

The pH range evaluated in TSPA 1993 was from 6.0 - 9.0. Figures 2-39 to 2-41 show the scatter plots for release relative to pH for the three APDs at 10,000 years and 100,000 years. These simulations use the Stahl failure distribution conceptualization and saturation dependent corrosion initiation. These plots include only the aqueous releases from the waste package (i.e.,  $^{14}\text{C}$  is not included in the total release on these scatter plots. The correlation of pH to release disappears from the 10,000-year plot to the 100,000-year plot for both the 141 and 70.4 kW/ha (57 and 28.5 kW/acre) cases. This trend can be traced to the observation that most of the release over 100,000 years is due to  $^{210}\text{Pb}$ , a daughter of U. Due to the lower solubility at high pH, the parents of  $^{210}\text{Pb}$  stay in the waste package thus yielding higher  $^{210}\text{Pb}$  releases but lower releases of the parents at high pH. The exception to this is the highest APD case which has a general increase in release with increasing pH. This may be due to the higher temperatures present at time of failure. Solubility of Np changes more rapidly per degree change at higher temperatures than at lower temperatures.

The effect of pH on solubility as it affects  $^{237}\text{Np}$  release is depicted in Figures 2-42 to 2-44. The figures are very similar to Figures 2-39 to 2-41, indicating that evaluating the solubility of Np as a function of pH is crucial to evaluating the overall release from the waste package. The normalized release at 10,000 years for all three APDs shows a gradual decrease from a pH of approximately 7.5 to 9. The normalized release at 100,000 years shows a greater independence of pH except for the 141 and 70.4 kW/ha (57 and 28.5 kW/acre) cases at the upper pH bound (9.0).

As a final scatter plot example, the Lamont failure distribution case for 141 kW/ha (57 kW/acre) is presented in Figures 2-45 to 2-46, first for total release and then for Np. The trends are similar to those shown in Figures 2-39 to 2-41. The normalized release at 10,000 years decreases as pH increases from 7.5 to 9. At 100,000 years, the normalized release appears independent of pH. The  $^{237}\text{Np}$  normalized release shows correlation with pH both for the 10,000- and 100,000-year simulations, though the pH at which normalized release begins to decrease is around 8.5 for 100,000 years and around 7 to 7.5 for 10,000 years.

### 2.3 CONCLUSIONS FROM WASTE PACKAGE ANALYSES

Several conclusions may be drawn from the waste package analysis results described in this section. These conclusions are highlighted below and discussed in greater detail in Section 4.

- For the assumptions and conceptualizations presented, the releases from the waste package according to thermal load are lowest from 70.4 kW/ha (28.5 kW/acre), 282 kW/ha (114 kW/acre), and then 141 kW/ha (57 kW/acre).
- As might be expected, the increase in container thickness provides a decrease in release from the waste package for the time periods evaluated (up to 100,000 years). However, the increase from 20 cm to 45 cm provided a substantially greater relative decrease in the total release. This is due primarily to the significant number of intact 45-cm overpack containers at 100,000 years.

- The temperature dependent corrosion initiation proved to be less conservative than the saturation dependent corrosion initiation conceptualization. Considerable uncertainty and disagreement as to the appropriate conceptualization appears to exist.
- Dry oxidation rates appear inconsequential in the Stahl conceptualization even for very high temperatures (500°C). The Lamont conceptualization, however, provides significantly greater penetration at high temperatures. The high temperatures expected in a backfilled repository lead to significantly different release values when using the Stahl or Lamont conceptualization.
- Both the Stahl and Lamont conceptualization appear to rapidly fail the inner container (formerly the SCP case).

Additional work is required in order to reduce uncertainty related to several aspects of the waste package analyses including: (1) corrosion rates (dry oxidation, general aqueous corrosion, pitting corrosion), (2) corrosion initiation conditions (saturation, temperature dependencies), and (3) radionuclide solubilities (especially  $^{237}\text{Np}$ ). These factors contribute to the major radionuclide releases from the waste package. Thus, reduction of the uncertainty in these parameters would significantly reduce uncertainty in the waste package model.

Table 2-1. Summary of Analysis Variations Evaluated in TSPA 1993

Areal Power Density (kW/acre)	Outer Container (cm)	Inner Container (cm)	Failure Conceptualization <sup>1</sup>	Case Label
28.5	10	.95	S1	28.5/10/.95/S1
	20	.95	S1	28.5/20/.95/S1
	45	.95	S1	28.5/45/.95/S1
57	10	.95	S1, L1, S2, L2	57/10/.95/S1 57/10/.95/L1 57/10/.95/S2 57/10/.95/L2
	10	3.5	L1, L2	57/10/3.5/L1 57/10/3.5/L2
	20	.95	S1	57/20/.95/S1
	45	.95	S1	57/45/.95/S1
114	10	.95	S1, S2, L2	114/10/.95/S1 114/10/.95/S2 114/10/.95/L2
	10	3.5	L1	114/10/3.5/L1
	20	.95	S1	114/20/.95/S1
	45	.95	S1	114/45/.95/S1

- <sup>1</sup> S1 = Stahl Failure Model; corrosion initiation is dependent on saturation - residual (8%)  
 S2 = Stahl Failure Model; corrosion initiation is dependent on temperature - boiling (100°C)  
 L1 = Lamont Failure Model; corrosion initiation is dependent on saturation - residual (8%)  
 L2 = Lamont Failure Model; corrosion initiation is dependent on temperature - boiling (100°C).

Table 2-2. Spent Fuel Waste Inventory

ISOTOPE	ORIGEN2 30 year Inventory <sup>1</sup> (Ci/MTHM)	SCP Design (Ci/Container) <sup>2</sup>	Multibarrier Waste Package Design (Ci/Container) <sup>3</sup>
<sup>227</sup> Ac	1.97E-5	4.14E-5	1.92E-4
<sup>241</sup> Am	3.92E3	8.23E3	3.82E4
<sup>242M</sup> Am	2.34E1	4.91E1	2.28E2
<sup>243</sup> Am	2.82E1	5.92E1	2.75E2
<sup>14</sup> C	1.48E0	3.11E0	1.44E1
<sup>36</sup> Cl <sup>4</sup>	1.18E-2	2.48E-2	1.15E-1
<sup>244</sup> Cm	1.41E3	2.95E3	1.37E4
<sup>245</sup> Cm	4.27E-1	8.97E-1	4.16E0
<sup>246</sup> Cm	9.38E-2	1.97E-1	4.14E-1
<sup>135</sup> Cs	5.67E-1	1.19E0	5.52E0
<sup>129</sup> I	3.72E-2	7.81E-2	3.62E-1
<sup>93M</sup> Nb	1.98E0	4.16E0	1.93E1
<sup>94</sup> Nb	8.91E-1	1.87E0	8.68E0
<sup>59</sup> Ni	2.52E0	5.29E0	2.45E1
<sup>63</sup> Ni	3.31E2	6.95E2	3.22E3
<sup>237</sup> Np	4.87E-1	1.02E0	4.74E0
<sup>231</sup> Pa	3.59E-5	7.54E-5	3.50E-4
<sup>210</sup> Pb	7.15E-7	1.50E-6	6.96E-6
<sup>107</sup> Pd	1.37E-1	2.88E-1	1.33E0
<sup>238</sup> Pu	3.57E3	7.50E3	3.48E4
<sup>239</sup> Pu	3.75E2	7.88E2	3.65E3
<sup>240</sup> Pu	5.73E2	1.20E3	5.58E3
<sup>241</sup> Pu	3.56E4	7.48E4	3.47E5
<sup>242</sup> Pu	2.18E0	4.58E0	2.12E1
<sup>226</sup> Ra	2.64E-6	5.54E-6	2.57E-5
<sup>228</sup> Ra	3.36E-10	7.06E-10	3.27E-9
<sup>79</sup> Se	4.80E-1	1.01E0	4.67E0

Table 2-2. Spent Fuel Waste Inventory (Continued)

ISOTOPE	ORIGEN2 30 year Inventory <sup>1</sup> (Ci/MTHM)	SCP Design (Ci/Container) <sup>2</sup>	Multibarrier Waste Package Design (Ci/Container) <sup>3</sup>
<sup>151</sup> Sm	3.77E2	7.92E2	3.67E3
<sup>126</sup> Sn	9.25E-1	1.94E0	9.01E0
<sup>99</sup> Tc	1.51E1	3.17E1	1.47E2
<sup>229</sup> Th	4.32E-7	9.07E-7	4.21E-6
<sup>230</sup> Th	3.79E-4	7.96E-4	3.69E-3
<sup>232</sup> Th	4.71E-10	9.89E-10	4.59E-9
<sup>233</sup> U	7.82E-5	1.64E-4	7.62E-4
<sup>234</sup> U	1.43E0	3.00E0	1.39E2
<sup>235</sup> U	1.68E-2	3.53E-2	1.64E-2
<sup>236</sup> U	2.93E-1	6.15E-1	2.85E0
<sup>238</sup> U	3.14E-1	6.59E-1	3.06E0
<sup>93</sup> Zr	2.58E0	5.41E0	2.51E1

<sup>1</sup> Assumes 40,747 MTHM PWR with burnup 42,300 Mwd/MTHM  
Assumes 22,253 MTHM BWR with burnup 32,250 Mwd/MTHM. See Appendix C. ORIGEN2  
(Croff, 1983).

<sup>2</sup> 2.1 MTHM/container.

<sup>3</sup> 9.74 MTHM/container, 21 PWR case.

<sup>4</sup> Chlorine inventory assumed to be nongaseous release.

Table 2-3. High-Level Waste Inventory

Isotope	TSPA 1993 HLW Inventory (Ci/Container) <sup>1</sup>	Isotope	TSPA 1993 HLW Inventory (Ci/Container) <sup>1</sup>
<sup>227</sup> Ac	6.02E-4	<sup>239</sup> Pu	4.73E0
<sup>241</sup> Am	8.65E1	<sup>240</sup> Pu	3.30E0
<sup>242m</sup> Am	2.06E-2	<sup>242</sup> Pu	5.02E-3
<sup>243</sup> Am	3.67E-2	<sup>241</sup> Pu	1.48E2
<sup>244</sup> Cm	1.14E1	<sup>226</sup> Ra	9.37E-8
<sup>245</sup> Cm	5.64E-5	<sup>79</sup> Se	9.18E-2
<sup>246</sup> Cm	6.39E-6	<sup>99</sup> Tc	3.30E0
<sup>135</sup> Cs	1.15E-1	<sup>229</sup> Th	1.51E-5
<sup>129</sup> I	1.90E-6	<sup>230</sup> Th	1.24E-5
<sup>94</sup> Nb	3.02E-5	<sup>232</sup> Th	1.05E-4
<sup>93m</sup> Nb	5.48E-1	<sup>233</sup> U	5.84E-4
<sup>59</sup> Ni	2.70E-2	<sup>234</sup> U	5.00E-2
<sup>237</sup> Np	2.83E-2	<sup>235</sup> U	7.93E-5
<sup>231</sup> Pa	9.74E-4	<sup>236</sup> U	4.35E-4
<sup>210</sup> Pb	2.72E-8	<sup>238</sup> U	3.78E-3
<sup>238</sup> Pu	4.00E2	<sup>93</sup> Zr	7.01E-1

<sup>1</sup> Assumed 4 canisters per container. Source: DOE (1987).

Table 2-4. Elicited General Corrosion Rates for Overpack (After Lamont, 1993)

Temperature (°C)	General Corrosion Rate (mm/yr)	Expected Failure (yr) <sup>1</sup>		
		10 cm overpack	20 cm overpack	45 cm overpack
20	.12	833	1667	3750
80	.38	263	526	1184
100	.20	500	1000	2250

<sup>1</sup> Failure times are calculated assuming corrosion begins at time = 0 and failure occurs when penetration = overpack thickness.

Table 2-5. Pitting Corrosion Rates (After Lamont, 1993)

Growth Condition	Inner Container Thickness											
	.95 cm						3.5 cm					
	70°C			100°C			70°C			100°C		
	g (mm/yr)	p	Time to Failure (yr) <sup>1</sup>	g (mm/yr)	p	Time to Failure (yr) <sup>1</sup>	g (mm/yr)	p	Time to Failure (yr) <sup>1</sup>	g (mm/yr)	p	Time to Failure (yr) <sup>1</sup>
Low growth rate (5 percentile)	.003	.033	95960	.299	.033	963	.003	.033	353,535	.299	.033	3547
Median growth rate (50 percentile)	.030	.033	9596	2.994	.033	96	.030	.033	35,354	2.994	.033	354
High growth rate (95 percentile)	.299	.033	963	29.939	.033	10	.299	.033	3547	29.939	.033	35

<sup>1</sup> Time to failure is calculated external to Lamont's model assuming growth of a pit occurs each year at the given probability. The time required for the penetration of the inner container by the pit is called time to failure.

Note: g = growth rate  
p = probability

Table 2-6. Failure Time and Fraction of Container Susceptible to Certain Temperature Zone (Bullen, 1993)

Parameter	28.5 kW/acre - conduction		57 kW/acre - conduction		114 kW/acre - conduction	
	SCP	Steel	SCP	Steel	SCP	Steel
Mean early failure time (yrs)			500	500	500	500
Mean failure time - alpha (yrs)			2400	2400	2400	2400
Mean failure time - beta (yrs)			400	425	400	425
Failure rate parameter - alpha and beta			2	2	2	2
Dry-out time - alpha (yrs)	0	0	2000	2000	2000	2000
Fraction failed at emplacement	.001	.001	.001	.001	.001	.001
Fraction susceptible to early failure	.004	.004	.004	.004	.004	.004
Fraction - alpha - wet	.02	.02	.05	.05	.005	.005
Fraction - alpha - dry	.325	.325	.65	.65	.045	.045
Fraction - beta - wet	.04	.04	.01	.01	0	0
Fraction - beta - dry	.56	.56	.09	.09	0	0

Note: Alpha and beta represent different thermal profiles.

**Table 2-7a. Calculated Time to Failure (Years) Due to General Corrosion  
Using Stahl Corrosion Model - 28.5 kW/acre<sup>1</sup>**

RING	Overpack Thickness		
	10 cm	20 cm	45 cm
1	>100,000	>100,000	>100,000
2	>100,000	>100,000	>100,000
3	>100,000	>100,000	>100,000
4	>100,000	>100,000	>100,000
5	>100,000	>100,000	>100,000
6	>100,000	>100,000	>100,000
7	>100,000	>100,000	>100,000

**Table 2-7b. Calculated Time to Failure (Years) Due to Pitting Corrosion  
Using Stahl Corrosion Model - 28.5 kW/acre<sup>1</sup>**

RING	Overpack Thickness		
	10 cm	20 cm	45 cm
1	4400	38,000	>100,000
2	4800	40,000	>100,000
3	5200	42,000	>100,000
4	5600	45,000	>100,000
5	6500	50,000	>100,000
6	8000	56,000	>100,000
7	12,000	68,000	>100,000

<sup>1</sup> Assumes corrosion begins at time = 0 years.

Table 2-8a. Calculated Time to Failure (Years) Due to General Corrosion  
Using Stahl Corrosion Model - 57 kW/acre<sup>1</sup>

RING	Overpack Thickness		
	10 cm	20 cm	45 cm
1	52,000	>100,000	>100,000
2	57,500	>100,000	>100,000
3	62,000	>100,000	>100,000
4	69,000	>100,000	>100,000
5	77,500	>100,000	>100,000
6	92,000	>100,000	>100,000
7	>100,000	>100,000	>100,000

Table 2-8b. Calculated Time to Failure (Years) Due to Pitting Corrosion  
Using Stahl Corrosion Model - 57 kW/acre<sup>1</sup>

RING	Overpack Thickness		
	10 cm	20 cm	45 cm
1	660	3500	79,000
2	690	3925	84,000
3	730	4400	90,000
4	820	5025	96,000
5	970	6200	>100,000
6	1425	8900	>100,000
7	3100	19,300	>100,000

<sup>1</sup> Assumes corrosion begins at time = 0 years.

Table 2-9a. Calculated Time to Failure (Years) Due to General Corrosion  
Using Stahl Corrosion Model - 114 kW/acre<sup>1</sup>

RING	Overpack Thickness		
	10 cm	20 cm	45 cm
1	46,800	>100,000	>100,000
2	48,300	>100,000	>100,000
3	51,400	>100,000	>100,000
4	54,400	>100,000	>100,000
5	35,900	>100,000	>100,000
6	42,100	>100,000	>100,000
7	19,100	>100,000	>100,000

Table 2-9b. Calculated Time to Failure (Years) Due to Pitting Corrosion  
Using Stahl Corrosion Model - 114 kW/acre<sup>1</sup>

RING	Overpack Thickness		
	10 cm	20 cm	45 cm
1	6250	13,600	61,300
2	6350	14,800	64,300
3	6450	15,100	67,300
4	6650	16,350	68,900
5	3950	8400	51,100
6	4250	9500	57,600
7	950	2950	81,700

<sup>1</sup> Rings 1-4 have dryout of 3160 years, Rings 5-6 have dryout of 1780 years, and Ring 7 has no dryout period.

Table 2-10. Calculated Time to Failure (Years) Due to Pitting Corrosion Using Stahl Corrosion Models - 57 kW/acre and 114 kW/acre - 100°C switchpoint

RING	57 kW/acre - 100°C switchpoint <sup>1</sup>	114 kW/acre - 100°C switchpoint <sup>3</sup>
	Overpack Thickness 10 cm <sup>2</sup>	Overpack Thickness 10 cm <sup>4</sup>
1	4840	15,750
2	2710	15,150
3	3370	14,370
4	2560	13,670
5	1210	13,060
6	1710	11,250
7	3810	6540

<sup>1</sup> Assumes corrosion initiation begins at the following times: Rings 1-3 = 1,000 years; Ring 4 = 316 years; Rings 5-7 = 0 years.

<sup>2</sup> 57/10/.95/S2.

<sup>3</sup> Assumes corrosion begins at the following times: Ring 1 = 6,600 years; Ring 2 = 6,400 years; Ring 3 = 6,000 years; Ring 4 = 5,700 years; Ring 4 = 5,700 years; Ring 5 = 5,300 years; Ring 6 = 4,800 years; for Ring 7, corrosion occurs from 0 - 300 years and then stops until 3,600 years.

<sup>4</sup> 114/10/.95/S2.

Table 2-11a. RIP Implementation of Failure Time for 28.5 kW/acre  
Using Stahl Corrosion Model (Pitting)<sup>1</sup>

Ring	10 cm		20 cm		45 cm	
	Start	Duration	Start	Duration	Start	Duration
1	3300	2200	28,000	19,500	100,000	100,000
2	3600	2400	30,000	20,000	100,000	100,000
3	3900	2600	31,500	21,000	100,000	100,000
4	4200	2800	33,750	22,500	100,000	100,000
5	4875	3250	37,500	25,000	100,000	100,000
6	6000	4000	42,000	28,000	100,000	100,000
7	9000	6000	51,000	34,000	100,000	100,000

Table 2-11b. RIP Implementation of Failure Time for 57 kW/acre  
Using Stahl Corrosion Model (Pitting)<sup>1</sup>

Ring	10 cm		20 cm		45 cm	
	Start	Duration	Start	Duration	Start	Duration
1	495	330	2625	1750	59,250	39,500
2	520	340	2945	1965	63,000	42,000
3	550	360	3300	2200	67,500	45,000
4	615	410	3770	2510	72,000	48,000
5	730	480	4650	3100	100,000	100,000
6	1070	710	6675	4450	100,000	100,000
7	2325	1550	14,475	9650	100,000	100,000

Table 2-11c. RIP Implementation of Failure Time for 114 kW/acre  
Using Stahl Corrosion Model (Pitting)<sup>1,2</sup>

Ring	10 cm		20 cm		45 cm	
	Start	Duration	Start	Duration	Start	Duration
1	4690	2850	10,200	6800	46,000	30,600
2	4760	3180	11,100	7400	48,200	32,200
3	4840	3220	11,300	7550	50,450	33,700
4	4990	3320	12,250	8200	51,650	34,500
5	2960	1980	6300	4200	38,300	25,600
6	3190	2120	7100	4800	43,200	28,800
7	710	480	2200	1500	61,250	40,900

<sup>1</sup> .95 cm inner container thickness.

<sup>2</sup> Time to resaturate above 8 percent saturation for each of the rings is as follows: Rings 1-4 are 3160 years; Rings 5-6 are 1780 years; Ring 7 is 0 years.

Note: All times are in years.

Table 2-12. RIP Implementation of Failure Time for 57 kW/acre and 114 kW/acre Using Stahl Corrosion Model (Pitting) - 100°C switch to aqueous corrosion

Ring	57 kW/acre		114 kW/acre	
	10 cm		10 cm	
	Start	Duration	Start	Duration
1	3630	2420	11,800	7880
2	2340	1550	11,350	7580
3	2510	1680	10,750	7200
4	1910	1280	10,250	6830
5	900	610	9800	6525
6	1290	860	8430	5630
7	2850	1910	4900	3275

Note: All times are in years.

Table 2-13. Calculated Time to Failure for General Corrosion Using Lamont Corrosion Model - 57 kW/acre<sup>1</sup>

Ring	Overpack Thickness		
	10 cm	20 cm	45 cm
1	650	1150	2025
2	600	1050	1900
3	575	975	1800
4	475	850	1650
5	400	725	1500
6	300	600	1300
7	275	500	1175

<sup>1</sup> Assumes corrosion begins at time = 0 years.

Note: All times are in years.

Table 2-14. Calculated Time to Failure for Pitting Corrosion Using Lamont Corrosion Model - 57 kW/acre (10 cm overpack)

Ring	.95 cm <sup>1</sup>			3.5 cm <sup>2</sup>		
	median	5th	95th	median	5th	95th
1	750	1500	700	1050	>100,000	700
2	700	28,000	625	1050	>100,000	650
3	650	43,000	525	1200	>100,000	600
4	600	58,000	450	1700	>100,000	500
5	700	70,000	400	10,000	>100,000	500
6	1200	82,000	300	20,000	>100,000	525
7	4400	91,000	250	30,000	>100,000	650

<sup>1</sup> 57/10/.95/L1 = See Table 2-1.

<sup>2</sup> 57/10/3.5/L1 = See Table 2-1.

Note: All times are in years.

Table 2-15a. Calculated Time to Failure for Pitting Corrosion Using Lamont Corrosion Model and 57 kW/acre - 100°C switchpoint

Ring	.95 cm <sup>1</sup>			3.5 cm <sup>2</sup>		
	median	5th	95th	median	5th	95th
1	1600	62,800	1380	3850	>100,000	1440
2	1390	67,300	1160	7400	>100,000	1220
3	1110	64,800	930	4700	>100,000	970
4	910	66,300	670	6100	>100,000	730
5	750	69,800	410	9900	>100,000	490
6	1230	81,100	310	21,500	>100,000	520
7	4300	89,900	260	29,800	>100,000	640

<sup>1</sup> 57/10/.95/L2

<sup>2</sup> 57/10/3.5/L2

Table 2-15b. Calculated Time to Failure for Pitting Corrosion Using Lamont Corrosion Model and 114 kW/acre - 100°C switchpoint

Ring	.95 cm <sup>1</sup>			3.5 cm <sup>2</sup>		
	median	5th	95th	median	5th	95th
1	7160	9470	7030	7560	>100,000	7070
2	6970	8800	6840	7350	99,000	6880
3	6570	8330	6430	6940	>100,000	6480
4	6220	8000	6100	6600	>100,000	6140
5	5860	7850	5730	6280	>100,000	5770
6	5350	7600	5230	5800	>100,000	5260
7	3790	5250	3690	4100	>100,000	3720

<sup>1</sup> 114/10/.95/L2.

<sup>2</sup> 114/10/3.5/L2.

Note: All times are in years.

Table 2-16. RIP Implementation of Pitting Corrosion for Inner Container with 10 cm overpack for 57 kW/acre Using Lamont Corrosion Model - 8 percent saturation - Weibull distribution<sup>1</sup>

Ring	Inner Container Thickness					
	.95 cm			3.5 cm		
	Start	Slope	Duration	Start	Slope	Duration
1	700	2.112	59.5	700	0.259	1439.7
2	625	0.249	326.7	650	0.265	1591.5
3	525	0.252	536.3	600	0.286	2157.0
4	450	0.246	664.1	500	0.331	3627.5
5	400	0.269	1171.7	500	0.623	17,106.4
6	300	0.325	2780.5	525	0.897	29,296.8
7	250	0.475	8979.2	650	1.200	39,830.0

<sup>1</sup> Assumes corrosion begins at time = 0.

Note: All times are in years.

Table 2-17a. RIP Implementation of Pitting Corrosion for Inner Container with 10 cm overpack for 57 kW/acre Using Lamont Corrosion Model - 100°C switchpoint - Weibull distribution<sup>1</sup>

Ring	Inner Container Thickness					
	.95 cm <sup>2</sup>			3.5 cm <sup>3</sup>		
	Start	Slope	Duration	Start	Slope	Duration
1	1380	0.260	901.3	1440	0.394	6103.6
2	1160	0.259	949.3	1220	0.528	12,370.6
3	930	0.249	783.1	970	0.446	8478.0
4	670	0.261	978.2	730	0.502	11,147.9
5	410	0.275	1287.8	490	0.621	16,985.2
6	310	0.327	2821.4	520	0.940	30,978.4
7	260	0.472	8779.1	640	1.194	39,637.6

<sup>1</sup> Assumes corrosion begins at the following times: Rings 1-3 = 1,000 years; Ring 4 = 316 years; Rings 5-7 = 0 years.

<sup>2</sup> 57/10/.95/L2.

<sup>3</sup> 57/10/3.5/L2.

Table 2-17b. RIP Implementation of Pitting Corrosion for Inner Container with 10 cm overpack for 114 kW/acre Using Lamont Corrosion Model - 100°C switchpoint - Weibull distribution<sup>1</sup>

Ring	Inner Container Thickness					
	.95 cm <sup>2</sup>			3.5 cm <sup>3</sup>		
	Start	Slope	Duration	Start	Slope	Duration
1	7030	0.524	261.5	7070	0.279	1822.2
2	6840	0.539	256.4	6880	0.277	1762.3
3	6430	0.561	270.0	6480	0.275	1740.7
4	6100	0.530	239.6	6140	0.275	1742.3
5	5730	0.524	261.5	5770	0.280	1884.2
6	5220	0.503	269.2	5260	0.283	1969.38
7	3690	0.533	198.9	3720	0.264	1519.5

<sup>1</sup> Assumes that corrosion begins at the following times: Ring 1 = 6,600 years; Ring 2 = 6,400 years; Ring 3 = 6,000 years; Ring 4 = 5,700 years; for Ring 7, corrosion occurs from 0-300 years and then stops until 3,600 years.

<sup>2</sup> 114/10/.95/L2.

<sup>3</sup> 114/10/3.5/L2.

Note: All start times are in years.

Table 2-18. Solubilities for TSPA 1993

RN	Solubility (g/m <sup>3</sup> )	Functional Form	Source
Ac	f(T)--Same as Am	Same as Am	Elicitation, (Nitsche et al., 1992a,b)
Am	f(T)	See Table 2-19a	Nitsche et al., (1992a,b)
C	NA (gaseous)	NA (gaseous)	Golder (1993)
Cm	f(T)	T ≤ 55°C, [LT: 1.2e-6, 1.2e-5, 1.2e-4] T > 55°C, [LT: 1.5e-10, 1.5e-9, 1.5e-8]	Wilson (1990)
Cs	LT: 1.2, 3.9e+2, 2.1e+3	LT: 1.2, 3.9e+2, 2.1e+3	Golder (1993), EPRI (1992)
I	NA (gaseous)	NA (gaseous)	Golder (1993)
Nb	LU: 9.3e-5, 9.3e-3	LU: 9.3e-5, 9.3e-3	Elicitation
Ni	LB: 5.9e-2, 5.9e+3, 105, 0.25	10**[2.0212*(0.25*DIST3+1)]	Elicitation
Np	f(T)	See Table 2-19b	Nitsche et al., (1992a,b)
Pa	LU: 2.3e-5, 2.3	10**(5*DIST2-4.6383)	Elicitation
Pb	LB: 2.1e-3, 2.1, 6.6e-2, 0.08	10**[-1.1805*(0.08*DIST3+1)]	Elicitation
Pu	f(T)	See Table 2-19c	Nitsche et al., (1992a,b)
Ra	LB: 2.3e-4, 2.3, 2.3e-2, 0.1	10**[-1.6383*(0.1*DIST1+1)]	Elicitation
Se	LT: 7.9e+2, 7.9e+3, 5.5e+5	LT: 7.9e+2, 7.9e+3, 5.5e+5	Golder (1993), EPRI (1992)
Sm	f(T)--Same as Am	Same as Am	Elicitation, (Nitsche et al., 1992a,b)
Sn	U: 1.3e-6, 1.3e-2	0.013*DIST2+1.3e-6	Elicitation
Sr	LB: 9.0e-2, 90, 9.0, 0.12	10**[0.9542*(0.12*DIST1+1)]	Elicitation
Tc	LT: 3.5e-2, 1e+2, 9.9e+5	LT: 3.5e-2, 1e+2, 9.9e+5	Golder (1993), EPRI (1992)

RN	Solubility (g/m <sup>3</sup> )	Functional Form	Source
Th	LU: 2.3e-5, 2.3e-2	10**(3*DIST2-4.6383)	Elicitation
U	f(T)--Same as Np	Same as Np	Elicitation, (Nitsche et al., 1992a,b)
Zr	LU: 9.1e-8, 9.1e-3	10**(5*DIST2-7.0410)	Elicitation

**Explanation:**

RN = radionuclide

All solubilities have units of g of element/m<sup>3</sup> of solution.

DIST1 = Normal distribution with  $\mu = 0$  and  $\sigma = 1$ ; for Ra and Sr.

DIST2 = 0 to 1; Uniform; for Pa, Sn, Th, Zr.

DIST3 = Normal distribution with  $\mu = 0$  and  $\sigma = 1$ ; for Ni and Pb.

pH = 6 to 9, uniform.

LB = log-beta distribution; min, max, expected value, coefficient of variation.

These are approximated by a log-normal distribution.

LT = log-triangular distribution; min, expected value, max.

LU = log-uniform distribution; min, max.

N = normal distribution; mean, standard deviation.

U = uniform distribution; min, max.

e+ = positive power of ten.

e- = negative power of ten.

Table 2-19a. Temperature- and pH-Dependent Solubilities for Americium

pH	Solubility for the given temperature range (gm/m <sup>3</sup> )		
	T ≤ 42.5°C	42.5°C < T < 75°C	75°C < T
≤ 6.5	N: 4.4e-4, 1.5e-4	N: 6.1e-1, 1.7e-1	N: 4.1e-4, 4.1e-4
6.5 < pH ≤ 7.75	N: 2.9e-4, 0.7e-4	N: 2.4e-3, 2.2e-3	N: 7.5e-5, 4.1e-5
> 7.75	N: 5.8e-4, 4.6e-4	N: 2.9e-3, 2.9e-3	N: 8.3e-5, 5.1e-5

N: Normal distribution; mean, standard deviation

Table 2-19b. Temperature- and pH-Dependent Solubilities for Neptunium

pH	Solubility for the given temperature range (gm/m <sup>3</sup> )		
	T ≤ 42.5°C	42.5°C < T < 75°C	75°C < T
≤ 6.5	N: 1.3e+3, 0.07e+3	N: 1.5e+3, 0.09e+3	N: 2.8e+2, 0.2e+2
6.5 < pH ≤ 7.75	N: 3.1e+1, 0.5e+1	N: 2.3e+2, 0.2e+2	N: 3.6e+1, 0.9e+1
> 7.75	N: 1.0e+1, 0.2e+1	N: 2.4e+1, 0.2e+1	N: 2.1e+1, 0.09e+1

N: Normal distribution; mean, standard deviation

Table 2-19c. Temperature- and pH-Dependent Solubilities for Plutonium

pH	Solubility for the given temperature range (gm/m <sup>3</sup> )		
	T ≤ 42.5°C	42.5°C < T < 75°C	75°C < T
≤ 6.5	N: 2.6e-1, 1.0e-1	N: 6.5e-3, 2.6e-3	N: 1.5e-3, 0.5e-3
6.5 < pH ≤ 7.75	N: 5.5e-2, 3.4e-2	N: 8.9e-3, 2.2e-3	N: 2.1e-3, 0.2e-3
> 7.75	N: 7.0e-2, 1.9e-2	N: 2.9e-2, 0.2e-2	N: 1.8e-3, 0.1e-3

N: Normal distribution; mean, standard deviation

Table 2-20. Comparison of TSPA 1991 Container Parameters With TSPA 1993 Container Parameters

RIP MODEL PARAMETER	TSPA 1991 RIP BASE CASE	TSPA 1993 RIP SCP BASE CASE	TSPA 1993 RIP MPC BASE CASE 21PWR 57 kW/acre
No. packages	PWR -- 19,980 BWR -- 13,320 no HLW	30,000 -- Spent Fuel 14,000 -- HLW	6468 - Spent Fuel (1078/ring) 3829 -- HLW
Waste burnup (MWd/MTHM)	PWR -- 33,000 BWR -- 27,500	38,747 -- Combined	42,300 - PWR 32,250 - BWR 39,075 combined
Mass waste/pkg = MTHM in repository/# of waste containers	2.1 MTHM/pkg	2.1 MTHM/pkg for PWR/BWR .5 MTHM/pkg-HLW	9.74 MTHM/pkg for PWR/BWR 1.828 MTHM/pkg-HLW

Table 2-21a. Comparison of TSPA 1991 Inventory Parameters With TSPA 1993 Parameters

INVENTORY	TSPA 1991 RIP BASE CASE (Ci/container <sup>2</sup> )	TSPA 1993 RIP SCP BASE CASE <sup>1</sup> (Ci/container <sup>2</sup> )	TSPA 1993 RIP MPC BASE CASE <sup>1</sup> (Ci/container <sup>3</sup> )
<sup>243</sup> Am	32.34	59.2	274.668
<sup>14</sup> C	1.54	3.29	14.4
<sup>135</sup> Cs	.7371	1.19	5.52
<sup>129</sup> I	.06195	.0781	3.62
<sup>237</sup> Np	2.352	1.02	4.74
<sup>239</sup> Pu	646.8	788.	3.65
<sup>79</sup> Se	.8001	1.01	4.67
<sup>126</sup> Sn	1.5015	1.94	9.01
<sup>99</sup> Tc	25.83	31.7	1.47
<sup>234</sup> U	3.969	3.0	1.39

<sup>1</sup> TSPA 1991 is for 10-year-old fuel. TSPA 1993 inventory is for 30-year-old fuel. 28 additional radionuclides are included in the TSPA 1993 inventory, which includes parents of <sup>237</sup>Np.

<sup>2</sup> Ci/container = Ci/MTHM \* 2.1 MTHM/container.

<sup>3</sup> Ci/container = Ci/MTHM \* 9.2 MTHM/container.

Table 2-21b. Comparison of TSPA 1991 Inventory Parameters With TSPA 1993 Parameters

INVENTORY	TSPA 1991 RIP BASE CASE Gap Fraction	TSPA 1993 RIP SCP BASE CASE Gap Fraction	TSPA 1993 RIP MPC BASE CASE Gap Fraction
<sup>243</sup> Am	0	0	0
<sup>14</sup> C	.02	.02	0.0125 → 0.0575: Uniform
<sup>135</sup> Cs	.02	.02	.02
<sup>129</sup> I	.02	.02	.02
<sup>237</sup> Np	0	0	0
<sup>239</sup> Pu	0	0	0
<sup>79</sup> Se	.02	.02	.02
<sup>126</sup> Sn	0	0	0
<sup>99</sup> Tc	.02	.02	.02
<sup>234</sup> U	0	0	0

Table 2-21c. Comparison of TSPA 1991 Inventory Parameters With TSPA 1993 Parameters

INVENTORY	TSPA 1991 RIP BASE CASE Solubility (g/m <sup>3</sup> )	TSPA 1993 RIP SCP BASECASE Solubility (g/m <sup>3</sup> )	TSPA 1993 RIP MPC BASE CASE Solubility (g/m <sup>3</sup> )
<sup>243</sup> Am	LU: 2.92E-6, 9.2E-4, 1.6E-4	(see Table 2-19)	(see Table 2-19)
<sup>14</sup> C	gas	gas	gas
<sup>135</sup> Cs	infinite	LT:1.2,3.9E2,2.1E3	LT:1.2,3.9E2,2.1E3
<sup>129</sup> I	infinite	gas	gas
<sup>237</sup> Np	LU: 1.40E-5, 4.50E-3, 7.82E-4	(see Table 2-19)	(see Table 2-19)
<sup>239</sup> Pu	LU: 3.82E-5, 1.22E-2, 2.10E-3	(see Table 2-19)	(see Table 2-19)
<sup>79</sup> Se	infinite	LT:7.9E2,7.9E3, 5.5E5	LT:7.9E2,7.9E3, 5.5E5
<sup>126</sup> Sn	LU: 1.26E-4, 4.03E-2, 6.93E-3	(see Table 2-18)	(See Table 2-18)
<sup>99</sup> Tc	infinite	LT:3.5E-2, 1E2, 9.9E5	LT:3.5E-2,1E2, 9.9E5
<sup>234</sup> U	LU: 1.66E-5, 5.38E-3, 9.36E-4	(see Table 2-18)	(see Table 2-18)

LU = Log-uniform: min, max, expected values

LT = Log-triangular: min, middle, max

Table 2-21d. Comparison of TSPA 1991 Inventory Parameters With TSPA 1993 Parameters

<b>INVENTORY</b>	<b>TSPA 1991 RIP BASE CASE Activity (Ci/g)</b>	<b>TSPA 1993 RIP SCP BASE CASE Activity (Ci/g)</b>	<b>TSPA 1993 RIP MPC BASE CASE Activity (Ci/g)</b>
<sup>243</sup> Am	2.E-1	2.E-1	2.E-1
<sup>14</sup> C	62.4 Ci/mol	62.4 Ci/mol	62.4 Ci/mol
<sup>135</sup> Cs	1.15E-3	1.15E-3	1.15E-3
<sup>129</sup> I	1.77E-4	1.77E-4	1.77E-4
<sup>237</sup> Np	7.06E-4	7.06E-4	7.06E-4
<sup>239</sup> Pu	6.22E-2	6.22E-2	6.22E-2
<sup>79</sup> Se	6.98E-2	6.98E-2	6.98E-2
<sup>126</sup> Sn	2.84E-2	2.84E-2	2.84E-2
<sup>99</sup> Tc	1.7E-2	1.7E-2	1.7E-2
<sup>234</sup> U	6.26E-3	6.26E-3	6.26E-3

Table 2-22. Comparison of TSPA 1991 Waste Package Failure Parameters With TSPA 1993 Parameters

TSPA 1991 MODEL PARAMETER	TSPA 1991 RIP BASE CASE	TSPA 1993 RIP BASE CASE
Beginning of resaturation period (yr)	500 yrs: constant	varies with thermal load
Duration of resaturation period (yr)	300 -1300 yrs: uniform	varies with thermal load
Container lifetime when wet (yr)	(1) Weibull:1, 1650 (2) LU: 500-10,000; gradual failure (3) LU: 500-10,000; all fail at once (4) LU: 500-10,000; sample maximum failure and fail gradually to that time	varies with thermal load

LU = Log-uniform: min, max, expected value

Table 2-23. Comparison of TSPA 1991 Exposure Parameters With TSPA 1993 Exposure Parameters

TSPA 1991 MODEL PARAMETER	RIP MODEL PARAMETER	TSPA 1991 RIP BASE CASE	TSPA 1993 RIP BASE CASE
Fraction of containers with rubble in air gap	(1) fraction of containers in water contact mode 3 - moist continuous (2) Fraction of waste wetted (3) ECA <sup>1</sup> (4) EDC <sup>3</sup>	(1) dependent on flux (2) .5 (3) 0 (4) SNL moist diff. coeff. (3.E-6 - 3.E-4: LU) <sup>2</sup>	(1) dependent on flux, temperature, saturation (2) 1.0 (3) 8.5-46.5 m <sup>2</sup> (4) Conca Curve
Fraction of fuel wet with seepage	(1) fraction of containers in water contact mode 2 - wet drip (2) Fraction of waste wetted (3) ECA (4) EDC	(1) dependent on flux (2) .5 (3) 1 (4) 0	N/A
Fraction of fuel wet and diffusing	(1) fraction of containers in water contact mode 1 - wet feet (2) Fraction of waste wetted (3) ECA (4) EDC	(1) dependent on flux (2) .5 (3) 1 (4) SNL wet diff. coeff. (9.E-4 - 9.E-3: LU)	N/A
Nominal case - no release	(1) fraction of containers in water contact mode 4 - nominal case	(1) dependent on flux	N/A
	Air alteration rate	0	0
Matrix alteration rate (1/yr)	Matrix dissolution rate (g/m <sup>2</sup> /yr)	LU: 5E-5, 1E-3, 3.17E-4	Temp. dependent (see text)

Table 2-23. Comparison of TSPA 1991 Exposure Parameters With TSPA 1993 Exposure Parameters (Continued)

TSPA 1991 MODEL PARAMETER	RIP MODEL PARAMETER	TSPA 1991 RIP BASE CASE	TSPA 1993 RIP BASE CASE
	Surface area of matrix (m <sup>2</sup> /g) (combined with matrix dissolution rate)	1	SF: ASF/(1.10062E7): ASF = ASF1*ASF2 Spent fuel = 78-107 uniform ASF2 = 1-100 uniform HLW: AHL/(7.012E6): AHL = 200-600
Prompt alteration rate (1/yr)	N/A -- radionuclides put in gap fraction	N/A	N/A
Spent fuel surface area (m <sup>2</sup> ) per package	Included in water volume contacting matrix (m <sup>3</sup> ) (= surface area * water film thickness * fraction of fuel wet)	.07	N/A
Water film thickness (mm)	Included in water volume contacting matrix (m <sup>3</sup> )	.07	Water volume contacting matrix: ASF*D WATER : D WATER = .001 thickness of water layer contacting matrix

2-56

<sup>1</sup> ECA = effective catchment area

<sup>2</sup> LU = log-uniform: min, max, expected value

<sup>3</sup> EDC = effective diffusion coefficient

Table 2-24. Comparison of TSPA 1991 Transport Parameters With TSPA 1993 Transport Parameters

TSPA 1991 MODEL PARAMETER	RIP MODEL PARAMETER	TSPA 1991 RIP BASE CASE	TSPA 1993 RIP BASE CASE
Moist diffusion coefficient (m <sup>2</sup> /yr)	Effective diffusion coefficient (m <sup>2</sup> /yr)	LU: 3E-6, 3E-4, 6.45E-5	- curve fit to Conca data
Wet diffusion coefficient (m <sup>2</sup> /yr)	Effective diffusion coefficient (m <sup>2</sup> /yr)	LU: 9E-4, 9E-3, 3.52E-3	- curve fit to Conca data
Flux coefficient of variation	None	N/A	N/A
Percolation rate (mm/yr)	Repository infiltration rate (m/yr)	Beta: .001,.0009,0,.039 (only for contact modes 1,2)	VTOUGH results
Effective diffusion area (m <sup>2</sup> )	Geometric factor for diffusion (m)	.1 (only for contact modes 1,3)	28.05*N*(fs): N = porosity of backfill = .1-.3; fs = 1 if sat>.08
Water collection area (A <sub>cross</sub> ) (m <sup>2</sup> )	Effective catchment area (m <sup>2</sup> ) = water collection area * fraction of seepage entering container	contac 1 = 1 contac 2 = 1 contac 3 = 0 contac 4 = 0	see ECA
Rubble thickness (cm)	Delay pathway (only in moist continuous)	(1) 3 cm air gap (2) did not evaluate in-drift emplacement	In-drift emplacement: .5 m crushed tuff zone

LU = Log-uniform: min, max, expected value

Table 2-25. Waste Package Configurations —57 kW/acre (Memory, 1993)

Characteristic		21 PWR		
		.95/10 cm	.95/20 cm	.95/45 cm
# of Waste Packages	SF	7674	7674	7674
	HLW	3257	3257	3257
Length		4.831	5.031	5.531
Diameter		1.7519	1.9519	2.4519

Table 2-26. Normalized Cumulative Release from the Waste Package for Reference Case

ISOTOPE	Normalized Cumulative Release (10,000 yr)	Normalized Cumulative Release (100,000 yr)
<sup>227</sup> Ac	4.52E-3	1.77E1
<sup>241</sup> Am	6.48E-2	1.37E-1
<sup>242M</sup> Am	1.64E-7	1.64E-7
<sup>243</sup> Am	9.59E-2	1.67E0
<sup>14</sup> C	2.59E0	3.13E0
<sup>36</sup> Cl	1.48E-2	4.84E-2
<sup>244</sup> Cm	3.96E-16	3.96E-16
<sup>245</sup> Cm	3.93E-8	1.83E-3
<sup>246</sup> Cm	4.96E-9	1.14E-5
<sup>135</sup> Cs	1.61E-1	5.17E-1
<sup>129</sup> I	9.95E-2	3.25E-1
<sup>93M</sup> Nb	1.42E-15	1.42E-15
<sup>94</sup> Nb	2.66E-3	3.24E-2
<sup>59</sup> Ni	6.14E-1	1.76E0
<sup>63</sup> Ni	1.91E-2	1.91E-2
<sup>237</sup> Np	3.69E0	1.34E1
<sup>231</sup> Pa	1.05E-2	2.70E-1
<sup>210</sup> Pb	1.81E-1	3.19E2
<sup>107</sup> Pd	3.46E-2	1.19E-1
<sup>238</sup> Pu	1.60E-6	1.60E-6
<sup>239</sup> Pu	4.13E-2	1.30E0
<sup>240</sup> Pu	2.78E-2	1.06E-1
<sup>241</sup> Pu	1.30E-14	1.30E-14
<sup>242</sup> Pu	1.76E-4	2.47E-2

Table 2-26. Normalized Cumulative Release from the Waste Package for Reference Case  
(Continued)

ISOTOPE	Normalized Cumulative Release (10,000 yr)	Normalized Cumulative Release (100,000 yr)
<sup>226</sup> Ra	9.69E-1	2.07E1
<sup>228</sup> Ra	1.93E-2	1.29E-1
<sup>79</sup> Se	1.30E-1	3.37E-1
<sup>151</sup> Sm	4.45E-4	4.45E-4
<sup>126</sup> Sn	1.31E-3	1.59E-2
<sup>99</sup> Tc	4.25E-1	1.28
<sup>229</sup> Th	1.21E-4	5.78E-3
<sup>230</sup> Th	2.17E-2	2.44E-1
<sup>232</sup> Th	8.33E-8	1.22E-6
<sup>233</sup> U	9.52E-4	4.32E-2
<sup>234</sup> U	8.76E-2	6.57E-1
<sup>235</sup> U	1.69E-4	3.37E-3
<sup>236</sup> U	2.87E-3	5.22E-2
<sup>238</sup> U	3.51E-3	4.28E-2
<sup>93</sup> Zr	7.71E-7	9.86E-6

Normalized to 40 CFR 191 Table 1

Table 2-27. Summary Results for 10,000 and 100,000 Year Normalized Cumulative Release from the Waste Package

Design <sup>1</sup>	Total Normalized Cumulative Release	<sup>14</sup> C Total Normalized Cumulative Release	<sup>237</sup> Np Total Normalized Cumulative Release	<sup>99</sup> Tc Total Normalized Cumulative Release	<sup>210</sup> Pb Total Normalized Cumulative Release
57/10/95/S1	9.3 / 383.	2.6 / 3.13	3.7 / 13.4	0.43 / 1.28	0.18 / 319.
57/20/95/S1	4.3 / 369.	1.1 / 1.70	1.9 / 13.1	0.21 / 1.22	0.05 / 309.
57/45/95/S1	0 / 28.9	0 / 1.4E-4	0 / 2.3	0 / 0.18	0 / 23.
114/10/95/S1	5.5 / 326.	1.3 / 2.14	1.2 / 14.3	0.31 / 1.36	0.35 / 14.
114/20/95/S1	2.0 / 304.	0.1 / 0.89	0.3 / 14.0	0.06 / 1.31	0.02 / 12.5
114/45/95/S1	0 / 145.	0 / 4.3E-3	0 / 9.9	0 / 0.82	0 / 6.1
28.5/10/95/S1	2.9 / 315.	0.7 / 1.22	1.2 / 11.7	0.14 / 1.06	0.02 / 263.
28.5/20/95/S1	0 / 182.	0 / 0.02	0 / 8.4	0 / 0.70	0 / 154.
28.5/45/95/S1 <sup>2</sup>	0/0	0/0	0/0	0/0	0/0
57/10/95/L1	7.7 / 362.	2.1 / 2.64	3.0 / 12.8	0.35 / 1.20	0.14 / 302.
57/10/3.5/L1	5.0 / 330.	1.4 / 1.82	2.0 / 11.9	0.22 / 1.09	0.08 / 277.
57/10/95/S2	7.1 / 375.	1.8 / 2.36	3.0 / 13.3	0.33 / 1.26	0.08 / 313.
57/10/95/L2	6.8 / 352.	1.8 / 2.33	2.8 / 12.5	0.31 / 1.17	0.10 / 294.
57/10/3.5/L2	3.5 / 315.	0.9 / 1.34	1.5 / 11.6	0.16 / 1.06	0.04 / 265.
114/10/95/S2	1.1 / 301.	0.02 / .76	0.05 / 14.0	0.02 / 1.31	0 / 12.3
114/10/95/L2	4.2 / 322.	0.9 / 1.82	0.85 / 14.2	0.25 / 1.35	0.21 / 13.8
114/1G/3.5/L2	3.0 / 290.	0.7 / 1.38	0.59 / 13.2	0.17 / 1.24	0.15 / 12.3

Format: 10,000 / 100,000

Normalized to 40 CFR 191 Table 1

<sup>1</sup> S1 = Stahl Failure Model; corrosion initiation is saturation dependent.

S2 = Stahl Failure Model; corrosion initiation is temperature dependent.

L1 = Lamont Failure Model; corrosion initiation is saturation dependent

L2 = Lamont Failure Model; corrosion initiation is temperature dependent

<sup>2</sup> No releases due to no container failures.

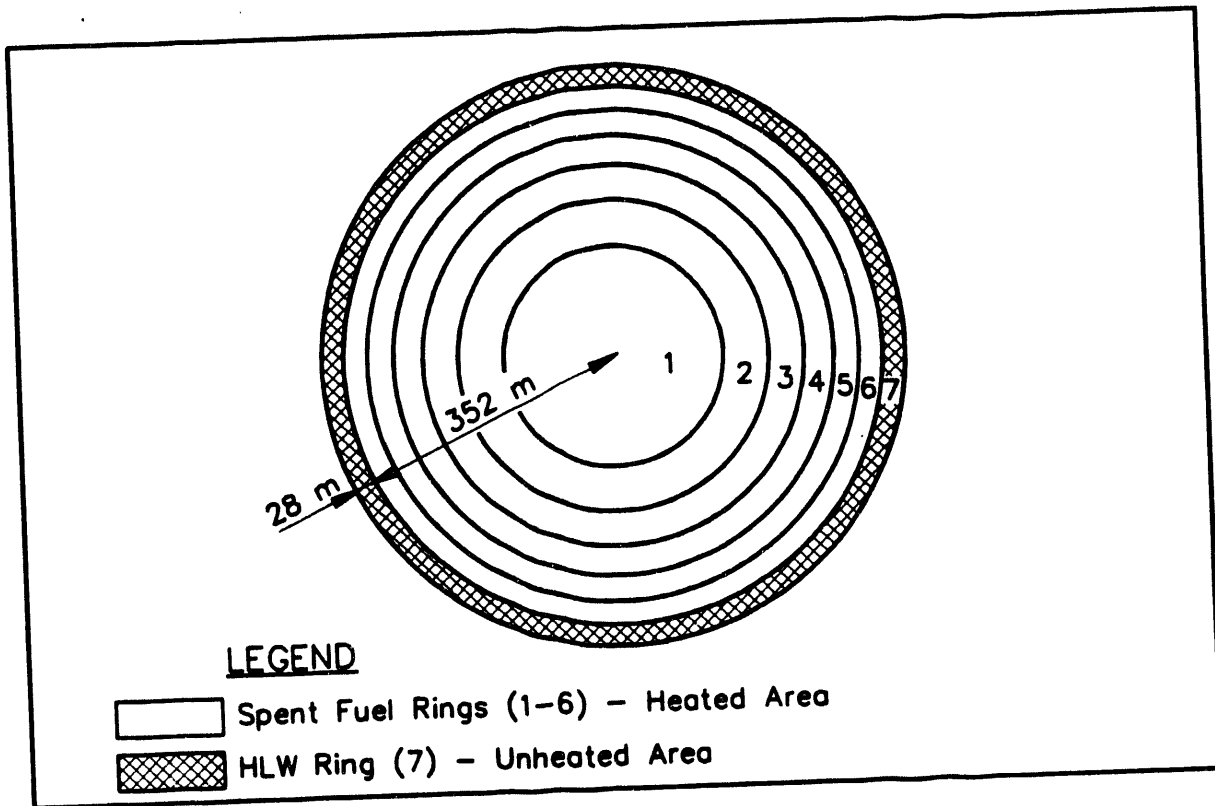


Figure 2-1. Repository Panel Conceptualization (Plan View)

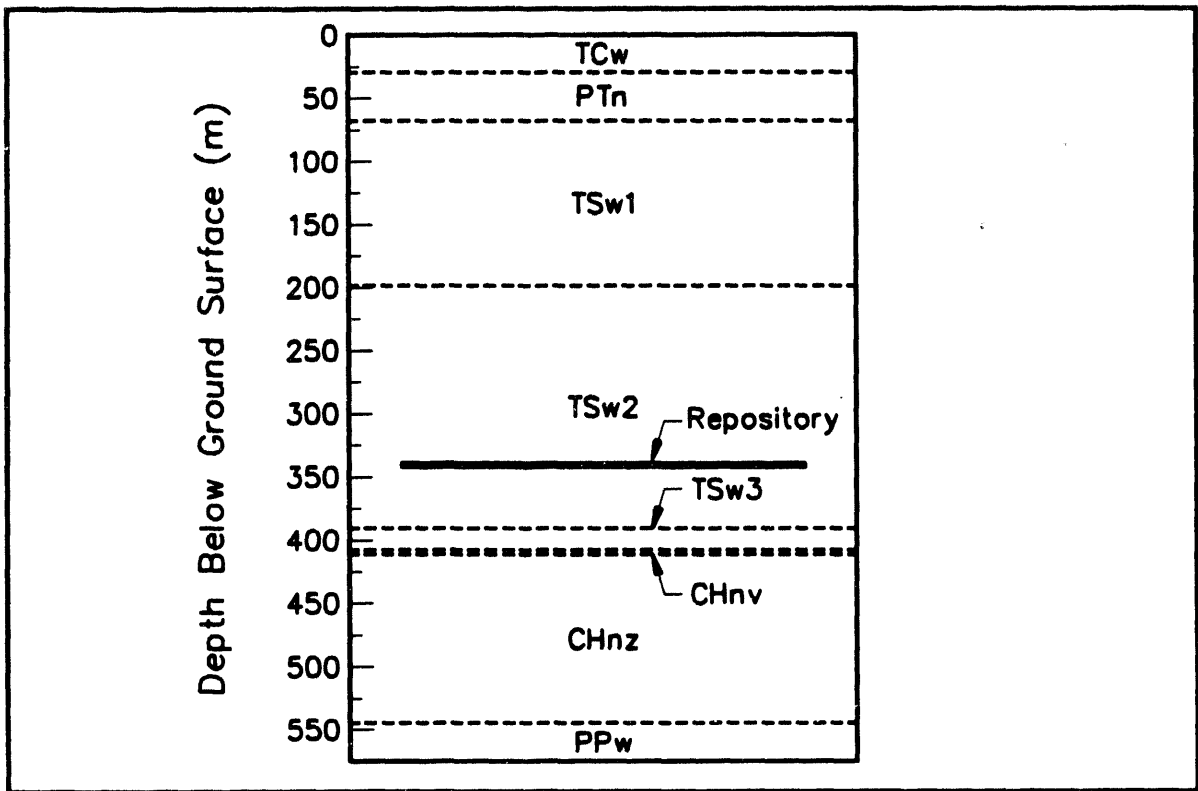


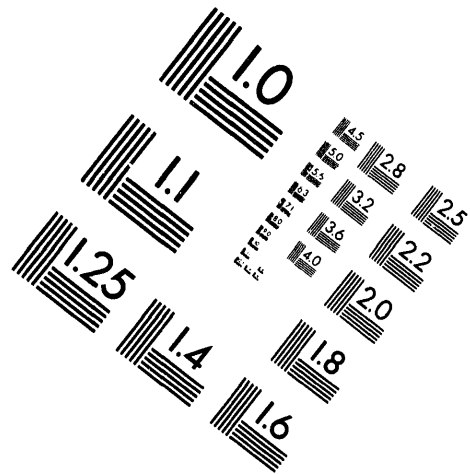
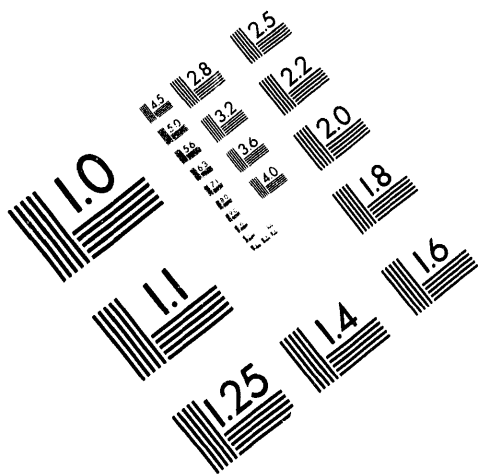
Figure 2-2. Repository Panel Conceptualization (Cross-Section)



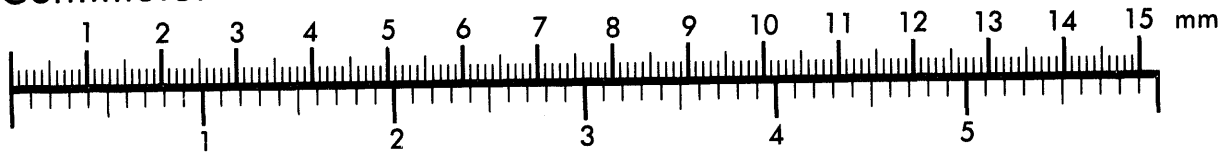
**AIM**

**Association for Information and Image Management**

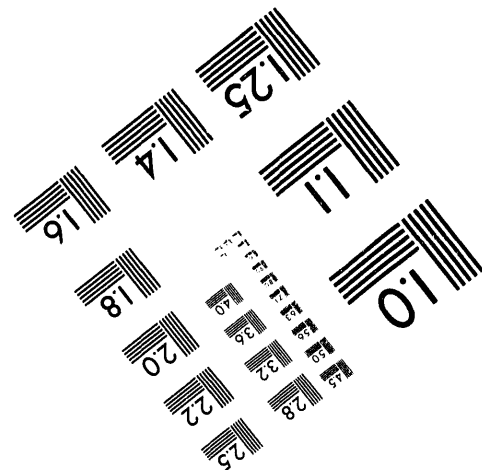
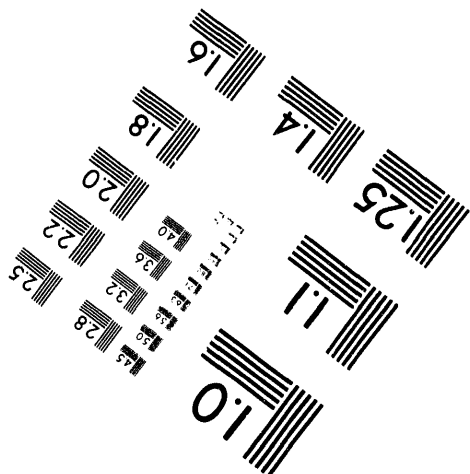
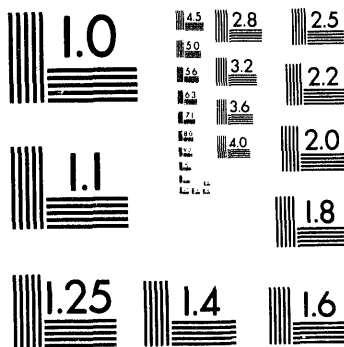
1100 Wayne Avenue, Suite 1100  
Silver Spring, Maryland 20910  
301/587-8202



Centimeter



Inches



MANUFACTURED TO AIM STANDARDS  
BY APPLIED IMAGE, INC.

**2 of 5**

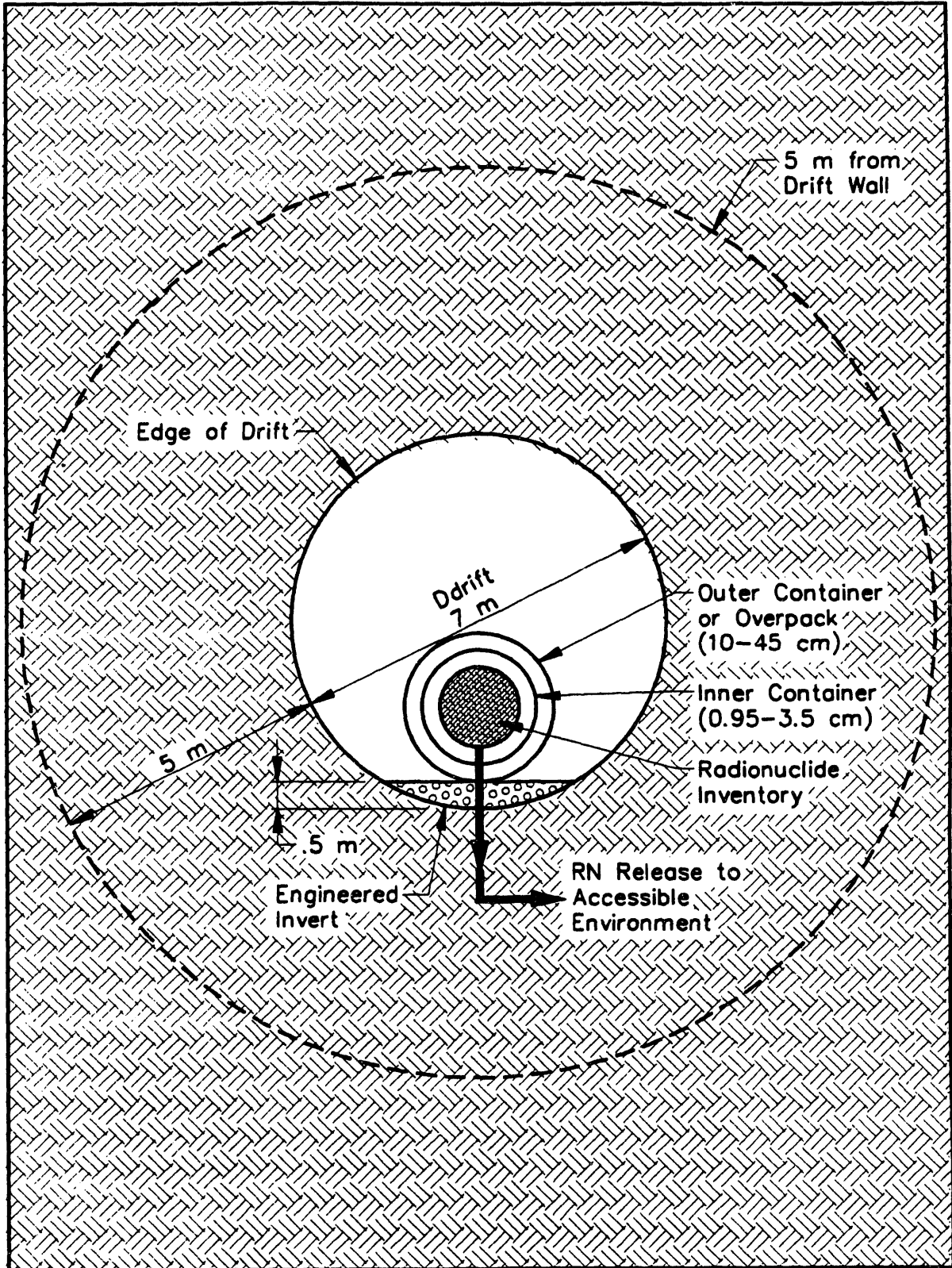


Figure 2-3. Waste Package/Engineered Barrier System Schematic

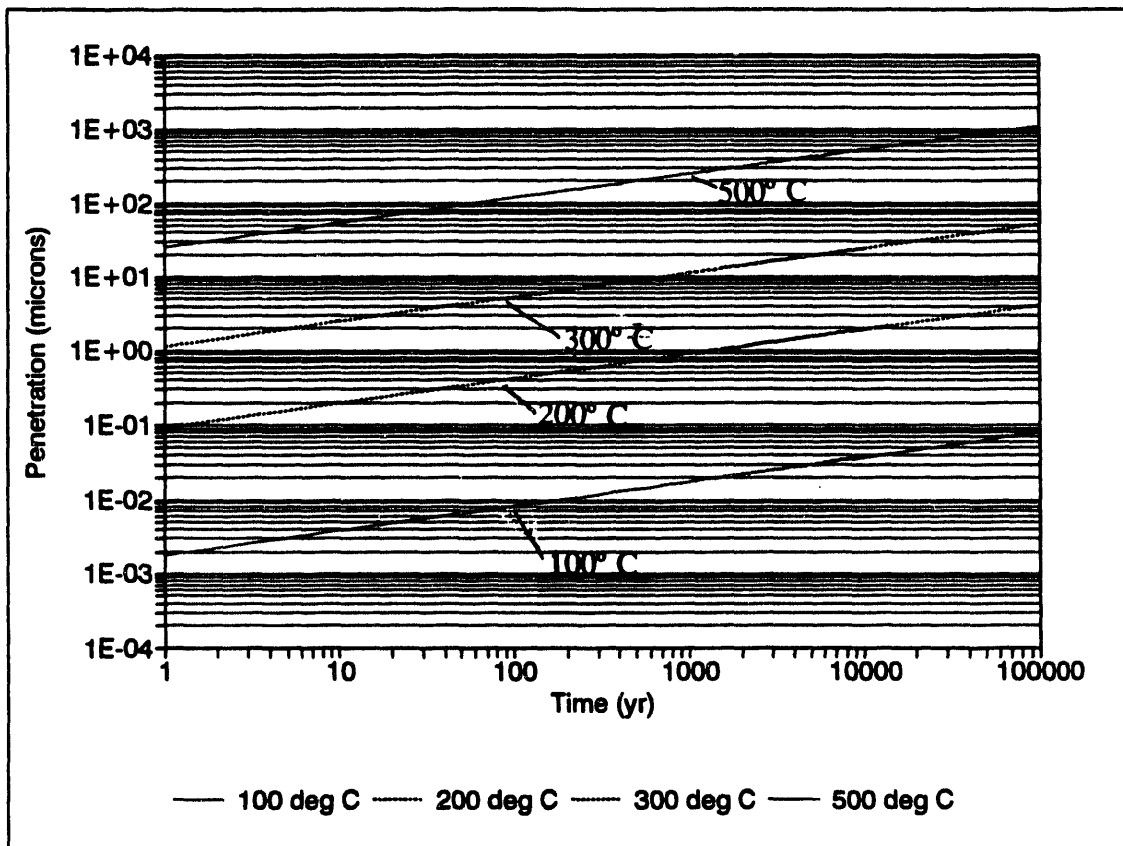


Figure 2-4. Dry Oxidation Penetration Depths (Stahl, 1993)

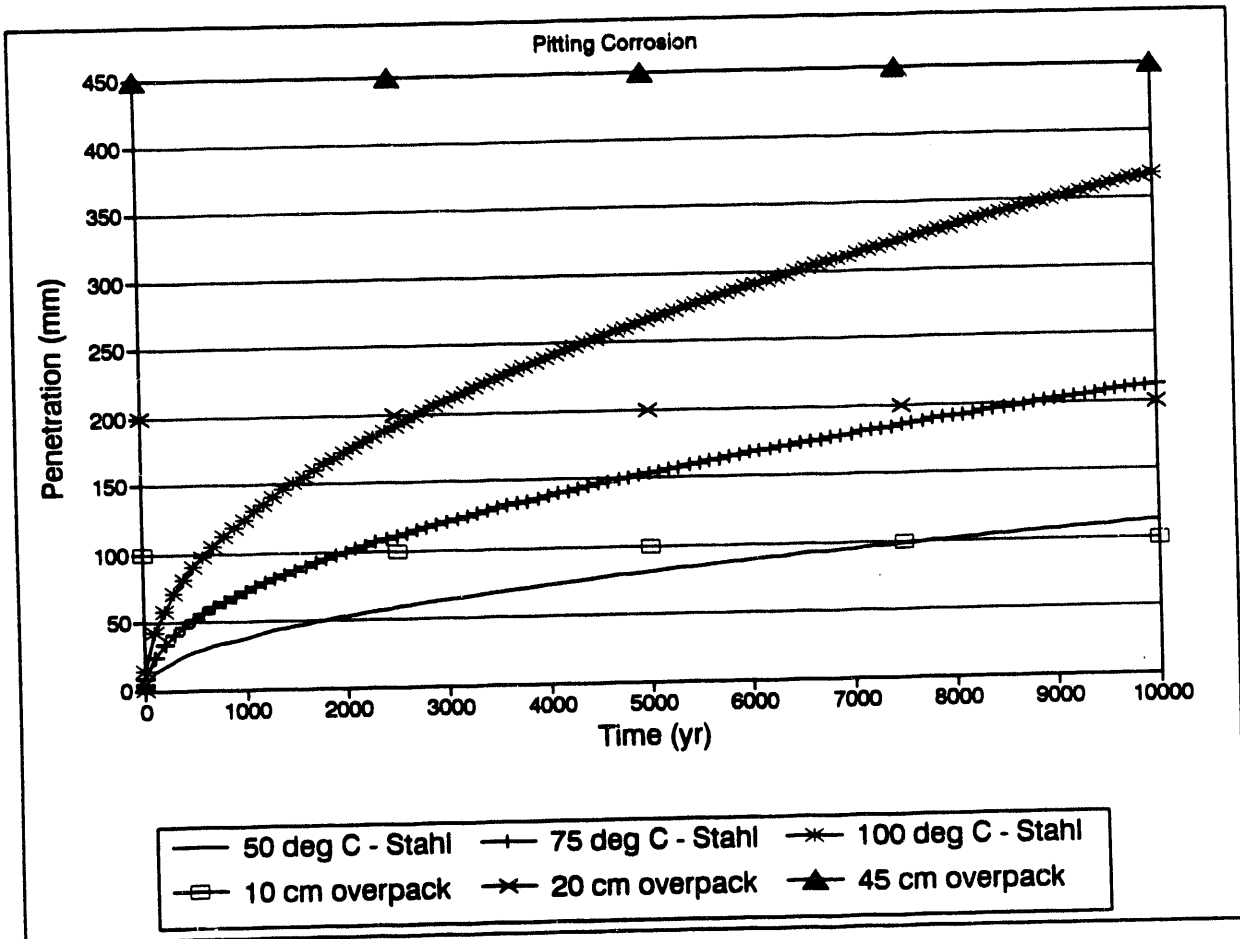


Figure 2-5. Pitting Corrosion Penetration Depths (Stahl, 1993)

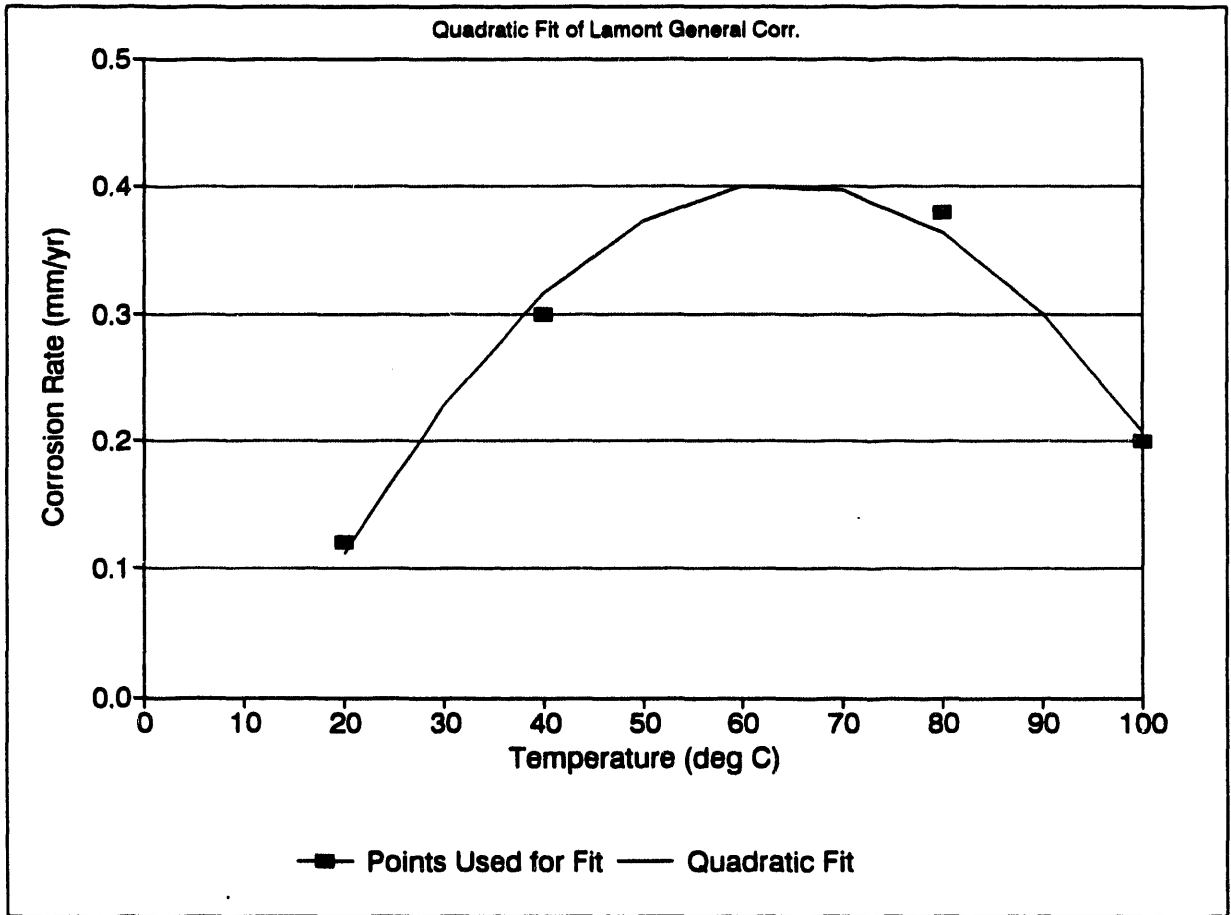
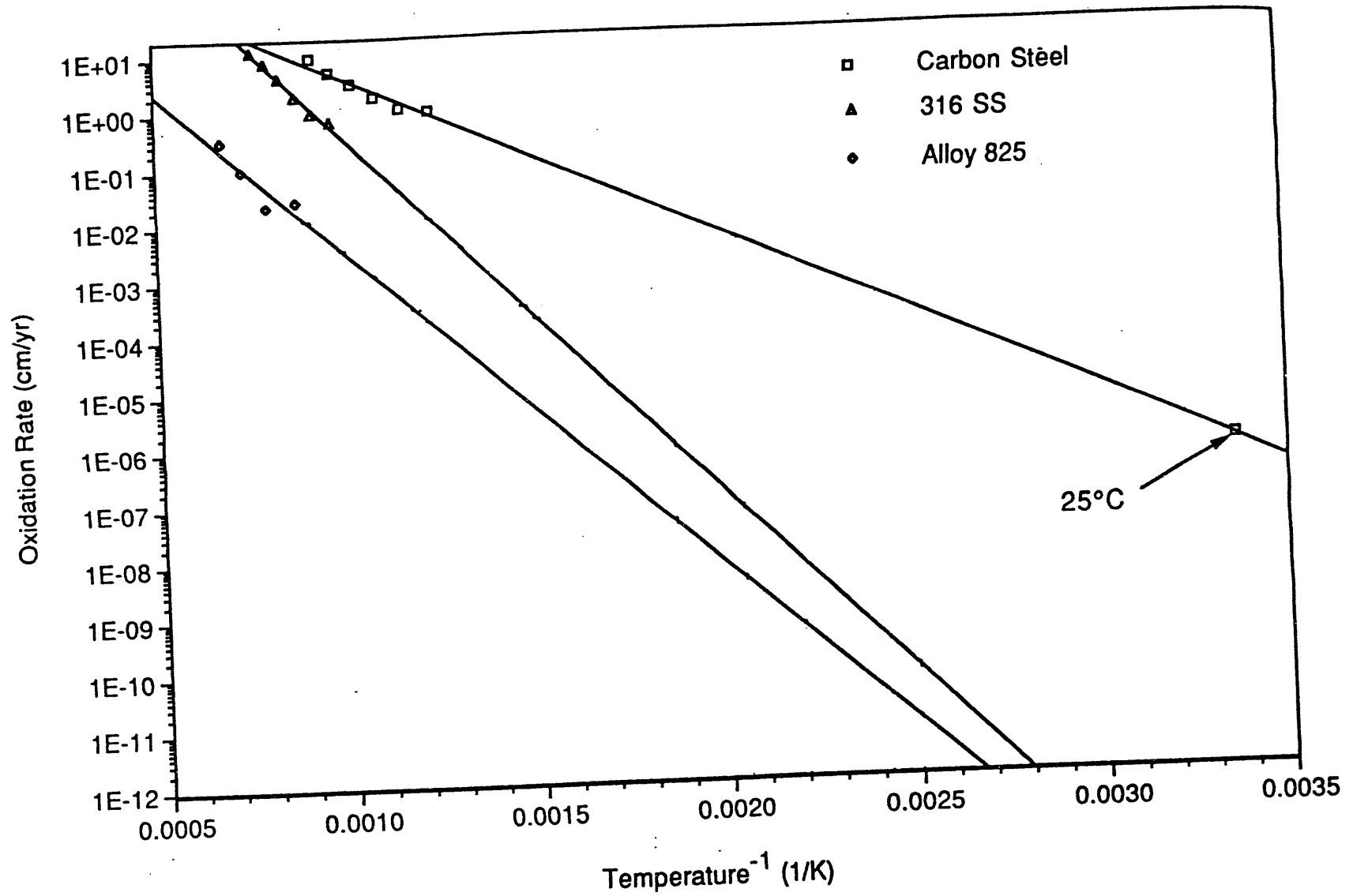


Figure 2-6. Quadratic Fit of Penetration Rates for General Aqueous Corrosion (Lamont, 1993)

# Air Oxidation Rates for Candidate Container Materials



2-68

Figure 2-7. Dry Oxidation Rates (Bullen, 1993)

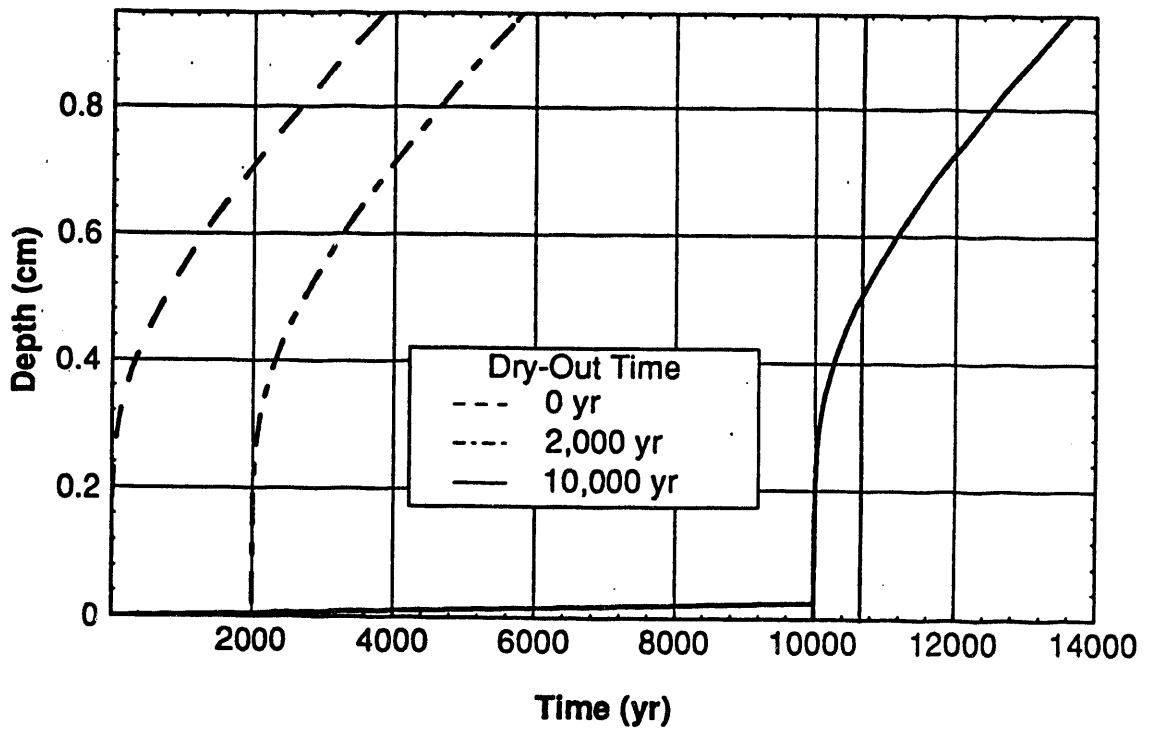


Figure 2-8. Aqueous Corrosion Penetration Rates (Bullen, 1993)

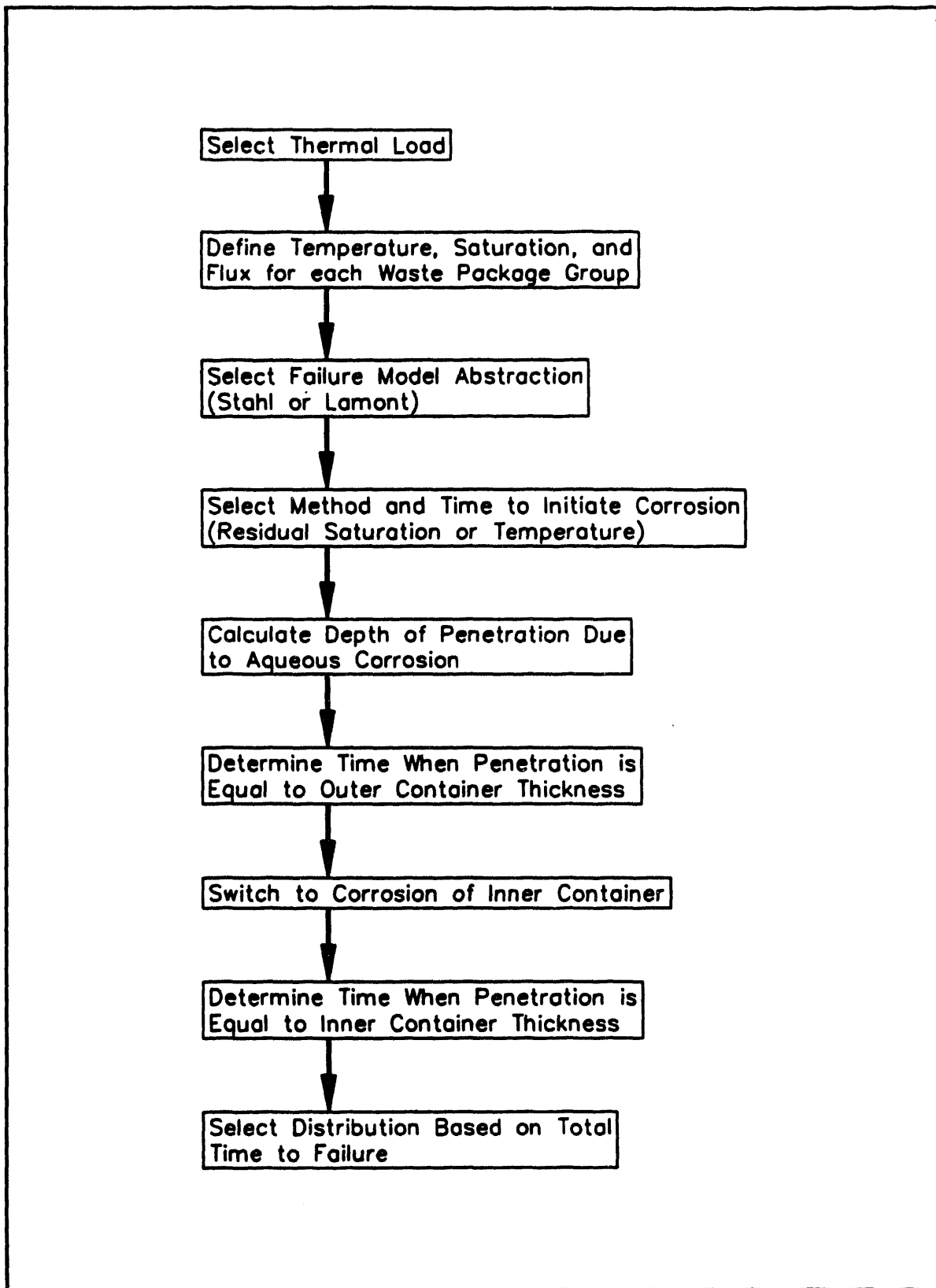


Figure 2-9. Method to Determine Failure Distribution

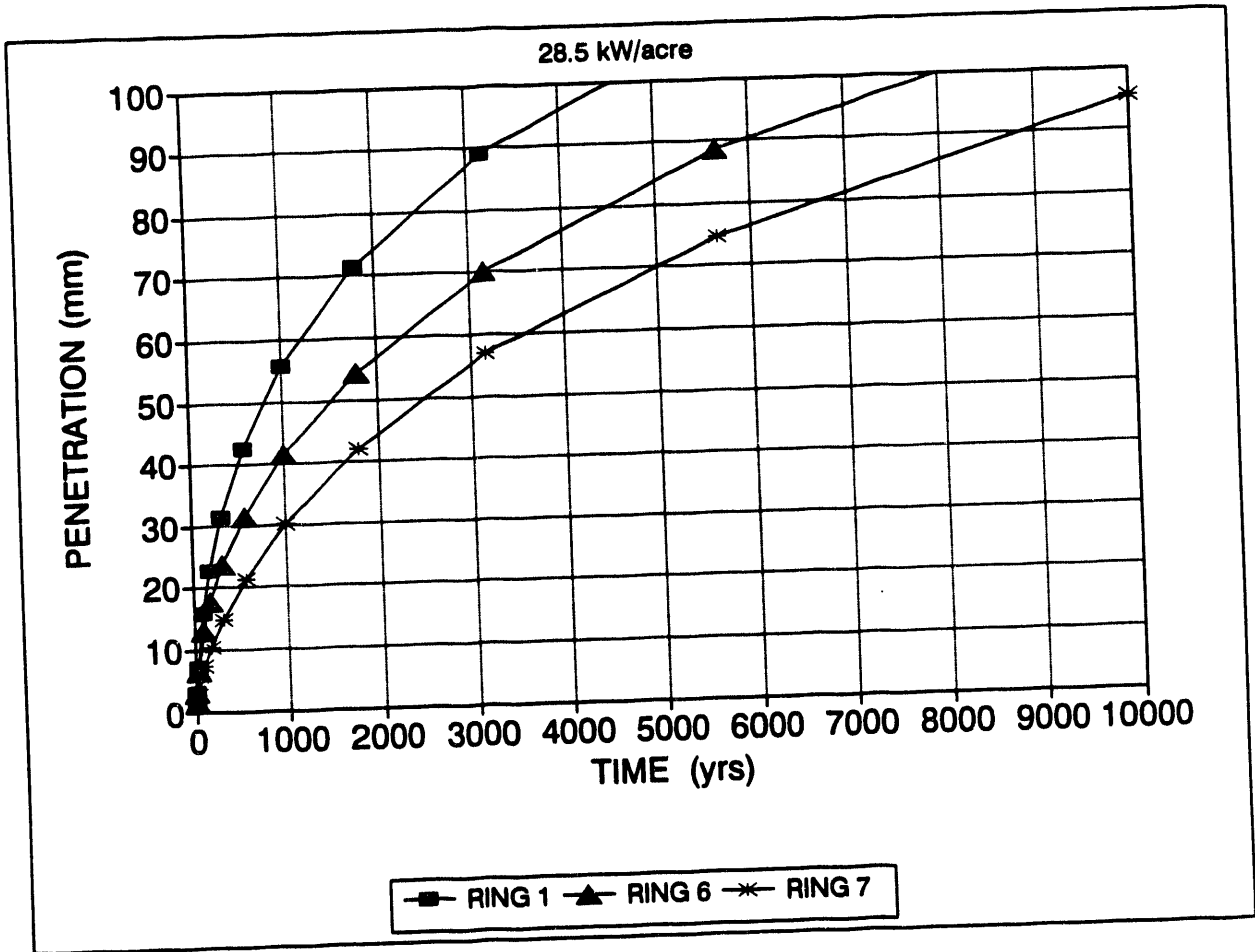


Figure 2-10. Penetration Depth due to Pitting Corrosion Using Stahl Corrosion Model - 28.5 kW/acre

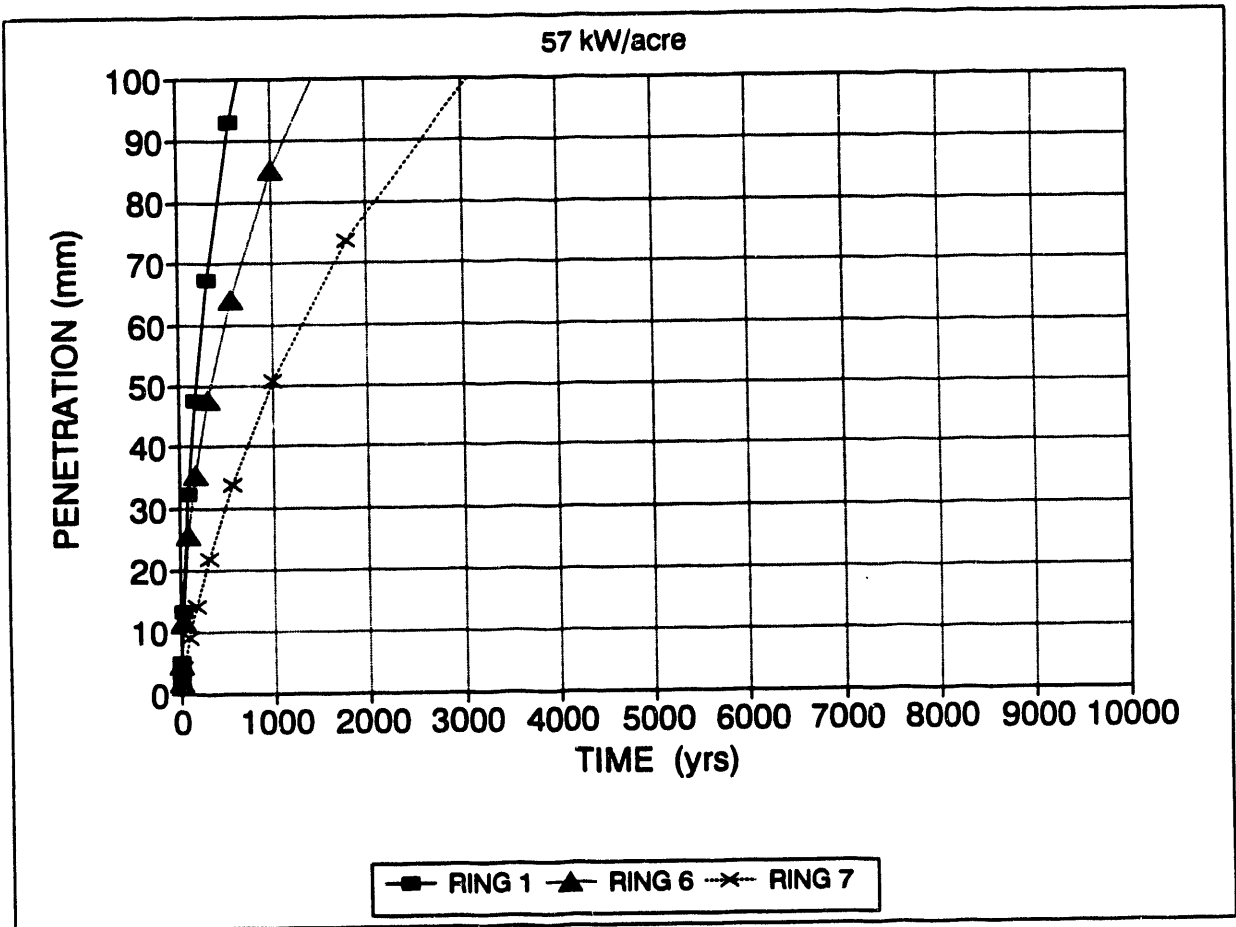


Figure 2-11. Penetration Depth due to Pitting Corrosion Using Stahl Corrosion Model - 57 kW/acre

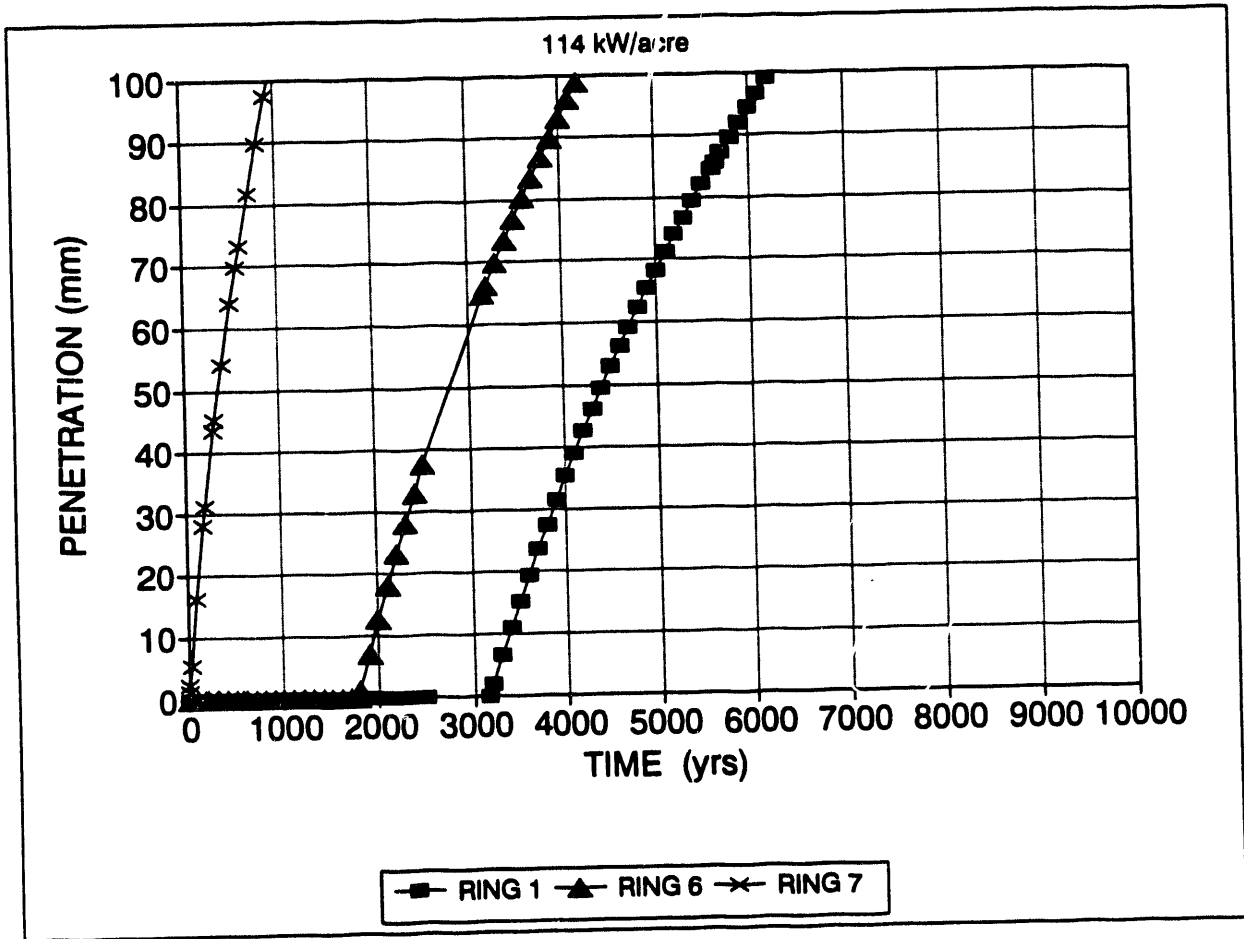


Figure 2-12. Penetration Depth due to Pitting Corrosion Using Stahl Corrosion Model - 114 kW/acre

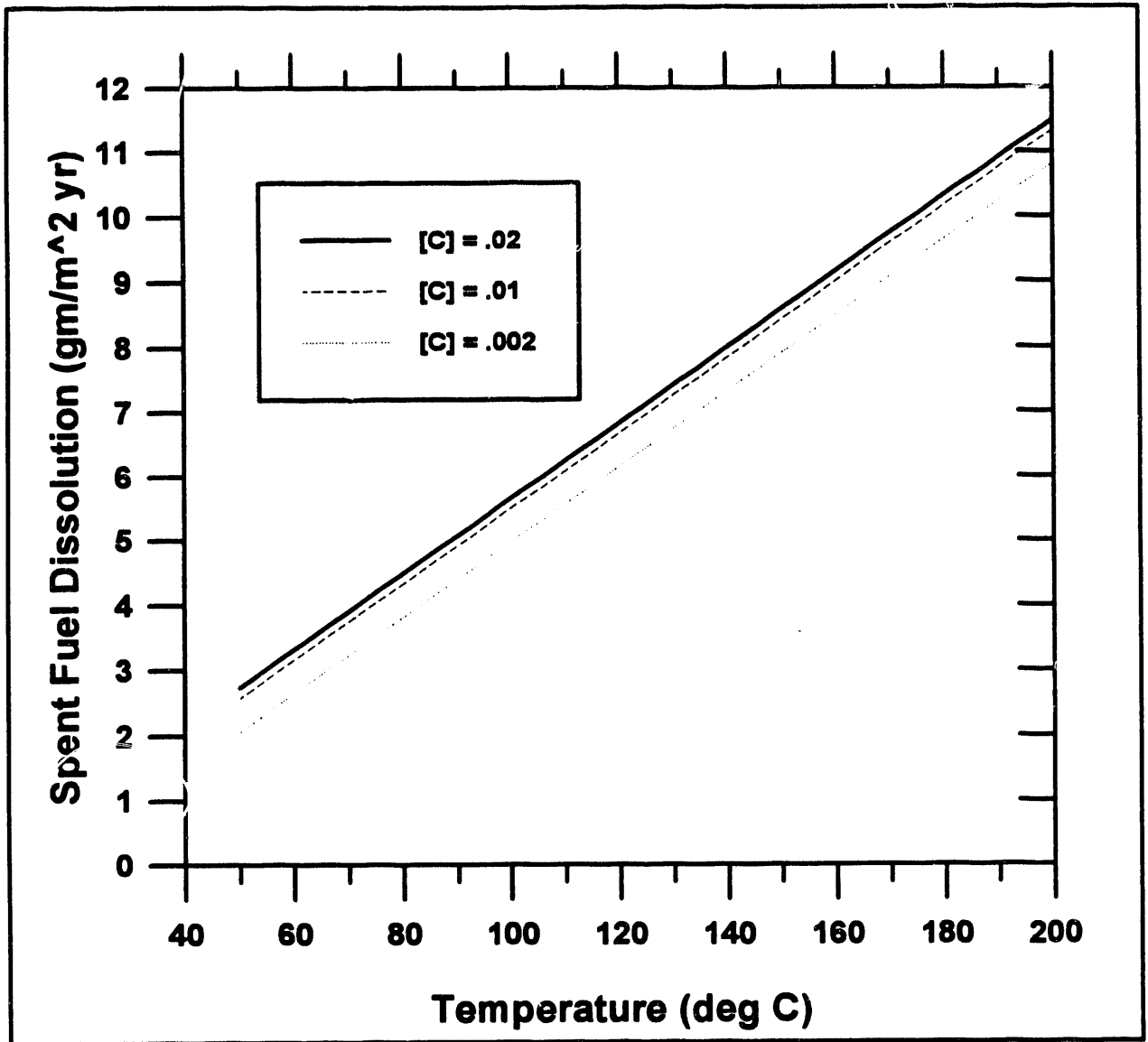


Figure 2-13. Spent Fuel Dissolution as a Function of Temperature and Total Carbonate

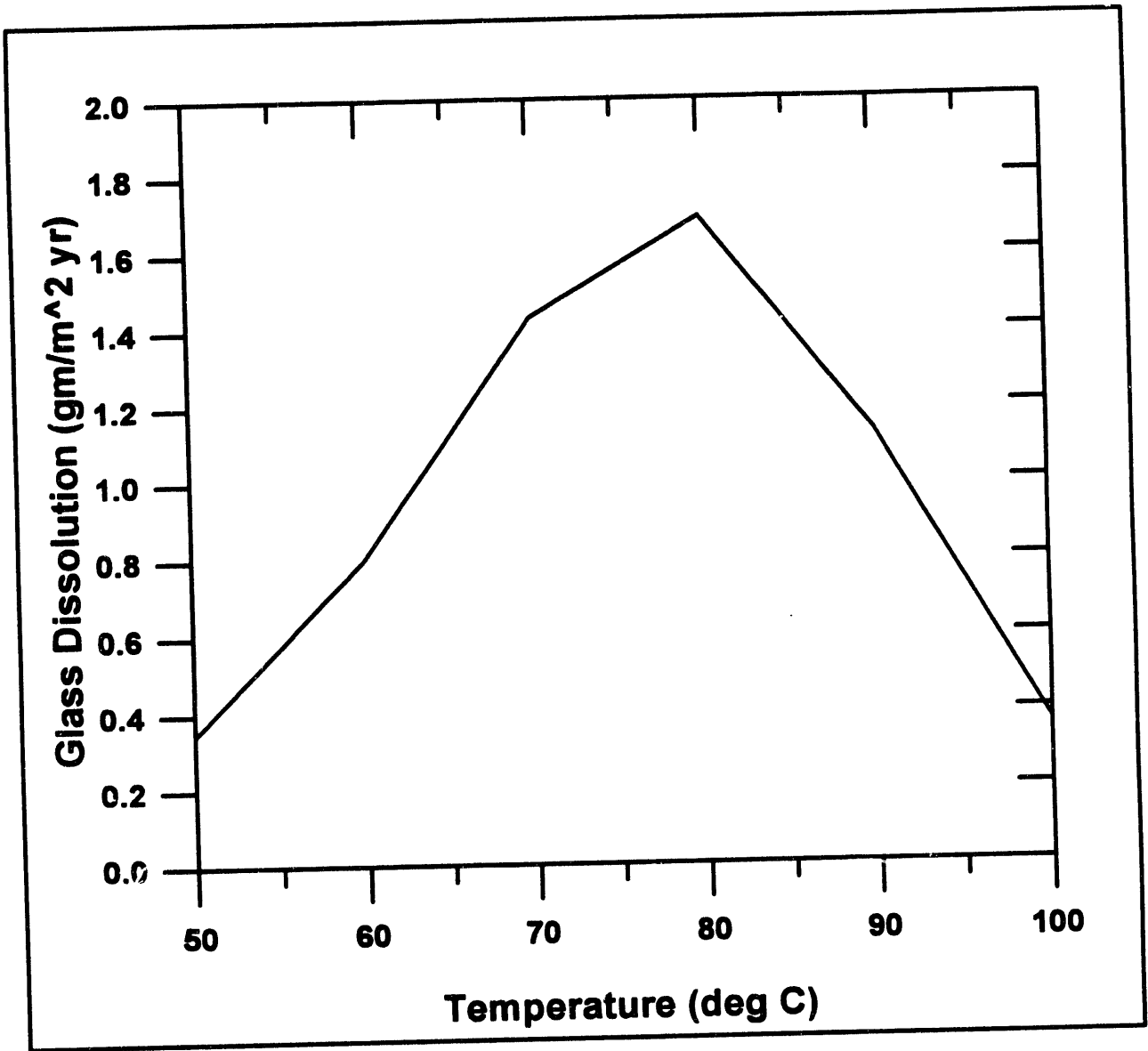


Figure 2-14. Glass Dissolution as a Function of Temperature (pH = 7)

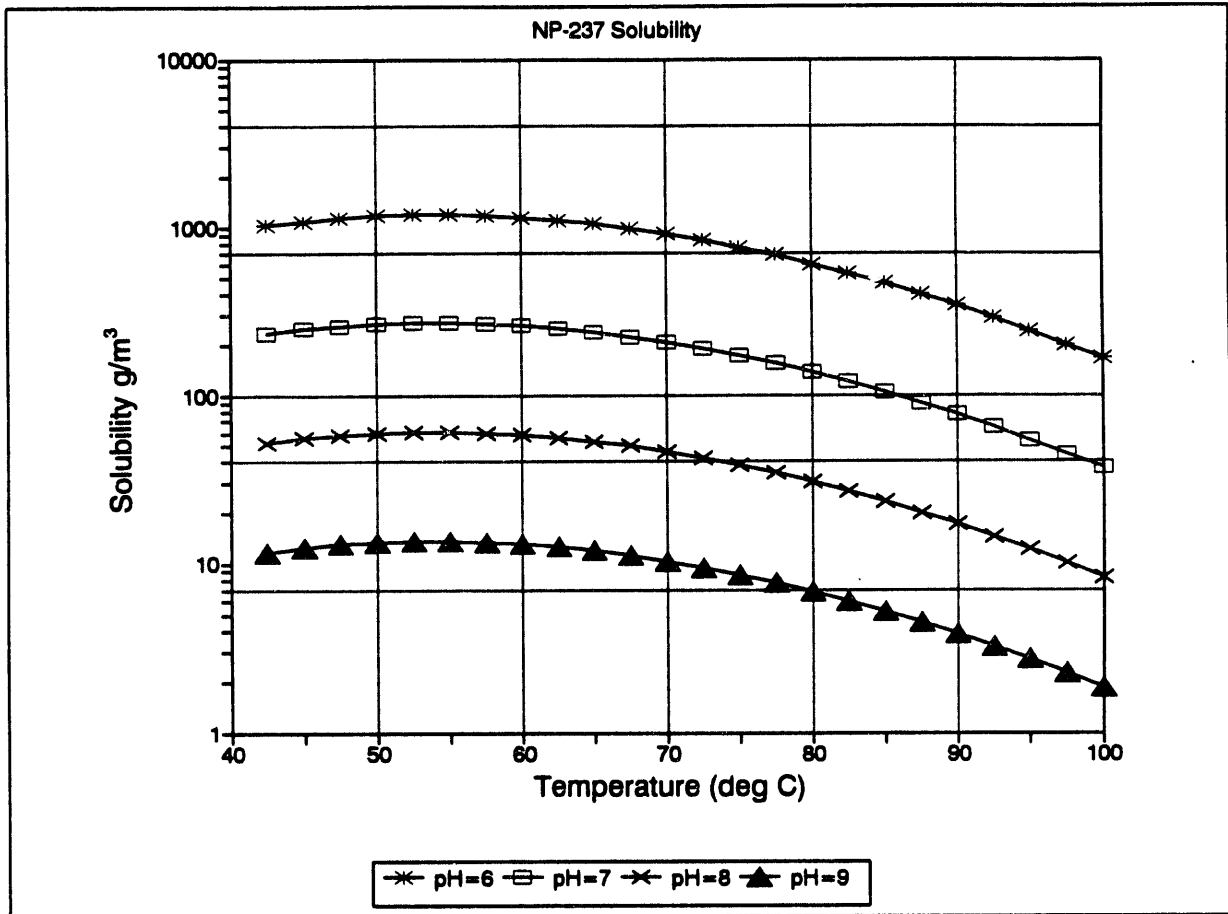


Figure 2-15. Neptunium Solubility as a Function of pH and Temperature

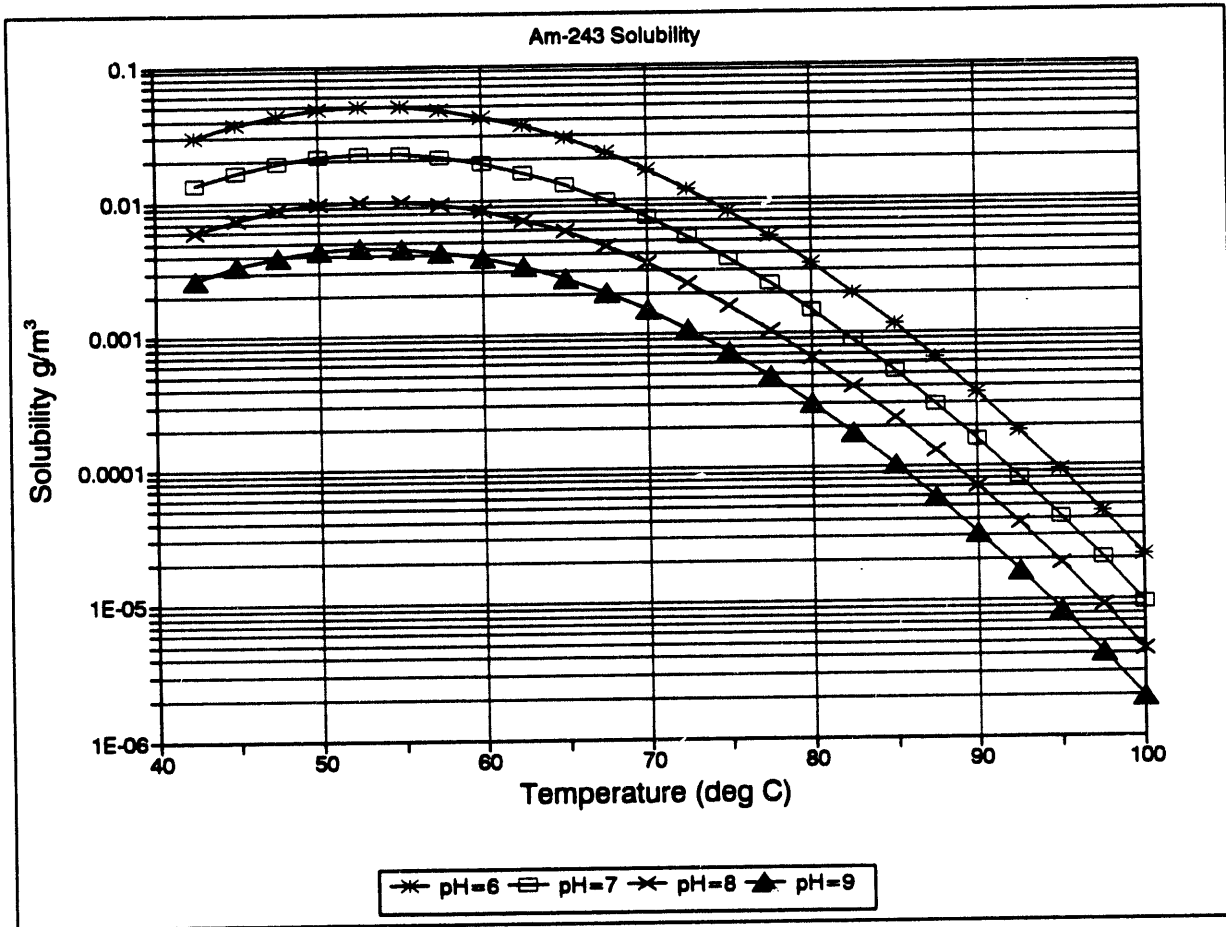


Figure 2-16. Americium Solubility as a Function of pH and Temperature

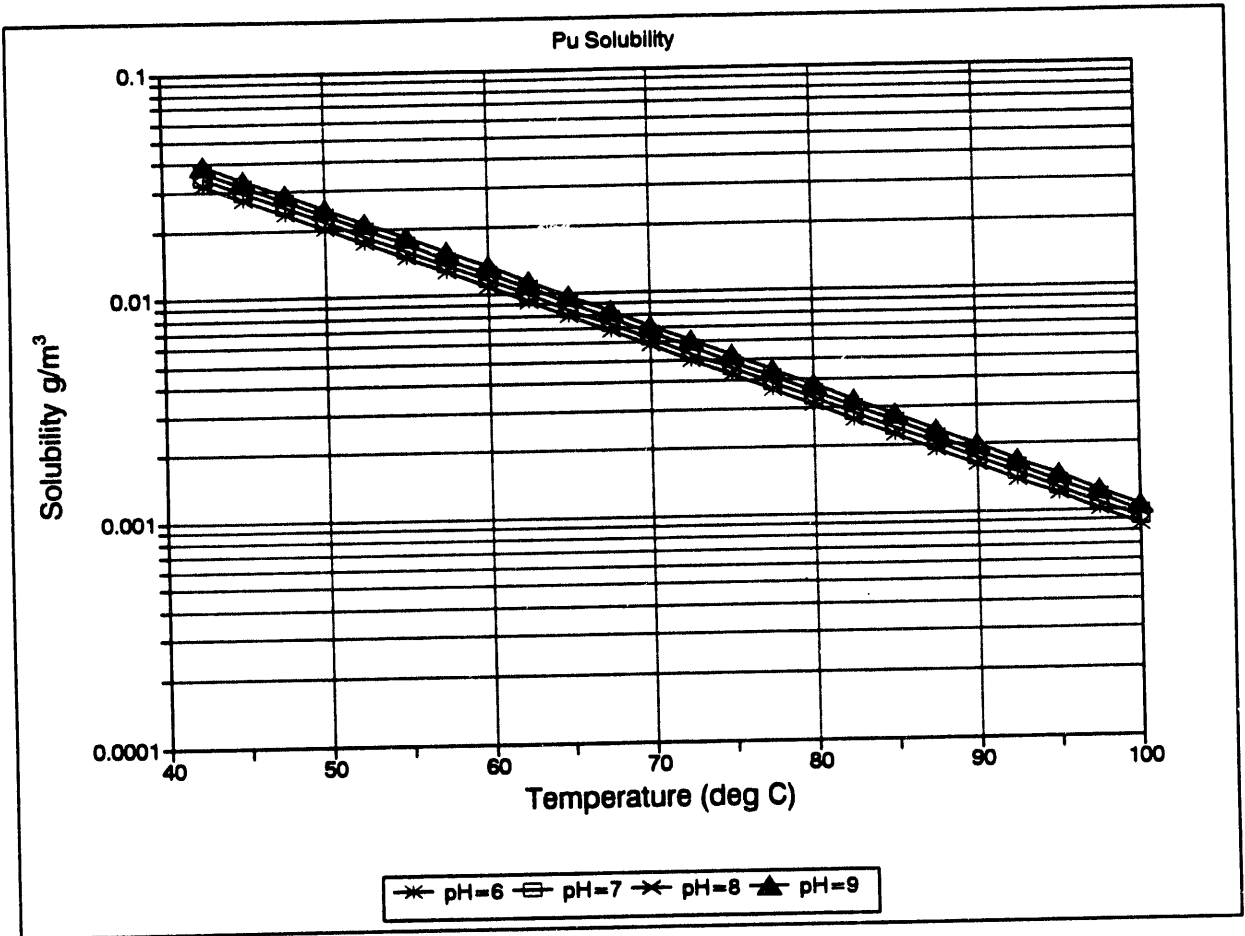


Figure 2-17. Plutonium Solubility as a Function of pH and Temperature

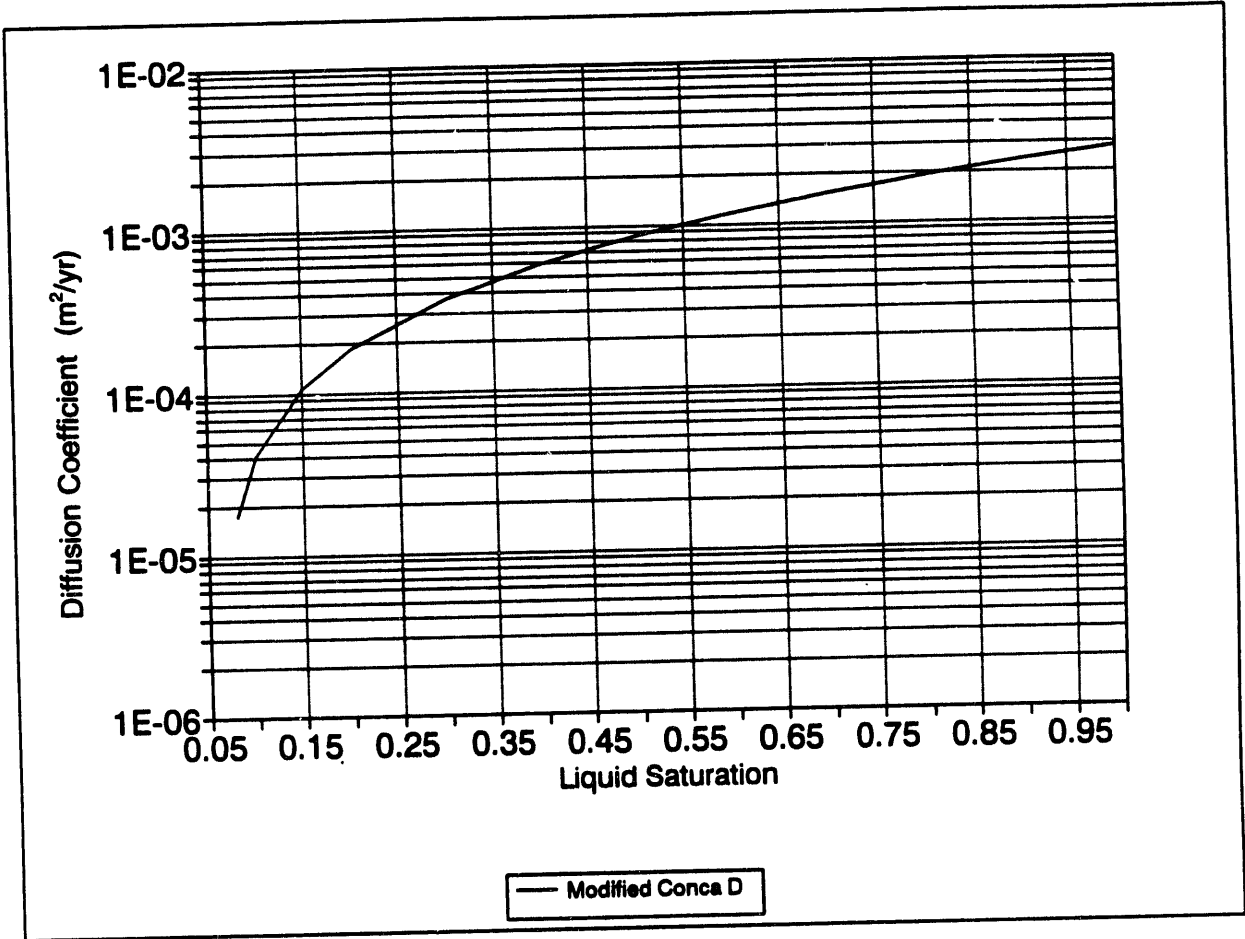


Figure 2-18. Conca Diffusion Coefficient Curve (Conca, 1990)

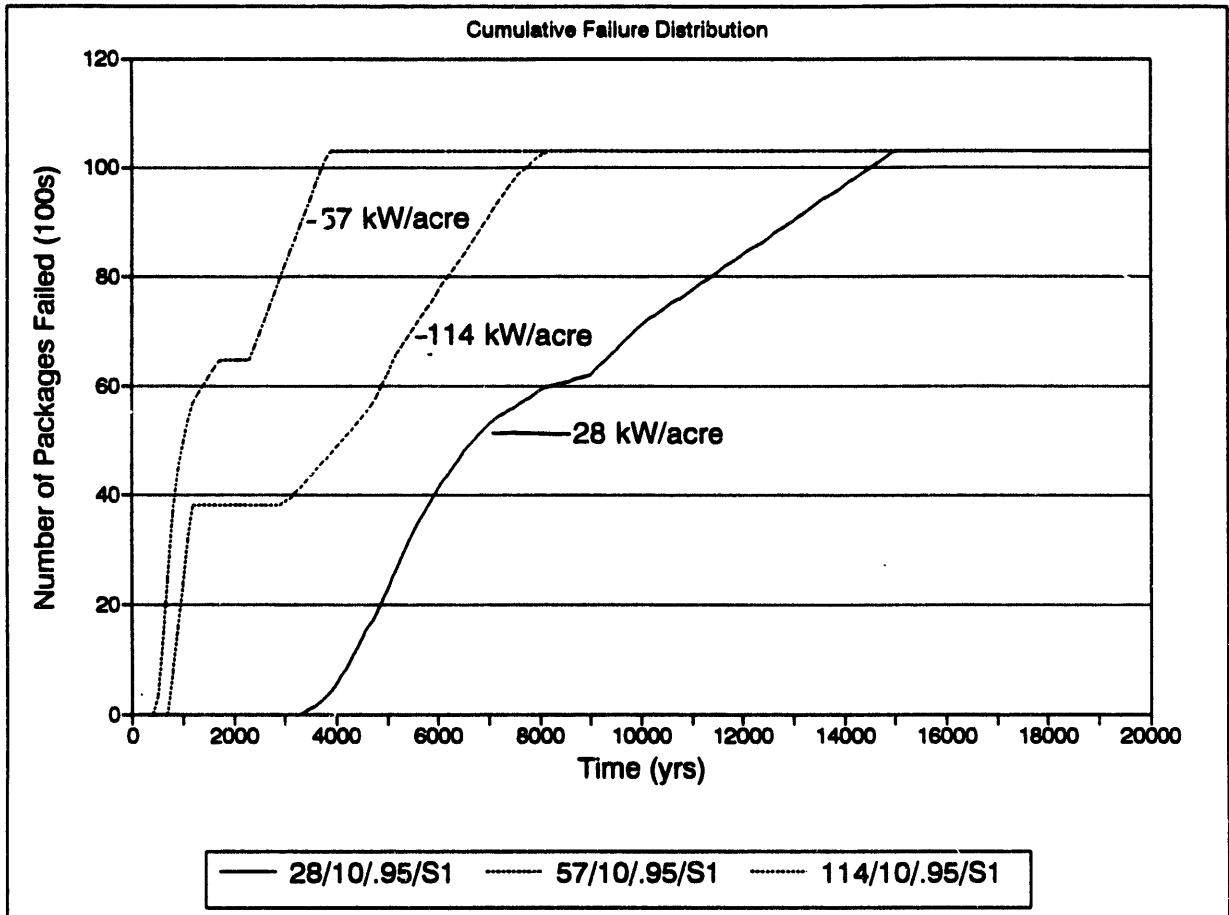


Figure 2-19a. Cumulative Waste Package Failure Distribution - APD Cases

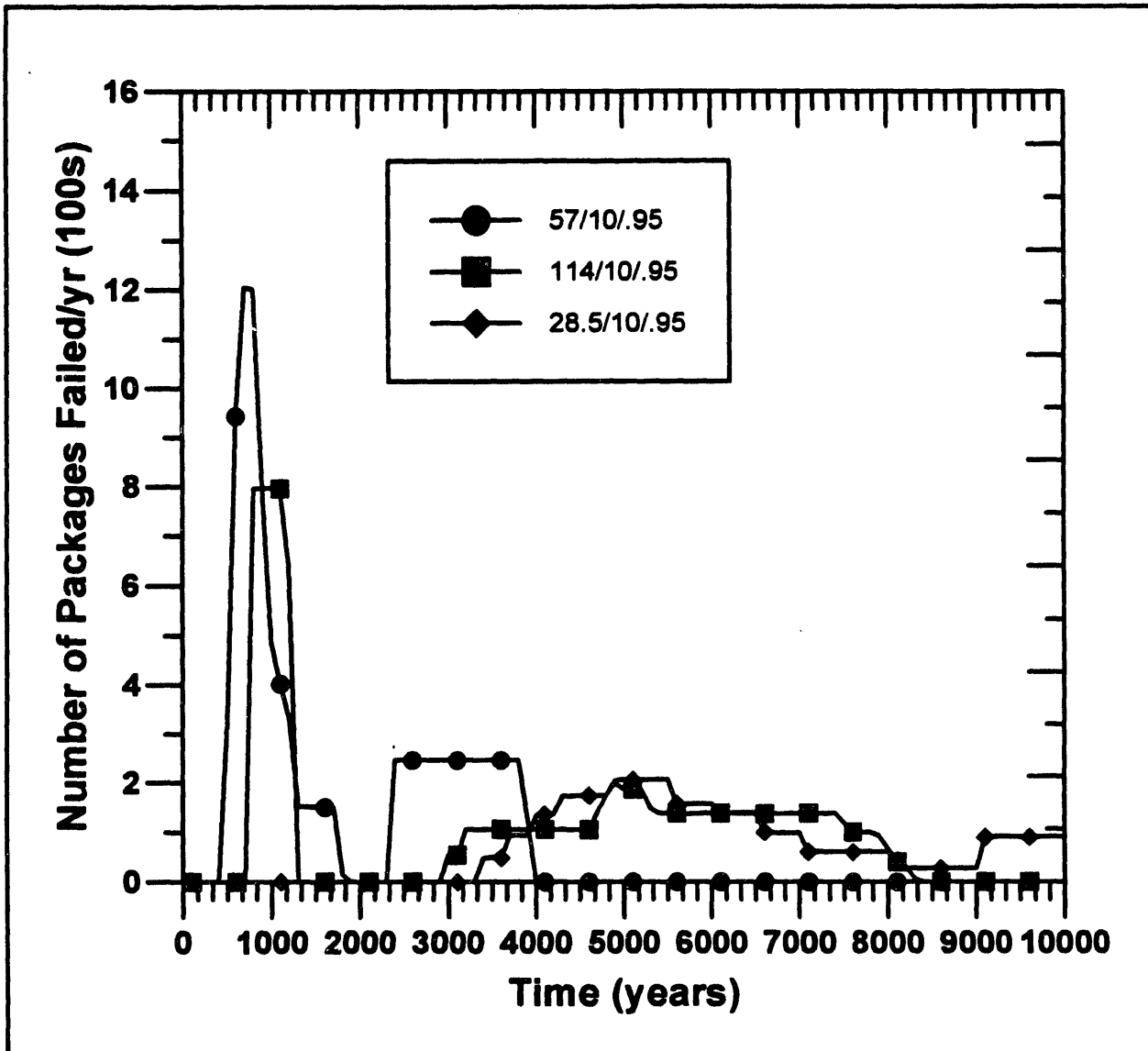


Figure 2-19b. Actual Waste Package Failure Distribution - APD Cases

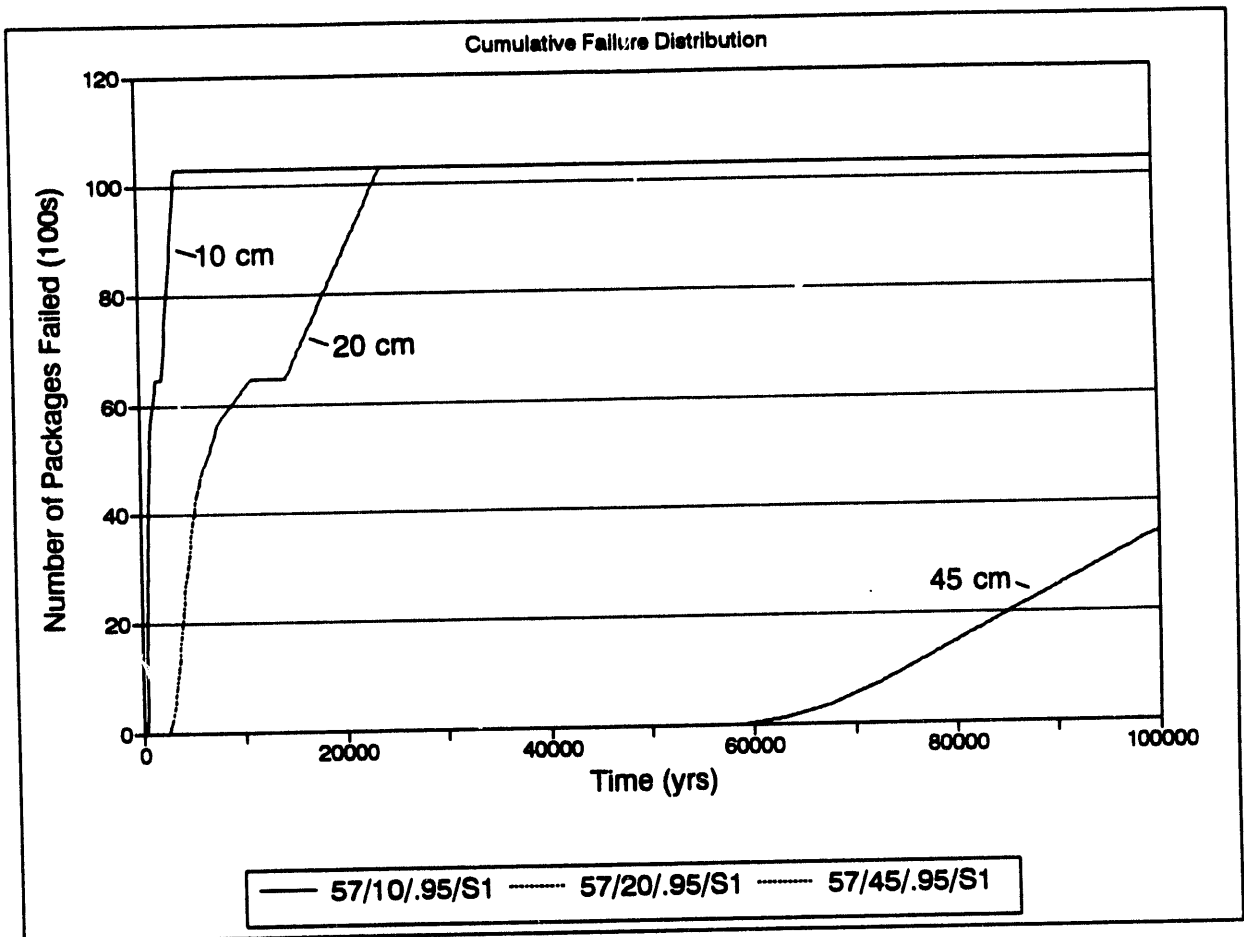


Figure 2-20. Waste Package Failure Distribution - Outer Container Thickness Cases

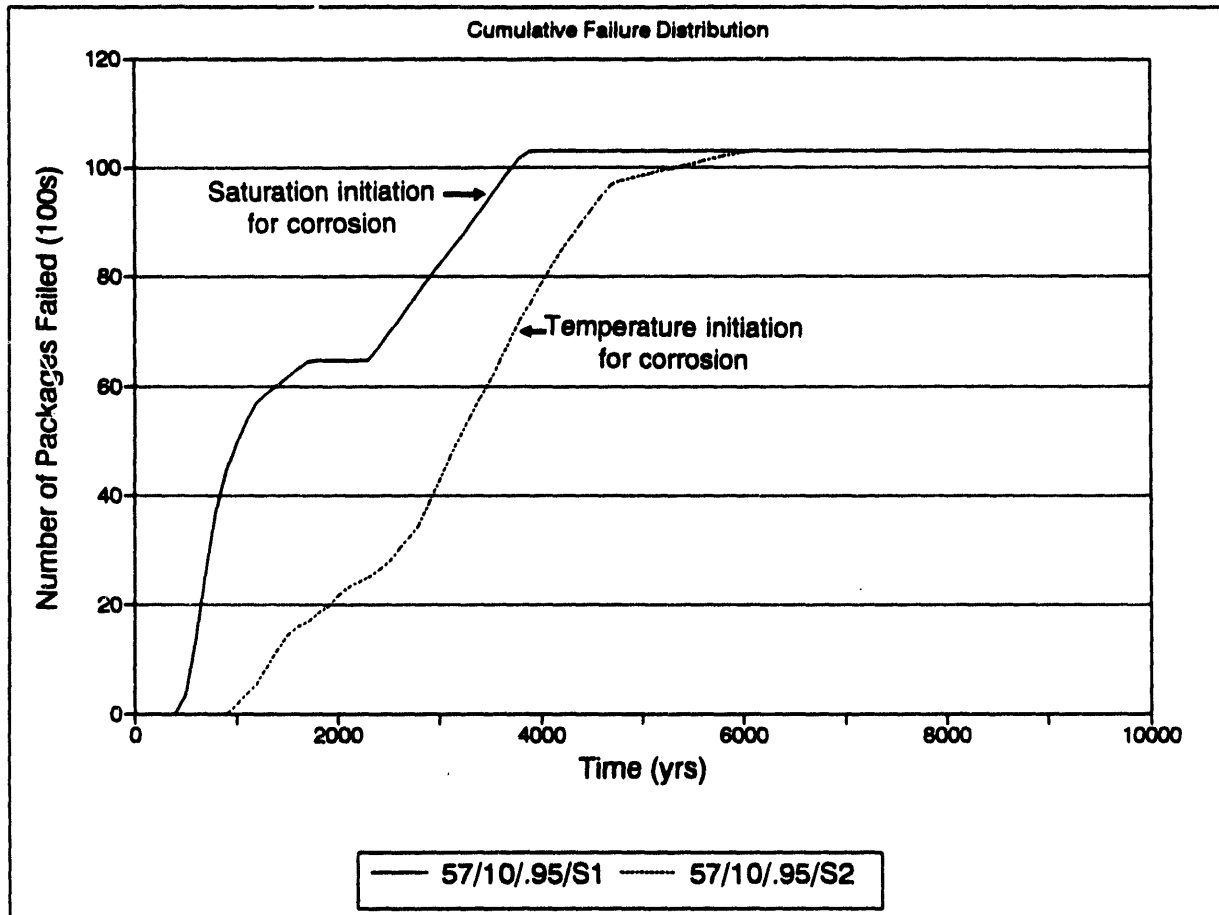


Figure 2-21. Waste Package Failure Distribution - Saturation vs. Temperature Cases - Stahl Model

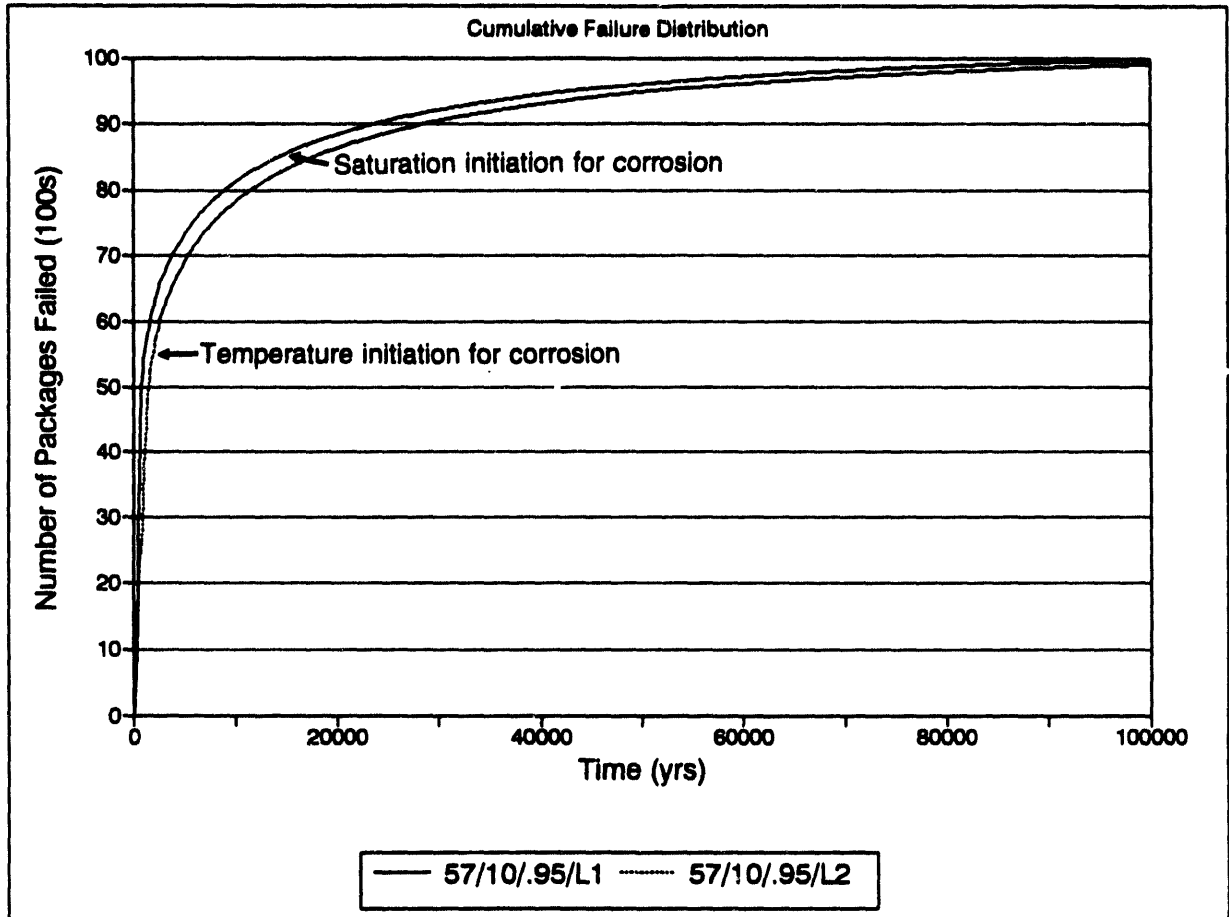


Figure 2-22a. Cumulative Waste Package Failure Distribution - Saturation vs. Temperature Cases - Lamont Model

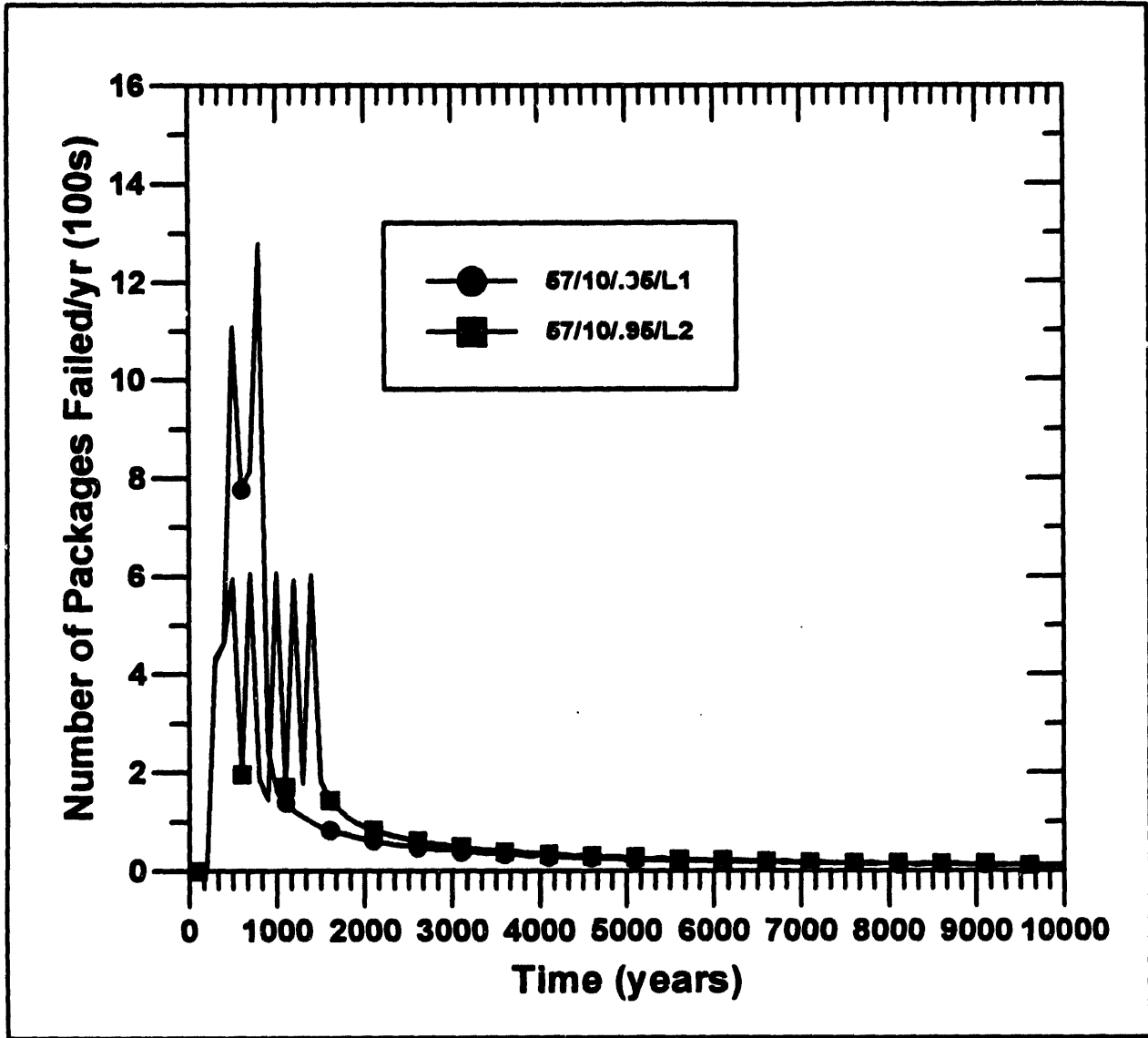


Figure 2-22b. Actual Waste Package Failure Distribution - Saturation vs. Temperature Cases - Lamont Model

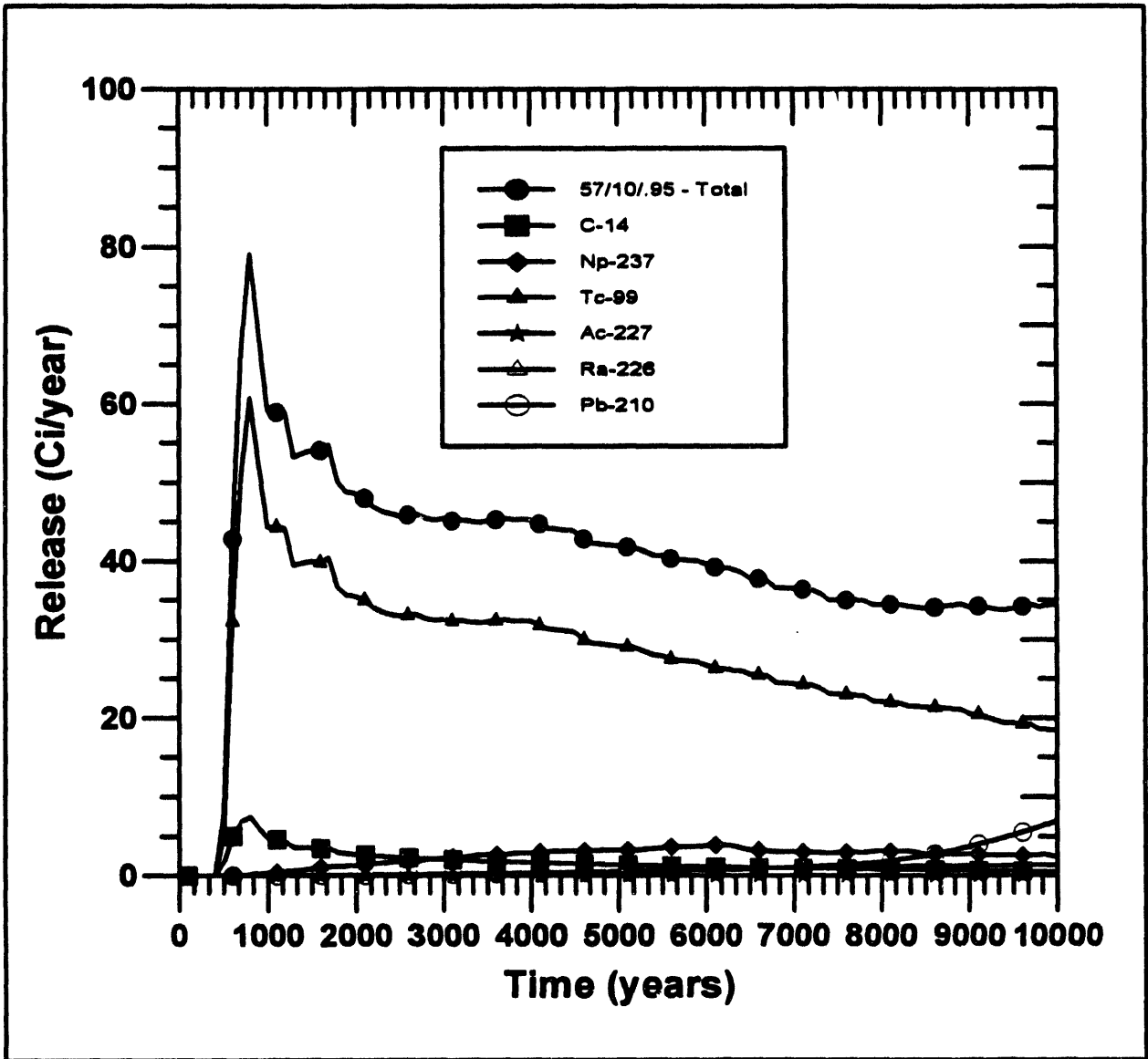


Figure 2-23a. Waste Package Release Rate: Reference Case - Expected Value Case - 10,000 Years

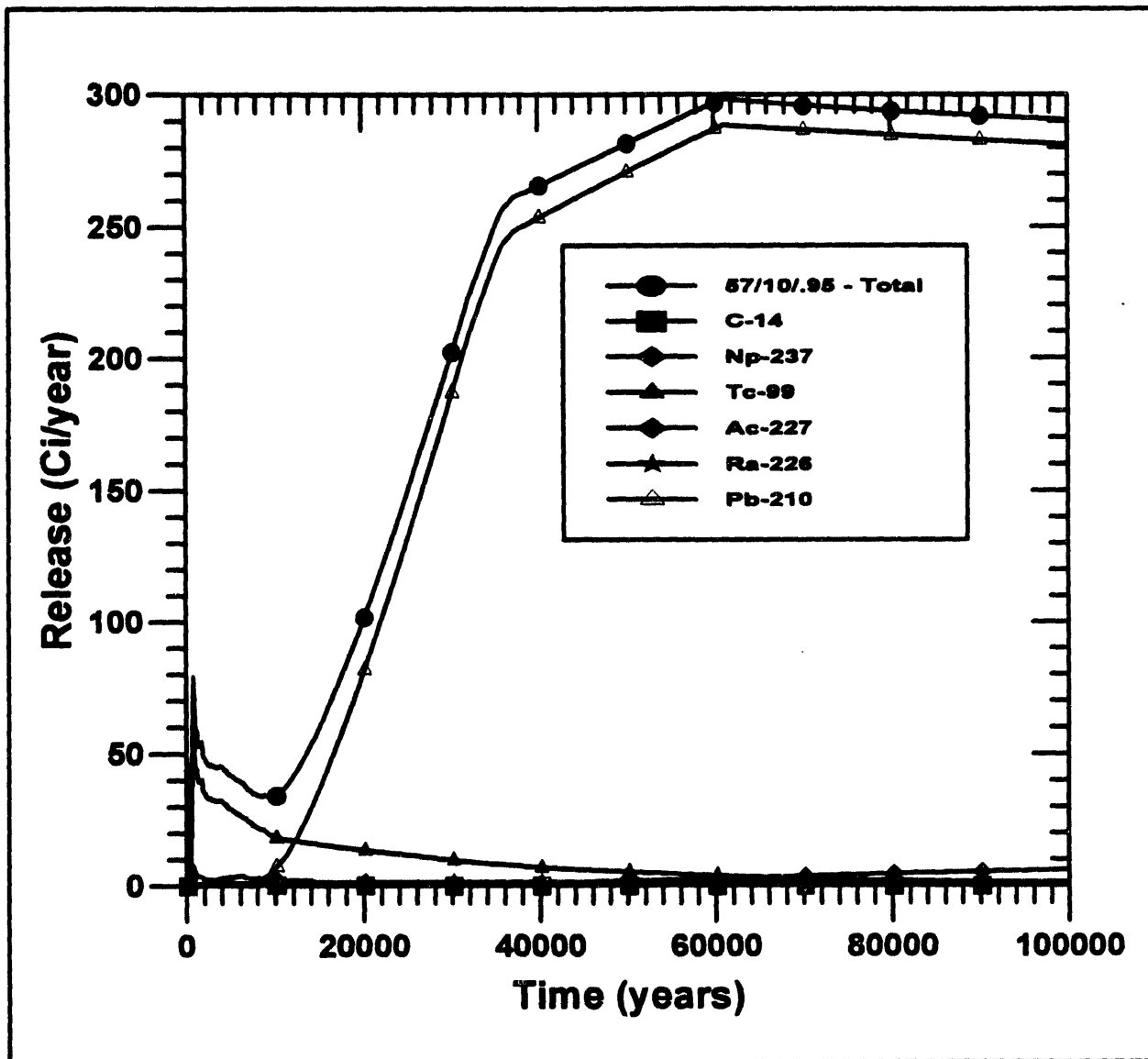


Figure 2-23b. Waste Package Release Rate: Reference Case - Expected Value Case - 100,000 Years

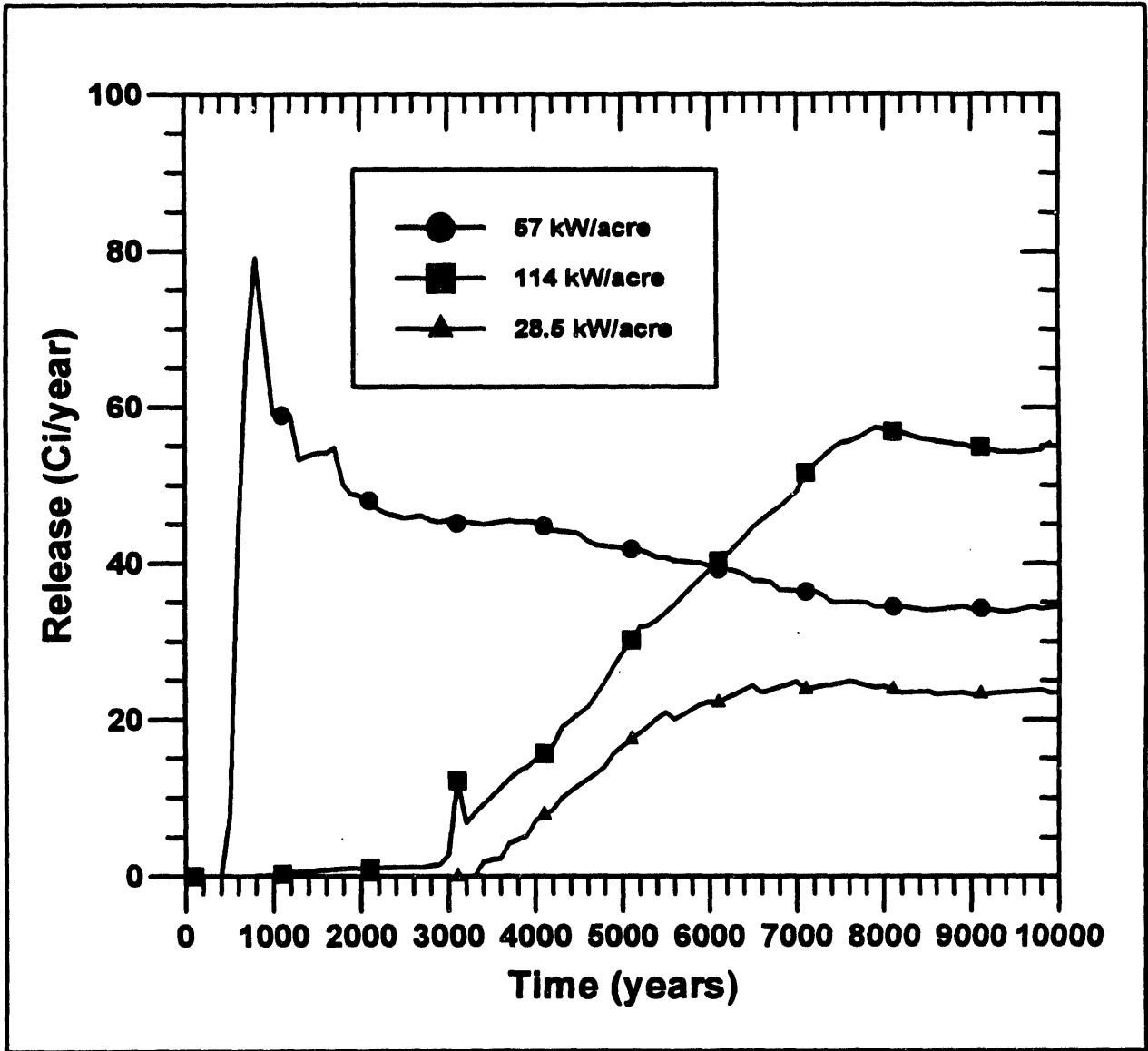


Figure 2-24a. Waste Package Release Rate: Thermal Loading Cases - 10,000 Years

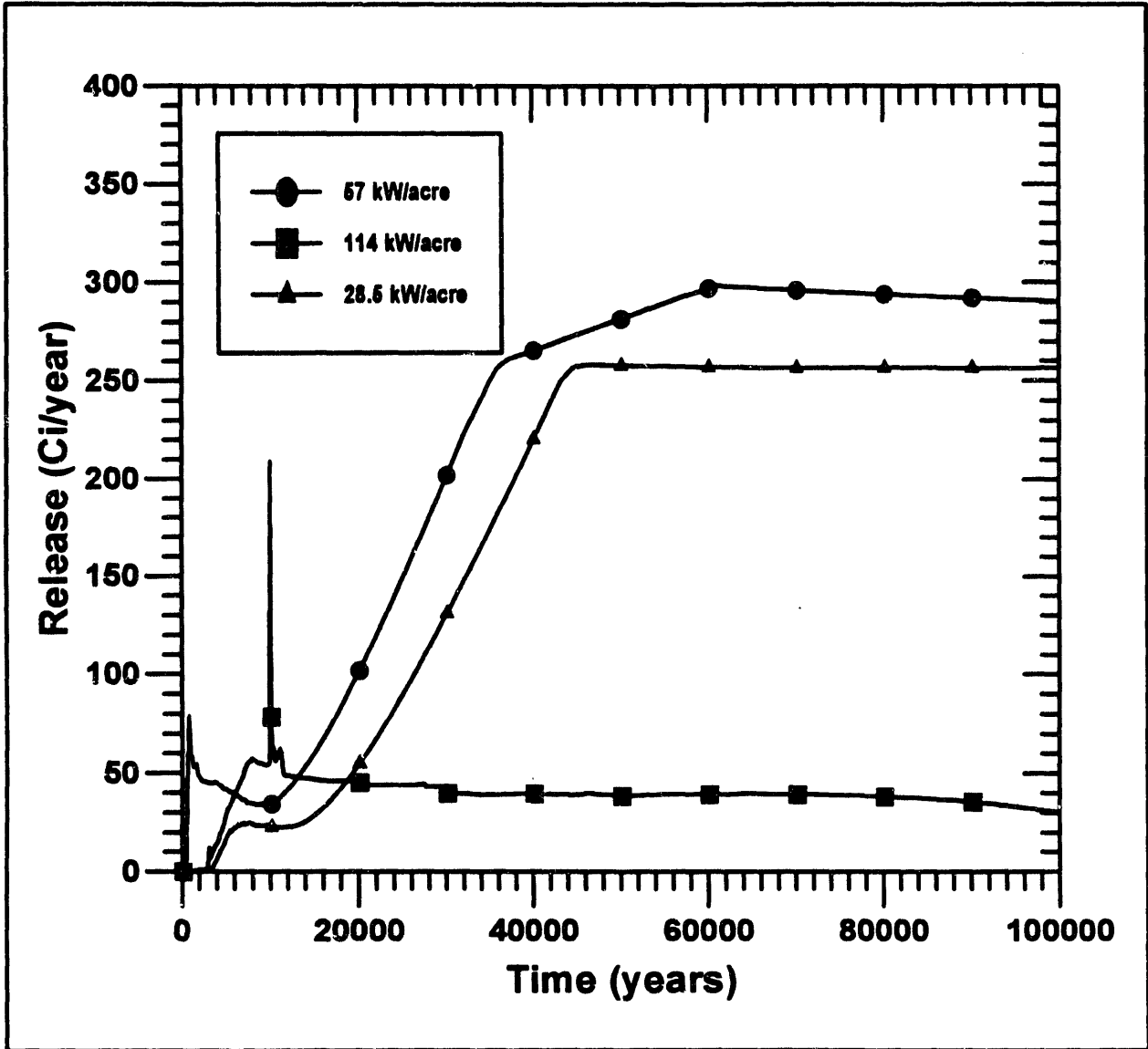


Figure 2-24b. Waste Package Release Rate: Thermal Loading Cases - 100,000 Years

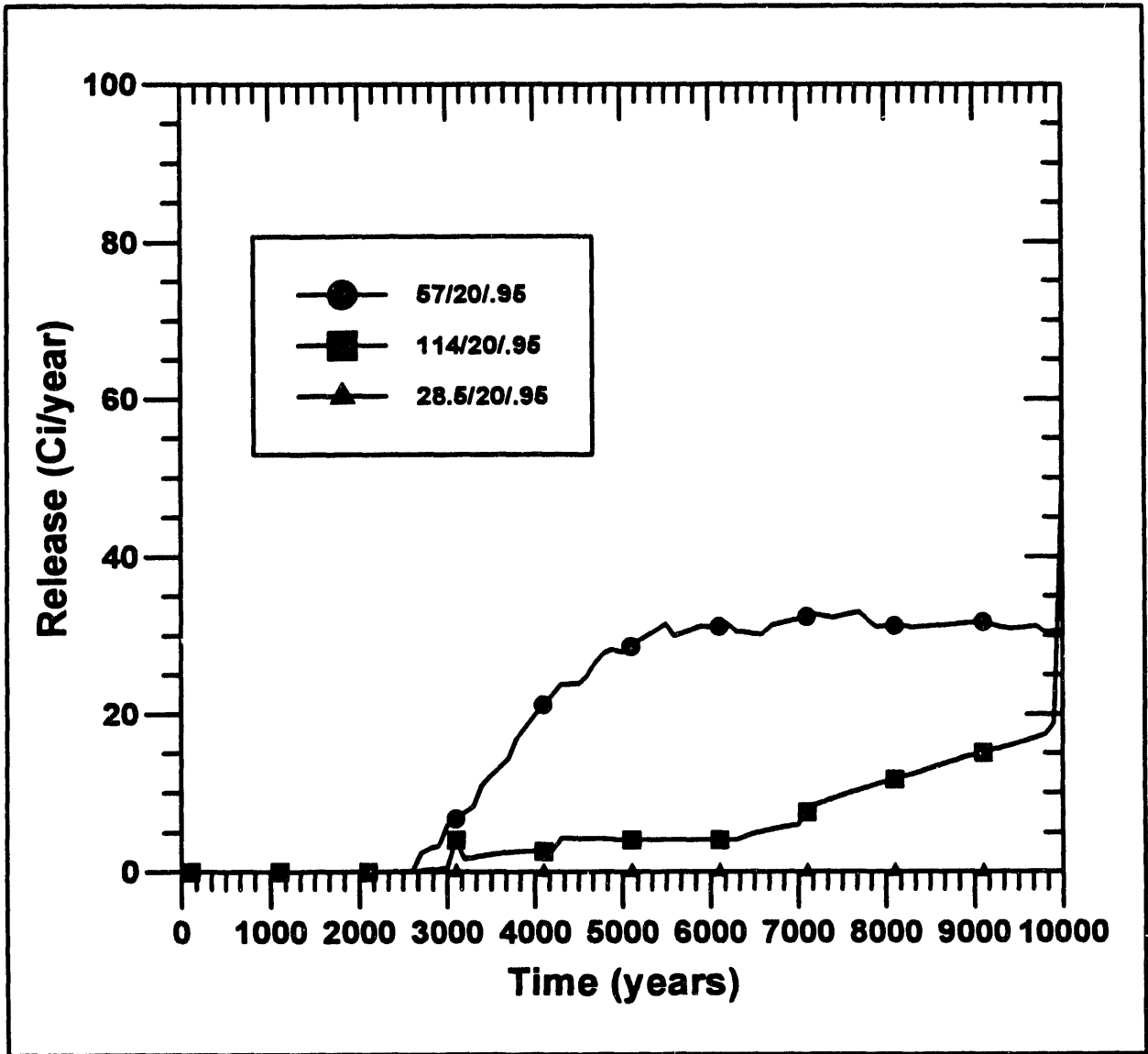


Figure 2-25a. Waste Package Release Rate: Thermal Loading Cases - 20 cm overpack - 10,000 Years

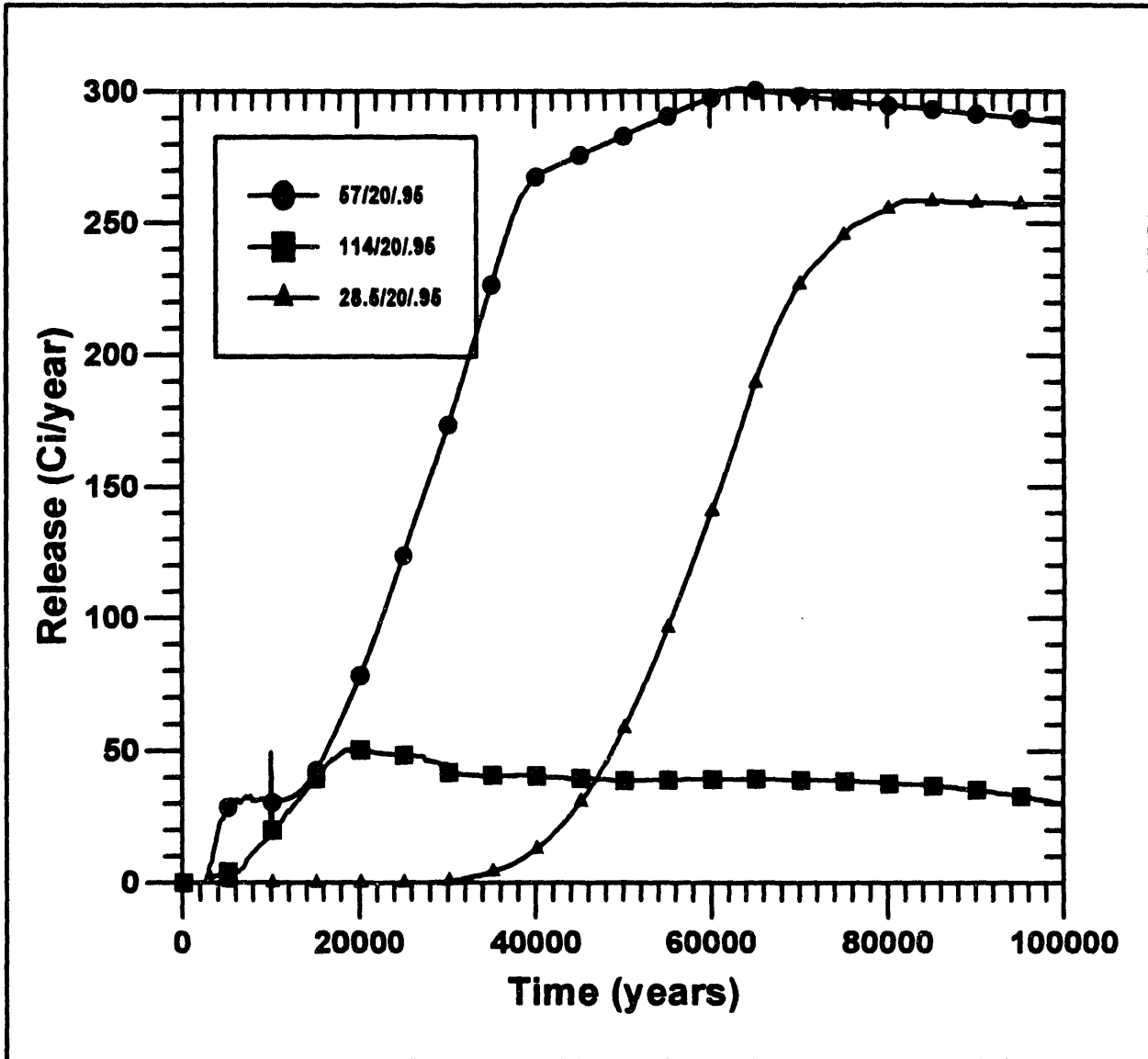


Figure 2-25b. Waste Package Release Rate: Thermal Loading Cases - 20 cm overpack - 100,000 Years

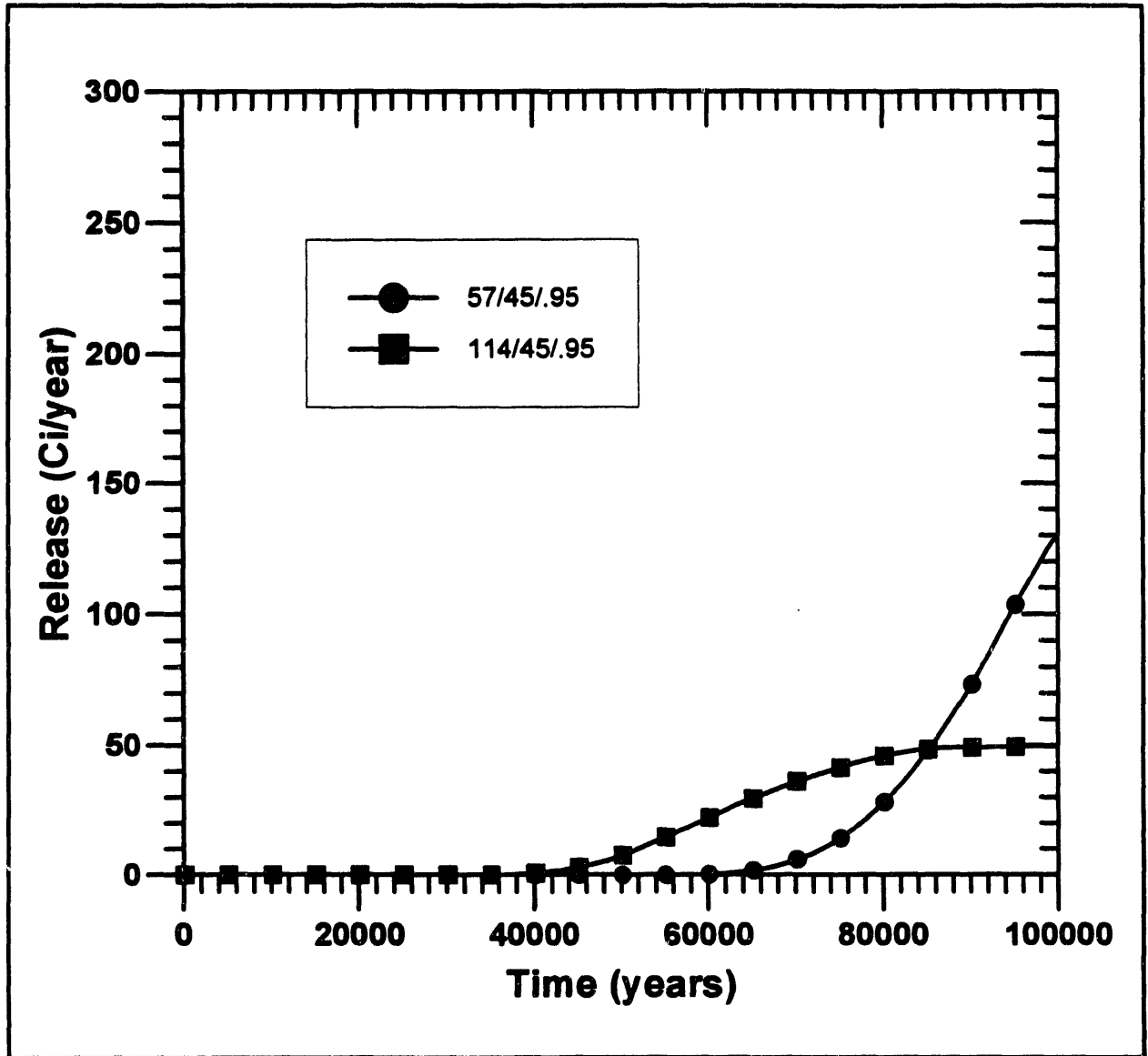


Figure 2-26. Waste Package Release Rate: Thermal Loading Cases - 45 cm overpack - 100,000 Years

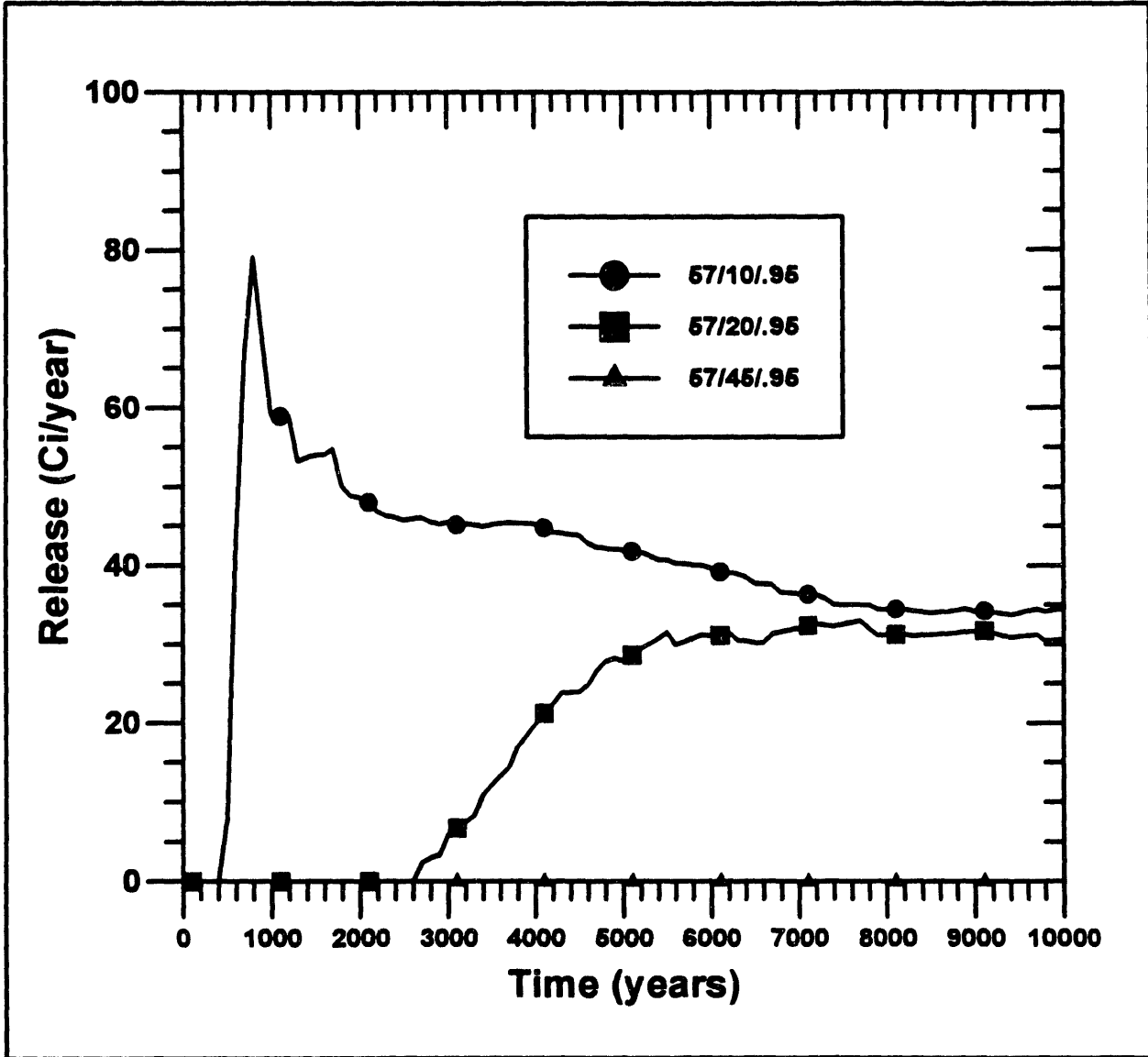


Figure 2-27a. Waste Package Release Rate: Overpack Cases - 57 kW/acre - 10,000 Years

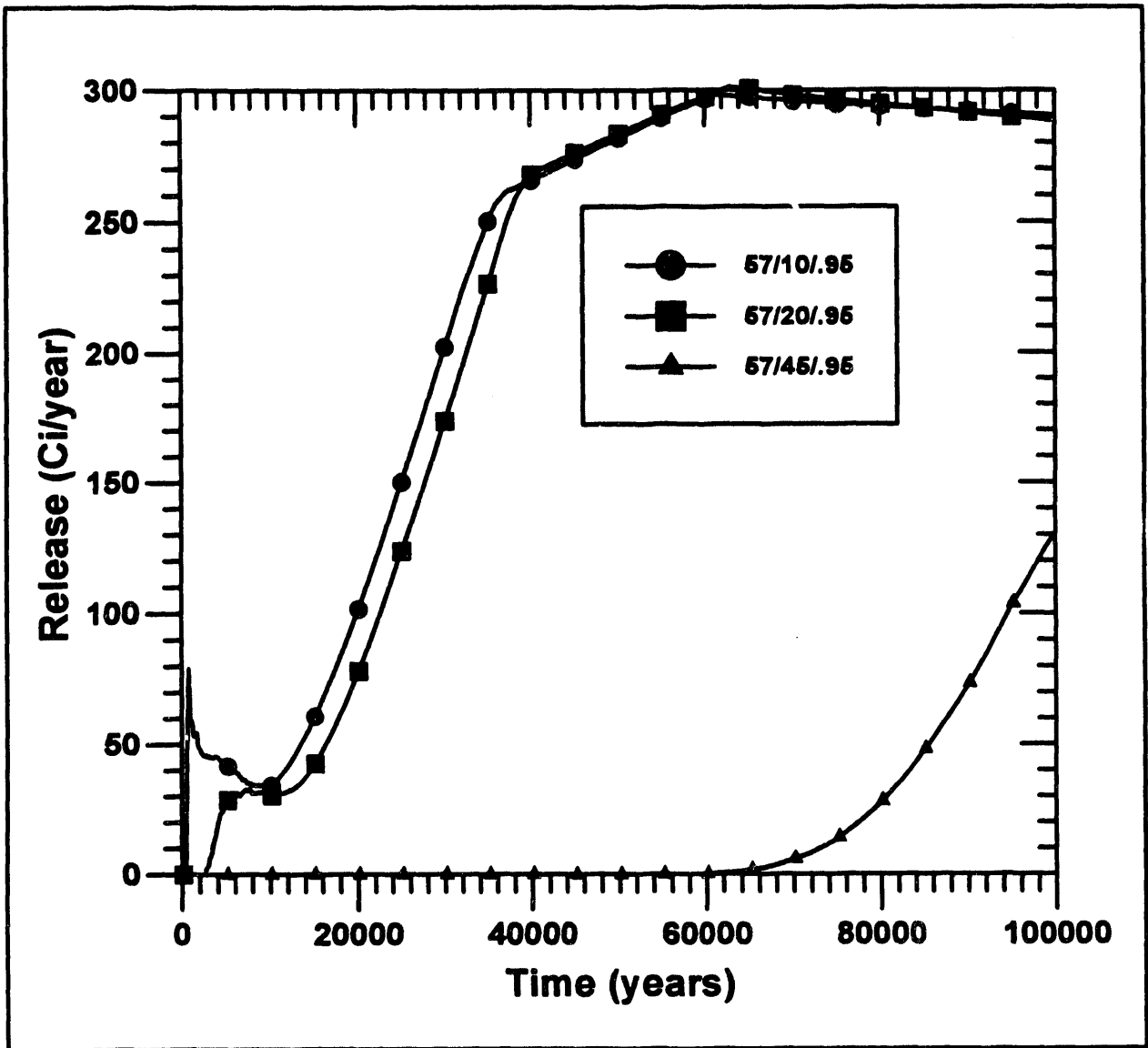


Figure 2-27b. Waste Package Release Rate: Overpack Cases - 57 kW/acre - 100,000 Years

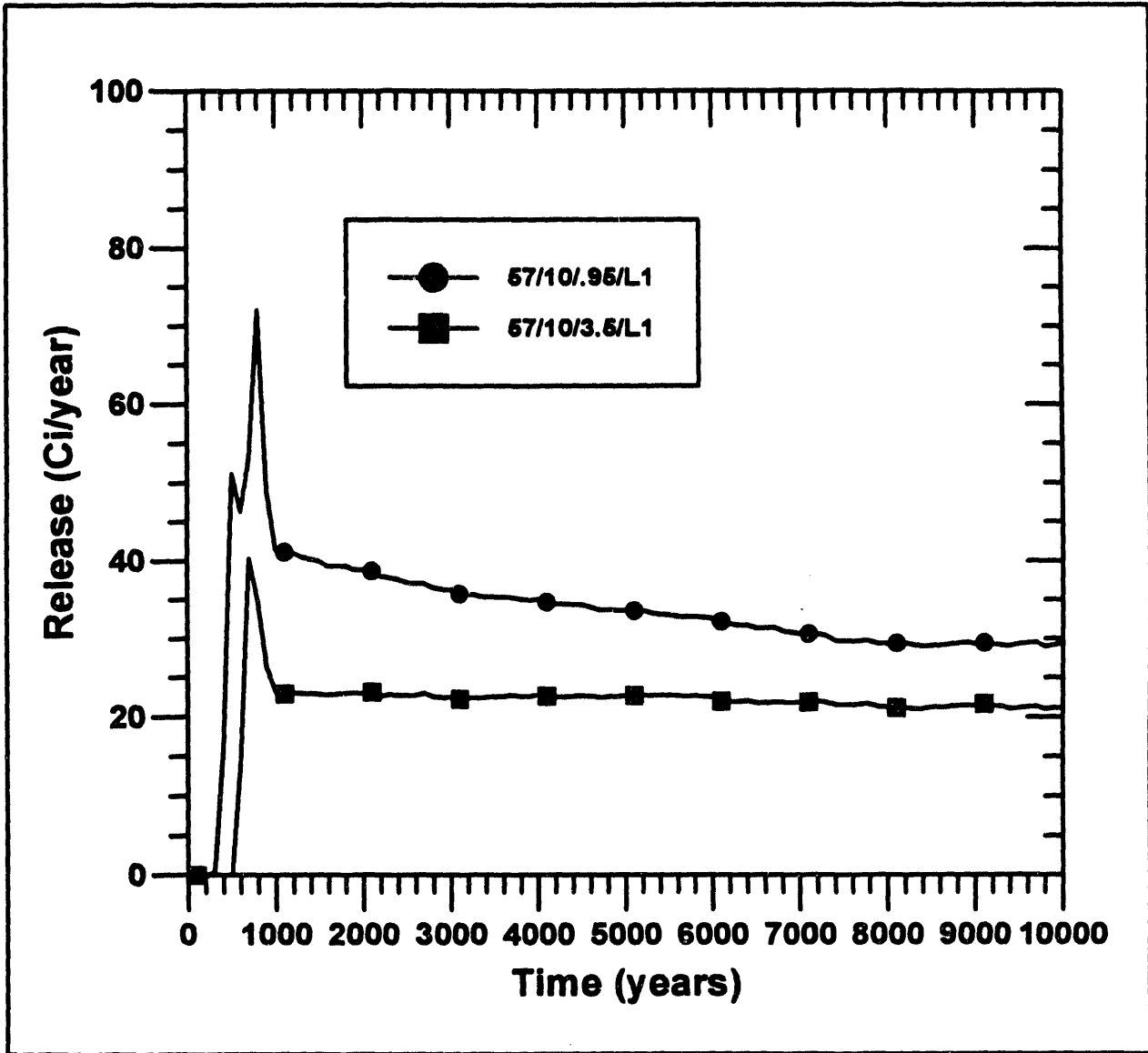


Figure 2-28a. Waste Package Release Rate: Inner Container Cases - 10,000 Years

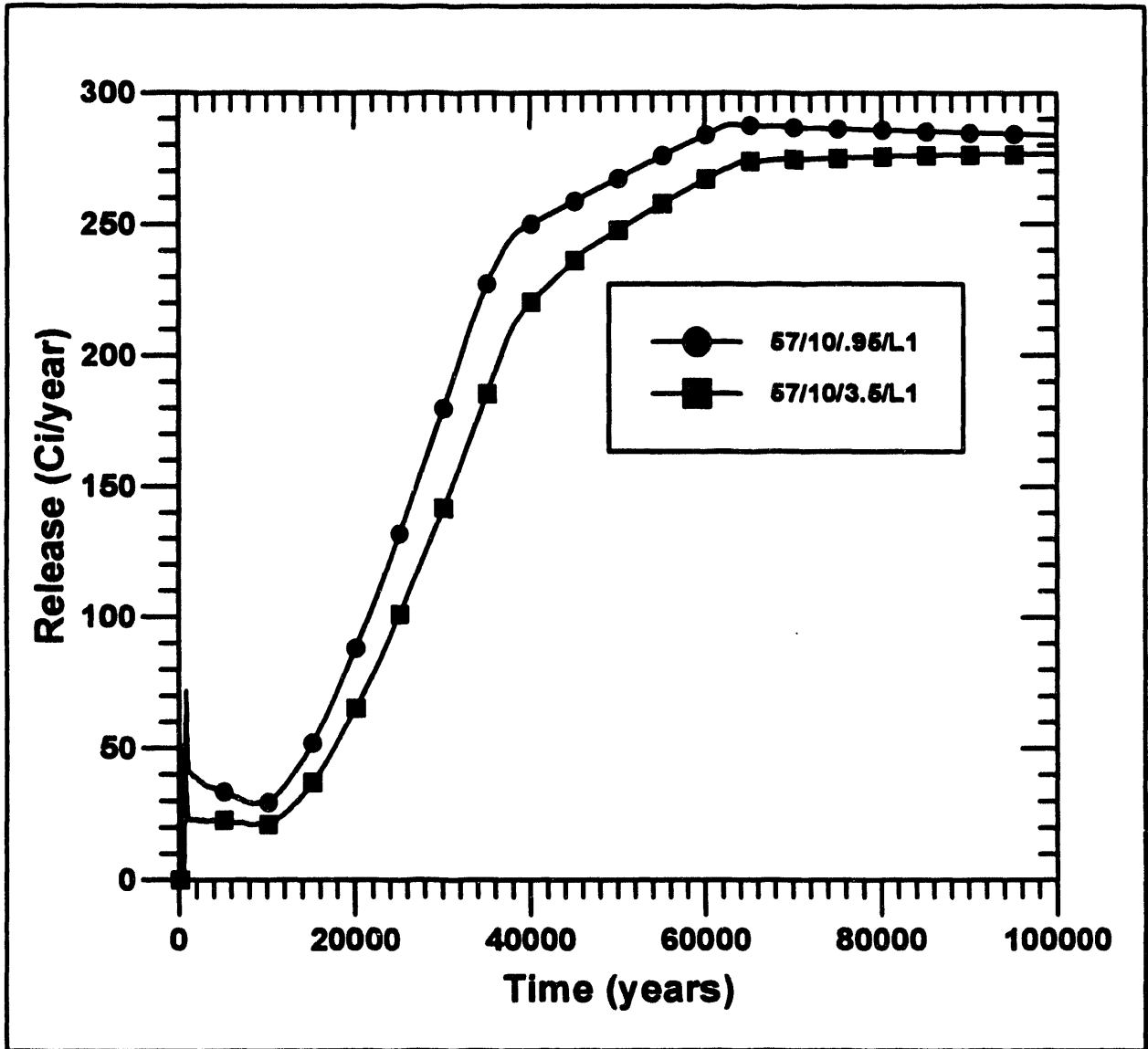


Figure 2-28b. Waste Package Release Rate: Inner Container Cases - 100,000 Years

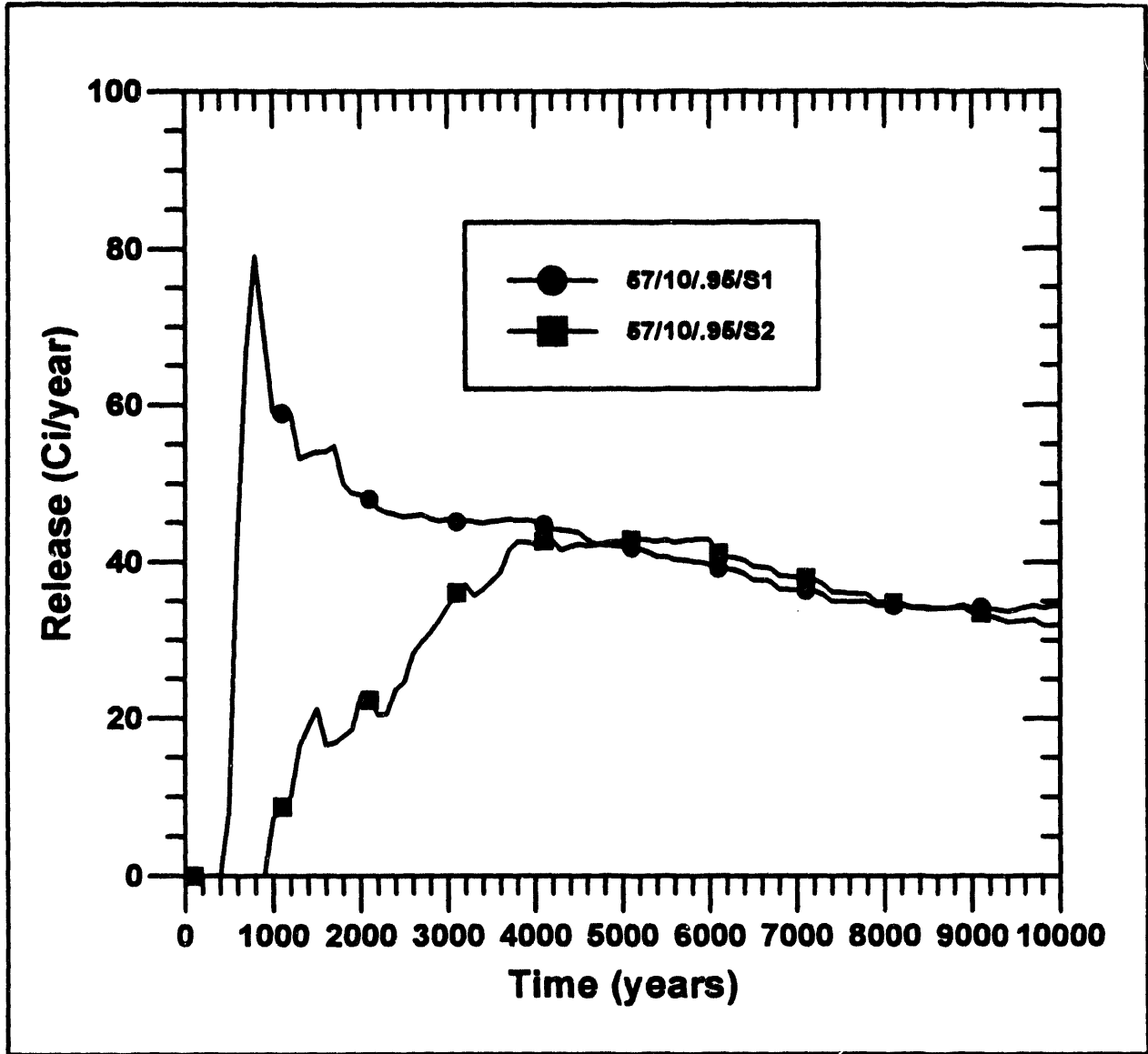


Figure 2-29a. Waste Package Release Rate: Saturation vs. Temperature Dependent Corrosion Initiation - 10,000 Years (after Stahl, 1993)

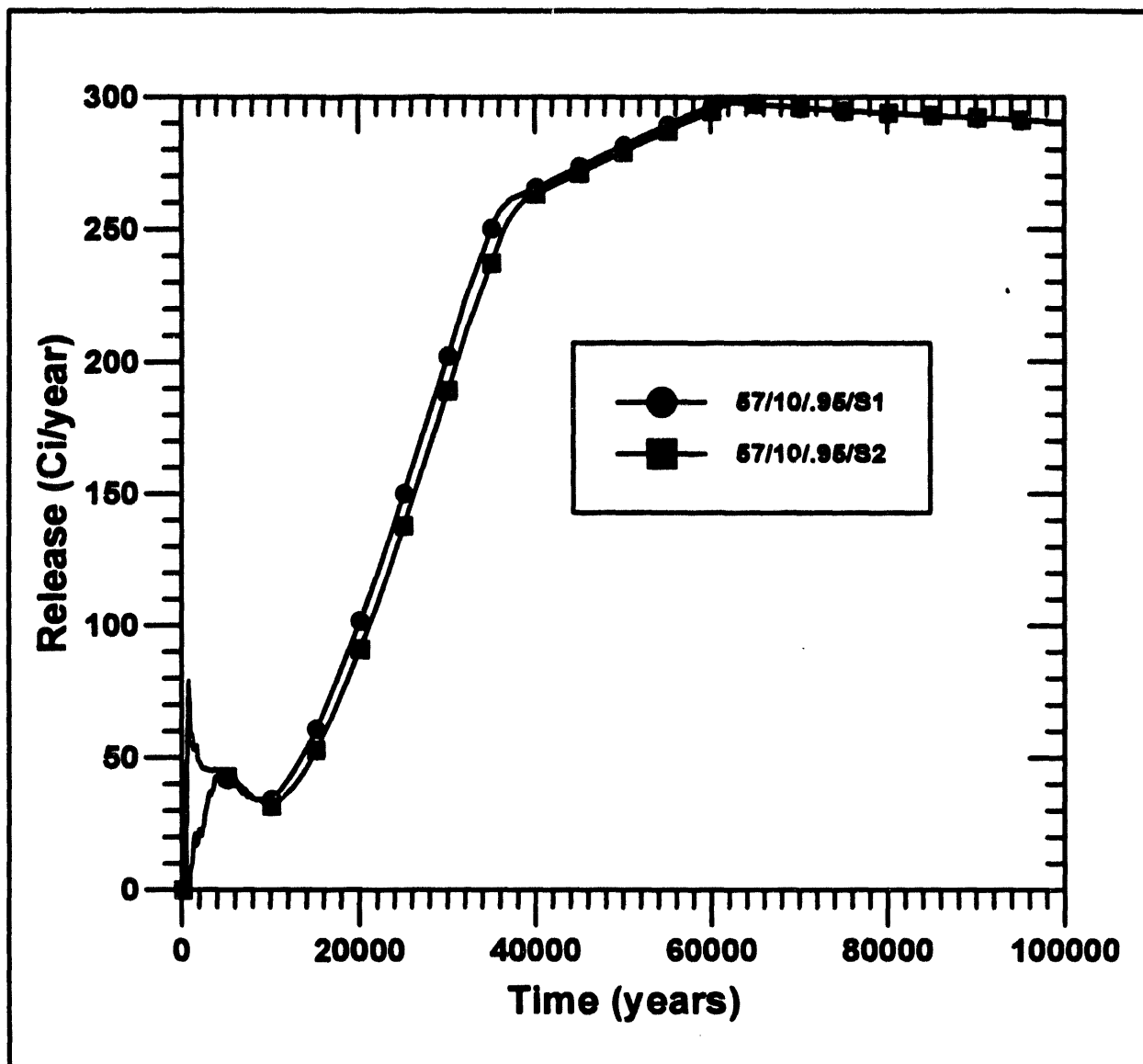


Figure 2-29b. Waste Package Release Rate: Saturation vs. Temperature Dependent Corrosion Initiation - 100,000 Years (after Stahl, 1993)

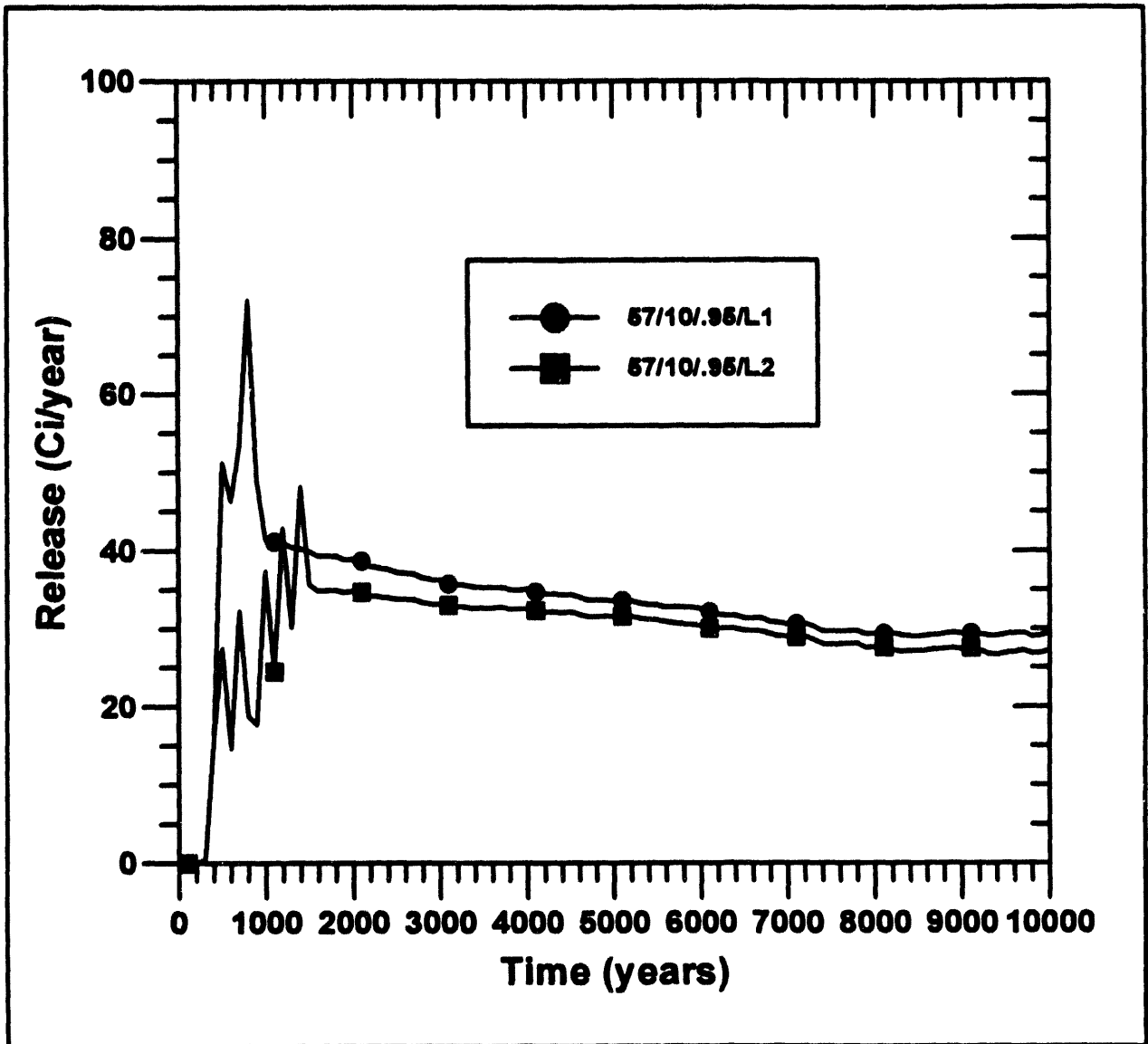


Figure 2-30a. Waste Package Release Rate: Saturation vs. Temperature Dependent Corrosion Initiation - 10,000 Years (after Lamont, 1993)

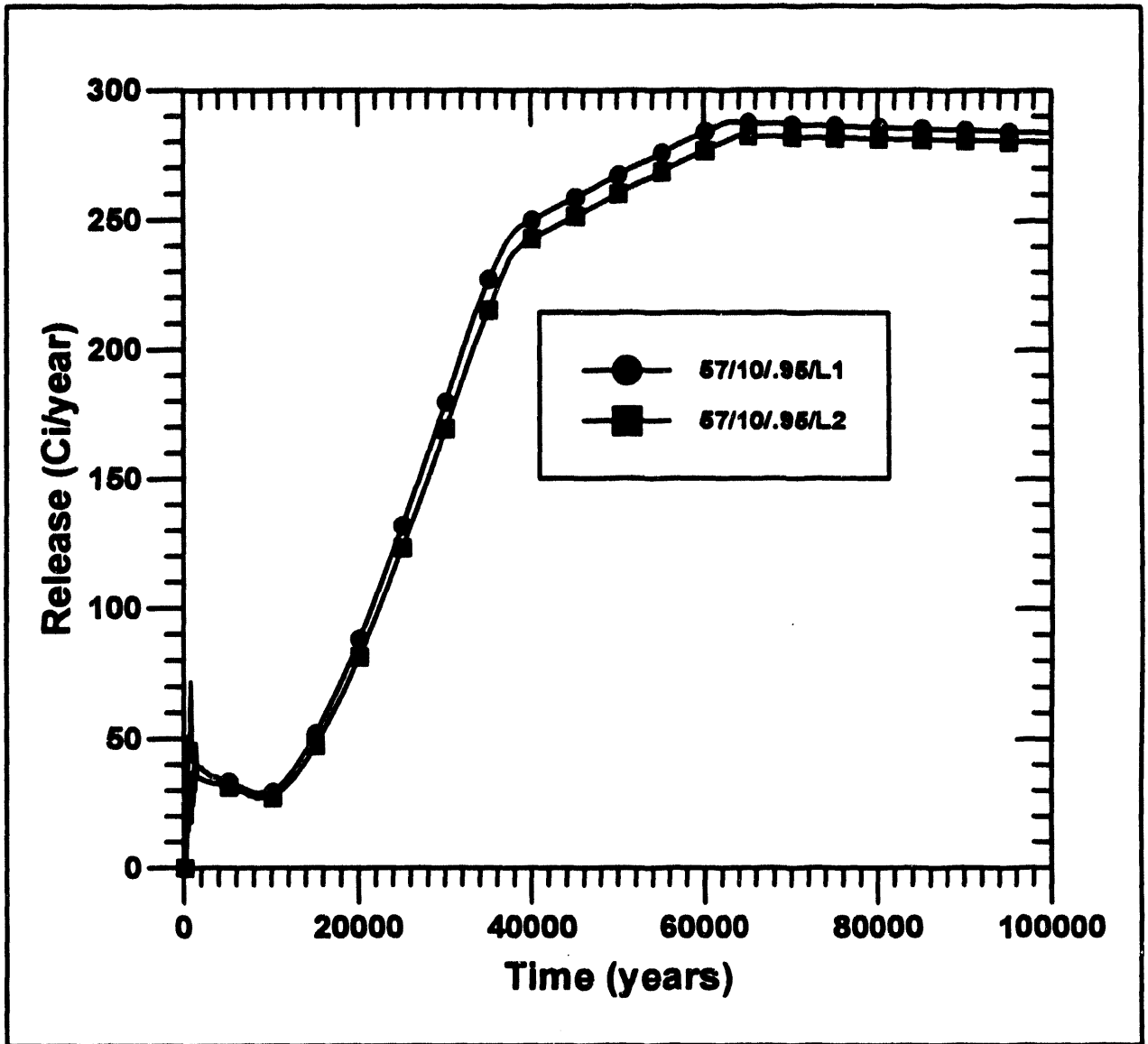


Figure 2-30b. Waste Package Release Rate: Saturation vs. Temperature Dependent Corrosion Initiation - 100,000 Years (after Lamont, 1993)

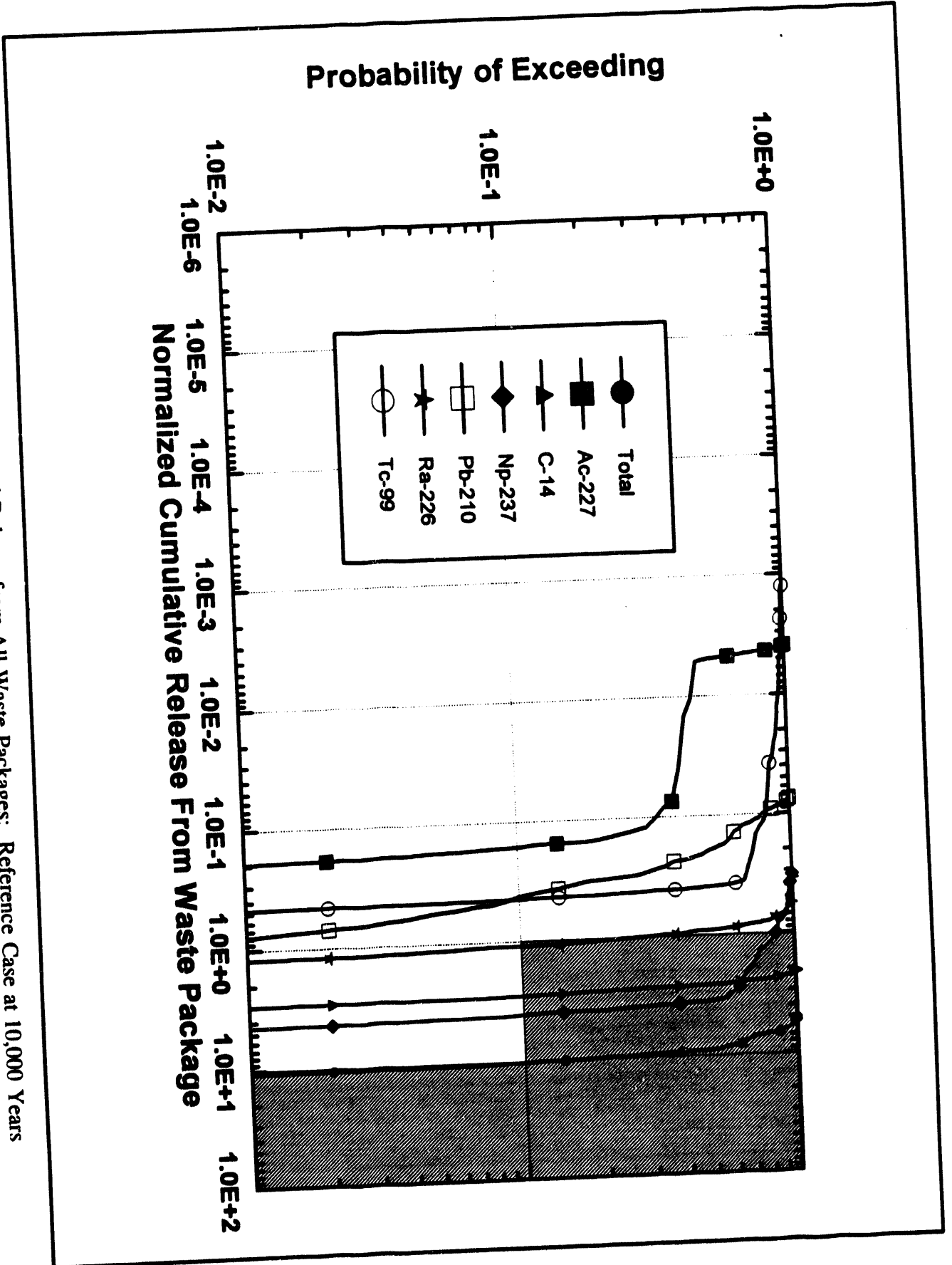


Figure 2-31. CCDF of Normalized Release from All Waste Packages: Reference Case at 10,000 Years

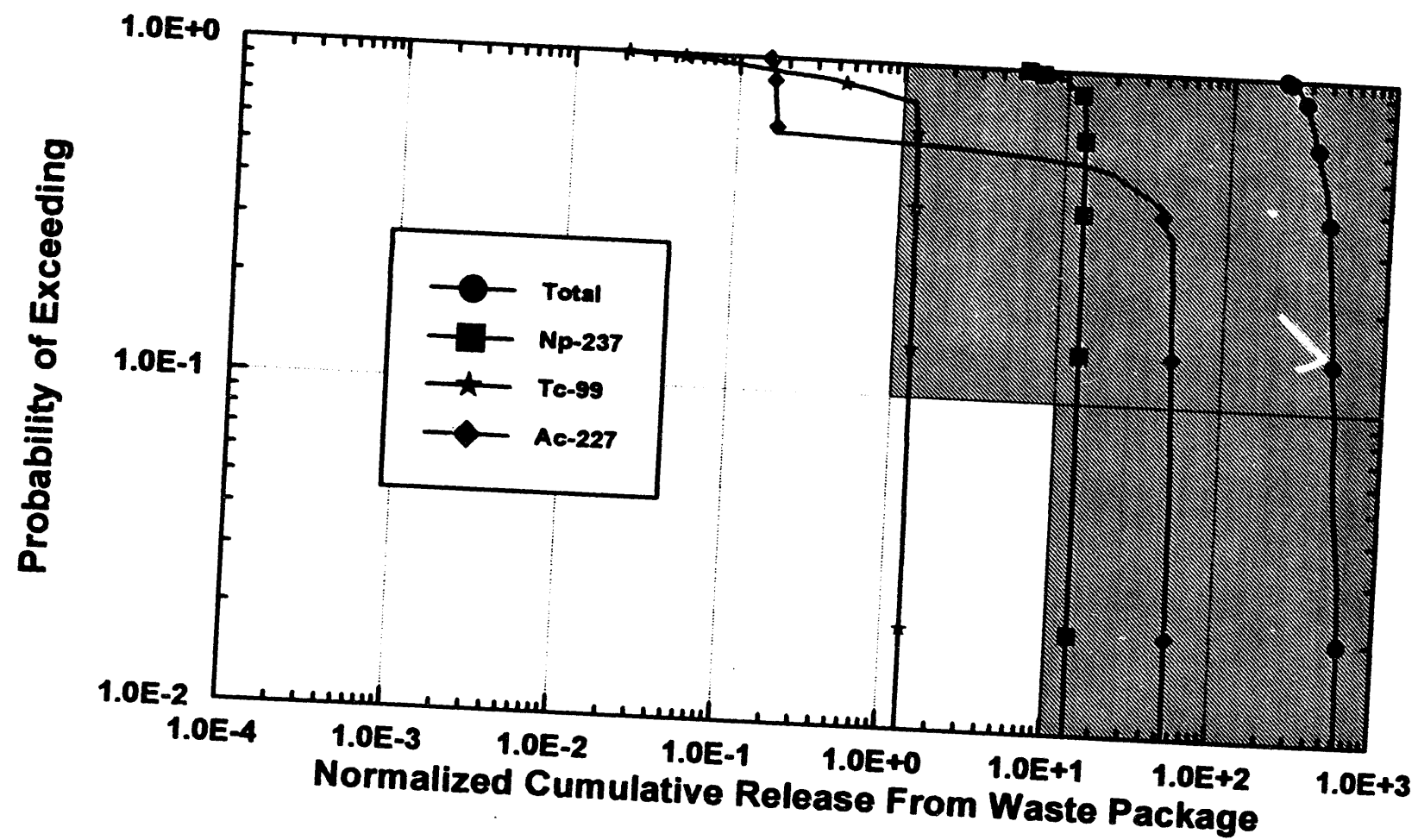


Figure 2-32. CCDF of Normalized Release from All Waste Packages: Reference Case at 100,000 Years

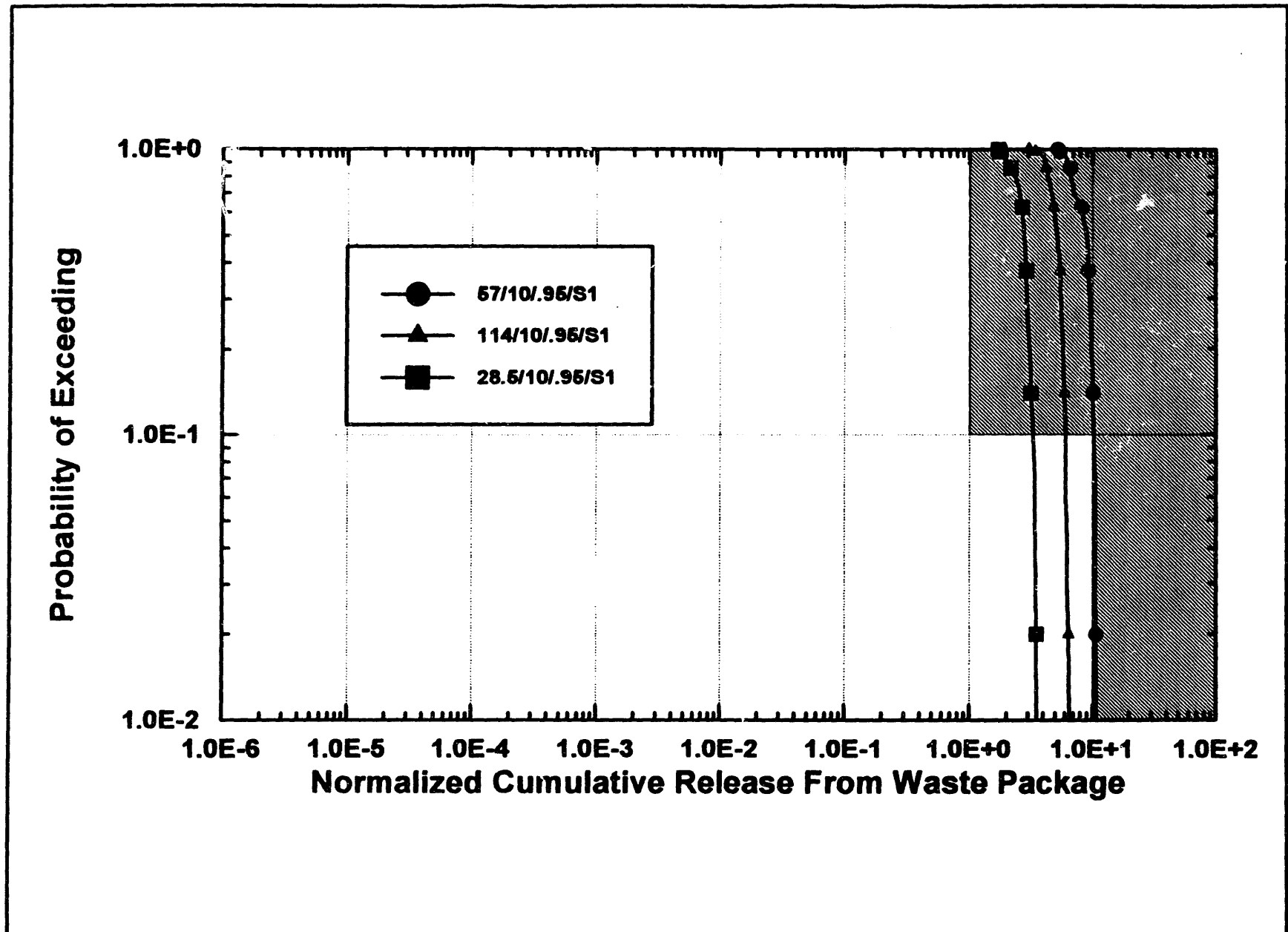


Figure 2-33. CCDF of Normalized Release from All Waste Packages: Thermal Load Cases at 10,000 Years

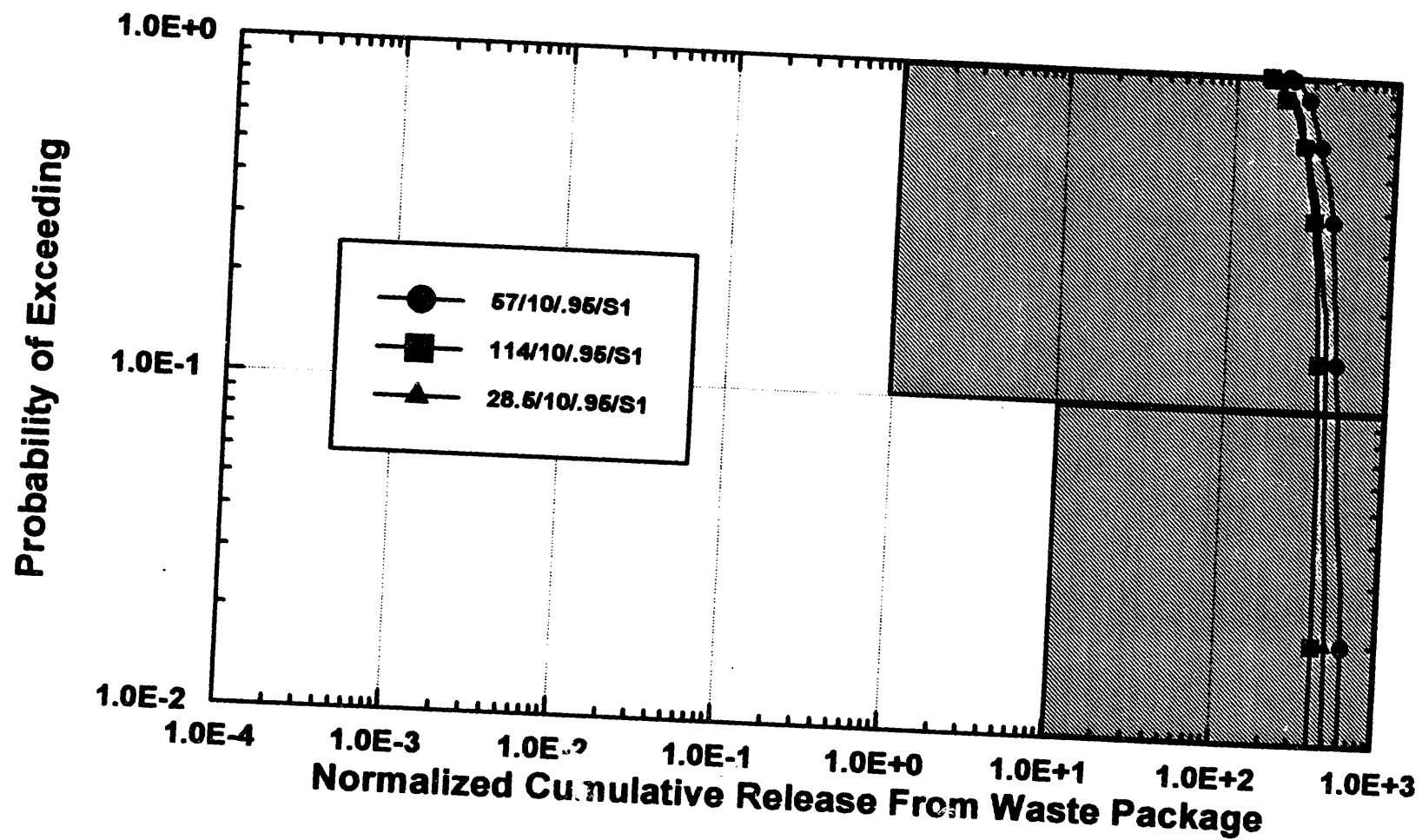


Figure 2-34. CCDF of Normalized Release from All Waste Packages: Thermal Load Cases at 100,000 Years

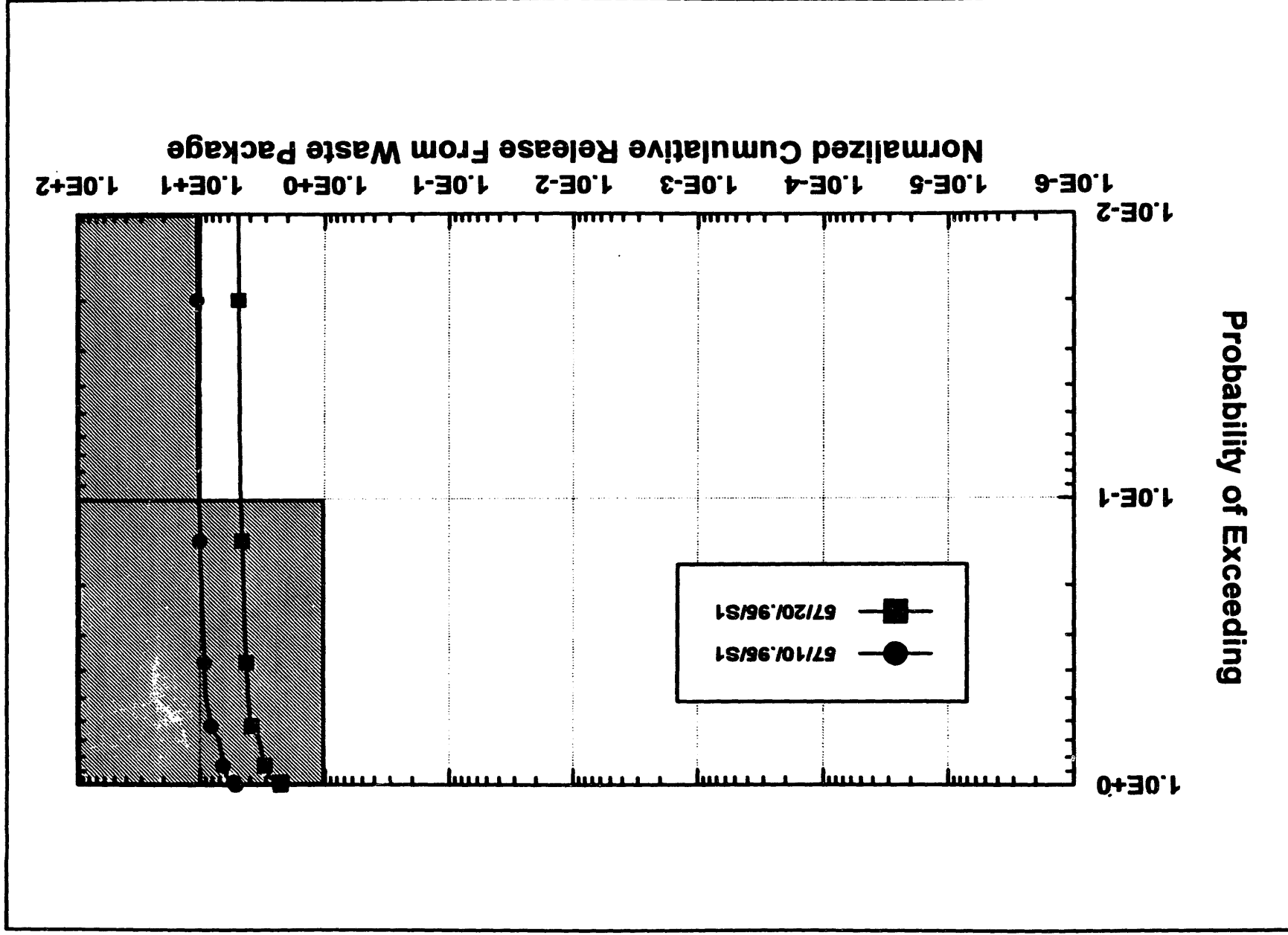


Figure 2-35. CCDF of Normalized Release from All Waste Packages: Outer Container Thickness Cases at 10,000 Years

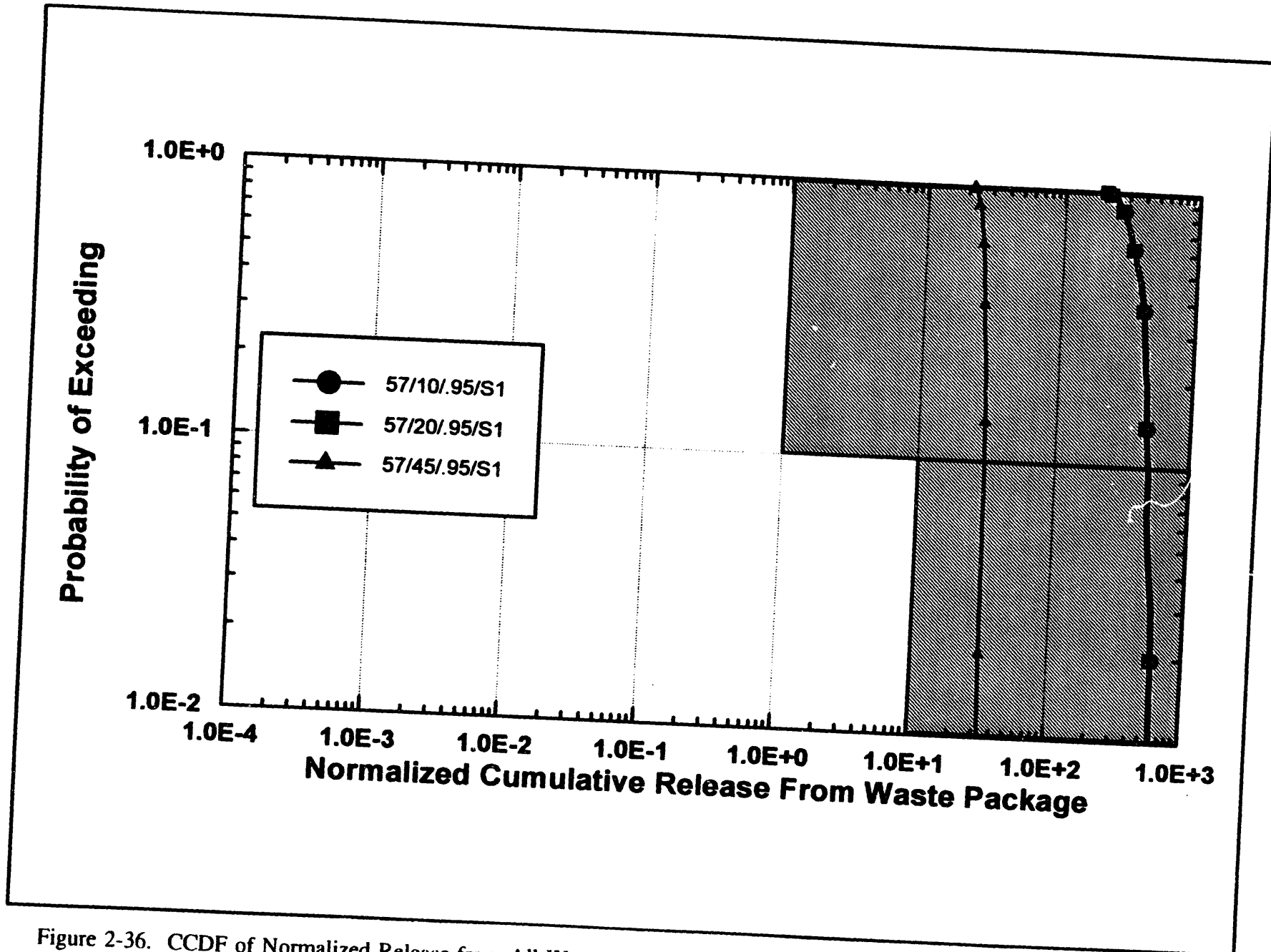


Figure 2-36. CCDF of Normalized Release from All Waste Packages: Outer Container Thickness Cases at 100,000 Years

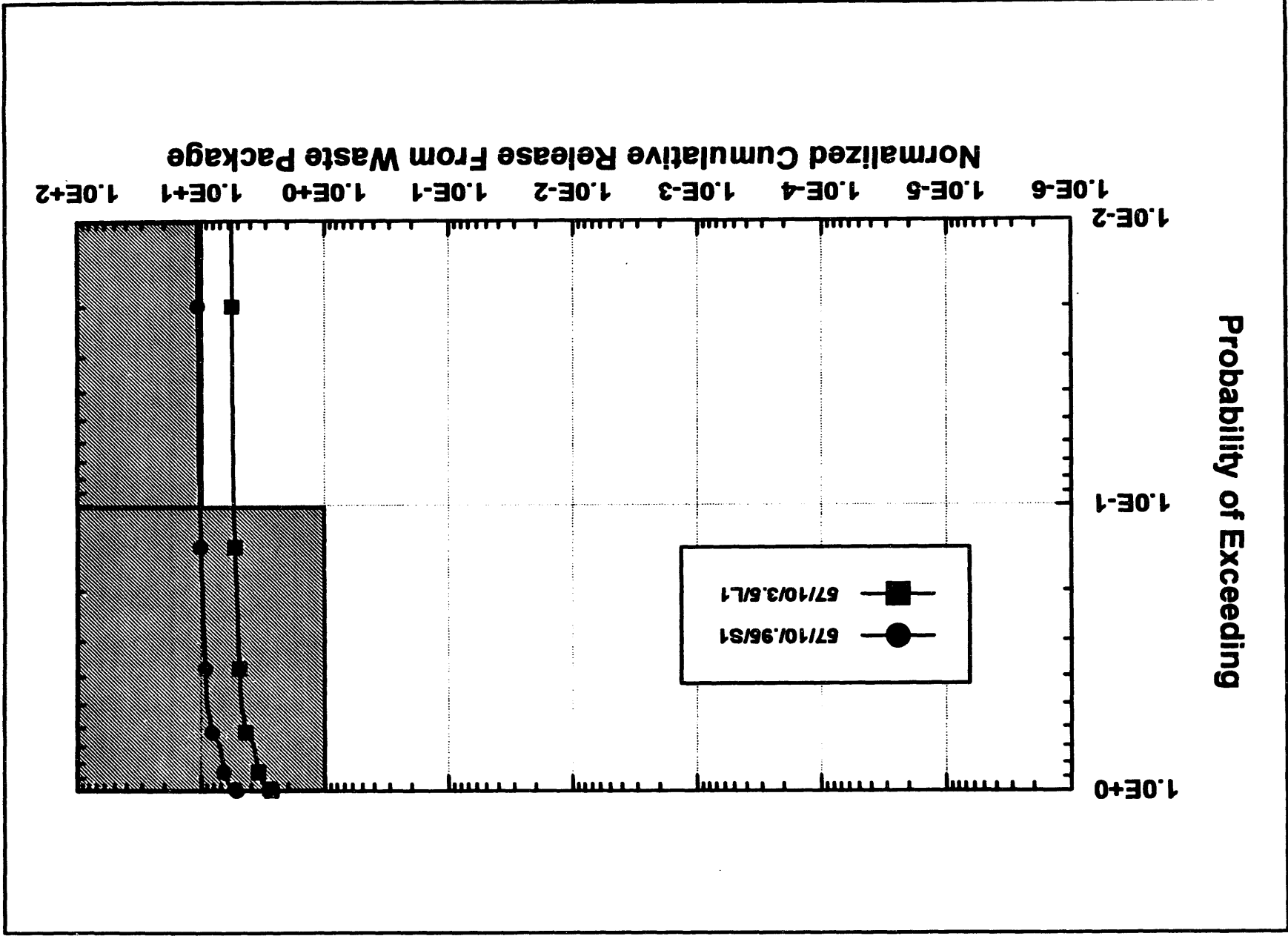


Figure 2-37. CCDF of Normalized Release from All Waste Packages: Corrosion Initiation Sensitivity Cases at 10,000 Years

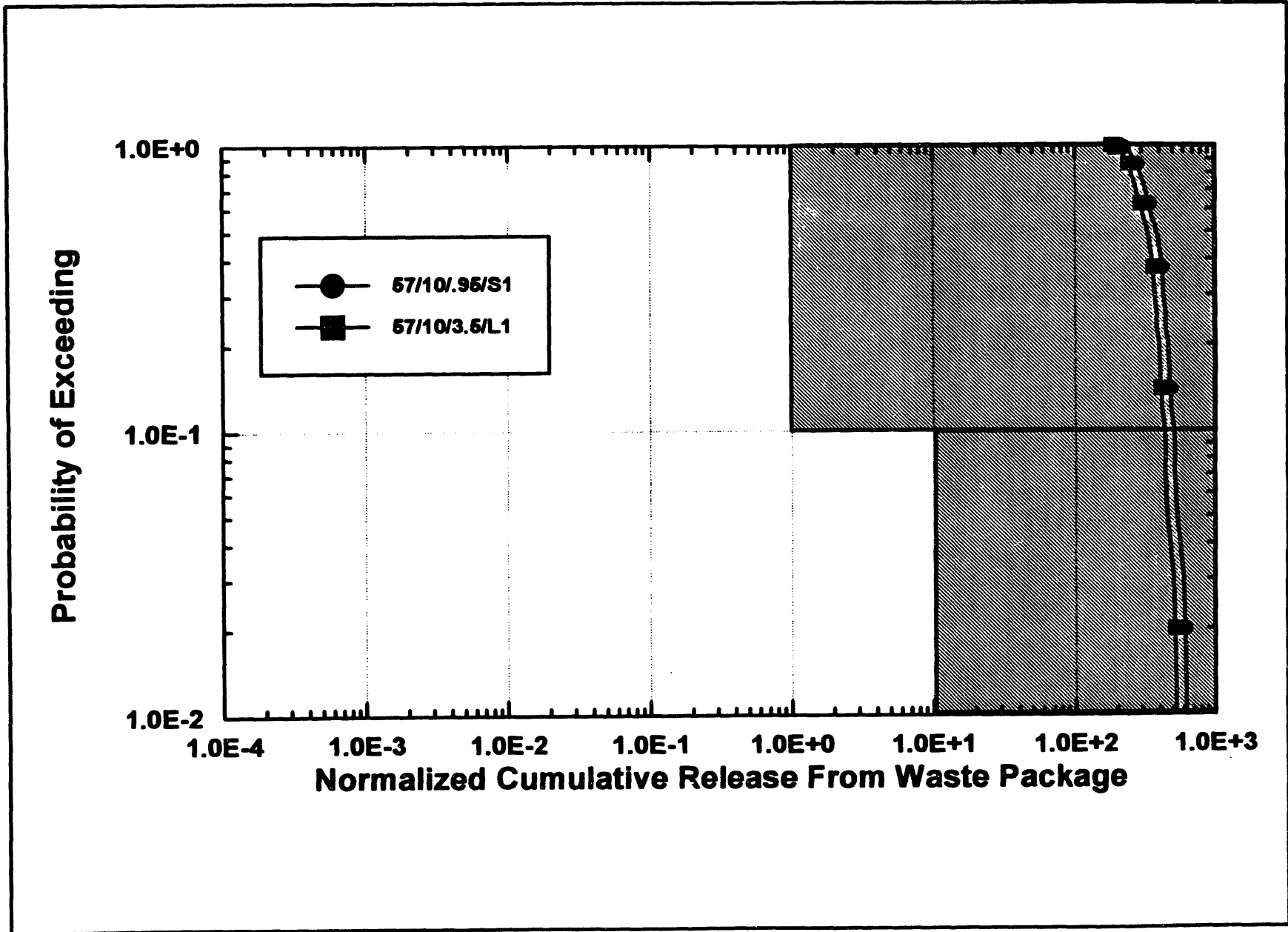


Figure 2-38. CCDF of Normalized Release from All Waste Packages: Corrosion Initiation Sensitivity Cases at 100,000 Years

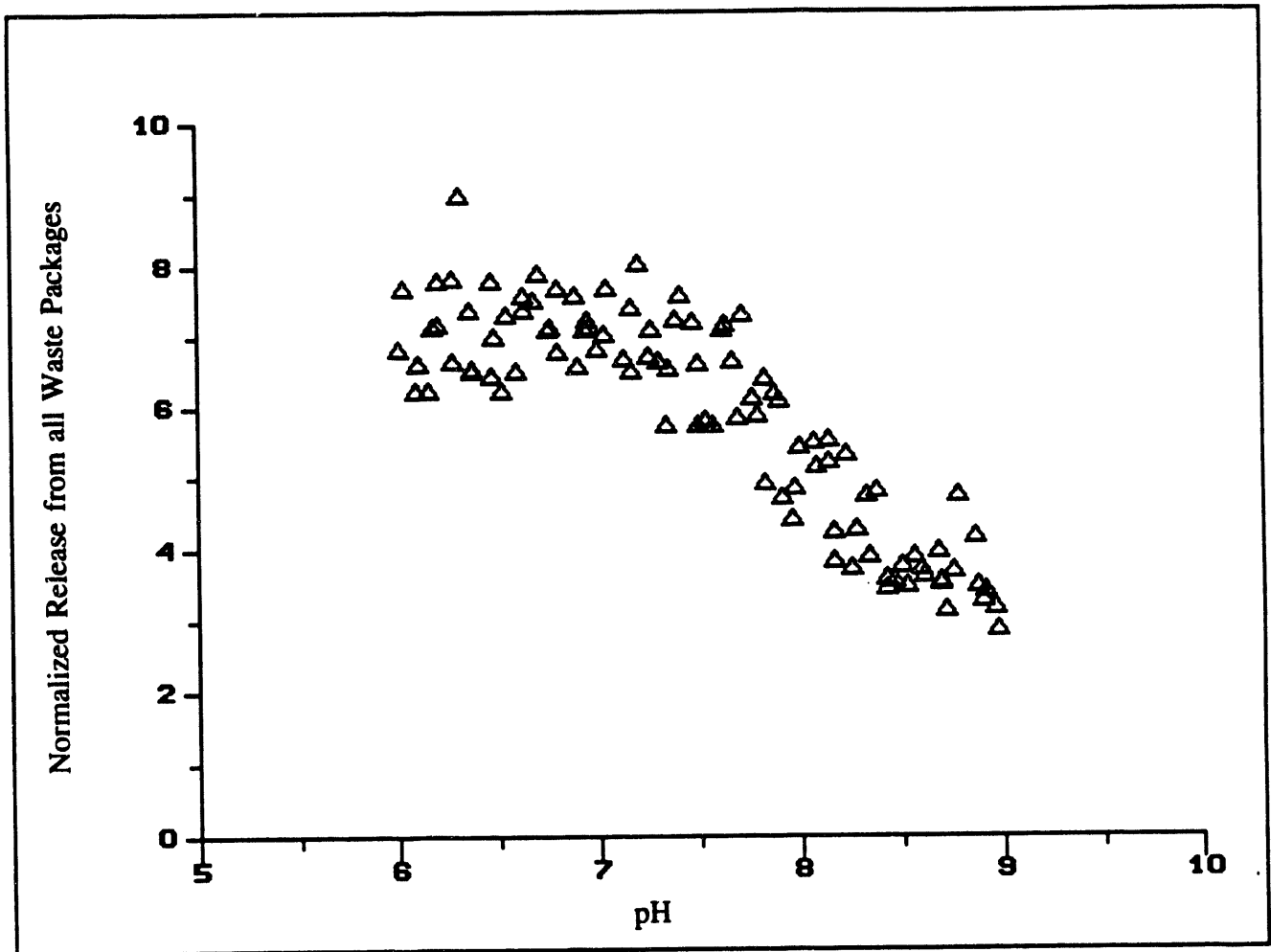


Figure 2-39a. Scatter Plot of pH vs. Total Normalized Release - Reference Case - 10,000 Years

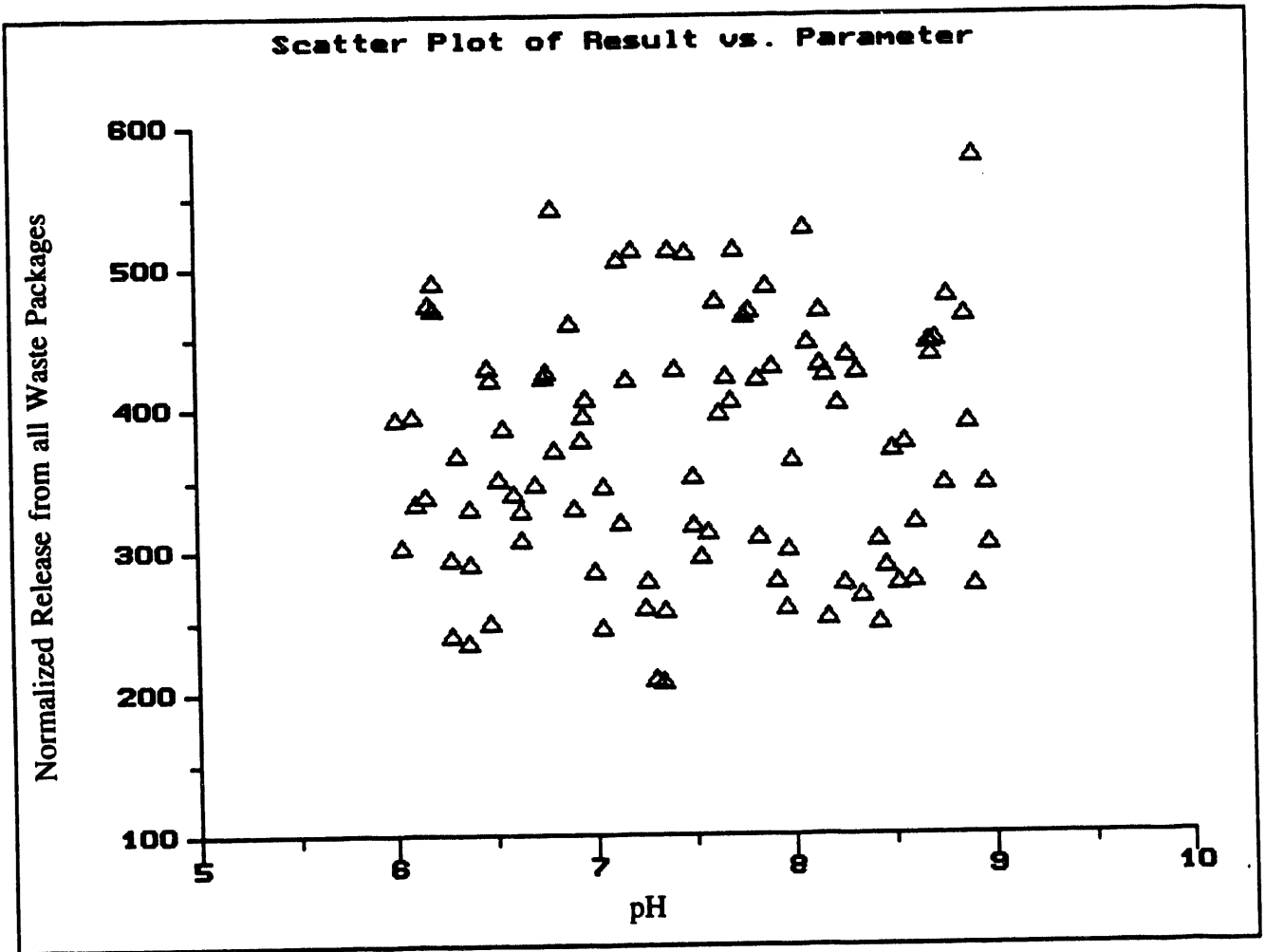


Figure 2-39b. Scatter Plot of pH vs. Total Normalized Release - Reference Case - 100,000 Years

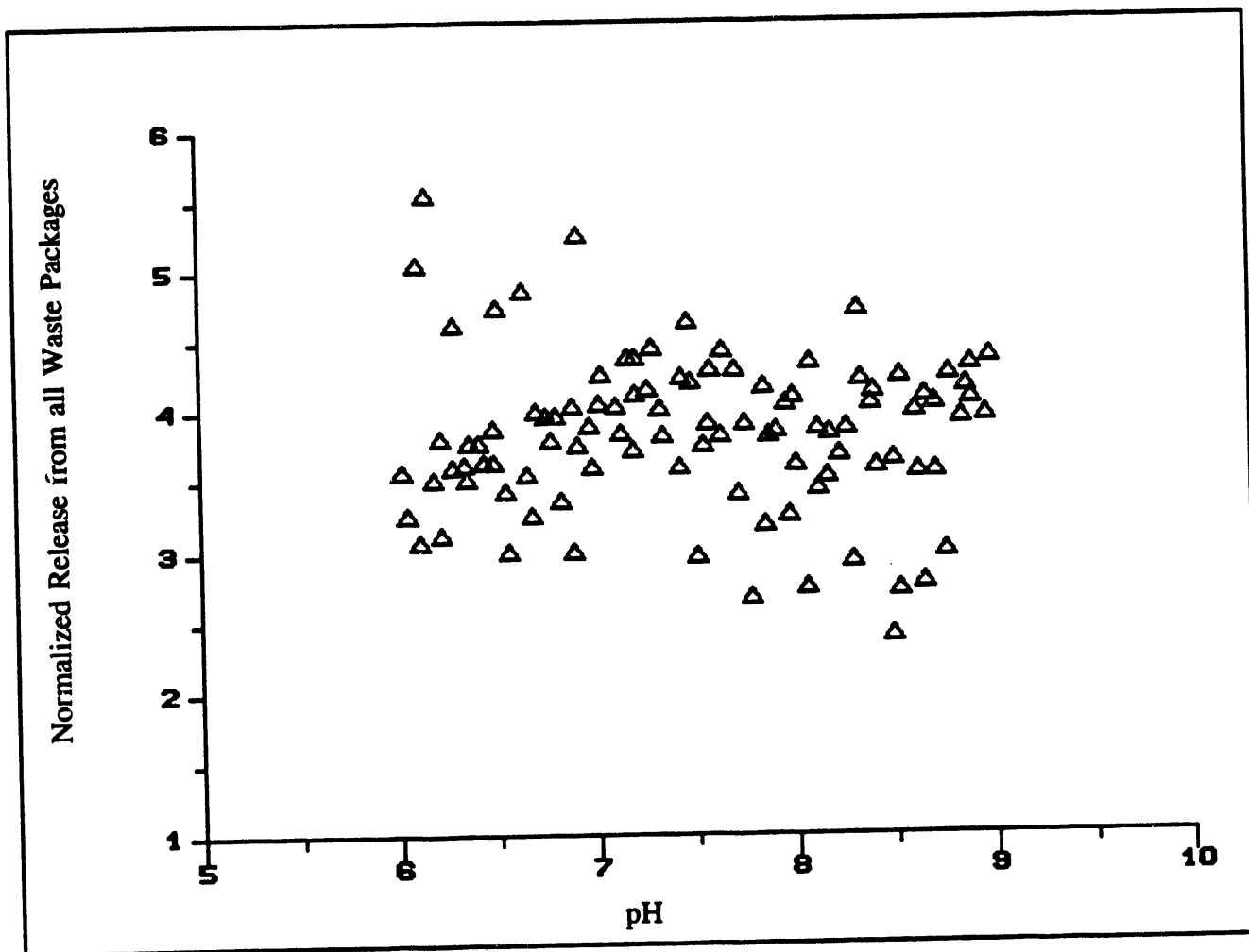


Figure 2-40a. Scatter Plot of pH vs. Total Normalized Release - 114 kW/acre - 10,000 Years

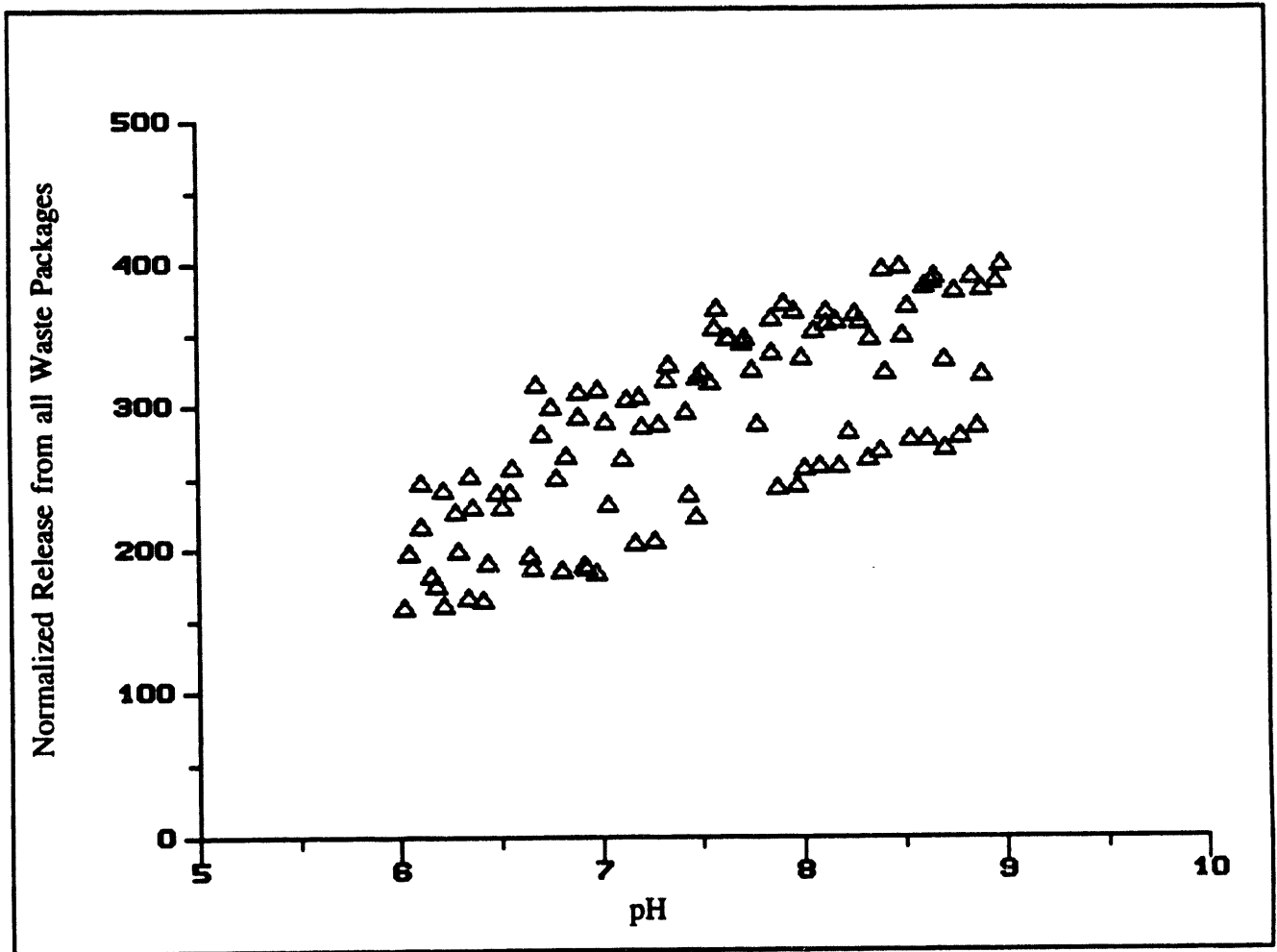


Figure 2-40b. Scatter Plot of pH vs. Total Normalized Release - 114 kW/acre  
100,000 Years

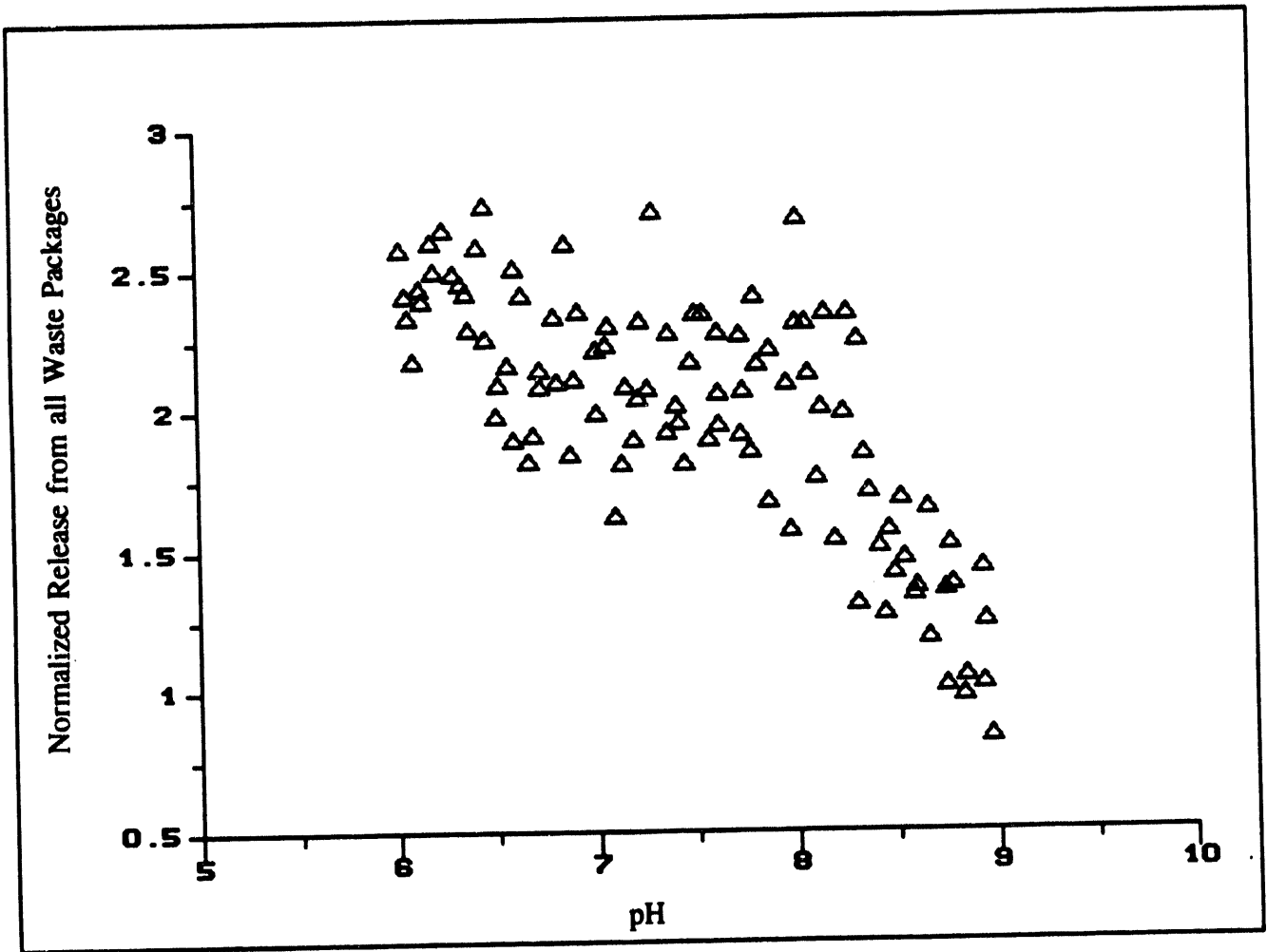


Figure 2-41a. Scatter Plot of pH vs. Total Normalized Release - 28.5 kW/acre - 10,000 Years

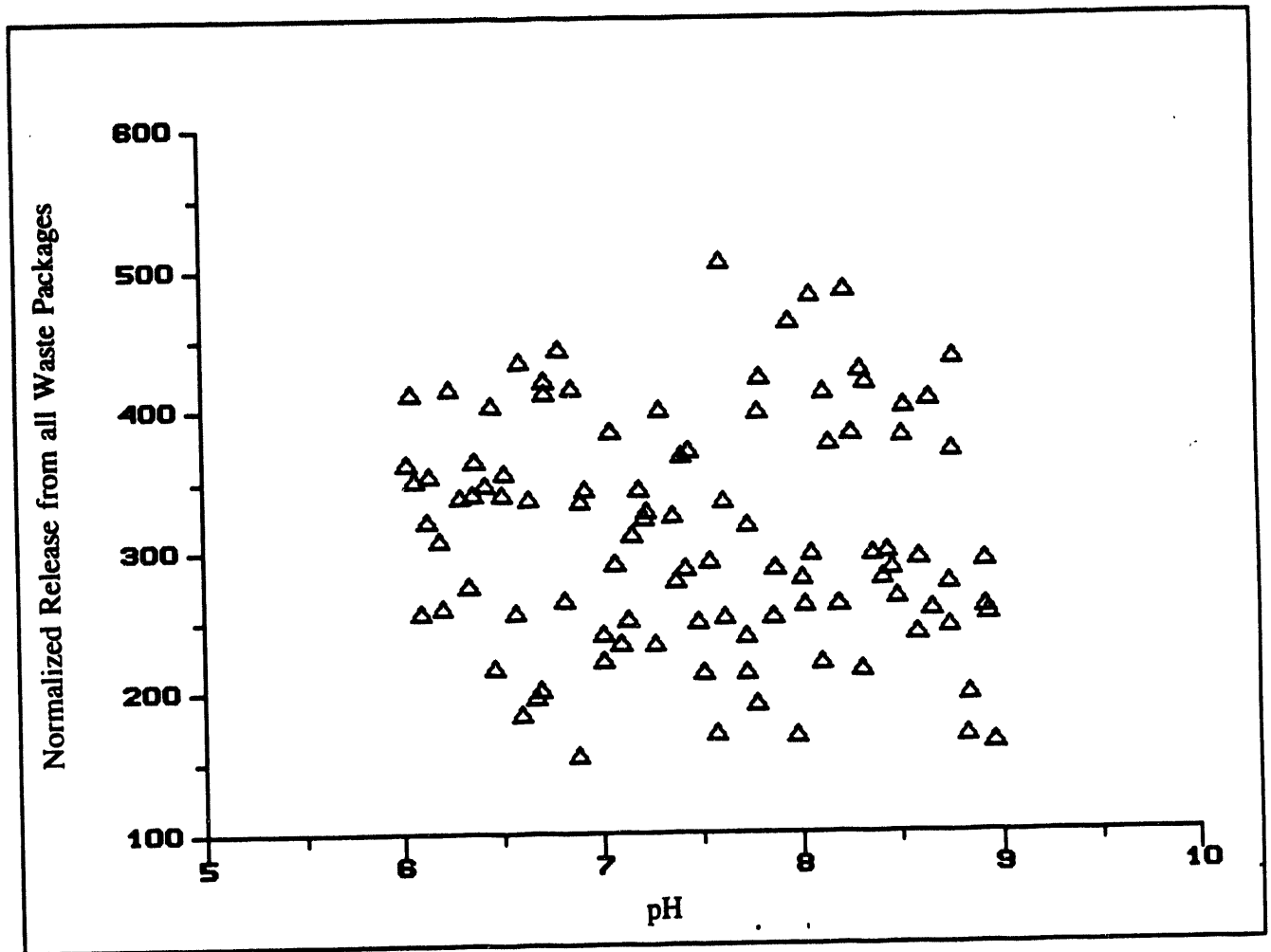


Figure 2-41b. Scatter Plot of pH vs. Total Normalized Release - 28.5 kW/acre - 100,000 Years

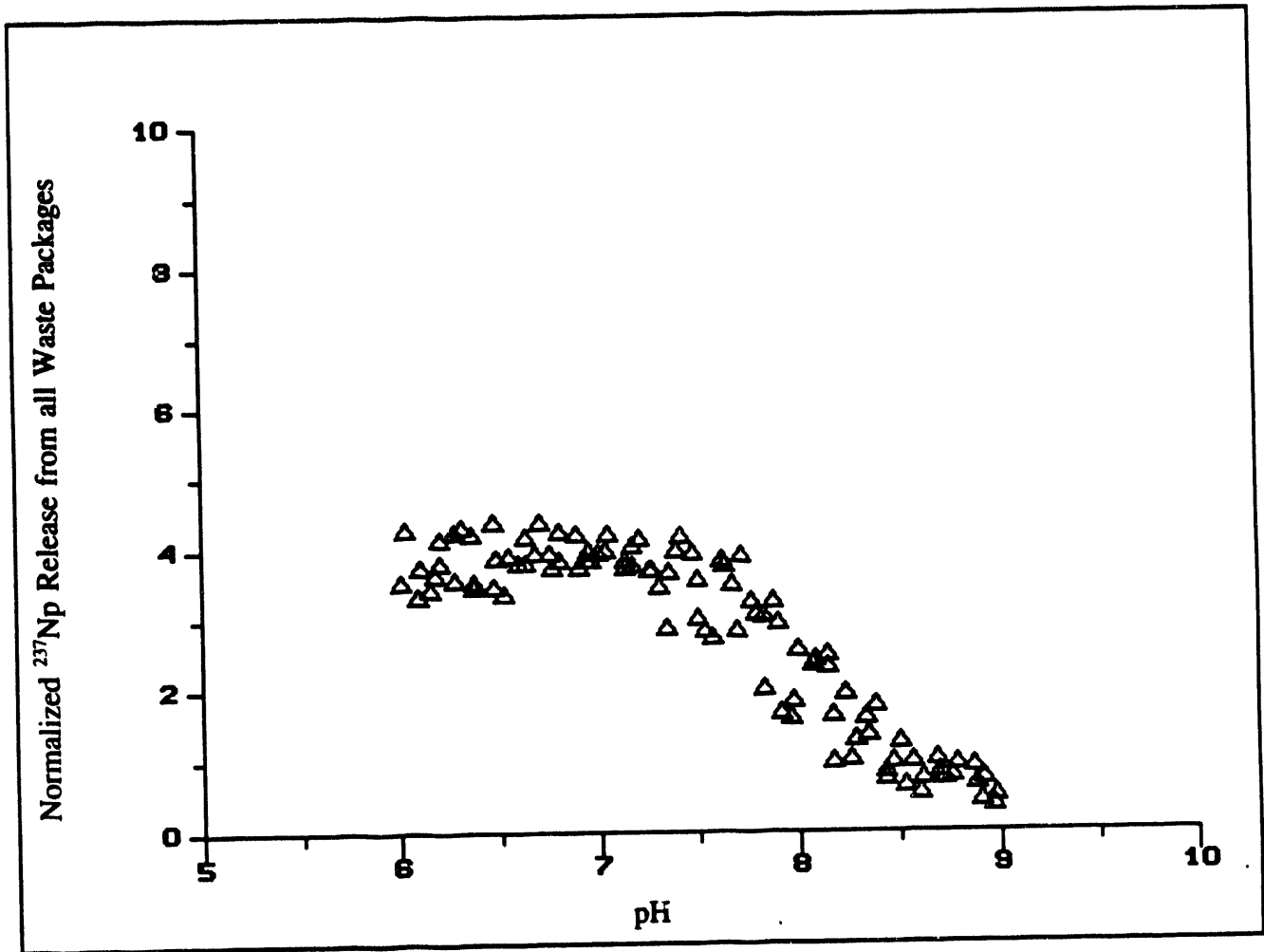


Figure 2-42a. Scatter Plot of pH vs. <sup>237</sup>Np Normalized Release - Reference Case - 10,000 Years

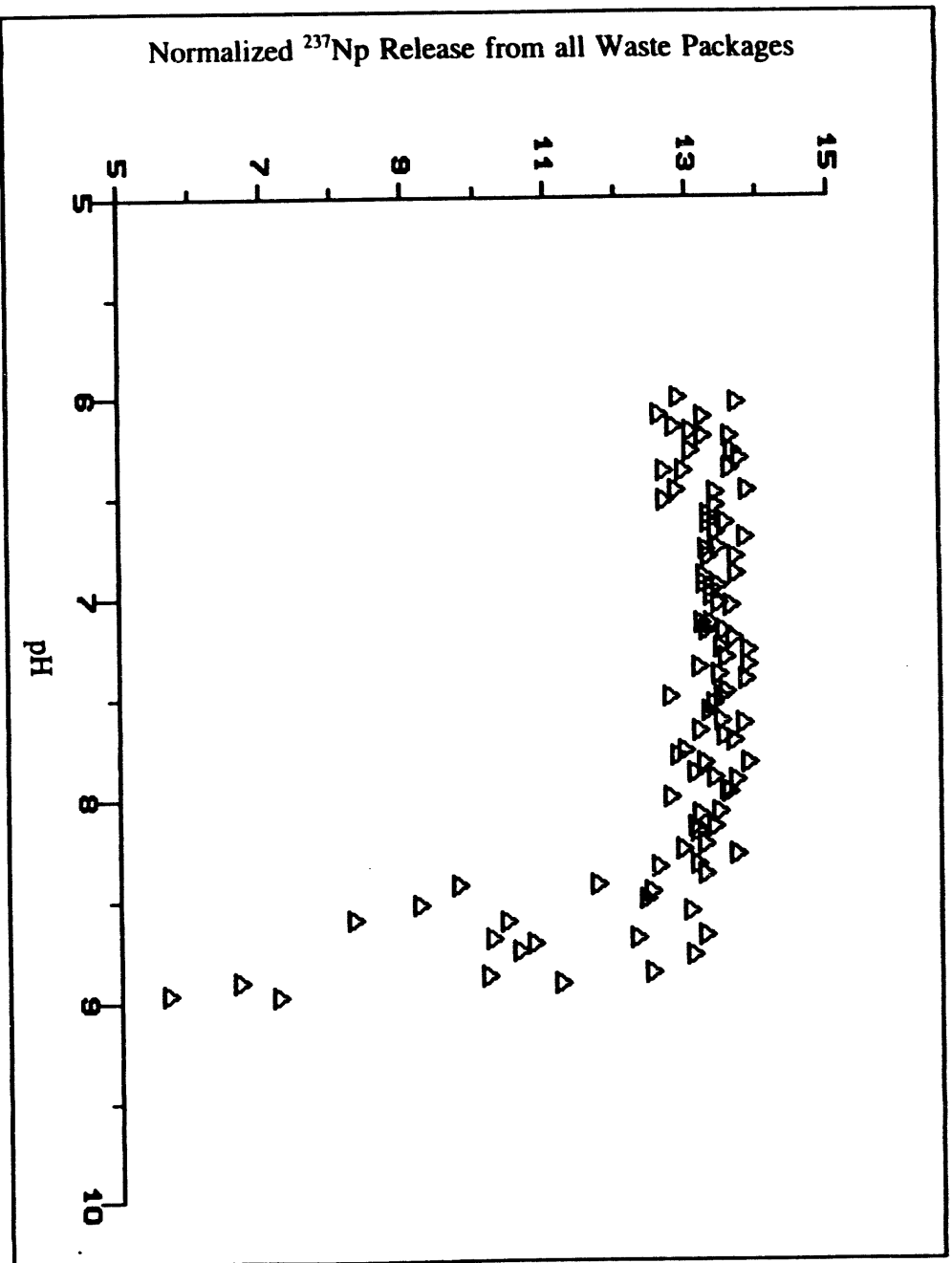


Figure 2-42b. Scatter Plot of pH vs. <sup>237</sup>Np Normalized Release - Reference Case - 100,000 Years

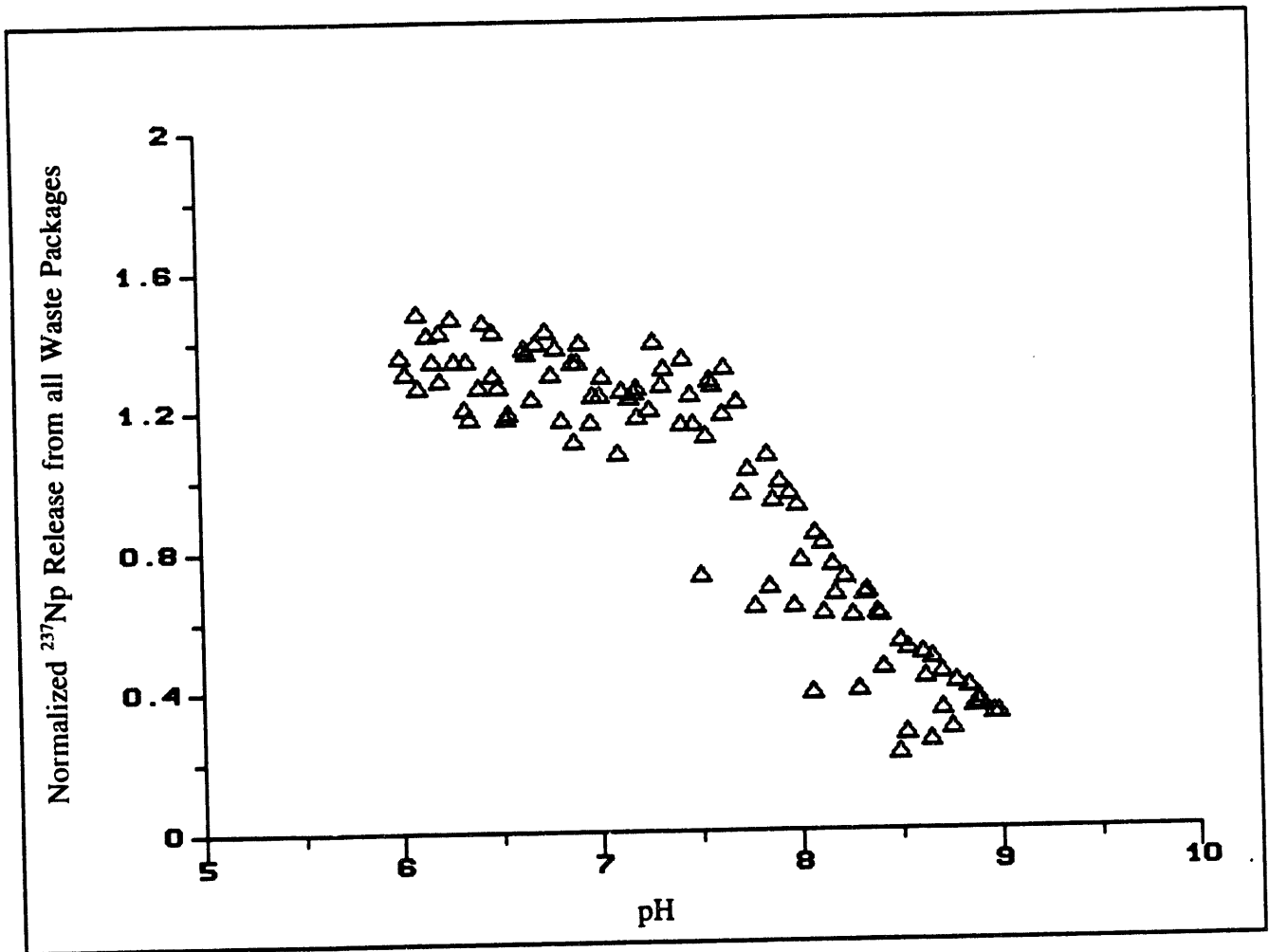


Figure 2-43a. Scatter Plot of pH vs.  $^{237}\text{Np}$  Normalized Release - 114 kW/acre - 10,000 Years

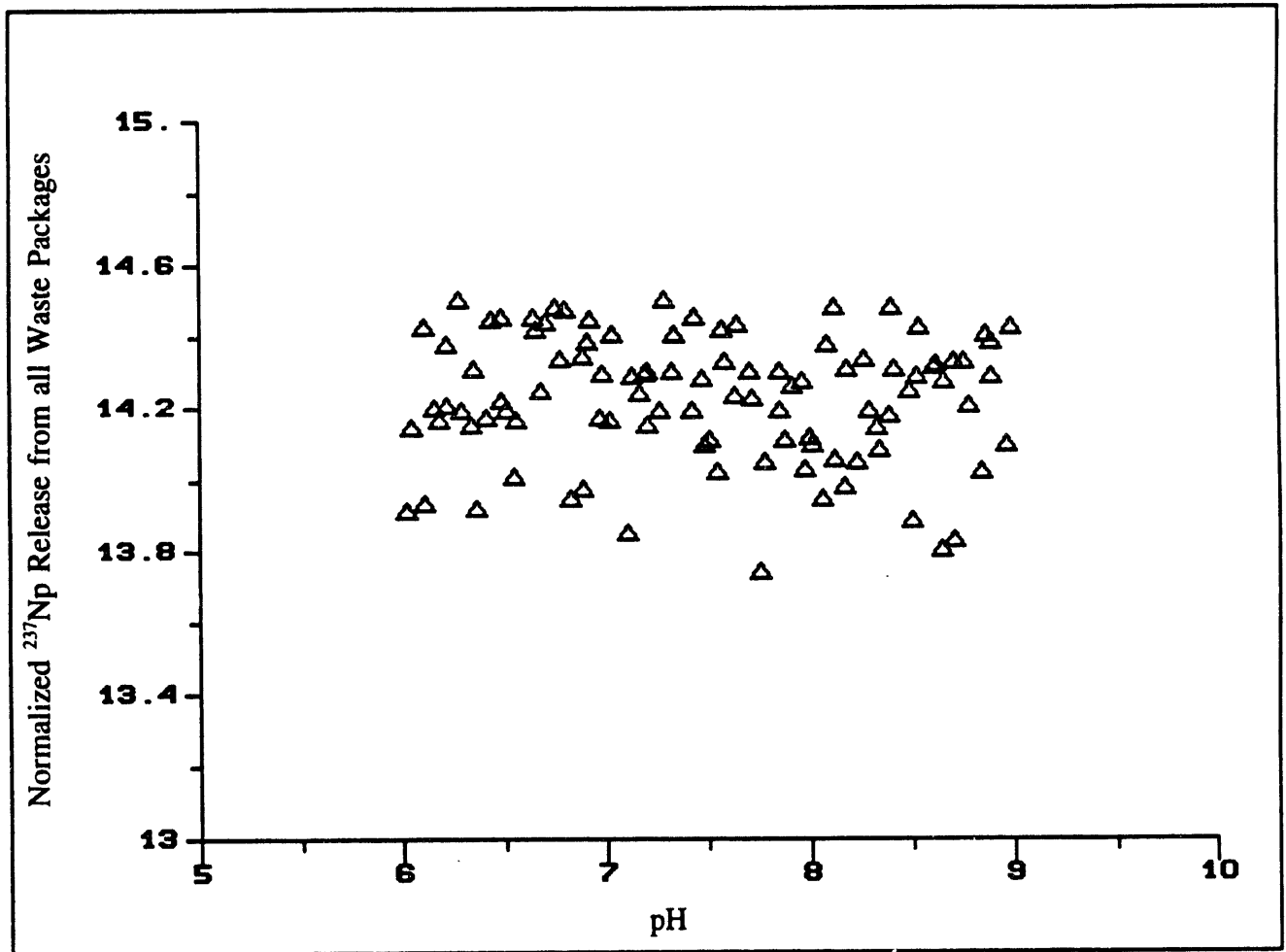


Figure 2-43b. Scatter Plot of pH vs. <sup>237</sup>Np Normalized Release - 114 kW/acre - 100,000 Years

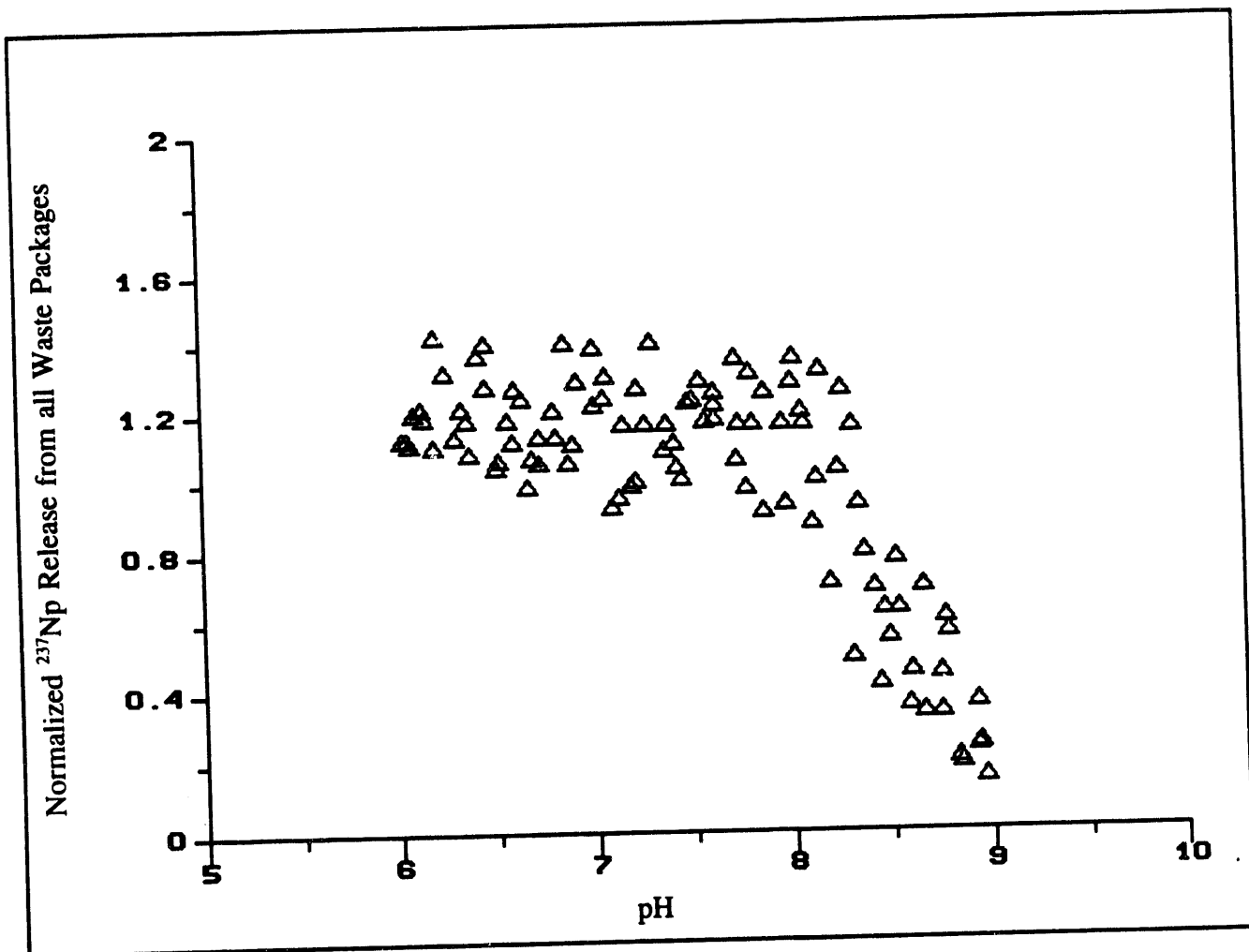


Figure 2-44a. Scatter Plot of pH vs. <sup>237</sup>Np Normalized Release - 28.5 kW/acre - 10,000 Years

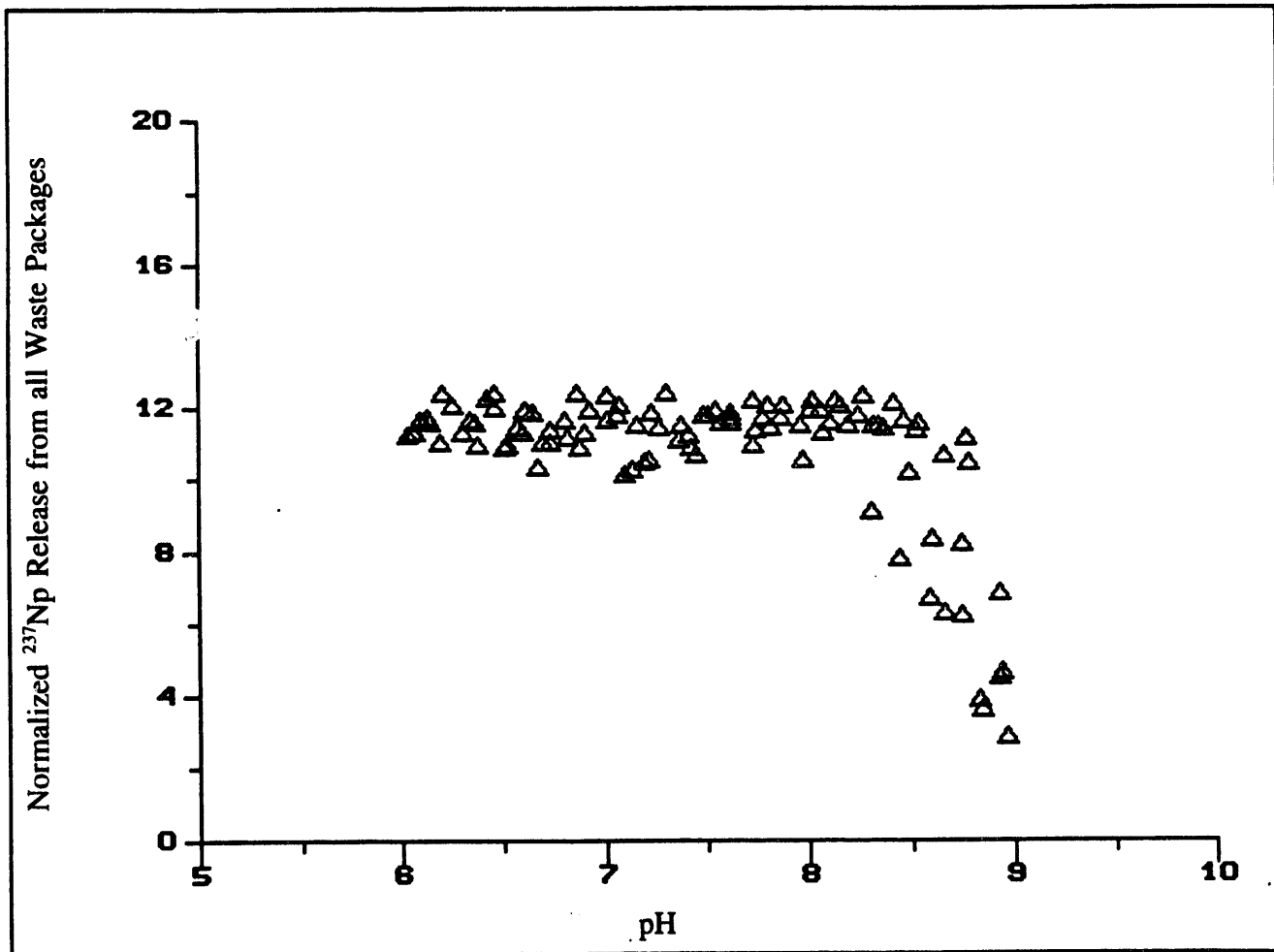


Figure 2-44b. Scatter Plot of pH vs.  $^{237}\text{Np}$  Normalized Release - 28.5 kW/acre  
100,000 Years

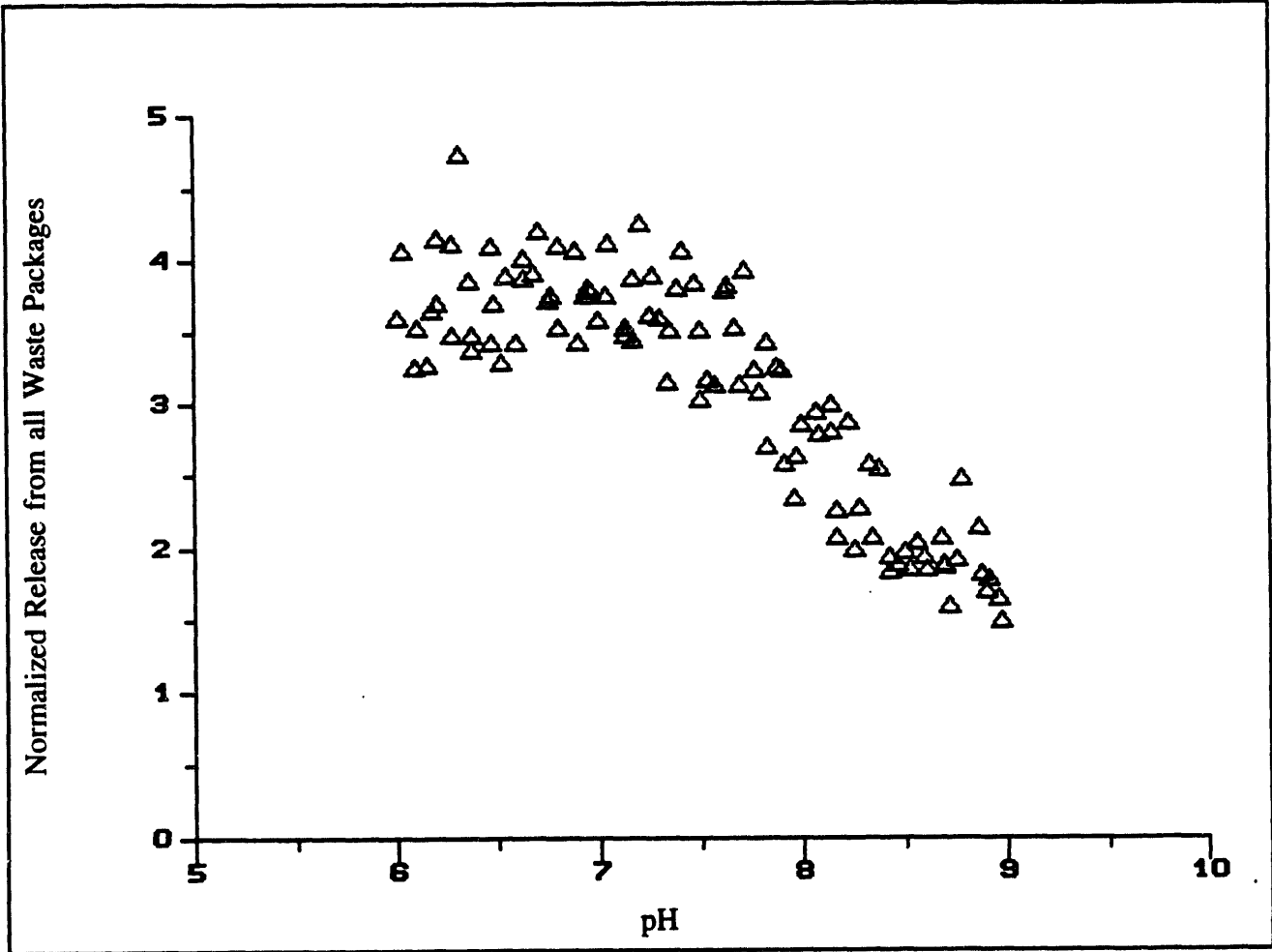


Figure 2-45a. Scatter Plot of pH vs. Total Normalized Release - Lamont Model Case - 10,000 Years

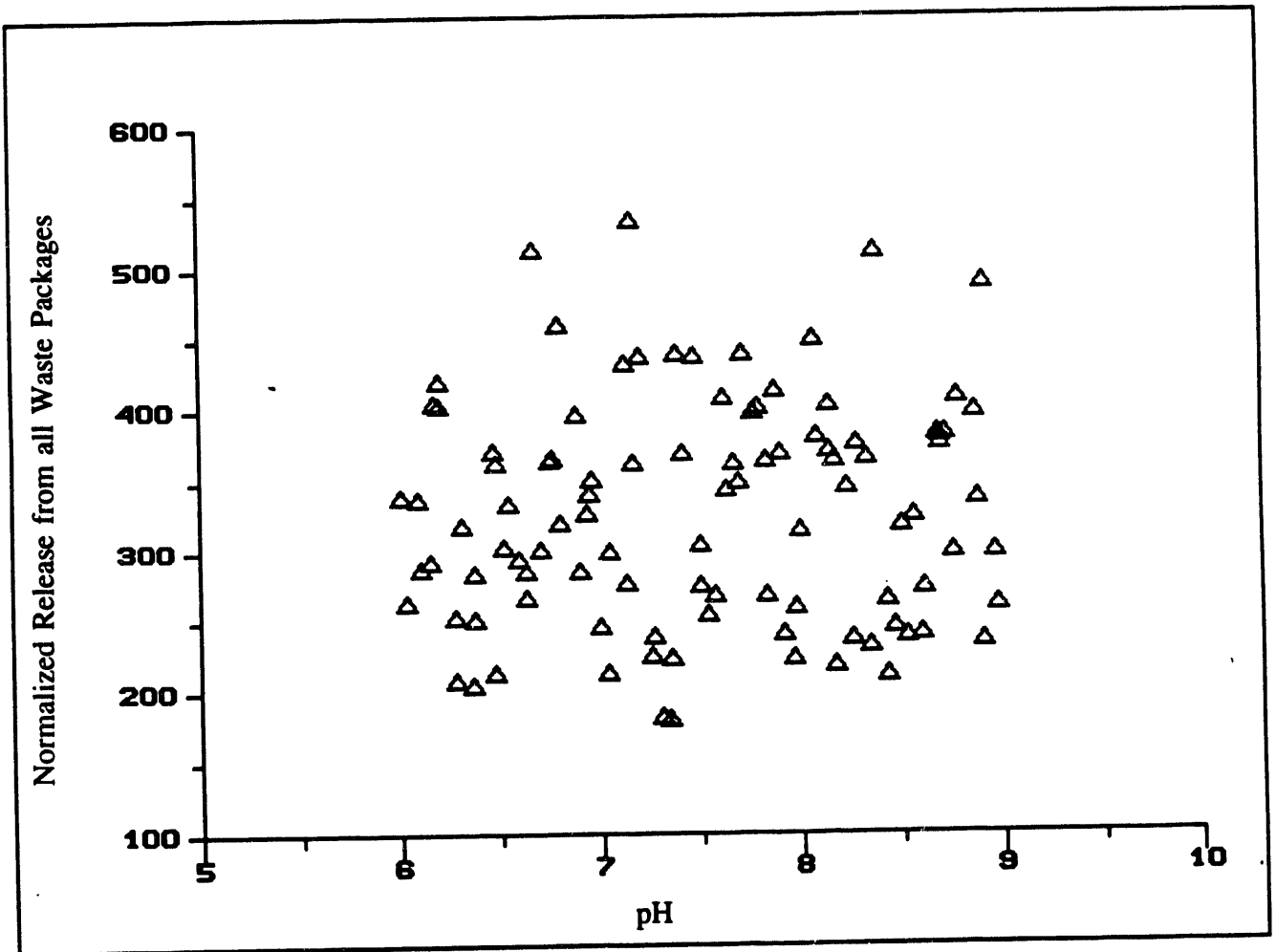


Figure 2-45b. Scatter Plot of pH vs. Total Normalized Release - Lamont Model Case - 100,000 Years

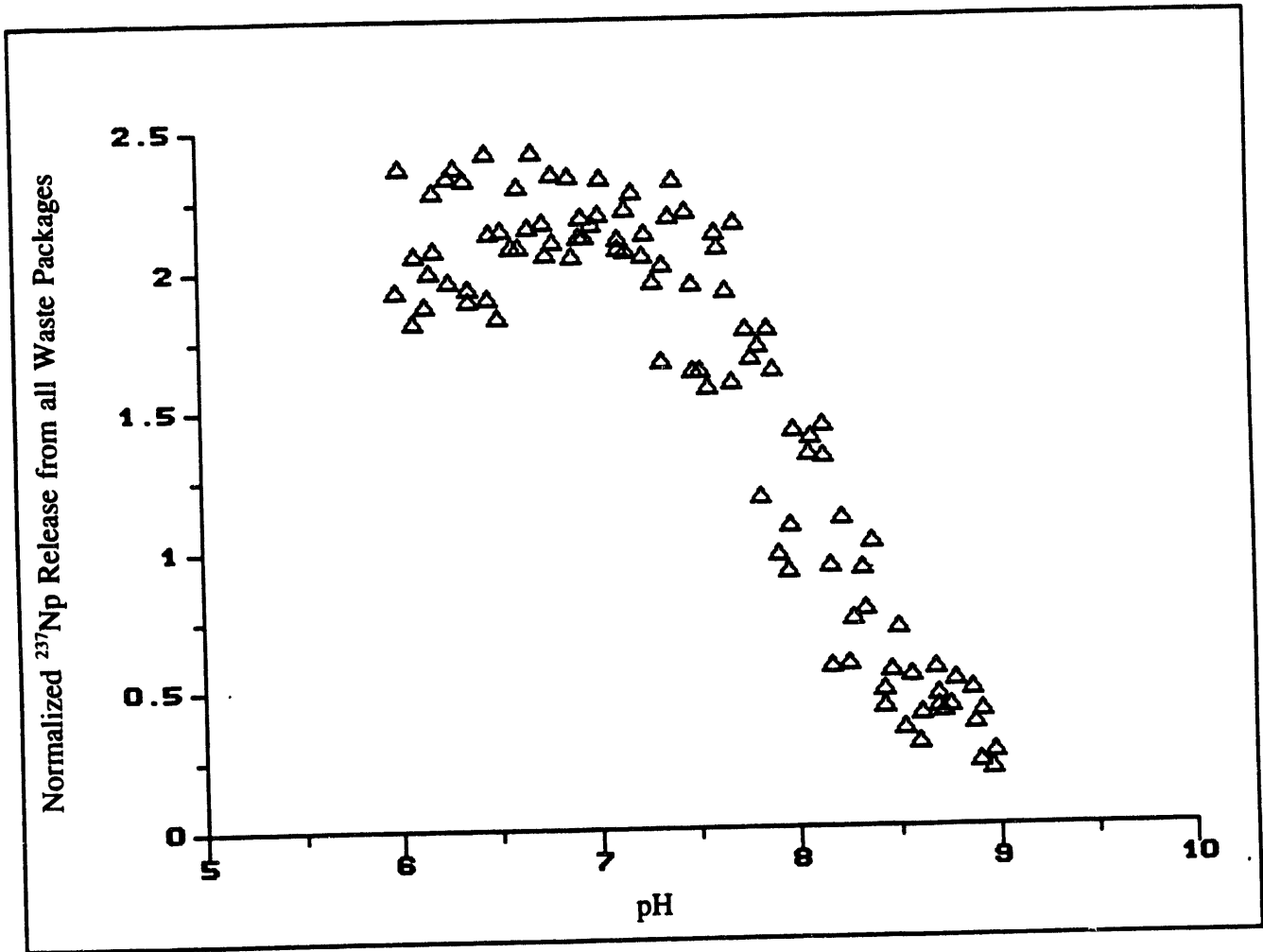


Figure 2-46a. Scatter Plot of pH vs. <sup>237</sup>Np Normalized Release - Lamont Model Case - 10,000 Years

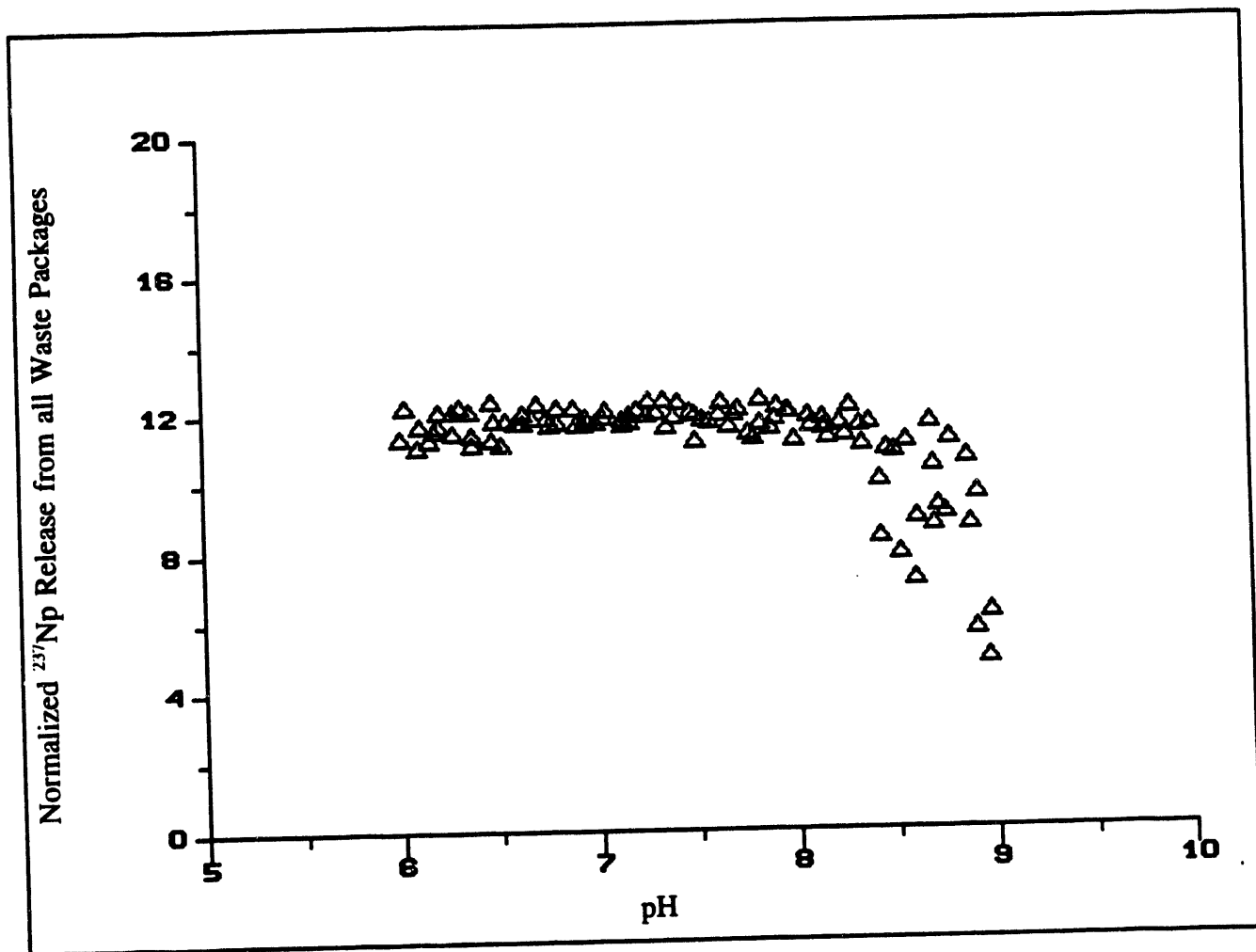


Figure 2-46b. Scatter Plot of pH vs.  $^{237}\text{Np}$  Normalized Release - Lamont Model Case - 100,000 Years

### **3. GASEOUS AND AQUEOUS FLOW AND TRANSPORT**

The gaseous and aqueous radionuclide releases to the accessible environment were determined using the total system performance code RIP. One feature within RIP allows for the different aspects of performance assessment considered in this study (i.e., waste package/engineered barrier system gaseous and aqueous transport, and dose) to be integrated into a single data set. The analyses presented below describe the system parameters for the aqueous transport, the gaseous transport, and the combined results for the radionuclide releases to the accessible environment. The dose analyses are a slight extension of the aqueous transport calculations and will be presented separately.

As discussed in Chapter 2, three different repository thermal-loading scenarios were considered (70.4, 141 and 282 kW/ha, or 28.5, 57, and 114 kW/acre) along with three different outer waste package thickness designs (10 cm, 20 cm and 45 cm) and two inner waste package thickness designs (0.95 cm and 3.5 cm). Two sets of waste package failure initiation scenarios were also investigated (Stahl and Lamont). Due to the large number of comparisons that could possibly be generated from each of these different scenarios, a few key waste package designs and failure initiation distributions had to be selected which would best demonstrate the variance in the radionuclide releases to the accessible environment. The analyses in TSPA 1993 are listed in Table 3-1 with the waste package scenario identifier used in the discussions below.

#### **3.1 UNSATURATED- AND SATURATED-ZONE AQUEOUS FLOW AND TRANSPORT**

##### **3.1.1 Conceptual Description**

For aqueous transport calculations, precipitation infiltrating Yucca Mountain was assumed to pass vertically through the repository. As the infiltrating water passed through the repository, any radionuclides that were present and available for transport were transferred into solution and moved from the EBS to the unsaturated zone beneath the repository. The radionuclides in solution were assumed to be transported vertically downgradient towards the saturated zone. The radionuclides that reached the base of the unsaturated zone were discharged into the saturated zone with the discharge from the saturated zone occurring downgradient at the accessible environment. The radionuclide transport in the unsaturated and saturated zone was considered to be undergoing attenuation due to sorption, including radioactive decay, while neglecting diffusion. These flow and transport assumptions are consistent for each of the different waste package/EBS configurations investigated.

The stratigraphy at Yucca Mountain consists of fractured, welded to nonwelded tuff units that dip easterly at 5° to 30°, with 500 to 750 m of unsaturated-zone thickness (Montazer and Wilson, 1984). The location of the proposed repository is approximately 225 m above the water table and approximately 350 m below the ground surface (Klavetter and Peters, 1986).

The unsaturated-zone stratigraphy between the proposed location of the repository and the water table includes the Topopah Spring Member of the Paintbrush Tuff, the rhyolites of the Calico

Hills, and the Prow Pass and Bullfrog Members of the Crater Flat Tuff. The unsaturated-zone stratigraphic differentiation used in this analysis follows that of the thermomechanical stratigraphy presented in Ortiz et al. (1985), with the addition of the Bullfrog Member. The thermomechanical stratigraphic designation was selected for the transport calculations in order to maintain consistency with the thermohydrologic analyses presented in this report (Appendix A) and by Buscheck and Nitao (1992; 1993).

The unsaturated-zone stratigraphy beneath the repository is separated into six distinct layers with the repository located in the middle unit of the Topopah Spring Member. The Topopah Spring Member includes a thick, devitrified, welded middle unit (TSw2) and a thin, densely welded, basal vitrophyre unit (TSw3). The units of the Calico Hills consist of an upper, nonwelded, vitric layer (CHn1v) and a lower, nonwelded, zeolitic layer (CHn1z). The Prow Pass (PPw) and Bullfrog (Bw) Members are both considered to be welded and devitrified units (Figure 3-1).

For the aqueous transport calculations, nine vertical columns were selected to incorporate the variability in the unsaturated-zone thickness and stratigraphy beneath the repository. The ground surface locations for each of the nine columns are presented in Figure 3-2. These locations are taken as the centroid location of nine panels used in a hydrothermal analysis conducted by Ryder (1993). These nine panels were selected based on the repository design of the Site Characterization Plan (DOE, 1988b) for a thermal loading of 141 kW/ha (57 kW/acre). A set of USGS (1993) published cross sections oriented along the proposed ramps and drifts in the Topopah Springs and Calico Hills units (Figure 3-1) were used to determine the stratigraphic thicknesses of the six layers directly beneath each centroidal location. Using the cross-sectional lines and a linear extrapolation, the stratigraphic thickness of each layer was determined for all nine columns (Table 3-2).

The stratigraphic designations and groupings on the USGS (1993) cross-sectional lines do not correlate directly to those of the thermomechanical stratigraphy (Ortiz et al., 1985). Therefore, a correlation between the two stratigraphic groupings was generated (Table 3-3). Several modifications were necessary to maintain consistency with the thermomechanical stratigraphy. The single Calico Hills unit (Tht) present in the USGS (1993) stratigraphy was divided into the two individual vitric (CHn1v) and zeolitic (CHn1z) layers of the thermomechanical stratigraphy. The hydrothermal analysis presented in Appendix A used a split of 3.4 percent of the total thickness of the (Tht) assigned to the vitric layer and the remaining 96.6 percent assigned to the zeolitic layer. These same percentages were used in determining the fraction of the single Calico Hills (Tht) layer assigned to the individual vitric (CHn1v) and zeolitic (CHn1z) layers in this analysis. The basal vitrophyre of the Topopah Spring (TSw3) and a portion of the upper vitric layer in the Calico Hills (CHn1v) were combined into a single unit (Tv) in the USGS (1993) cross sections. For consistency with the thermomechanical stratigraphy designations, the basal vitrophyre (TSw3) unit was maintained at a constant thickness of 10 m (D. Hoxie, personal communication, 1993) with the remaining thickness of the Tv unit added to the CHn1v unit. The thickness of the lowermost units in the unsaturated zone (PPw or Bw) was dependent on the location of the water table. Using three points where the water-table elevation was known (Table 3-4), the water-table elevations, and thus the thickness of the lower layer at the centroidal locations were estimated (Table 3-2).

Thermal effects on the movement of water in the unsaturated zone due to various repository thermal loadings were investigated (Appendix A). The analysis provided profiles of temperature, Darcy flux, and liquid saturation in each stratigraphic layer as a function of time for each thermal load, assuming a zero background or ambient infiltration. These profiles were used to determine the extent and duration of the dryout zone within the near-field environment. However, in TSPA 1993, ambient unperturbed hydrologic conditions were maintained in the far field once the radionuclides were released from the EBS to the geosphere. The effects of an ambient infiltration on the thermal perturbation of the far-field hydrologic conditions is still uncertain. Further analyses of the non-zero ambient infiltration effect on the transient nature of temperature, liquid flux, and liquid saturations are necessary to better define the far-field environment.

### 3.1.2 Parameter Values

The aqueous transport model input parameters used in this TSPA analysis are a combination of parameters from the TSPA 1991 (Barnard et al., 1992) analysis, expert elicitation workshops, and recently published studies. The primary emphasis in the generation of this report was to demonstrate the effects of various repository thermal-loading scenarios on the radionuclide releases from the EBS and to the accessible environment.

The one-dimensional advective-dispersion transport option within RIP was selected to perform the aqueous transport calculations. This option requires the input of the pathway volumetric flow rate and pathway area to generate the velocity term in the transport equation. Also required were the longitudinal dispersivity and the individual radionuclide retardation coefficients in each layer.

The effective ground-water velocity for each layer in the unsaturated and saturated zones was calculated using the following relation:

$$V_j = \frac{u_j}{n_j S_j}$$

where  $V_j$  is the effective ground-water velocity (m/yr),  $u_j$  is the Darcy (or percolation) flux (m/yr),  $n_j$  is the bulk porosity, and  $S_j$  is the liquid saturation.

The Darcy flux for both the unsaturated and saturated zones was taken as a constant value per realization selected from a specified distribution. Table 3-5 presents the flux distributions for both the unsaturated and saturated zones. The unsaturated-zone Darcy flux distribution was determined by selecting an exponential distribution with a mean value of  $5 \times 10^{-4}$  m/yr (0.5 mm/yr) (Wilson et al., 1994, in press). The saturated-zone Darcy flux distribution was obtained from the saturated-zone flow analysis conducted by Barr (1993). The flux values in each of the individual grid blocks within the entire model domain were averaged to obtain a mean value of 2.0 m/yr with minimum and maximum values of  $4.7 \times 10^{-6}$  m/yr and 390 m/yr, respectively. Due to the large range of values used in the averaging process, a modification of the distribution was conducted to narrow the range.

The potential increase in the infiltration at Yucca Mountain due to climatic changes has been incorporated into the analysis. Long and Childs (1993) expect a 2.5 times increase in the rate

of infiltration under full glacial (pluvial) conditions. These glacial conditions were not considered to occur for another 50,000 to 100,000 years (Long and Childs, 1993). To incorporate the potential increase in the infiltration into this analysis, an infiltration flux multiplier distribution was defined with a mean of 2.5, and a minimum and maximum of 1.0 and 5.0. A single value from this distribution was selected for each realization and multiplied by the unsaturated-zone flux to obtain the increase in flux due to climatic changes. It was considered that the unsaturated-zone flux would not drop below current conditions, as defined in this analysis. The transition from present day conditions to a glacial climate was considered to occur gradually (linearly) over a 100,000-year period. Over the next 100,000 years, the conditions would linearly transition back to present day conditions. This cycle was repeated throughout the entire 1,000,000-year simulation time.

At the start of each realization, a single unsaturated-zone flux and flux multiplier value is selected from the respective distributions. As the climate transitions over the first 100,000 years to glacial conditions, the unsaturated-zone flux is linearly increased from the unmodified value to the modified value calculated using the multiplier. During the next 100,000 years, the unsaturated-zone flux value is linearly decreased from the higher modified flux value back to the unmodified flux. Figure 3-3 demonstrates this transitioning for a selected unsaturated-zone flux of  $5.0 \times 10^{-4}$  m/yr (0.5 mm/yr), a flux multiplier of 5.0, and a simulation time of  $10^6$  years. Since the transition time occurs over a 100,000-year time frame, the releases to the accessible environment generated at 10,000 and 100,000 years should not show the effects of climate change.

Table 3-6 presents a correlation of the TSPA 1991 stratigraphy designations and the stratigraphy used in this report. The bulk porosity data for the unsaturated zone were taken directly from the TSPA 1991 analysis (Barnard et al., 1992). Included in Table 3-7 is a listing of the bulk porosity data distributions input into the aqueous transport calculations. For each realization, a single porosity value was selected per layer and held constant throughout the simulation. The saturated-zone bulk porosity was held constant at two percent, based on the saturated-zone flow analysis conducted by Barr (1993).

The liquid saturation (Table 3-8) for each unsaturated zone layer was selected as the averaged, pre thermal loading ambient steady-state saturation determined from the hydrothermal analysis (Appendix A). The saturation values were determined for no background infiltration and therefore are lower than the values expected for the system with a background infiltration higher than zero. The use of lower than expected saturation values will lead to an increase in the particle velocity and a corresponding decrease in the particle travel times to the accessible environment. The saturation for each unsaturated-zone layer was held constant at the steady-state value for each realization.

Since the aqueous transport is specified to be one-dimensional, only the longitudinal component of dispersion is considered in the transport calculations. The transport of radionuclides is considered to be dominated by advection, therefore diffusion is not considered. The longitudinal dispersivity was arbitrarily specified as 10 percent of the individual unsaturated-zone layer thicknesses and 10 percent of the saturated-zone length.

The use of distribution coefficients ( $k_d$ ) is a simplified approach in estimating the amount of radionuclide partitioning that occurs between the solid (rock) and liquid (water) phases during transport. Table 3-9 presents a listing of the  $k_d$  distributions used for each radionuclide for three different types of tuff: devitrified (D), vitric (V), and zeolitic (Z). These values were obtained from expert-elicitation workshops (Appendix H). The quantities in parentheses in Table 3-9 are modifications to the original data required prior to implementation within RIP. These numbers are very similar to the values used in the TSPA 1991 document (Barnard et al., 1992).

Bulk density data for each stratigraphic unit were determined from the Technical Data Base (CRWMS M&O, 1993) and Healey et al. (1986). Direct measurements were taken from Well USW G-4 and the sample depths were correlated to the USGS (1993) stratigraphy. The measurements were averaged within each stratigraphic unit to obtain the bulk density values (Table 3-10).

The retardation factors for each radionuclide and each stratigraphic unit were determined based on the following:

$$R_{ij} = 1 + \frac{\rho_{bj}}{n_{bj}} \cdot k_{dij}$$

where  $R_{ij}$  is the retardation for radionuclide  $i$  for stratigraphic unit  $j$ ,  $k_{dij}$  is the distribution coefficient for radionuclide  $i$  for stratigraphic unit  $j$  (mL/g),  $\rho_{bj}$  is the bulk density of stratigraphic unit  $j$  (g/mL), and  $n_{bj}$  is the bulk porosity of stratigraphic unit  $j$ . Table 3-11 presents expected-value retardation factors for several key radionuclides for each stratigraphic unit considered. The expected value is the retardation factor determined using the mean values of the included parameter distributions. These values are similar to the retardation factors used in TSPA 1991 (Barnard et al., 1992).

### 3.1.3 Aqueous Flow Regime

For aqueous transport, the release of radionuclides from the repository was assumed to be divided equally among nine vertical columns (Figure 3-4). These nine, equal-area one-dimensional columns were used to simulate the transport of nuclides through the unsaturated zone. The radionuclides that reached the base of these nine unsaturated-zone columns were released to a single saturated-zone pathway (Figure 3-4). The accessible environment for aqueous releases was designated to be located at the end of the single saturated-zone pathway.

The aqueous transport of radionuclides within the unsaturated and saturated zones was assumed to be in equilibrium between the fractures and matrix such that an equivalent-continuum medium (single porosity) could be utilized. The transport algorithm incorporated the one-dimensional, advection-dispersion equation with the addition of retardation and radioactive decay.

The flow in the nine unsaturated-zone columns was assumed to be one-dimensional with no cross-flow between columns. In columns 4 and 5 (Table 3-2), the water table is located within the Bullfrog welded tuff (Bw). The Bullfrog welded tuff was assumed to be equivalent to the Prow Pass welded tuff (PPw).

The saturated zone was assumed to be a single, horizontal pathway extending 5000 m from beneath the repository to the accessible environment. The hydrologic parameters of the saturated zone were assumed to be equivalent to the Prow Pass welded tuff. The radionuclide releases from each of the nine unsaturated-zone columns were discharged into the same location within the saturated zone, 5000 m upgradient from the accessible environment.

## **3.2 UNSATURATED-ZONE GASEOUS FLOW AND TRANSPORT**

### **3.2.1 Conceptual Description**

The transport of gas from the repository to the ground surface at Yucca Mountain has been investigated because of fast travel-time estimates of gas transport, relative to aqueous transport, in the unsaturated zone (Ross, 1993). The analysis presented below only considered the release of  $^{14}\text{C}$  from the repository due to a relatively large inventory in the spent fuel and the fact that the release of  $^{14}\text{C}$  is governed by the alteration of the waste and not by solubility controls. Also, a significant portion of the  $^{14}\text{C}$  is located outside of the actual waste form and is immediately available for release once the inner container has failed.

For gaseous ( $^{14}\text{C}$ ) transport in the unsaturated zone at Yucca Mountain, the results presented by Ross (1993) formed the foundation for this section of the TSPA analysis. Ross (1993) conducted simulations which determined the travel-time distribution for the movement of  $^{14}\text{C}$  to the atmosphere, part of the accessible environment, as a function of release time from the repository. Figure 3-5 presents Ross' (1993) repository areal conceptualization for a thermal loading of 141 kW/ha (57 kW/acre), showing the location of the three cross sections used in determining the stratigraphic pathways for the  $^{14}\text{C}$  transport (Figure 3-6). These three pathways extended from below the repository to the ground surface. In every 25-m section where these vertical sections intersected the repository,  $^{14}\text{C}$  was released at a random location within the 25-m interval and the travel time to the surface was determined. This procedure was repeated every 1,000 years, for 18,000 years, in order to capture the repository thermal effects on the flow of gas within Yucca Mountain.

Figure 3-7 presents a probability density function (PDF) for the travel time of  $^{14}\text{C}$  released at 1,000 years. This PDF incorporates the effects of retardation, thermal loading and surface topography on the particle travel times. Figure 3-8 presents the conversion of this PDF to a cumulative density function (CDF). A CDF similar to Figure 3-8 was generated for each of the 18 travel-time PDFs, representing the  $^{14}\text{C}$  travel times from 1,000 to 18,000 years (Appendix I).

A single repository thermal load of 141 kW/ha (57 kW/acre) was used in the Ross (1993)  $^{14}\text{C}$  travel-time calculations. However, in this TSPA analysis, three thermal-loading scenarios were considered (70.4, 141 and 282 kW/ha or 28.5, 57, and 114 kW/acre). In each thermal-loading scenario, the  $^{14}\text{C}$  travel-time distributions generated for a thermal loading of 141 kW/ha (57 kW/acre) were incorporated into the data set. The use of the 141 kW/ha (57 kW/acre) travel-time distributions for the lower and higher thermal loadings does incorporate some error into the analysis results. For the 141 kW/ha (57 kW/acre) thermal load, the largest travel-time is approximately 2,000 years, for  $^{14}\text{C}$  released at 18,000 years. With the increase to a 282 kW/ha (114 kW/acre) thermal loading, the travel times would be expected to be faster. With a decrease

to a 70.4 kW/ha (28.5 kW/acre) thermal loading the travel times would be expected to be slower. However, the expected change in the travel times is not considered to incorporate significant errors in the overall shape of the  $^{14}\text{C}$  release curves. Therefore, the 141 kW/ha (57 kW/acre) travel-time calculations for  $^{14}\text{C}$  were incorporated into the other repository thermal-loading scenarios.

### 3.2.2 Unsaturated-Zone Gaseous Flow Regime

The  $^{14}\text{C}$  inventory of 1.48 Ci/MTHM was located entirely within the spent fuel waste packages (Rings 1 through 6). A fraction of the  $^{14}\text{C}$  inventory was located between the inner container and the actual waste forms, thereby allowing instantaneous release of this fraction upon failure of the inner container. The quick-release fraction was calculated as a uniform distribution ranging from 1.25 to 5.75 percent of the total inventory. This distribution was specified as a percentage of the total  $^{14}\text{C}$  inventory used in the release calculations and is the same percentage used in the analysis performed in TSPA 1991 (Barnard et al., 1992).

The unsaturated-zone gaseous transport calculations were performed in the same manner as the aqueous transport calculations. Within RIP, the one-dimensional, advection-dispersion transport equation was used. Each of the eighteen travel-time CDF curves were broken down into a series of five or six step functions that described the general shape of the CDF curve (Figure 3-9). The step function values (travel time vs. cumulative probability) for the CDF in Figure 3-9 are tabulated and presented in Table 3-12.

Ross (1993) provided a single  $^{14}\text{C}$  travel-time for the particles released within the repository at 1,000-year increments, from 1,000 to 18,000 years. In TSPA 1993, if the release of  $^{14}\text{C}$  from the EBS occurred within plus or minus 500 years of one of the 1,000-year release times, the released  $^{14}\text{C}$  traveled according to the travel-time distribution for that release time. For example, if a quantity of  $^{14}\text{C}$  was released between 1,500 and 2,500 years, it would travel according to the travel-time distribution for  $^{14}\text{C}$  released at 2,000 years in Ross' (1993) simulations. Table 3-13 presents the time frames over which each travel-time distribution was applied. Sometimes the travel-time distributions for more than one release period were very similar. This is the case for release times of 1,000 and 4,000 years and for 2,000 and 3,000 years. If two curves were very similar, they were combined into a single curve and applied over the time frames associated with both curves.

As stated above, the travel-time distributions incorporated the variability in the distance between the repository and the ground surface based on the topography of Yucca Mountain. In this analysis, the use of the generated travel-time distributions allows for this variable distance to be removed from the calculations. If these step-function travel times are inverted to obtain one over the travel time, a unit average linear velocity can be calculated that specifies the magnitude of the gaseous flow (length per time) through a 1.0-m or unit thickness layer. The calculation of the velocity was generated assuming a bulk porosity of 1.0. This was necessary since RIP transport calculations require a pathway travel velocity, formation bulk porosity, and length. Table 3-12 presents the calculated average linear velocities for  $^{14}\text{C}$  that corresponds to the travel-time PDF presented in Figure 3-9.

The unsaturated-zone gaseous transport within RIP was performed by discharging the  $^{14}\text{C}$  released from the EBS into one of a number of pathways. The pathway at which the  $^{14}\text{C}$  was discharged into was a function of the time since the simulation started (Table 3-13). Each pathway contained a different average linear velocity distribution, so as the  $^{14}\text{C}$  was discharged into the pathway, the velocity was dependent on the value selected from the distribution. As the simulation time increased, the discharged  $^{14}\text{C}$  was shifted between pathways. Once an amount of  $^{14}\text{C}$  was discharged into a pathway and assigned an average linear velocity, it maintained a constant velocity until released into the accessible environment. Figure 3-10 presents a schematic of the  $^{14}\text{C}$  pathway and average linear velocity designations for a release time frame of 5,500 to 6,500 years.

### 3.3 RESULTS

#### 3.3.1 Results of Releases to the Accessible Environment at 10,000 Years

The transport of radionuclides in both the gaseous and aqueous phases have been combined into a single data set. The gaseous and aqueous transport occurs in different pathways within RIP model. This section presents the releases to the accessible environment as an extension of the releases from the EBS presented in Chapter 2. The releases from the EBS were presented for 17 different waste package/EBS configuration scenarios. However, the TSPA analyses for only 6 of these cases were extended into the geosphere (Table 3-14). The radionuclide releases to the accessible environment are calculated for simulation times of 10,000 years and 100,000 years. For each EBS scenario and simulation time investigated, both expected-value time-history plots of mass release rate vs. time, and CCDF plots of the total normalized mass release for 100 realizations have been generated. To demonstrate the variation in the release to the accessible environment based on varying the waste package/EBS configuration, only the releases for  $^{14}\text{C}$ ,  $^{99}\text{Tc}$ ,  $^{237}\text{Np}$ , and the total summation of all nuclides will be presented in the results analysis. These radionuclides were selected as examples of gaseous ( $^{14}\text{C}$ ), alteration-limited ( $^{99}\text{Tc}$ ), and solubility-limited ( $^{237}\text{Np}$ ) radionuclides. These three are determined to be the major release and dose contributors from the analyses performed, but the releases to the accessible environment from all 39 radionuclides in the waste package are included in the "total" curves.

A shorthand will be used to describe the waste package/EBS configurations/scenarios. In parentheses will be shown the thermal loading in kW/acre, the outer container barrier thickness in centimeters, the inner container barrier thickness in centimeters, and the corrosion model and initiating mode (S = Stahl, L = Lamont, 1 = saturation, 2 = temperature). The reference case (57/10/0.95/S1) will be used as the simulation with which all other runs will be compared. Figure 3-11 presents an expected-value plot for the releases to the accessible environment during the first 10,000 years after closure. The expected-value curves are the results generated from a single realization using the mean or expected value of all stochastic input parameters. In the first 10,000 years, the release to the accessible environment is dominated by the gaseous release of  $^{14}\text{C}$ , with only a minor contribution from the release of  $^{99}\text{Tc}$  from the aqueous domain. By integrating the area underneath the curve, the cumulative mass released to the accessible environment can be calculated. This integration is performed for each radionuclide and then normalized to the Table 1 EPA limits for releases to the accessible environment at 10,000 years. Table 3-14 presents the normalized cumulative releases for the total release and the release of

$^{14}\text{C}$ ,  $^{99}\text{Tc}$ , and  $^{237}\text{Np}$  at 10,000 years for the reference case (57/10/0.95/S1). The total normalized cumulative release to the accessible environment was 2.37 with virtually all of this attributable to the gaseous release of  $^{14}\text{C}$ . The aqueous release of  $^{99}\text{Tc}$  is insignificant with a normalized release of less than  $10^{-6}$  and no measurable release of  $^{237}\text{Np}$  occurs over 10,000 years.

Using the same data set as the expected-value case, a simulation comprised of 100 realizations is generated which incorporates the stochastic nature of the input parameters. Figure 3-12 shows the CCDF of the cumulative normalized release of  $^{14}\text{C}$ ,  $^{99}\text{Tc}$ , and the total to the accessible environment. As in the expected-value simulation, the total release to the accessible environment is dominated by  $^{14}\text{C}$  with only a slight increase in the maximum release in  $^{99}\text{Tc}$ . Several realizations have releases of  $^{237}\text{Np}$  to the accessible environment, but these are significantly lower than a cumulative normalized release of  $10^{-6}$ . The magnitude of the early-time gaseous releases in this analysis is primarily a function of the frequency of the waste package failures. If the waste packages fail at early times, the transport velocities will be higher and the amount of  $^{14}\text{C}$  decay that has occurred is smaller. Therefore, if a large number of waste packages fail at or during an early-time period, a large portion of the  $^{14}\text{C}$  quick-release fraction will be released early, creating an initial early-time spike (Figure 3-11).

The effects of repository thermal loading on the releases to the accessible environment are determined by increasing (282 kW/ha or 114 kW/acre) and decreasing (70.4 kW/ha or 28.5 kW/acre) the thermal load. Figure 3-13 combines the expected-value curves for the total release and the release of  $^{14}\text{C}$  to the accessible environment for 57/10/0.95/S1, 28.5/10/0.95/S1, and 114/10/0.95/S1. This figure shows that as the repository thermal loading is varied, with all other factors being the same, the release to the accessible environment is predominantly comprised of  $^{14}\text{C}$ . For the higher and lower thermal load, there is no  $^{99}\text{Tc}$  or  $^{237}\text{Np}$  released to the accessible environment. The total normalized cumulative release for the expected-value cases (Table 3-14) show that the thermal loading of 141 kW/ha (57 kW/acre) yields the highest total release at 10,000 years, with 282 kW/ha (114 kW/acre) and 70.4 kW/ha (28.5 kW/acre) releasing approximately 55 and 74 percent less, respectively.

Figure 3-14 presents three CCDF curves for the  $^{14}\text{C}$  and total normalized cumulative release to the accessible environment for the 57/10/0.95/S1, 28.5/10/0.95/S1, and 114/10/0.95/S1 scenarios, using 100 realizations. As in the expected-value case, the release of  $^{14}\text{C}$  dominates the total release to the accessible environment for all three thermal-loading scenarios. The releases from the thermal loads of 141 kW/ha (57 kW/acre) and the 282 kW/ha (114 kW/acre) are above the EPA limits, as shown in the cross-hatched area in Figure 3-14. The thermal load of 141 kW/ha (57 kW/acre) has a greater probability of releasing a larger amount of mass than either the 70.4 kW/ha (28.5 kW/acre) or the 282 kW/ha (114 kW/acre) loading. Since more waste packages fail sooner in the 141 kW/ha (57 kW/acre) scenario, more  $^{14}\text{C}$  is available for transport at the higher linear-particle velocities used in the gaseous transport.

The effects of varying the waste package inner or outer container thickness on the releases to the accessible environment have been investigated. While maintaining a thermal load of 141 kW/ha (57 kW/acre), three waste package container-thickness variations are generated. The outer thickness is increased from 10 cm (57/10/0.95/S1), to 20 cm (57/20/0.95/S1), and then to 45 cm (57/45/0.95/S1). The inner thickness is also increased from 0.95 cm to 3.5 cm, while maintaining

the outer thickness at 10 cm (57/10/3.5/L1). This last simulation also investigated the use of the Lamont waste package failure distributions.

Figure 3-15 presents the expected-value plots for the total and  $^{14}\text{C}$  release rates to the accessible environment for the four simulations. The curve for 57/45/0.95/S1 is not presented since no waste package failures occur within the first 10,000 years. Figure 3-15 and Table 3-14 show that the release of  $^{14}\text{C}$  dominates the total release to the accessible environment for 10,000 years. As the thickness of either the inner or outer waste package increases, the time to waste package failure increases, causing a decrease in the release to the accessible environment. The normalized cumulative release of  $^{99}\text{Tc}$  is less than  $10^{-6}$  for all cases and there is no release of  $^{237}\text{Np}$  to the accessible environment within 10,000 years. The total normalized cumulative release of  $^{14}\text{C}$  to the accessible environment decreased by approximately 60 percent for the 20-cm outer thickness and 45 percent for the 3.5-cm inner thickness.

Figure 3-16 presents the results of 100 realizations for the four different waste package thickness scenarios. The plot shows the CCDFs of the  $^{14}\text{C}$  and total normalized cumulative releases to the accessible environment for 57/10/0.95/S1, 57/20/0.95/S1, and 57/10/3.5/L1. The CCDFs show that the release to the accessible environment is also controlled by  $^{14}\text{C}$  and that the thicker inner or outer waste package barriers yield lower releases over 10,000 years. The scenario with a 45-cm outer waste package thickness (57/10/3.5/L1) still had no releases to the accessible environment within 10,000 years.

The release of radionuclides to the accessible environment within the first 10,000 years after waste emplacement is dominated by  $^{14}\text{C}$ . Varying the thermal load and waste package container thickness did have an effect on the total amount and rate of  $^{14}\text{C}$  released. When the repository thermal loading was increased and decreased, the large spike of  $^{14}\text{C}$  released at early times was not present due to an increase in the time of container failure initiation. This resulted in the 141 kW/ha (or 57 kW/acre) thermal load yielding the highest total releases to the accessible environment. As the waste package container thicknesses were increased from the reference case values, the total normalized cumulative releases to the accessible environment decreased. This is especially true of the 45-cm outer thickness container in which no waste package failures occurred within 10,000 years.

### 3.3.2 Results of Releases to the Accessible Environment at 100,000 Years

The same comparisons between different thermal loading and waste package thickness scenarios have been carried out for a total simulation time of 100,000 years. The reference case (57/10/0.95/S1) simulation was continued from 10,000 years to 100,000 years, and will again be used as the reference case. Figure 3-17 presents the expected-value plots for the total,  $^{14}\text{C}$ , and  $^{99}\text{Tc}$  release to the accessible environment. At early times (<20,000 years), the release is dominated by  $^{14}\text{C}$ , as discussed above, but at late times (>20,000 years) the release is dominated by  $^{99}\text{Tc}$ . The release of  $^{237}\text{Np}$  to the accessible environment is measurable, but insignificant within 100,000 years. Table 3-14 shows that the total normalized cumulative release for the expected-value simulation is approximately 70 percent  $^{14}\text{C}$  and 20 percent  $^{99}\text{Tc}$ . The mass releases calculated at 100,000 years and normalized in Table 3-14 were normalized to the EPA limit designed for the releases to the accessible environment at 10,000 years. Since there is no

standard for normalizing releases at times other than 10,000 years, the 10,000-year EPA limit was maintained in the analysis.

The effects of the three thermal-loading scenarios, 57/10/0.95/S1, 28.5/10/0.95/S1, and 114/10/0.95/S1, on the releases to the accessible environment at 100,000 years have been investigated. Figure 3-18 presents the expected-value plots for the total releases to the accessible environment for the three thermal loads. The lower and higher thermal loads also show a bimodal release curve with  $^{14}\text{C}$  dominating at early times and  $^{99}\text{Tc}$  dominating at late times. As in the 10,000 year simulations, the normalized cumulative release of  $^{14}\text{C}$  to the accessible environment was highest for the 141 kW/ha (57 kW/acre) thermal load (Table 3-14). For the release of  $^{99}\text{Tc}$ , the 282 kW/ha (114 kW/acre) thermal load yielded the highest releases. The total normalized cumulative release for the expected-value cases show that the thermal loading of 141 kW/ha (57 kW/acre) yields the highest total release at 100,000 years, with 282 kW/ha (114 kW/acre) and 70.4 kW/ha (28.5 kW/acre) releasing approximately 33 and 62 percent less, respectively.

The radionuclide releases to the accessible environment as a function of waste package inner or outer container thickness also have been investigated for the 100,000-year time frame. The analysis is exactly as for the 10,000 year simulation with the same four container thickness scenarios considered (57/10/0.95/S1, 57/20/0.95/S1, 57/45/0.95/S1, and 57/10/3.5/L1). Figure 3-19 presents the total expected-value plots for the release to the accessible environment based on the four waste package designs. The 20-cm outer container thickness simulation (57/20/0.95/S1) results are similar to the reference case except for a slight delay in arrival at the accessible environment and 45 percent less  $^{14}\text{C}$  released during the time period up to 20,000 years (Table 3-14). The 3.5-cm inner container thickness simulation (57/10/3.5/L1) is also similar to the reference case but with approximately 40 percent less  $^{14}\text{C}$  and 20 percent less  $^{99}\text{Tc}$  released. The increase in the outer container thickness to 45 cm (57/45/0.95/S1) had a significant impact on the total releases to the accessible environment. Due to the longer waste package container lifetimes, the release of  $^{14}\text{C}$ , with a half-life of 5,700 years, was almost eliminated. The initial release of a significantly measurable amount to the accessible environment occurred at greater than 70,000 years (Figure 3-19), with  $^{99}\text{Tc}$  contributing the majority of the total release (Table 3-14).

The relative effects of repository thermal loading and waste package container thickness on the releases to the accessible environment at 100,000 years are similar to the 10,000-year simulations. The reference case thermal loading scenario (57/10/0.95/S1) yielded total normalized cumulative releases to the accessible environment that are greater than the 70.4 kW/ha (28.5 kW/acre) and 282 kW/ha (114 kW/acre) thermal load cases. The waste package configuration with the thinnest outer and inner containers (57/10/0.95/S1) yielded the highest releases due to the higher waste package failure rates at early times. As the inner or outer container thicknesses are increased, the overall release to the accessible environment decreased and its arrival to the accessible environment is delayed, especially for the 45-cm outer container thickness.

Using simulations of 100 realizations, a set of CCDF curves representing the effects of varying the repository thermal load and the waste package container thickness at 100,000 years on the releases to the accessible environment have been generated. These simulations were conducted

with the  $^{14}\text{C}$  inventory removed. This will allow for the total releases at the accessible environment to be based solely on aqueous releases.

A simulation of 100 realizations was conducted using the reference case data set (57/10/0.95/S1) for a simulation time of 100,000 years. Figure 3-20 presents the generated CCDF for the total aqueous releases and the release of  $^{99}\text{Tc}$  and  $^{237}\text{Np}$  to the accessible environment. The curve representing total release to the accessible environment crosses over the cross-hatched EPA limits, however, the releases are normalized to a 10,000-year standard and not a 100,000-year standard. The total normalized cumulative aqueous releases to the accessible environment for the 100,000-year simulation are greater than the aqueous releases (based on  $^{99}\text{Tc}$ ) for the 10,000-year simulation by several orders of magnitude. It should be noted that the normalized cumulative releases to the accessible environment for  $^{14}\text{C}$  at 10,000 years, yielded higher releases than the total aqueous releases at 100,000 years for over 90 percent of the realizations (compare Figures 3-11 and 3-20). If the normalized cumulative releases for  $^{14}\text{C}$  at 100,000 years were simulated and included, the total curve in Figure 3-20 would be shifted further to the right to incorporate the higher total releases.

The effects of varying the repository thermal load have been investigated by generating simulations of 100 realizations each, for the three thermal load scenarios (57/10/0.95/S1, 28.5/10/0.95/S1, and 114/10/0.95/S1). Figure 3-21 presents a CCDF of the total normalized cumulative release to the accessible environment for all three thermal loads. These curves show that at a time frame of 100,000 years after waste emplacement, the cumulative release to the accessible environment is almost insensitive to the repository thermal loading.

The effects of varying the waste package inner and outer container thicknesses have been investigated by generating simulations of 100 realizations each, for the four different container thickness scenarios (57/10/0.95/S1, 57/20/0.95/S1, 57/45/0.95/S1, and 57/10/3.5/L1). Figure 3-22 presents a CCDF of the total normalized cumulative release to the accessible environment for all four scenarios. This plot shows that the release to the accessible environment at 100,000 years is not reduced by increasing the outer container thickness to 20 cm. However, decreases of one to two orders of magnitude are obtained by increasing the outer container thickness to 45 cm. Using the Lamont corrosion rates and an inner container thickness of 3.5 cm, the releases at 100,000 years are very similar to the reference case using the Stahl failure initial criteria and an inner container thickness of 0.95 cm (Figure 3-22).

In taking the TSPA analysis of the radionuclide releases to the accessible environment out to 100,000 years, it has been shown that the releases are rather invariant for the thermal loads and container configurations investigated (except for 57/45/0.95/S1). The exception shows that by increasing the outer container thickness to 45 cm, the releases to the accessible environment can be significantly reduced, in terms of both magnitude and arrival times.

### 3.3.3 Scatter Plots of Releases

Scatter plots showing the correlation of individual parameter values to normalized cumulative aqueous releases at the accessible environment have been generated for selected parameters. The scatter plots are presented for simulation times of 10,000 and 100,000 years. An equivalent set

of scatter plots have been generated for each repository thermal load and waste package container thickness scenario investigated. However, only the scatter plots from the reference case (57/10/0.95/S1) will be presented due to the similarity in the results. That is, the selected parameters have the same effect on the transport of the radionuclides to the accessible environment, with the different waste package/EBS configuration/scenarios only contributing to shifting the times of arrival and the magnitude of the releases.

The scatter plots generated for the aqueous releases at 10,000 years are presented for  $^{99}\text{Tc}$ , since the total release is dominated by the gaseous release of  $^{14}\text{C}$ . The scatter plots generated for the aqueous releases at 100,000 years are presented for the summation of all radionuclides transported in the aqueous phase. Figures 3-23 through 3-25 present scatter plots of the unsaturated-zone flux, saturated-zone flux, and pH vs. the normalized cumulative release of  $^{99}\text{Tc}$  to the accessible environment at 10,000 years. These plots show that no releases of  $^{99}\text{Tc}$  were obtained until the unsaturated-zone flux was greater than approximately  $4.0 \times 10^{-4}$  m/yr (0.4 mm/yr). Once unsaturated-zone flux was above this value, the releases were dependent on the unsaturated-zone flux, and not significantly dependent on either the pH of the ground water or the saturated-zone flux. The strong dependency on unsaturated-zone flux is due to the location of the  $^{99}\text{Tc}$  dispersive front within the saturated zone. At a flux of approximately  $4.0 \times 10^{-4}$  m/yr, the initial edge of the  $^{99}\text{Tc}$  plume has arrived at the accessible environment. As the flux is increased over approximately one order of magnitude, the release to the accessible environment increases due to a greater portion of the dispersive front being released to the accessible environment. The concentration gradient within the dispersive front is nonlinear, so as the portion of the dispersive front that releases to the accessible environment is increased by increasing the unsaturated-zone flux, the cumulative  $^{99}\text{Tc}$  releases do not increase linearly. This is seen by an approximately 11 orders of magnitude increase in the release, due to an increase in the unsaturated-zone flux by one order of magnitude. This behavior is also seen in the release to the accessible environment for the 100,000-year simulations presented below. The lack of dependence on the saturated-zone flux is primarily due to the longer retention times in the unsaturated zone as compared to the saturated zone.

Figures 3-26 through 3-28 present scatter plots of the unsaturated-zone flux, saturated-zone flux, and pH vs. the total normalized cumulative aqueous releases to the accessible environment at 100,000 years. As in the 10,000-year simulations, the magnitude of the release is primarily dependent on the unsaturated-zone flux. As with the 10,000-year releases to the accessible environment, the increase in the unsaturated-zone flux by over one order of magnitude results in more than one order of magnitude increase in release. At a flux of approximately  $2.0 \times 10^{-4}$  m/yr, the breakthrough has reached a level such that the entire dispersive front of the  $^{99}\text{Tc}$  has been released to the accessible environment, and the increase in the releases as a function of unsaturated-zone flux levels off on the log-log plot. This leveling off is due to the majority of the  $^{99}\text{Tc}$  mass being released to the accessible environment, as seen in Figure 3-17 for the expected-value case.

### **3.3.4 Radiation Dose Exposures from Aqueous Pathways**

In addition to determining the mass or activity releases at the accessible environment, the aqueous dose exposures have also been determined. The dose exposure was calculated over a

1,000,000-year time frame in order to capture the peak doses for certain radionuclides. The dose analyses have been conducted using the same data sets and EBS scenarios as presented above, and a simulation time of  $10^6$  years. The  $^{14}\text{C}$  inventory was removed from the waste packages to obtain only the exposures due to aqueous transport.

The dose calculations within RIP are conducted using the following:

$$D_i = \frac{M_i}{Q_m} DCF_i$$

where  $D_i$  is the dose for radionuclide  $i$  (rem/yr),  $M_i$  is the mass rate of release for radionuclide  $i$  (gm/yr),  $Q_m$  is the mixing volumetric flow rate ( $\text{m}^3/\text{yr}$ ), and  $DCF_i$  is the dose conversion factor for radionuclide  $i$  (rem- $\text{m}^3/\text{gm-yr}$ ). The dose conversion factors for each radionuclide were compiled from several sources (Eslinger et al., 1993; NAS, 1984) and are presented in Table 3-15. The mixing volumetric flow rate was assumed to be

$$Q_m = A_c u$$

where  $A_c$  is the cross-sectional area of the saturated-zone ( $\text{m}^2$ ) and  $u$  is the saturated-zone flux ( $\text{m/yr}$ ). The cross-sectional area was held constant equal to the footprint of the repository at  $2.0 \times 10^5 \text{m}^2$  with an arbitrarily assumed mixing depth of 50 m (Wilson et al., 1994, in press).

The dose exposure generated over  $10^6$  years is the maximally exposed individual whole body dose for a person that obtains all of his/her drinking water and crop irrigation water from the contaminated saturated zone. This assumption is conservative because a person would be expected to obtain food and drink from other sources as well. Therefore, the peak doses presented below should be considered to be the maximum likely doses.

The effects of varying the repository thermal load and the waste package container thickness on the dose exposures have been investigated for a time frame of  $10^6$  years. The results will be presented in two different formats. The first is an expected-value plot of dose (rem/yr) vs. time (yr), where the expected-value run is a single realization generated using the mean or expected values of all the stochastic parameters. The second format is a CCDF of the probability of exceeding the peak dose (rem/yr) for a simulation consisting of 100 realizations with the stochastic nature of the specified parameters incorporated. The peak dose is defined as the single point maximum dose exposure (rem/yr) over the entire simulation.

Figure 3-29 presents the expected-value plots for the reference-case repository thermal load of 141 kW/ha or 57 kW/acre (57/10/0.95/S1). This plot shows a bimodal character with  $^{99}\text{Tc}$  contributing the peak dose at times less than 300,000 years and  $^{237}\text{Np}$  contributing the peak dose from 300,000 to  $10^6$  years. The  $^{99}\text{Tc}$  peak dose of approximately 1.2 rem/yr occurred around 70,000 years, with the  $^{237}\text{Np}$  peak dose, within  $10^6$  years, of approximately 40 rem/yr around 800,000 years. Other radionuclides of interest in the results presented below are  $^{129}\text{I}$  and  $^{210}\text{Pb}$ .

The early arriving  $^{129}\text{I}$  is another alteration-limited, non-retarded radionuclide, while  $^{210}\text{Pb}$  is a solubility-limited radionuclide with a large retardation factor.

Figures 3-30 and 3-31 present the expected-value plots for the 70.4 kW/ha or 28.5 kW/acre (28.5/10/0.95/S1) and the 282 kW/ha or 114 kW/acre (114/10/0.95 S1) thermal-loading scenarios, respectively. For 28.5/10/0.95 S1 (Figure 3-30), the dose exposures for the alteration-limited radionuclides ( $^{99}\text{Tc}$  and  $^{129}\text{I}$ ) peaked at slightly lower values and larger times but were releasing higher doses than the reference case (57/10/0.95 S1) from 200,000 to 900,000 years. The dose exposures of  $^{237}\text{Np}$  for the 70.4 kW/ha (28.5 kW/acre) case were the same as in the 141 kW/ha (57 kW/acre) reference case. Figure 3-31 shows that for a thermal loading of 282 kW/ha (114 kW/acre) (114/10/0.95/S1), the alteration-limited rates are slightly higher than the reference case at early times, and the  $^{237}\text{Np}$  rates are the same as the reference case. Figure 3-31 also shows that the  $^{210}\text{Pb}$  doses (along with other highly retarded solubility-limited radionuclides) arrived approximately 100,000 years earlier with an increase in peak dose of about one order of magnitude.

Figure 3-32 presents a CCDF generated from 100 realizations for each of the three thermal-loading scenarios. The CCDF curves show the probability of exceeding a certain peak dose. The three CCDFs for peak dose over  $10^6$  years are very similar with the only differences of significance being the very low probability realizations. Here, the magnitude of the 282 kW/ha (114 kW/acre) case exposures are slightly higher than those for the 141 kW/ha (57 kW/acre) and the 70.4 kW/ha (28.5 kW/acre) cases.

The peak dose exposures over  $10^6$  years are very insensitive to an increase or decrease in the repository thermal load. There is some variation in the peak dose for certain radionuclides, however, the variance is not that significant when compared to the overall magnitude of the dose exposures. The main dose contributors of  $^{99}\text{Tc}$  at early times (<200,000 years) and  $^{237}\text{Np}$  at later time (>200,000 years) are consistent for each of the three scenarios, with little change in the expected-value peak dose within  $10^6$  years.

The effects of varying the waste package container thickness on the dose exposures have also been investigated for the  $10^6$ -year time frame. The waste package outer and inner container thicknesses were varied as in the 10,000- and 100,000-year simulations presented above. Figures 3-33 through 3-35 present the expected-value plots for the 57/20/0.95/S1, 57/45/0.95/S1 and 57/10/3.5/L1 scenarios, respectively. The increase in the outer container thickness to 20 cm has no significant effect on reducing the peak dose, as compared to the reference case (57/10/0.95/S1), over the  $10^6$ -year simulation. However, increasing the outer container thickness to 45 cm does have a significant impact on the early time dose. The peak dose for  $^{99}\text{Tc}$  is delayed by approximately 50,000 years with the magnitude of the peak dose lowered by sixty percent. The effect on the late-arriving solubility-limited radionuclides (such as  $^{237}\text{Np}$ ) is only to delay the build up to the peak dose by the same 50,000 years, but the peak dose is of the same magnitude and arrival time. The approximately 50,000-year delay is due to the increase in the waste package failure times of the larger outer container. Figure 3-35 shows only a slight decrease in the  $^{99}\text{Tc}$  peak dose for the simulation using the 3.5-cm inner container and the Lamont waste package failure model.

Figure 3-36 presents the CCDFs for each of the four different waste package container thickness scenarios, each for a simulation of 100 realizations. Only in the case of the 45-cm outer container is there a significant difference in the CCDFs. The 57/45/0.95/S1 simulation shows lower peak-dose exposures for only 30 percent of the simulations. This peak dose corresponds to the peak  $^{237}\text{Np}$  dose exposure, which was shown not to vary significantly in magnitude for times greater than 600,000 years. The lower peak doses for 30 percent of the realizations represent the realizations when the delay in the waste package failure times created a corresponding delay in the arrival of the  $^{237}\text{Np}$  peak-dose exposure beyond the  $10^6$  simulation time.

### 3.3.5 Scatter Plots of Dose

Scatter plots showing the correlation of individual parameter values to the peak-dose exposure over  $10^6$  years have been generated. An equivalent set of scatter plots have been generated for each repository thermal load and waste package container thickness scenario investigated. However, only the scatter plots from the reference case (57/10/0.95/S1) will be presented due to the similarity of the results for all the waste package configurations and EBS scenarios. Figures 3-37 through 3-39 present scatter plots of the saturated-zone flux, the unsaturated-zone flux, and the pH of the ground water. Figure 3-37 shows that the peak-dose exposure over  $10^6$  years is more dependent on the unsaturated-zone flux than the saturated-zone flux, as increasing the unsaturated zone flux decreases the water travel time and therefore increases the peak concentrations and dose. Figure 3-38 shows that the peak dose exposure over  $10^6$  years is slightly dependent on the saturated-zone flux, as increasing the saturated flux linearly decreases the concentration and the corresponding dose. Figure 3-39 shows that over  $10^6$  years, the value of the pH has no effect on the peak dose value. It was expected that the saturated-zone flux would be the more dominant controlling factor on the peak dose, since as the magnitude of the flux increases, and thus the mixing volume, the peak-dose exposure would decrease. However, it was shown that this was not the case. Since the majority of the radionuclide travel time is attributed to flow through the unsaturated zone, the unsaturated-zone flux was the dominant dose controlling factor.

The effect of the climate change multiplier on the releases to the accessible environment was not observed on the expected-value plots or from the scatter plot results. Due to limitations of the RIP model, a scatter plot of the modified flux could not be presented. This lack of an effect on the releases is due to the magnitude of the change in unsaturated-zone flux. The flux multiplier only varied between one and five, resulting in less than one-half order of magnitude increase in the unsaturated-zone flux. This variance is small in comparison to the three orders of magnitude over which the unmodified unsaturated-zone flux distribution extended. Therefore, the change in the unsaturated-zone flux due to the flux multiplier is too small, in comparison to the overall magnitude of the flux, to demonstrate a controlling effect on the releases to the accessible environment over  $10^6$  years.

Table 3-1. Simulation Identifiers Based on Waste Package/Engineered Barrier System Configurations

Waste Package/Engineered Barrier System Scenario	Thermal Load (kW/acre)	Waste Package Outer Thickness (cm)	Waste Package Inner Thickness (cm)	Waste Package Failure Mode	Saturation (1) or Temperature (2)
57/10/0.95/S1	57	10	0.95	Stahl	Saturation
57/20/0.95/S1	57	10	0.95	Stahl	Saturation
57/45/0.95/S1	57	10	0.95	Stahl	Saturation
57/10/3.5/L1	57	10	3.5	Lamont	Saturation
28.5/10/0.95/S1	28.5	10	0.95	Stahl	Saturation
114/10/0.95/S1	114	10	0.95	Stahl	Saturation

Table 3-2. Stratigraphic Thicknesses of the Nine Unsaturated-Zone Columns Used in the Aqueous Transport Simulations

Layer Number	Layer	Column #1	Column #2	Column #3	Column #4	Column #5	Column #6	Column #7	Column #8	Column #9
1	TSw2	131	143	109	75	45	68	100	89	78
2	TSw3	10	10	10	10	10	10	10	10	10
3	CHn1v	34	32	35	40	38	32	30	31	33
4	CHn1z	69	77	74	62	62	75	78	69	60
5	PPw	28	25	73	130	130	119	71	74	77
6	Bw	0	0	0	3	36	0	0	0	0

**Table 3-3. Stratigraphic Column Correlations between the Thermomechanical (Ortiz et al., 1985) and the USGS (1993) Stratigraphies as used in TSPA 1993**

ORTIZ et al., 1985	USGS, 1993
TSw2	Tmn
	Tl
	Tln
TSw3	Tv
CHn1v	
CHn1z	Tht
PPw	Tcp
<sup>1</sup> Bw	Tcb

<sup>1</sup>not present in Ortiz et al., (1985)

Table 3-4. Reference Points for the Calculation of the Water-Table Elevation

Well	Elevation (m)	Northerly Coordinates (ft)	Easterly Coordinates (ft)
USW H-5	775.11	766,600	559,000
UE-25a#1	730.93	764,800	566,300
USW WT-7	775.60	756,600	555,700

Table 3-5. TSPA 1993 Unsaturated- and Saturated-Zone Aqueous Flux Distributions (m/yr)

Zone	Distribution Type	Mean Value	Standard Deviation	Minimum	Maximum
Unsaturated	beta	5.00E-04	4.80E-04	0.00E+00	1.25E-02
Saturated	log-normal	2.00E+00	3.16E+00		

Table 3-6. Correlation of TSPA 1993 and TSPA 1991 (Barnard et al., 1992) Stratigraphic Designations

TSPA 1991 (Barnard et al., 1992)	TSPA 1993
Welded	TSw2
Vitrophyre	TSw3
Vitric	CHnlv
Zeolitic	CHnlz
Partially Welded	PPw
Partially Welded	Bw

Table 3-7. TSPA 1993 Eta Bulk Porosity Distributions (Barnard et al., 1992)

Layer	E[x]	CV[x]	S.D. <sup>1</sup>	Min	Max
TSw2	0.11	0.2	0.022	0.044	0.197
TSw3	0.09	0.2	0.018	0.037	0.161
CHnlv	0.21	0.2	0.042	0.000	1.000
CHnlz	0.41	0.2	0.082	0.000	1.000
PPw	0.24	0.2	0.048	0.000	1.000
Bw <sup>2</sup>	0.24	0.2	0.048	0.000	1.000

<sup>1</sup> Standard deviation = E[x] x CV[x]

<sup>2</sup> Bw is assumed to be the same as PPw in TSPA 1993

Table 3-8. TSPA 1993 Ambient Unsaturated-Zone Liquid Saturations (Appendix A)

Layer	Liquid Saturation
TSw2	0.681
TSw3	0.763
CHn1v	0.080
CHn1z	0.922
PPw	0.988
Bw <sup>1</sup>	0.988

<sup>1</sup> Bw is assumed to be the same as PPw in TSPA 1993

Table 3-9. TSPA 1993 Distribution Coefficient Distributions (mL/g) (Appendix H) (Page 1 of 3)

ELEMENT	ROCK TYPE	DIST	E[x]	CV[v] (S.D.) <sup>1</sup>	MIN	MAX	COMMENTS
Am	D <sup>2</sup>	uniform			100	2000	Same for Ac, Cm, Nb, Sm, and Zr
	V <sup>3</sup>	beta	~380	0.2 (~76)	100	1000	
	Z <sup>4</sup>	uniform			100	1000	
Cs	D	uniform			100	200	
	V	uniform			100	200	
	Z	uniform			500	3000	
Ni	D	normal	(250)	(65)	0	500	<p>The min and max are 3σ apart The mean (μ) is 250 for all 3 distributions</p> <p>These were obtained in a memo dated June 4, 1993, from M.D. Siegel, SNL, 6115, to Jack Gauthier.</p>
	V	normal	(250)	(65)	0	500	
	Z	normal	(250)	(65)	0	500	
Np	D	exponential (gamma)	2	1 (2)	0	50	
	V	exponential (beta)	0.5	(0.5)	0	12.5	

Table 3-9. TSPA 1993 Distribution Coefficient Distributions (mL/g) (Appendix H) (Page 2 of 3)

ELEMENT	ROCK TYPE	DIST	E[x]	CV[v] (S.D.) <sup>1</sup>	MIN	MAX	COMMENTS
Np (Continued)	Z	exponential (beta)	4	(4)	0	100	
Pa	D	exponential (beta)	2	(2)			Extremely limited data
	V	exponential (beta)	0.5	(0.5)			
	Z	exponential (beta)	4	(4)			
Pb	D	uniform			100	500	Limited data
	V	uniform			100	500	
	Z	uniform			100	500	
Pu	D	beta	100	0.25 (25)	50	200	
	V	beta	100	0.25 (25)	50	200	
	Z	beta	40	0.15 (6)	30	70	

Table 3-9. TSPA 1993 Distribution Coefficient Distributions (mL/g) (Appendix H) (Page 3 of 3)

ELEMENT	ROCK TYPE	DIST	E[x]	CV[v] (S.D.) <sup>1</sup>	MIN	MAX	COMMENTS
Ra	D	uniform			100	500	
	V	uniform			100	500	
	Z	uniform			1000	5000	
Sn	D	uniform			20	200	
	V	uniform			20	200	
	Z	uniform			100	300	
U	D	uniform			0	5	Same for Se to be conservative
	V	uniform			0	4	
	Z	uniform			5	20	
Cl, I, Tc	All		0				

<sup>1</sup> S.D. = E[x] x CV[v]

<sup>2</sup> D = Devitrified tuff

<sup>3</sup> V = Vitric tuff

<sup>4</sup> Z = Zeolitic tuff

Table 3-10. TSPA 1993 Beta Bulk Density Distributions (g/mL)

<b>Layer</b>	<b>Mean Value</b>	<b>Standard Deviation</b>	<b>Minimum</b>	<b>Maximum</b>
TSw2	2.24	0.092	2.0	2.4
TSw3	2.15	0.191	1.7	2.5
CHn1v	1.68	0.220	1.3	2.1
CHn1z	1.68	0.220	1.3	2.1
PPw	2.00	0.181	1.7	2.4
Bw	2.00	0.181	1.7	2.4

Table 3-11. Expected-Value Retardation Factors for Selected Radionuclides

Layer	U	Np	Cs	Pu	Pb
TSw2	52	42	3055	2037	6110
TSw3	49	13	3584	2389	7168
CHnlv	17	5	1201	801	2401
CHnlz	42	17	7172	165	1230
PPw	22	18	125	834	2501
Bw	22	18	1251	834	2501
SZ-PPw	26	21	1501	1001	3000

Table 3-12. Step-function Travel Times and Unit Average Linear Velocities for  $^{14}\text{C}$  at 1000 Years (modified from Ross, 1993)

Percentage	Travel Time (yrs)	Unit-Average Linear Velocity (m/yr)
2	225	4.44E-3
28	275	3.64E-3
32	360	2.78E-3
3	460	2.17E-3
23	530	1.89E-3
12	610	1.64E-3

Table 3-13. Time Frames for <sup>14</sup>C Travel-Time Designations

<b>Ross (1993) Release Time (yr)</b>	<b>TSPA 1993 Start Time (yr)</b>	<b>TSPA 1993 End Time (yr)</b>
1,000	0	1,500
2,000	1,600	2,500
3,000	2,600	3,500
4,000	3,600	4,500
5,000	4,600	5,500
6,000	5,600	6,500
7,000	6,600	7,500
8,000	7,600	8,500
9,000	8,600	9,500
10,000	9,600	10,500
11,000	10,600	11,500
12,000	11,600	12,500
13,000	12,600	13,500
14,000	13,600	14,500
15,000	14,600	15,500
16,000	15,600	16,500
17,000	16,600	17,500
18,000	17,600	--

Table 3-14. Normalized Cumulative Release to the Accessible Environment for the Expected-value Simulations at 10,000 and 100,000 Years

Waste Package/ Engineered Barrier System Scenario	Total		<sup>14</sup> C		<sup>99</sup> Tc		<sup>237</sup> Np	
	10,000 yrs	100,000 yrs	10,000 yrs	100,000 yrs	10,000 yrs	100,000 yrs	10,000 yrs	100,000 yrs
57 / 10 / 0.95 / S1 <sup>1</sup>	2.37	4.19	2.37	2.91	<1E-6	0.89	0.00	<1E-6
57 / 20 / 0.95 / S1	0.92	2.73	0.92	1.56	<1E-6	0.84	0.00	<1E-6
57 / 45 / 0.95 / S1	0.00	0.03	0.00	0.0001	0.00	0.02	0.00	<1E-6
57 / 10 / 3.5 / L1	1.26	2.73	1.26	1.69	<1E-6	0.72	0.00	<1E-6
114 / 10 / 0/95 / S1	1.09	3.36	1.09	1.95	0.00	0.98	0.00	<1E-6
28.5 / 10 / 0.95 / S1	0.61	2.12	0.61	1.11	0.00	0.70	0.00	<1E-6

<sup>1</sup> Design Case #1 (Reference Case) Simulation: 57 = 57 kW/acre; 10 = 10-cm outer container thickness; 0.95 = 0.95-cm inner container thickness; and S1 = Stahl failure criteria with initiation at saturation >8%.  
- All releases are normalized to the 40 CFR 191 Table 1 values

Table 3-15. TSPA 1993 Dose Conversion Factors

ISOTOPE	DOSE-CONVERSION FACTOR (rem-m <sup>3</sup> /gm-yr)	ISOTOPE	DOSE-CONVERSION FACTOR (rem-m <sup>3</sup> /gm-yr)
<sup>227</sup> Ac	2.28E9	<sup>239</sup> Pu	1.24E4
<sup>241</sup> Am	2.81E7	<sup>240</sup> Pu	4.56E4
<sup>242</sup> Am	3.08E4	<sup>241</sup> Pu	3.96E5
<sup>242m</sup> Am	7.67E7	<sup>242</sup> Pu	7.25E2
<sup>243</sup> Am	1.63E6	<sup>226</sup> Ra	8.79E6
<sup>14</sup> C	1.72E6	<sup>79</sup> Se	1.10E5
<sup>243</sup> Cm	2.93E8	<sup>126</sup> Sn	6.08E4
<sup>244</sup> Cm	3.65E8	<sup>99</sup> Tc	7.72E2
<sup>245</sup> Cm	1.44E6	<sup>229</sup> Th	4.38E5
<sup>246</sup> Cm	2.57E6	<sup>230</sup> Th	6.00E3
<sup>135</sup> Cs	1.23E3	<sup>232</sup> Th	1.62E-1
<sup>129</sup> I	2.05E2	<sup>233</sup> U	1.36E3
<sup>94</sup> Nb	2.42E5	<sup>234</sup> U	4.56E2
<sup>237</sup> Np	1.31E5	<sup>235</sup> U	1.48E-1
<sup>231</sup> Pa	1.12E6	<sup>236</sup> U	4.48E0
<sup>210</sup> Pb	2.17E9	<sup>238</sup> U	3.63E-2
<sup>238</sup> Pu	3.10E6		

Qac Surficial deposits, poorly sorted, sand to boulders, nonlithified to partly indurated, some caliche

**TIMBER MOUNTAIN TUFF**

**RAINIER MESA MEMBER**

Tmrn Nonwelded tuff; vitric

Tmrw Welded tuff; partly to moderately welded, devitrified

**PAINTBRUSH TUFF**

**TIVA CANYON MEMBER**

Cu Undifferentiated; quartz latite to rhyolite, nonwelded to densely welded, vitric to devitrified, with and without lithophysae

Ccr Quartz latite caprock; moderately to densely welded, vitric to devitrified, sparse lithophysae

Cuc Upper cliff; moderately to densely welded, devitrified, abundant lithophysae

Cul Upper lithophysal; moderately to densely welded, devitrified, abundant lithophysae

Cks Clinkstone; moderately welded, devitrified

CII Lower lithophysal; moderately to densely welded, devitrified, abundant lithophysae

Ch Hackly; moderately to densely welded, devitrified

Cc Columnar; nonwelded to densely welded, partly vitric

**Bedded Tuff**

Bt Poorly to moderately bedded, some crossbedded

**YUCCA MOUNTAIN MEMBER**

Tpy Nonwelded to densely welded lithophysae

**Bedded Tuff**

Bt Pumiceous, poorly bedded

**PAH CANYON MEMBER**

Tpp Nonwelded to moderately welded

**Bedded Tuff**

Bt Nonwelded, reworked, moderate

**TOPOPAH SPRING MEMBER**

Tc Quartz latite caprock; nonwelded crystals

Tcl Quartz latite caprock lithophysal crystals, lithophysae

Tul Upper lithophysal; moderately abundant lithophysae

Tmn Middle nonlithophysal; moderately sparse lithophysae

TII Lower lithophysal; moderately abundant lithophysae

TIn Lower nonlithophysal; densely

Tv Vitrophyre; densely welded to at base of member, partly zeolitic

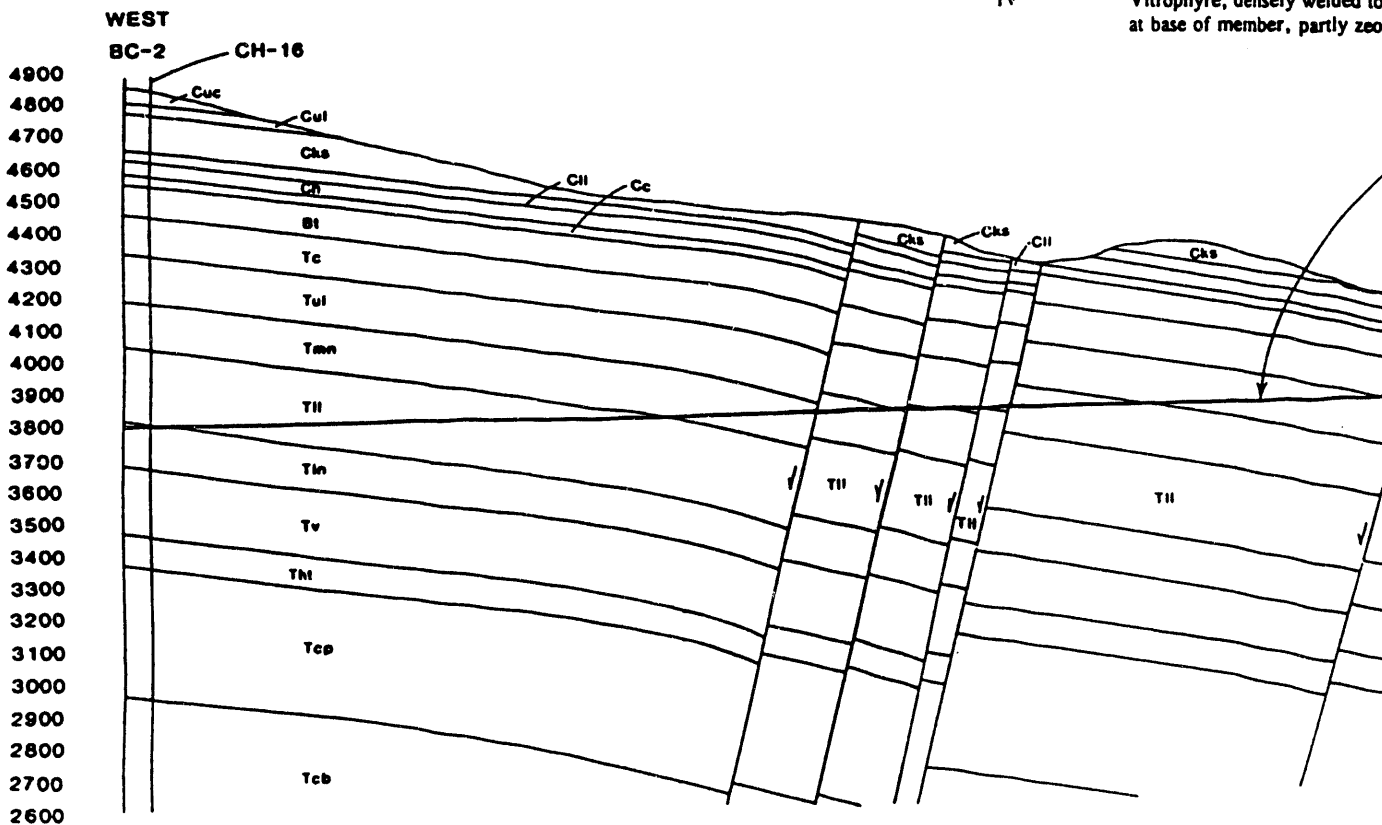


Figure 3-1 Stratigraphic Cross-Section Through Yucca Mountain on a Line from the Topopal Spring South Portal, West to the Intersection with the Proposed Repository at BC-2 (modified from USGS, 1993)



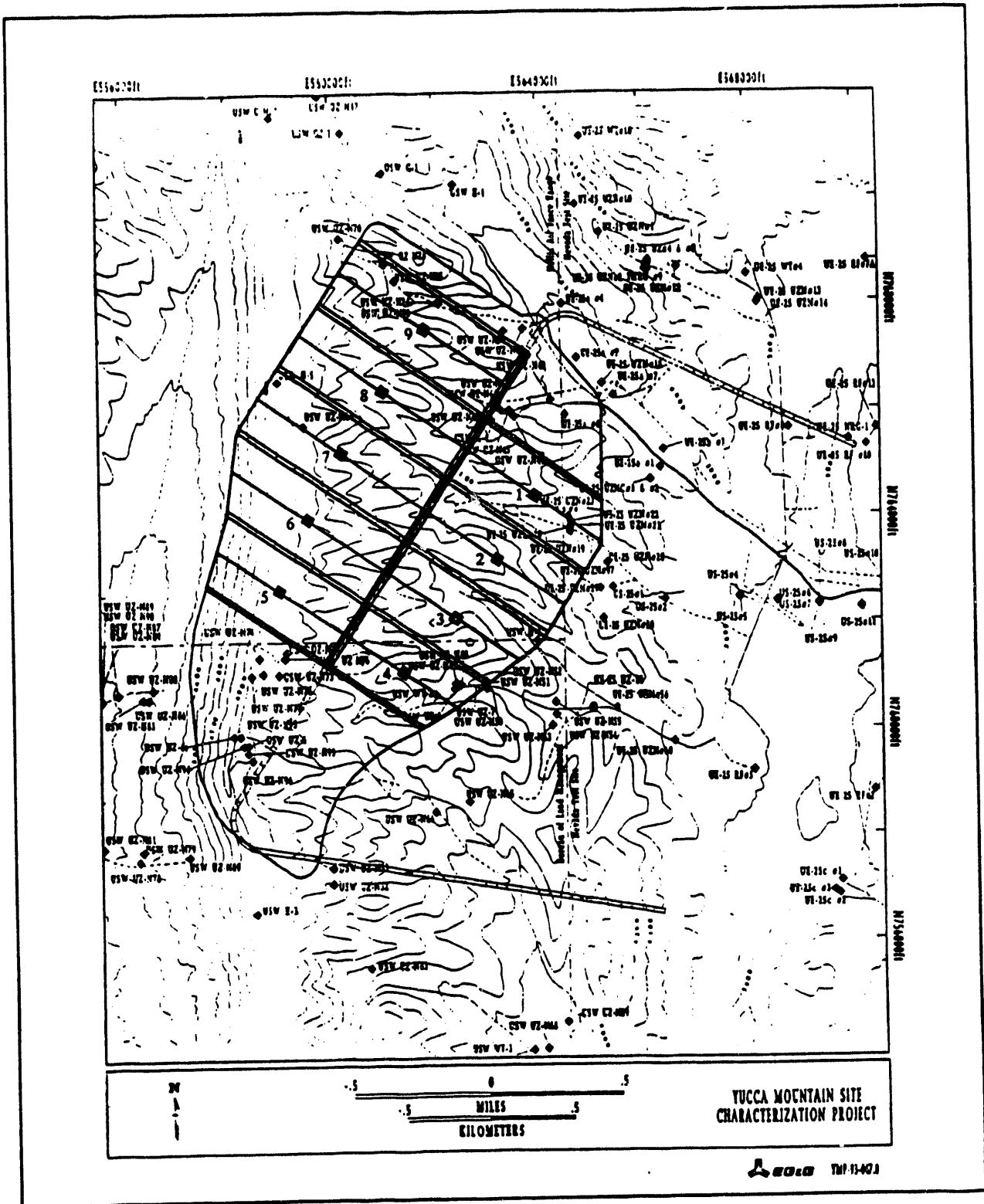


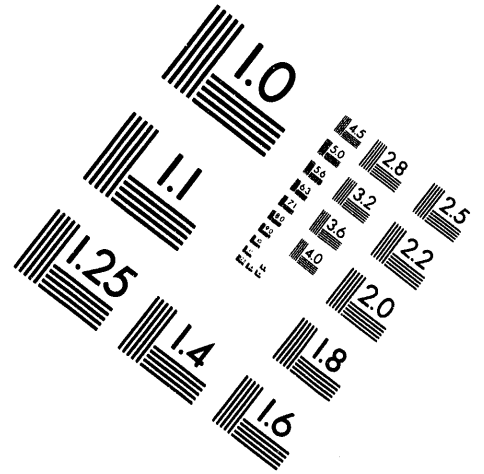
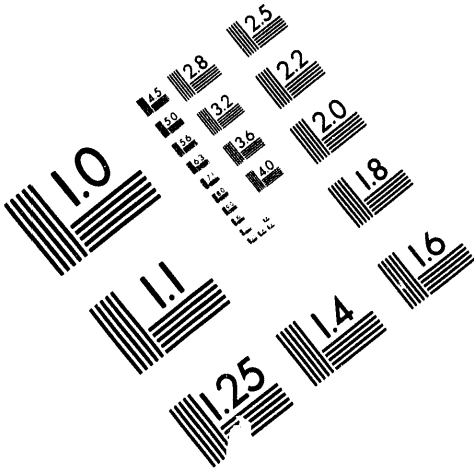
Figure 3-2. Areal Repository Conceptualization Showing Centroidal Locations of the Nine Unsaturated-Zone Columns (modified after Ryder (1993))



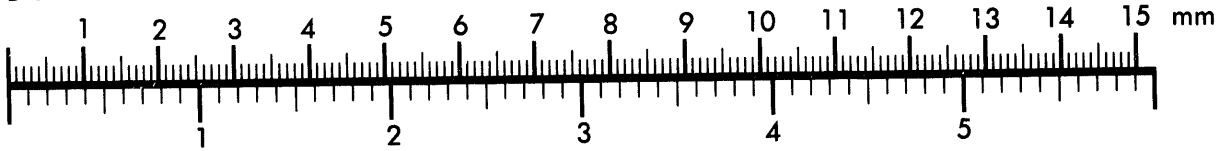
**AIM**

**Association for Information and Image Management**

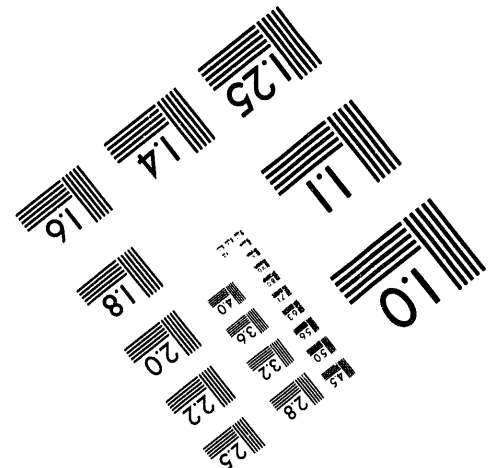
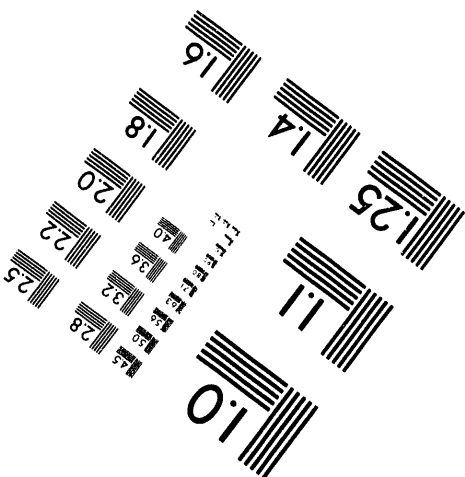
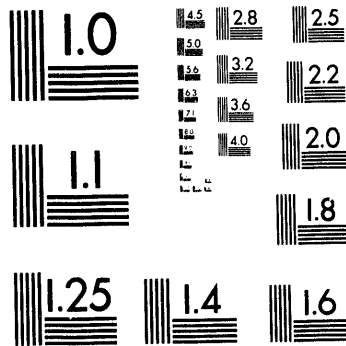
1100 Wayne Avenue, Suite 1100  
Silver Spring, Maryland 20910  
301/587-8202



**Centimeter**



**Inches**



MANUFACTURED TO AIM STANDARDS  
BY APPLIED IMAGE, INC.

**3 of 5**

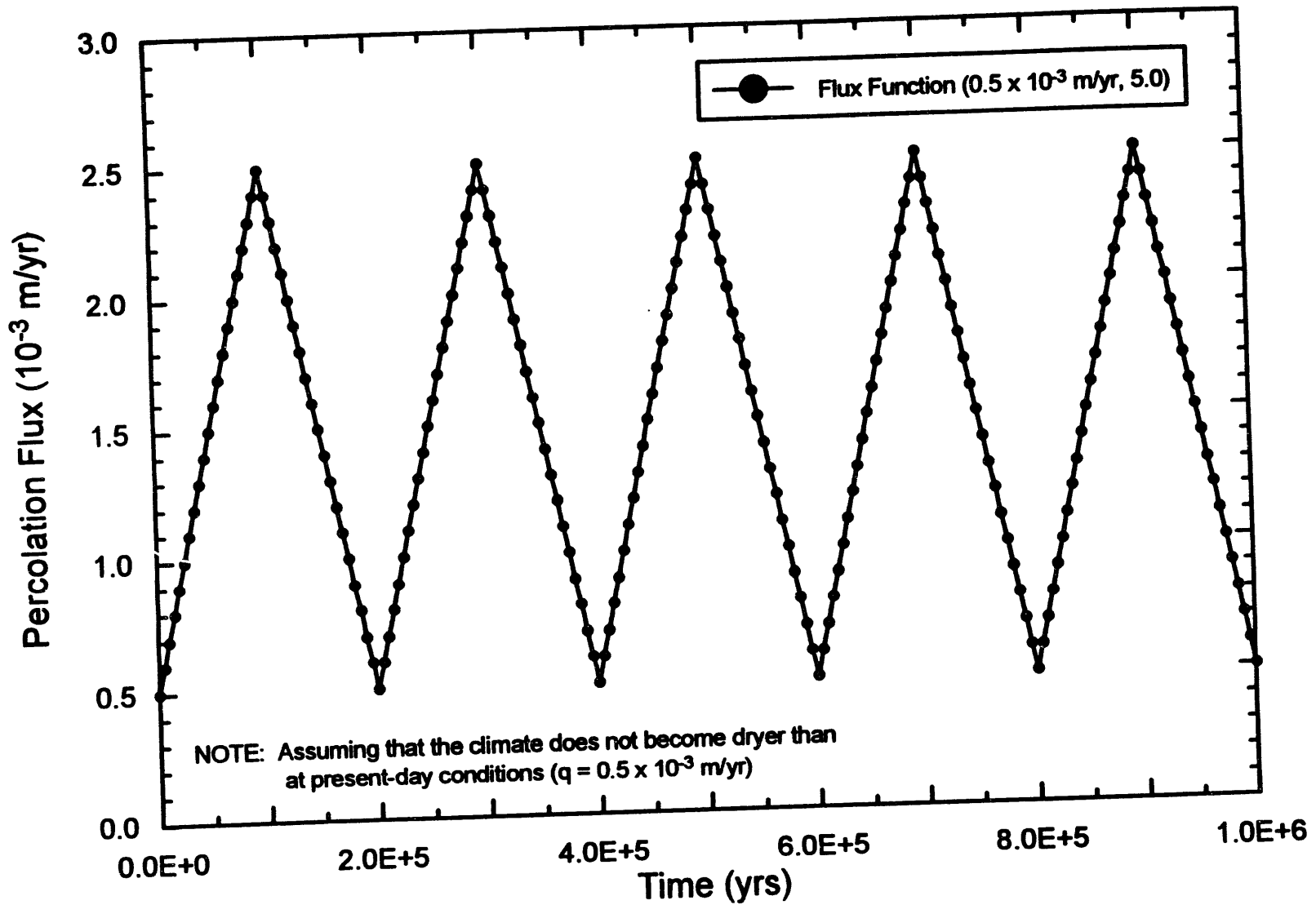


Figure 3-3. Percolation Flux Change Over One Million Years Due to the Expected Climate Changes

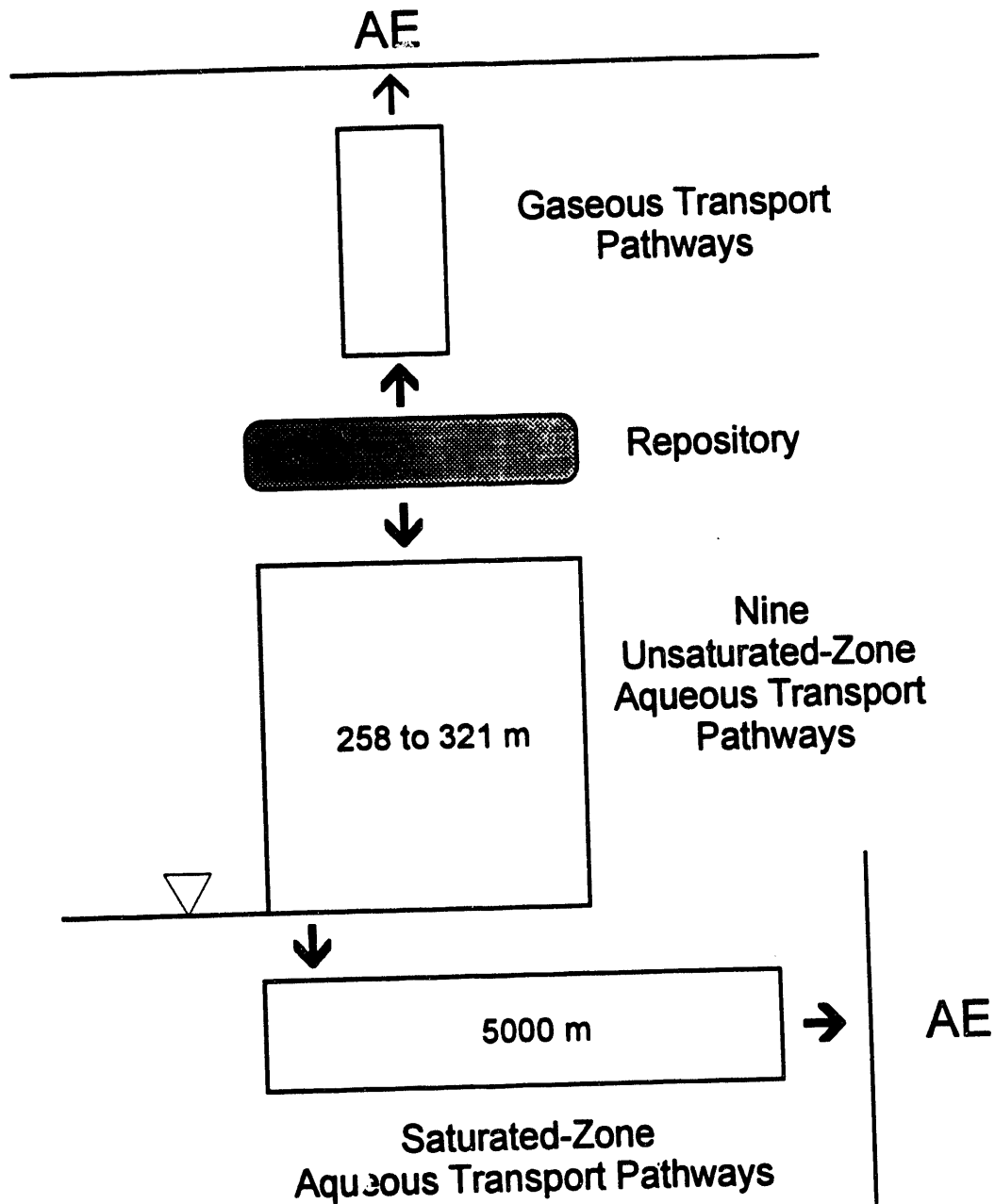


Figure 3-4. Aqueous Transport Pathway Conceptualizations

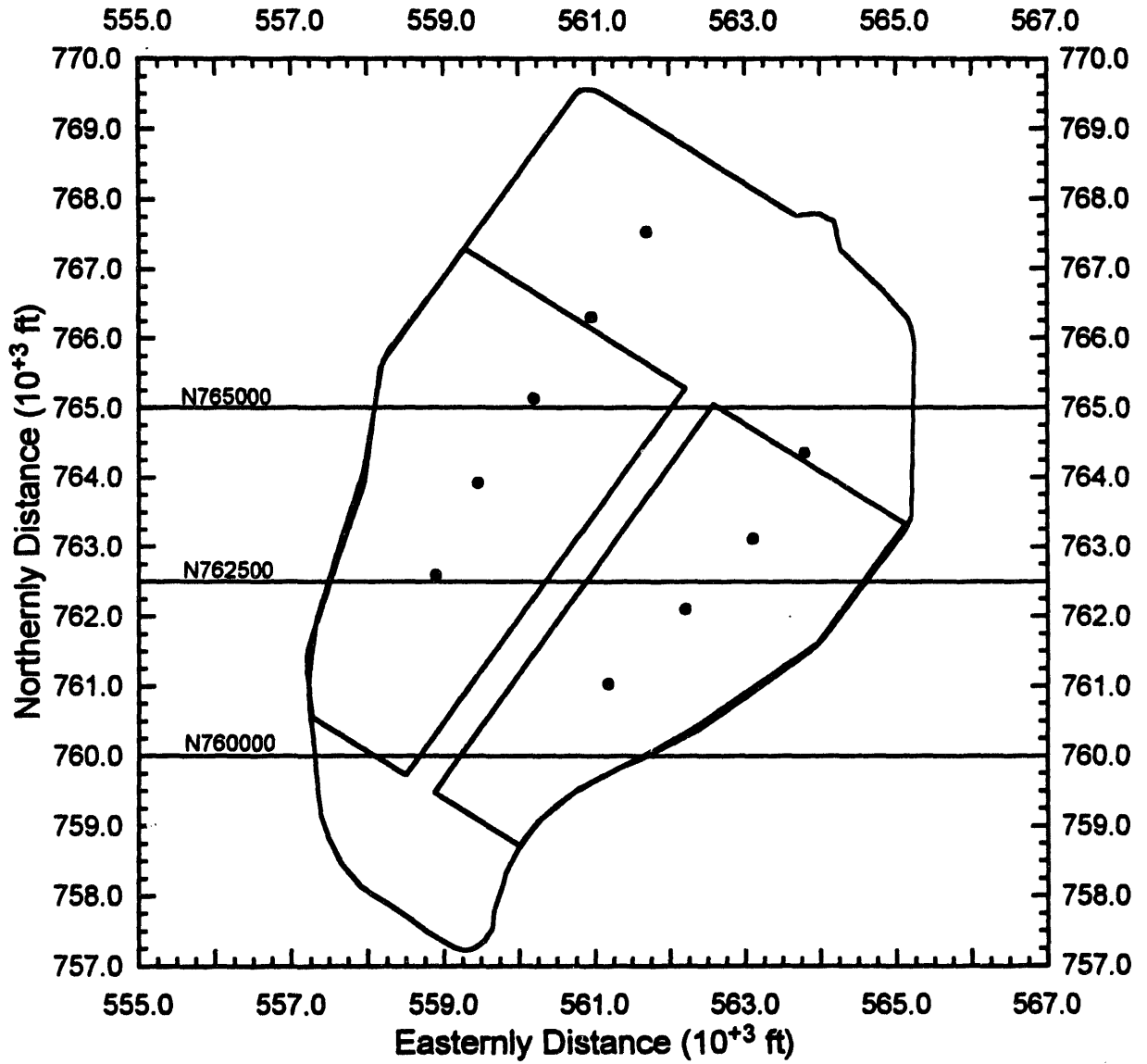


Figure 3-5. Ross (1993) Areal Repository Conceptualization Showing Cross-Sectional Lines N765000, N762500 and N760000

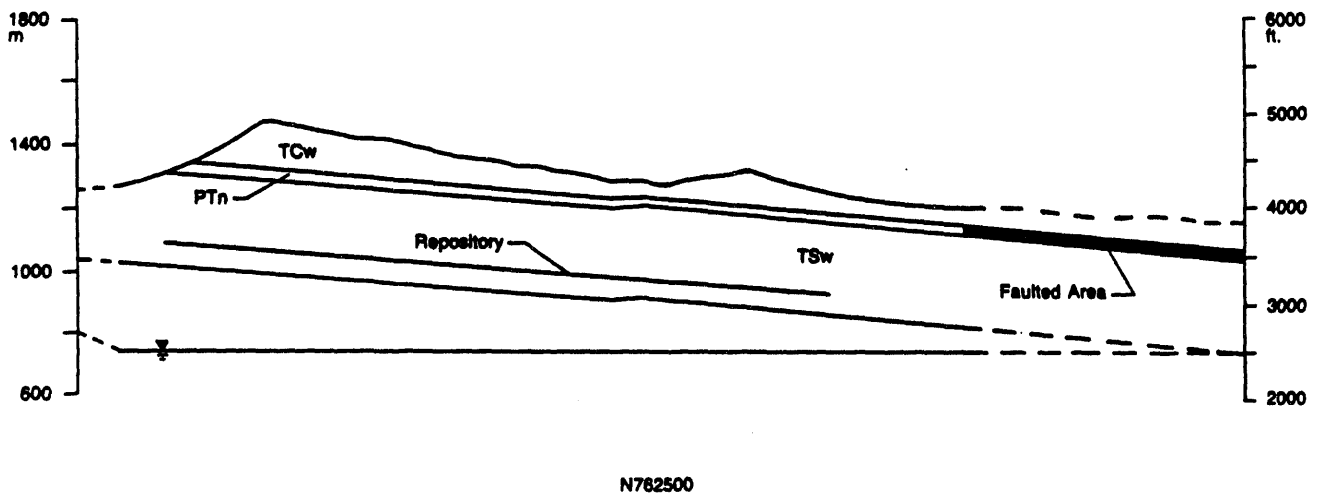


Figure 3-6. Cross-sectional View Through Yucca Mountain along the N762500 Line (taken from Ross et al., 1992)

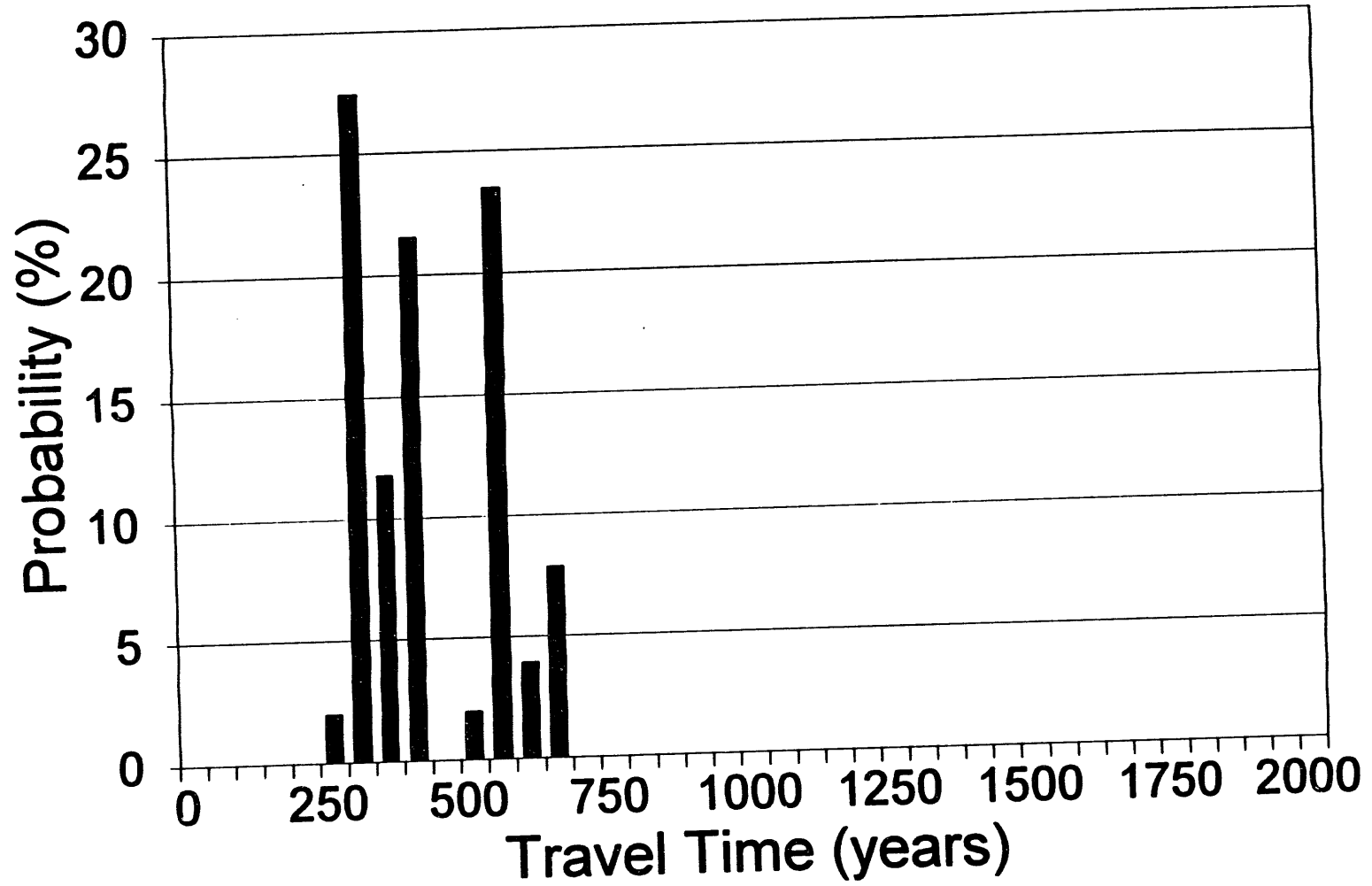


Figure 3-7. Probability Density Function of the Retarded  $^{14}\text{C}$  Travel Times for Particles Released at 1,000 Years (Ross, 1993)

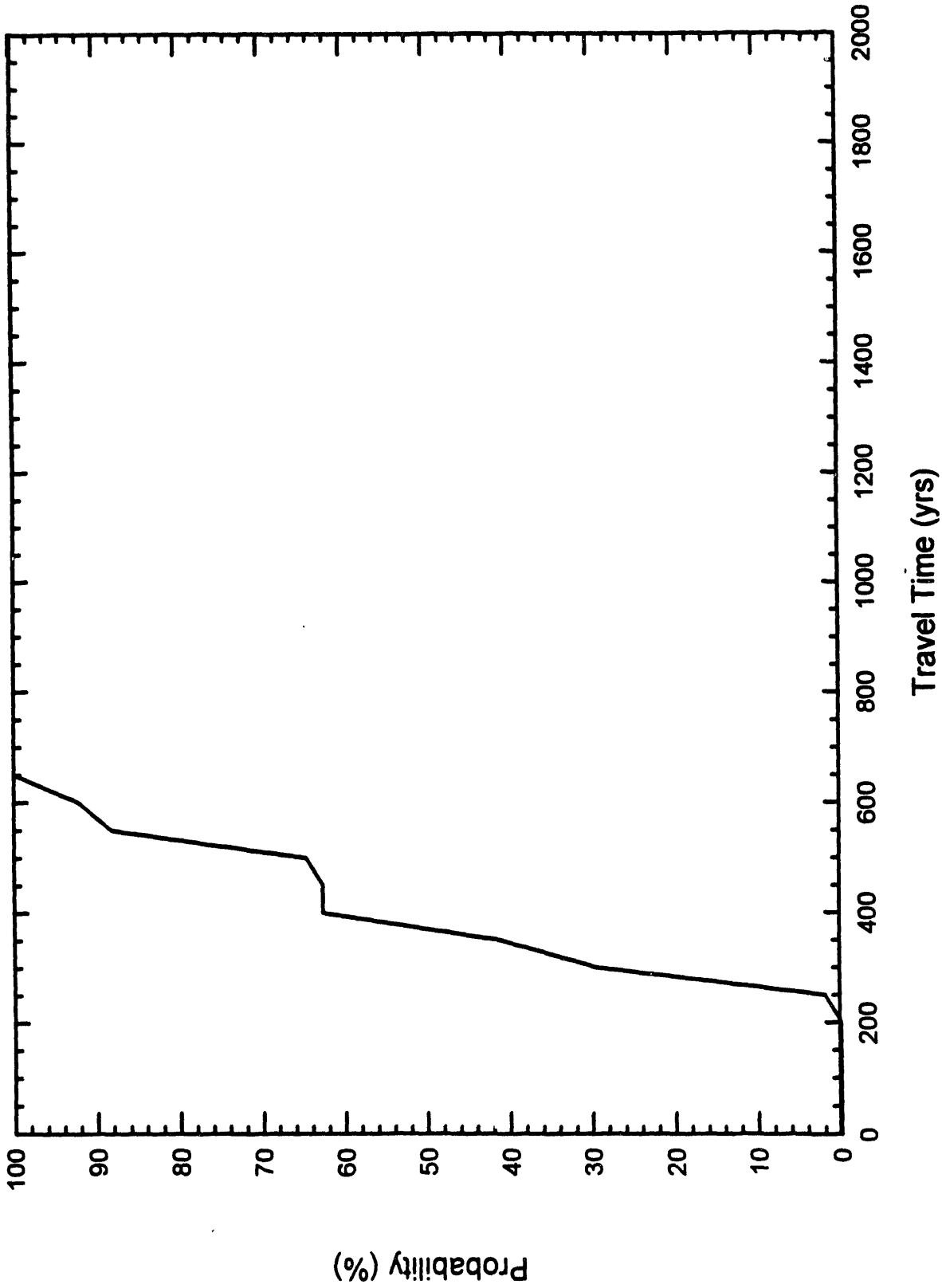


Figure 3-8. Cumulative Density Function of <sup>14</sup>C Travel Times for Releases at 1,000 Years

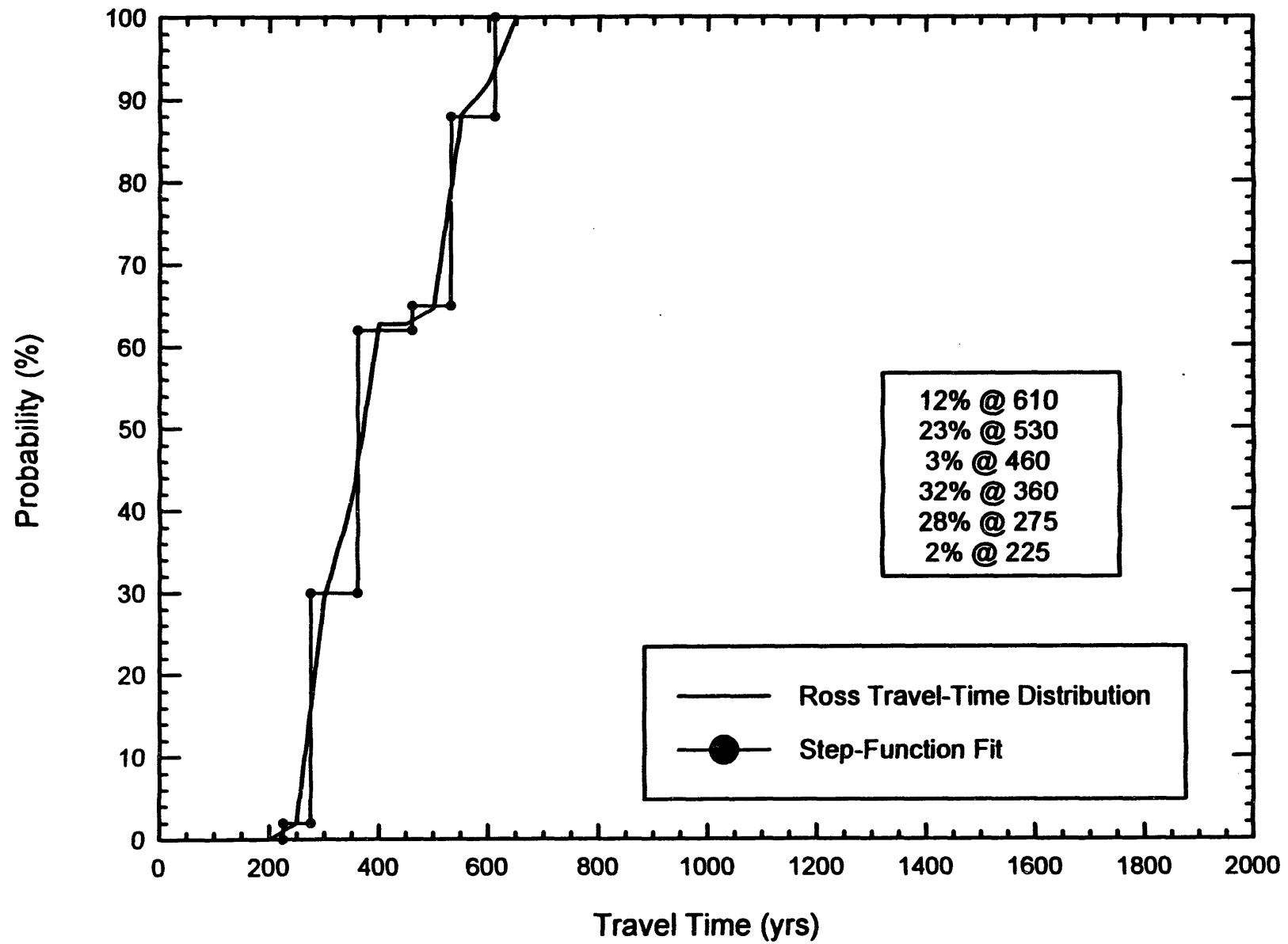


Figure 3-9. TSPA 1993 Step-function Fit of the cumulative Density Function of  $^{14}\text{C}$  Travel Times for Releases at 1,000 Years

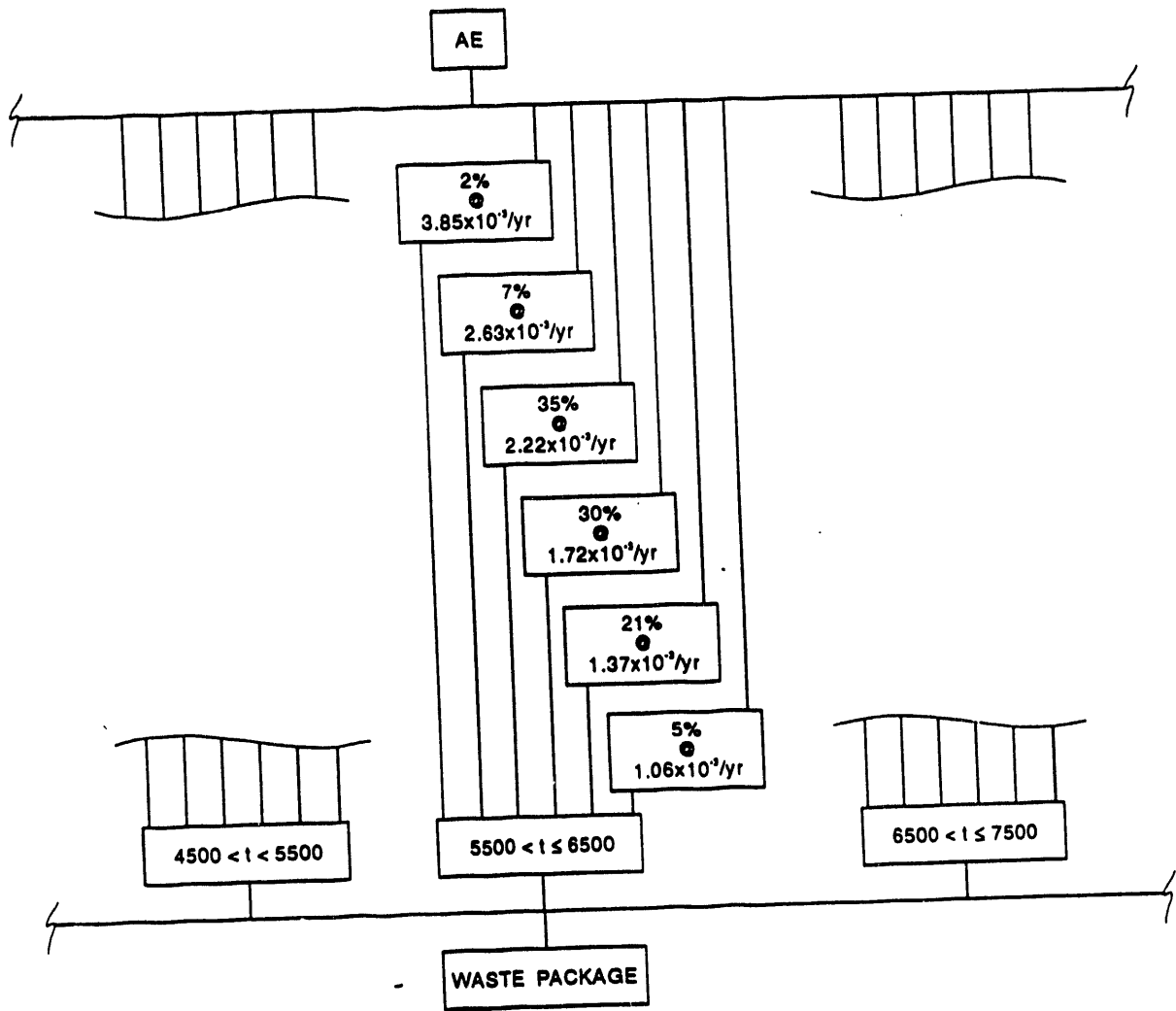


Figure 3-10. Partial Presentation of <sup>14</sup>C Travel Pathway Configurations within the RIP

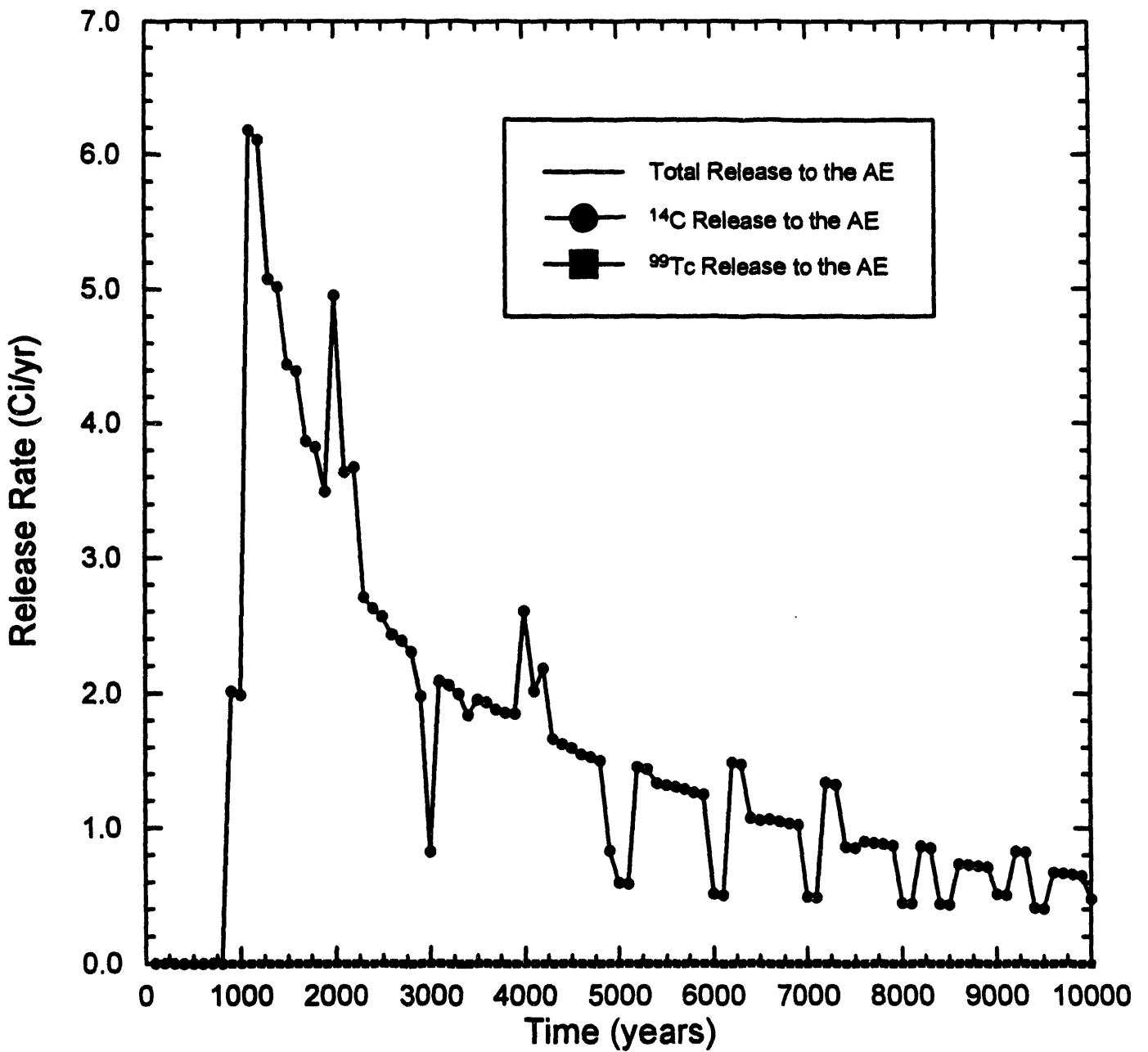


Figure 3-11. Expected-Value Releases to the Accessible Environment over 10,000 Years for 57/10/0.95/S1

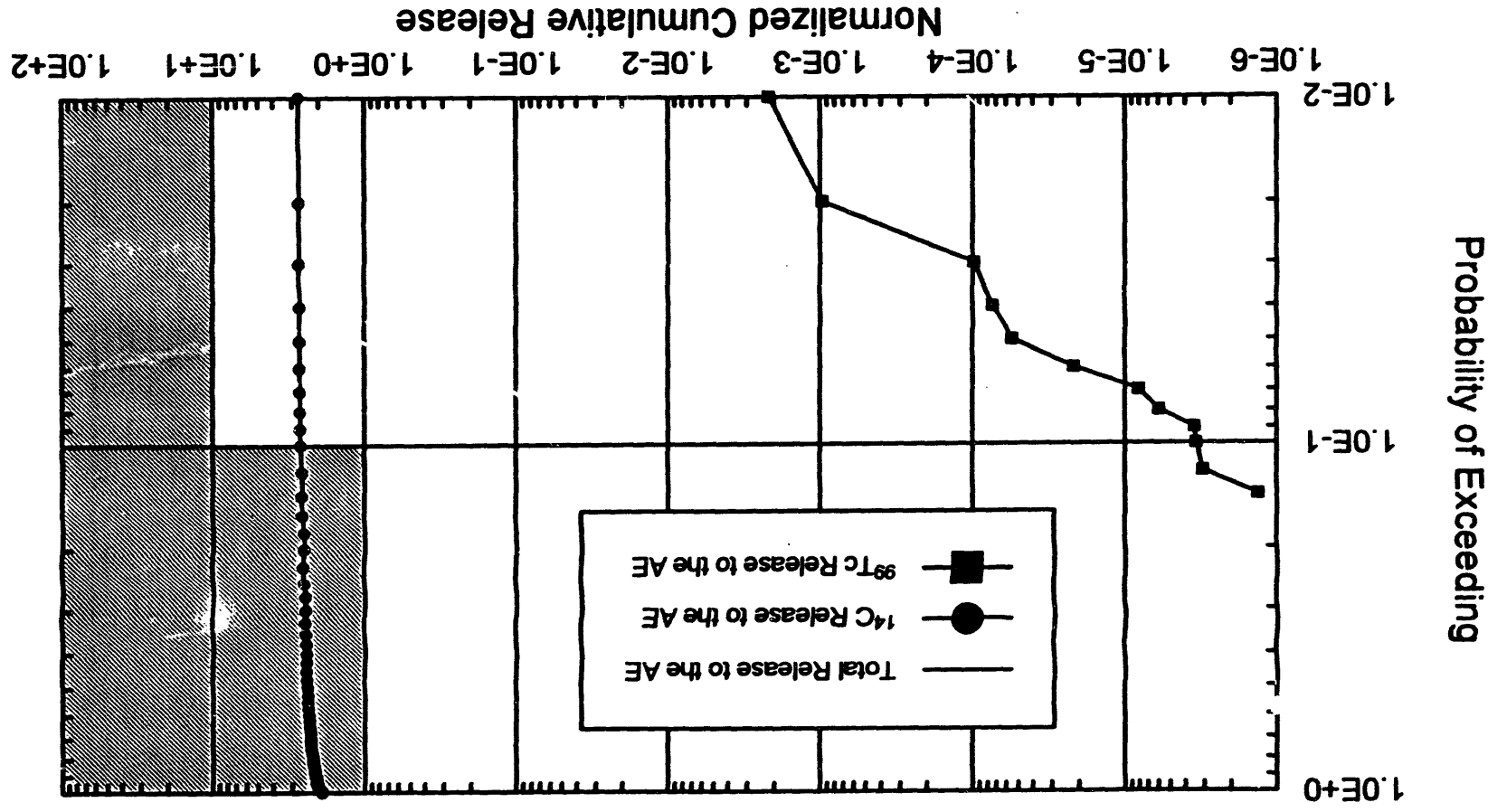


Figure 3-12. CCDF of Normalized Cumulative Release to the Accessible Environment at 10,000 Years for 57/10/0.95/S1

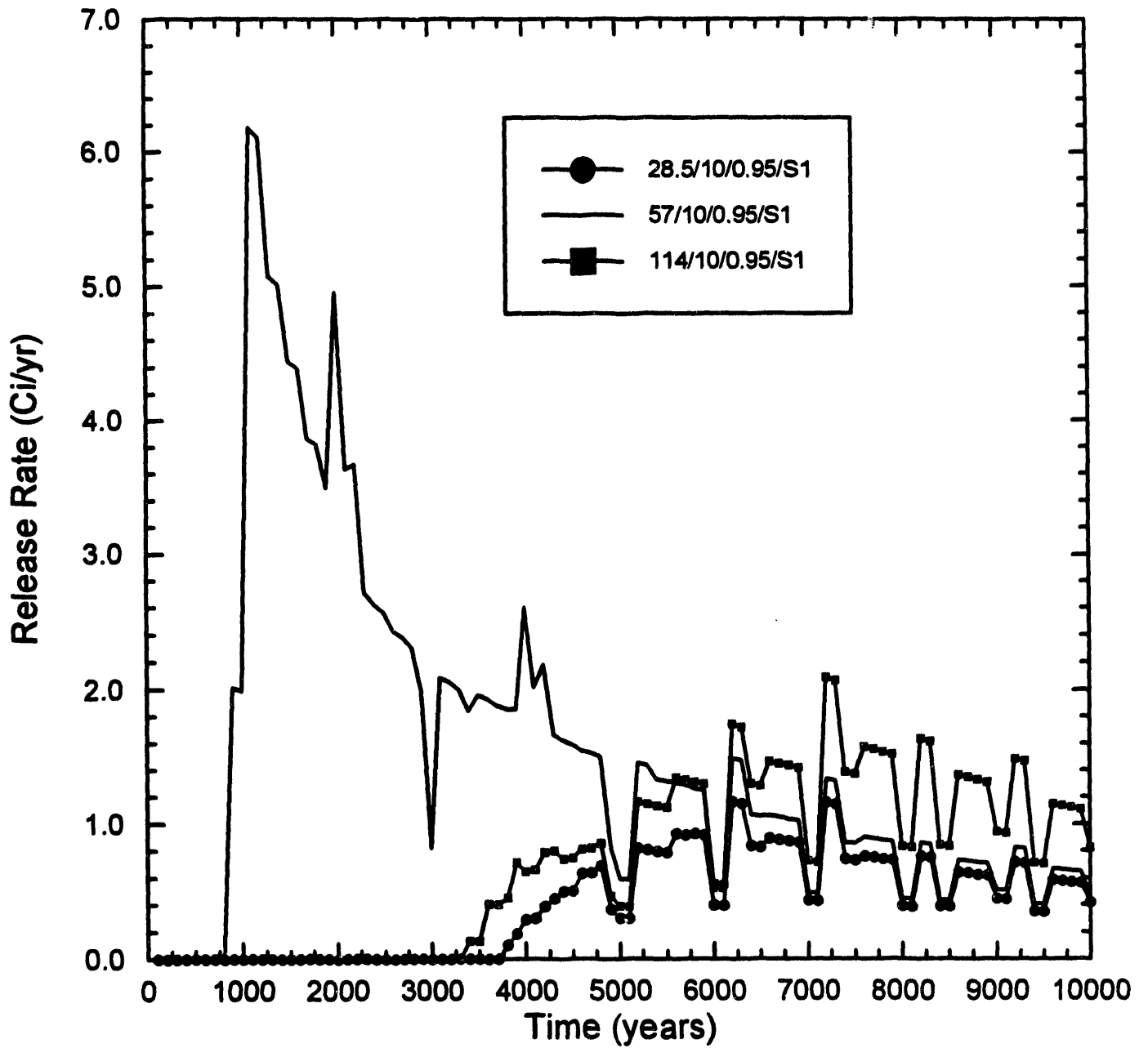


Figure 3-13. Expected-Value Releases to the Accessible Environment over 10,000 Years for 28.5/10/0.95/S1, 57/10/0.95/S1, and 114/10/0.95/S1

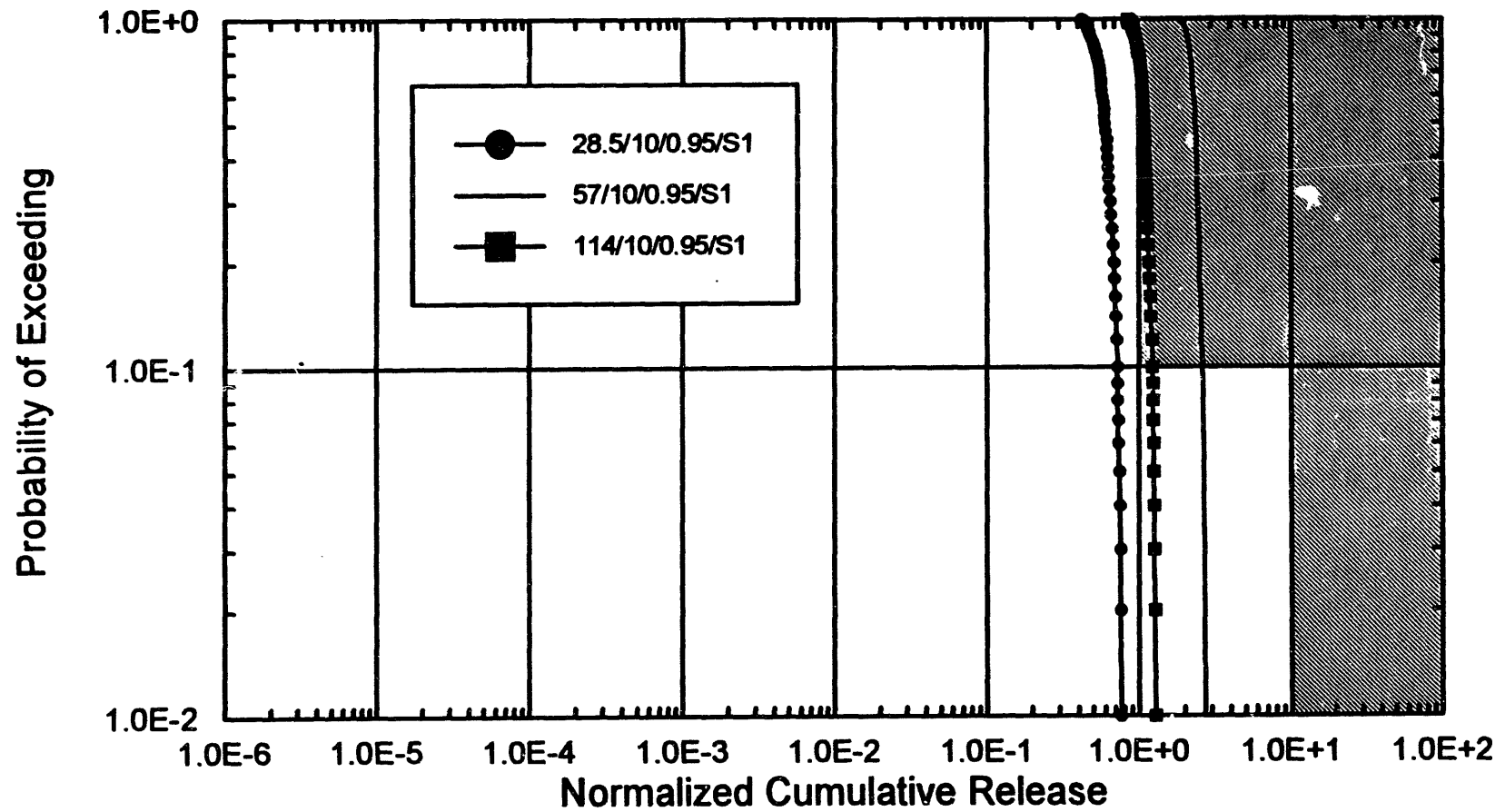


Figure 3-14. CCDF of Normalized Cumulative Releases to the Accessible Environment at 10,000 Years for 28.5/10/0.95/S1, 57/10/0.95/S1 and 114/10/0.95/S1 ,

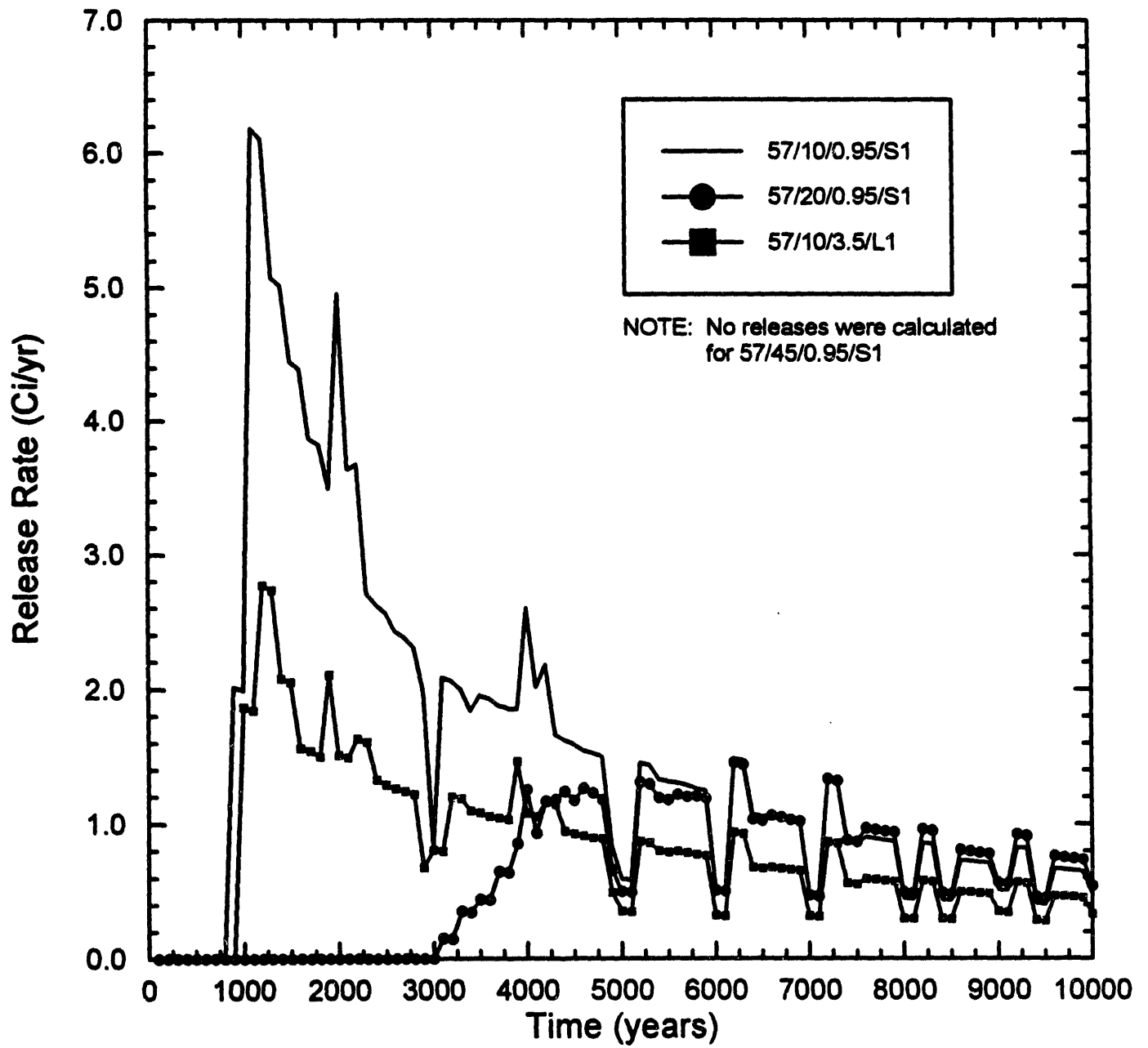


Figure 3-15. Expected-Value Releases to the Accessible Environment over 10,000 Years for 57/10/0.95/S1, 57/20/0.95/S1, and 57/10/3.5/L1

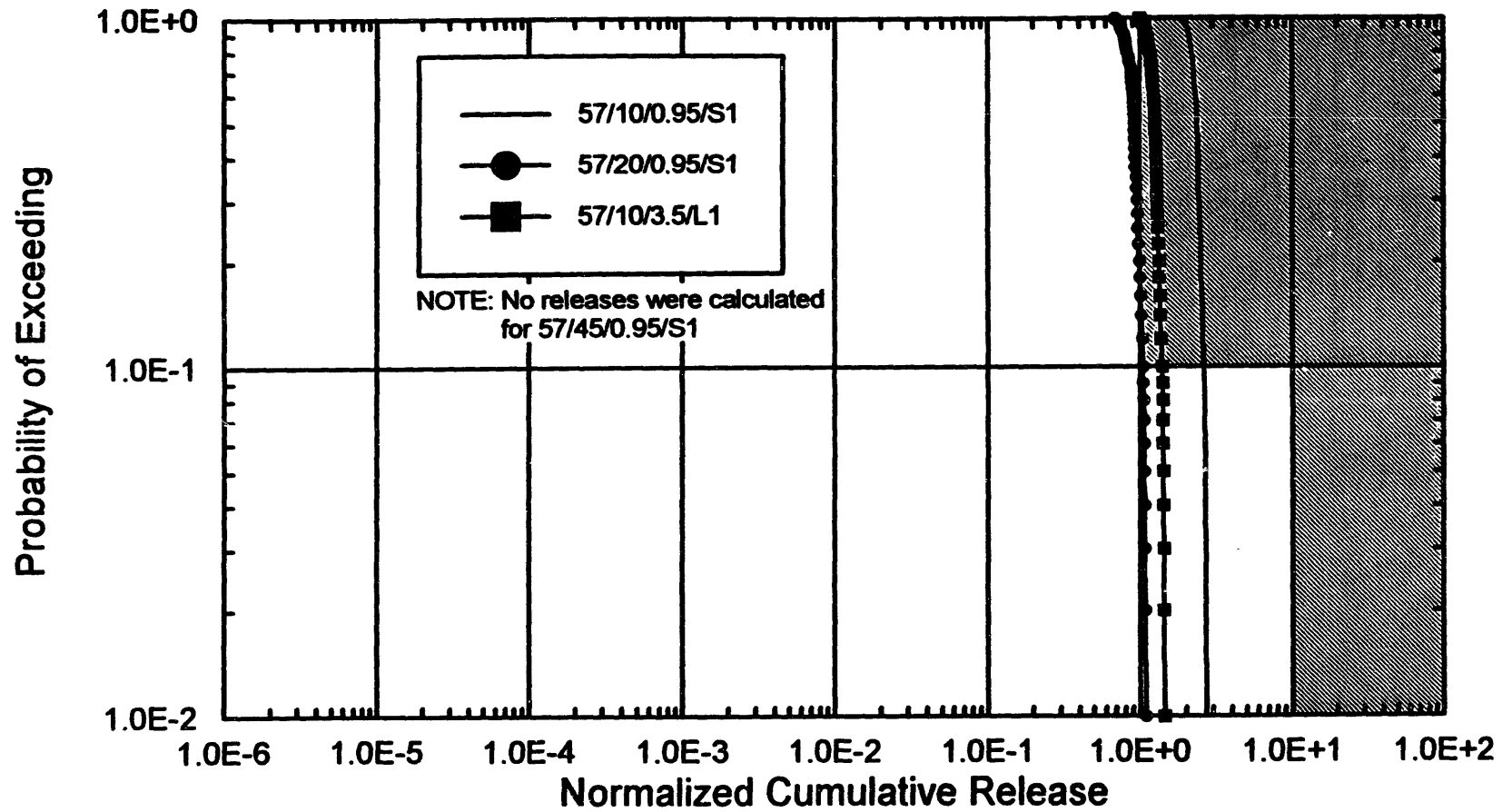


Figure 3-16. CCDF of Normalized Cumulative Release to the Accessible Environment at 10,000 Years for 57/10/0.95/S1, 57/20/0.95/S1, and 57/10/3.5/L1

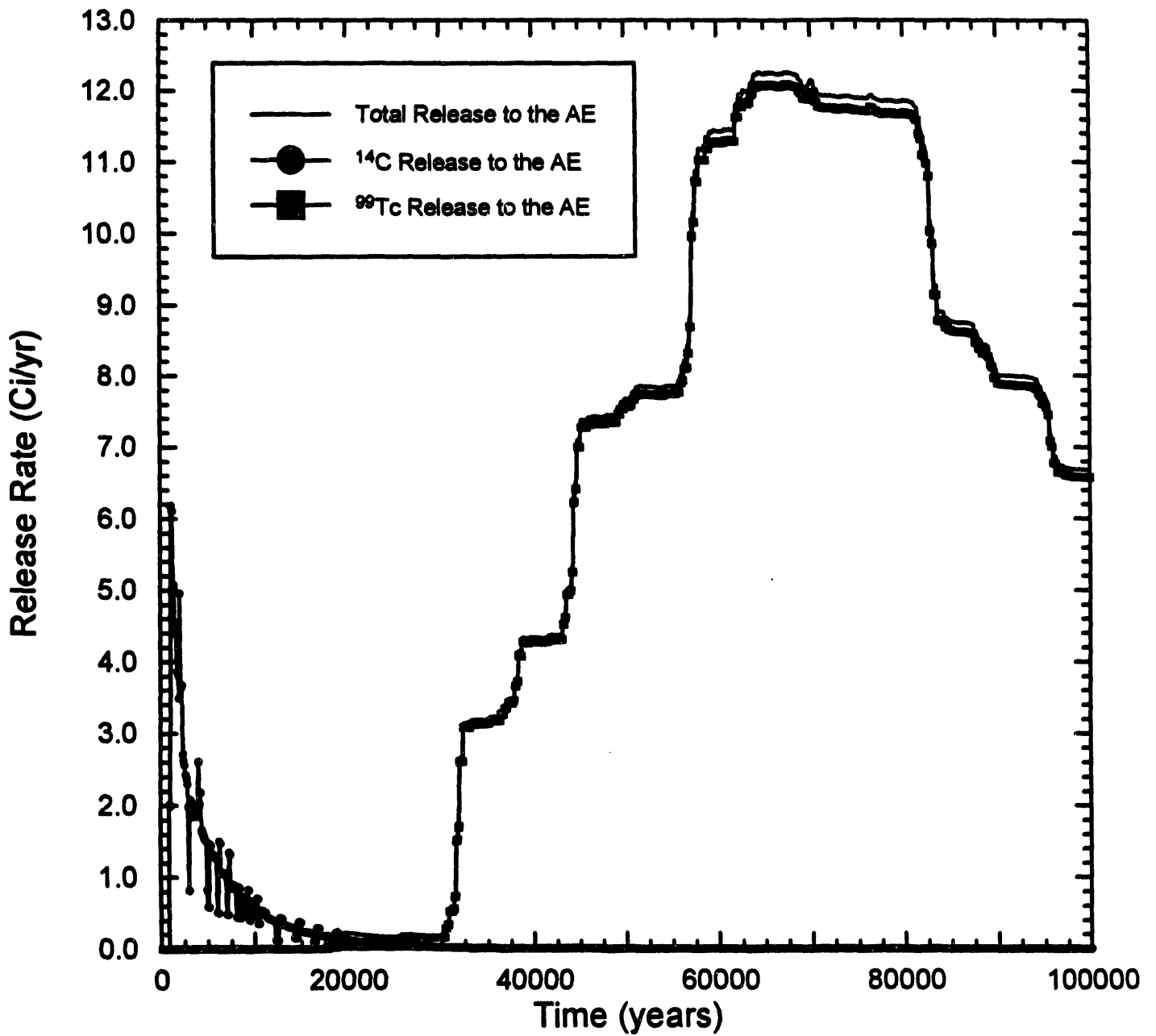


Figure 3-17. Expected-Value Releases to the Accessible Environment over 100,000 Years for 57/10/0.95/S1

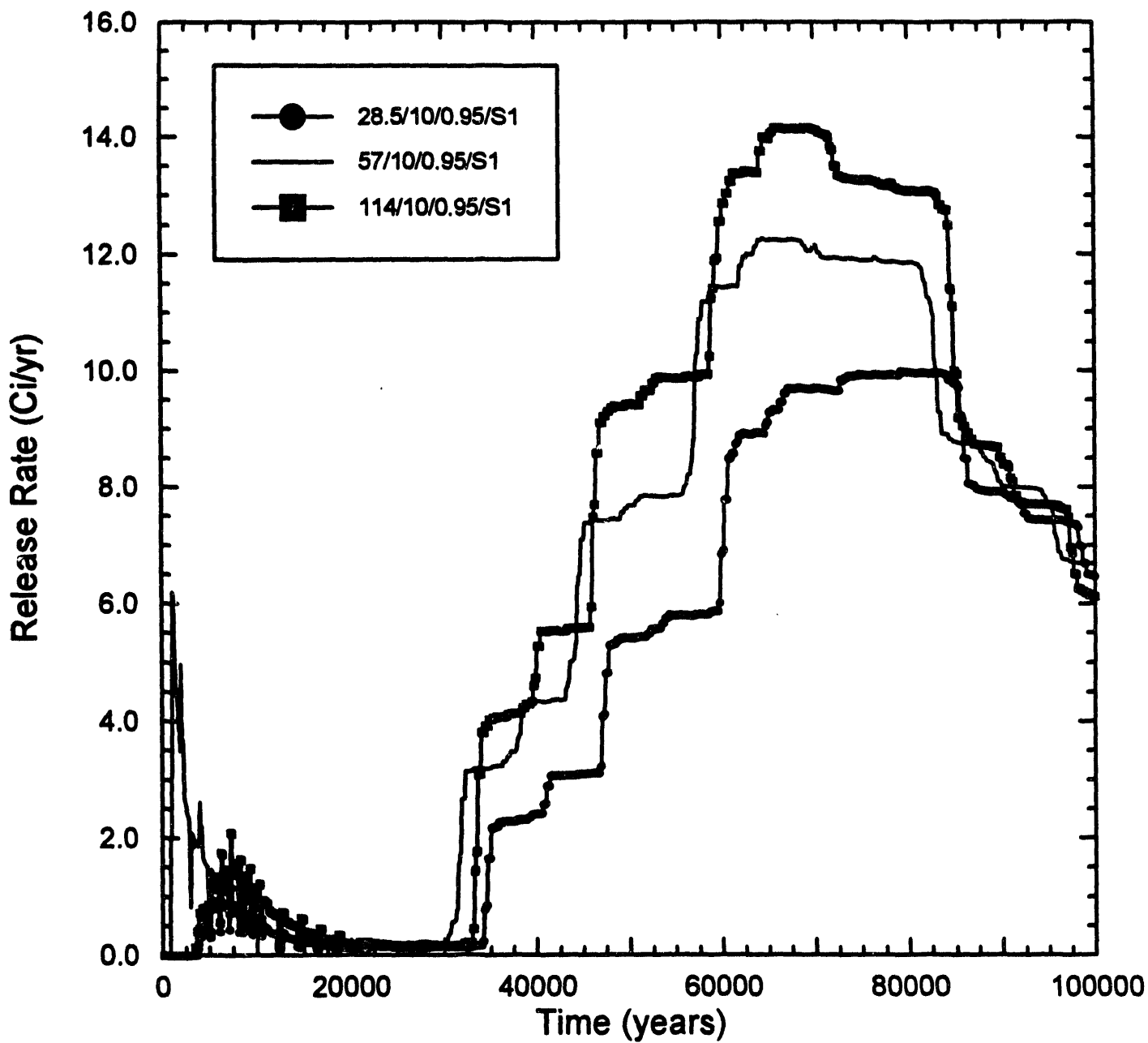


Figure 3-18. Expected-Value Releases to the Accessible Environment over 100,000 Years for 28.5/10/0.95/S1, 57/10/0.95/S1, and 114/10/0.95/S1

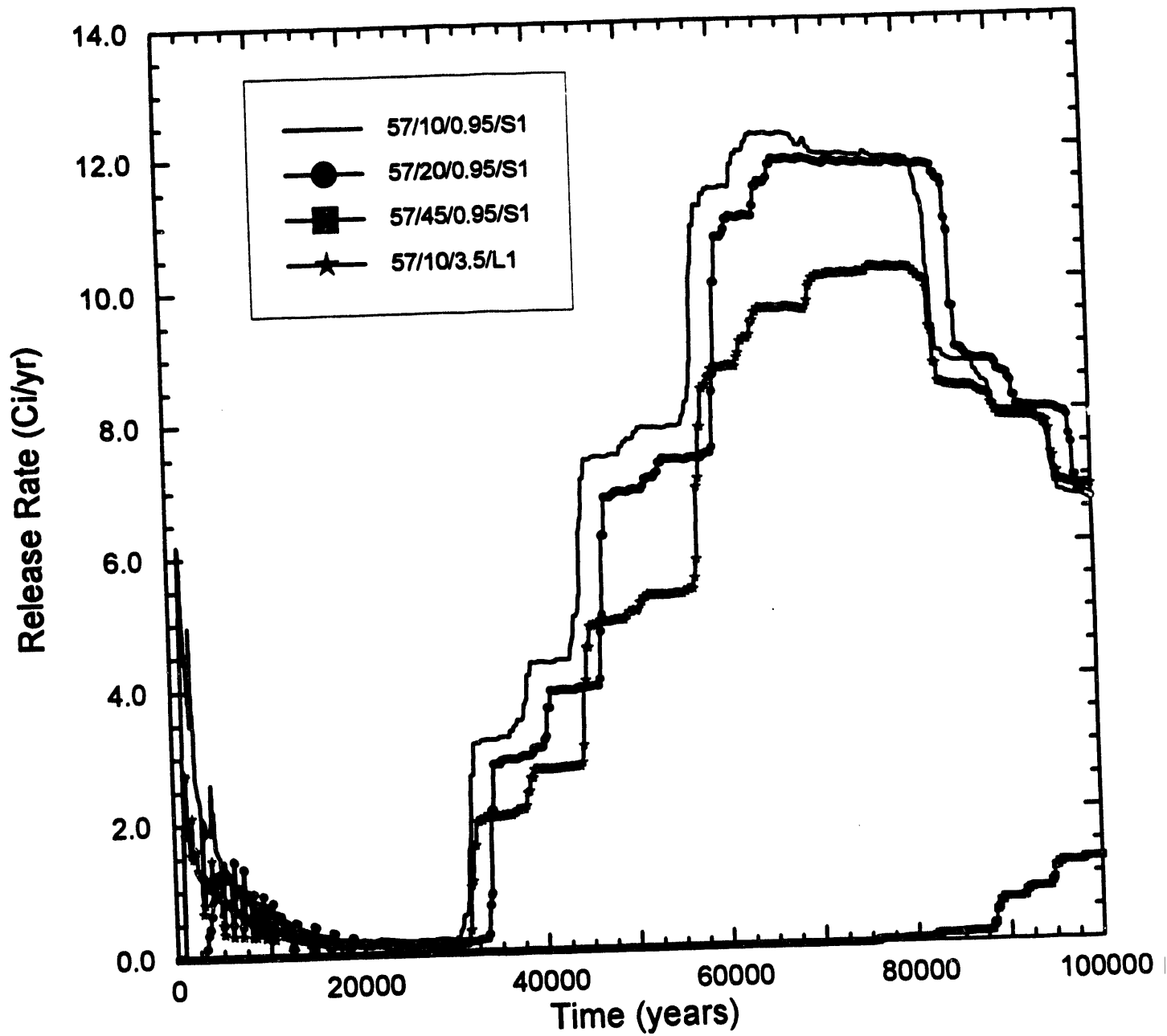


Figure 3-19. Expected-Value Releases to the Accessible Environment over 100,000 Years for 57/10/0.95/S1, 57/20/0.95/S1, 57/45/0.95/S1, and 57/10/3.5/L1

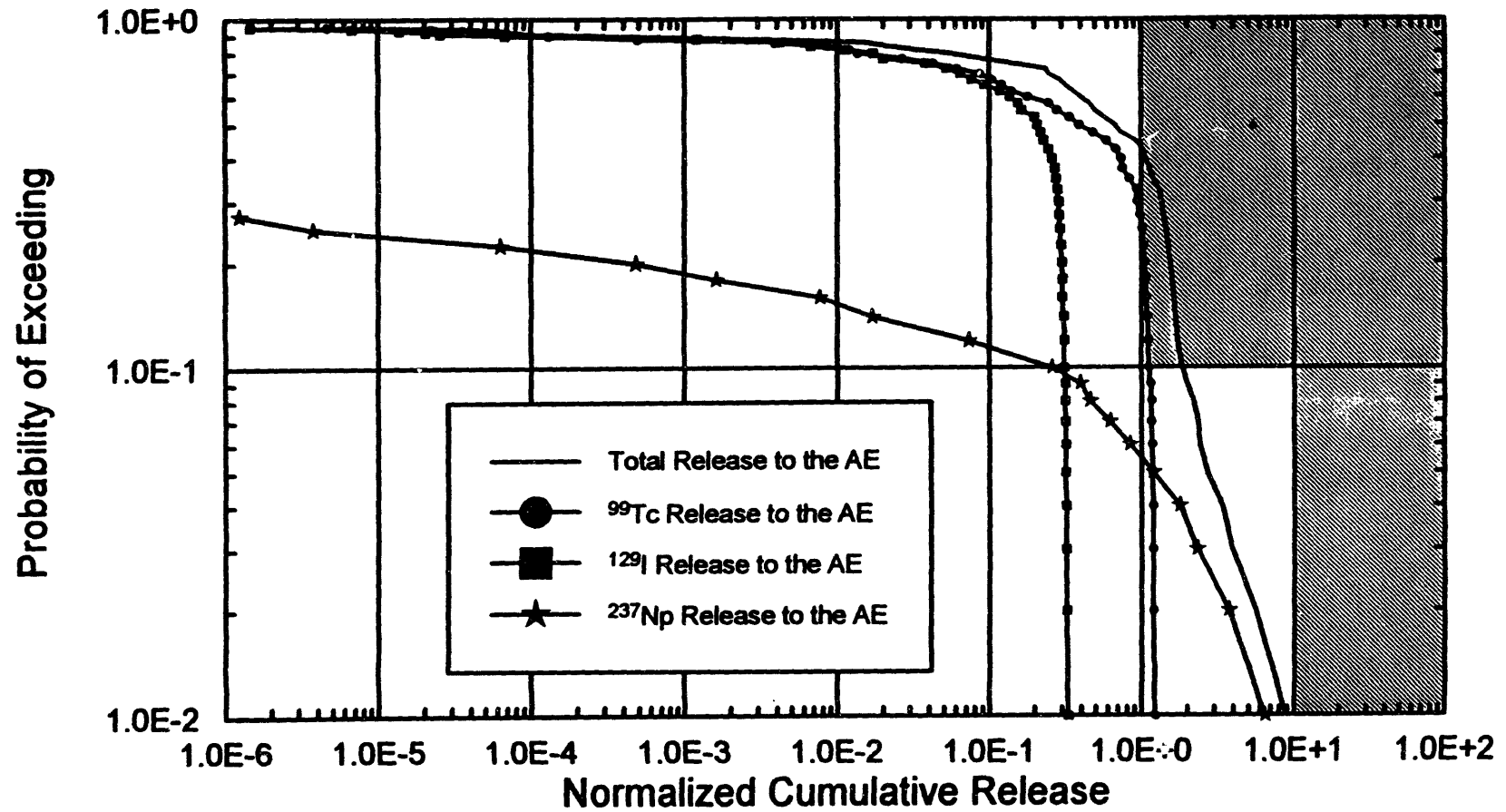


Figure 3-20. CCDF of Normalized Cumulative Release to the Accessible Environment at 100,000 Years for 57/10/0.95/S1

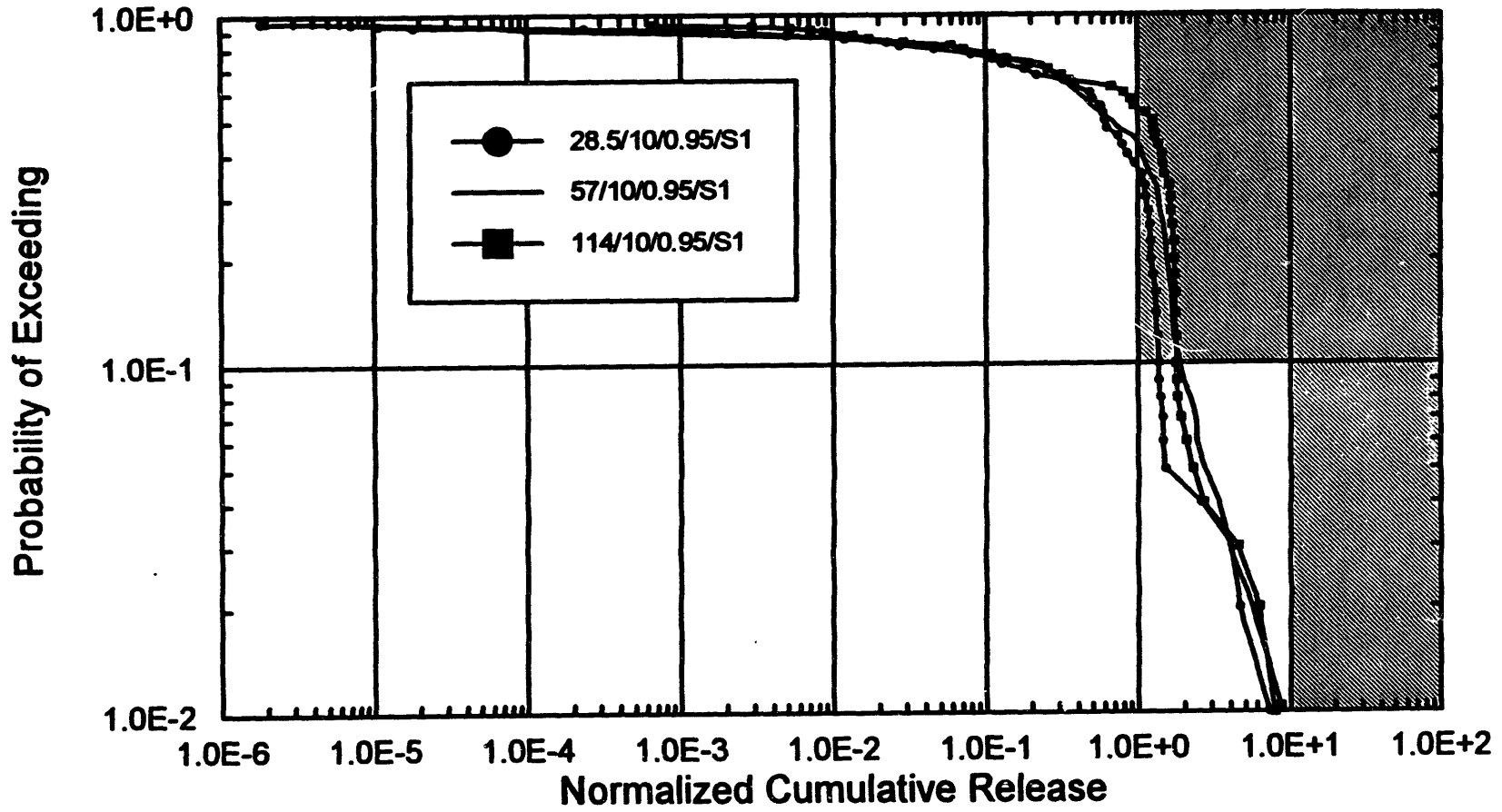


Figure 3-21. CCDF of Normalized Cumulative Release to the Accessible Environment at 100,000 Years for 28.5/10/0.95/S1, 57/10/0.95/S1, and 144/10/0.95/S1

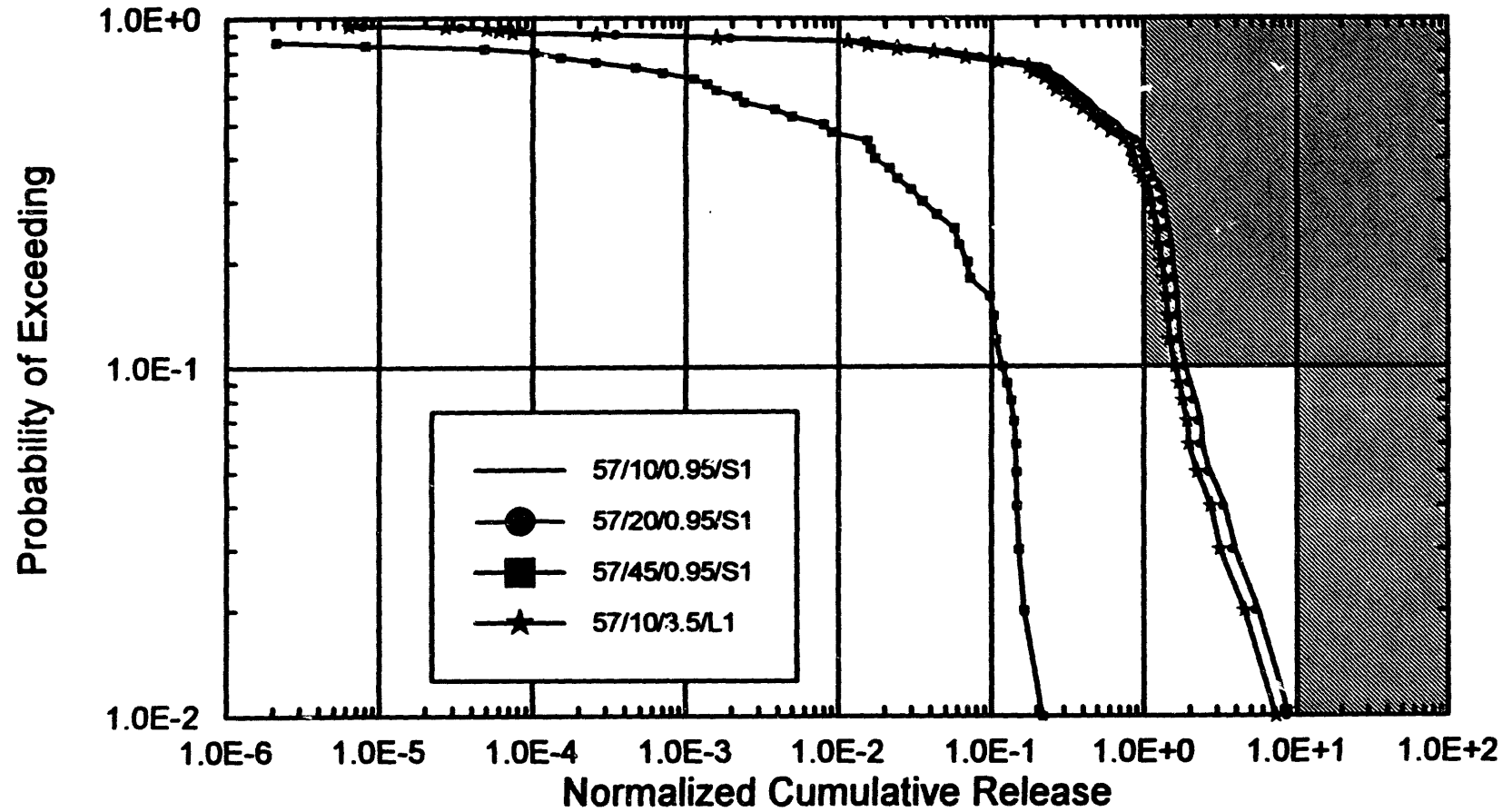


Figure 3-22. CCDF of Normalized Cumulative Release to the Accessible Environment at 100,000 Years for 57/10/0.95/S1, 57/20/0.95/S1, and 57/10/3.5/L1

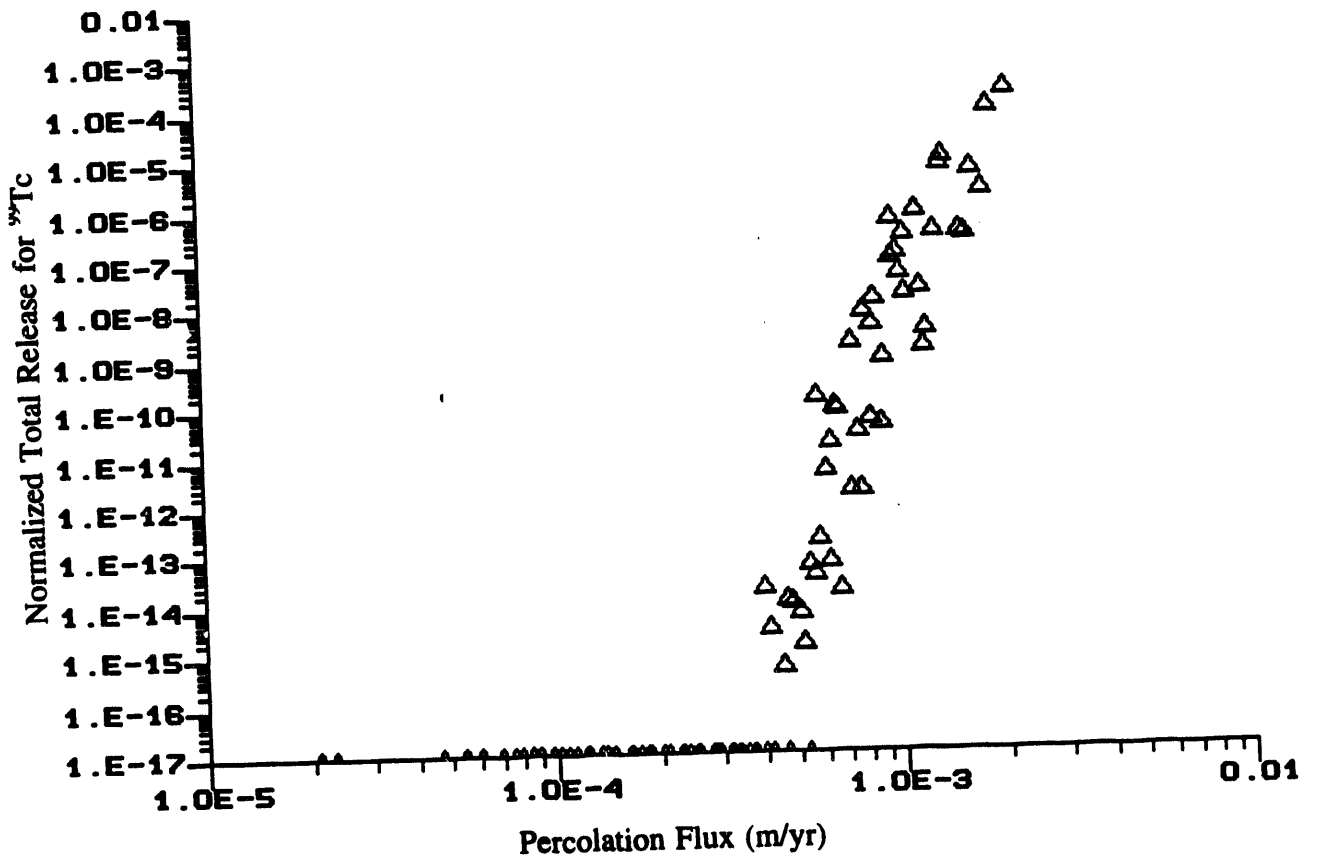


Figure 3-23. Scatter Plot of Unsaturated-Zone Flux vs. Normalized Release of <sup>99</sup>Tc to the Accessible Environment at 10,000 Years for 57/10/0.95/S1

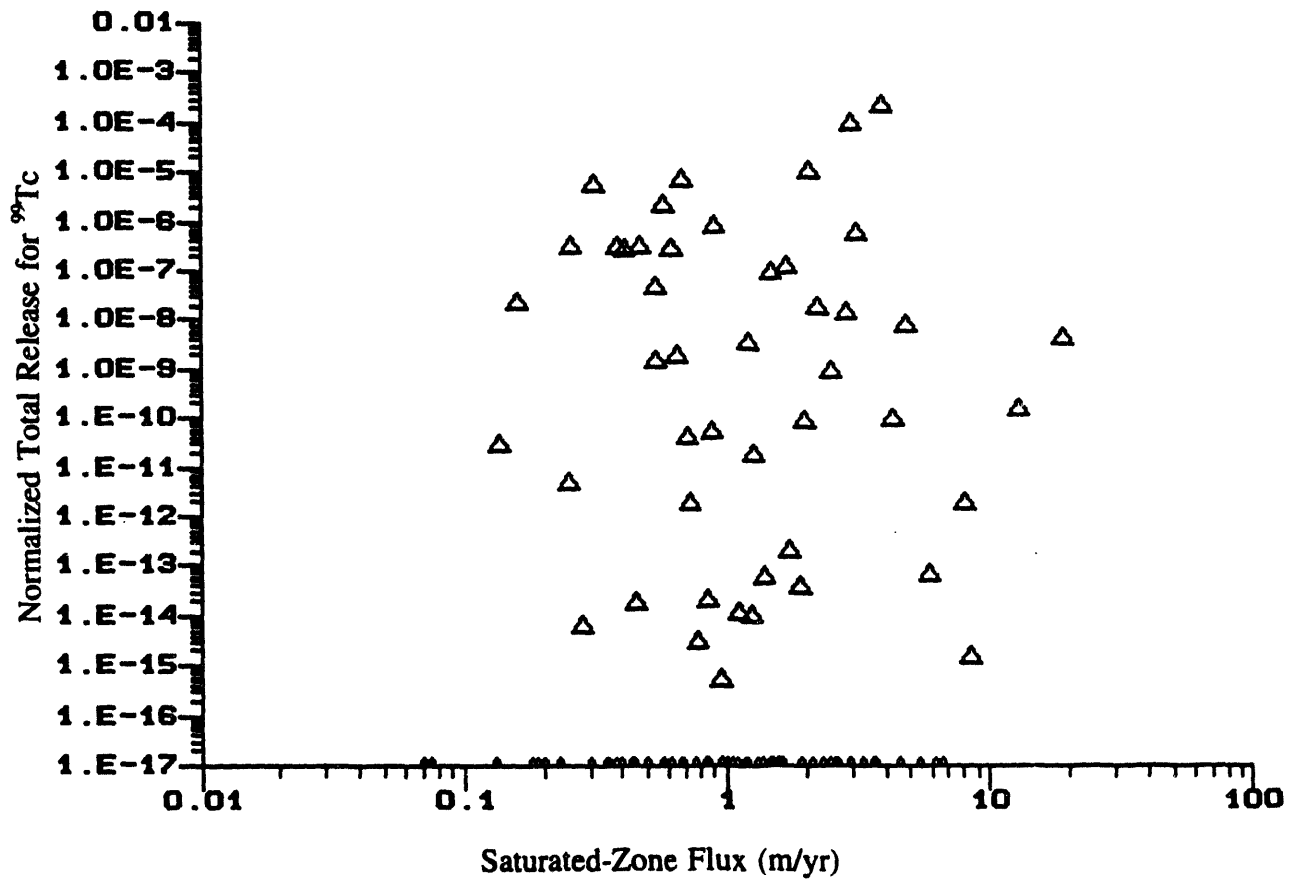


Figure 3-24. Scatter Plot of Saturated-Zone Flux vs. Normalized Release of <sup>99</sup>Tc to the Accessible Environment at 10,000 Years for 57/10/0.95/S1

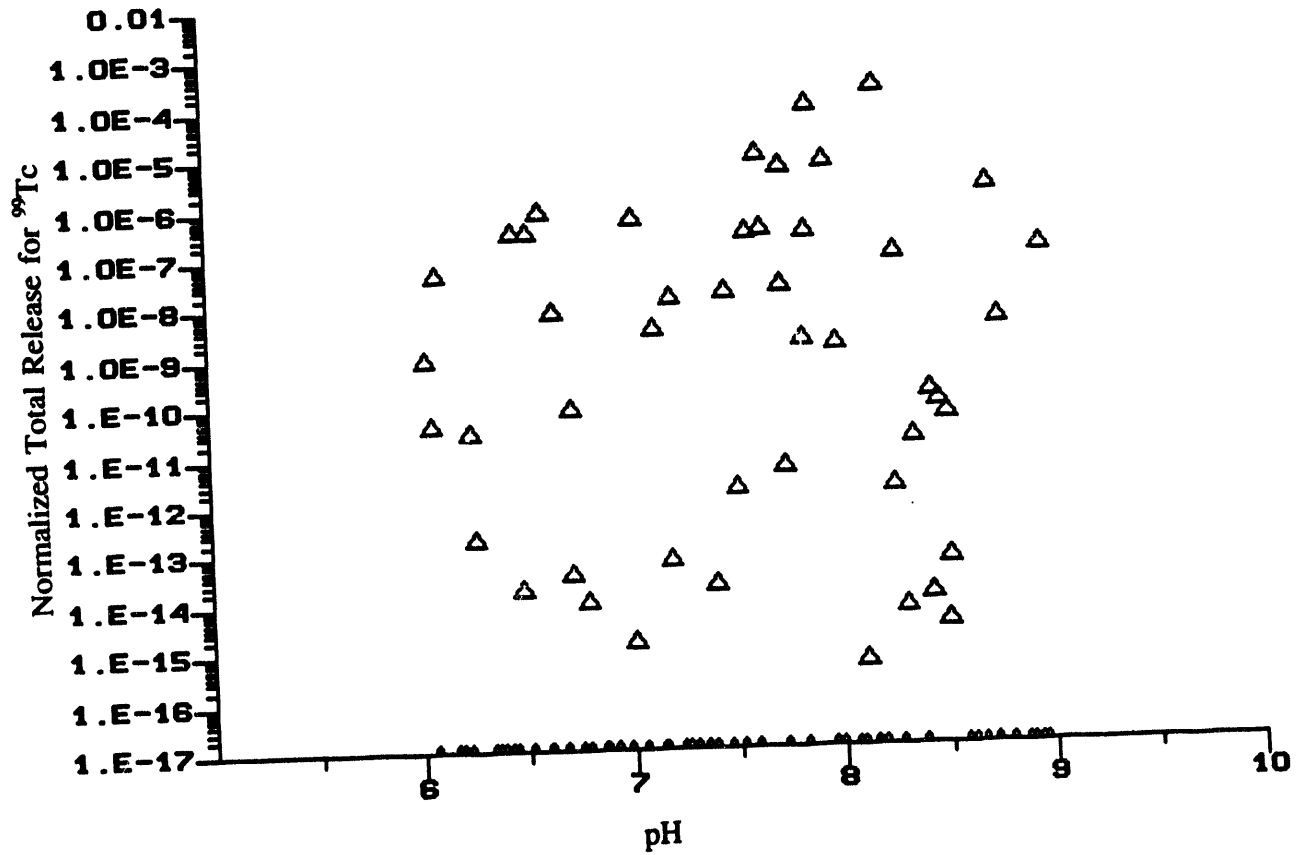


Figure 3-25. Scatter Plot of pH vs. Normalized Release of <sup>99</sup>Tc to the Accessible Environment at 10,000 Years for 57/10/0.95/S1

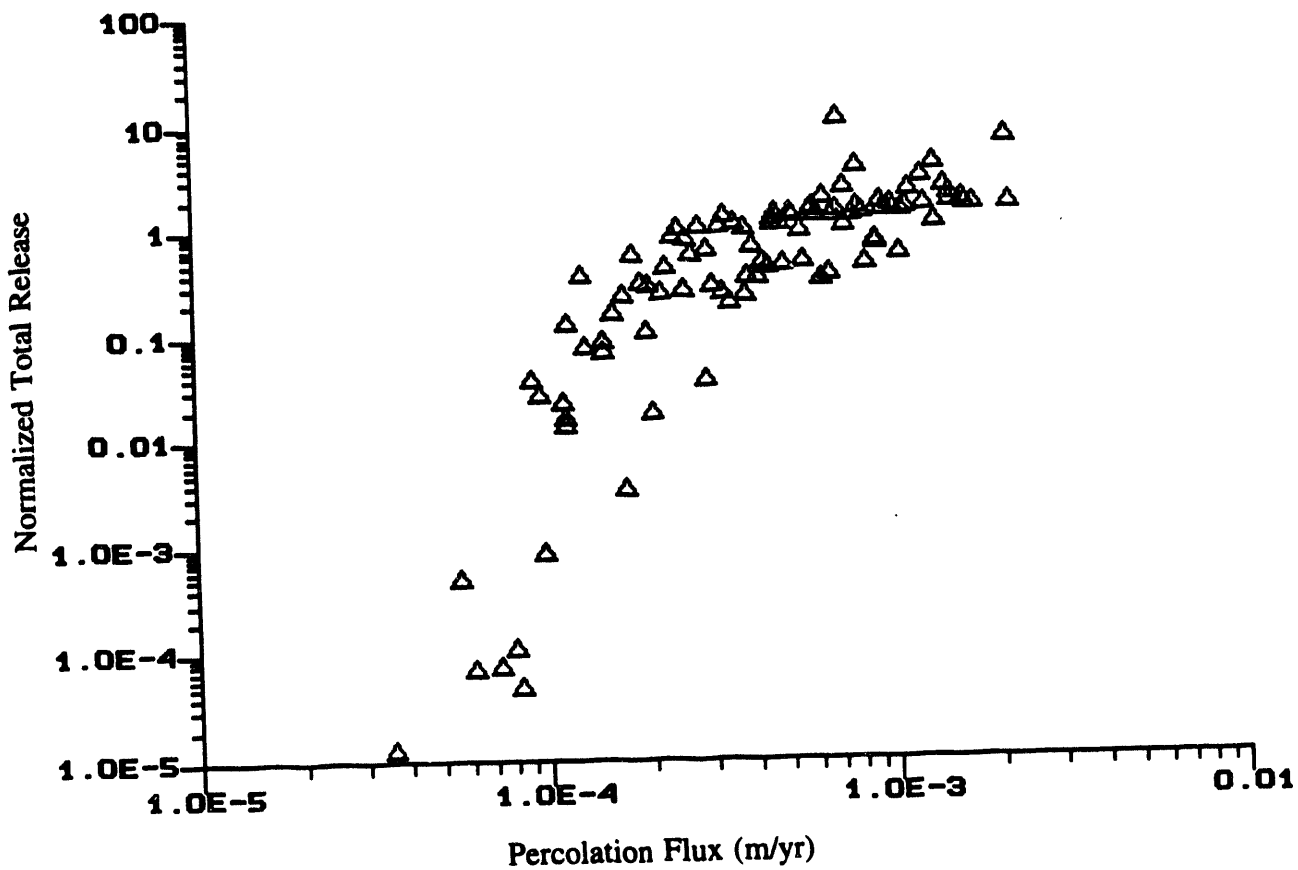


Figure 3-26. Scatter Plot of Unsaturated-Zone Flux vs. Normalized Total Release to the Accessible Environment at 100,000 Years for 57/10/0.95/S1

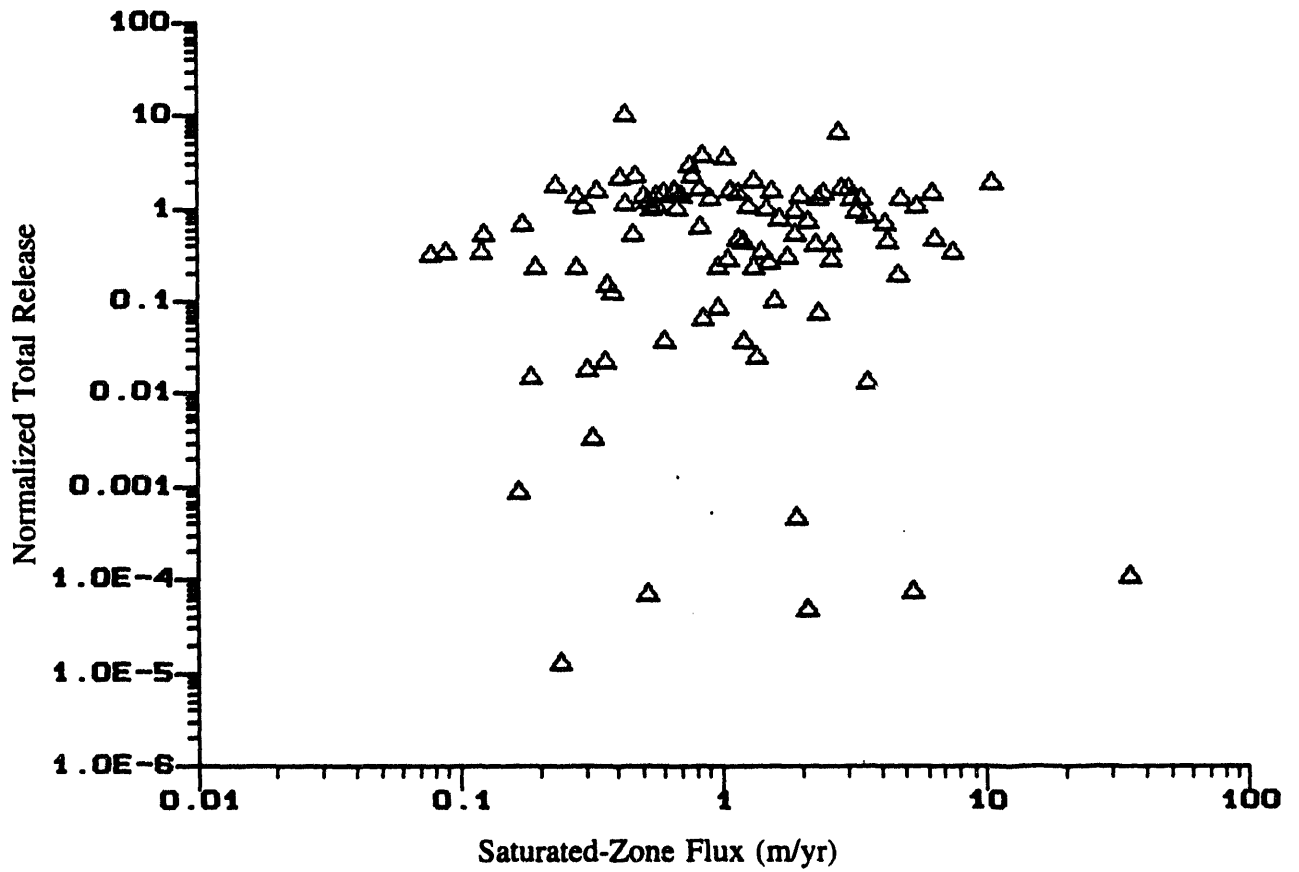


Figure 3-27. Scatter Plot of Saturated-Zone Flux vs. Normalized Total Release to the Accessible Environment at 100,000 Years for 57/10/0.95/S1

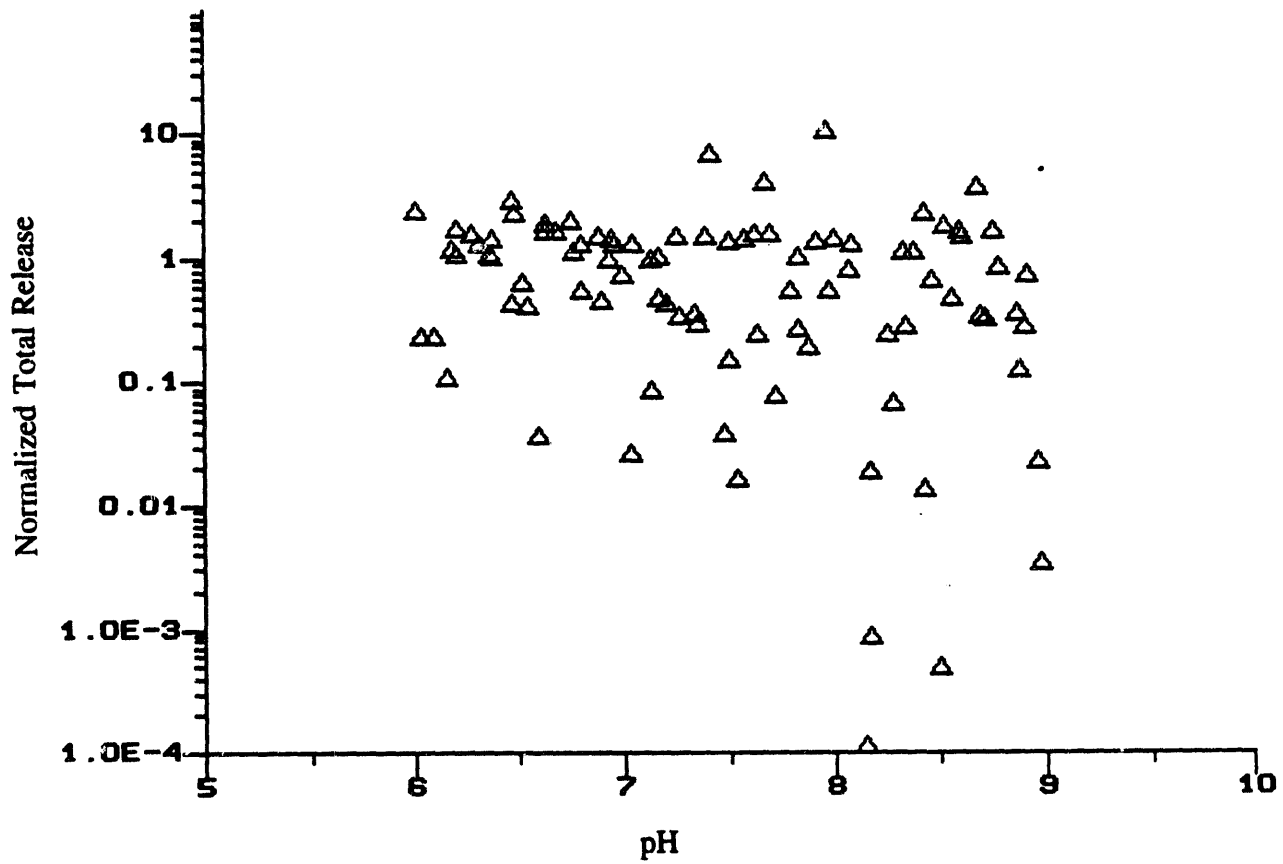


Figure 3-28. Scatter Plot of pH vs. Normalized Total Release to the Accessible Environment at 100,000 Years for 57/10/0.95/S1

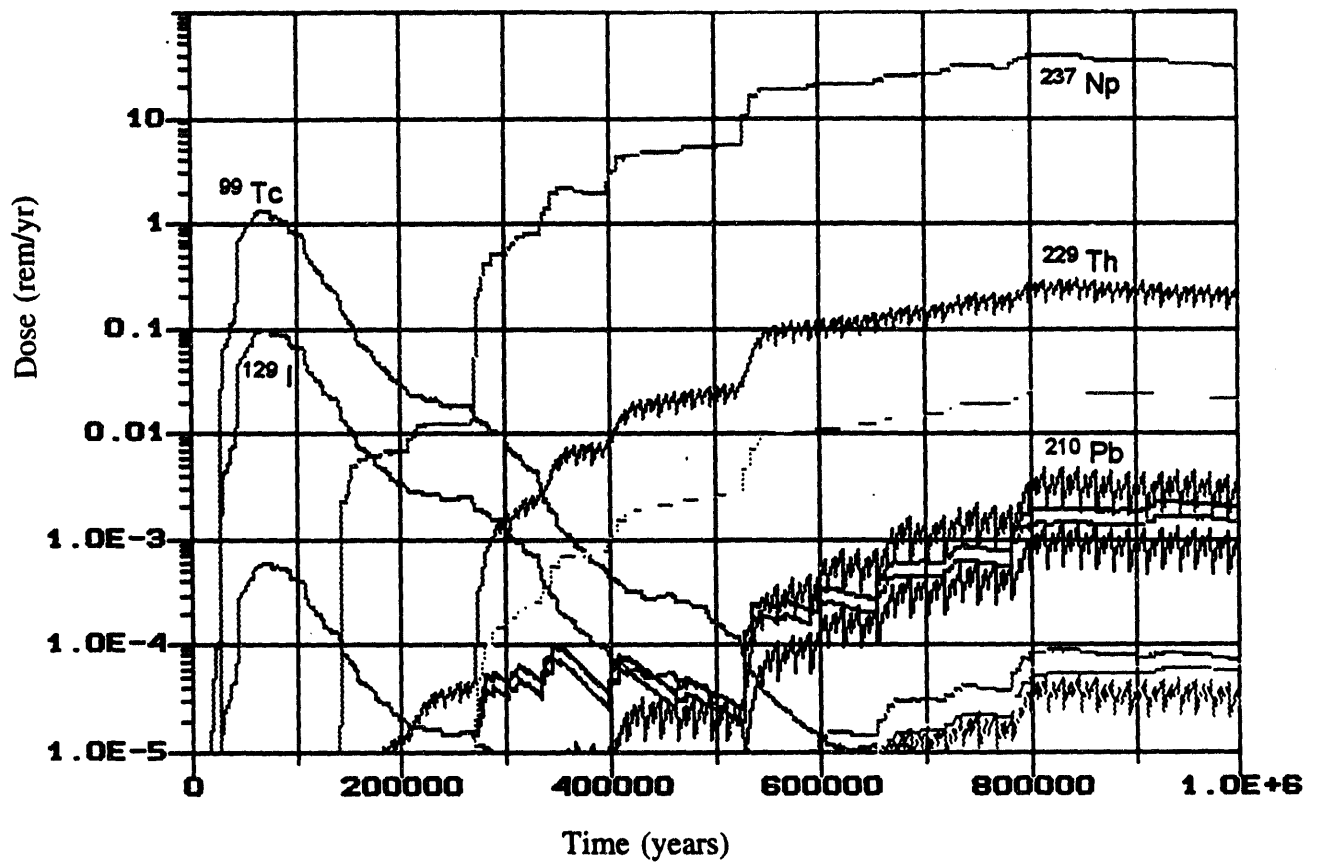


Figure 3-29. Expected-Value Dose Exposures over 1,000,000 Years for 57/10/0.95/S1

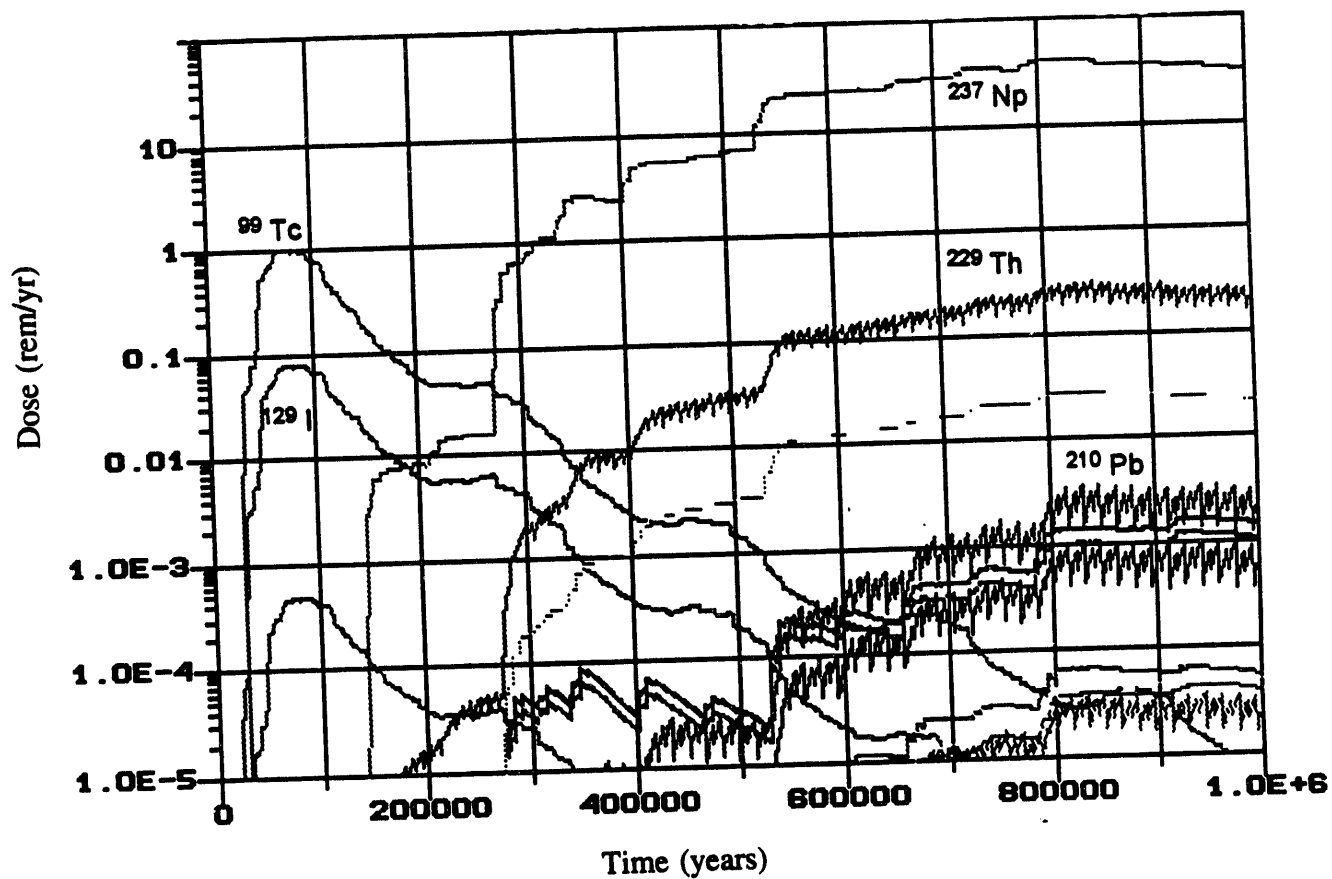


Figure 3-30. Expected-Value Dose Exposures over 1,000,000 Years for 28.5/10/0.95/S1

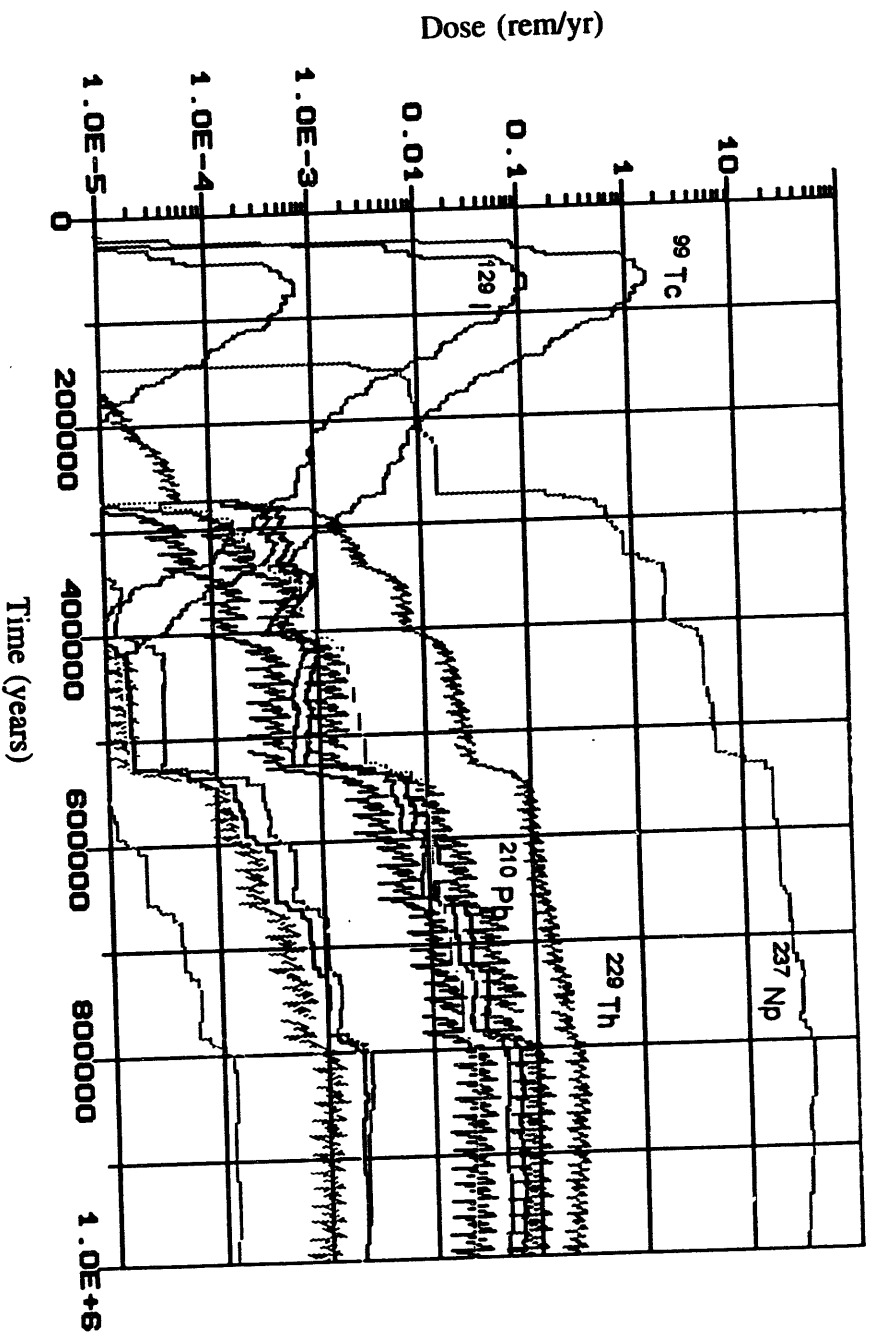


Figure 3-31. Expected-Value Dose Exposures over 1,000,000 Years for 114/10/0.95/S1

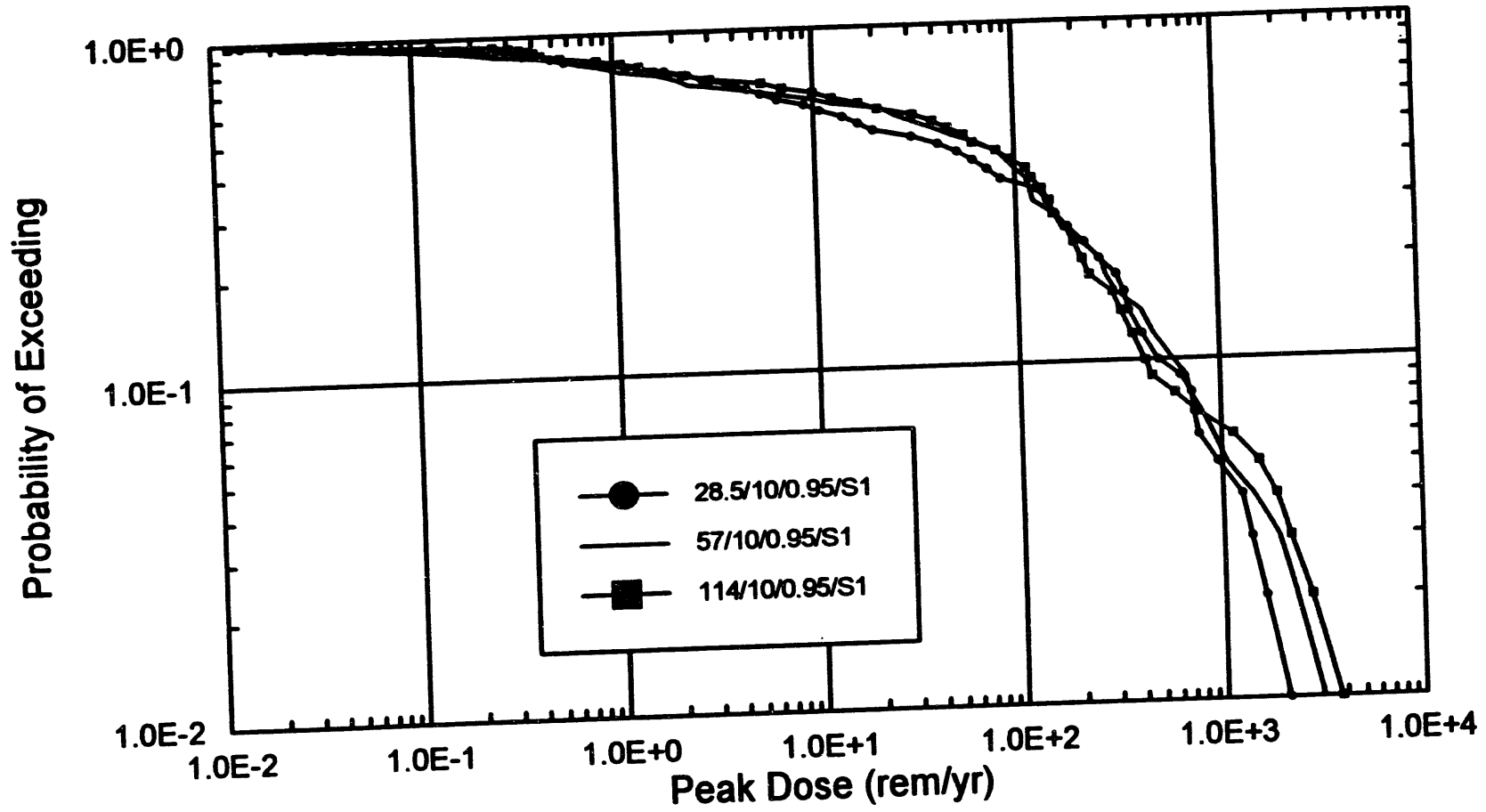


Figure 3-32. CCDF of Peak Dose Exposures over 1,000,000 Years for 28.5/10/0.95/S1, 57/10/0.95/S1, and 114/10/0.95/S1

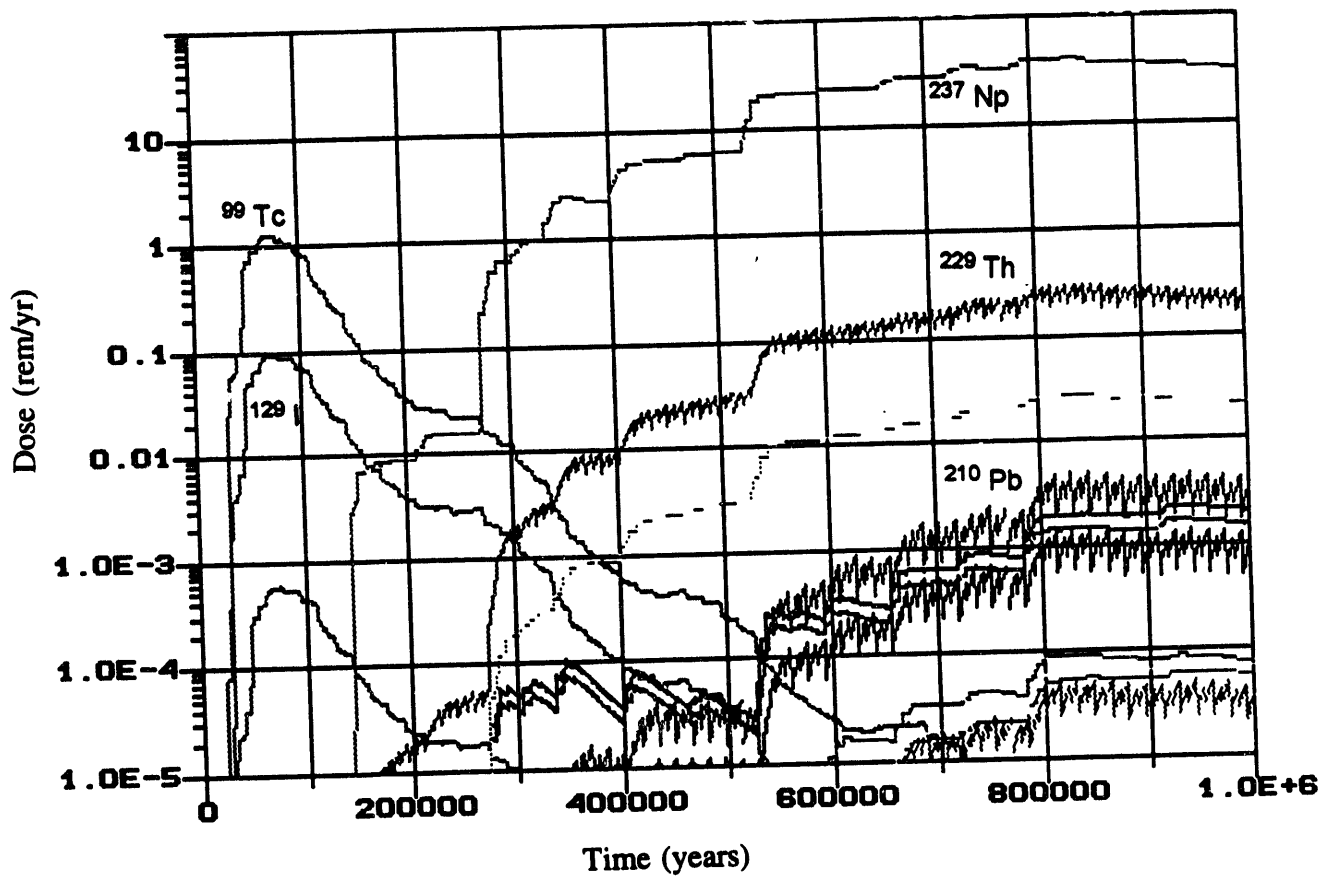


Figure 3-33. Expected-Value Dose Exposures over 1,000,000 Years for 57/20/0.95/S1

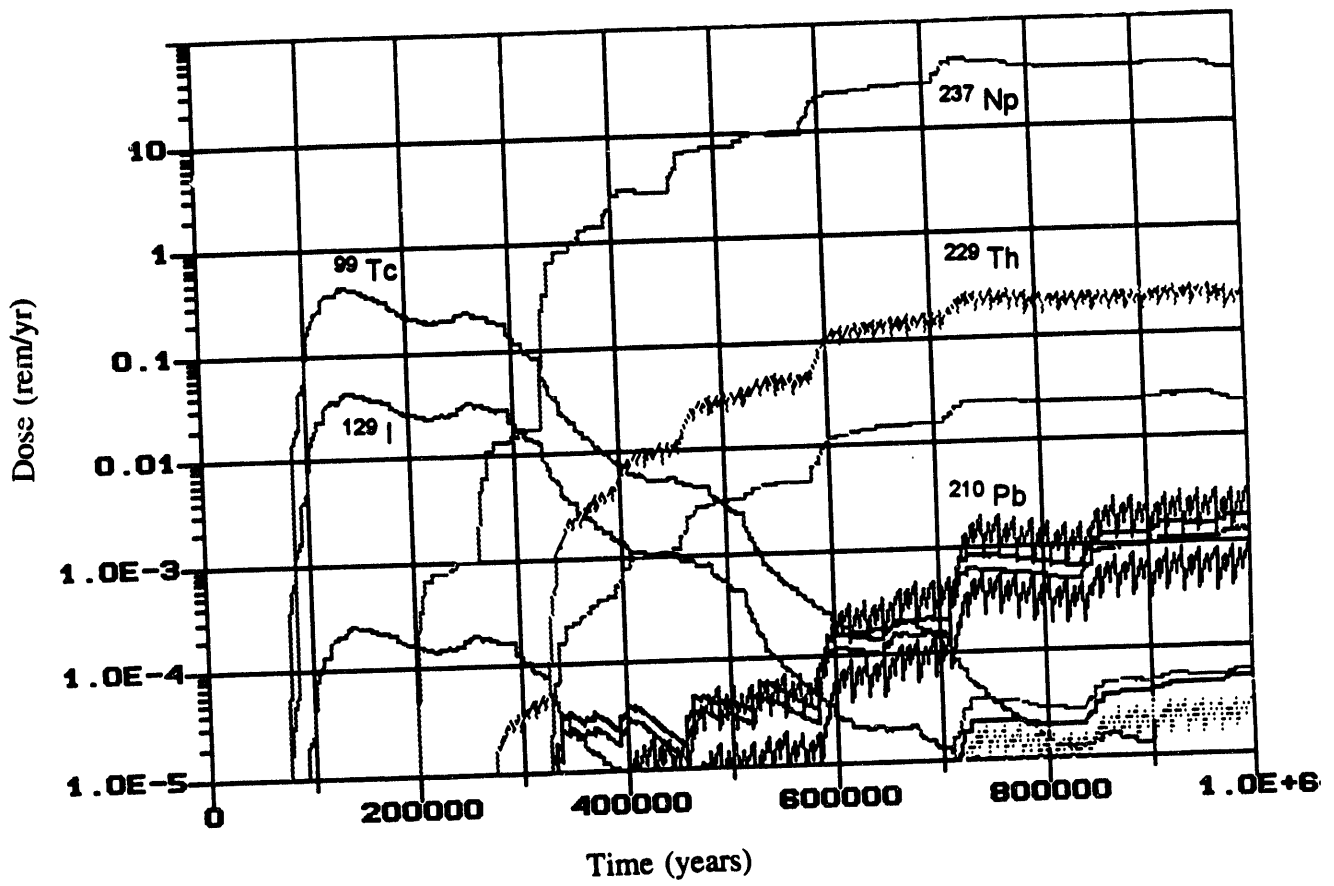


Figure 3-34. Expected-Value Dose Exposures over 1,000,000 Years for 57/45/0.95/S1

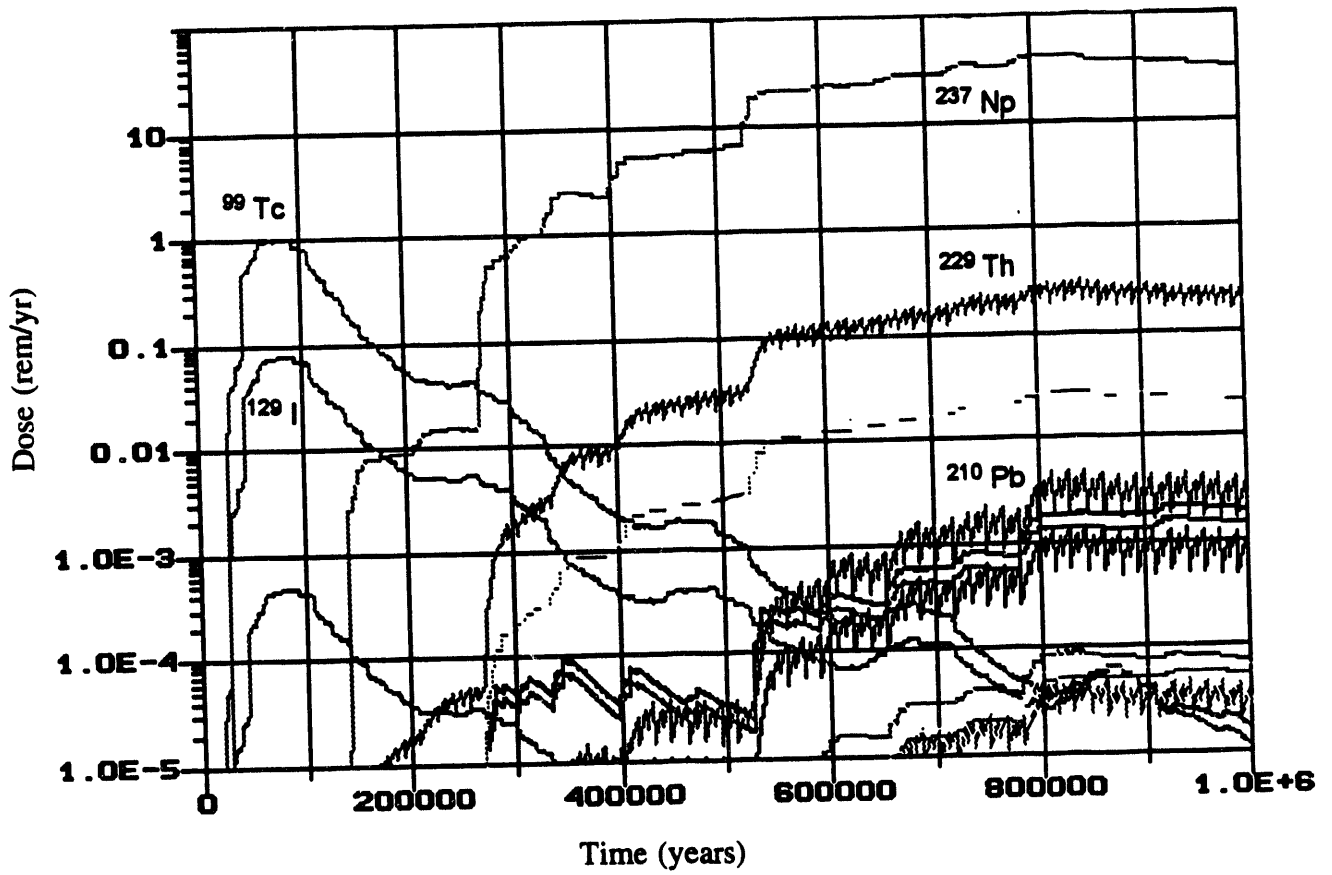


Figure 3-35. Expected-Value Dose Exposures over 1,000,000 Years for 57/10/3.5/L1

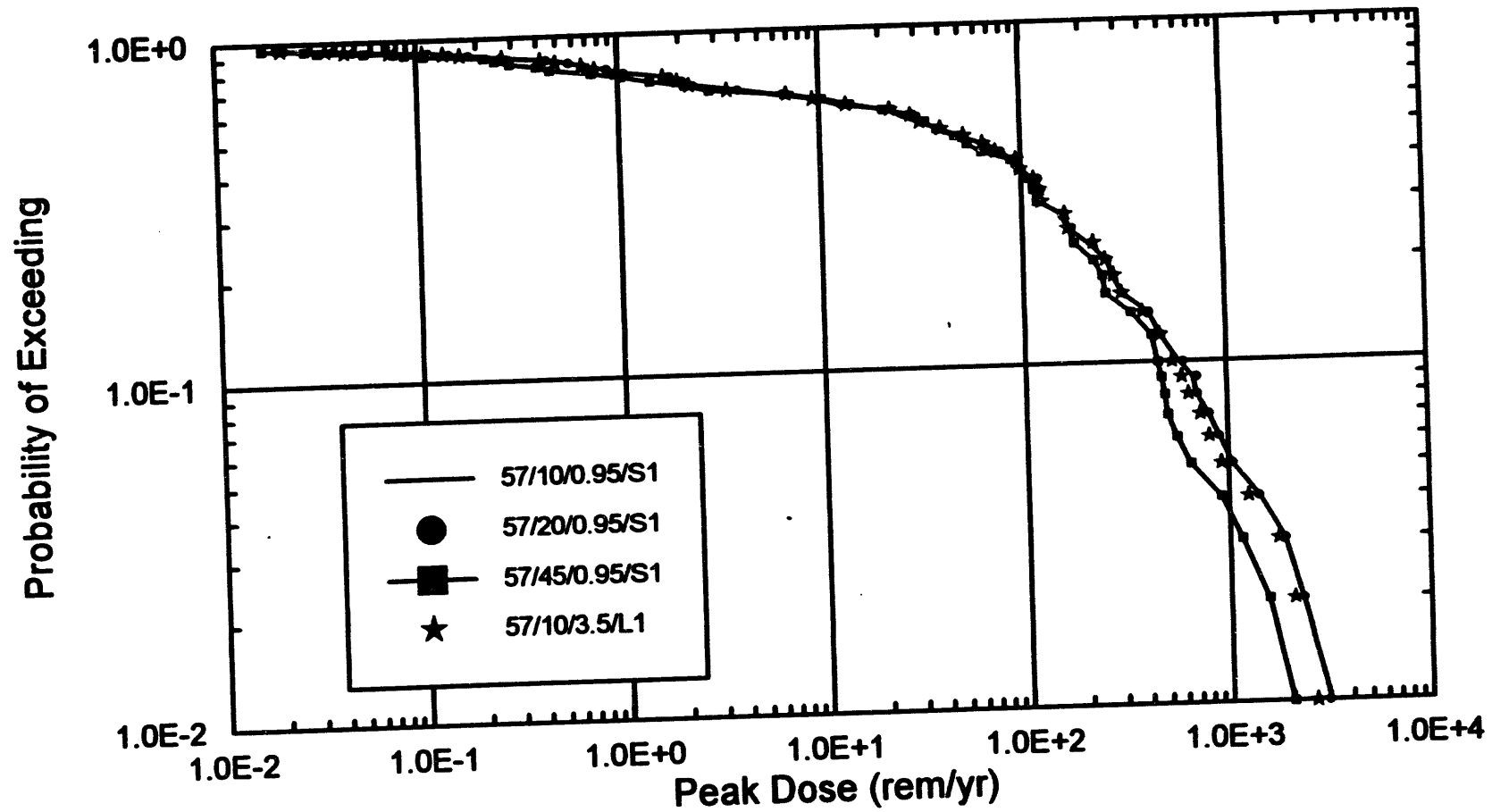


Figure 3-36. CCDF of Peak Dose Exposures over 1,000,000 Years for 57/10/0.95/S1, 57/20/0.95/S1, 57/45/0.95/S1, and 57/10/3.5/L1

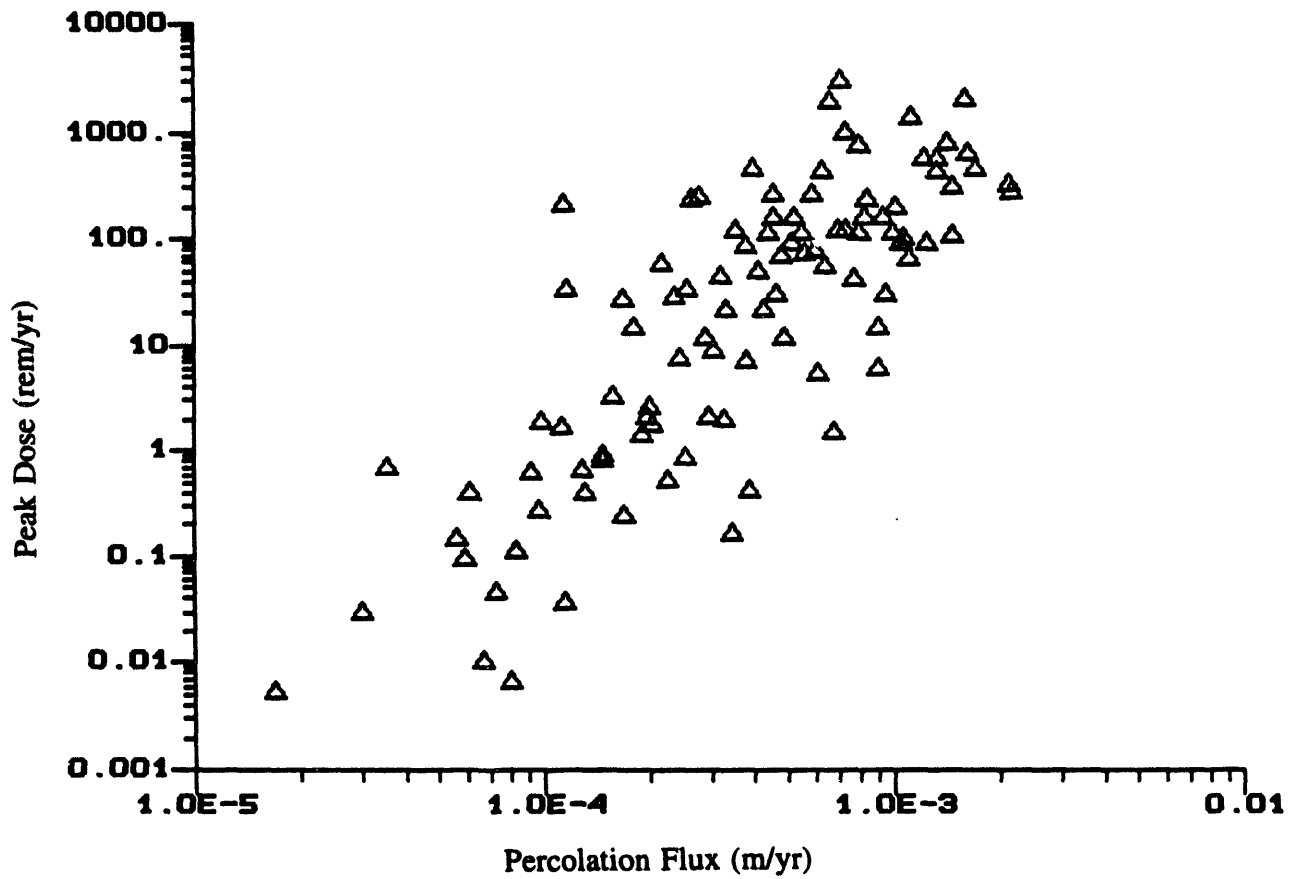


Figure 3-37. Scatter Plot of Unsaturated-Zone Flux vs. Peak Dose Exposure over 1,000,000 Years for 57/10/0.95/S1

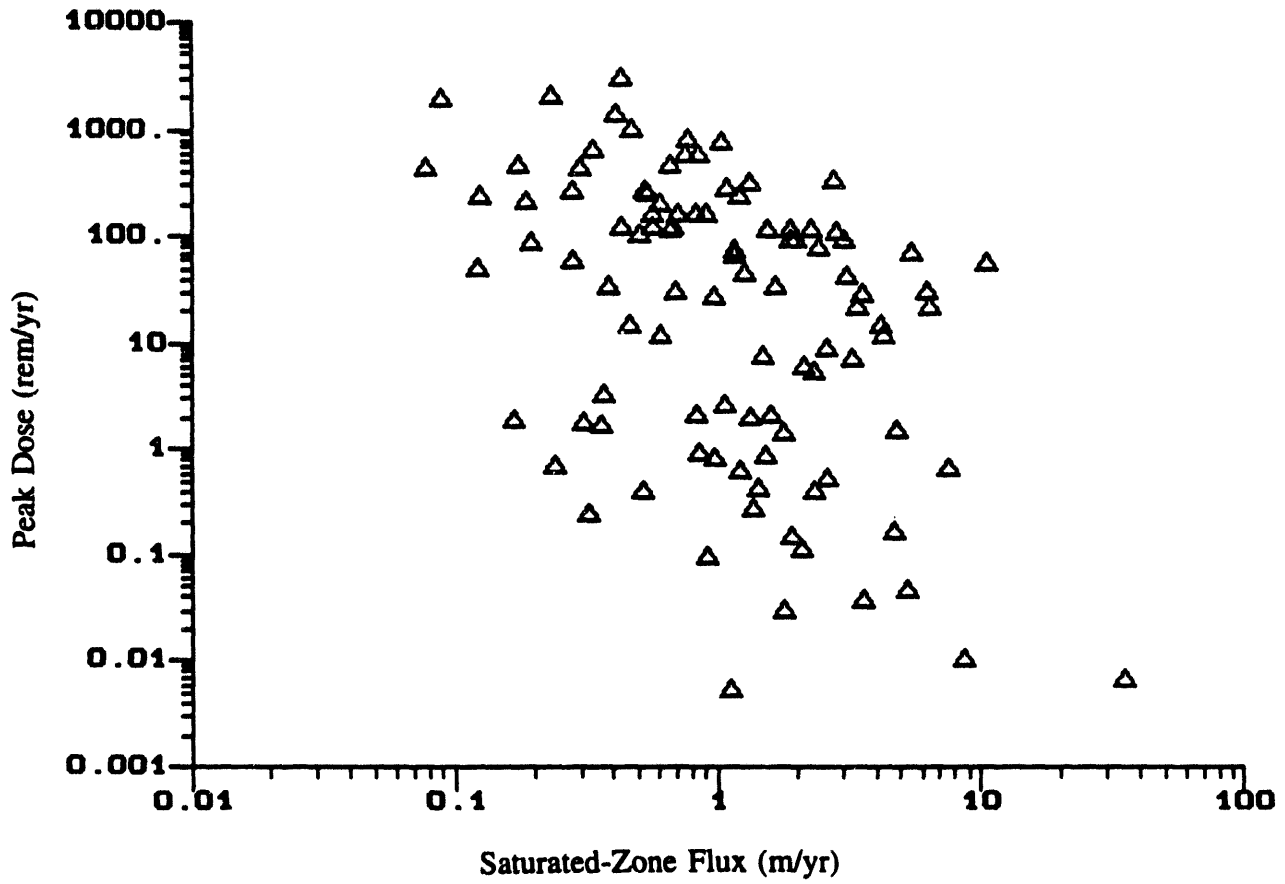


Figure 3-38. Scatter Plot of Saturated-Zone Flux vs. Peak Dose Exposure over 1,000,000 Years for 57/10/0.95/S1

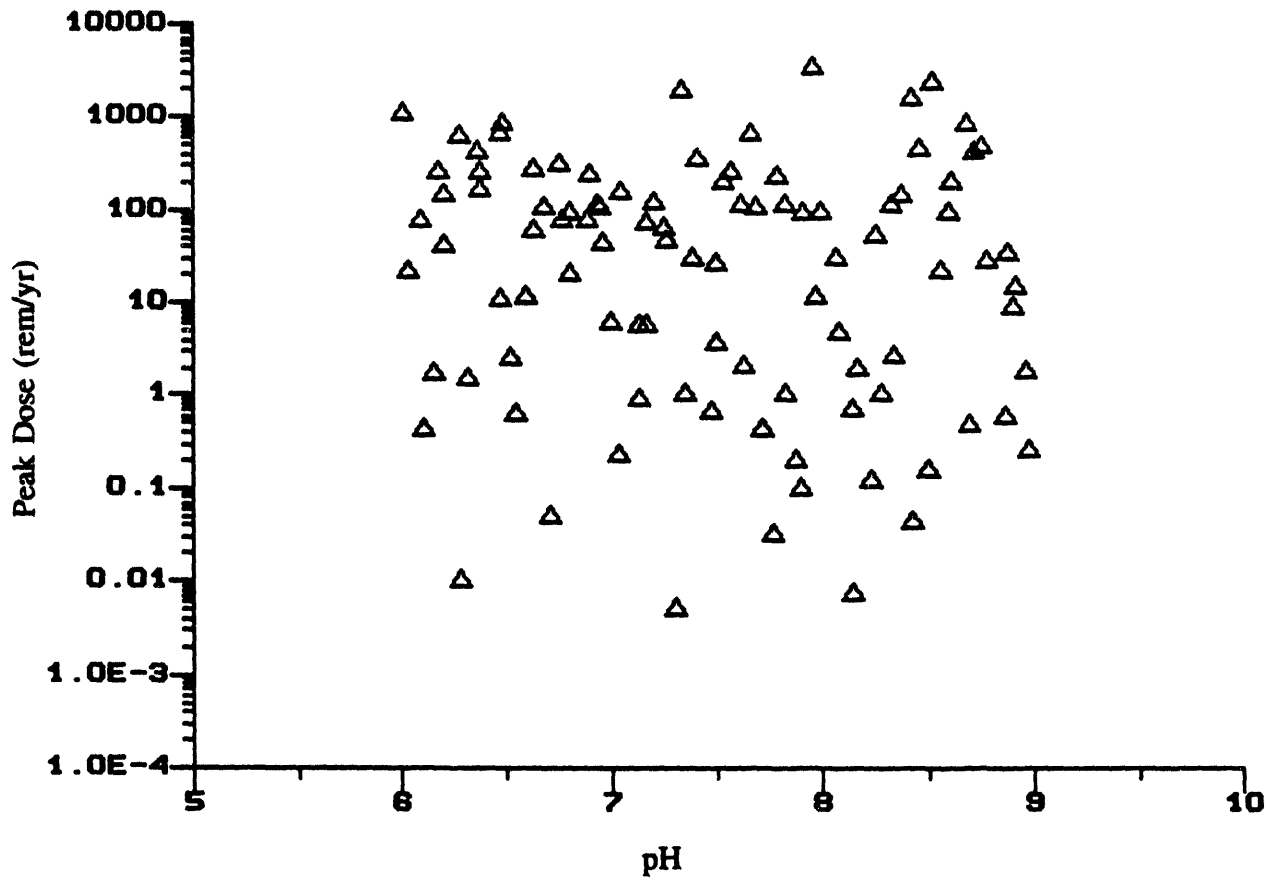


Figure 3-39. Scatter Plot of pH vs. Peak Dose Exposure over 1,000,000 Years for 57/10/0.95/S1

## **4. SUMMARY AND CONCLUSIONS**

The preceding chapters have detailed the specific assumptions regarding the input parameter distributions and dependencies/correlations and the resulting postclosure total system performance as defined by both the cumulative radionuclide release at the accessible environment boundary and the maximum individual dose associated with the release. In the following discussion some of the key assumptions and remaining uncertainties (both conceptual as well as parametric) are reiterated, with special emphasis on those that are different from those made in either TSPA 1991 or in the SNL contribution to TSPA 1993. The significant results are then summarized with focus on the sensitivity of the results to the key design issues (namely the thermal load and waste package design), conceptual representations of aqueous corrosion, the time period of regulatory concern, and the type of environmental standard. A series of recommendations for additional analyses of detailed processes are presented to develop more defensible abstractions as well as additional site and design information that would significantly enhance the representativeness of future TSPA iterations.

### **4.1 SIGNIFICANCE OF KEY ASSUMPTIONS**

#### **4.1.1 Waste Package/Engineered Barrier System Assumptions**

Numerous assumptions have been employed in TSPA 1993 that have a significant effect on the predicted performance. These assumptions include the definition of the near-field environment, the processes affecting the initiation of aqueous corrosion, the aqueous corrosion rates, and the thermally dependent properties affecting radionuclide mobilization and release from the EBS. These assumptions are fundamentally different than those employed in TSPA 1991 in which (1) it was assumed that the thermally induced delay for aqueous corrosion was an uncertain time ranging from 300 to 1,300 years, (2) the time to failure of the waste packages was assumed to be from 500 to 10,000 years following the thermally induced delay, and (3) no thermally dependent processes or parameters were directly incorporated (but the parameter ranges were expanded to incorporate the uncertainty due to potential thermal effects).

The near-field environment used in TSPA 1993 has been based on thermohydrologic analyses conducted at the panel scale of the repository. The simulations were performed at the sub-repository scale to capture the potential edge effects caused by unheated portions of the total repository area due to the presence of the main axis drift and associated side drifts, the set-back of any waste packages from these drifts, and the existence of the lower thermal output from the defense high-level waste. Although the model used in this analysis has the advantage over earlier analyses (such as Buscheck and Nitao, 1993 or Tsang and Pruess, 1993) of incorporating the edge effects which Ryder (1993) has determined to be important in controlling the duration of above boiling conditions, it has the disadvantage of not allowing heat or water to be transported radially away from the panel. This assumption may be conservative from a hydrologic perspective as the water remains within the cylinder of the panel rather than being shed away from the repository block. This assumption may be either conservative or nonconservative from a thermal perspective because, while the time before aqueous corrosion is initiated may be slightly greater (due to the temperatures being slightly higher than what would occur if radial heat transport

outside of the panel cylinder were allowed) the corrosion rates and other temperature-dependent parameters would also be slightly increased (such as increasing most radionuclide solubilities and alteration rates).

For the hydrothermal analyses, the entire repository was divided into nine panels of equal area and each panel was divided into seven equal area concentric rings, with the inner rings containing the spent fuel waste packages and the outer ring containing the HLW packages. As a result of these analyses, the spatially and temporally variable temperatures, water saturations and liquid water fluxes were incorporated in the assessment of the waste package/EBS performance. These analyses were conducted at three thermal loads to determine the sensitivity of the thermohydrologic regime to this important design variable.

The results of the thermohydrologic analyses are employed to determine the near-field environment. These analyses do not consider the very-near-field (i.e., drift- or waste package-scale) thermohydrologic regime which will ultimately control the thermally dependent processes of potential significance to waste package/EBS performance. To determine the thermal regime in the vicinity of the waste packages themselves, additional thermal calculations assuming conduction in the rock and radiation from the waste package to the rock have been conducted. These analyses indicated that the waste package surface temperature at early times (several hundred years) was significantly greater (on the order of 100°C) than the rock temperature 5 m away from the drift wall. However, at times ranging from 500 to 1,000 years, the temperature in the rock and at the package surface were within about 10°C of each other. Because of general concern with the time period when the temperatures fall below the boiling point or when the water saturations are above their residual values, using the rock temperatures and saturations as indicative of the near-field environment is considered to be reasonable and conservative in the absence of more rigorous very-near-field thermohydrologic analyses. The very-near-field thermal calculations conducted as part of TSPA 1993, which considered the effects of a backfilled repository, illustrate the significant increase in the waste package surface temperatures at early times, which are dependent on the assumed thermal properties of the backfill. [Note: The SNL baseline thermal analyses included a backfill placed at 75 years following emplacement, which caused a large temperature increase at the waste package surface for the first few hundred years for the in-drift emplacement mode. After this time, the thermal profiles of the rock and waste package surface again begin to converge (Eric Ryder, personal communication, 1993; Wilson et al., 1994, in press; see also Appendix B).]

The direct incorporation of the thermohydrologic regime, even though this regime is uncertain and not at the drift/waste package scale, is a considerable improvement in the conceptual representation of the relevant processes over the simple assumption incorporated in TSPA 1991. The primary significance of the assumed thermohydrologic environment is the delay for the initiation of waste package degradation processes (principally aqueous corrosion). This delay may be considered to be controlled by either temperature or water saturation. Significant uncertainty exists as to the nature of the very-near-field environment which will dictate the initiation (and ultimately the continuation) of aqueous corrosion processes (McCright, 1993). The physical-chemical properties of the outer precipitated layer, which consists of porous oxides and oxihydroxides, will control the likelihood that a liquid layer can exist in equilibrium with the ambient air, thus allowing the corrosion processes to continue. It is acknowledged that this uncertainty exists, and two different criteria (rock saturation at the repository level and rock

temperature) have been assumed for the initiation of aqueous corrosion in order to test the sensitivity of the failure times and waste package/EBS releases to this uncertainty.

The results of the analyses indicate that when a temperature rather than a saturation cutoff is used as the criterion for the initiation of aqueous corrosion, then the delay times in TSPA 1993 generally range from a few hundred to about 1,000 years for the 141 kW/ha (57 kW/acre) thermal load (very similar to the assumed range in TSPA 1991), while if saturation is used as the criterion, the aqueous corrosion can begin immediately following closure. This time difference is of very little consequence to the waste package/EBS release when integrated over 10,000 years (on the order of 20 percent difference). At low thermal loads, whether temperature or saturation is used as the criterion for aqueous corrosion initiation makes no difference as both criteria indicate that corrosion can be initiated as soon as the repository is closed. At high thermal loads, the temperature criterion leads to the initiation of aqueous corrosion from 4,500 to 6,300 years after emplacement (depending on location within the panel) while the saturation criterion leads to corrosion initiation ranging from zero (for the case of packages located near the edge of the heated portion) to almost 4,000 years (for packages located near the center of the panels). As a result, at the high thermal loads, the integrated 10,000-year release is predicted to be much less when a temperature rather than a saturation cutoff criterion is employed. In all cases, however, when the waste package/EBS release is integrated over 100,000 years, the differences caused by different assumptions on the initiation of aqueous corrosion processes are minimal (less than 10 percent). Therefore, the importance of the assumed criterion on the initiation of aqueous corrosion appears to be not that significant *except* at high thermal loads when considering the releases over 10,000 years. Although the effect of this conceptual uncertainty for waste package designs that include thicker outer container walls has not been investigated, the differences are expected to be more pronounced because delaying the initiation of aqueous corrosion generally had a significant effect on the time of failure and release rates or cumulative releases from the thicker packages.

An important difference between the SNL TSPA 1993 analyses and those reported on in this document is the temperature of the very-near field at early times following closure. Due to the thermal properties of the backfill, SNL calculates very high temperatures (i.e., above 500°C) at early times for the in-drift emplacement mode (Eric Ryder, personal communication, 1993; Wilson et al., 1994, in press). For the in-borehole emplacement, the temperatures are only 100 to 150°C above the rock temperature. This temperature difference has a significant effect on performance because the dry oxidation rate of mild steel at such elevated temperatures can be over 1 mm/yr (Bullen, personal communication), implying an outer barrier lifetime of less than 100 years for the base case 10-cm outer barrier thickness. In this case, the waste package surface temperatures rarely exceed 200°C, even in the case of a 282 kW/ha (114 kW/acre) thermal load. At this temperature, the dry oxidation rate is less than 0.01 mm/yr (Bullen, personal communication) and decreases rapidly as the temperature drops, so that this process can be neglected in assessments of waste package lifetimes. This difference should be kept in mind when comparing the results of these analyses with those presented in the SNL TSPA 1993.

In addition to uncertainty on the relevant processes affecting the initiation of aqueous corrosion, different sources exist with which to define the corrosion rates (both general and pitting) applicable for the outer corrosion-allowance barrier and the inner corrosion-resistant barrier. These differences, which are detailed in Chapter 2 as well as Appendixes E and F, are due to

different interpretations of the literature available with which to define corrosion rates for the materials of interest in the multibarrier waste package design incorporated in TSPA 1993. The corrosion rates for the outer barrier are not that dissimilar at early times, but at late times the rates can decrease significantly due to the exponential relationship included in Stahl's rates (Appendix E). While this yields only a slight reduction in failure times for the 10-cm-thick outer barrier, it would have a pronounced effect on the thicker outer barrier designs (i.e., increasing the time for the outer barrier "failure" by increasing the thickness has a positive compounding effect of also decreasing the aqueous corrosion rate due to the Arrhenius time relationship).

The corrosion rates for the inner corrosion-resistant barrier are significantly different between Stahl and Lamont (Appendixes E and F, respectively). Stahl conservatively assumes the maximum pitting corrosion rate (about 1 mm/yr) is applicable to all waste packages. Lamont considers the pitting corrosion rate to be variable (from package to package or from pit to pit on a single package) and uncertain and highly dependent on the temperature. Neither Stahl nor Lamont consider the possible benefit to be gained by cathodic protection of the inner Alloy 825 barrier caused by the lower corrosion potential of the carbon steel outer barrier (McCright, 1993). Although one could conservatively consider the maximum pitting corrosion rate provided by Lamont to define the deepest pits on each container (i.e., the "extreme value distribution" of pit depths), this assumption would not adequately address the variability due to environmental differences (primarily geochemistry, hydrology, temperature, and the possible presence of man-made materials) from area to area in the repository as well as the variability in the materials and welding used in the fabrication of the containers themselves. If the maximum corrosion rate presented by Lamont had been considered, the failure of the inner corrosion-resistant barrier would have been the few 10s of years assumed by Stahl.

When combining the different assumptions presented by Stahl and Lamont for the corrosion of the outer and inner barrier materials used in the base case waste package design, it was found that, in general, the Lamont assumptions lead to a slightly reduced (less than 20 percent) waste package release over 10,000 years. This is probably due to the fact that not all of the packages have failed in 10,000 years as a result of the variability in the corrosion rates of the inner barrier. As before, when integrating over 100,000 years the differences caused by the assumed corrosion rates are insignificant (although they may be more pronounced for the thicker waste package designs). The incorporation of the 3.5-cm inner corrosion-resistant barrier reduces the 10,000-year cumulative release from the waste package/EBS by about 30 percent, while reducing the 100,000-year cumulative release by only 10 percent. As an aside, it is interesting to note that while employing the Lamont assumptions regarding corrosion rates yields a slightly lower release from the waste package than does the use of the Stahl assumption for the 141 kW/ha (57 kW/acre) thermal load, the reverse is true when using the 282 kW/ha (114 kW/acre) thermal load. This is probably a result of the exponential relationship imbedded in Stahl's representation of aqueous pitting corrosion of the outer barrier, which tends to reduce the pitting corrosion rate at larger times (once aqueous corrosion is initiated).

In summary, the differences between the conceptual interpretation of the processes affecting the initiation of aqueous corrosion (i.e., temperature or saturation criteria) as well as the uncertainty in the appropriate representation of the aqueous general and pitting corrosion rates (i.e., Stahl or Lamont), do not have a significant effect on the predicted release from the waste package over 10,000 years. The differences are even less pronounced when integrating the release over

100,000 years. This is not to say that a more defensible representation of the very-near-field (i.e., emplacement drift and waste package scale) thermohydrologic regime is not necessary to more confidently predict the temporal and spatial variability of the relevant environmental factors affecting the initiation of the corrosion processes. Also, the detailed mechanistic understanding of the corrosion rates of the outer barrier under different thermohydrologic conditions, as well as the cathodic protection of the inner corrosion-resistant barrier, need to be enhanced in order to gain increased confidence of the actual waste package behavior. In addition, the actual definition of what is meant by "failure" of the containment provided by the waste package needs to be further investigated. The present analyses conservatively assume that when a pit breaches the inner container, that the entire waste package has effectively disintegrated and all the waste is available for alteration and dissolution. This neglects any protection provided by the cladding.

This iteration of TSPA considers the thermal dependency of a number of properties affecting radionuclide release from the waste package/EBS. The alteration rate of the spent fuel and the dissolution rate of the HLW are dependent on temperature. The solubilities of many of the radionuclides are also temperature dependent. In addition, the advective flux past the waste packages and the effective diffusion coefficient for transport from the waste package to the host rock are also dependent on the thermohydrologic environment. None of these properties was thermally dependent in TSPA 1991, although a distribution was assigned to each property value to account for the uncertainty in the property, with a portion of that uncertainty being potentially ascribable to the impact the near-field environment has on the property. In addition to pointing out the properties that were considered to be thermally dependent, it is important to also acknowledge those properties which were assumed not to vary with temperature or other near-field environmental conditions. These include (1) the effective normalized surface area of the spent fuel and glass waste forms (i.e., the possible increase in surface area that could result if the uranium oxide form changes to the higher volume  $U_3O_8$  was not considered), (2) the fraction of the surface area of the fuel matrix that is wet (conservatively assumed to be equal to 1.0 in contrast to TSPA 1991 where it was assumed to equal 0.5), and (3) the fraction of the waste surface in contact with diffusive pathways (also conservatively assumed to be equal to 1.0). The impact of these assumptions in comparison to those made in TSPA 1991 is difficult to directly determine. In the cases where little or no information exists on the conditions inside the waste package once the package has failed, conservative deterministic values have been used, rather than consideration of some assumed uncertainty in the property. It is felt this is a more justified approach at the present level of understanding and given the general objectives of the TSPA 1993 iteration.

A major difference between TSPA 1993 and TSPA 1991 is the incorporation of a more complete radionuclide inventory. In this iteration, 39 radionuclides have been included in the spent fuel inventory and 7,000 MTHM of defense high-level waste for the nominal scenario. For the key radionuclides determined to be of greatest significance to release and dose, this difference is, in fact, minor as those radionuclides were also included in TSPA 1991. The more complete inventory allows one to state that by incorporating this inventory in the analyses, the results do not change appreciably, which is a very useful conclusion. Although the defense waste has a different isotopic makeup than the spent fuel and the defense waste packages may fail either earlier (in the cases where they are cooler and therefore aqueous corrosion is initiated sooner) or later (in the cases where they are cooler and therefore the aqueous corrosion rate is slower) than the spent fuel waste packages, the inclusion of this waste form did not have a significant

impact on the results. In the future it may be useful to break out the contribution to the total release and dose attributable to the different waste forms to determine what the real impact of including the defense waste is on the result.

In general, the release of radionuclides may be classified into those that are alteration-rate limited and those that are solubility limited. In this iteration of TSPA 1993, the solubilities are in some cases significantly different from those used in TSPA 1991. In particular, the solubility of Np is six orders of magnitude greater for low pH values and four orders of magnitude greater for high pH values than those used in Barnard et al. (1992). These values are similar to those used by Eslinger et al. (1993). This difference is primarily the result of new laboratory testing conducted by Los Alamos at more oxidizing conditions likely to be representative of in situ conditions at Yucca Mountain. This difference in the magnitude of Np solubility results in much greater releases from the waste package/EBS and correspondingly greater releases and doses at the accessible environment at times very distant in the future. In TSPA 1993, the solubilities are temperature and pH dependent, rather than being an uncertain parameter distribution. Although the actual solubility value at any particular time may vary from waste package group to waste package group, the value itself is not considered to be uncertain. The net result of incorporating the functional dependency may not be dissimilar to including a broad uncertainty in the parameter distribution.

In TSPA 1993, the solubilities are defined by the element not the radionuclide. If several different isotopes of the same element are being considered (for example, the five principal isotopes of U:  $^{233}\text{U}$ ,  $^{234}\text{U}$ ,  $^{235}\text{U}$ ,  $^{236}\text{U}$ , and  $^{238}\text{U}$ ), the temporally varying mass fraction of each isotope is used to determine the mass of each isotope that is dissolvable (up to the solubility limit) and available for diffusive or advective transport. This is the internally consistent method of assuring that the correct mass of each radionuclide is released. The incorporation of this refinement in TSPA 1993 probably has little significance on the key radionuclides because they are dominated by a single isotope, but may impact the releases and doses associated with daughters of some of the radionuclide chains if the parents' release is controlled by the mass fraction of another isotope of the same element.

#### **4.1.2 Geosphere Flow and Transport Assumptions**

In general, only minor modifications have been made in TSPA 1993 to the geosphere representations for gaseous phase flow and transport and aqueous phase flow and transport in the unsaturated and saturated zones. These modifications have been predicated on additional process-level modeling and site information acquired since TSPA 1991. In addition, TSPA 1993 has directly incorporated a simplified representation of climate change to evaluate the potential effects on release and dose.

The hydrostratigraphy used in TSPA 1993 is based on USGS cross sections along the planned drift axes. The unit thicknesses depicted on these cross sections have been modified slightly to make the vitrophyre thickness consistent with observations from well logs (D. Hoxie, personal communication, 1993). The thickness of each unit is considered to be constant within each column, rather than being sampled as SNL assumes in TSPA 1993 (T. Robey, personal

communication, 1993; Wilson et al., 1994, in press). This distinction is considered to be insignificant as long as the total thickness of the unsaturated zone is equivalent.

The porosity values used in TSPA 1993 are identical to those used in TSPA 1991. The bulk density values used in TSPA 1993 were from measurements in USW G-4. Although SNL has completed detailed well log analyses to update these parameters for their TSPA 1993, the differences appear to be slight.

The unsaturated zone percolation flux remains an uncertain parameter in this iteration of TSPA. To be consistent with SNL's TSPA 1993, a similar exponential percolation flux distribution with a mean of 0.5 mm/yr has been used. The flux based on the saturated matrix conductivity of the Topopah Spring welded unit (TSw2) has not been modified, as SNL has done (M. Wilson, personal communication, 1993; Wilson et al., 1994, in press). Therefore, it is possible that slightly higher flux values are used when higher values are sampled. Due to the use of a factor of two lower percolation flux in TSPA 1993 than TSPA 1991, the advective travel time to the accessible environment is increased by a factor of almost two as most of the travel time is in the unsaturated zone. This factor alone contributes significantly to the differences in cumulative aqueous releases integrated over 10,000 years between those presented here and those documented earlier (Barnard et al., 1992; INTERA, 1993). This difference also makes the dispersion more significant for the 10,000-year cumulative aqueous release as it is generally the dispersed early arrival mass which contributes most significantly to the predicted release.

As in TSPA 1991, a large matrix-fracture coupling for transport has been used (i.e., it is assumed that the transport is matrix-dominated, either due to matrix imbibition of water due to capillary forces or matrix diffusion of radionuclides due to a concentration gradient between the fractures and matrix). In earlier analyses to compare RIP with TSPA 1991, a different conceptualization of fracture-matrix coupling was experimented with by using a Markovian approximation of the transition between fractures and matrix (INTERA, 1993). For a moderate amount of fracture-matrix interaction (corresponding physically to fracture lengths on the order of one-tenth of the pathway length), it was found that the equivalent matrix-dominated transport gave similar results, while for small fracture-matrix couplings, the releases were increased slightly. The degree of matrix-dominated transport needs to be addressed further in future TSPA iterations as well as additional process-level models and in situ observations.

The radionuclide retardation values used in TSPA 1993 have been based on recent laboratory tests conducted by Los Alamos under expected in situ environments. While the laboratory tests were conducted using different reference waters under varying temperature and pH conditions, the range of distribution coefficients did not vary appreciably. Therefore, the retardation was not made dependent on any environmental properties, but the uncertainty expressed by the experts was considered.

Dispersion in the unsaturated zone can have a significant effect on the 10,000-year releases to the accessible environment, especially in those cases where the expected water travel time is greater than 10,000 years (as it is in almost all realizations). Large dispersion coefficients cause the leading edge of the radionuclide breakthrough curve to precede the center of mass (corresponding to the 50 percent arrival time) by several thousand years. In TSPA 1993, a dispersivity equal to one-tenth the pathway length (i.e., ranging from about 1 to 10 m) has been

used. In TSPA 1991, Barnard et al. (1992) used a range from 10 to 25 m. In TSPA 1993, SNL used a dispersivity value of one-tenth the total pathway length (i.e., 20 to 30 m). The larger dispersivity will generate earlier arrivals of mass at the accessible environment, which will result in slightly larger cumulative releases when integrating over 10,000 years. This fact should be kept in mind by the interested reader when comparing the results presented in this document with those presented in the SNL TSPA 1993.

The possible modification in percolation flux due to climatic changes as a linearly increasing and decreasing function with the maximum increase being an uncertain factor ranging from one (i.e., no change from ambient) to five has been approximated. In contrast, SNL has assumed a step-function change in percolation which can occur any time over the next 100,000 years (for example, a 1 percent chance of occurring in the next 1,000 years or a 10 percent chance of occurring in the next 10,000 years), with a revised percolation flux of about a factor of 20 (M. Wilson, personal communication, 1993; Wilson et al., 1994, in press). This difference will be significant when comparing integrated releases over 10,000 years calculated using the two assumptions.

The saturated zone ground-water flux used in TSPA 1993 has been based on process-level modeling conducted by Barr (1993). These fluxes are slightly higher than those employed in TSPA 1991. However, because most of the total water travel time to the accessible environment occurs in the unsaturated zone, this increase does not create a significant impact on the releases to the accessible environment.

The gaseous-phase velocity distribution has been based on process-level modeling of thermally perturbed gas flow and  $^{14}\text{C}$  transport conducted by Ross (1993). These analyses are a significant improvement on the simplifying assumptions made in TSPA 1991. In particular, the gas travel time is fully transient based on a particle-tracking routine which uses the two-dimensional transient gas phase velocity field calculated with the computer code, TGIF, (Ross, 1993). Although gas phase velocities were only calculated with the 141 kW/ha (57 kW/acre) thermal load, the travel times are generally very short in comparison to the 10,000 year time period so increasing the thermal load to 282 kW/ha (114 kW/acre) would be expected to have only a minimal impact on the release to the accessible environment. The effect of decreasing the thermal load on the gas phase velocities and corresponding  $^{14}\text{C}$  travel times has yet to be investigated.

#### **4.1.3 Biosphere Assumptions**

Analyses of individual dose have been incorporated in TSPA 1993. In addition to defining the aqueous releases to the accessible environment (in the form of cumulative mass or activity), the radionuclide concentration in the ground water and the likely pathways that may lead to humans ingesting these radionuclides now need to be determined.

The radionuclide concentration will be dependent on the volume of water into which the radionuclides are mixed or diluted. In TSPA 1993, the assumption is made that the mixing occurs within a cross-sectional area equal to the repository width (about 4000 m) times a mixing depth of 50 m. This value was chosen to be midway between the 5 to 500 m assumed by SNL.

in their TSPA 1993 (M. Wilson, personal communication, 1993; Wilson et al., 1994, in press). The mixing depth is more dependent on the assumed production interval for ground-water extraction wells. If one considered that the well was producing from only a thin zone at the top of the saturated zone (which would be unrealistic due to the lowering of the water table which would ensue after ground water discharge had commenced) then the mixing depth would be controlled by the vertical mixing caused by advection and transverse dispersion. If one considered that the well was drilled and slotted to intercept the maximum yield, then the mixing depth would be the entire transmissive thickness of the saturated zone (assumed by EPA to be 2400 m). It is felt there is little justification for any particular value for the mixing depth and a reasonable value was selected. The dose results are linearly dependent on this parameter. Therefore, it is recommended that any dose-based environmental standard be tied to some specified mixing depth.

In addition to concentration, the dose analyses require some definition of the quantity of water which the individual consumes (for varying personal or agricultural purposes) and the means by which radionuclides may be ingested by that individual. In the present analyses, it is assumed that the individual pumps the water and uses 700 l/yr for personal consumption and the remainder for personal use (showers, cooking, etc.) and irrigation. The same dose conversion factors developed by PNL as part of TSPA 1991 were used (Eslinger et al., 1993). In cases where no dose conversion values were available (because those radionuclides were not considered as part of TSPA 1991), values from the Waste Isolation Systems Panel study (NAS, 1983) or EPA (EPA, 1988) were used. As SNL only considered the dose associated with drinking the water, their doses would be expected to be slightly lower than those predicted here.

## **4.2 SENSITIVITY AND SIGNIFICANCE OF RESULTS**

### **4.2.1 Significance of Results to Design**

Several different design options have been investigated as part of the sensitivity analyses conducted in TSPA 1993. Based on the results presented in Chapters 2 and 3, it is possible to make some general conclusions on the impact of the different design options on performance, where the performance is defined with respect to either the cumulative radionuclide release or the peak individual dose. The conclusions are dependent on the time period of concern, so some remarks are made on the relative performance associated with different design options over different times.

Any conclusion regarding the relative advantages or disadvantages of a particular design that may be reached based on this total system performance assessment analyses, must be predicated at this stage on the understanding of the fundamental processes and parameters affecting performance. That is, the robustness of the results is closely linked to the confidence placed in the current conceptualization of the system and its components. As significant uncertainties remain in the understanding of the very-near-field environment and its effect on the waste package lifetime and EBS release, some caution should be used prior to unconditionally accepting the comparisons that are presented below. To a limited extent, the impact of some of the uncertainty has been tested on the expected performance for different design options. In particular, the significance of alternate criteria has been investigated for the initiation of aqueous

corrosion and alternate conceptualizations and parameterizations for aqueous corrosion rates. However, these sensitivity analyses are not exhaustive and should be expanded to account for new process-level understanding that is generated as the advanced conceptual design matures.

Various thermal loads have been proposed for the potential repository at Yucca Mountain. The performance at three representative loads corresponding to 70.4, 141 and 282 kW/ha (28.5, 57, and 114 kW/acre) has been evaluated. The 141 kW/ha (57 kW/acre) case corresponds to the SCP thermal load. For each thermal load, thermohydrologic analyses to determine the water saturations and temperatures in the vicinity of the waste packages (considered to be 5 m into the rock) have been conducted. These parameters are then used to define the initiation of aqueous corrosion and a range of thermally dependent properties affecting the waste package/EBS release.

In general, it may be concluded that when considering the integrated release from the waste package over 10,000 years, the 282 kW/ha (114 kW/acre) case generates lower releases than the 141 kW/ha (57 kW/acre) case. This reduction, which is dependent on the waste package design and the conceptual representation of aqueous corrosion, is by about a factor of two. This reduction is primarily a result of the delay in the initiation of aqueous corrosion due to the higher thermal load. Although the HLW packages tend to fail earlier under the higher thermal load of the spent fuel packages because they are "wetter" earlier, this is more than offset by the increased time to failure of the spent fuel packages. The use of temperature as the cutoff criterion for the initiation of aqueous corrosion tends to enhance the difference in release between the two thermal loads. The use of the Lamont corrosion conceptualization tends to decrease the difference in 10,000-year performance between the two thermal loads.

In general, the conclusions reached for the 10,000-year integrated release for different thermal loads are also germane to the 100,000-year time period. However, instead of the differences in release between the two thermal loads being on the order of 100 percent, they are on the order of 10 to 20 percent. This is as expected as the primary benefit of a very high thermal load is to delay the initiation of aqueous corrosion. Once corrosion is initiated and failure occurs, the integrated releases tend to be similar. The exception to this observation occurs when the thick outer corrosion allowance material is used, in which case the higher thermal load caused an increase in the 100,000-year cumulative release from the waste package. This apparent anomaly can be explained by the realization that although the initiation of aqueous corrosion is delayed for the higher thermal load, the corrosion rates are accelerated for longer periods of time due to the temperature-dependent rates employed in the model.

Although the impact of using a lower thermal load has not been exhaustively tested (i.e., the effect alternate conceptual representations of aqueous corrosion initiation and rate might have on the results has not been evaluated) it may be concluded that, in general, the lower thermal load (represented by a 70.4 kW/ha or 28.5 kW/acre thermal load) provides for lower releases from the waste package than does the 141 kW/ha (57 kW/acre) case. This difference is pronounced for the 10,000-year integrated release (being about a factor of three for the 10-cm outer barrier thickness) and again is less significant when integrating over 100,000 years. This improvement in performance for the lower thermal load is a direct result of the temperature dependence of the aqueous corrosion rate. For low thermal loads, the temperatures are significantly cooler, which decreases the rate of pitting and general corrosion, thereby increasing the lifetime of the waste

packages. This result occurs regardless of whether a temperature or saturation corrosion initiation criterion is used.

The impact of different thermal loads on releases to the accessible environment mimic the observations made above concerning releases from the waste package. As has been noted in recent assessments of postclosure total system performance at Yucca Mountain, the gaseous releases (i.e.,  $^{14}\text{C}$ ) dominate the cumulative 10,000-year release when normalized to the Table 1 limits of 40 CFR Part 191. As the gaseous releases to the accessible environment are controlled by the waste package lifetime (because the travel times from the repository to the accessible environment are short in comparison to the 10,000-year time period), the gaseous releases illustrate the same sensitivity as the waste package/EBS release; that is the 141 kW/ha (57 kW/acre) case yields greater releases than either the 282 kW/ha (114 kW/acre) or the 70.4 kW/ha (28.5 kW/acre) thermal load. [Note: It is expected that the gaseous releases over 10,000 years would be lower than those presented in Chapter 3 for the 70.4 kW/ha (28.5 kW/acre) thermal load if the gaseous flow regime had been modeled at this lower thermal load. However, Ross (1993) only conducted thermally dependent gas phase modeling at the 141 kW/ha (57 kW/acre) thermal load.]

The integrated aqueous releases to the accessible environment over 10,000 years are extremely small, generally less than about  $10^{-6}$  of the EPA Table 1 values, and tend to reinforce the conclusion that very high and very low thermal loads yield lower releases than the moderate 141 kW/ha (57 kW/acre) thermal load. When integrating releases to the accessible environment over 100,000 years, one observes that the very high and very low thermal loads yield lower releases than the moderate thermal load case. However, when considering only the aqueous releases, the cumulative releases decrease as the thermal load is lowered. Although this decrease is small (about 10 percent from 282 to 141 kW/ha (114 to 57 kW/acre) and about 20 percent from 141 to 70.4 kW/ha (57 to 28.5 kW/acre), it is explainable by the increase in several of the waste package/EBS release properties at elevated temperatures. In particular, the alteration rate of spent nuclear fuel is generally greater at higher temperatures.

The effect of the thermal loading design on the peak individual dose over a 1,000,000-year time period is insignificant. If one were to consider other postclosure performance measures over this time period one would reach a similar conclusion. This is a direct result of the fact that while the thermal load can cause differences in expected releases over the time period that the thermal regime is most significant, at larger times these effects have no impact on the consequences.

In summary, for time periods on the order of 10,000 years, the high and low thermal loads provide better overall postclosure performance than the medium 141 kW/ha (57 kW/acre) load. The low thermal load generally provides lower releases from the waste package/EBS due to the lower corrosion rates, while the high thermal load provides lower releases due to the delay in the initiation of aqueous corrosion. When considering releases to the accessible environment, a similar relationship between effect of alternate thermal loads is observed primarily due to the significance of the gaseous releases. In considering the aqueous releases to the accessible environment, one must examine the 100,000-year releases to discern an effect, as the releases over 10,000 years are of little significance. Over the 100,000-year time period, the effect of the very-near-field environment and the thermohydrologically-dependent processes and parameters

becomes less pronounced as the results for all three thermal loads are within 50 percent of each other.

It bears noting that the long term "dryout" of the geosphere caused by very high thermal loads was not directly evaluated in this study, as a sufficient suite of process-level thermohydrologic analyses conducted over a wide range of possible ambient percolation fluxes was not available. This so-called "extended-dry" concept would have the benefit of delaying the advective transport in the geosphere until such time as the velocity vectors are oriented downward, but with the drawback that once the downward flux is reinstated, the magnitude of the flux will be increased several fold (M. Reeves, personal communication, 1993). Future TSPAs should consider more rigorously the geosphere aspects of the hydrothermal perturbation.

In addition to the repository thermal load, the effects of alternate waste package designs on the postclosure total system performance were investigated. The impact of alternate thicknesses of the outer corrosion-allowance material and the inner corrosion-resistant material was also investigated. In general, one may make the obvious observation that as the thickness of the barrier increases, the releases decrease because the time to failure of the waste packages is increased. However, the response is definitely not linear over the range of thicknesses considered. The differences between a 10-cm and a 20-cm outer mild steel barrier on integrated releases over 10,000 years is slightly more than a factor of two (except at the low thermal loads). However, there is virtually no release over 10,000 years when the 45-cm outer barrier is considered. This is a direct result of the compounding effect that decreased temperature and increased time cause in decreasing the pitting corrosion rate of mild steel; so as one increases the time at which failure may occur, one is buying additional safety by the simple fact that the temperatures are cooler. This also tends to reduce some of the thermally dependent release parameters such as the alteration/dissolution rate.

When one considers releases from the waste package/EBS over 100,000 years, the differences between the 10-cm and 20-cm outer barriers are insignificant (less than 10 percent), while again the 45-cm outer barrier provides considerable containment. It is interesting to note that the 45-cm outer barrier performs worse in the case of the 282 kW/ha (114 kW/acre) thermal load than it does in the 141 kW/ha (57 kW/acre) case. This is due to the increased alteration/dissolution of the spent fuel and HLW glass and the increased solubility of some of the radionuclides at the higher temperatures once the waste packages have failed.

When one considers releases to the accessible environment, one notices a similar dramatic improvement in performance when going from the 20-cm to the 45-cm outer barrier. For the base-case thermal load of 141 kW/ha (57 kW/acre), the aqueous releases decrease by a factor of 40 and the gaseous releases decrease by a factor of 10,000 (primarily due to the decay of  $^{14}\text{C}$  during the containment period provided by the increased time to failure).

The use of the 3.5-cm inner corrosion resistant barrier makes no difference to postclosure performance when one considers the Stahl concept of pitting corrosion to represent the maximum pit growth rate. However, if one uses the spatially variable pit growth rate postulated by Lamont (and not the extreme bounding case also put forward by Lamont), then increasing the inner barrier to 3.5 cm (from the base case of 0.95 cm) generally causes a reduction of the releases over 10,000 years by between 30 and 100 percent depending on the thermal load and assumed

criterion for the initiation of aqueous corrosion. As noted several times previously, when extending the time frame to 100,000 years, the improvement in performance afforded by the increased inner barrier thickness is less pronounced (generally about 10 percent). The same relative performance is observed when considering releases to the accessible environment.

As noted earlier, the waste package design has little impact on the peak individual dose over the 1,000,000 year time period. Even if one postulates a mechanism to delay the release of activity from the waste package/EBS by more than 100,000 years (as would be the case for a 45-cm outer barrier waste package placed in a 28.5 kW/acre thermal load), the release and transport of some key long-lived radionuclides (in particular,  $^{237}\text{Np}$ ) will eventually occur. Although the peak doses may not occur until several hundred thousand years following closure, they will be at about the same magnitude irrespective of the containment provided by the waste package. [However, as discussed below, the near-field environment will have a significant effect on the release and corresponding dose, due to the solubility of the key radionuclides in the small amount of water in contact with the waste.]

In summary, the 45-cm outer barrier appears to provide a significant improvement to the waste package lifetime and hence to the EBS release and release to the accessible environment. When combining the beneficial aspects of the thicker outer barrier with a lower temperature environment (corresponding to a lower thermal load), one can with a relatively high certainty assure that the waste packages will last more than 100,000 years using the current understanding of the conceptual representation of container failure mechanism. The effects of either a 10-cm or 20-cm outer barrier are less pronounced, as is the small additional benefit provided by the 3.5-cm inner barrier.

Many conservative aspects have been assumed in the current TSPA that could also add significantly to the overall performance. The potential positive effects (i.e., additional postclosure safety) that could result from (1) cathodic protection of the Alloy 825 inner barrier, (2) the ability of the cladding to delay alteration, and (3) the limited surface area available for diffusive releases have not been considered. On the other hand, the potential negative effects that could result from (1) increasing the spent-fuel surface area due to high-temperature oxidation of the waste form, (2) natural or human-induced colloid transport, or (3) non-equilibrium fracture-dominated reflux of water from the thermally perturbed hydrologic regime (which may be mitigated by ventilation during the operational phase of the repository) have not been considered.

#### **4.2.2 Significance of Results to Site Characterization**

The primary focus of this iteration of TSPA was to evaluate the impact of alternate repository and waste package designs on the expected cumulative release of radionuclides to the accessible environment and the corresponding individual dose associated with that release. As a result of this objective, less emphasis was placed on evaluating the uncertainty in release caused by the uncertainty in the conceptualization and parameterization of the geosphere. However, this uncertainty is important and impacts the near-field thermohydrologic regime as well as the far-field aqueous and gaseous flow and transport. In this section, the sensitivity of the results to this uncertainty are examined briefly.

As has been noted in several assessments of the performance of a potential repository at Yucca Mountain, the key issue affecting the ability of the site and engineered barriers to contain and isolate radioactive wastes from the accessible environment is the conceptual model for flow and transport through the fractured-porous media as well as the magnitude of the percolation flux through the unsaturated zone. In the present assessment of total system performance, it is assumed that transport through the unsaturated zone is dominated by the matrix, either because of the large capillary pressure differences between the fractures and matrix *or* the large matrix diffusion due to the concentration gradient between the fractures and matrix. This assumption is equivalent to the large fracture-matrix coupling employed in TSPA 1991 and continued in the SNL TSPA 1993 (M. Wilson, personal communication, 1993; Wilson et al., 1994, in press). In an earlier assessment, the significance of this assumption using a Markovian approximation of fracture-matrix flow and transport was tested (INTERA, 1993), but in that analysis there was little physical justification for the parameter ranges used to approximate the transition between fracture and matrix flow. Most analyses of the hydrologic flow regime in the unsaturated zone at Yucca Mountain (whether under ambient or thermally perturbed conditions) assume the composite porosity flow model. The validity of this assumption as well as the impact of this assumption on the predicted performance should be more rigorously evaluated.

As in TSPA 1991, the ambient percolation flux was considered to be uncertain. In contrast to TSPA 1991, the uncertainty has been broken into two distributions, one representing the uncertainty in the current conditions and the other representing the uncertainty in the percolation flux due to future climates. The uncertainty in the expected percolation flux at the repository depth is large. Estimates range from the flux being upward (i.e., corresponding to a current net drying of the unsaturated zone at Yucca Mountain), to essentially zero, to a downward flux of between 0.01 and 1.0 mm/yr (see Hevesi and Flint, 1993; Nichols, 1987; Conrad, 1993; Gauthier, 1993; and Long and Childs, 1993, among others). An exponential distribution for the current percolation flux with an expected value of 0.5 mm/yr was used. This distribution implies that 63 percent of the values sampled will be less than 0.5 mm/yr and 37 percent of the values will be greater than 0.5 mm/yr. This distribution is exactly a factor of two less than that used in TSPA 1991. This difference is not so much due to new insights or new information as it is to the fact that climate change is modeled explicitly as a multiplier on the expected ambient flux distribution instead of embedding the climate change implicitly in the distribution as was assumed in TSPA 1991. This distribution has been used to be consistent with the range selected by SNL in their TSPA 1993.

The importance of the percolation flux on release and dose is clearly illustrated in the scatter plots presented in Chapter 3. The significance of this parameter will continue to be high in future assessments of total system performance. The need for more defensible estimates of this parameter and its uncertainty continues to be a high priority for the site characterization of Yucca Mountain. Estimates of the percolation flux can be made from shallow surface-based observations, deep surface-based observations, or observations made from the Exploratory Studies Facility (ESF). Direct quantification of the percolation flux from shallow observations is difficult due to the temporal and spatial variability inherent in this parameter and the fact that the net infiltration below the root zone is a complex function of slope (both angle and direction), vegetation, atmospheric conditions, precipitation (type, intensity and duration), antecedent conditions in the surface soil/rock, and the physical/hydrologic characteristics of the surficial materials, among other factors. Indirect quantification of the percolation flux from deep surface-

based observations (such as vertical saturation-depth profiles) is also difficult unless one is confident of the lateral representativeness of the hydraulic properties and the saturation/capillary pressure and saturation/relative permeability relationships. In both instances, it must be acknowledged that point measurements are being made of a process that is inherently variable in space. The best means of confidently and unambiguously determining the ambient aqueous percolation flux at the repository horizon is by direct observation following the excavation of the ESF. Even in this case, however, care must be exercised to minimize the disturbance to the in situ hydrologic conditions caused by ventilation, as large quantities of water may be evaporated from the rock face.

In addition to the uncertainty in the ambient percolation flux at the potential repository horizon, the representation of the possible increase in flux that may be attributable to future climate changes is also uncertain. The flux change is described as a linearly increasing and decreasing function from the current value (which is assumed to represent a "dry" climate), based on a proposal put forward by Long and Childs (1993). For the expected value of the flux multiplier of three which applies to the maximum glacial period assumed to be 100,000 years from now, the average percolation flux over 100,000 years would be increased by a factor of two times the ambient flux. Given the large uncertainty in the ambient flux, this factor of two has little added significance. Clearly future iterations of total system performance assessment will continue to investigate alternate conceptualizations of likely climate changes and their impact on the repository level percolation flux.

As in TSPA 1991, several geosphere properties were considered to be uncertain in this iteration of TSPA 1993. These include matrix porosity, bulk density, and retardation. In contrast to TSPA 1991, the uncertainty in fracture properties was not included because it was assumed that the matrix controlled the transport of radionuclides in the geosphere. The fracture properties may be significant for the realizations where the sampled percolation flux exceeds the saturated hydraulic conductivity of the matrix if one assumes that matrix diffusion does not occur. While the matrix properties play a role in retarding the radionuclides from reaching the accessible environment, they are relatively insignificant over the ranges that have been evaluated. The retardation coefficients of some key radionuclides such as  $^{237}\text{Np}$  can play a more significant role for releases over the 100,000-year time frame if they are found to be significantly less than the current conservative estimates based on laboratory measurements conducted under varying geochemical and thermal environments.

More sophisticated analyses of thermally perturbed gaseous flow and  $^{14}\text{C}$  transport in the unsaturated zone as well as aqueous flow in the saturated zone have been incorporated in this iteration of TSPA 1993. These process-level models are not based so much on new data as they are on a more rigorous modeling approach. Both models rely on the bulk permeability of the fractured-porous media in the vicinity of Yucca Mountain. In general, it may be concluded that the gaseous release to the accessible environment is relatively insensitive to the gaseous flow in the unsaturated zone because the  $^{14}\text{C}$  travel times are short in comparison to the expected life of the waste packages. In addition, the aqueous release to the accessible environment is relatively insensitive to the aqueous flow in the saturated zone because the travel times of radionuclides in this domain is short in comparison to the travel time through the unsaturated zone. However, the dose attributable to aqueous releases at the accessible environment is directly related to the horizontal flux through the saturated zone, because as the flux increases the dilution increases

and the dose decreases. Therefore, if a dose-based standard is promulgated, a greater understanding of the flow in the saturated zone will be required.

#### **4.2.3 Significance of Results to Alternate Environmental Standards**

The analyses performed as part of TSPA 1993 were conducted over a range of time periods and addressed individual dose in addition to radionuclide release as the performance measure of interest for postclosure safety. The conclusions reached regarding the relative performance associated with different design options, as well as the relative importance of certain conceptual models and parameters, are dependent on the performance measure and time period considered.

The primary justifications for conducting analyses over time periods greater than the 10,000 years required in 40 CFR Part 191 are to: (1) evaluate the consequences associated with some long-lived radionuclides that are not released in 10,000 years due to the waste package lifetime and/or the retarded geosphere travel time, (2) provide "better insight on the long-term performance of disposal alternatives" (EPA, 1993), (3) compare results with other countries which consider dose over time periods greater than 10,000 years, and (4) prepare for discussions with the NAS Committee on the Review of Applicable Environmental Standards for Yucca Mountain. It is realized that times greater than 10,000 years are not currently regulated in any environmental standard (see, for example, the Land Withdrawal Act applicable to the Waste Isolation Pilot Plant and the Resource Conservation and Recovery Act requirements applicable to deep-well injection permitting) and that increased uncertainty exists regarding future climates and human behavior at larger times. However, interesting insights can be gained by evaluating performance at times very distant in the future, as well as employing alternate measures of performance.

When considering the 10,000-year time period, virtually all (greater than 99.99 percent) of the release to the accessible environment is the result of  $^{14}\text{C}$ . The cumulative aqueous release to the accessible environment has about a 90 percent probability of being less than  $10^{-6}$  of the EPA limit. Because the cumulative releases over 10,000 years are controlled by the gaseous releases, the results are sensitive to the thermal load and waste package design. The aqueous releases are generally insignificant over 10,000 years for the percolation flux distribution considered. However, the aqueous releases are very sensitive to the percolation flux and the conceptual model for fracture-matrix interaction.

When considering the 100,000-year time period, the gaseous release accounts for over half of the total release to the accessible environment. The remainder is provided by unretarded aqueous species, primarily  $^{99}\text{Tc}$ . In general, the cumulative aqueous radionuclide release over 100,000 years is insensitive to the thermal load and outer barrier thicknesses less than 20 cm. Outer barrier thicknesses on the order of 45 cm, especially when combined with low thermal loads, yields waste package lifetimes that can last the entire 100,000 years. For those radionuclides that do reach the accessible environment in 100,000 years or less, the results are very sensitive to the percolation flux.

When considering the 1,000,000-year time period, the dose performance measure was chosen for comparison of alternatives. In general, the peak dose is attributable to  $^{237}\text{Np}$ . The only instances where this is not the case are the result of either a very low percolation flux through the

unsaturated zone, a very high retardation in the unsaturated zone, or a very low solubility. The peak dose over 1,000,000 years is insensitive to thermal loads and waste package designs. The peak dose is very sensitive to the percolation flux, the Np solubility, and the assumed mixing depth in the saturated zone. The dose will also be sensitive to the assumed dose conversion factor, which is suggested should be prescribed by the regulatory agencies *if* this performance measure is adopted as being the best means to assure the long-term safety of high-level radioactive waste disposal facilities.

### **4.3 RECOMMENDATIONS FOR ADDITIONAL ANALYSES/INFORMATION**

While the TSPA analyses presented in this document have significantly extended the analyses documented in TSPA 1991 (primarily by the abstraction of detailed process modeling results and the use of recent laboratory understanding of thermally dependent processes and parameters), many uncertainties still remain. Some of these uncertainties were identified in TSPA 1991, while others have manifested themselves either because of a desire to incorporate the thermohydrologic and corrosion processes directly into the analyses or because the abstraction of process model results has indicated areas which require greater attention in order to reduce the existing uncertainty. As performance assessment is an iterative procedure, it is important to point out the most critical assumptions and uncertainties which need to be reduced in order to produce a more robust safety argument.

The thermohydrologic analyses used in this iteration of TSPA 1993 are a first attempt to incorporate results abstracted from a more detailed process model into a more simplified representation of the system. While this is an excellent start, additional thermohydrologic analyses are required at the panel, drift and waste package scales to evaluate the effect of uncertain and spatially variable thermohydrologic properties, uncertain fracture-matrix conceptual models, and uncertain ambient percolation fluxes on the expected far-field, near-field and very-near-field thermal and hydrologic regimes as a function of time and space. It has been shown that it is relatively straightforward to abstract the results from the detailed models; what is now required is more complete sensitivity and uncertainty analyses using the more detailed process models.

In addition to the uncertainty associated with the expected thermohydrologic environment in the vicinity of the waste packages, considerable uncertainty remains regarding the processes affecting the initiation and rate of aqueous corrosion of the mild steel outer barrier and the Alloy 825 inner barrier. Greater understanding is required of the cathodic protection of the inner barrier, the processes affecting the growth of pits, and even the definition of waste package "failure" in order to provide a more defensible argument for the range of possible waste package lifetimes and early release mechanisms.

The ambient unsaturated zone flux remains a very significant parameter in this iteration of total system performance. Any direct or indirect observations to better quantify the expected value and its uncertainty should be used, although it is acknowledged that until underground observations can be made of the undisturbed conditions the current uncertainty will remain. It is foreseen that the preliminary site-scale unsaturated zone model should be the basis for the representation of the geosphere in subsequent TSPAs.

The conceptual understanding of how water moves through the unsaturated zone at Yucca Mountain, in particular the potential role of episodic fracture flow, also should be improved before initiating a future iteration of TSPA. Assumptions are made that appear to be justified if the composite porosity model is applicable, but additional testing is required to determine the validity of this assumption. This testing may include numerical "experiments" to determine the relative importance of different conceptual representations on some surrogate of postclosure performance. One may look at this testing as developing the justification or basis for the proper level of abstraction of process modeling results for inclusion in the TSPA analyses.

In addition to the conceptual understanding of flow, there is a need to validate the representation of radionuclide transport through the unsaturated zone. The simplified  $K_d$  approach has been used to approximate the complex physical-chemical processes affecting transport of dissolved species. This approximation, as well as the parameter ranges used, need to be justified by detailed laboratory and field tests to be conducted as part of the site characterization program.

## 5. REFERENCES

- Allard, B., 1982. "Solubilities of Actinides in Neutral or Basic Solutions," in Actinides in Perspective, Proceedings of the Actinides--1981 Conference, Pacific Grove, CA, N. M. Edelstein (ed.), Pergamon Press, NY.
- Altenhofen, M. K., and P. W. Eslinger, 1990. "Evaluation of Near-Field Thermal Environmental Conditions for a Spent Fuel Repository in Tuff," in Proceedings of the International Topical Meeting on High Level Radioactive Waste Management, Las Vegas, NV, April 8-12, 1990, Vol. 1, American Nuclear Society, La Grange Park, IL and American Society of Civil Engineers, New York, NY, pp. 402-409.
- Apps, J. A., C. L. Carnahan, P. C. Lichtner, M. C. Michel, D. Perry, and R. J. Silva, 1983. Status of Geochemical Problems Relating to the Burial of High-Level Radioactive Waste, 1982," LBL-151103, Lawrence Berkeley Laboratory, Berkeley, CA.
- Apted, M. J., W. J. O'Connell, K. H. Lee, A. T. MacIntyre, T.-S. Ueng, T. H. Pigford, and W.W.-L. Lee, 1991. "Preliminary Calculation of Release Rates from Spent Fuel in a Tuff Repository," in Proceedings of the High Level Radioactive Waste Management Second Annual International Conference, Las Vegas, NV, April 28-May 3, 1991, American Nuclear Society, La Grange Park, IL and American Society of Civil Engineers, New York, NY.
- Ballou, L. B., 1990. "Thermal Analyses--Effect of Spent Fuel Receipt Characteristics," presented to the Nuclear Waste Technical Review Board, Lawrence Livermore National Laboratory, January 1990.
- Barnard, R. W., M. L. Wilson, H. A. Dockery, J. H. Gauthier, P. G. Kaplan, R. R. Eaton, F. W. Bingham, and T. H. Robey, 1992. TSPA 1991: An Initial Total-System Performance Assessment for Yucca Mountain, SAND91-2795, Sandia National Laboratories, Albuquerque, NM.
- Bourcier, W. L., 1990. "Dissolution of Nuclear Waste Glass as a Function of pH, Time and Temperature," Materials Research Society Symposium Proceedings, Vol. 212, Materials Research Society, Pittsburgh, PA, pp. 371-381.
- Bourcier, W. L., 1991. "Overview of Chemical Modeling of Nuclear Waste Glass Dissolution," Materials Research Society Symposium Proceedings, Vol. 212, Materials Research Society, Pittsburgh, PA, pp. 3-18.
- Bourcier, W. L., 1993. Memo to R. Stout March 17, 1993, re: Conceptualization for Dissolution of the Glass Waste Form.
- Bradley, D. J., C. O. Harvey, and R. P. Turcotte, 1979. Leaching of Actinides and Technetium from Simulated High-Level Waste Glass, PNL-3152, Pacific Northwest Laboratory, Waste Isolation Assessment Program, Richland, WA.

- Buscheck, T. A., and J. J. Nitao, 1992. "The Impact of Thermal Loading on Repository Performance at Yucca Mountain," in Proceedings of the High Level Radioactive Waste Management Third Annual Conference, Las Vegas, NV, April 12-16, 1992, American Nuclear Society, La Grange Park, IL and American Society of Civil Engineers, New York, NY.
- Buscheck, T. A., and J. J. Nitao, 1993. "The Analysis of Repository-Heat-Driven Hydrothermal Flow at Yucca Mountain," in Proceedings of the High Level Radioactive Waste Management Fourth Annual Conference, Las Vegas, NV, April 26-30, 1993, American Nuclear Society, La Grange Park, IL and American Society of Civil Engineers, New York, NY, pp 847-865.
- Chambré, P. L., T. H. Pigford, W.W.-L. Lee, J. Ahn, S. Kajiwara, C. L. Kim, H. Kimure, H. Lung, W. J. Williams, and S. J. Zavoshy, 1985. Mass Transfer and Transport in a Geologic Environment, LBL-19430, Lawrence Berkeley Laboratory, Berkeley, CA.
- Conca, J., 1990. "Diffusion Barrier Transport Properties of Unsaturated Paintbrush Tuff Rubble Backfill," in Proceedings of the International Topical Meeting on High Level Radioactive Waste Management, Las Vegas, NV, April 8-12, 1990, American Nuclear Society, La Grange Park, IL and American Society of Civil Engineers, New York, NY, pp. 394-401.
- Conrad, S. H., 1993. "Using Environmental Tracers to Estimate Recharge through an Arid Basin," in Proceedings of the High Level Radioactive Waste Management Fourth Annual Conference, Las Vegas, NV, April 26-30, 1993, American Nuclear Society, La Grange Park, IL and American Society of Civil Engineers, New York, NY, pp. 132-137.
- CRWMS M&O (Civilian Radioactive Waste Management System Management and Operating Contractor), 1993. Characteristics Database: LWR Radiological PC Database, A00000000-02268-1200-20002 V1.0, VA-MO4-20002.021.C014, Vienna, VA.
- Daniels, W. R., K. Wolfsberg, R. S. Rundberg, A. E. Ogard, J. F. Kerrisk, and C. J. Duffy, 1982. Summary Report on the Geochemistry of Yucca Mountain and Environs, LA-9328-MS, Los Alamos National Laboratory, Los Alamos, NM.
- Doctor, P. G., P. W. Eslinger, D. M. Elwood, D. W. Engel, M. D. Freshley, A. M. Liebetrau, P. W. Reimus, D. L. Strenge, J. E. Tanner, and A. E. Van Luik, 1992. An Example Postclosure Risk Assessment Using the Yucca Mountain Candidate Site, PNL-8081, Pacific Northwest Laboratory, Richland, WA.
- DOE (U.S. Department of Energy), 1986. Final Environmental Assessment, Yucca Mountain Site, Nevada Research and Development Area, Nevada, 3 volumes, DOE/RW-0073, Office of Civilian Radioactive Waste Management, Washington, D.C.
- DOE (U.S. Department of Energy), 1987. Characteristics of Spent-Fuel, High-Level Waste, and Other Radioactive Wastes Which May Require Long-Term Isolation, DOE/RW-0184, Office of Civilian Radioactive Waste Management, Washington, D.C.

- DOE (U.S. Department of Energy), 1988a. Internal Dose Conversion Factors for Calculation of Dose to the Public, DOE/EH-0071, Office of Environment and Health, Washington, D.C.
- DOE (U.S. Department of Energy), 1988b. Site Characterization Plan: Yucca Mountain Site, Nevada Research and Development Area, Nevada, DOE/RW-0199, Office of Civilian Radioactive Waste Management, Washington, D.C.
- Einzigler, R. E., S. C. Marschman, and H. C. Buchanan, 1991. "Spent-Fuel Dry-Bath Oxidation Testing," Nuclear Technology, Vol. 94, pp. 383-393.
- Einzigler, R. E., 1991. "Effects of an Oxidizing Atmosphere in a Spent Fuel Packaging Facility," presented at Focus '91, Nuclear Waste Packaging, Las Vegas, NV, September 29-October 2, 1991.
- EPA (U.S. Environmental Protection Agency), 1988. Limiting Values of Radionuclide Intake and Air Concentration and Dose Conversion Factors for Inhalation, Submersion, and Ingestion, EPA-520/1-88-020, Washington, D.C.
- EPRI (Electric Power Research Institute), 1992. "Source Term in the EPRI Performance Assessment," R. Shaw, presented to Nuclear Waste Technical Review Board, Las Vegas, NV, October 15, 1992.
- Eslinger, P. W., L. A. Doremus, D. W. Engel, T. B. Miley, M. T. Murphy, W. E. Nichols, M. D. White, D. W. Langford, and S. J. Ouderkerk, 1993. Preliminary Total-System Analysis of a Potential High-Level Nuclear Waste Repository at Yucca Mountain, PNL-8444, Pacific Northwest Laboratory, Richland, Washington.
- Garisto, N. C., E. R. Vance, S. Stroes-Gascoyne, and L. H. Johnson, 1989. Instant-Release Fractions for the Assessment of Used Nuclear Fuel Disposal, AECL-9892, Whiteshell Nuclear Research Establishment, Pinawa, Canada.
- Gauthier, J. H., 1993. "The Most Likely Groundwater Flux through the Unsaturated Tuff Matrix at USW H-1," in Proceedings of the High Level Radioactive Waste Management Fourth Annual Conference, Las Vegas, NV, April 26-30, 1993, American Nuclear Society, La Grange Park, IL and American Society of Civil Engineers, New York, NY, pp. 146-151.
- Golder Associates Inc., 1993. Application of RIP (Repository Integration Program) to the Proposed Repository at Yucca Mountain: Conceptual Model and Input Data Set, 923-1171, Redmond, WA.
- Gray, W. and C. Wilson, 1990. "Effects of Water Composition and Temperature on the Dissolution Rate of  $UO_2$ ," presented at the 1990 Spent Fuel Workshop, Manitoba, Canada.
- Gray, W. J., H. R. Leider, and S. A. Steward, 1992. "Parametric Study of LWR Spent Fuel Dissolution Kinetics," Journal of Nuclear Materials, Vol. 190, pp. 46-52.

- Healey, D. L., F. G. Clutson, and D. A. Glover, 1986. Borehole Gravity Meter Survey in Drill Hole USW G-4, Yucca Mountain Area, Nye County, Nevada, USGS-OFR-86-205, Open-File Report, U.S. Geological Survey, Denver, CO.
- Hevesi, J. A., and A. L. Flint, 1993. "The Influence of Seasonal Climatic Variability of Shallow Infiltration at Yucca Mountain," in Proceedings of the High Level Radioactive Waste Management Fourth Annual Conference, Las Vegas, NV, April 26-30, 1993, American Nuclear Society, La Grange Park, IL and American Society of Civil Engineers, New York, NY, pp. 122-131.
- INTERA, Inc, 1993. A Comparative Application of the Repository Integration Model (RIP) to Total System Performance Assessment - 1991, B00000000-01717-2200-00010-00, Civilian Radioactive Waste Management System Management and Operating Contractor, Las Vegas, NV.
- Klavetter, E. A., and R. R. Peters, 1986. Estimation of Hydrologic Properties of an Unsaturated, Fractured Rock Mass, SAND84-2642, Sandia National Laboratories, Albuquerque, NM.
- Knauss, K. G., W. L. Bourcier, K. D. McKeegan, C. I. Merzbacher, S. N. Nguyen, F. J. Ryerson, D. K. Smith, H. C. Weed, and L. Newton, 1990. "Dissolution Kinetics of a Simple Analogue Nuclear Waste Glass as a Function of pH, Time, and Temperature," Materials Research Society Symposium Proceedings, Vol. 176, pp. 371-381.
- Kossik, R., and J. Hachey, 1993 (in press). RIP Repository Performance Assessment and Strategy Evaluation Model: User's Guide Version 3.00, Golder Associates Inc., Redmond, WA.
- Lamont, A., 1993. Personal communication (reproduced in Appendix F).
- Long, A., and S. W. Childs, 1993. "Rainfall and Net Infiltration Probabilities for Future Climate Conditions at Yucca Mountain," in Proceedings of the High Level Radioactive Waste Management Fourth Annual Conference, Las Vegas, NV, April 26-30, 1993, American Nuclear Society, La Grange Park, IL and American Society of Civil Engineers, New York, NY, pp. 112-121.
- McCright, R. D., 1993. "Corrosion Aspects under Various Thermal Scenarios," presented to Nuclear Waste Technical Review Board, Denver, CO, July 13, 1993.
- McGuire, R. K., D. B. Bullen, N.G.W. Cook, K. J. Coppersmith, J. M. Kemeny, A. Long, F. J. Pearson, Jr., F. Schwartz, M. Sheriden, and R. R. Youngs, 1990, Demonstration of a Risk-Based Approach to High-Level Waste Repository Evolution, NP-7057, Electric Power Research Institute, Palo Alto, CA.

- McGuire, R. K., M. J. Apted, D. B. Bullen, S. Childs, N.G.W. Cook, K. J. Coppersmith, R. L. Keeney, J. M. Kemeny, A. Long, F. J. Pearson, Jr., F. Schwartz, M. Sheriden, and R. R. Youngs, 1992. Demonstration of a Risk-Based Approach to High-Level Waste Repository Evolution: Phase 2, NP-100384, Electric Power Research Institute, Palo Alto, CA.
- Meijer, A., 1993. Personal communication (reproduced in Appendix H).
- Miller, I., R. Kossik, and M. Cunnane, 1992. "A New Methodology for Site Suitability Evaluation," in Proceedings of the High Level Radioactive Waste Management Third Annual Conference, Las Vegas, Nevada, April, 8-12, 1990, Vol. 1, American Nuclear Society, La Grange Park, IL and American Society of Civil Engineers, New York, NY, pp. 494-501.
- Miller, I., R. Kossik, and J. Hachey, 1993 (in press). RIP Repository Performance Assessment and Strategy Evaluation Model: Theory and Capabilities Version 3.00, Golder Associates Inc., Redmond, WA.
- Montazer, P., and W. E. Wilson, 1984. Conceptual Hydrologic Model of Flow in the Unsaturated Zone, Yucca Mountain, Nevada, USGS-WRI-84-4345, Water-Resources Investigations Report, U.S. Geological Survey, Denver, CO.
- NAS (National Research Council, National Academy of Sciences), 1983. Board on Radioactive Waste Management-Waste Isolation System Panel, A Study of the Isolation System for Geologic Disposal of Radioactive Wastes, National Academy Press, Washington, D.C.
- Nichols, W. D., 1987. Geohydrology of the Unsaturated Zone at the Burial Site for Low-Level Radioactive Waste near Beatty, Nye County, Nevada, USGS-WSP-2312, Water-Supply Paper, U.S. Geological Survey, Washington, D.C., 57 pp.
- Nitao, J. J., 1989. V-TOUGH - An Enhanced Version of the TOUGH Code for the Thermal and Hydrologic Simulation of Large-Scale Problems in Nuclear Waste Isolation, UCID-21954, Lawrence Livermore National Laboratory, Livermore, CA.
- Nitsche, H., R. C. Gatti, E. M. Standifer, S. C. Lee, A. Mueller, T. Prussin, R. S. Deinhammer, H. Maurer, K. Becraft, S. Leung, and S. A. Carpenter, 1992a. Measured Solubilities and Speciations of Neptunium, Plutonium, and Americium in a Typical Groundwater (J-13) from the Yucca Mountain Region, LBL-30958, Lawrence Berkeley Laboratory, Berkeley, CA.
- Nitsche, H., K. Roberts, T. Prussin, A. Mueller, K. Becraft, D. Keeney, S. A. Carpenter, and R. C. Gatti, 1992b. Measured Solubilities and Speciations from Oversaturation Experiments of Neptunium, Plutonium, and Americium in UE25P#1 Well Water from the Yucca Mountain Region, LBL-32897, Lawrence Berkeley Laboratory, Berkeley, CA.

- NRC (U.S. Nuclear Regulatory Commission), 1981. Estimates of Internal Dose Equivalent to 22 Target Organs for Radionuclides Occurring in Routine Releases from Fuel-cycle Facilities, Vol. III, Dunning, D., Killough, G., Bernard, S., Pleasant, J., and Walsh, P. NUREG/CR-0150 Vol. 3 (ORNL/NUREG/TM-190/V3), U.S. Nuclear Regulatory Commission, Washington, D.C.
- NRC (U.S. Nuclear Regulatory Commission), 1990. Phase 1 Demonstration of the Nuclear Regulatory Commission's Capability to Conduct a Performance Assessment for a High-Level Waste Repository, Division of High-Level Waste Management, NMSS, U.S. Nuclear Regulatory Commission, Washington, D.C.
- O'Connell, W. J., and R. S. Drach, 1986. Waste Package Performance Assessment: Deterministic System Model Program Scope and Specification, UCRL-53761, Lawrence Livermore National Laboratory, Livermore, CA.
- Ortiz, T. S., R. L. Williams, F. B. Nimick, B. C. Whittel, and D. L. South, 1985. A Three Dimensional Model of Reference Thermal/Mechanical and Hydrological Stratigraphy at Yucca Mountain, Southern Nevada, SAND84-1076/UC-70, Sandia National Laboratories, Albuquerque, NM.
- Oversby, V., 1987. "Spent Fuel as a Waste Form--Data Needs to Allow Long-Term Performance Assessment Under Repository Disposal Conditions," in Scientific Basis for Nuclear Waste Management X, J. K. Bates and W. B. Seefeld, (eds.), Vol. 84, Materials Research Society, Pittsburgh, PA.
- Oversby, V., and C. N. Wilson, 1986. "Derivation of a Waste Package Source Term for the NNWSI From the Results of Laboratory Experiments," in Scientific Basis for Nuclear Waste Management IX, L. O. Werme, (ed.), Vol. 66, Materials Research Society, Pittsburgh, PA.
- Park, U., and C. G. Pflum, 1990. "Requirements for Controlling a Repository's Releases of Carbon-14 Dioxide; the High Costs and Negligible Benefits," in Proceedings of the International Topical Meeting on High Level Radioactive Waste Management, Las Vegas, NV, April 8-12, 1990, Vol. 2, American Nuclear Society, La Grange Park, IL and American Society of Civil Engineers, New York, NY, pp. 1158-1164.
- Pigford, T. H., P. L. Chambre, and W.W.-L Lee, 1990. A Review of Near-Field Mass Transfer in Geologic Disposal Systems, LBL-27045, Lawrence Berkeley Laboratory, Berkeley, CA.
- Pruess, K., and Y. Tsang, 1993. "Modeling of Strongly Heat-Driven Flow Processes at a Potential High-Level Nuclear Waste Repository at Yucca Mountain, Nevada," in Proceedings of High Level Radioactive Waste Management Fourth Annual Conference, Las Vegas, NV, April 26-30, 1993, American Nuclear Society, La Grange Park, IL and American Society of Civil Engineers, New York, NY, pp. 568-575.
- Roddy, J. W., H. C. Clairborn, R. C. Ashline, P. J. Johnson, B. T. Rhyne, 1986. Physical and Decay Characteristics of Commercial LWR Spent Fuel, ORNL/TM-9591/V1&R1, Oak Ridge National Laboratory, Oak Ridge, TN.

- Ross, B., S. Amter, and N. Lu, 1991. Numerical Studies of Rock-Gas Flow in Yucca Mountain, SAND91-7034, Sandia National Laboratories, Albuquerque, NM.
- Ross, B., S. Amter, and N. Lu, 1992. Numerical Studies of Rock-Gas Flow in Yucca Mountain, SAND91-7034/UC-814, Sandia National Laboratories, Albuquerque, NM.
- Ross, B., 1993. Memo to Mike Wilson re Carbon-14 Travel Time Distribution Simulation Data (reproduced in Appendix I).
- Ryder, E., 1993. "Comparison of Predicted Far-Field Temperatures for Discrete and Smearred Heat Sources," in Proceedings of High Level Radioactive Waste Management Fourth Annual International Conference, Las Vegas, NV, April 26-30, 1993, American Nuclear Society, La Grange Park, IL and American Society of Civil Engineers, New York, NY, pp. 841-846.
- Sass, J., and A. Lachenbruch, 1983. Preliminary Interpretation of Thermal Data from the Nevada Test Site, USGS-OFR-82-973, Open-File Report, U.S. Geological Survey, Denver CO.
- Shaw, R., R. F. Williams, J. C. Stepp, and R. McGuire, 1992. "Performance Assessment for a High-Level Waste Repository at Yucca Mountain," in Proceedings of the High Level Radioactive Waste Management Third Annual Conference, Las Vegas, NV, April 12-16, 1992, Vol. 1, American Nuclear Society, La Grange Park, IL and American Society of Civil Engineers, New York, NY, pp. 869-873.
- Shaw, R. A. and R. K. McGuire, 1993. "Demonstration of a Risk-Based Approach to High-Level Repository Evaluation 'Phase II,'" in Proceedings of the High Level Radioactive Waste Management Fourth Annual International Conference, Las Vegas, NV, April 26-30, 1993, Vol. 1, American Nuclear Society, La Grange Park, IL and American Society of Civil Engineers, New York, NY, pp. 1-5.
- Sinnock, S., Y. Lin, and J. Brannen, 1984. Preliminary Bounds on the Postclosure Performance of the Yucca Mountain Repository Site, Southern Nevada, SAND84-1492, Sandia National Laboratories, Albuquerque, NM.
- Sinnock, S., Y. T. Lin, and J. P. Brannen, 1987. "Preliminary Bounds on the Expected Post-closure Performance of the Yucca Mountain Repository Site, Southern Nevada," Journal of Geophysical Research, Vol. 92, No. B8, pp. 7820-7842.
- SPSS, 1993. SPSS for Windows (Release 6). SPSS, Inc., Chicago, IL.
- Stahl, 1993. Personal communication. (reproduced in Appendix E).
- Thompson, F. L., F. H. Dove, and K. M. Krupka, 1984. Preliminary Upper-Bound Consequence Analysis for a Waste Repository at Yucca Mountain, Nevada, SAND83-7475, Sandia National Laboratories, Albuquerque, New Mexico.
- Triay, 1993. Personal communication (reproduced in Appendix G).

- Uhlig, H. H. (ed.), 1948. Corrosion Handbook, John Wiley & Sons, New York, NY.
- U.S. Congress, 1992. Energy Policy Act of 1992, Public Law 102-486, Signed into Law by the President on October 24, 1992.
- USGS (U.S. Geological Survey), 1993. "Geological Cross Sections of Proposed Underground Excavations Exploratory Studies Facility," DTN:GS930308314221.009, Water Resources Division, U.S. Geological Survey, Denver, CO.
- Van Konynenburg, R. A., C. F. Smith, H. W. Culham, and H. D. Smith, 1987. "Carbon-14 in Waste Packages for Spent Fuel in a Tuff Repository," in Scientific Basis for Nuclear Waste Management X, J. K. Bates and W. B. Seefeld, (eds.), Vol. 84, Materials Research Society, Pittsburgh, PA.
- Wilson, C. N., and W. J. Gray, 1990. "Measurement of Soluble Nuclide Dissolution Rates from Spent Fuel," in Materials Research Society Symposia Proceedings, Volume 176, V. M. Oversby and P. W. Brown (eds.), Materials Research Society, Pittsburg, PA, pp. 489-498.
- Wilson, W. E., 1985. Letter to Dr. D. L. Vieth (December 24, 1985), Unsaturated-zone flux at Yucca Mountain, Nevada, U.S. Geological Survey, Denver, CO.
- Wilson, M. L., 1993. "Sensitivity Analyses for Total-System Performance Assessment," in Proceedings of the High Level Radioactive Waste Management Fourth Annual Conference, Las Vegas, NV, April 26-30, 1993, Vol. 1, American Nuclear Society, La Grange Park, IL and American Society of Civil Engineers, New York, NY, pp. 14-21.
- Wilson, M. L., J. H. Gauthier, R. W. Barnard, G. E. Barr, H. A. Dockery, E. Dunn, R. R. Eaton, D. C. Guerin, N. Lu, M. J. Martinez, R. Nilson, C. A. Rautman, T. H. Robey, B. Ross, E. E. Ryder, A. R. Schenker, S. A. Shannon, L. H. Skinner, W. G. Halsey, J. Gansemer, L. C. Lewis, A. D. Lamont, I. R. Triay, A. Meijer, and D. E. Morris, 1994 (in press). Total-System Performance Assessment for Yucca Mountain -- SNL Second Iteration (TSPA-1993), SAND93-2675, Sandia National Laboratories, Albuquerque, NM.

#### CODES AND REGULATIONS

- 10 CFR Part 60 (Code of Federal Regulations), 1993. Title 10, Energy, Part 60, Disposal of High-Level Radioactive Wastes in Geologic Repositories, U.S. Government Printing Office, Washington, D.C.
- 40 CFR Part 191, (Code of Federal Regulations), 1993. Title 40, Protection of Environment, Part 191, Environmental Standards for the Management and Disposal of Spent Nuclear Fuel, High-Level and Transuranic Radioactive Wastes, U.S. Government Printing Office, Washington, D.C.

## 6. ACRONYMS AND ABBREVIATIONS

APD	areal power density
BWR	boiling water reactor
CCDF	complementary cumulative distribution function
CDF	cumulative density function
DHLW	defense high-level waste
DOE	U.S. Department of Energy
EBS	Engineered Barrier System
ECM	equivalent continuum model
EPA	U.S. Environmental Protection Agency
EPRI	Electric Power Research Institute
HLW	high-level waste
LLNL	Lawrence Livermore National Laboratory
Los Alamos	Los Alamos National Laboratory
M&O	Civilian Radioactive Waste Management System Management and Operating Contractor
MTHM	metric tons of heavy metal
MTIHM	metric tons of initial heavy metal
MTU	metric tons of uranium
NAS	National Academy of Sciences
NRC	U.S. Nuclear Regulatory Commission
PDF	probability density function
PNL	Pacific Northwest Laboratory
PWR	pressurized-water reactor
RIP	Repository Integration Program
SCP	Site Characterization Plan
SNL	Sandia National Laboratories
TSPA	Total System Performance Assessment
USGS	U.S. Geological Survey
YMP	Yucca Mountain Site Characterization Project
YMPO	Yucca Mountain Site Characterization Project Office

**APPENDIX A**

**FAR-FIELD THERMOHYDROLOGIC CALCULATIONS**

**Srikanta Mishra**

## INTRODUCTION

The U.S. Department of Energy is currently investigating the suitability of Yucca Mountain, Nevada, as a potential repository for the nation's spent nuclear fuel and high-level radioactive waste. The wastes are expected to be emplaced within densely-welded, fractured tuff units in the unsaturated zone, approximately 300 m below land surface and 200 m above the water table. Heat generated from radioactive decay will initiate processes such as conductive and convective heat transfer, boiling and condensation, capillary adsorption and vapor pressure lowering, thermal buoyancy driven vapor flow, etc., all of which can alter the distribution and movement of heat and/or water in the vicinity of the repository. Thus, flow and transport predictions for the geosphere during the postclosure period of the repository require the use of concepts and models that are likely to be substantially different from those used to describe the ambient behavior of water-air flow in the unsaturated zone.

Several modeling studies of heat transport and/or fluid flow induced by repository heating at Yucca Mountain have been presented in the recent past. These include: numerical analyses of coupled heat and fluid flow processes at the repository scale (Pollock, 1986; Tsang and Pruess, 1987; Nitao, 1988; Buscheck and Nitao, 1992; Pruess and Tsang, 1993; Buscheck and Nitao, 1993), as well as near- and far-field temperature predictions via space-time superpositions of conduction-only analytical solutions (Ryder, 1993). Recent studies of hydrothermal effects at Yucca Mountain have relied on simplified axisymmetric models which treat the entire repository as a single, smeared heat source (Buscheck and Nitao, 1992; Pruess and Tsang, 1993; Buscheck and Nitao, 1993). Such a representation of repository heating, which ignores the spatial heterogeneity in thermal loading due to the access drifts and defense high-level wastes with negligible heat generation, has been shown to overpredict the temporal persistence of thermal effects (Ryder, 1993).

Although thermohydrologic models are useful for predicting the response of the geosphere to waste emplacement, a total system performance assessment (TSPA) exercise to demonstrate compliance with regulatory requirements must also consider the performance of the waste package and other engineered barriers due to all significant events and processes. The overall complexity of such an assessment, often carried out in a probabilistic framework, precludes the use of detailed process models for predicting the behavior of subsystems such as the waste package and/or the geosphere. Analyses of total system performance thus require simplified descriptions and/or abstractions of individual subsystem behavior to be developed as the first step from detailed calculations using lower-level process models.

Previous iterations of TSPA for the Yucca Mountain site have either ignored the impact of thermal effects on total system performance (Barnard and Dockery, 1991), or have used a simplistic attenuation model to represent repository dryout due to waste heat and the subsequent delay in the onset of water flow past the waste packages (Barnard et al., 1992; INTERA, Inc., 1993). The Civilian Radioactive Waste Management System Management and Operating Contractor's (M&O) current exercise for TSPA at Yucca Mountain seeks to improve upon these studies by incorporating thermal dependencies on waste package failure and radionuclide release from the engineered barriers. This requires that functional relationships between thermal load and temperature, aqueous flux, gaseous flux, liquid saturation and relative humidity be abstracted from detailed calculations of coupled heat and fluid flow in the geosphere. Such a numerical

model, which is essentially similar to that presented by Buscheck and Nitao (1993), but customized to the scale of a typical waste-emplacement panel, is described in this appendix.

## MODEL DESCRIPTION

### Computational Tool

The computational tool used in this study for modeling panel-scale thermohydrologic behavior is V-TOUGH (Nitao, 1989), which is capable of simulating coupled multidimensional transport of water, vapor, air and heat in porous and fractured media. V-TOUGH can take into account: (i) fluid flow in both liquid and gas phases under pressure, viscous and gravity forces, (ii) capillary and phase adsorption for the liquid phase, (iii) vapor pressure lowering due to capillary effects, (iv) binary diffusion in the gas phase, and (v) heat transport due to conduction, convection and binary diffusion. V-TOUGH is Lawrence Livermore National Laboratory's (LLNL) enhanced and vectorized version of the widely-used TOUGH code (Pruess, 1987).

### Model Geometry

Figure A-1 shows the location of the individual waste-emplacement panels within the potential repository area at Yucca Mountain. The nine numbered panels identified therein represent the locations of the waste package/engineered barrier system, as well as the origins of the one-dimensional pathways for aqueous and gaseous transport in the geosphere. As depicted by the cross section in Figure A-2, a typical panel is assumed to contain spent fuel assemblies in the middle, surrounded by defense high-level wastes, with access drifts forming an outer shell around the wastes. The corresponding dimensions represent average values for waste emplacement areas and operational areas (i.e., drifts) for the nine panels shown in Figure A-1. For computational convenience, the rectangular cross section of a typical panel is converted into an equivalent circular cross section, as also shown in Figure A-3. This process preserves the relative proportions of the area occupied by spent fuel, defense wastes and access drifts.

Assuming that an axisymmetric ( $r$ - $z$ ) model with the circular cross section of Figure A-3 can adequately represent panel-scale hydrothermal behavior implies that a panel does not interact with other panels or with the surrounding rock body. Figure A-1 suggests that this is a reasonable simplification for the panel-panel interfaces, where no-flow conditions for both heat and fluid flow can be invoked for symmetry reasons. Use of a no-flux boundary condition for the panel-rock interface, on the other hand, would not allow heat to dissipate into the host rock, nor would condensate shedding (from the panel into the surrounding rock) be allowed to occur. Although not realistic, such an assumption is expected to have only a minor impact on fluid saturation and temperature distributions within the panel. This has been confirmed by comparing to repository-scale analyses by Buscheck and Nitao (1993).

### Stratigraphy and Hydrogeologic/Thermal Properties

The stratigraphy and parametrization used to describe the unsaturated zone at the panel scale are similar to those used by Buscheck and Nitao (1993), and are based on data from Klavetter and Peters (1986). The unsaturated zone consists of a series of variably fractured and variably

welded tuffaceous rock units, with matrix and fracture hydraulic properties as given in Table A-1. The choice of an axisymmetric model geometry for computational convenience prevents the observed tilting of the various stratigraphic units to be taken into account. Thermal rock properties correspond to those given in Version 4 of the Reference Information Base (DOE, 1991).

Table A-1. Matrix and Fracture Hydraulic Properties

Unit Name	Thickness (m)	Permeability (m <sup>2</sup> )	Porosity (-)	van Genuchten (1980) Parameters		
				$\alpha$ (Pa <sup>-1</sup> )	$\beta$ (-)	$S_r$ (-)
TCw	29.3	9.70E-19	0.08	8.40E-7	1.558	0.002
PTn	38.1	3.90E-14	0.04	1.53E-6	6.873	0.100
TSw1	130.1	1.90E-18	0.11	5.80E-7	1.798	0.080
TSw2	143.2	1.90E-18	0.11	5.80E-7	1.798	0.080
Repo	4.6	1.90E-18	0.11	5.80E-7	1.798	0.080
TSw2	41.9	1.90E-18	0.11	5.80E-7	1.798	0.080
TSw3	15.8	1.50E-19	0.07	4.51E-7	2.058	0.080
CHn1v	4.6	2.70E-14	0.46	1.64E-6	3.872	0.041
CHn1z	131.7	2.00E-18	0.28	3.15E-7	1.602	0.110
PPw	298.7	4.50E-16	0.24	1.44E-6	2.639	0.066
Fractures	--	8.33E-10	3.33E-4	1.315E-3	4.230	0.0395

The hydraulic properties given above for the various units correspond to those of the matrix only. Fracture properties are taken to be the same for all rock types, and are calculated assuming three 100  $\mu\text{m}$  fractures to occur per meter of rock (Buscheck and Nitao, 1992). The bulk absolute permeability, defined as the porosity-weighted permeability of the fracture and the matrix, is computed to be approximately  $2.8\text{E-}13 \text{ m}^2$  (280 millidarcies) for all units.

#### Equivalent Continuum Model

The paucity of data on geometric/hydraulic characteristics of fractures at Yucca Mountain, as well as the computational complexity associated with modeling hydrothermal behavior in a discrete fracture network, necessitates the use of an equivalent continuum model (ECM) (Pruess et al.,

1985). The ECM formulation assumes capillary pressure and thermal equilibrium between the fractures and the matrix, which allows equivalent continuum properties to be derived by volume averaging fracture and matrix characteristics. The assumption of capillary pressure continuity implies that for most cases of fracture density and permeability, the fractures will be dry as long as the matrix is not close to full liquid saturation. In other words, the ECM forces liquid movement to occur primarily within the matrix and to be controlled by the matrix permeability, whereas air/vapor movement takes place primarily in the fractures and is controlled by the fracture permeability.

Discretization

As indicated earlier, the model developed in this study treats a typical panel as an equivalent right circular cylinder in two-dimensional axisymmetric geometry. The vertical discretization is based on the Klavetter and Peters (1986) stratigraphy and includes approximately 1 km of the saturated zone. The nine stratigraphic units are discretized into 42 layers with thickness ranging from 4.6 m at the repository horizon to ~200 m at the bottom of the model. Areally, the model domain is divided into eight concentric rings of equal cross-sectional area. At the repository horizon, the inner six rings are assumed to contain the spent-fuel assemblies, the seventh ring is assumed to contain the defense high-level wastes, and the last ring is taken to represent the drifts.

Thermal Loading

Because heat generation from the defense wastes is negligible compared to that from the spent fuel, the outer two rings at the repository horizon (i.e., 25 percent of the panel area) are taken to be unheated at all times. Thermal characteristics of the emplaced spent fuel assemblies are computed assuming "youngest fuel first" for 10-year out-of-core waste with a 22:41 mix of boiling water reactor (BWR) and pressurized-water reactor (PWR), which results in an average age of 23 years, a burnup of 39 GWd/MTU and an initial heat output of 1.05 kW/MTU (see Appendix D). The thermal decay curve for this blended fuel is shown in Figure A-4. The emplaced quantity, average age and burnup values for the BWR and PWR assemblies are given in Table A-2.

Table A-2. Characteristics of Emplaced Spent Fuel

Attribute	BWR	PWR
Amount (10 <sup>3</sup> MTU)	22.25	40.75
Average age (yr)	23.5	22.5
Burnup (GWd/MTU)	32.2	42.2

[Note: These are slightly different than those presented by King in Appendix D.]

## Initial Conditions

Initial conditions for the panel-scale model are calculated with V-TOUGH assuming capillary-gravity equilibrium for the anticipated geothermal gradient under zero net surficial infiltration. Since all flows are expected to be vertical for these conditions, a two-step initialization is carried out with a one-dimensional model having the same vertical discretization/parametrization as the full two-dimensional axisymmetric model. Following the approach taken by Pruess and Tsang (1993), the pressure-temperature equilibrium is first established for the zero permeability case. In the second step, the full two-phase flow problem is solved for the appropriate values of permeabilities. The resulting steady-state vertical saturation profile, shown in Figure A-5, is found to be essentially identical to the results from Buscheck and Nitao (1993) for the zero net infiltration case.

## Boundary Conditions

For the steady-state calculations of initial conditions described above (as well as for the subsequent transient simulations under thermal loading) the boundary conditions are set as follows. The lateral boundaries are taken to be closed for both heat and fluid flow. The upper boundary is assigned constant pressure (0.86 atm) and constant temperature (13°C) conditions representative of the atmospheric contact. The lower boundary, located 1 km into the saturated zone, is taken to be at a constant temperature of 53°C and a constant pressure of 15 atm.

# RESULTS AND DISCUSSION

## Simulation Scenarios

Beginning from the initial conditions described previously, thermohydrologic behavior for the waste-emplacement panel is simulated over a 100,000 year time period for areal power densities (APD) of 70.4, 141, and 282 kW/ha (28.5, 57 and 114 kW/acre). Performance measures of interest are temperature and liquid saturation in each of the eight concentric rings as a function of time. In what follows, time histories for these variables are provided at three spatial locations: (i) at the center of the panel,  $r = 72$  m; (ii) at the edge of the heated area of the panel,  $r = 336$  m; and (iii) at the edge of the panel (i.e.,  $r = 393$  m). The temperature history provides a baseline for determining thermal dependencies in corrosion-related parameters and flow/transport coefficients. The saturation history serves to establish the presence or absence of liquid water in the pore spaces as affected by thermal loading, and its impact on the onset of aqueous corrosion. For TSPA purposes, the temporal evolution in liquid saturation and temperature in the inner six rings (i.e., the area containing the heat-generating waste) have been provided in tabular form.

## Model Results

Figure A-6 shows temporal variations in temperature and saturation for the 28.5 kW/acre APD case. In this and all subsequent figures, the time axis is plotted on a logarithmic scale so as to accentuate early-time effects during which temperatures first build up rapidly to a maximum and then show a gradual decline to ambient conditions. No part of the modeled domain is predicted

to experience above-boiling temperatures, with the temperature at the center of the panel peaking only at 70°C. As expected, saturation changes from the ambient are negligible everywhere within the panel.

Temperature and liquid saturation histories for the 57 kW/acre APD case are given in Figure A-7. The temperature at the center of the panel is shown to peak at ~110°C, cooling down to below-boiling conditions after 1,000 years. Corresponding liquid saturation levels are reduced to approximately 10 percent over a similar (i.e., 1,000 year) time period. Although temperatures at the edge of the heated area, as well as at the edge of the panel, do show increases to 70°-80°C, only minor changes in saturation from ambient conditions are indicated there.

Temperature and saturation histories for the 282 kW/ha (114 kW/acre) APD case are presented in Figure A-8. For the 282 kW/ha (114 kW/acre) APD case, the nominal boiling point (96°C) is seen to be exceeded everywhere within the panel, at least for some period of time. The temperature reaches a maximum of ~18°C at the center of the panel, and stays above boiling for approximately 8,000 years. The edge of the heated area peaks at ~130°C and remains under above-boiling conditions for over 5,000 years. The edge of the panel exceeds the nominal boiling point only around 500 years and stays in that condition for 2,000 years.

As shown in Figure A-8, complete dryout (i.e., zero liquid saturation conditions) is predicted to occur only at the center of the panel for ~1000 years, even though above-boiling temperature conditions prevail for substantially longer periods of time. This effect is caused by vapor-pressure lowering (and the associated increase in boiling point) due to capillarity in an unsaturated medium. Vapor-pressure lowering effects also have an effect at the edge of the heated area in the panel, where liquid saturation drops to only 5 percent despite temperatures that reach ~130°C. Partial dryout conditions are also predicted at the edge of the panel.

### Discussion

Although the numerical model used here to simulate panel-scale hydrothermal response is essentially similar to that used by Buscheck and Nitao (1993) for simulating repository-scale thermohydrologic performance, the interpretation of model results is somewhat different than that presented in the LLNL study. This difference is primarily due to the emphasis on using temperature as the key performance measure in Buscheck and Nitao (1993) as compared to the use of both temperature and saturation as performance measures in this study. Some insights gained in this process, as demonstrated in Figures A-6 through A-8, are summarized below:

- The thermal load influences the extent to which the boiling point is increased from the nominal value of 96°C due to vapor-pressure lowering effects.
- The period during which complete dryout occurs is much shorter than the period corresponding to above-boiling temperatures (i.e.,  $T > 96^\circ\text{C}$ ).
- Using 96°C as the threshold for liquid disappearance due to vaporization (and liquid reappearance due to condensation) tends to increase the predicted duration of extended-dry conditions at the repository horizon.

Thus, temperature-based predictions of the spatial and temporal persistence of rock dryout generated from thermohydrologic simulations (Buscheck and Nitao, 1992; Buscheck and Nitao, 1993) (or from conduction-only model calculations [Ryder, 1993]) will be enhanced. The important implication here is that the waste packages will be predicted to be dry for a longer period of time than will actually be the case.

Far-field results represent averages over several meters, and do not necessarily reflect temperature and saturation conditions locally in the vicinity of waste packages. Appendix B describes a simplified methodology for converting far-field temperatures into waste-package surface (and drift wall) temperatures assuming no change in hydrologic conditions. The lack of a similar procedure for predicting near-field saturation is an important limitation for the current TSPA exercise.

### **CONCLUDING REMARKS**

A two-dimensional axisymmetric (r-z) model has been developed to provide thermohydrologic input for the current iteration of TSPA at Yucca Mountain. The model uses a series of concentric rings to represent spent-fuel emplaced areas, regions containing defense high-level wastes with negligible heat generation, and the unheated drift regions in a typical waste-emplacment panel. Using a vertical stratigraphy similar to that used by Buscheck and Nitao (1993), and beginning from capillary-gravity-thermal equilibrium conditions, hydrothermal behavior at the panel scale is simulated with V-TOUGH for thermal loads of 70.4, 141, and 282 kW/ha (28.5, 57 and 114 kW/acre). Temperature and saturation histories calculated for each of the rings are used in the TSPA calculations to define thermal dependencies of various mechanistic/phenomenological coefficients, and also to determine the onset aqueous corrosion.

Simplified models such as the one described in this appendix are useful tools for understanding the coupling between heat and fluid flow due to thermal loading, as well as for developing methodologies to incorporate thermal effects in the TSPA process. However, several caveats remain with respect to the representativeness of such models, viz: (i) demonstration of the validity (or lack thereof) of the ECM assumption for various combinations of fracture properties and thermal loads, (ii) uncertainty in characterizing the spatial distribution and connectivity of permeable fractures, (iii) inconsistency in using far-field model results to predict near-field (waste-package scale) hydrologic conditions, and (iv) the importance of a finite surficial percolation flux on near- and far-field hydrothermal regimes. These questions should be addressed prior to the abstraction of hydrothermal model results for future TSPA exercises.

### **REFERENCES**

Barnard, R. W. and H. A. Dockery (eds.), 1991. Technical Summary of the Performance Assessment Calculational Exercises for 1990 (PACE-90), Volume 1: "Nominal Configuration" Hydrogeologic Parameters and Calculational Results, SAND90-2726, Sandia National Laboratories, Albuquerque, NM.

- Barnard, R. W., M. L. Wilson, H. A. Dockery, J. H. Gauthier, P. G. Kaplan, R. R. Eaton, F. W. Bingham, and T. H. Robey, 1992. TSPA 1991: An Initial Total-System Performance Assessment for Yucca Mountain, SAND91-2795, Sandia National Laboratories, Albuquerque, NM.
- Buscheck, T. A., and J. J. Nitao, 1992. "The Impact of Thermal Loading on Repository Performance at Yucca Mountain," in Proceedings of the High Level Radioactive Waste Management Third Annual Conference, Las Vegas, NV, April 12-16, 1992, American Nuclear Society, La Grange Park, IL and American Society of Civil Engineers, New York, NY.
- Buscheck, T. A., and J. J. Nitao, 1993. "The Analysis of Repository-Heat-Driven Hydrothermal Flow at Yucca Mountain," in Proceedings of the High Level Radioactive Waste Management Fourth Annual Conference, Las Vegas, NV, April 26-30, 1993, American Nuclear Society, La Grange Park, IL and American Society of Civil Engineers, New York, NY, pp 847-865.
- DOE (U.S. Department of Energy), 1991. The Yucca Mountain Site Characterization Project Reference Information Base, Version 4, Rev. 4, YMP/CC-0002, Yucca Mountain Site Characterization Project Office, Las Vegas, NV.
- INTERA, Inc, 1993. A Comparative Application of the Repository Integration Model (RIP) to Total System Performance Assessment - 1991, B00000000-01717-2200-00010-00, Civilian Radioactive Waste Management System Management and Operating Contractor, Las Vegas, NV.
- Klavetter, E. A., and R. R. Peters, 1986. Estimation of Hydrologic Properties of an Unsaturated, Fractured Rock Mass, SAND84-2642, Sandia National Laboratories, Albuquerque, NM.
- Nitao, J. J., 1988. Numerical Modeling of the Thermal and Hydrological Environment Around a Nuclear Waste Package Using the Equivalent Continuum Approximation: Horizontal Emplacement, UCID-21444, Lawrence Livermore National Laboratory, Livermore, CA.
- Nitao, J. J., 1989. V-TOUGH - An Enhanced Version of the TOUGH Code for the Thermal and Hydrologic Simulation of Large-Scale Problems in Nuclear Waste Isolation, UCID-21954, Lawrence Livermore National Laboratory, Livermore, CA.
- Pollock, D. W., 1986. "Simulation of Fluid Flow and Energy Transport Processes Associated with High-Level Radioactive Waste Disposal in Unsaturated Alluvium," Water Resources Research, Vol. 22, No. 5, pp. 765-775.
- Pruess, K., Y. W. Tsang, and J. S. Y. Wang, 1985. "Modeling of Strongly Heat-Driven Flow in Partially Saturated Fractured Porous Media," in Memoirs, International Association of Hydrogeologists, XXVII, pp. 486-497.
- Pruess, K., 1987. TOUGH User's Guide, NUREG/CR-4645, SAND86-7104, LBL-20700, U.S. Nuclear Regulatory Commission, Washington, D.C.

- Pruess, K., and Y. Tsang, 1993. "Modeling of Strongly Heat-Driven Flow Processes at a Potential High-Level Nuclear Waste Repository at Yucca Mountain, Nevada," in Proceedings of High Level Radioactive Waste Management Fourth Annual Conference, Las Vegas, NV, April 26-30, 1993, American Nuclear Society, La Grange Park, IL and American Society of Civil Engineers, New York, NY, pp. 568-575.
- Ryder, E., 1993. "Comparison of Predicted Far-Field Temperatures for Discrete and Smeared Heat Sources," in Proceedings of High Level Radioactive Waste Management Fourth Annual International Conference, Las Vegas, NV, April 26-30, 1993, American Nuclear Society, La Grange Park, IL and American Society of Civil Engineers, New York, NY, pp. 841-846.
- Tsang, Y. W. and K. Pruess, 1987. "A Study of Thermally Induced Convection near a High-Level Nuclear Waste Repository in Partially Saturated Fractured Tuff," Water Resources Research, Vol. 23, No. 10, pp. 1958-1966.
- van Genuchten, M. Th., 1980. "A Closed-Form Equationj for Predicting the Hydraulic Conductivity of Unsaturated Soils," Soil Science Society of America Journal, Vol. 44, No. 4, pp. 892-898.

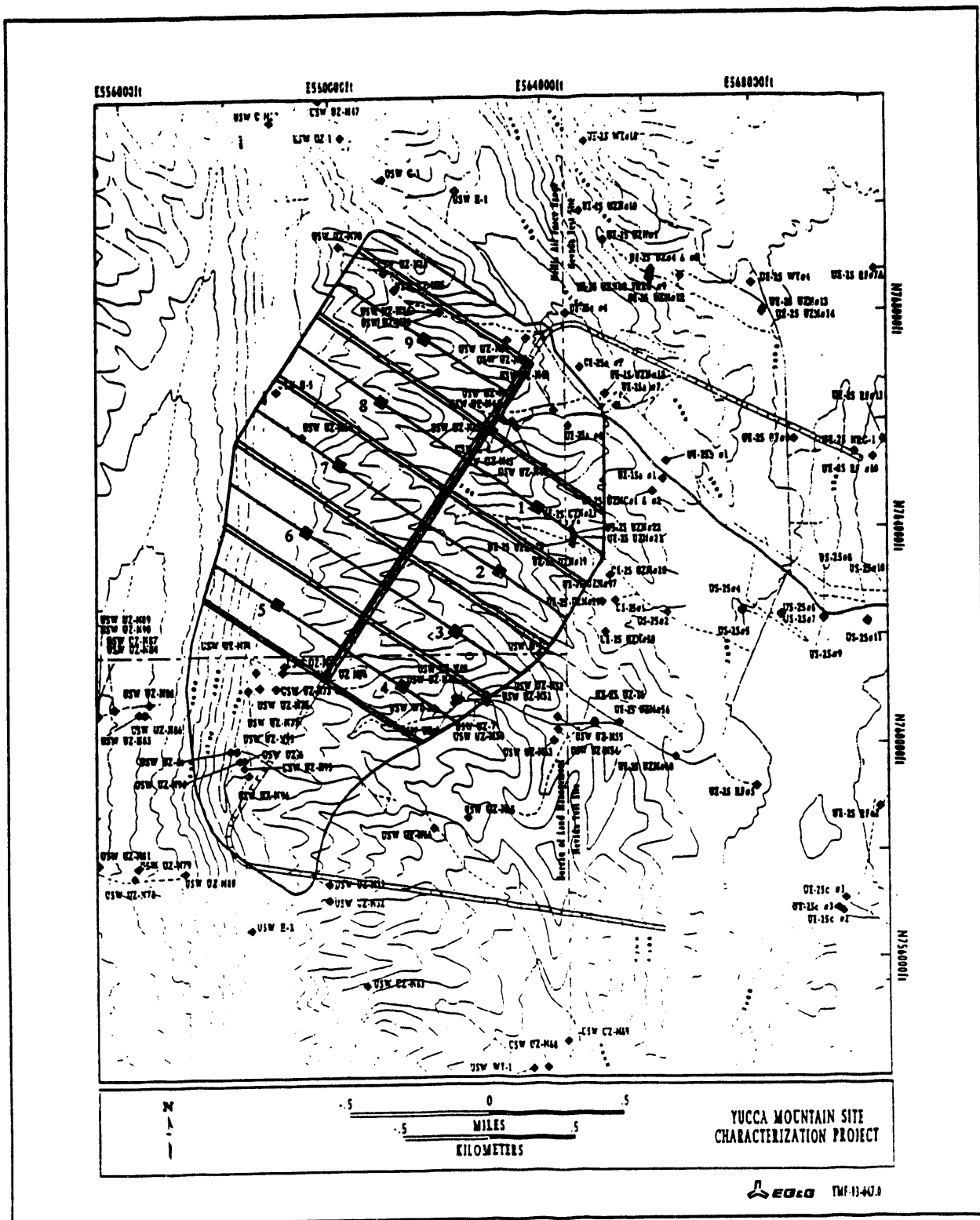


Figure A-1. Location of Individual Waste Emplacement Panels Within the Potential Repository Area at Yucca Mountain

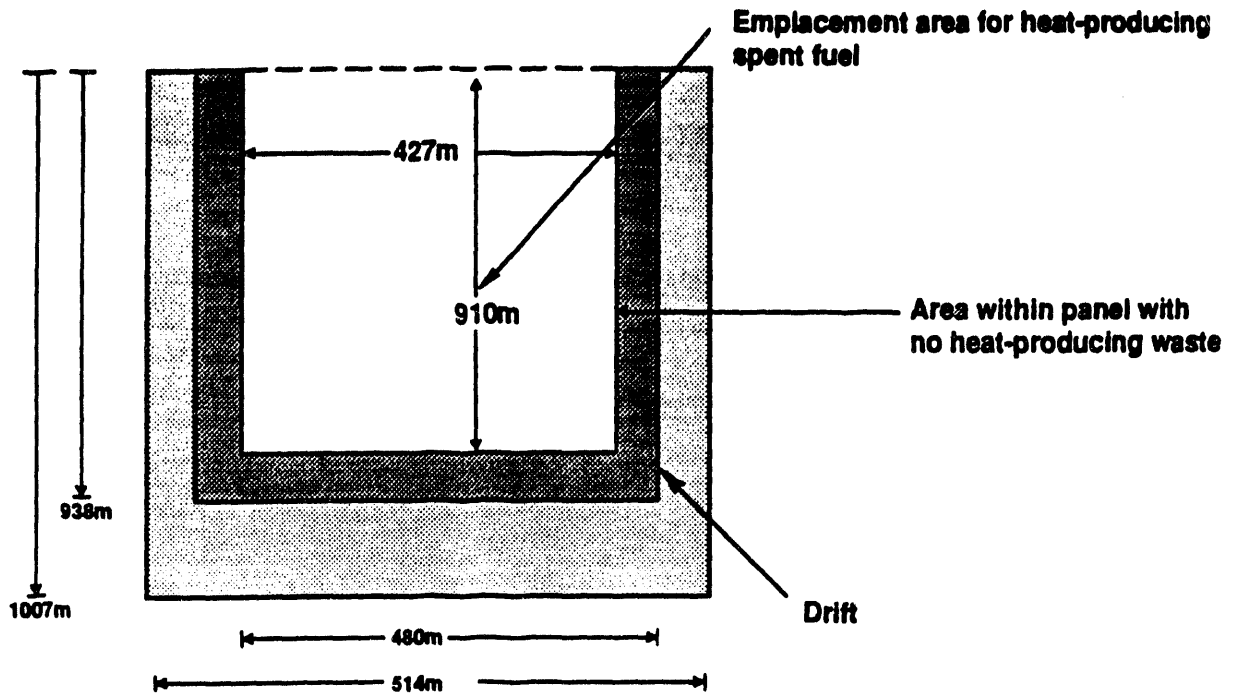


Figure A-2. Actual Rectangular Cross Section of a Typical Panel

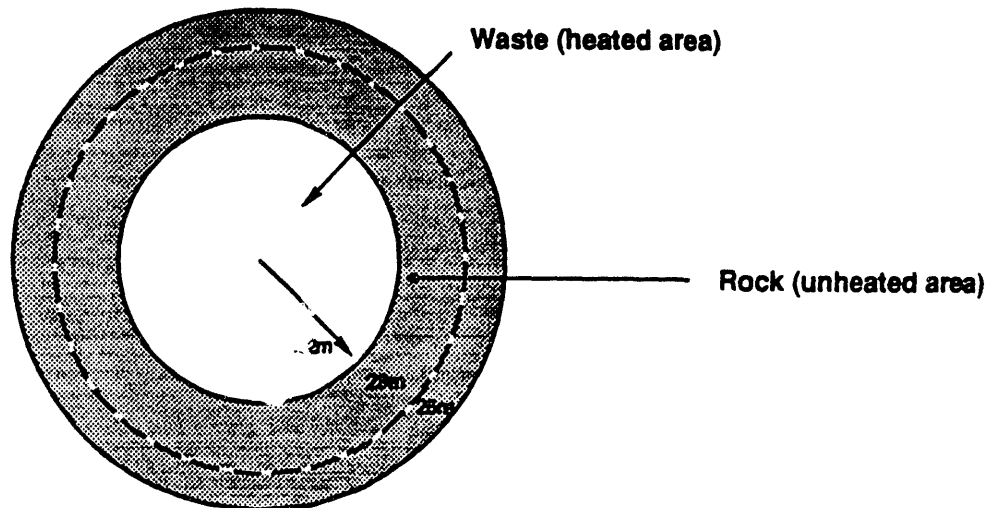
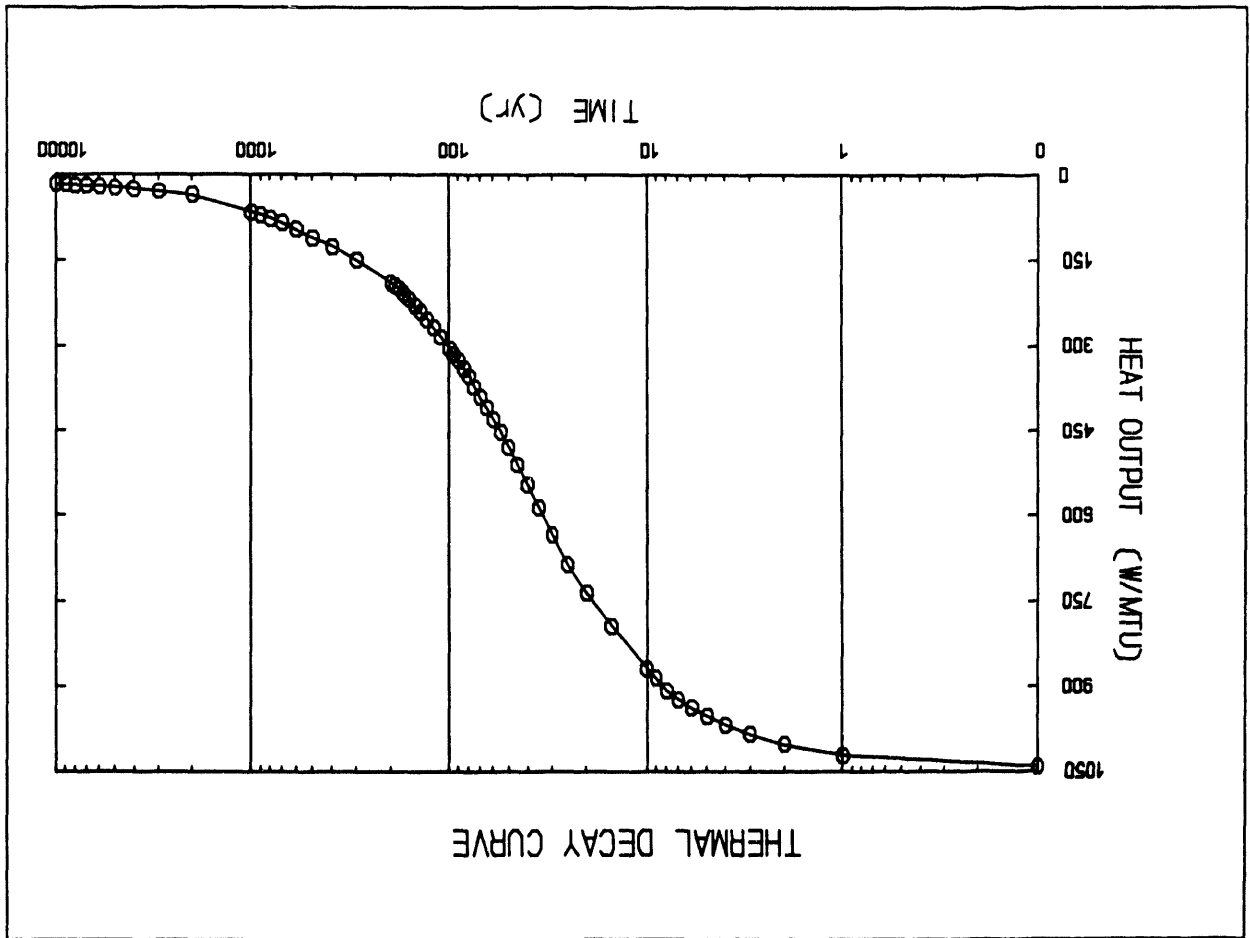


Figure A-3. Approximation of the Panel Cross Section Shown Above by an Equivalent Circular Cross Section

Figure A-4. Thermal Decay Curve for Reference Blended Fuel



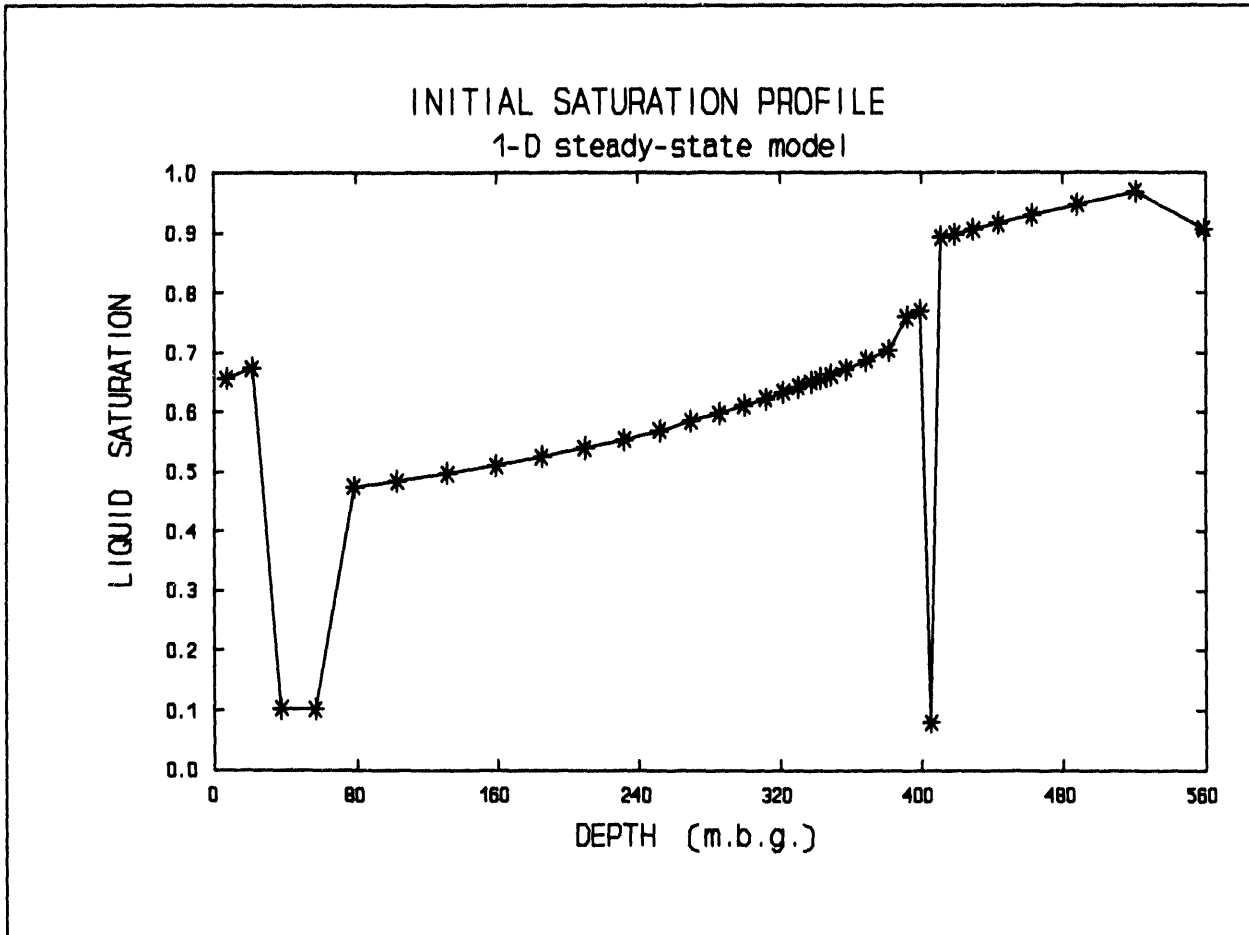


Figure A-5. Steady-State Saturation Profile Calculated Along the Vertical for Zero Net Surficial Infiltration Conditions

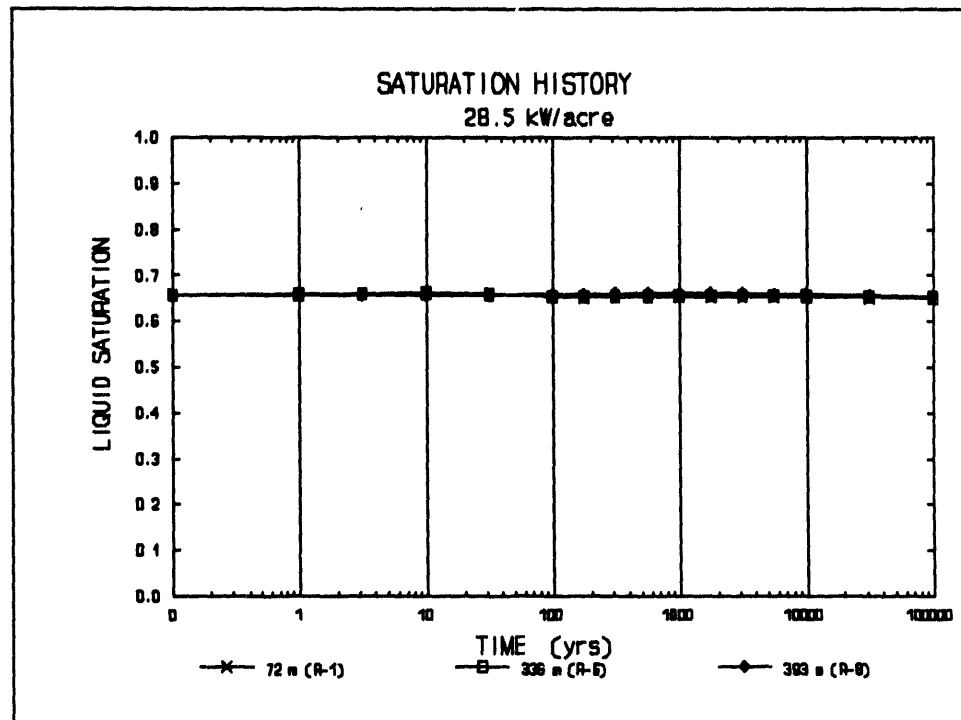
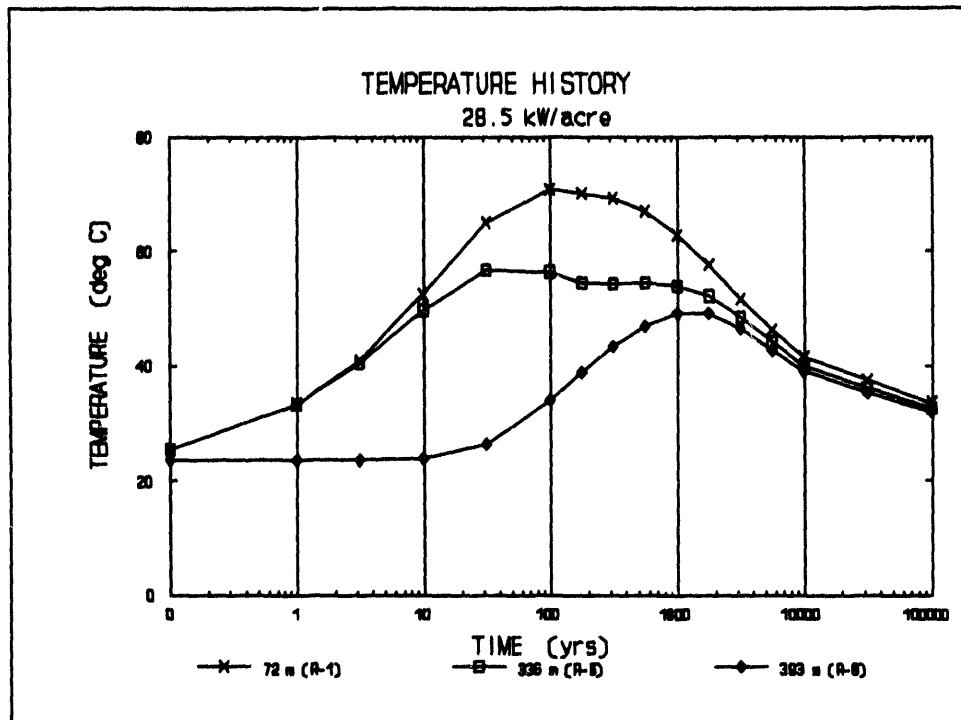


Figure A-6. Temperature and Saturation Histories at Three Spatial Locations Within the Panel for the 28.5 kW/Acre APD Case

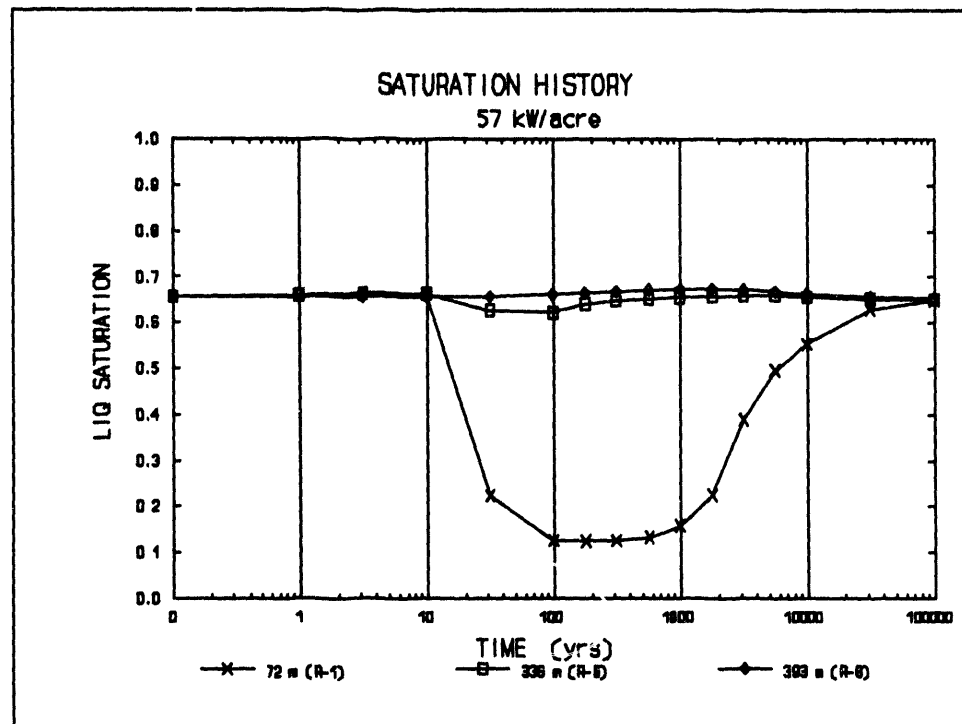
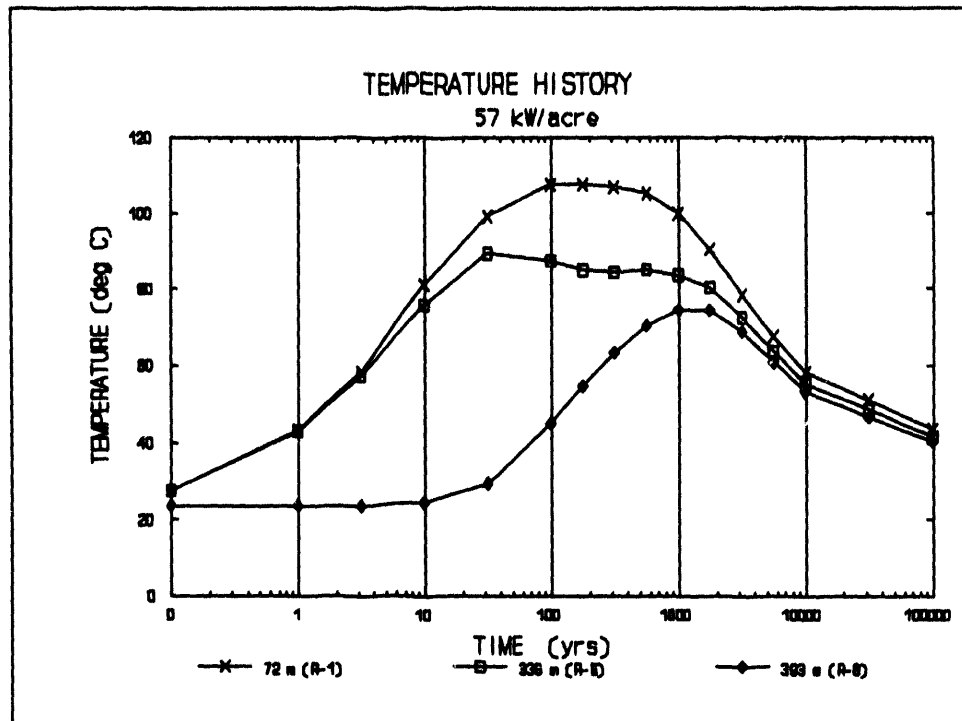


Figure A-7. Temperature and Saturation Histories at Three Spatial Locations Within the Panel for the 57 kW/Acre APD Case

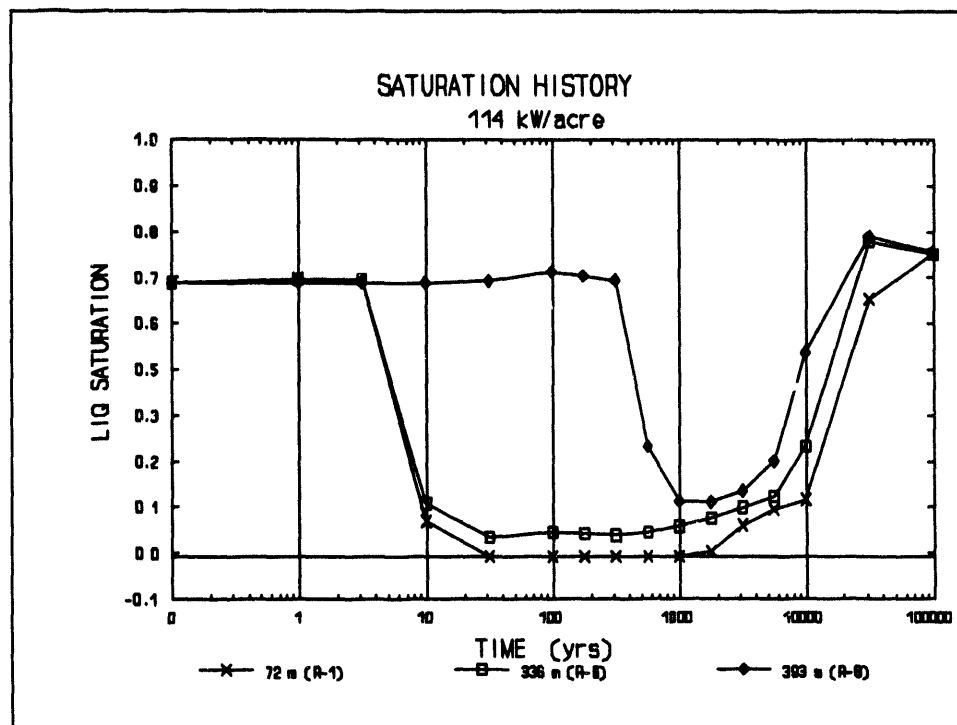
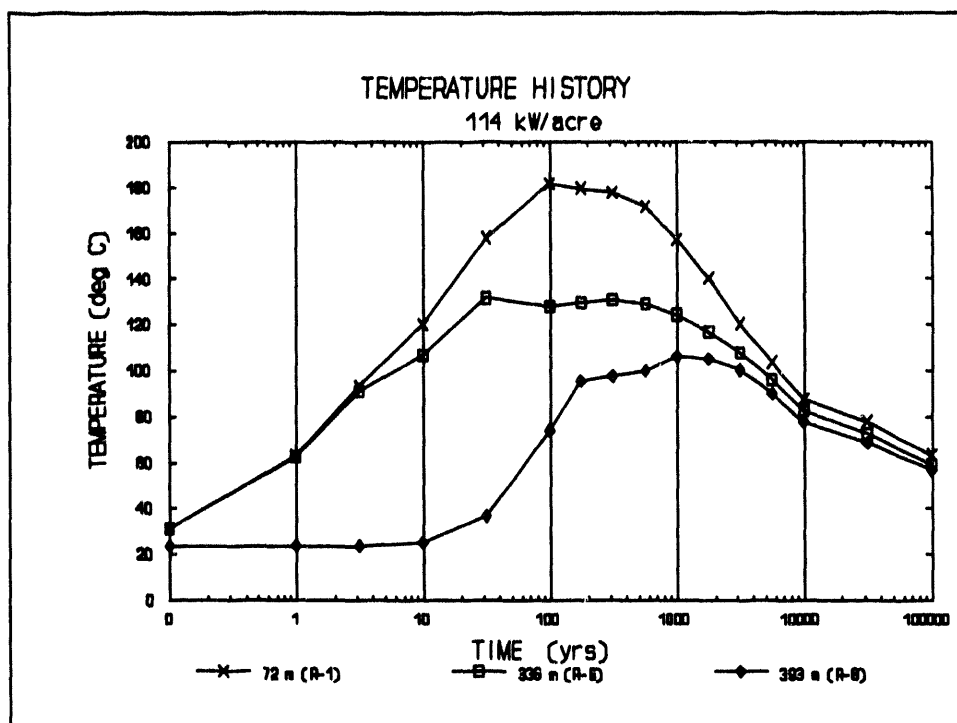


Figure A-8. Temperature and Liquid Saturation Histories at Three Spatial Locations Within the Panel for the 114 kW/Acre APD Case

**APPENDIX B**

**NEAR-FIELD THERMAL CALCULATIONS**

**Suresh Lingineni**

## INTRODUCTION

The simulation of waste package containment and release requires information about the near-field environment conditions. The Civilian Radioactive Waste Management System Managing and Operating Contractor's (M&O) current exercise for Total System Performance Assessment (TSPA) at Yucca Mountain (TSPA 1993), uses the Repository Integration Program (RIP) code (Golder Associates Inc. 1993) as the computational model. The RIP code assumes that most important near-field parameters are the moisture content and temperature conditions. The temperature conditions at the edge of each waste package (as a function of time) are explicitly included in RIP to determine the time at which waste packages rewet after a thermal period. The near-field thermal conditions are also needed as input to waste package models such as AREST (Liebostrau et al., 1987) so that temperature-dependent effects are accounted for in the containment, waste form release and coupled transport models.

Much of the performance assessment modeling at Yucca Mountain has largely focused on predicting far-field thermal conditions at ambient conditions as well as at different thermal loadings. These studies rely upon simplified models which treat the entire repository as a single, smeared heat source, and fail to provide accurate near-field thermal conditions and their dependence on the waste emplacement characteristics. A method of determining the waste package temperatures from the time history of the average repository temperature, is presented in this appendix. The average repository temperatures are obtained from a subrepository scale hydrothermal model developed by the M&O in support of TSPA 1993 (Mishra, 1993; Appendix A). The subrepository scale calculations are performed for a single emplacement panel that is defined as a rectangular area of 427 m by 937 m. For ease of computation, the rectangular panel is represented as a circular disk of equal area, which is further divided into eight concentric rings of equal cross-section area. At the repository horizon, the inner six rings are assumed to contain the heat sources, with the outer two rings taken to be unheated. The repository temperature distributions are calculated for zero net recharge under conditions of capillary-gravity equilibrium with the existing geothermal gradient.

The far-field thermal calculations for TSPA 1993 are carried out for different values of areal power densities (APD) and the resulting average repository temperatures are assumed to be independent of the waste emplacement mode (vertical borehole or horizontal in-drift), waste package spacing in the emplacement drift, waste package capacities, and sizes of the emplacement drifts or boreholes. Using these average repository temperatures as the boundary conditions for the waste package scale analysis, the near-field thermal profiles are generated as a function of waste emplacement parameters such as drift spacing, waste package spacing and the waste package capacities.

## MODEL DESCRIPTION

The following analysis describes a thermal model that has been developed to calculate the waste package temperatures as a function of time, using the average repository temperatures obtained from subrepository scale hydrothermal analysis as input. This model is applicable for in-drift emplacement mode, and it also accounts for the effects of backfilling the drift. The modeled region considered in these simulations consists of a single, infinitely long emplacement drift, surrounded by the host rock. The analysis is carried out in a one-dimensional radial coordinate system (Figure B-1). It is assumed that the average repository temperature is the temperature of the host rock at a distance of 5 m from the drift wall. Thus, the waste packages only perceive the 5-m temperatures as the surrounding environment, and are not affected by the surrounding drifts. This implies that the drift spacing cannot be considered as a direct parameter in the following analysis for near-field thermal model.

The main processes included in this model are radiation heat transport from the waste package surface to the drift wall and conductive heat transport into the host rock. Moisture effects and convective heat transport in the near field are not included in the present model. The resulting governing equation that describes the variation of host rock temperatures as a function of time, can be written as:

$$\rho_h c_{ph} \frac{\partial T_h}{\partial t} = \frac{k_h}{r} \frac{\partial}{\partial r} \left[ r \frac{\partial T_h}{\partial r} \right] \quad (\text{B-1})$$

with the following initial and boundary conditions:

$$T_h(r,0) = T_i ; \quad R_d \leq r \leq (5+R_d) \quad (\text{B-2})$$

$$\epsilon \sigma F_{12} A_{wp} (T_{wp}^4(t) - T_h^4(R_d, t)) = -k_h A_h \left( \frac{\partial T_h}{\partial r} \right)_{R_d, t} ; \quad t > 0 \quad (\text{B-3})$$

$$T_h(5+R_d, t) = T_{rep}(t) ; \quad t > 0 \quad (\text{B-4})$$

where

- $T_h(r,t)$  = Temperature distribution in the host rock at time t
- $T_{wp}(t)$  = Temperature of the waste package at time t
- $T_i$  = Initial temperature of the host rock as set by geothermal gradient
- $T_{rep}(t)$  = Average repository temperatures obtained the subrepository scale hydrothermal analysis
- $\rho_h$  = Average density of the host rock
- $c_{ph}$  = Average specific heat of the host rock
- $k_h$  = Thermal conductivity of the host rock
- $\epsilon$  = Emissivity of the waste package
- $\sigma$  = Stefan - Boltzmann constant
- $R_d$  = Drift radius
- $F_{12}$  = View factor between the waste package and the drift wall

The boundary condition given by equation (B-3) is an interfacial heat flux condition written at the drift wall corresponding to a drift without backfill. It is obtained by equating the radiative heat transfer rate from the waste package to the conductive heat transfer rate into the host rock at the drift wall location. The surface areas  $A_{wp}$  and  $A_h$  correspond to the waste package surface area and the surface area of drift wall in a unit cell as shown in Figure B-1. The second boundary condition at a radial distance of 5 m from the drift wall results from the assumption that the host rock temperature at that location is equal to the average repository temperature obtained from subrepository scale hydrothermal analysis. When the drift is backfilled, the interfacial boundary condition at the drift wall should be modified by equating the conductive heat transfer rates in the backfill and host rock, as:

$$k_b \left( \frac{\partial T_b}{\partial r} \right)_{(R,r,t)} = k_h \left( \frac{\partial T_h}{\partial r} \right)_{(R,r,t)} \quad (B-5)$$

where

- $T_b(r,t)$  = Temperature distribution in the backfill
- $k_b$  = Thermal conductivity of the backfill

Similarly, the governing equation that describes the variation of the waste package temperature with time can be written as:

$$\rho_{wp} c_{pwp} \frac{\partial T_{wp}}{\partial t} = q(t) - \epsilon \sigma (T_{wp}^4 - T_h^4(R_d, t)) \quad (B-6)$$

with the following initial condition:

$$T_{wp}(0) = T_i \quad t=0 \quad (B-7)$$

where

- $\rho_{wp}$  = Average density of the waste package
- $c_{pwp}$  = Average specific heat of the waste package
- $q(t)$  = Volumetric heat generation in the waste package

In writing equation (B-6), it is assumed that the waste package has a uniform temperature profile. However, due to the heat generation within the waste package, a parabolic temperature profile develops within the waste package, with maximum temperature at the center of the waste package. The heat generation rate ( $q(t)$ ) in the waste package as a function of time, is calculated from the thermal characteristics of the fuel (in terms of W/MTU), and the number of fuel assemblies in the waste package. The waste package temperatures calculated by the above analysis are assumed to be valid at the waste package surface and the interior temperatures of the waste package at the centerline are determined using the following method. The temperature distribution in a long, solid cylinder with uniform internal heat generation rate is given by:

$$T_{wp}(r) = \frac{q(t) r_{wp}^2}{4k_{wp}} \left[ 1 - \frac{r^2}{r_{wp}^2} \right] + T_{wp,s} \quad (B-8)$$

Thus, the centerline waste package temperature and the waste package surface temperature can be determined, which are the maximum and minimum temperatures within the waste package. A representative average value for the waste package temperature can be determined by volumetrically averaging the above temperature distribution using the following definition:

$$T_{wp,av} = 4\pi \int_0^{R_{wp}} \frac{T_{wp}(r) r dr}{V_{wp}} \quad (B-9)$$

Rock thermal characteristics were obtained for the middle Topopah Spring unit (TSw2) of the Paintbrush welded tuff from the Reference Information Base. Thermal properties of the waste form and container materials were obtained from the waste package design group (Table B-1,

Bahney and Doering, 1993). Waste packages are assumed to be loaded with ten-year out-of-core fuel with a burnup rate of 45 GWd/MTU.

## **RESULTS**

In this work, waste package temperatures are calculated for three APDs of 70.4, 141, and 282 kW/ha (28.5, 57 and 114 kW/acre). For each of these power densities, average repository temperatures of the six rings with heat sources are provided as input from the subrepository scale analysis. These average repository temperatures in the six rings as a function of time after waste emplacement are shown in Figures B-2 to B-4. It can be seen from these data that the average repository temperatures increase to a peak value in the initial period of 100 years and begin to decrease in the following periods. For a given areal power density, the highest repository temperatures are observed in Ring 1 and temperatures are found to reduce in the subsequent outer rings.

The near-field temperature conditions are determined using the analysis described in the previous section for various average repository temperature histories. For a given repository temperature history, the very near-field (waste package or drift scale) thermal conditions are dependent upon the choice of drift diameter, waste package spacing, waste package geometry, and the number of fuel assemblies placed in the waste package. The effect of each of these parameters on the near-field thermal conditions is discussed in this section. Figures B-5 to B-10 show the near-field temperatures as a function of time after waste emplacement. The plots are provided for the three APDs considered in this work, and for rings with the highest and lowest temperature histories. The results are obtained for a drift diameter of 7 m (23 ft), waste package spacing of 8 m, and 21 PWR fuel assemblies placed in the waste package. Each plot shows temporal variation of the drift wall temperature, waste package centerline temperature, waste package surface temperature and the volume averaged waste package temperature.

The following observations can be made from the data presented in Figures B-5 to B-10. Temperatures of the waste packages increase steadily following the waste emplacement and peak temperatures are observed within the first 10 years. The difference between the waste package temperatures and the repository temperatures is the greatest at the initial time and decreases steadily with time. This can be attributed to the heat generation profiles of the emplaced waste (i.e., heat generation rate is the highest at the time of emplacement which would require a maximum temperature gradient between the waste package and the surrounding host rock in order to dissipate the heat). Thus, the excess heat generated within the package that cannot be transferred into the host rock will increase the waste package temperature. As the heat generated in the waste package decreases with time, smaller temperature gradients are sufficient to transfer heat and the waste package temperatures begin to reduce. It can be noted that the time at which

peak repository temperature occurs may not coincide with the time of peak waste package temperature. Typically, waste package temperatures peak much earlier than repository temperatures and the difference between these temperatures diminishes to less than 50°C within 100 years after waste emplacement. As the APD increases, the peak waste package temperature increases and the time taken to reach this peak value also increases.

The results presented in Figures B-5 to B-10 correspond to the case of in-drift emplacement mode with no backfill, where radiation heat transfer is the predominant mode of heat transport between the waste package and the host rock boundary. The effect of backfilling the drift after waste emplacement, on the near-field thermal conditions, can be seen in Figures B-11 to B-14. The results in these figures are shown for Rings 1 and 6, and for two APDs of 70.4 and 282 kW/ha (28.5 and 114 kW/acre). The backfill material is assumed to be noncompacted crushed tuff. The porosity of this backfill is assumed to be 60 percent. The presence of backfill in the drift has the following effects on the near-field thermal conditions. The temperatures of waste packages placed in a backfilled drift are much higher than the corresponding case with no backfill. This is due to the fact that larger thermal gradients are required to transfer the heat through the backfill where conductive heat transfer is the predominant heat transport mode. Peak waste package temperatures occur at earlier time levels when the drift is backfilled, and the difference between waste package temperature and the repository temperature reduces to less than 50°C about 1,000 years after waste emplacement.

The sensitivity of the near-field thermal conditions to the waste emplacement parameters such as drift diameter and waste package spacing has also been analyzed using the present thermal model. The results are presented for the case in which maximum repository temperatures are observed (i.e., for an APD of 282 kW/ha (114 kW/acre and for Ring 1. Three drift diameters of 7 m (23 ft), 5.5 m (18 ft), and 4.6 m (15 ft) are chosen for sensitivity analysis. The number of fuel assemblies in the waste package is taken to be 21 and the waste package spacing of 8 m is chosen. Results of time variation in waste package temperatures as a function of drift diameter, with and without backfill, are shown in Figures B-15 and B-16. It is interesting to note that increasing drift diameters have opposite effects on the near-field thermal conditions depending on whether the drift is backfilled or not. In the absence of backfill, increasing drift diameters tend to reduce the waste package temperatures. With increasing drift diameter higher surface areas are available for radiation heat transfer from the waste package as well as for conduction heat transport into the host rock and lesser thermal gradients are created in the near field. However, when the drift is backfilled, the most significant resistance to the heat transport from the waste package is due to the conduction through the backfill. When the drift diameter is increased, the effective distance through which conduction has to take place in the backfill increases, thus giving rise to higher waste package temperatures. Also, the sensitivity of the near-field temperatures to the drift diameter is greater in the case of backfilled drifts.

The effect of waste package spacing on the waste package temperatures is shown in Figures B-17 and B-18, in which three waste package spacings of 5 m, 8 m and 10 m are considered. These results correspond to a drift diameter of 7 m (23 ft) and 21 fuel assemblies are assumed in the waste package. Increasing the waste package spacing results in lower waste package temperatures independent of the presence of backfill. Higher waste package spacing results in increased surface area of the drift wall through which heat can be conducted into the host rock, within each unit cell. Waste package temperatures are found to be more sensitive to waste package spacing when the drift is backfilled.

## **SUMMARY**

A thermal model is presented to determine the near-field temperatures using the average repository temperatures obtained from a subrepository scale hydrothermal model. The effects of waste emplacement characteristics such as drift diameter, waste package spacing, number of fuel assemblies and the backfill are incorporated into this model. Waste package temperatures are calculated for three different APDs and for various waste emplacement configurations. The results indicated that significant difference can exist between the waste package temperature and average repository temperature within the initial period of 100 years. When the drift is backfilled, the observed waste package temperatures are much higher, and they differ considerably from the repository temperature for as long as 1,000 years. The time at which a peak in the waste package temperature occurs does not coincide with the peak repository temperature.

The near-field thermal conditions are found to be more sensitive to the waste package spacing and drift diameter in the cases where the drifts are backfilled. Increasing the drift diameter is found to produce opposite effects on the near-field thermal conditions, depending on whether the drifts are backfilled or not.

## **REFERENCES**

- Bahney R. H., and T. W. Doering, 1993. "Waste Package Inputs to Systems Studies," Interoffice Correspondence, April 1, 1993, Las Vegas, NV.
- Golder Associates Inc., 1993. Application of RIP (Repository Integration Program) to the Proposed Repository at Yucca Mountain: Conceptual Model and Input Data Set, 923-1171, Redmond, WA.
- Liebetrau, A. M., M. J. Apted, D. W. Engel, M. K. Altenhofen, D. M. Strachan, C. R. Reid, C. F. Windisch, R. L. Erikson, and K. I. Johnson, 1987. The Analytical Repository Source-Term (AREST) Model: Description and Documentation, PNL-6346, Pacific Northwest Laboratory, Richland, WA.

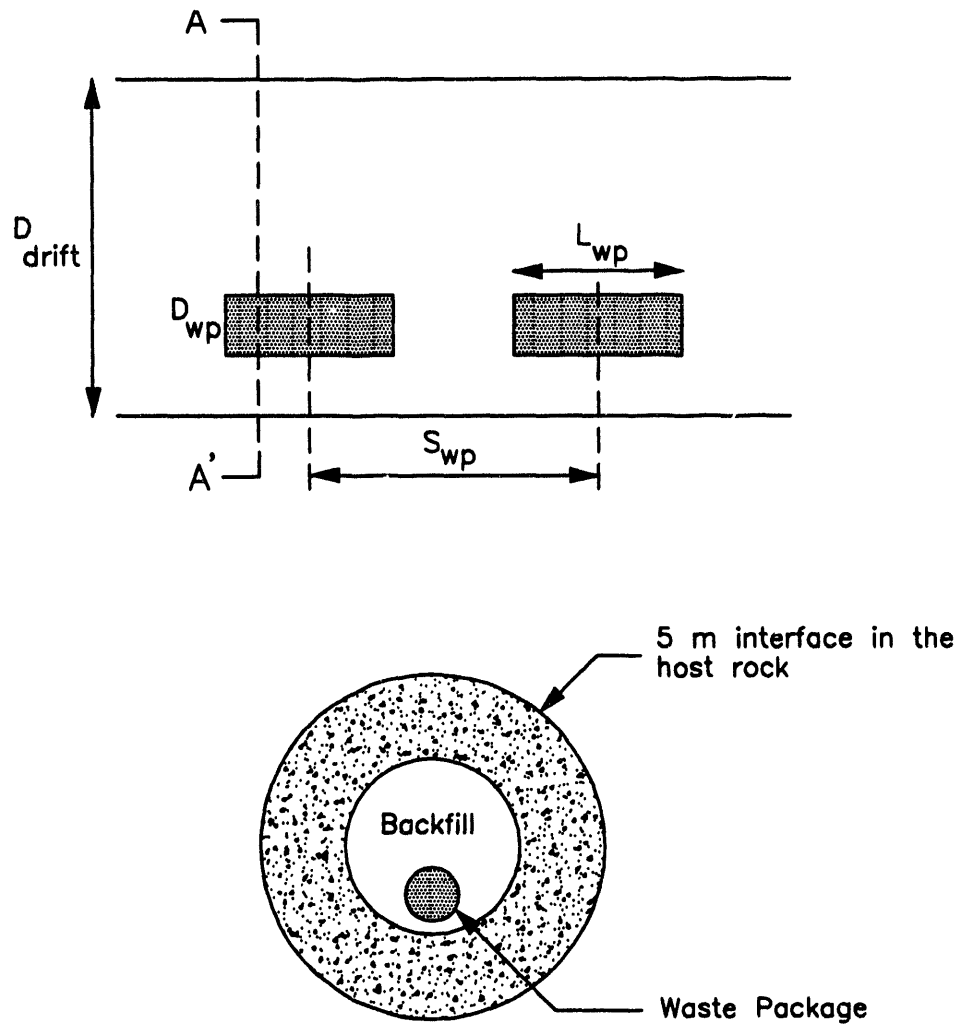


Figure B-1. Schematic of the Waste Packages Inside the Drift and Cross-sectional View of the Waste Packages

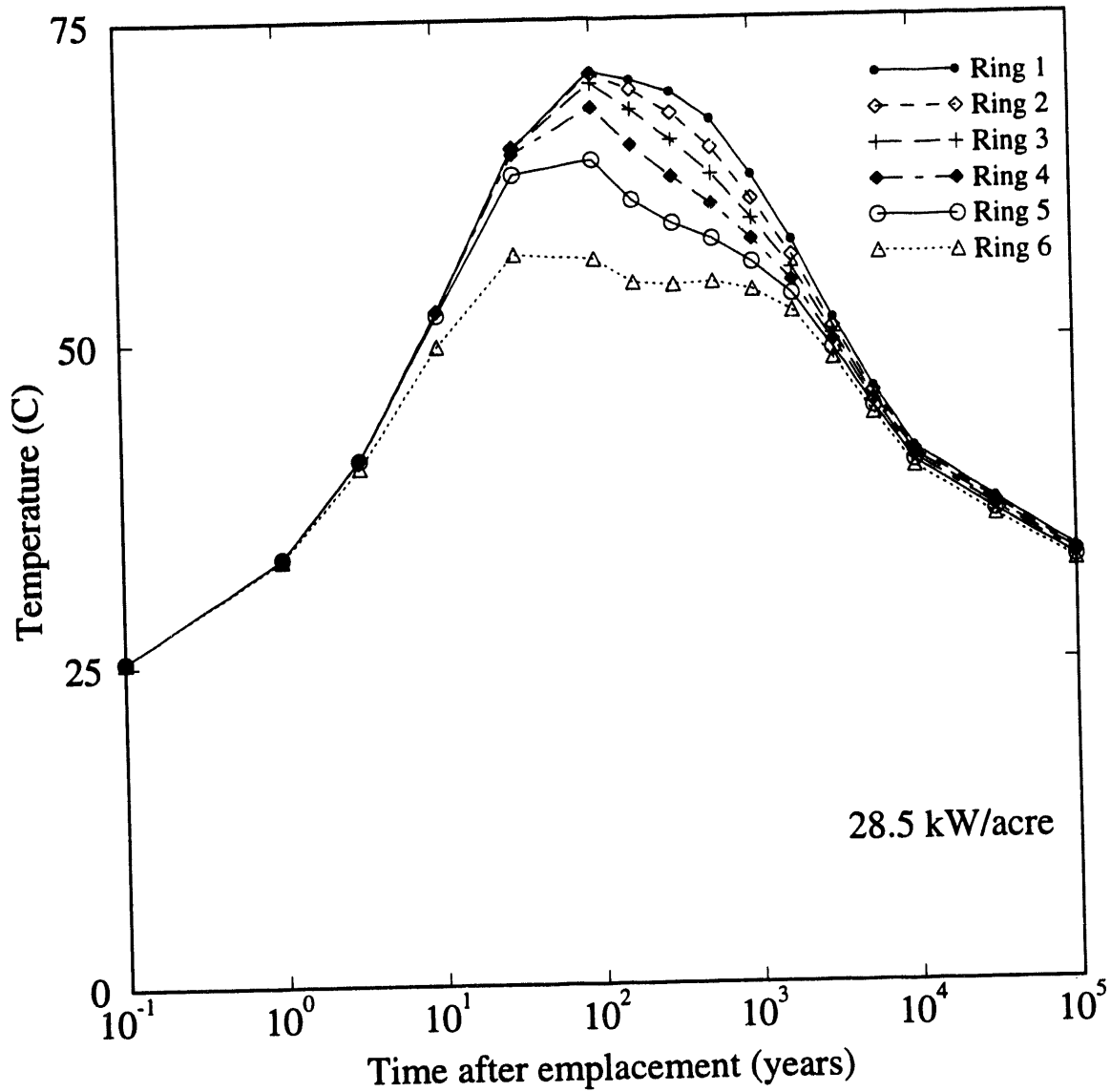


Figure B-2. Average Repository Temperatures as a Function of Time  
(After Mishra, 1993; Appendix A)

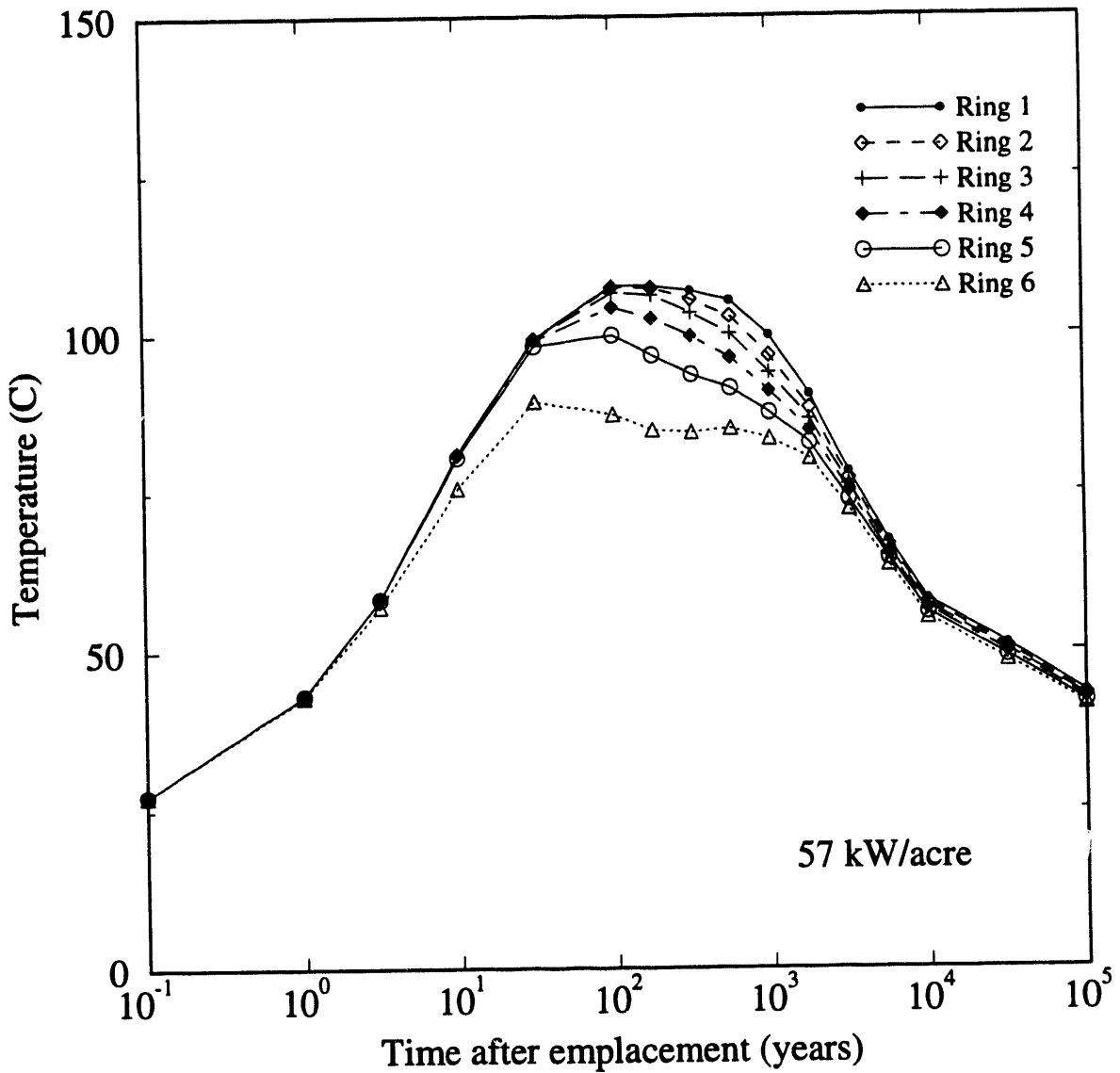


Figure B-3. Average Repository Temperatures as a Function of Time  
(After Mishra, 1993; Appendix A)

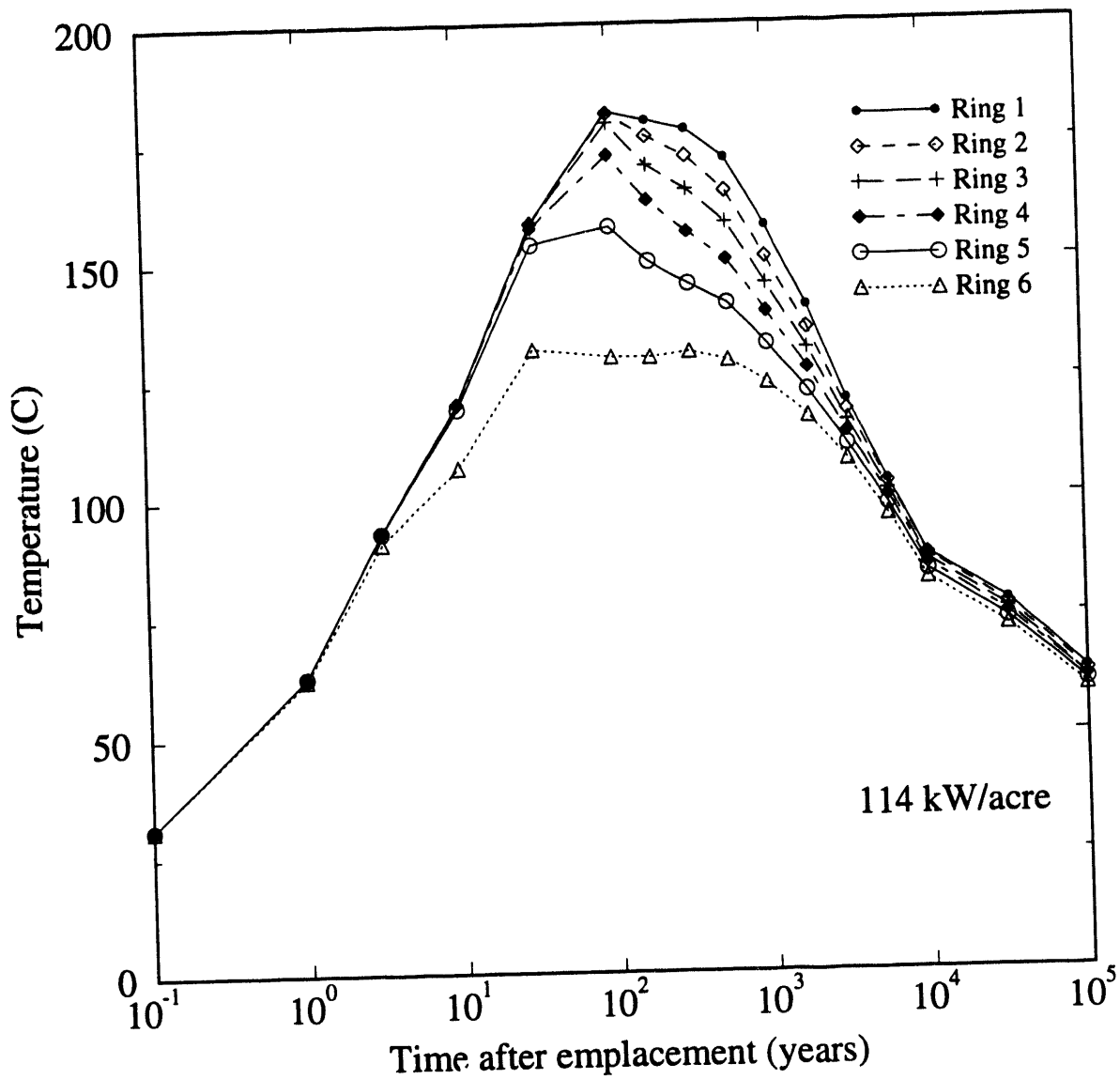


Figure B-4. Average Repository Temperatures as a Function of Time (After Mishra, 1993; Appendix A)

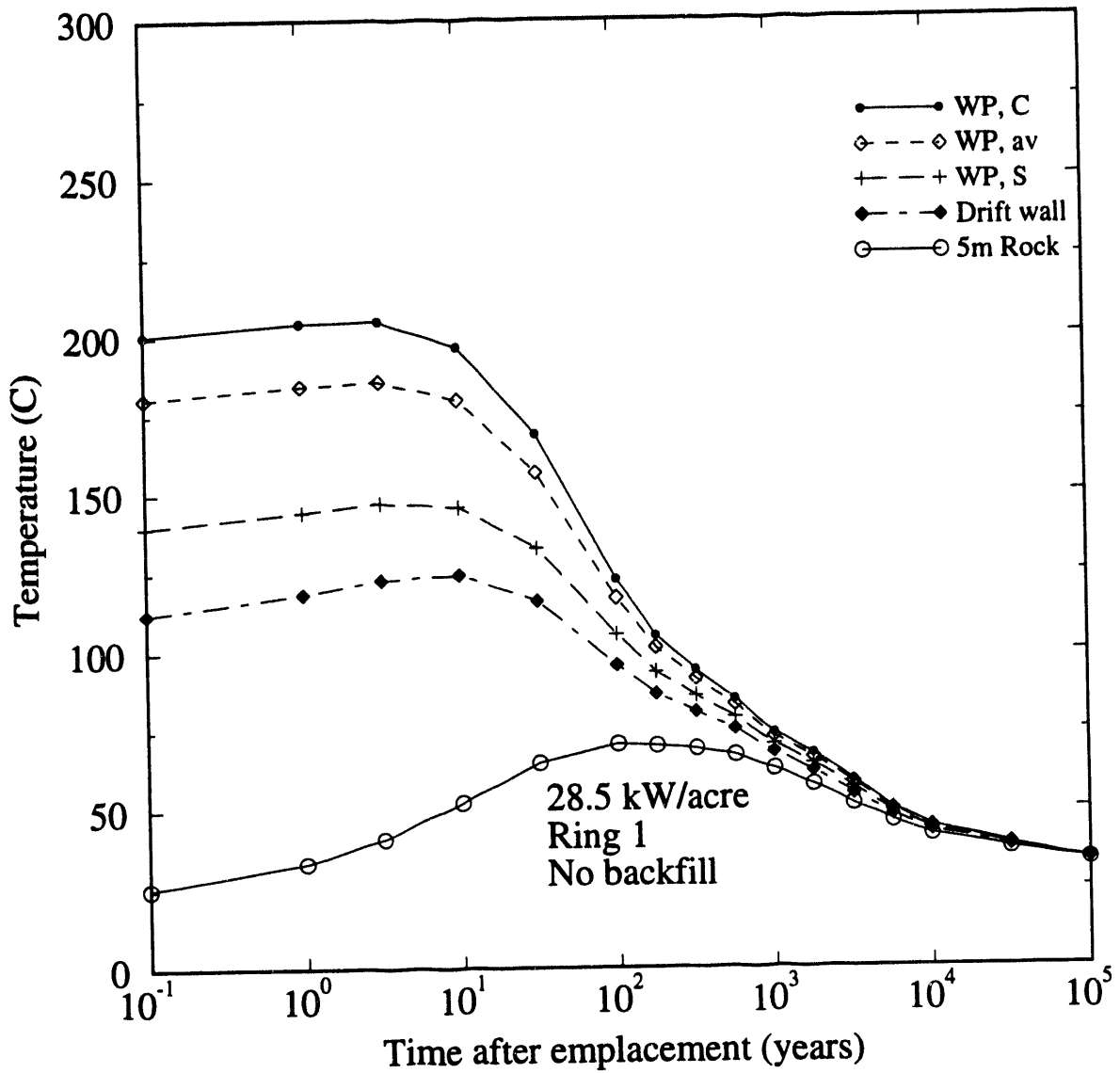


Figure B-5. Temperatures in the Near Field as a Function of Time  
 (21 PWR assemblies per package, 7 m drift diameter, 8 m waste package spacing)  
 (C = center; av = average; S = surface)

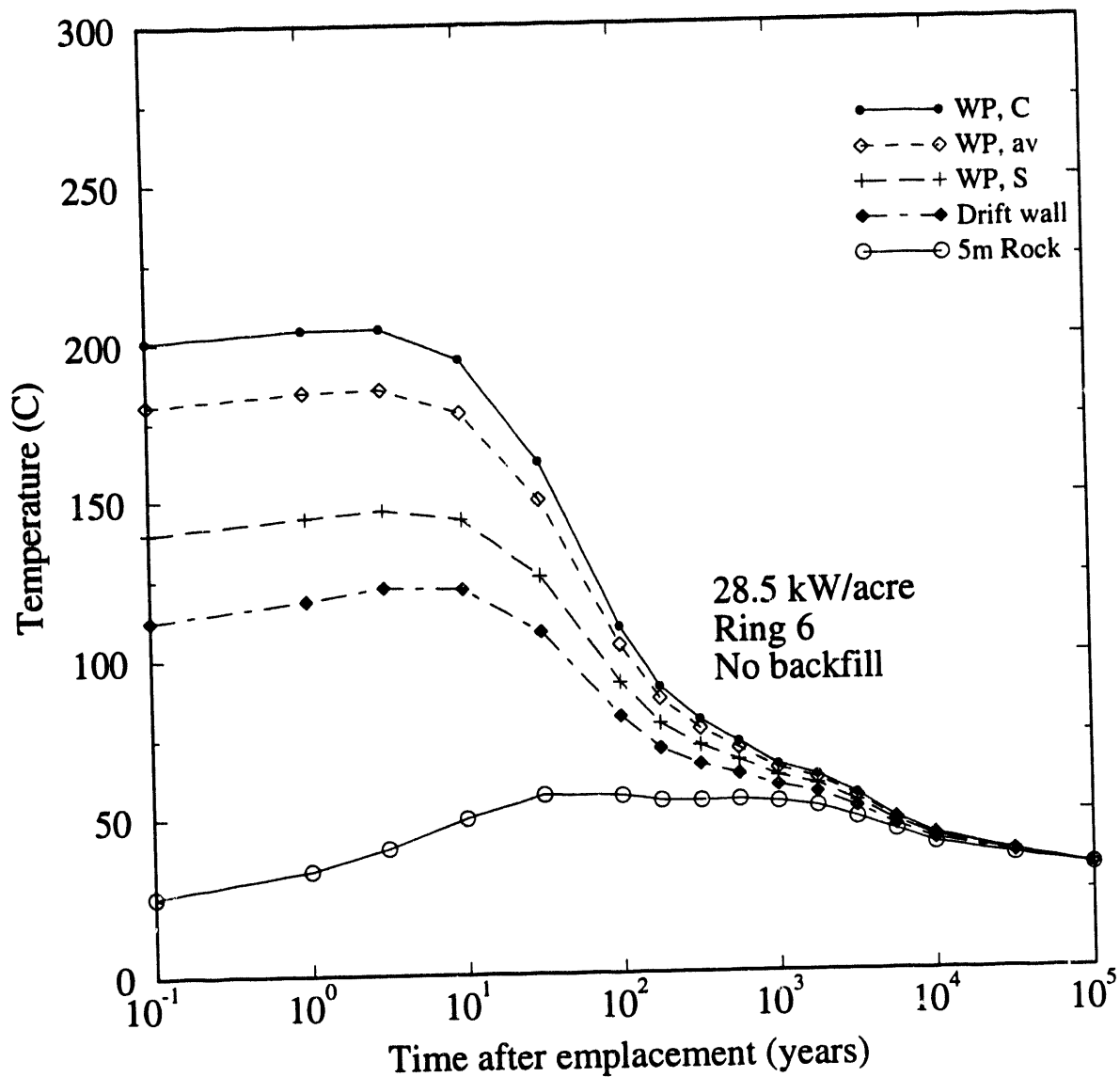


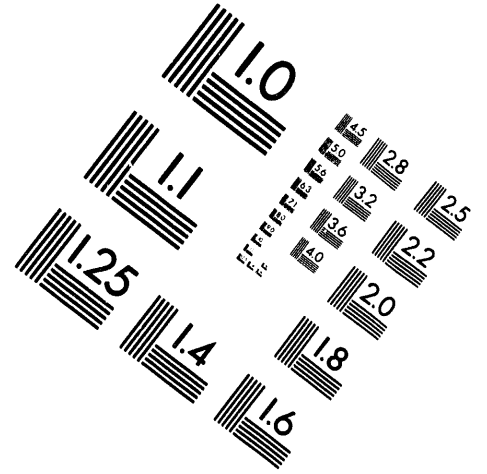
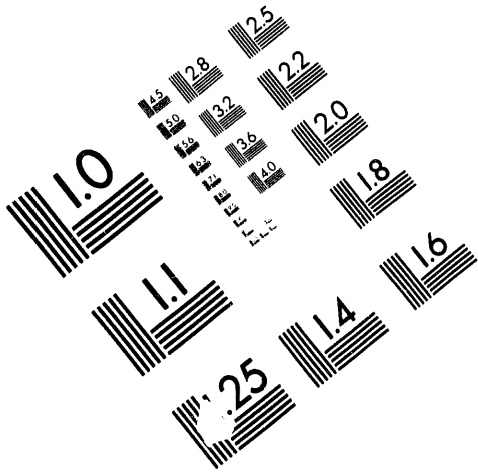
Figure B-6. Temperatures in the Near Field as a Function of Time  
 (21 PWR assemblies per package, 7 m drift diameter, 8 m waste package spacing)  
 (C = center; av = average; S = surface)



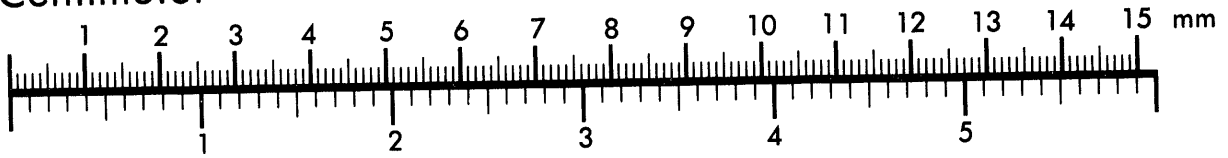
**AIM**

**Association for Information and Image Management**

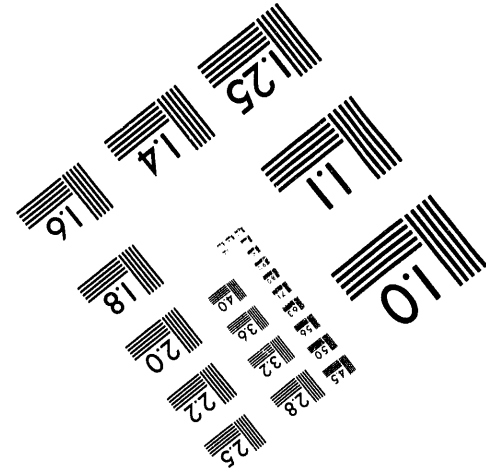
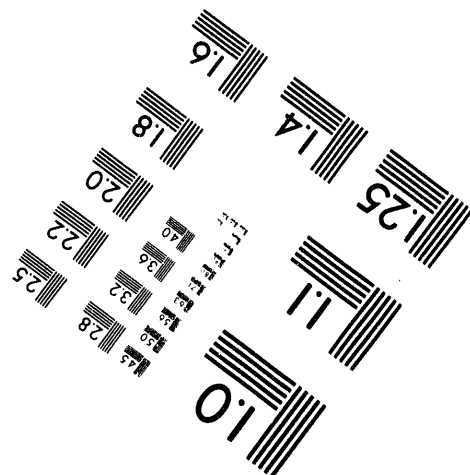
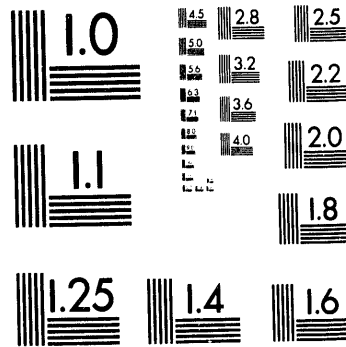
1100 Wayne Avenue, Suite 1100  
Silver Spring, Maryland 20910  
301/587-8202



Centimeter



Inches



MANUFACTURED TO AIM STANDARDS  
BY APPLIED IMAGE, INC.

**4 of 5**

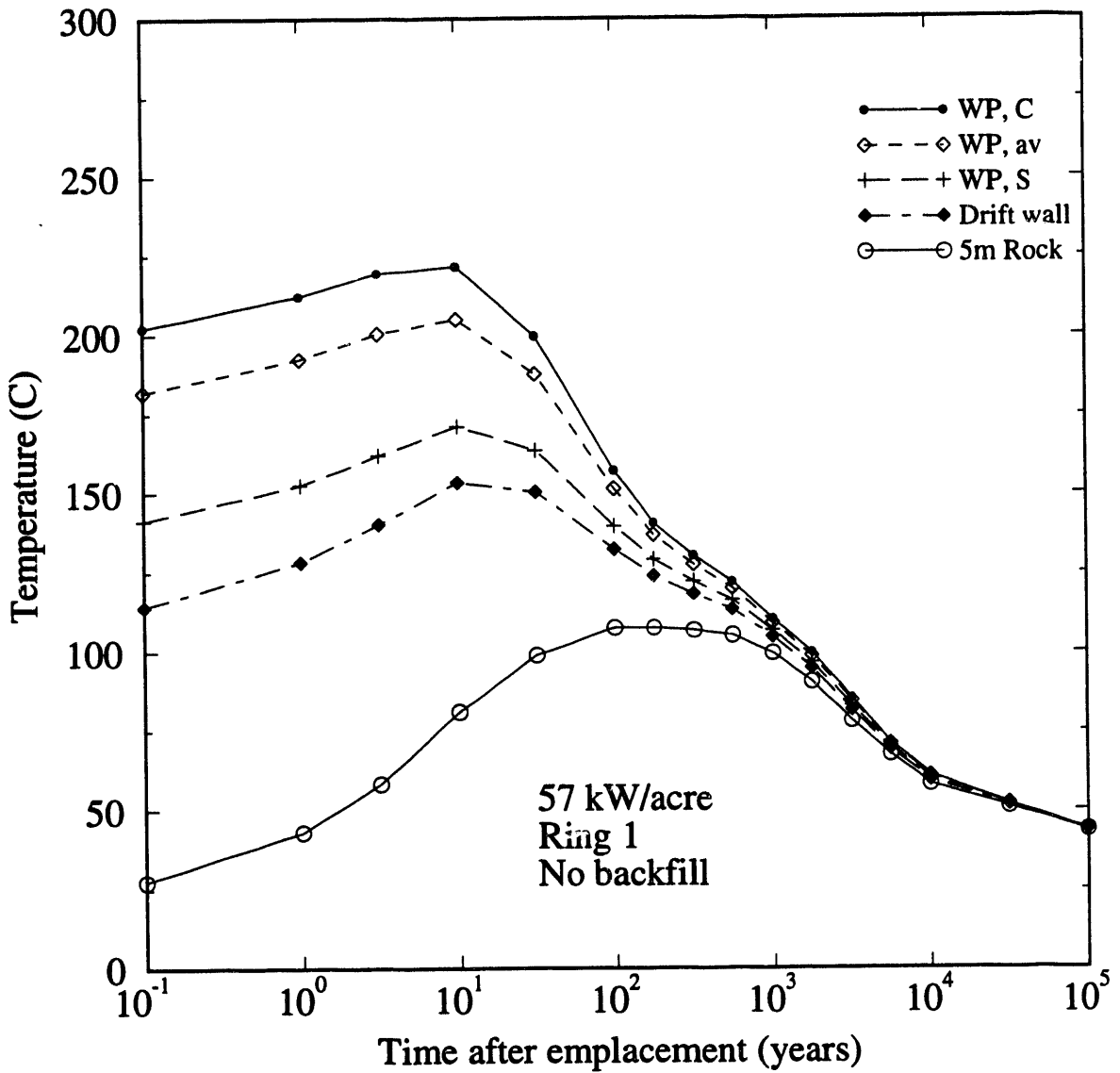


Figure B-7. Temperatures in the Near Field as a Function of Time  
 (21 PWR assemblies per package, 7 m drift diameter, 8 m waste package spacing)  
 (C = center; av = average; S = surface)

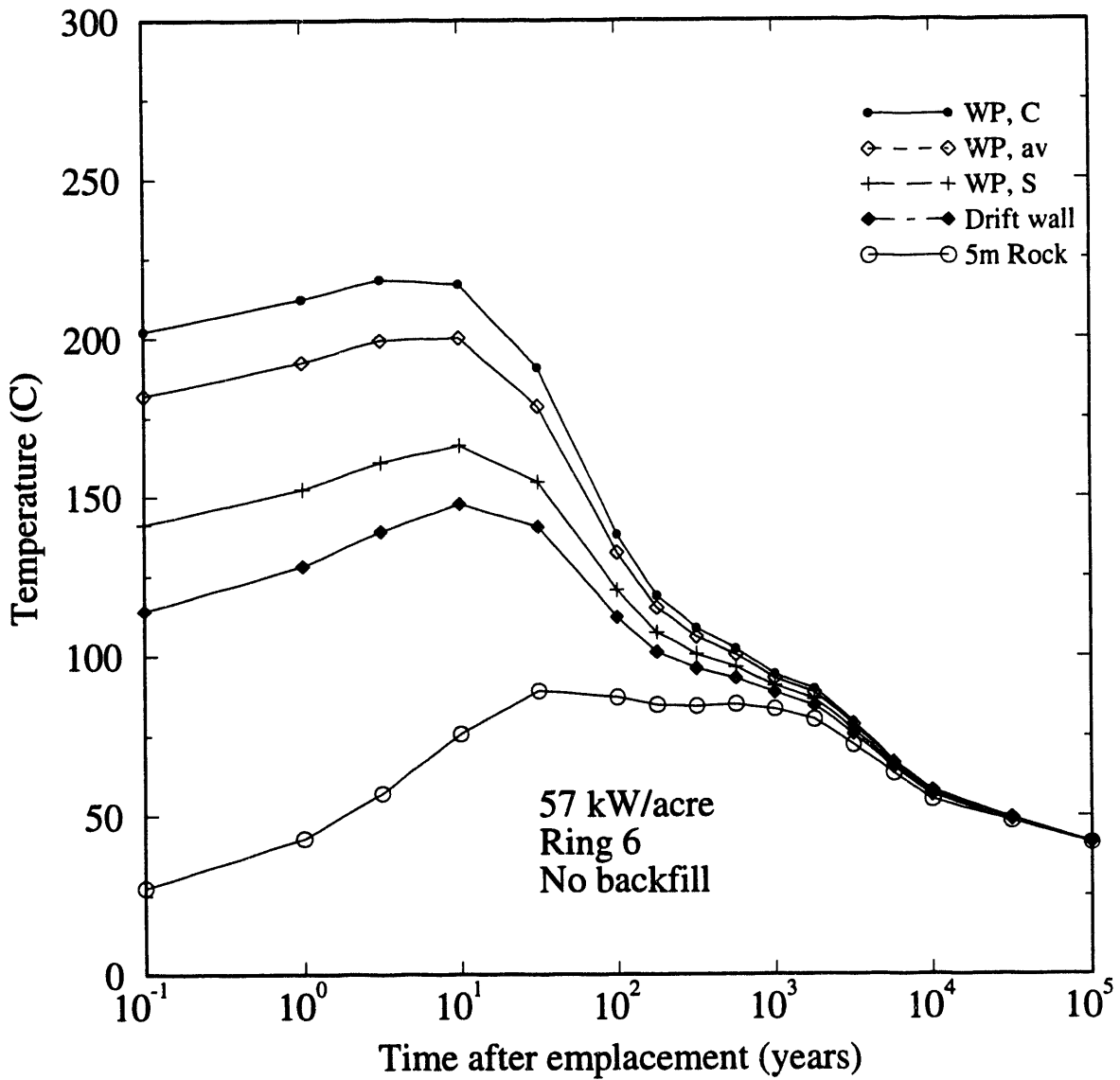
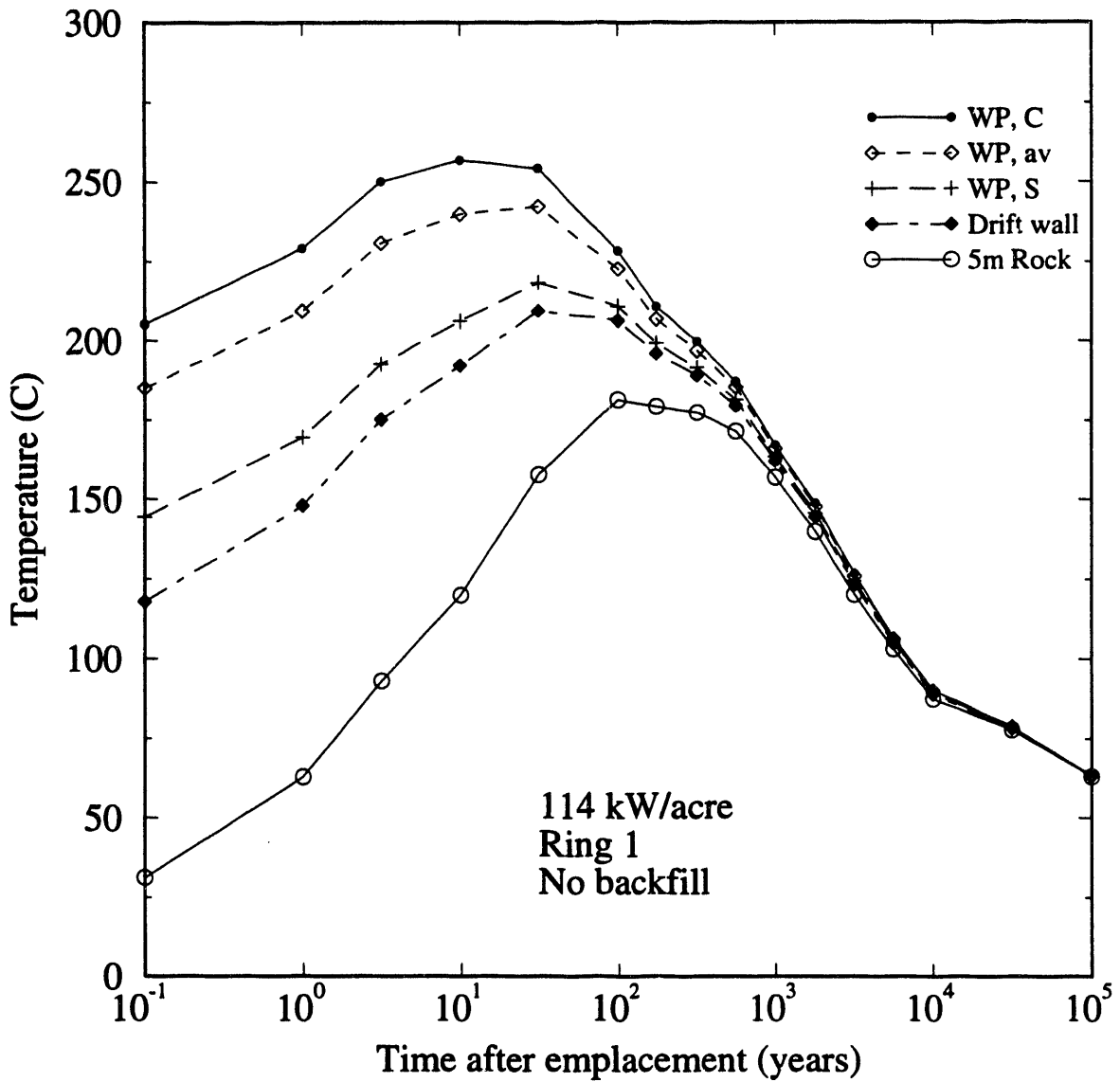


Figure B-8. Temperatures in the Near Field as a Function of Time  
 (21 PWR assemblies per package, 7 m drift diameter, 8 m waste package spacing)  
 (C = center; av = average; S = surface)



**Figure B-9. Temperatures in the Near Field as a Function of Time**  
 (21 PWR assemblies per package, 7 m drift diameter, 8 m waste package spacing)  
 (C = center; av = average; S = surface)

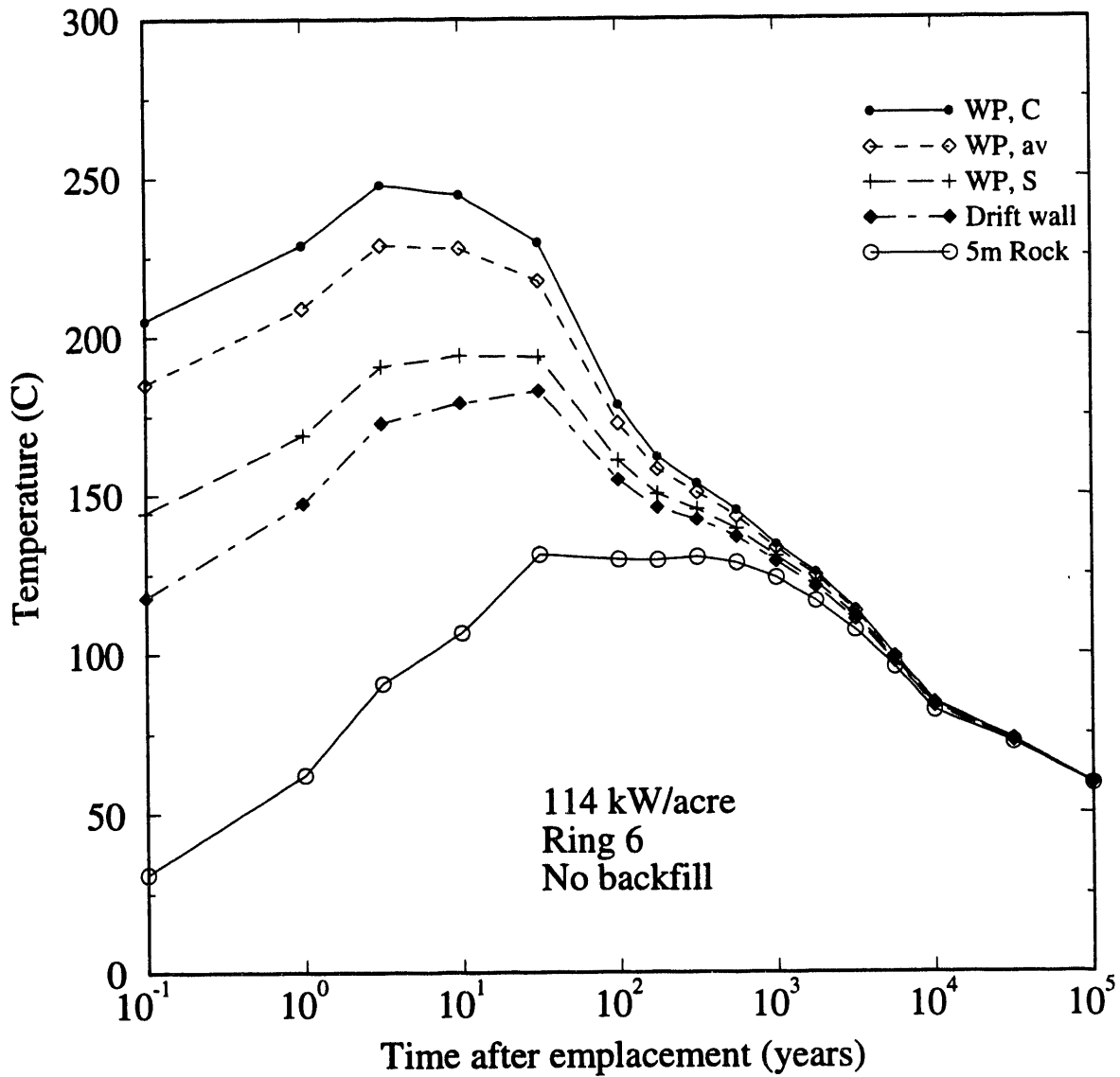


Figure B-10. Temperatures in the Near Field as a Function of Time  
 (21 PWR assemblies per package, 7 m drift diameter, 8 m waste package spacing)  
 (C = center; av = average; S = surface)

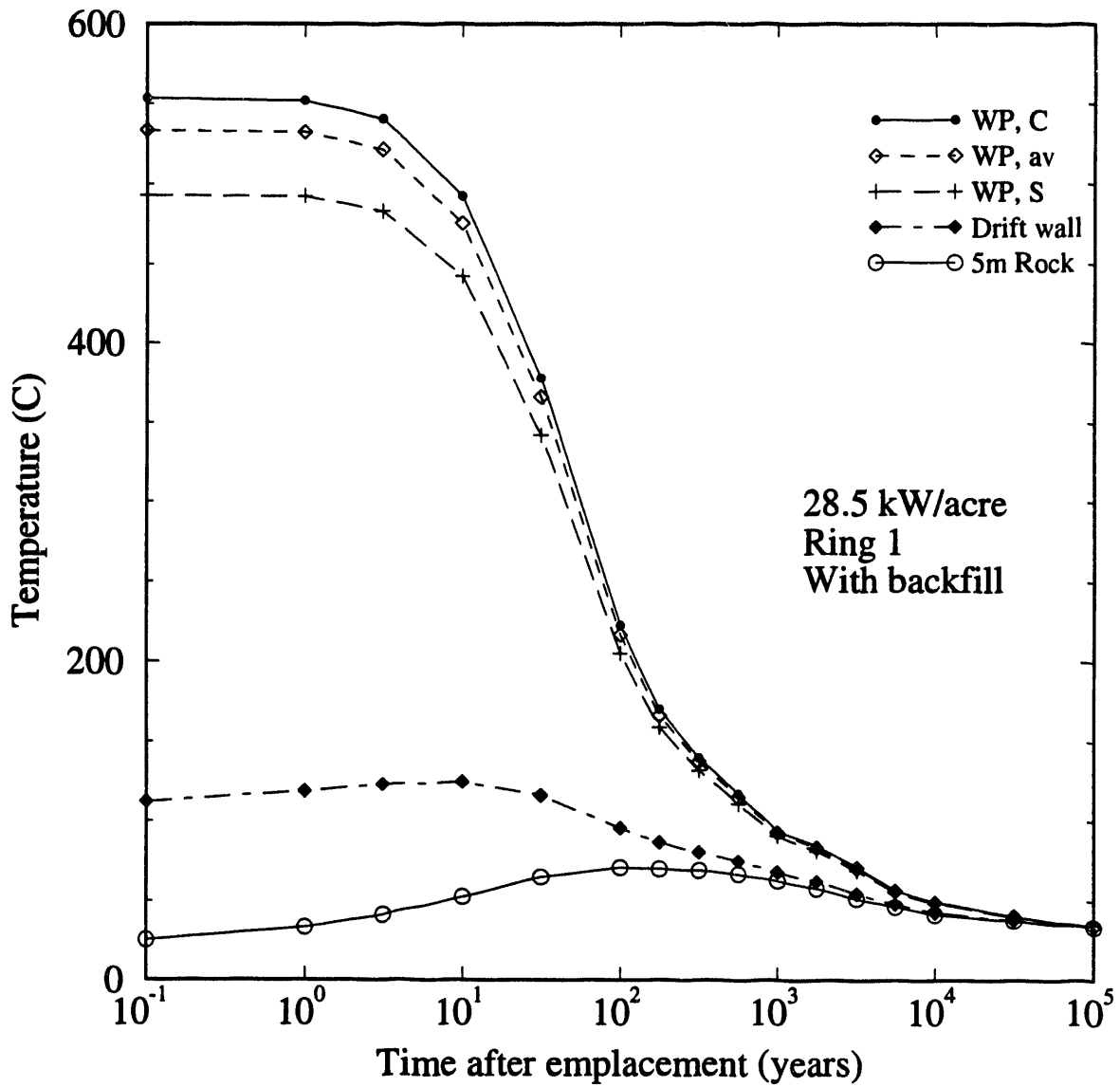


Figure B-11. Temperatures in the Near Field as a Function of Time  
 (21 PWR assemblies per package, 7 m drift diameter, 8 m waste package spacing)  
 (C = center; av = average; S = surface)

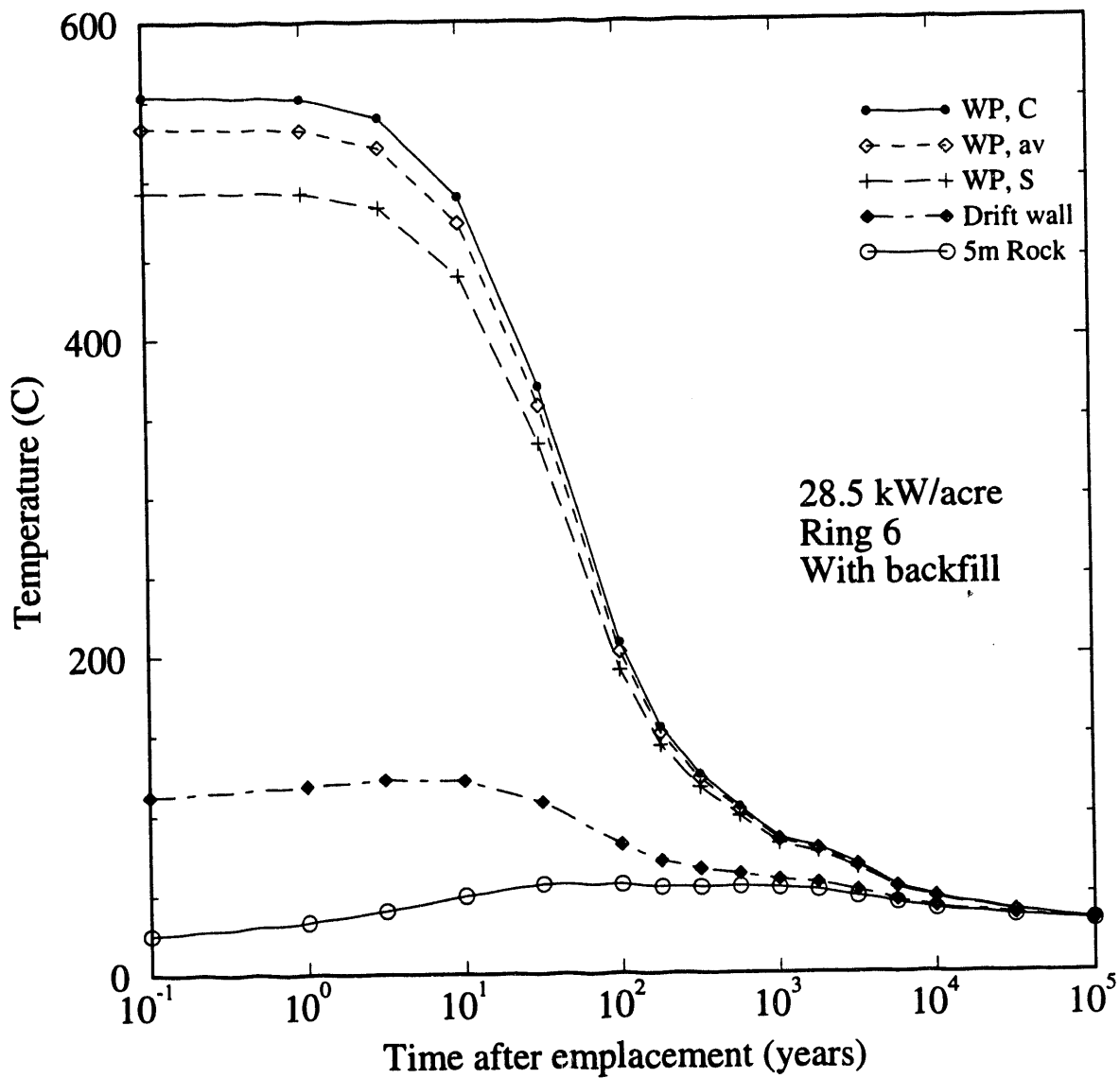
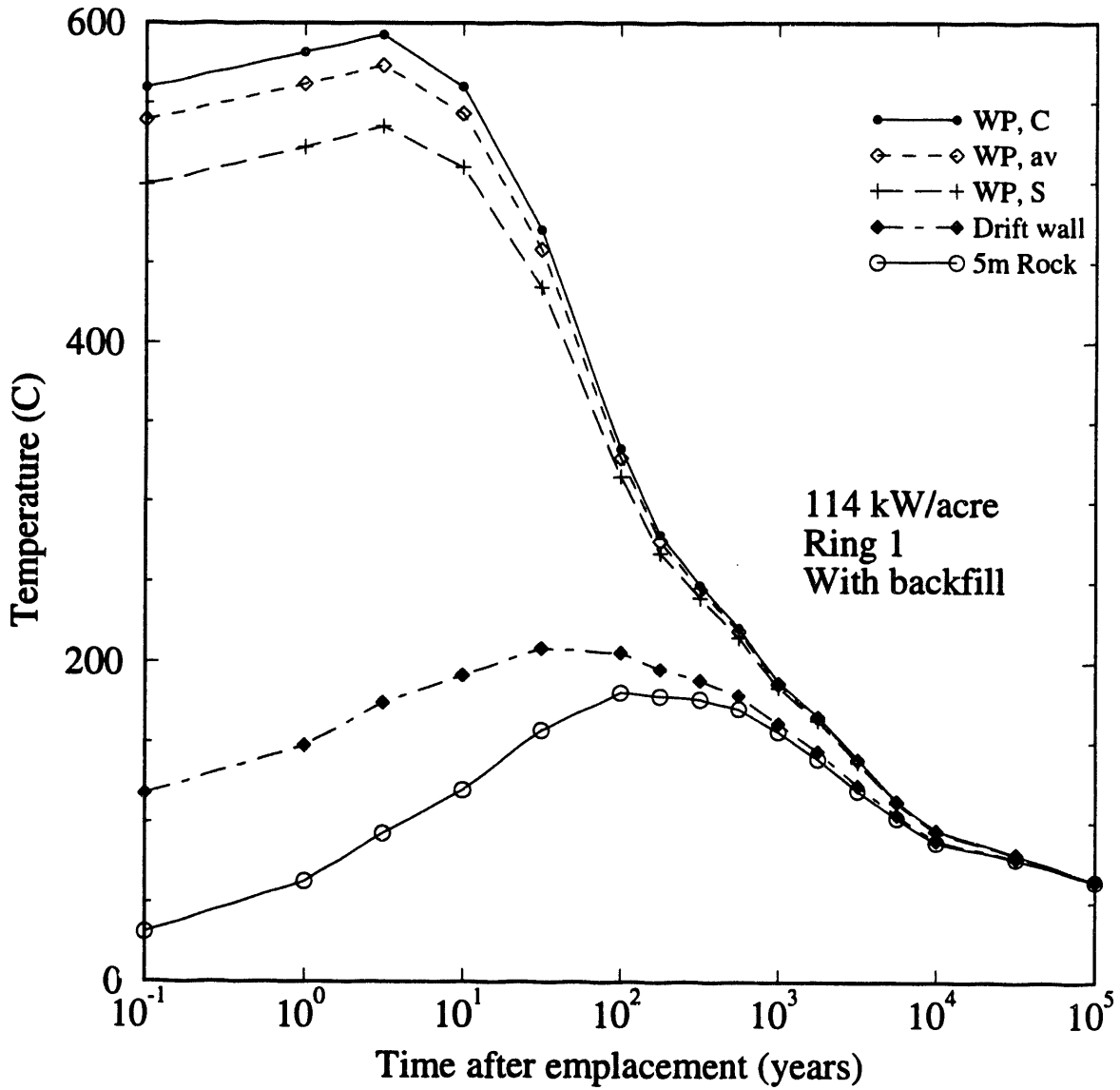


Figure B-12. Temperatures in the Near Field as a Function of Time  
 (21 PWR assemblies per package, 7 m drift diameter, 8 m waste package spacing)  
 (C = center; av = average; S = surface)



**Figure B-13. Temperatures in the Near Field as a Function of Time**  
 (21 PWR assemblies per package, 7 m drift diameter, 8 m waste package spacing)  
 (C = center; av = average; S = surface)

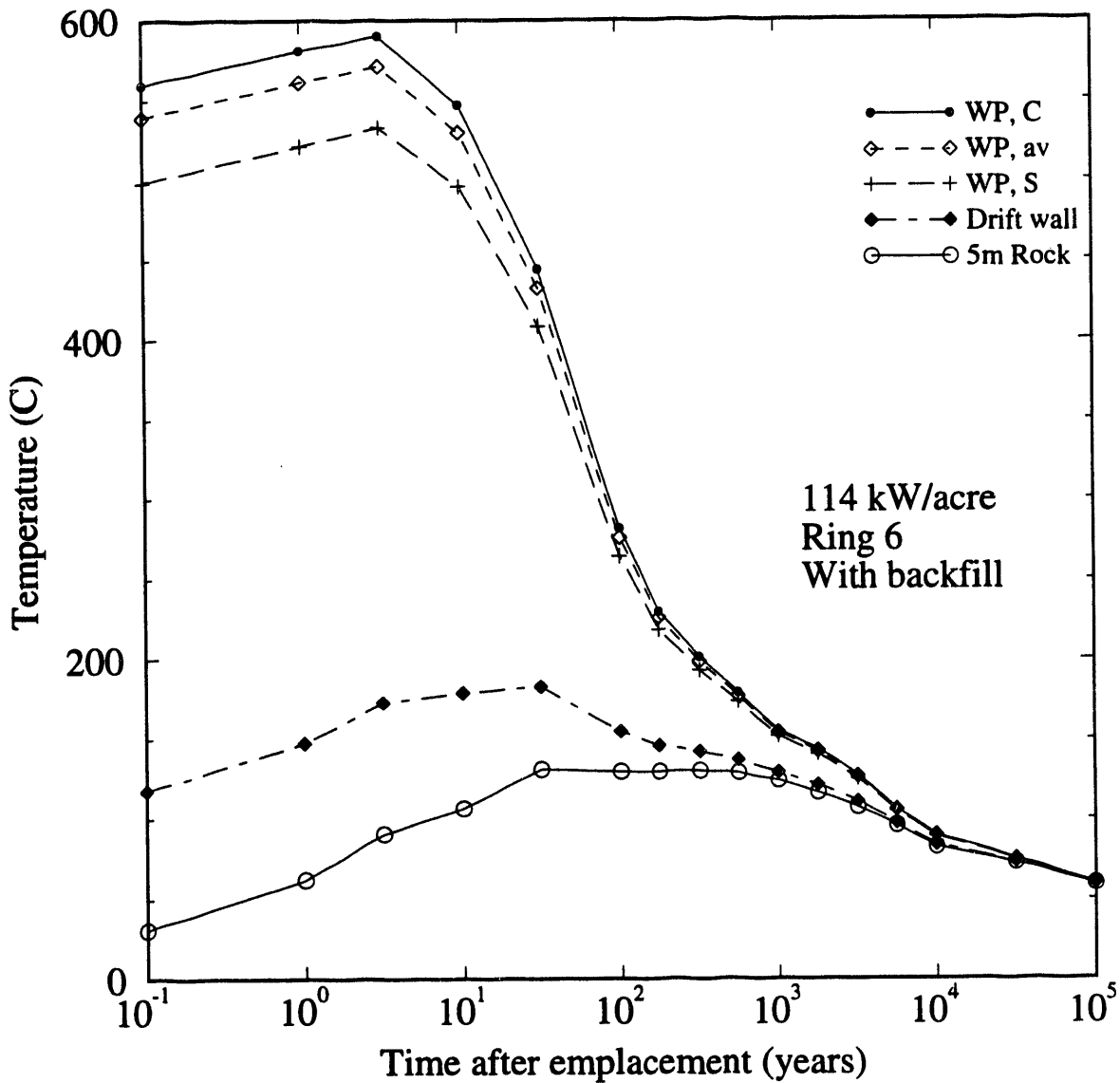


Figure B-14. Temperatures in the Near Field as a Function of Time  
 (21 PWR assemblies per package, 7 m drift diameter, 8 m waste package spacing)  
 (C = center; av = average; S = surface)

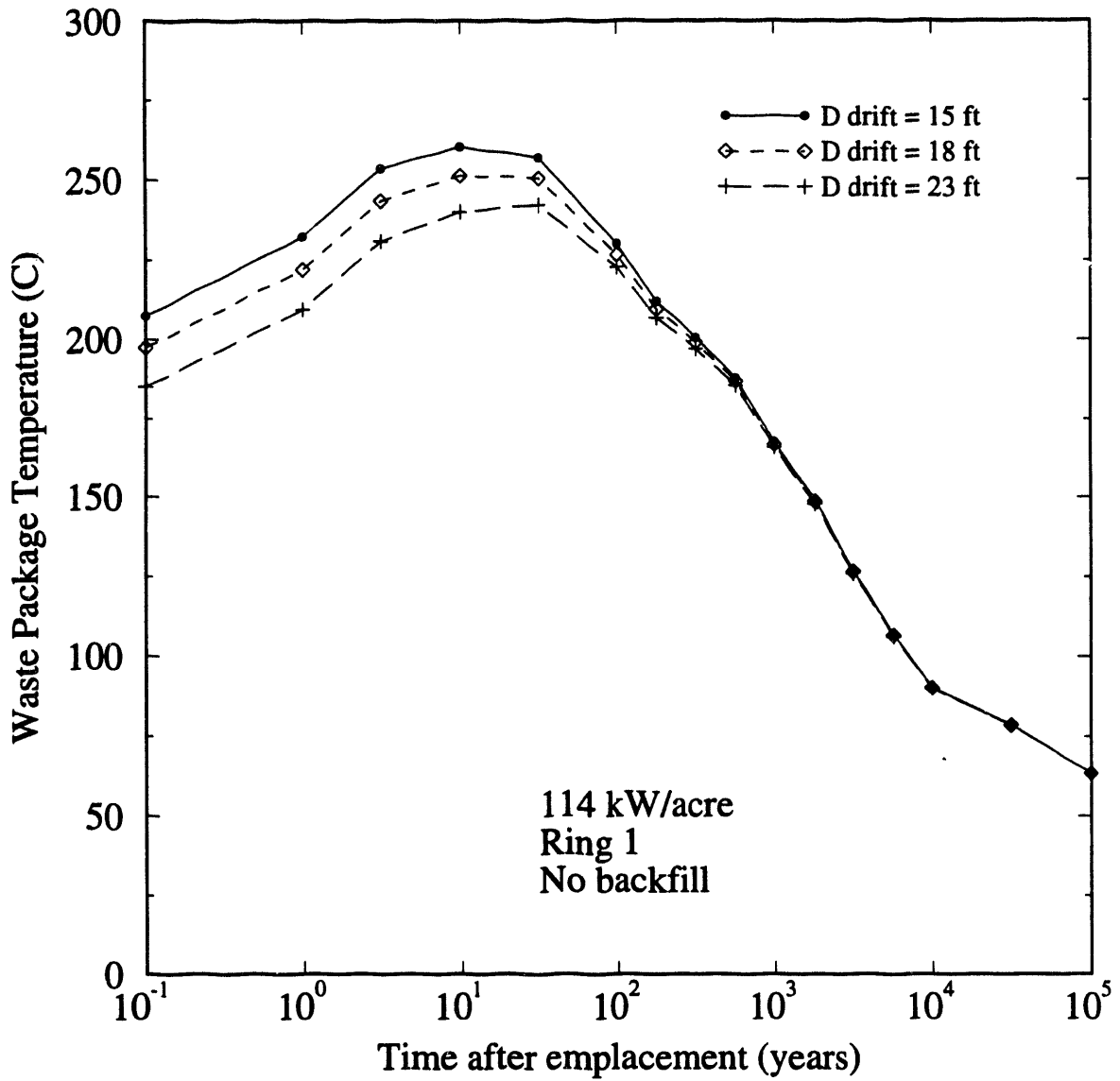


Figure B-15. Sensitivity of Average Waste Package Temperatures to the Drift Diameter  
(21 PWR assemblies per package, 8 m waste package spacing)

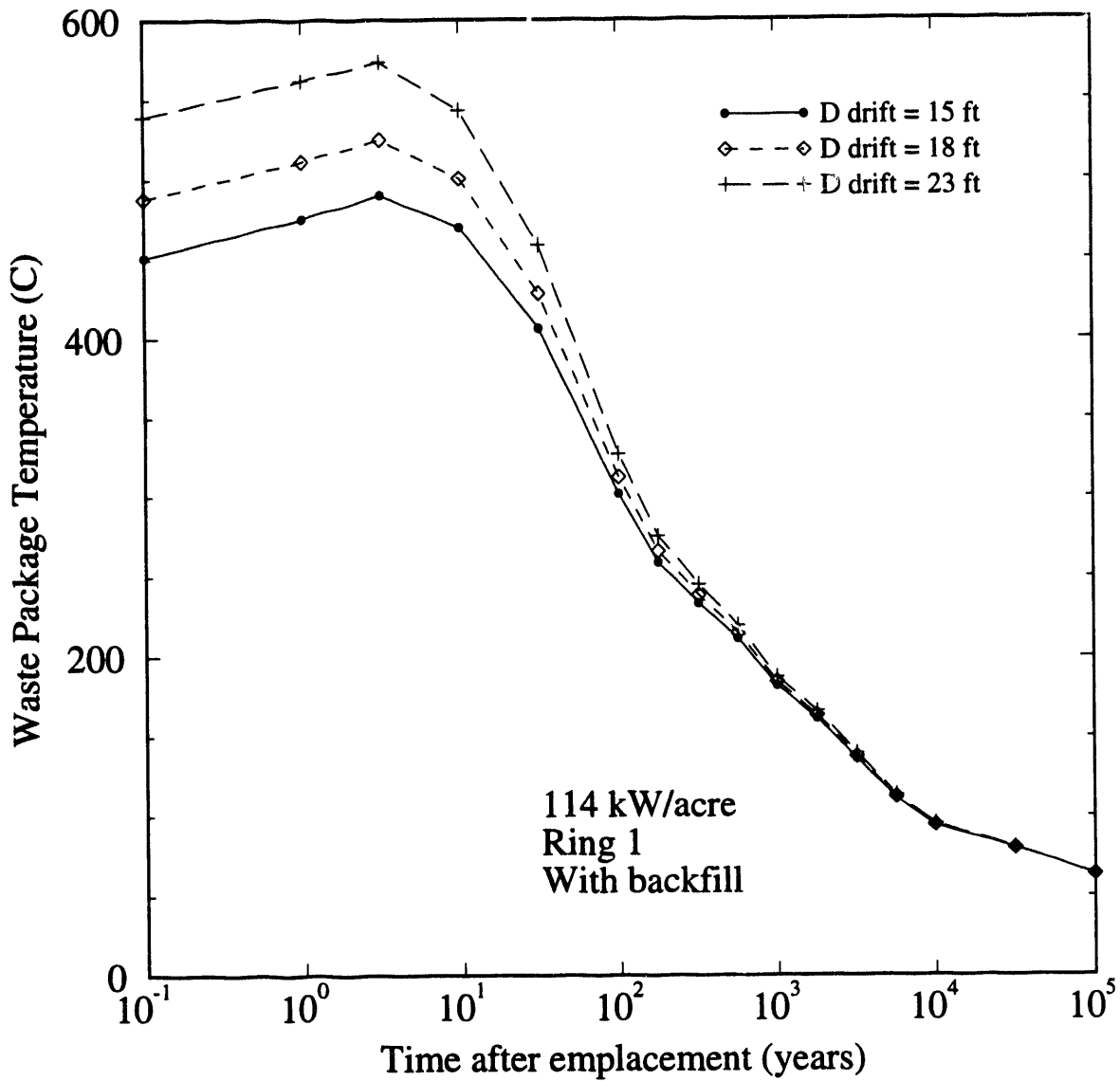
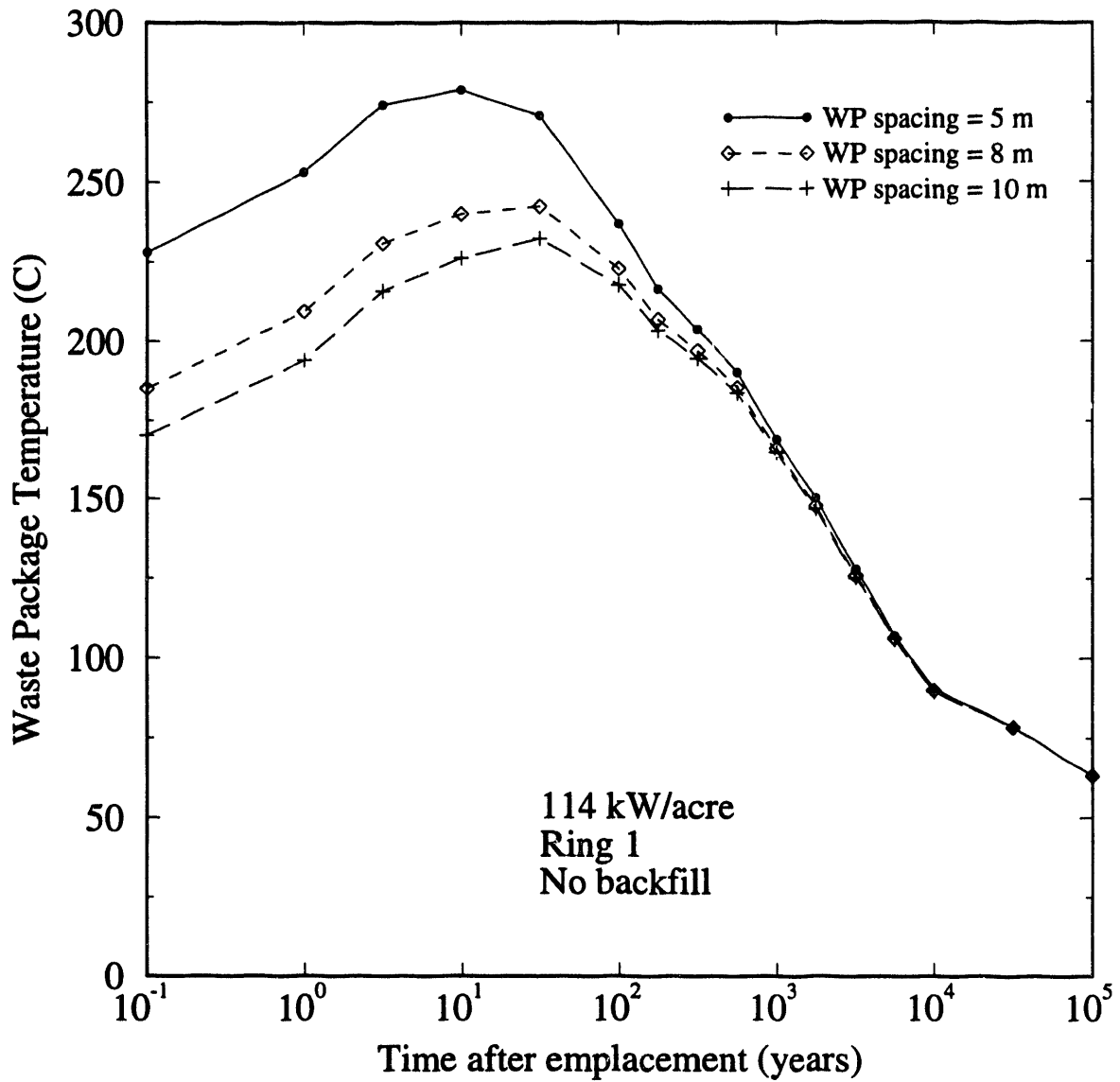


Figure B-16. Sensitivity of Average Waste Package Temperatures to the Drift Diameter  
(21 PWR assemblies per package, 8 m waste package spacing)



**Figure B-17. Sensitivity of Average Waste Package Temperatures to the Waste Package Spacing**  
(21 PWR assemblies per package, 7 m drift diameter)

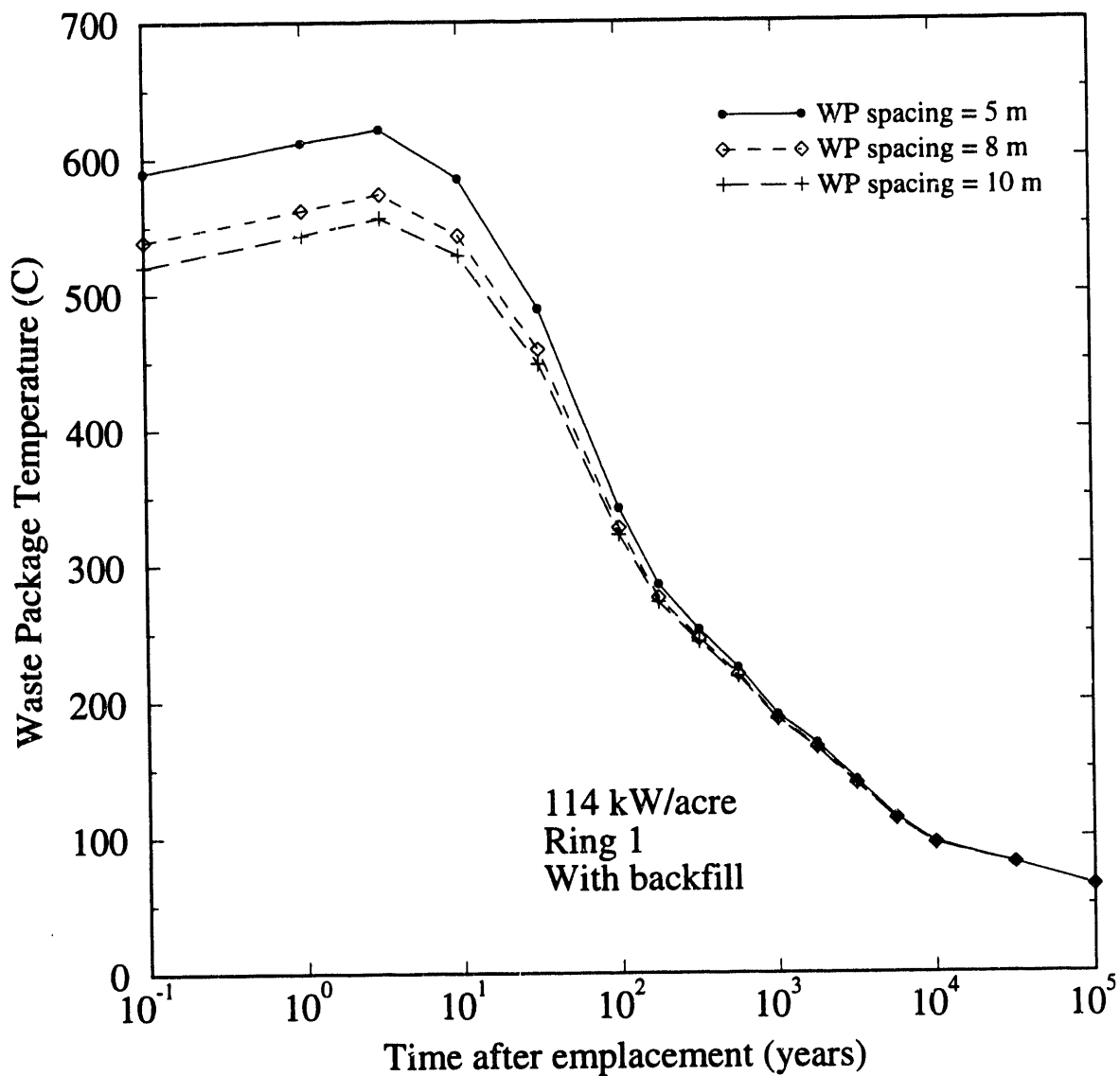


Figure B-18. Sensitivity of Average Waste Package Temperatures to the Waste Package Spacing  
(21 PWR assemblies per package, 7 m drift diameter)

**APPENDIX C**

**RADIONUCLIDE INVENTORY FOR TSPA 1993**

**Anthony Smith**

## **INTRODUCTION**

An important component in any assessment of the release of radionuclides to the accessible environment is the definition of the initial inventory available for alteration/dissolution and transport. While one might expect that the inventory of the spent fuel and high-level defense waste that may ultimately be disposed at a potential repository should be fairly well quantified, there are many factors which will affect the actual inventory at receipt which cause the initial inventory to be uncertain. In addition, performance assessment calculations generally do not consider the entire inventory because a large fraction of the total radionuclide constituents either have such short half-lives or low inventories to be of no consequence over the time periods of interest (although they may be significant for assessments of preclosure occupational and public safety). The rationale for and the determination of the inventory used in TSPA 1993 are documented in the discussion which follows.

The approach taken to determine the initial inventory for use in TSPA 1993 consisted of the following steps:

1. Determine the pressurized-water reactor (PWR), boiling water reactor (BWR), and defense high-level waste (DHLW) inventories for all radionuclides from the Characteristic Data Base (CDB) (Oak Ridge National Laboratory, 1992).
2. Determine the weighted average spent fuel inventory for the average burnups, averaged fuel ages out of reactor, and relative amounts of PWR and BWR fuel.
3. Conduct screening of the total inventory based on the potential contribution of each radionuclide normalized to the 40 CFR 191 Table 1 values to release over time periods from 1,000 to 1,000,000 years.
4. Conduct screening based on the potential contribution of each radionuclide to the average annual whole body dose over time periods from 1,000 to 1,000,000 years.
5. Compare the results of both screening methods to determine the appropriate inventory.

The fundamental source of information on the physical and radiological properties of the radioactive wastes that may be accepted by U.S. Department of Energy (DOE) for emplacement in a high-level waste repository is the CDB. The CDB serves as the official source of information for the characterization of those materials that will (or may) become the responsibility of Office of Civilian Radioactive Waste Management. The radiological characteristics are derived from radioactive isotopes created in the reactors from either nuclear fission (fission products), activation of lighter isotopes (activation products), or neutron capture by the heavy metals (actinides). Calculation of the quantities of each radionuclide present as a function of fuel enrichment, burnup and age for various kinds of spent fuel (PWR and BWR) are determined with the ORIGEN2 code (Croff, 1983). The basic function of ORIGEN2 is to quantify the generation of individual nuclides resulting from neutron-induced fission, neutron capture, or other transmutation reactions and the depletion (and concurrent buildup) of nuclides resulting from natural decay processes. Although ORIGEN2 contains approximately

1,400 radionuclides, 194 radionuclides remain in the 30-year CDB inventory. These radionuclides are indicated in Table C-1.

The current plans for disposal of commercially-generated and DHLW consist of accepting 63,000 metric tons of initial heavy metal (MTIHM) of spent fuel and 7,000 MTIHM of DHLW. Based on current best estimates of repository receipt schedules and fuel enrichments, it has been estimated by King (1993; see Appendix D) that the spent fuel would consist of 40,747 MTIHM of PWR fuel with an average burnup of 42.3 GWd/MTIHM and 22,253 MTIHM of BWR fuel with an average burnup of 32.25 GWd/MTIHM. In both cases, it is assumed that the fuel is 30 years out-of-reactor at the time of disposal. The DHLW is assumed to be contained within 14,000 containers (i.e., 0.5 MTIHM per container) which are proportionately derived from the total inventories at West Valley, Idaho National Engineering Laboratory, Savannah River Laboratory, and Hanford.

The first screening method used the inventory of the 63,000 MTIHM of spent fuel at times ranging from 1,000 to 1,000,000 years determined from the CDB, and normalized each inventory activity (in Curies/MTIHM) by the release limits specified in Table 1 of 40 CFR 191. Although it must be acknowledged that these release limits may not be the best indicators of relative performance because they apply to cumulative releases at the accessible environment over 10,000-year time periods, they provide a useful comparison to assure that the most significant potential contributors to release are identified. By examining time periods up to 1,000,000 years, we are approximating the effects of arrival time delay due to a combination of waste package lifetime and retarded radionuclide transport in the geosphere. Table C-2 presents the principal radionuclides potentially contributing to the U.S. Environmental Protection Agency (EPA) sum. If one were to consider those radionuclides contributing at least some fraction of the total potential release over the time periods of interest as relevant for incorporation in the TSPA 1993 inventory, then one could determine a representative inventory. If one considered a cut-off of  $10^{-6}$  of the total release normalized by the EPA Table 1 values as well as the parents of daughters which contribute to at least  $10^{-6}$  of the potential release, then 86 radionuclides would remain in the inventory.

The second screening method also used the inventory of the 63,000 MTIHM of spent fuel and employed a simple spreadsheet release, dilution, and ingestion model to determine the potential contribution of each radionuclide to the individual dose over time periods up to 1,000,000 years. Starting with the CDB-derived inventories of all radionuclides, the waste form was assumed to alter at  $10^{-5}$  of the total inventory per year. Each element was assumed to dissolve in water at the reasonable solubilities based primarily on the WISP analyses (NAS, 1983). The advective release of each radionuclide from the repository was assumed using a percolation flux of 0.1 mm/yr and a cross-sectional area of all waste packages of 33,000 m<sup>2</sup>. The released radionuclides were then mixed in the saturated zone with a lateral flow of 10<sup>4</sup> m<sup>3</sup>/yr. The diluted radionuclides were then assumed to be ingested by drinking 700 l/yr of the water derived from the saturated zone aquifer. The ingested dose was then determined by using the maximum dose conversion factors from a number of published sources (Eckerman, 1988; DOE, 1988; Dunning, 1981). The fractional contribution of each radionuclide to the total individual dose was then determined. All radionuclides contributing to 99.999 percent of the potential total dose at any time ranging from 1,000 to 1,000,000 years (or the parents of daughters which contribute at least  $10^{-5}$  to the

potential total dose) are then retained in the inventory for use in TSPA 1993. The most significant radionuclides resulting from using this screening method are tabulated in Tables C-3a to C-3d for time periods of 1,000, 10,000, 100,000, and 1,000,000 years, respectively. A total of 37 radionuclides meet this criterion.

In comparing the results of the two screening methods, it is not surprising that the same radionuclides appear as the most significant on both lists. This perhaps reflects the similarity between a population-dose based standard (which is fundamentally the basis for the EPA Table 1 values) and an individual dose-based criterion. While one can always question the use of a particular cut-off for delimiting the radionuclides to include in an assessment of total system performance, we feel it is justified to include those which may potentially contribute to the individual dose of an exposed population. As a result, we have chosen the 37 radionuclides contributing 99.999 percent of the potential individual dose over any time period from 1,000 to 1,000,000 years. This assures us of including the long-lived radionuclides which may be unimportant as far as the Table 1 release limits are concerned but which may be significant contributors to dose. The 37 radionuclides are tabulated in Table C-4 along with their 30-year inventories. The corresponding DHLW inventories for the important dose-contributing radionuclides are shown in Table C-5.

## REFERENCES

Croff, A. G., 1983. "ORIGEN2: A versatile computer code for Calculating the Nuclide Compositions and Characteristics of Nuclear Materials," Nuclear Technology, Vol. 62, pp. 335-352.

DOE/EH-0071, 1988. Internal Dose Conversion Factors for Calculation of Dose to the Public.

Dunning, D. E., et al., 1981. Estimates of Internal Dose Equivalent to 22 Target Organs for Radionuclides Occurring in Routine Releases from Nuclear Fuel-Cycle Facilities. NUREG/CR-0150.

Eckerman, K. F. et al., 1988. Limiting Values of Radionuclide Intake and Air Concentration and Dose Conversion Factors for Inhalation, Submersion, and Ingestion, EPA--520/1-88-020.

NAS (National Research Council, National Academy of Sciences), 1983. Board on Radioactive Waste Management-Waste Isolation System Panel, A Study of the Isolation System for Geologic Disposal of Radioactive Wastes, National Academy Press, Washington, D.C.

Oak Ridge National Laboratory, 1992. Characteristics of Potential Repository Wastes, DOE/RW-0184-R1, prepared for the U.S. Department of Energy Office of Civilian Radioactive Waste Management, Washington, D.C.

Table C-1. Radionuclides Considered

H 3	Sn 119m	Re 187	Th 234
Be 10	Sn 121m	Re 188	Pa 231
C 14	Sn 123	Ir 192	Pa 233
Si 32	Sn 126	Pt 193	Pa 234
P 32	Sb 124	Tl 206	Pa 234m
S 35	Sb 125	Tl 207	U 232
Cl 36	Sb 126	Tl 208	U 233
Ar 39	Sb 126m	Tl 209	U 234
K 40	Te 123	Pb 204	U 235
Ca 41	Te 123m	Pb 205	U 236
Ca 45	Te 125m	Pb 209	U 237
Sc 46	Te 127	Pb 210	U 238
V 50	Te 127m	Pb 211	U 240
Mn 54	I 129	Pb 212	Np 235
Fe 55	Cs 134	Pb 214	Np 236
Co 58	Cs 135	Bi 208	Np 237
Co 60	Cs 137	Bi 210	Np 238
Ni 59	Ba 137m	Bi 210m	Np 239
Ni 63	La 138	Bi 211	Np 240m
Zn 65	Ce 142	Bi 212	Pu 236
Se 79	Ce 144	Bi 213	Pu 238
Kr 81	Pr 144	Bi 214	Pu 239
Kr 85	Pr 144m	Po 210	Pu 240
Rb 87	Nd 144	Po 211	Pu 241
Sr 90	Pm 146	Po 212	Pu 242
Y 90	Pm 147	Po 213	Pu 243
Y 91	Sm 146	Po 214	Pu 244
Zr 93	Sm 147	Po 215	Am 241
Zr 95	Sm 148	Po 216	Am 242
Nb 93m	Sm 149	Po 218	Am 242m
Nb 94	Sm 151	At 217	Am 243
Nb 95	Eu 150	Rn 219	Am 244
Nb 95m	Eu 152	Rn 220	Cm 242
Mo 93	Eu 154	Rn 222	Cm 243
Tc 98	Eu 155	Fr 221	Cm 244
Tc 99	Gd 152	Fr 223	Cm 245
Ru 106	Gd 153	Ra 223	Cm 246
Rh 102	Tb 160	Ra 224	Cm 247
Rh 106	Ho 166m	Ra 225	Cm 248
Pd 107	Tm 170	Ra 226	Bk 249
Ag 108	Tm 171	Ra 228	Cf 249
Ag 108m	Lu 176	Ac 225	Cf 250
Ag 109m	Lu 177	Ac 227	Cf 251
Ag 110	Lu 177m	Ac 228	Cf 252
Ag 110m	Hf 175	Th 227	
Cd 109	Hf 182	Th 228	
Cd 113m	Ta 182	Th 229	
In 113m	W 181	Th 230	
In 115	W 185	Th 231	
Sn 113	W 188	Th 232	

**Table C-2**  
**Inventory / EPA Limit**

Decay 10 <sup>3</sup> yrs		Decay 10 <sup>4</sup> yrs		Decay 10 <sup>5</sup> yrs		Decay 10 <sup>6</sup> yrs	
Am241	1.09E+04	Pu239	2.86E+03	Pu239	2.18E+02	Th230	5.24E+01
Pu240	5.21E+03	Pu240	2.01E+03	Th230	1.42E+02	Th229	1.18E+01
Pu239	3.65E+03	Am243	1.11E+02	U234	2.14E+01	At217	1.18E+01
Am243	2.57E+02	U234	2.68E+01	Pu242	1.82E+01	Ac225	1.18E+01
U234	2.73E+01	Th230	2.31E+01	Np237	1.47E+01	Bi213	1.18E+01
Np239	2.57E+01	Pu242	2.14E+01	Ra226	1.43E+01	Fr221	1.18E+01
Pu238	2.21E+01	Np237	1.52E+01	Rn222	1.43E+01	U233	1.17E+01
Pu242	2.18E+01	Np239	1.11E+01	Po210	1.43E+01	Po213	1.15E+01
C14	1.32E+01	C14	4.44E+00	Po218	1.43E+01	Np237	1.10E+01
Np237	1.30E+01	U236	3.99E+00	Po214	1.43E+01	Po218	5.25E+00
Cm245	3.95E+00	U238	3.15E+00	U233	5.28E+00	Ra226	5.25E+00
U238	3.14E+00	Zr93	2.57E+00	Th229	4.82E+00	Rn222	5.25E+00
U236	3.09E+00	Nb93m	2.44E+00	Ac225	4.82E+00	Po214	5.25E+00
Zr93	2.58E+00	Ni59	2.31E+00	At217	4.82E+00	Po210	5.25E+00
Ni59	2.50E+00	Am241	1.90E+00	Fr221	4.82E+00	U234	4.59E+00
Nb93m	2.45E+00	Cm245	1.89E+00	Bi213	4.82E+00	U236	4.41E+00
Cm242	2.31E+00	Ra226	1.80E+00	Po213	4.72E+00	Pu242	3.63E+00
Th230	2.27E+00	Po210	1.80E+00	U236	4.53E+00	U238	3.15E+00
Tc99	1.51E+00	Rn222	1.80E+00	U238	3.15E+00	Zr93	1.64E+00
Pa233	1.30E+00	Po214	1.80E+00	Zr93	2.47E+00	Nb93m	1.56E+00
Sb126m	9.18E-01	Po218	1.80E+00	Nb93m	2.34E+00	Ra225	1.18E+00
Sn126	9.18E-01	Pa233	1.52E+00	Pa233	1.47E+00	Pb209	1.18E+00
Nb94	8.62E-01	Tc99	1.46E+00	Bi210	1.43E+00	Pa233	1.10E+00
Cm246	8.14E-01	Sb126m	8.63E-01	Pb214	1.43E+00	Bi214	5.25E-01
Cs135	5.67E-01	Sn126	8.63E-01	Bi214	1.43E+00	Pb214	5.25E-01
Se79	4.75E-01	Nb94	6.34E-01	Pb210	1.43E+00	Pb210	5.24E-01
Pu241	3.95E-01	U233	6.22E-01	Tc99	1.09E+00	Bi210	5.24E-01
I129	3.72E-01	Cs135	5.66E-01	Ni59	1.06E+00	Cs135	4.20E-01
Th234	3.15E-01	Se79	4.31E-01	Cs135	5.51E-01	I129	3.56E-01
Pa234m	3.14E-01	I129	3.72E-01	Pb209	4.82E-01	Th234	3.15E-01
Am242m	2.81E-01	Pa234m	3.15E-01	Ra225	4.82E-01	Pa234m	3.15E-01
Am242	2.80E-01	Th234	3.15E-01	Sb126m	4.62E-01	Ra223	3.00E-01
Ni63	2.22E-01	Cm246	2.18E-01	Sn126	4.62E-01	Po215	3.00E-01
Sm151	2.14E-01	At217	2.14E-01	I129	3.71E-01	Rn219	3.00E-01
U235	1.71E-01	Th229	2.14E-01	Th234	3.15E-01	Pa231	3.00E-01
Pd107	1.37E-01	Fr221	2.14E-01	Pa234m	3.15E-01	Bi211	3.00E-01
Sb126	1.29E-01	Ac225	2.14E-01	U235	2.93E-01	U235	3.00E-01
U233	4.28E-02	Bi213	2.14E-01	Bi211	2.40E-01	Th227	2.95E-01
Ra226	4.05E-02	Po213	2.09E-01	Ra223	2.40E-01	Pd107	1.23E-01
Rn222	4.05E-02	U235	2.00E-01	Pa231	2.40E-01	Tc99	5.84E-02

**Table C-2**  
**Inventory / EPA Limit**

Po218	4.05E-02	Pu241	1.90E-01	Po215	2.40E-01	Pb211	3.00E-02
Po210	4.05E-02	Bi214	1.80E-01	Rn219	2.40E-01	Ac227	3.00E-02
Po214	4.05E-02	Bi210	1.80E-01	Th227	2.37E-01	Th231	3.00E-02
Th231	1.71E-02	Pb214	1.80E-01	Se79	1.65E-01	Tl207	2.99E-02
Mo93	1.31E-02	Pb210	1.80E-01	Pu240	1.44E-01	Tl209	2.54E-02
Cl36	1.18E-02	Pd107	1.37E-01	Pd107	1.36E-01	Th232	2.20E-03
Pb214	4.05E-03	Sb126	1.21E-01	Sb126	6.47E-02	Cl36	1.18E-03
Bi210	4.05E-03	Po215	3.56E-02	Nb94	2.93E-02	Sb126m	9.04E-04
Bi214	4.05E-03	Bi211	3.56E-02	Th231	2.92E-02	Ln126	9.04E-04
Pb210	4.05E-03	Rn219	3.56E-02	Pb211	2.40E-02	Po211	8.39E-04
Rn219	3.81E-03	Ra223	3.56E-02	Ac227	2.40E-02	Ni59	4.35E-04
Po215	3.81E-03	Pa231	3.56E-02	Tl207	2.39E-02	Fr223	4.14E-04
Ra223	3.81E-03	Th227	3.51E-02	Am243	2.36E-02	Pa234	4.09E-04
Bi211	3.81E-03	Ra225	2.14E-02	Tl209	1.04E-02	Ra224	2.20E-04
Pa231	3.80E-03	Pb209	2.14E-02	Cl36	9.37E-03	Bi212	2.20E-04
Th227	3.75E-03	Th231	2.00E-02	Np239	2.36E-03	Th228	2.20E-04
Ho166m	2.51E-03	Cl36	1.15E-02	Am241	1.23E-03	Rn220	2.20E-04
At217	1.70E-03	Ac227	3.56E-03	Cm245	1.23E-03	Po216	2.20E-04
Ac225	1.70E-03	Pb211	3.56E-03	Po211	6.72E-04	Po212	1.41E-04
Bi213	1.70E-03	Tl207	3.55E-03	Pa234	4.09E-04	Sb126	1.27E-04
Fr221	1.70E-03	Mo93	2.20E-03	Fr223	3.31E-04	Ce142	3.17E-05

Table C-3a	
Major Potential Contributors to Dose at 10 <sup>3</sup> yrs (rem)	
Am243	3.92E-03
Np237	1.16E-03
Pu241	4.13E-04
Cm245	2.60E-04
Am241	9.56E-05
Pu239	7.37E-05
Cm246	5.28E-05
Pu240	5.17E-05
Pb210	2.11E-05
Tc99	1.54E-05
I129	7.19E-06
Cs135	4.49E-06
Nb94	4.31E-06
Ac227	3.94E-06
Ra226	3.92E-06
Se79	2.89E-06
Pa231	2.82E-06
C14	1.86E-06
Am242m	9.41E-07
Nb93m	8.95E-07
Th232	3.96E-07
Ni59	3.67E-07
Pu242	2.93E-07
U233	9.96E-08
Ni63	8.97E-08
Sm151	5.83E-08
Cl36	2.49E-08
Sn126	2.10E-08
Th229	2.01E-08
Pd107	1.43E-08
Mo93	1.24E-08
U235	1.03E-08
U234	9.95E-09
Ho166m	9.83E-09

Table C-3b	
Major Potential Contributors to Dose at 10 <sup>4</sup> yrs (rem)	
Np237	1.16E-03
Pb210	9.37E-04
Am241	3.30E-04
Cm245	2.73E-04
Ra226	1.74E-04
Pu240	5.86E-05
Pu239	4.11E-05
Ac227	3.69E-05
Cm246	3.08E-05
Pa231	2.63E-05
Tc99	1.50E-05
I129	7.19E-06
Am243	5.52E-06
Cs135	4.47E-06
Nb94	3.17E-06
Se79	2.63E-06
Nb93m	8.92E-07
C14	6.28E-07
Pu242	4.17E-07
Th232	3.87E-07
Ni59	3.39E-07
Th229	2.43E-07
U233	9.71E-08
Cl36	2.44E-08
Sn126	2.10E-08
Pd107	1.43E-08
U235	1.33E-08
U234	9.92E-09

Table C-3c	
Major Potential Contributors to Dose at 10 <sup>5</sup> yrs (rem)	
Pb210	7.43E-03
Ra226	1.38E-03
Np237	1.16E-03
Ac227	2.49E-04
Pa231	1.78E-04
Pu240	3.31E-05
Tc99	1.12E-05
Am241	7.82E-06
I129	7.16E-06
Cs135	4.35E-06
Pu242	2.63E-06
Se79	1.01E-06
Nb93m	8.56E-07
Th229	7.82E-07
Cm245	4.15E-07
Am243	3.95E-07
Th232	3.38E-07
Ni59	1.55E-07
Nb94	1.47E-07
U233	7.74E-08
Pu239	2.19E-08
Sn126	2.10E-08
Cl36	1.99E-08
U238	1.94E-08
U235	1.50E-08
Pd107	1.42E-08
U234	9.87E-09

Table C-3d	
Major Potential Contributors to Dose at 10 <sup>6</sup> yrs (rem)	
Pb210	2.73E-03
Np237	1.16E-03
Ra226	5.07E-04
Ac227	3.10E-04
Pa231	2.22E-04
I129	6.88E-06
Pu242	4.63E-06
Cs135	3.32E-06
Th229	7.56E-07
Tc99	5.98E-07
Nb93m	5.70E-07
Th232	4.97E-08
U238	4.28E-08
Ra228	3.46E-08
U233	1.66E-08
U235	1.46E-08
Sn126	1.33E-08
Pd107	1.29E-08
U234	9.87E-09

**Table C-4**  
**RADIONUCLIDES IN AVERAGE SNF RANKED BY POTENTIAL WHOLE BODY DOSE**  
**Alteration at 1E-5/Yr & Appropriate Solubilities**

	30 Yr Inventory (Ci/MTIHM)			30 Yr Inventory (Ci/MTIHM)	
ISOTOPE			ISOTOPE		
Percent of dose by incorporating isotopes to line (at times of 10 <sup>3</sup> , 10 <sup>4</sup> , 10 <sup>5</sup> & 10 <sup>6</sup> years).	Am243	2.82E+01	Vertical dots show decay chains needed to allow for time increase in daughter products. Note parent dose may be insignificant.	Cm244	1.41E+03
	Np237	4.87E-01		Pu240	5.73E+02
	Pb210	7.15E-07		Tc99	1.51E+01
	Ra226	2.64E-06		I129	3.72E-02
	Th230	3.79E-04		Cs135	5.67E-01
	U234	1.43E+00		Nb94	8.91E-01
	U238	3.14E-01		Se79	4.80E-01
	Pu238	3.57E+03		Th229	4.32E-07
	Pu242	2.18E+00		U233	7.82E-05
	Am242m	2.34E+01		Zr93	2.58E+00
	Cm246	9.38E-02		Nb93m	1.98E+00
	Am241	3.92E+03		C14	1.48E+00
	Pu241	3.56E+04		Th232	4.71E-10
	Cm245	4.27E-01		U236	2.93E-01
	Pa231	3.59E-05		Ni59	2.52E+00
	U235	1.68E-02		Ra228	3.36E-10
	Pu239	3.75E+02		Sm151	3.77E+02
	Ac227	1.97E-05		Sn126	9.25E-01
			Pd107	1.37E-01	

Inventory from a mixture of BWR 22253 MTIHM + PWR 40747 MTIHM  
with burnup of 42.3 GWd/MTIHM for PWR and 32.25 GWd/MTIHM for BWR.

**Table C-5  
DHLW Inventory**

Isotope	30 Yr Ci/container
Cm246	6.39E-06
Cm245	5.64E-05
Cm244	1.14E+01
Am243	3.67E-02
Pu242	5.02E-03
Am242m	2.06E-02
Am241	8.65E+01
Pu241	1.48E+02
Pu239	4.73E+00
U238	3.78E-03
Pu238	4.00E+02
Np237	2.83E-02
U235	7.93E-05
U234	5.00E-02
Pa231	9.74E-04
Th230	1.24E-05
Ac227	6.02E-04
Ra226	9.37E-08
Pb210	2.72E-08
Pu240	3.30E+00
Tc99	3.30E+00
Cs135	1.15E-01
I129	1.90E-06
Nb94	3.02E-05
Se79	9.18E-02
U236	4.35E-04
U233	5.84E-04
Th232	1.05E-04
Th229	1.51E-05
Nb93m	5.48E-01
Zr93	7.71E-01
Ni59	2.70E-02

**APPENDIX D**

**WASTE STREAM AND WASTE PACKAGE DESCRIPTIONS:  
YOUNGEST FUEL FIRST WITH MRS FLOW THROUGH  
EMPLACEMENT SCENARIO**

**John King**

**INTEROFFICE CORRESPONDENCE**  
Civilian Radioactive Waste Management System  
Management & Operating Contractor



TRW Environmental  
Safety Systems Inc.

WBS: 9.2.1.1.3  
QA: N/A

**Subject:**  
Data Transmittal for Phase 2  
Thermal Loading Study

**Date:**  
May 24, 1993  
VA.SE.JK.5/93.031

**From:**  
John King *JK*

**To:**  
S. Saterlie

**cc:**  
M. Abhold  
W. Bailey *WB*  
T. Doering (w/ Attachments)  
D. Gibson  
P. Gottlieb (w/ Attachments)  
J. Miller  
R. Memory  
L. Rickertson (w/ Attachments)  
RMS R&H (w/ Attachments)

**Location:**  
TES1/3500-M  
(703) 204-8740

In support of the Phase 2 Repository Thermal Loading Study, the attached data are provided. The attached waste stream and waste package data are for two system scenarios: 1) Oldest Fuel First (OFF) with MRS passthrough/flowthrough, and 2) Youngest Fuel First, greater than or equal to 10 years old (YFF(10)), with MRS passthrough/flowthrough. These two scenarios were run with the Waste Stream Model, CSCI: A00020025.AAXO1.0, which is a controlled but not QA'd model. Key parameters in the runs are: reference receipt rates (3000 MTU/yr) as documented in the System Throughput Rate Study, a western strategy (generic eastern MRS, western reactor fuel shipped directly to MGDS), OFF selection for dry storage when pools are full, full core reserves (FCRs) maintained, and dry storage fuel pickup is deferred until pools are empty or contain fuel less than five years old. Cask rounding parameters do not affect the results presented here. Note that average fuel characteristic values differ somewhat from those reported in the Phase 1 System Implications of Repository Thermal Loading study in which FCRs were not maintained (i.e. pools were allowed to fill to capacity) because blending was being analyzed, and the largest possible pool inventories were desired to explore the maximum impact of blending. The net effect of maintaining FCRs is that more (OFF) fuel goes into dry storage and either ages considerably before pickup or is never picked up, so the overall average age at emplacement is reduced by about one year when FCRs are maintained.

Per your request, the waste streams resulting from these two scenarios were packaged five different ways for a total of ten waste package inventories using the WPA3 code (currently not under formal configuration management). The waste package capacities are shown in Table 1 along with the resulting overall average heat at emplacement. Tables 2 and 3 show detailed (annual) waste characteristics for the unpackaged waste stream, and Tables 4(a) through 4(e) and Tables 5(a) through 5(e) show the annual waste package data for the various waste package capacities. Note the last line of these tables labeled "Avg" shows overall averages for the yearly parameters with the exception of the Number of WP's column which shows total waste packages. The waste packages are filled using a simple blending stream and assuming (for computational reasons) the entire year's inventory is available for blending. This assumption is probably not realistic, but for the highly aggregated data presented here this assumption should have only a second order effect at most. All heat output data are based on the Characteristics Database (CSCI:

A00020002.AAX01.0) as adapted for WSM and WPA3 using the methodology documented in Reference 1.

Tables 6(a) through 6(c) and Tables 7(a) through 7(c) give the generic heat decay curves requested for underground layout scoping calculations. These curves were derived as show in Figure 1 by taking overall average ages at emplacement, average burnups, and average enrichments for PWRs and BWRs and generating a generic heat decay curve based on the average values, and then mass weighting the two Watts/MTU curves by the relative MTUs of PWR and BWR assemblies in the scenario for an assembly type independent heat decay curve. Note that the PWR and BWR curves are noticeably different, so the combined curve should be used for scoping calculations only. Also, care should be used in linking the origin (in time) of these curves to an actual emplacement year. Since the data are based on overall average age at emplacement and a single curve is generated, the curve effectively represents an instantaneous emplacement of all the waste. Therefore, if the curve's time zero is assigned to a year, it should be the "centroid" year of the mass emplacement over time.

Equivalent annual thermal source terms for repository-scale thermal calculations have been computed for Eric Ryder (SNL) and are given in Tables 8(a) through 8(e) and 9(a) through 9(e). These source terms are computed by aggregating SNF characteristics on an annual basis (for each emplacement year) from individual waste packages. Details of the methodology may be found in Reference 2.

Since you have not yet received an InfoSTREAMS account, all the data in Tables 1 through 9 have been provided electronically by uploading them to the YMV4 network drive in the common area (\\YMV4\PCCOMMON) under a subdirectory called KINGDATA. The files are Read-Only and cannot be altered or deleted unless they are purposely unprotected.

Finally, Attachment I is the QAP-3-12 form for external transmission of design input data. This attachment is included to document the QA status of the data in case they are used in design related activities.

If you have any questions, please do not hesitate to call. Please keep me apprised of your progress on the Study and include me on any relevant documents' distribution.

## REFERENCES

1. "WSA Heat Calculations," IOC, E. Bogart to W. Bailey, et al., June 19, 1992.
2. "Improved Spent Nuclear Fuel Source Term Generation Capability for Performance Assessment and System Studies," IOC VA.SE.WB.3/93.180, J. King to R. Nelson, March 12, 1993.

## Attachments

5/18/03

Table 1. Waste Package Summary Data  
Phase 2 MGDS Thermal Loading Study

King

(1) SYSTEM SCENARIO	(Unpackaged) Assembly Averages				Waste Packages (3)					
	PWR		BWR		Cap.	PWR No. Pkgs	(2) Avg Heat	Cap.	BWR No. Pkgs	(2) Avg Heat
	Age	Burnup	Age	Burnup						
OFF	24.6	40366	25.7	31441	2	47,575	945	4	31,097	710
					4	23,787	1,890	6	20,731	1,065
					12	7,929	5,670	21	5,923	3,728
					16	5,946	7,560	32	3,887	5,681
					21	4,530	9,921	40	3,109	7,101
YFF(10)	22.3	42329	23.5	32232	2	47,591	1,124	4	31,163	818
					4	23,795	2,247	6	20,775	1,227
					12	7,931	6,742	21	5,935	4,293
					16	5,948	8,990	32	3,895	6,541
					21	4,532	11,799	40	3,116	8,177

D-3

- (1) "OFF" - OFF Acceptance/MRS Flowthrough  
"YFF(10)" - YFF >= 10 yrs old Acceptance/MRS Flowthrough
- (2) Average Heat Output at Emplacement in Watts/Package
- (3) Packaging assumes blending into packages with 3000 MTU "lag storage"

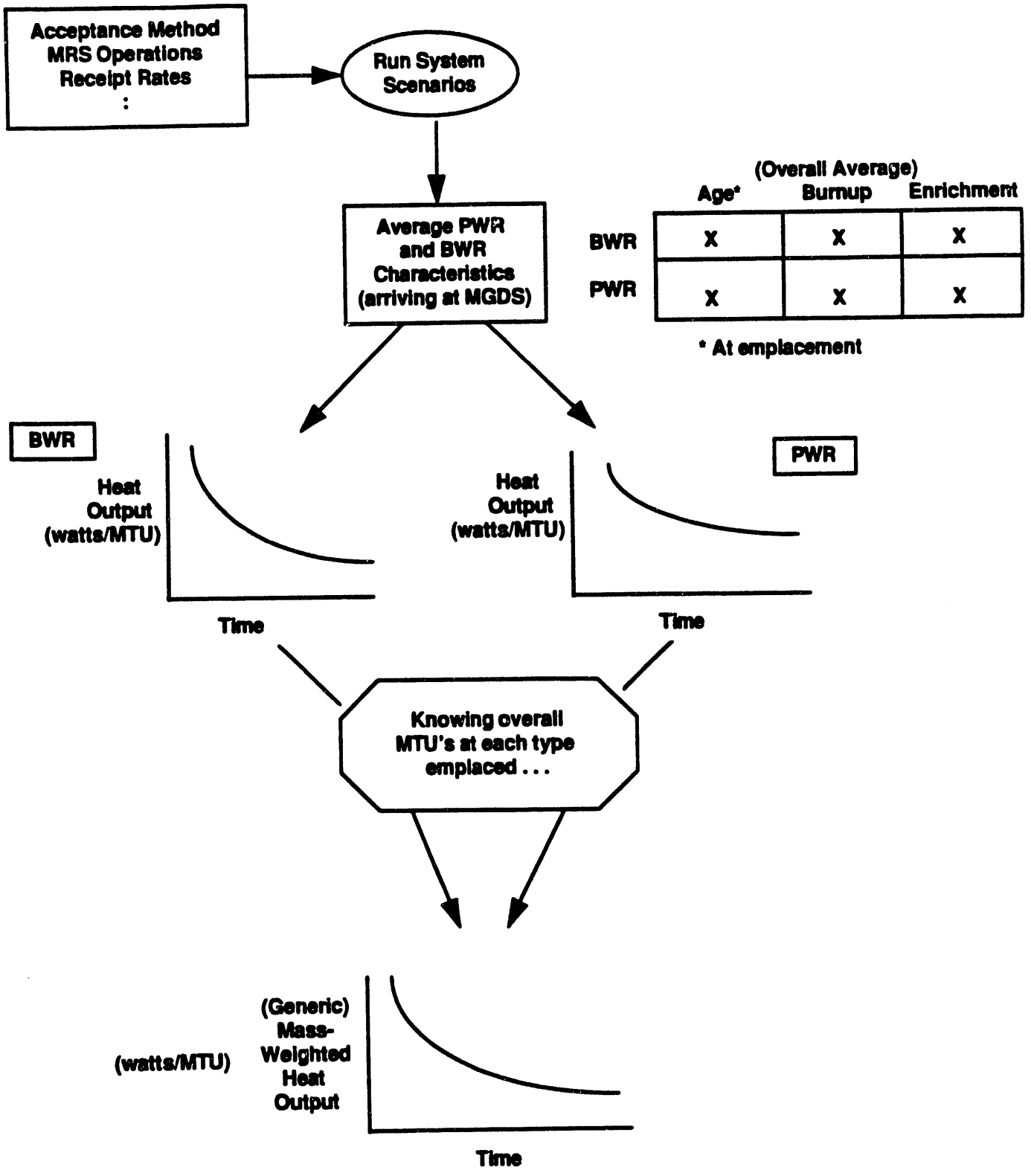


**Figure 1. Derivation of "Generic" Waste Package Heat Decay Curves**

Table 3

AVERAGE ANNUAL SPENT FUEL CHARACTERISTICS AT EMPLACEMENT 3/30/93 11:37  
 WFF10-3K, With Flowthrough, for Steve Saterlie, Phase II Thermal

MTU

	MTU	BURNUP MWD/MTU	HEAT WATTS/- MTU	AGE
2010	304	38619	1433	12.0
2011	597	39274	1449	11.3
2012	1200	40066	1463	12.4
2013	2001	39370	1406	14.0
2014	2965	40467	1398	15.0
2015	2986	40920	1460	14.7
2016	3040	41417	1464	15.2
2017	2991	40964	1427	16.2
2018	2953	42889	1588	14.2
2019	2992	40021	1325	19.2
2020	3058	40878	1441	17.1
2021	2965	41718	1458	17.3
2022	3037	40008	1407	18.1
2023	2993	38911	1299	19.9
2024	3009	38755	1375	17.9
2025	2981	38621	1337	20.7
2026	3014	36951	1260	23.9
2027	2983	34860	1168	27.1
2028	3019	32139	881	34.1
2029	2976	32697	642	40.3
2030	3014	35773	750	37.4
2031	2960	38562	862	34.4
2032	2993	38649	879	34.2
2033	1969	39229	883	34.7

Table 3 (Continued)

VERAGE ANNUAL SPENT FUEL CHARACTERISTICS AT EMPLACEMENT 3/30/93 11:37  
 FF10-3K, With Flowthrough, for Steve Saterlie, Phase II Thermal

PWR

	MTU	BURNUP MWD/MTU	HEAT WATTS/- MTU	AGE
2010	139	36308	1448	11.0
2011	197	34997	1343	12.6
2012	442	35920	1418	13.1
2013	781	34955	1284	15.2
2014	902	35085	1286	15.8
2015	1019	36628	1447	13.6
2016	988	35256	1290	16.2
2017	1048	35406	1351	15.1
2018	980	37525	1570	12.2
2019	883	33172	1168	19.1
2020	1101	33846	1304	16.2
2021	896	33904	1250	17.9
2022	1097	33847	1383	14.9
2023	948	31737	1161	20.3
2024	1037	30447	1209	16.6
2025	916	31290	1327	16.6
2026	1193	29645	1126	25.1
2027	1380	26797	959	30.2
2028	1220	23585	615	39.4
2029	1163	28121	553	41.3
30	1253	31410	667	38.5
31	1046	33600	789	35.2
2032	1114	31652	759	35.4
2033	510	32319	802	34.5

Table 3

AVERAGE ANNUAL SPENT FUEL CHARACTERISTICS AT EMPLACEMENT 3/30/93 11:37  
 FF10-3K, With Flowthrough, for Steve Saterlie, Phase II Thermal

MTU

	MTU	BURNUP MWD/MTU	HEAT WATTS/- MTU	AGE
2010	304	38619	1433	12.0
2011	597	39274	1449	11.3
2012	1200	40066	1463	12.4
2013	2001	39370	1406	14.0
2014	2965	40467	1398	15.0
2015	2986	40920	1460	14.7
2016	3040	41417	1464	15.2
2017	2991	40964	1427	16.2
2018	2953	42889	1588	14.2
2019	2992	40021	1325	19.2
2020	3058	40878	1441	17.1
2021	2965	41718	1458	17.3
2022	3037	40008	1407	18.1
2023	2993	38911	1299	19.9
2024	3009	38755	1375	17.9
2025	2981	38621	1337	20.7
2026	3014	36951	1260	23.9
2027	2983	34860	1168	27.1
2028	3019	32139	881	34.1
2029	2976	32697	642	40.3
2030	3014	35773	750	37.4
2031	2960	38562	862	34.4
2032	2993	38649	879	34.2
2033	1969	39229	883	34.7

Table 3 (Continued)

VERAGE ANNUAL SPENT FUEL CHARACTERISTICS AT EMPLACEMENT 3/30/93 11:37  
 FF10-3K, With Flowthrough, for Steve Saterlie, Phase II Thermal

PWR

	MTU	BURNUP MWD/MTU	HEAT WATTS/- MTU	AGE
2010	139	36308	1448	11.0
2011	197	34997	1343	12.6
2012	442	35920	1418	13.1
2013	781	34955	1284	15.2
2014	902	35085	1286	15.8
2015	1019	36628	1447	13.6
2016	988	35256	1290	16.2
2017	1048	35406	1351	15.1
2018	980	37525	1570	12.2
2019	883	33172	1168	19.1
2020	1101	33846	1304	16.2
2021	896	33904	1250	17.9
2022	1097	33847	1383	14.9
2023	948	31737	1161	20.3
2024	1037	30447	1209	16.6
2025	916	31290	1327	16.6
2026	1193	29645	1126	25.1
2027	1380	26797	959	30.2
2028	1220	23585	615	39.4
2029	1163	28121	553	41.3
30	1253	31410	667	38.5
31	1046	33600	789	35.2
2032	1114	31652	759	35.4
2033	510	32319	802	34.5

Table 3 (Continued)

AVERAGE ANNUAL SPENT FUEL CHARACTERISTICS AT EMPLACEMENT 3/30/93 11:37  
 YFF10-3K, With Flowthrough, for Steve Saterlie, Phase II Thermal

BWR

	MTU	BURNUP MWD/MTU	HEAT WATTS/- MTU	AGE
2010	165	40557	1421	12.9
2011	400	41386	1501	10.7
2012	758	42480	1490	12.0
2013	1220	42196	1484	13.2
2014	2062	42822	1447	14.7
2015	1966	43145	1467	15.2
2016	2052	44385	1548	14.7
2017	1943	43961	1468	16.7
2018	1973	45554	1597	15.1
2019	2109	42889	1390	19.3
2020	1958	44831	1517	17.6
2021	2069	45103	1549	17.0
2022	1940	43492	1420	19.9
2023	2045	42235	1363	19.7
2024	1973	43121	1462	18.6
2025	2065	41872	1341	22.5
2026	1821	41735	1348	23.1
2027	1603	41801	1348	24.4
2028	1799	37939	1061	30.4
2029	1813	35635	699	39.7
2030	1761	38880	809	36.7
2031	1914	41273	901	34.1
2032	1880	42795	951	33.5
2033	1458	41647	911	34.8
ALL YEARS	63001	38762	1235	22.7
BWR YEARS	22253	32232	1106	23.5 ✓
PWR YEARS	40747	42329	1305	22.3

Table 3 (Continued)

3/30/93

ANNUAL REPOSITORY INVENTORY  
FF10-3K, With Flowthrough, for Steve Saterlie, Phase II Thermal

TIME YEAR	METRIC TONS OF URANIUM	ASSEMBLY	AVERAGE HEAT WATTS/MTU	AGE	BURNUP MWD/MTU
ALL 2010	303.7	1174	1433	12.0	38619
ALL 2011	901.0	3204	1426	11.9	39054
ALL 2012	2101.2	7443	1425	12.6	39632
ALL 2013	4102.4	14628	1391	13.8	39504
ALL 2014	7067.0	24415	1368	14.9	39908
ALL 2015	10052.6	34720	1365	15.5	40209
ALL 2016	13092.7	45044	1356	16.2	40489
ALL 2017	16083.7	55458	1337	17.0	40578
ALL 2018	19036.6	65492	1344	17.4	40936
ALL 2019	22029.1	75326	1308	18.5	40812
ALL 2020	25087.3	85995	1293	19.2	40820
ALL 2021	28052.1	95847	1279	19.9	40915
ALL 2022	31089.2	106477	1261	20.6	40826
ALL 2023	34081.8	116494	1234	21.5	40658
ALL 2024	37091.1	126817	1216	22.1	40504
ALL 2025	40072.3	136729	1197	22.9	40364
ALL 2026	43086.4	147426	1173	23.9	40125
ALL 2027	46069.5	158618	1145	25.1	39784
ALL 2028	49088.1	169836	1102	26.6	39314
ALL 2029	52063.3	181132	1052	28.3	38936
ALL 2030	54727.9	190751	1019	29.6	38931
ALL 2031	57688.3	201146	991	30.8	38912
ALL 2032	60681.6	211942	967	31.9	38899
ALL 2033	61621.9	213933	958	32.5	39260

Table 3 (Continued)

3/30/93 11:

ANNUAL REPOSITORY INVENTORY  
 FF10-3K, With Flowthrough, for Steve Saterlie, Phase II Thermal

TYPE	YEAR	METRIC TONS OF URANIUM	ASSEMBLY	AVERAGE HEAT WATTS/MTU	AGE	BURNUP MWD/MTU
BWR	2010	138.5	781	1448	11.0	36308
BWR	2011	336.0	1871	1364	12.3	35537
BWR	2012	777.7	4350	1375	13.2	35755
BWR	2013	1558.8	8731	1307	14.7	35354
BWR	2014	2461.2	13768	1274	15.7	35256
BWR	2015	3480.4	19488	1298	15.8	35657
BWR	2016	4468.8	25036	1266	16.7	35569
BWR	2017	5516.6	30911	1253	17.2	35538
BWR	2018	6496.7	36379	1272	17.3	35837
BWR	2019	7379.9	41301	1227	18.4	35518
BWR	2020	8480.5	47447	1209	19.0	35301
BWR	2021	9376.6	52460	1183	19.8	35168
BWR	2022	10473.7	58618	1177	20.2	35029
BWR	2023	11421.3	63899	1146	21.1	34756
BWR	2024	12457.9	69674	1122	21.6	34398
BWR	2025	13373.8	74801	1108	22.2	34185
BWR	2026	14566.5	81323	1080	23.4	33813
BWR	2027	15946.6	88821	1042	24.9	33206
BWR	2028	17166.4	95673	985	26.8	32522
BWR	2029	18329.0	102583	934	28.7	32244
BWR	2030	19372.1	108399	906	30.0	32474
BWR	2031	20418.3	114289	882	31.2	32531
BWR	2032	21531.9	120597	859	32.3	32486
BWR	2033	21500.6	120401	857	32.7	32919

Table 3 (Continued)

3/30/93

ANNUAL REPOSITORY INVENTORY  
FF10-3K, With Flowthrough, for Steve Saterlie, Phase II Thermal

TYPE	YEAR	METRIC TONS OF URANIUM	ASSEMBLY	AVERAGE HEAT WATTS/MTU	AGE	BURNUP MWD/MTU
PWR	2010	165.2	393	1421	12.9	40557
PWR	2011	565.1	1333	1462	11.6	41144
PWR	2012	1323.5	3093	1455	12.3	41910
PWR	2013	2543.6	5897	1443	13.2	42047
PWR	2014	4605.9	10647	1418	14.4	42394
PWR	2015	6572.2	15232	1401	15.4	42619
PWR	2016	8623.9	20008	1403	16.0	43039
PWR	2017	10567.1	24547	1380	16.9	43209
PWR	2018	12539.9	29113	1381	17.5	43578
PWR	2019	14649.2	34025	1348	18.6	43478
PWR	2020	16606.8	38548	1336	19.4	43638
PWR	2021	18675.5	43387	1327	20.0	43800
PWR	2022	20615.5	47859	1304	20.9	43771
PWR	2023	22660.5	52595	1279	21.7	43633
PWR	2024	24633.2	57143	1264	22.4	43592
PWR	2025	26698.5	61928	1241	23.3	43459
PWR	2026	28519.9	66103	1220	24.2	43348
PWR	2027	30122.9	69797	1199	25.2	43266
PWR	2028	31921.7	74163	1165	26.4	42966
PWR	2029	33734.2	78549	1115	28.1	42572
PWR	2030	35355.8	82352	1081	29.3	42469
PWR	2031	37270.0	86857	1051	30.5	42408
PWR	2032	39149.8	91345	1026	31.6	42427
PWR	2033	40121.4	93532	1012	32.4	42659

Table 5(a)

## Waste Package Power Data (watts/package)

LEWIS OPTION USED LVY10204 (3000 MTU LAG) 3K MTU/YR - YFF(10) w/ FT

\* Packages containing 4 assemblies

Year	No. WP	Min	Max	Max - Min	Mean	% Del	S.D.	C.V.
010	184	982.	1057.	75.	1027.	0.00	24.3	2.4
011	279	790.	1027.	237.	956.	-6.96	67.8	7.1
012	646	771.	1125.	354.	1021.	6.80	96.0	9.4
013	1118	829.	974.	145.	917.	-10.15	44.0	4.8
014	1245	799.	994.	195.	911.	-0.68	54.5	6.0
015	1399	870.	1131.	261.	1035.	13.66	94.9	9.2
016	1389	802.	994.	192.	933.	-9.92	51.1	5.5
017	1452	773.	1074.	300.	959.	2.80	84.7	8.8
018	1398	859.	1216.	357.	1117.	16.52	95.7	8.6
019	1249	759.	892.	133.	833.	-25.39	38.1	4.6
020	1496	777.	1126.	349.	948.	13.75	108.2	11.4
021	1263	773.	1010.	236.	895.	-5.60	40.5	4.5
022	1531	884.	1123.	239.	983.	9.85	63.8	6.5
023	1285	624.	1156.	533.	846.	-13.98	135.2	16.0
024	1453	597.	1150.	553.	859.	1.59	114.7	13.4
025	1313	467.	1174.	707.	933.	8.57	124.8	13.4
026	1612	658.	1182.	524.	837.	-10.24	112.8	13.5
027	1876	349.	1060.	711.	713.	-14.81	218.9	30.7
028	1678	266.	965.	699.	430.	-39.77	191.8	44.7
029	1710	258.	405.	147.	385.	-10.32	22.4	5.8
030	1871	292.	464.	173.	448.	16.19	23.1	5.2
031	1511	361.	589.	229.	560.	25.11	29.4	5.3
032	1491	372.	613.	241.	564.	0.73	46.1	8.2
033	714	383.	670.	287.	513.	-8.96	107.1	20.8
Avg	31163	637.	965.	328.	818.	11.84	82.9	11.1

PWR Packages containing 2 assemblies

Year	No. WP	Min	Max	Max - Min	Mean	% Del	S.D.	C.V.
010	204	1062.	1264.	202.	1177.	0.00	50.6	4.3
011	466	1149.	1328.	179.	1280.	8.76	25.2	2.0
012	858	1179.	1381.	202.	1270.	-0.76	28.0	2.2
013	1382	813.	1334.	521.	1299.	2.26	41.5	3.2
014	2350	1202.	1303.	101.	1251.	-3.68	16.8	1.3
015	2406	706.	1378.	672.	1243.	-0.61	21.6	1.7
016	2329	1285.	1423.	139.	1337.	7.49	26.0	1.9
017	2264	778.	1602.	825.	1251.	-6.44	47.5	3.8
018	2320	1292.	1747.	455.	1388.	10.97	44.1	3.2
019	2455	817.	1427.	609.	1178.	-15.11	78.7	6.7
020	2252	610.	1433.	823.	1313.	11.49	48.7	3.7
021	2394	697.	1446.	749.	1330.	1.24	34.7	2.6
022	2254	788.	1556.	768.	1242.	-6.57	66.9	5.4
023	2342	701.	1428.	727.	1171.	-5.73	61.7	5.3
024	2272	643.	1504.	861.	1259.	7.51	41.8	3.3
025	2431	1009.	1449.	440.	1155.	-8.29	95.8	8.3
026	2056	561.	1543.	982.	1189.	3.00	79.2	6.7
027	1879	1050.	1474.	423.	1166.	-1.95	89.9	7.7
028	2161	594.	1357.	763.	910.	-21.99	193.2	21.2
029	2210	344.	590.	246.	565.	-37.92	35.0	6.2
030	2066	365.	686.	321.	667.	18.14	22.8	3.4
031	2218	642.	778.	136.	765.	14.66	14.2	1.9
032	2321	441.	811.	371.	790.	3.21	21.6	2.7
033	1701	691.	795.	104.	773.	-2.10	14.6	1.9
Avg	47591	809.	1293.	484.	1124.	8.69	50.0	4.6

Table 5(b)

## Waste Package Power Data (watts/package)

LENDING OPTION USED LVY10406 (3000 MTU LAG) 3K MTU/YR - YFF(10) w/ FT

A Packages containing 6 assemblies

Year	No. WP	Min	Max	Max - Min	Mean	% Del	S.D.	C.V.
2010	122	1472.	1585.	113.	1541.	0.00	36.0	2.3
2011	186	1227.	1541.	313.	1434.	-6.98	100.9	7.0
2012	431	1183.	1687.	504.	1531.	6.79	143.8	9.4
2013	746	1244.	1461.	217.	1376.	-10.13	66.1	4.8
2014	830	1174.	1491.	316.	1367.	-0.69	81.9	6.0
2015	932	1305.	1697.	392.	1553.	13.66	142.4	9.2
2016	926	1203.	1491.	288.	1399.	-9.92	76.7	5.5
2017	968	1227.	1611.	384.	1438.	2.79	127.0	8.8
2018	932	1321.	1824.	503.	1676.	16.52	143.4	8.6
2019	833	1144.	1367.	223.	1250.	-25.38	57.3	4.6
2020	997	1166.	1689.	523.	1422.	13.72	162.3	11.4
2021	842	1160.	1569.	409.	1343.	-5.58	60.9	4.5
2022	1021	1326.	1685.	359.	1475.	9.82	95.6	6.5
2023	856	935.	1700.	765.	1269.	-13.96	202.7	16.0
2024	969	790.	1725.	934.	1289.	1.56	172.8	13.4
2025	875	769.	1760.	991.	1399.	8.58	187.3	13.4
2026	1075	911.	1773.	862.	1256.	-10.25	169.7	13.5
2027	1251	523.	1589.	1067.	1070.	-14.81	328.2	30.7
2028	1118	407.	1447.	1040.	644.	-39.76	287.4	44.6
2029	1140	414.	607.	193.	578.	-10.34	33.6	5.8
2030	1248	495.	696.	202.	671.	16.20	34.7	5.2
2031	1007	581.	884.	303.	840.	25.12	44.1	5.3
2032	994	657.	919.	263.	846.	0.73	69.0	8.2
2033	476	575.	1005.	431.	770.	-8.97	160.5	20.8
Avg	20775	967.	1450.	483.	1227.	11.84	124.3	11.1

PWR Packages containing 4 assemblies

Year	No. WP	Min	Max	Max - Min	Mean	% Del	S.D.	C.V.
2010	102	2124.	2528.	404.	2353.	0.00	100.7	4.3
2011	233	2297.	2655.	358.	2560.	8.76	50.0	2.0
2012	429	2358.	2763.	405.	2540.	-0.76	55.9	2.2
2013	691	2063.	2668.	605.	2598.	2.26	81.3	3.1
2014	1175	2405.	2607.	202.	2502.	-3.68	33.6	1.3
2015	1203	2083.	2700.	617.	2487.	-0.61	38.6	1.6
2016	1164	2569.	2847.	278.	2673.	7.49	51.9	1.9
2017	1132	2100.	3204.	1104.	2501.	-6.44	93.6	3.7
2018	1160	2585.	3495.	910.	2775.	10.96	87.0	3.1
2019	1228	2154.	2849.	695.	2356.	-15.10	156.7	6.7
2020	1126	2025.	2866.	841.	2627.	11.48	94.4	3.6
2021	1197	2143.	2891.	749.	2659.	1.24	65.9	2.5
2022	1127	2308.	3111.	803.	2485.	-6.57	131.9	5.3
2023	1171	2129.	2856.	727.	2342.	-5.73	121.5	5.2
2024	1136	2146.	3008.	861.	2518.	7.51	79.5	3.2
2025	1215	2018.	2891.	873.	2309.	-8.29	191.6	8.3
2026	1028	1574.	3086.	1512.	2379.	2.99	157.9	6.6
2027	940	2101.	2948.	847.	2332.	-1.94	179.4	7.7
2028	1080	1252.	2715.	1462.	1820.	-21.97	385.6	21.2
2029	1105	856.	1180.	324.	1130.	-37.92	69.5	6.2
2030	1033	943.	1372.	429.	1334.	18.13	45.4	3.4
2031	1109	1284.	1557.	272.	1530.	14.67	28.6	1.9
2032	1161	1210.	1623.	413.	1579.	3.21	42.1	2.7
2033	850	1395.	1590.	195.	1546.	-2.10	29.0	1.9
Avg	23795	1922.	2584.	662.	2247.	8.69	98.8	4.6

Table 5(c)

## Waste Package Power Data (watts/package)

BLENDING OPTION USED LVY11221 (3000 MTU LAG) 3K MTU/YR - YFF(10) w/ FT

## 3) Packages containing 21 assemblies

Year	No. WP	Min	Max	Max - Min	Mean	% Del	S.D.	C.V.
2010	35	5170.	5576.	406.	5394.	0.00	128.8	2.4
2011	53	4213.	5422.	1209.	5018.	-6.97	358.7	7.1
2012	123	4191.	5896.	1705.	5358.	6.78	508.4	9.5
2013	213	4233.	5121.	888.	4817.	-10.11	239.5	5.0
2014	237	4291.	5240.	949.	4783.	-0.70	295.1	6.2
2015	266	4460.	5936.	1476.	5434.	13.61	503.1	9.3
2016	265	4074.	5722.	1648.	4899.	-9.84	281.6	5.7
2017	277	4179.	5642.	1464.	5034.	2.74	450.0	8.9
2018	266	4506.	6383.	1877.	5865.	16.51	505.5	8.6
2019	238	3998.	4739.	741.	4378.	-25.35	217.4	5.0
2020	285	3936.	5927.	1991.	4977.	13.67	577.2	11.6
2021	240	4062.	5357.	1296.	4701.	-5.54	232.5	4.9
2022	292	4284.	6121.	1837.	5159.	9.74	362.5	7.0
2023	245	3273.	6168.	2895.	4441.	-13.91	720.2	16.2
2024	276	3171.	6035.	2864.	4514.	1.64	612.8	13.6
2025	250	3037.	6128.	3091.	4895.	8.45	676.5	13.8
2026	307	3454.	5827.	2373.	4396.	-10.20	610.3	13.9
2027	358	1828.	5796.	3967.	3745.	-14.82	1156.6	30.9
2028	319	1397.	5272.	3875.	2256.	-39.75	1008.9	44.7
2029	326	1577.	2132.	555.	2021.	-10.41	120.5	6.0
2030	357	1949.	2463.	514.	2349.	16.22	125.4	5.3
2031	287	2193.	3103.	910.	2940.	25.13	156.7	5.3
2032	284	2258.	3218.	960.	2961.	0.71	243.5	8.2
2033	136	1917.	3519.	1601.	2694.	-9.00	564.1	20.9
<b>Avg</b>	<b>5935</b>	<b>3402.</b>	<b>5114.</b>	<b>1712.</b>	<b>4293.</b>	<b>11.82</b>	<b>444.0</b>	<b>11.3</b>

## PWR Packages containing 12 assemblies

Year	No. WP	Min	Max	Max - Min	Mean	% Del	S.D.	C.V.
2010	34	6386.	7584.	1198.	7060.	0.00	296.8	4.2
2011	77	7303.	7966.	663.	7679.	8.76	140.0	1.8
2012	143	7326.	8185.	859.	7619.	-0.78	164.0	2.2
2013	231	7051.	8004.	953.	7793.	2.28	237.2	3.0
2014	391	7214.	7793.	579.	7507.	-3.68	99.8	1.3
2015	401	6987.	7967.	980.	7461.	-0.61	112.1	1.5
2016	388	7637.	8449.	812.	8019.	7.48	156.0	1.9
2017	378	7141.	9613.	2472.	7504.	-6.41	278.3	3.7
2018	386	7763.	9991.	2228.	8326.	10.95	257.9	3.1
2019	410	6468.	8540.	2072.	7071.	-15.07	471.6	6.7
2020	375	7438.	8598.	1160.	7880.	11.44	277.2	3.5
2021	399	7639.	8673.	1035.	7978.	1.24	191.1	2.4
2022	376	7015.	9162.	2147.	7455.	-6.56	393.6	5.3
2023	390	6455.	8219.	1764.	7027.	-5.74	360.9	5.1
2024	379	7269.	9023.	1754.	7553.	7.49	231.9	3.1
2025	405	6053.	8637.	2584.	6928.	-8.28	575.1	8.3
2026	342	6575.	9257.	2682.	7136.	3.00	459.7	6.4
2027	314	6303.	8844.	2541.	6997.	-1.95	537.4	7.7
2028	360	3760.	8144.	4384.	5460.	-21.97	1156.2	21.2
2029	368	2567.	3539.	972.	3389.	-37.93	208.6	6.2
2030	344	3366.	4114.	749.	4003.	18.11	135.4	3.4
2031	370	3852.	4669.	817.	4590.	14.66	88.2	1.9
2032	387	4010.	4869.	858.	4738.	3.23	124.0	2.6
2033	283	4268.	4769.	501.	4639.	-2.09	84.5	1.8
<b>Avg</b>	<b>7931</b>	<b>6160.</b>	<b>7692.</b>	<b>1532.</b>	<b>6742.</b>	<b>8.68</b>	<b>293.2</b>	<b>4.5</b>

Table 5(d)

## Waste Package Power Data (watts/package)

LENDING OPTION USED LVY11632 (3000 MTU LAG) 3K MTU/YR - YFP(10) w/ FT

\* Packages containing 32 assemblies

Year	No. WP	Min	Max	Max - Min	Mean	± Del	S.D.	C.V.
010	23	7895.	8455.	560.	8219.	0.00	186.9	2.3
011	34	6552.	8217.	1666.	7642.	-7.02	550.7	7.2
012	81	6571.	8983.	2412.	8158.	6.75	764.9	9.4
013	140	6632.	8208.	1575.	7344.	-9.97	358.5	4.9
014	156	6749.	7950.	1202.	7289.	-0.75	434.2	6.0
015	174	6987.	9022.	2035.	8280.	13.58	760.9	9.2
016	174	6414.	8820.	2406.	7469.	-9.80	421.4	5.6
017	182	6547.	8589.	2042.	7670.	2.70	676.3	8.8
018	174	7046.	9727.	2680.	8934.	16.48	762.9	8.5
019	156	6100.	8813.	2713.	6686.	-25.17	346.2	5.2
020	187	6145.	9009.	2864.	7571.	13.25	867.9	11.5
021	158	6204.	8852.	2648.	7174.	-5.24	343.4	4.8
022	192	6726.	8988.	2261.	7858.	9.53	515.9	6.6
023	160	5006.	9067.	4060.	6775.	-13.79	1079.3	15.9
024	182	4825.	8855.	4030.	6869.	1.40	915.8	13.3
025	164	5709.	8987.	3278.	7461.	8.61	990.1	13.3
026	202	5263.	8441.	3177.	6695.	-10.27	898.7	13.4
027	234	2788.	8477.	5689.	5711.	-14.69	1750.9	30.7
028	210	2179.	7691.	5512.	3436.	-39.84	1527.2	44.5
029	214	2502.	3232.	729.	3081.	-10.33	179.0	5.8
030	233	3035.	3714.	679.	3580.	16.21	184.7	5.2
031	189	3480.	4713.	1233.	4475.	24.99	242.4	5.4
032	187	3553.	4904.	1350.	4512.	0.82	366.3	8.1
033	89	3064.	5362.	2297.	4104.	-9.05	856.0	20.9
Avg	3895	5332.	7795.	2462.	6541.	11.75	665.9	11.1

\*WR Packages containing 16 assemblies

Year	No. WP	Min	Max	Max - Min	Mean	± Del	S.D.	C.V.
2010	25	8591.	10112.	1522.	9432.	0.00	383.0	4.1
2011	58	9184.	10622.	1437.	10224.	8.39	226.3	2.2
2012	108	9778.	10948.	1170.	10161.	-0.62	217.7	2.1
2013	172	9353.	10672.	1319.	10390.	2.26	321.8	3.1
2014	294	9619.	10393.	774.	10010.	-3.66	134.4	1.3
2015	301	9687.	10511.	823.	9948.	-0.62	144.7	1.5
2016	291	10285.	11254.	969.	10692.	7.48	205.9	1.9
2017	283	9521.	11449.	1928.	10005.	-6.43	355.6	3.6
2018	290	10348.	12527.	2179.	11100.	10.95	335.0	3.0
2019	307	8621.	11096.	2474.	9427.	-15.07	626.3	6.6
2020	281	9818.	11464.	1645.	10505.	11.43	371.0	3.5
2021	300	10193.	11564.	1371.	10638.	1.27	256.1	2.4
2022	281	9353.	12194.	2840.	9939.	-6.58	523.1	5.3
2023	293	8607.	11197.	2589.	9371.	-5.72	484.8	5.2
2024	284	9600.	12031.	2431.	10069.	7.45	309.6	3.1
2025	304	8071.	11499.	3428.	9241.	-8.23	767.9	8.3
2026	257	8766.	12343.	3576.	9513.	2.95	611.2	6.4
2027	235	8404.	11792.	3388.	9329.	-1.93	714.5	7.7
2028	270	5014.	10858.	5844.	7283.	-21.93	1542.0	21.2
2029	276	3423.	4719.	1296.	4519.	-37.96	277.2	6.1
2030	258	4520.	5486.	966.	5336.	18.08	181.7	3.4
2031	278	5169.	6226.	1057.	6119.	14.67	119.3	1.9
2032	290	5281.	6492.	1210.	6317.	3.24	166.2	2.6
2033	212	5691.	6359.	668.	6185.	-2.10	112.6	1.8
Avg	5948	8204.	10158.	1954.	8990.	8.65	391.2	4.5

Table 5(e)

## Waste Package Power Data (watts/package)

BLENDING OPTION USED LVY12140 (3000 MTU LAG) 3K MTU/YR - YFF(10) w/ FT

## B. Packages containing 40 assemblies

Year	No. WP	Min	Max	Max - Min	Mean	± Del	S.D.	C.V.
2010	18	9869.	10568.	700.	10284.	0.00	231.8	2.3
2011	28	8189.	10272.	2083.	9559.	-7.05	670.4	7.0
2012	64	8394.	11206.	2812.	10193.	6.63	956.8	9.4
2013	112	8404.	11004.	2600.	9186.	-9.88	471.4	5.1
2014	125	8436.	9938.	1502.	9113.	-0.79	543.3	6.0
2015	140	8734.	11279.	2545.	10352.	13.60	951.5	9.2
2016	139	8061.	9919.	1858.	9328.	-9.89	507.1	5.4
2017	145	8179.	10735.	2556.	9586.	2.77	848.0	8.8
2018	140	8808.	12158.	3350.	11171.	16.53	954.1	8.5
2019	124	7634.	8903.	1269.	8340.	-25.34	377.0	4.5
2020	150	7672.	11261.	3589.	9464.	13.48	1087.9	11.5
2021	126	7764.	10429.	2665.	8966.	-5.26	411.5	4.6
2022	153	8274.	11230.	2956.	9819.	9.50	649.8	6.6
2023	129	6253.	11333.	5080.	8475.	-13.68	1354.0	16.0
2024	145	6068.	11071.	5003.	8597.	1.43	1130.7	13.2
2025	132	6984.	11233.	4249.	9310.	8.29	1255.1	13.5
2026	161	6579.	10562.	3983.	8374.	-10.05	1127.3	13.5
2027	187	3509.	10586.	7077.	7146.	-14.66	2182.0	30.5
2028	168	2728.	9620.	6892.	4295.	-39.89	1915.5	44.6
2029	171	3127.	4040.	913.	3850.	-10.38	225.5	5.9
2030	187	3816.	4642.	827.	4474.	16.21	232.6	5.2
2031	151	4350.	5891.	1541.	5594.	25.04	302.8	5.4
2032	149	4448.	6125.	1677.	5638.	0.78	457.3	8.1
2033	72	3830.	6702.	2872.	5141.	-8.82	1071.9	20.9
<b>Avg</b>	<b>3116</b>	<b>6671.</b>	<b>9613.</b>	<b>2942.</b>	<b>8177.</b>	<b>11.74</b>	<b>829.8</b>	<b>11.1</b>

## PWR Packages containing 21 assemblies

Year	No. WP	Min	Max	Max - Min	Mean	± Del	S.D.	C.V.
2010	19	11373.	13429.	2056.	12383.	0.00	517.7	4.2
2011	44	12082.	14098.	2016.	13416.	8.35	345.3	2.6
2012	82	12741.	14510.	1768.	13333.	-0.62	317.4	2.4
2013	132	12043.	14128.	2085.	13638.	2.29	444.1	3.3
2014	224	12370.	13993.	1623.	13137.	-3.68	253.7	1.9
2015	229	12480.	14194.	1714.	13057.	-0.61	279.9	2.1
2016	221	13135.	15104.	1969.	14034.	7.49	356.6	2.5
2017	216	12417.	16339.	3922.	13134.	-6.42	548.9	4.2
2018	221	13301.	16468.	3168.	14567.	10.92	489.1	3.4
2019	234	11248.	14904.	3657.	12376.	-15.04	870.7	7.0
2020	214	12848.	15644.	2796.	13786.	11.39	556.7	4.0
2021	228	13012.	14915.	1903.	13962.	1.28	441.7	3.2
2022	215	12133.	16598.	4465.	13050.	-6.53	754.6	5.8
2023	223	11259.	14896.	3637.	12299.	-5.75	692.0	5.6
2024	216	12389.	15883.	3494.	13214.	7.44	499.0	3.8
2025	232	10588.	15650.	5062.	12133.	-8.18	1058.2	8.7
2026	196	11357.	16326.	4969.	12485.	2.90	859.8	6.9
2027	179	10937.	16161.	5225.	12245.	-1.92	999.3	8.2
2028	206	6578.	14796.	8218.	9554.	-21.97	2049.6	21.5
2029	210	4320.	6227.	1907.	5930.	-37.93	372.3	6.3
2030	197	5939.	7217.	1278.	7004.	18.11	246.3	3.5
2031	211	6581.	8279.	1698.	8033.	14.69	174.8	2.2
2032	221	6766.	8581.	1814.	8291.	3.21	228.1	2.8
2033	162	7327.	8384.	1057.	8118.	-2.08	175.3	2.2
<b>Avg</b>	<b>4532</b>	<b>110634.</b>	<b>13614.</b>	<b>2979.</b>	<b>11799.</b>	<b>8.64</b>	<b>563.8</b>	<b>4.9</b>

Table 7(a)  
 YFF(10) w/ Flowthrough

Watts/MTU for BWRs

Age in years: 23.46  
 Age burnup : 32236.25  
 Average enrichment : 3.10  
 Total MTUs of BWRs : 22253.16

yrs decay	watts/MTU
0	860.14
1	844.64
2	829.66
3	815.06
4	800.84
5	787.13
7	762.48
10	724.45
15	668.42
20	618.66
30	534.55
50	413.05
100	259.45
300	133.78
500	98.41
1000	56.29
5000	18.34
10000	13.34

Table 7(b)  
 YFF(10) w/ Flowthrough

Watts/MTU for PWRs

Age in years: 22.48  
 Average burnup : 42210.76  
 Average enrichment : 3.92  
 Total MTUs of PWRs : 40747.22

yrs decay	watts/MTU
0	1126.24
1	1104.72
2	1084.28
3	1064.25
4	1044.80
5	1025.98
7	991.54
10	940.81
15	865.14
20	798.19
30	685.53
50	523.46
100	319.48
300	156.42
500	114.27
1000	66.54
5000	23.25
10000	16.89

Table 7(c)  
YFF(10) w/ Flowthrough

Watts/MTU for Average Weighted Package

! MTUs of PWRs & BWRs: 63000.38

yrs decay	watts/MTU
0	1032.24
1	1012.85
2	994.34
3	976.23
4	958.63
5	941.61
7	910.63
10	864.39
15	795.65
20	734.78
30	632.20
50	484.46
100	298.28
300	148.42
500	108.66
1000	62.92
5000	21.52
10000	15.64

**APPENDIX E**

**WASTE PACKAGE CORROSION RATES**

**David Stahl**

**Interoffice Correspondence**  
**Civilian Radioactive Waste Management System**  
**Management & Operating Contractor**



TRW Environmental  
Safety Systems Inc.

WBS: 1.2.2  
QA: N/A

**Subject:**  
Waste Package Corrosion Inputs

**Date:**  
June 21, 1993  
LV.WP.DS.06/93-107

**From:**  
D. Stahl

**To:**  
R. Memory  
S. Saterlie

**cc:**  
H. Benton  
K. McCoy  
R. Fish  
A. Roy  
B. Mann ✓

**Location/Phone**  
TES3/P110  
(702)794-7778  
  
CF-DS (M106)

This IOC is a follow up to IOC DS.03/93-048 dealing with Waste Package Inputs and concentrates on values (and variability) for dry oxidation and aqueous corrosion of the iron-based overpack as a function of time and temperature.

Dry oxidation data for iron-based materials in the 100-250°C is almost non-existent. Most of the data on dry oxidation is from atmospheric exposures over long periods in various environments including rural, semi-industrial, industrial, and marine. Data is available for many materials exposed for up to 20 years. The data, with the exception of those for marine environments, tend to fit an exponential equation with corrosion rates decreasing with time, suggesting the establishment of a protective film. (The chloride present in the mist in marine environments tends to inhibit the formation of protective films.) The time exponent usually falls between 0.3 and 0.6. Previously, this time effect was neglected in that a constant oxidation rate (20 µm/yr) was provided. From the environmental data given in the ASM Handbook for carbon steels I calculated an exponent of 0.57. This would yield an expression for penetration,  $P = 1.156 t^{0.57}$ , where t is in days. Thus, the penetration for one year is 33 µm, for two years it is 50 µm, and for 10 years it is 124 µm, which agrees with the data. The average penetration rates are then 33, 25 and 12 µm/yr, for one, two and ten years, respectively. The variation is on the order of +/- 25%.

The ASM Handbook provides one set of data at elevated temperature, 454°C (850°F) and 538°C (1000°F), for air oxidation of carbon steels for about one year. (Data, also are provided for a steam atmosphere which were similar.) The time exponent was about 0.3, suggesting that a more tenacious oxide film is developing at the higher temperatures than at the ambient temperatures discussed above. The penetration equations from the data provided are  $P = 2.01 t^{0.33}$  for 454°C and  $P = 5.35 t^{0.33}$  for 538°C. For one year, the penetrations would be 14 and 38 µm, respectively.

If the same process can be extrapolated to lower temperatures, then the penetration equation would follow the same form with the same exponent, but with a different coefficient. The coefficient can be estimated by using an Arrhenius approach (where the temperature effect is proportional to  $e^{-Q/RT}$ ) by plotting the data vs 1/T, where T is the absolute temperature, (Q is the activation energy, and R is the gas constant). (The coefficients for 300°C and 200°C are 0.2 and 0.02, respectively.) The activation energy for this process, which is presumably due to diffusion of oxygen through the oxide film, was calculated to be 57.1 kJ/mol. This compares favorably to data provided in a review by

**Interoffice Correspondence**  
**Civilian Radioactive Waste Management System**  
**Management & Operating Contractor**



**TRW Environmental**  
**Safety Systems Inc.**

R. Freer, which gives the activation energy for the diffusion of oxygen in FeO as 83.6 kJ/mol and in Fe<sub>3</sub>O<sub>4</sub> as 71 kJ/mol. The value of Q (57.1 kJ/mol), when divided by R, which is 8.3143 J/K-mol, yields a value of Q/R of 6870. Thus, the entire equation for penetration can now be written as  $P = 25,500 t^{0.33} e^{-6870/T}$ . If an expression for penetration is needed in years, the equation becomes  $P = 178,700 t(y)^{0.33} e^{-6870/T}$ .

This approach provides much smaller penetration values for temperatures in the range of repository interest. For example, the penetration at 200°C would be 0.09, 0.19, 0.40, 0.86 and 1.84 μm, after 1, 10, 100, 1000 and 10,000 years, respectively. The error is likely to be larger because of the method of extrapolation. However, even at 100%, these values are very low, which would make degradation by dry oxidation negligible.

The available data for corrosion of carbon steels in aqueous environments were also reviewed. Most of the data are for flowing river waters. These data follow a time dependency with an exponent ranging from 0.5 to 0.8. One set of data relate to static exposure in Gatun Lake for up to 16 years. This set of data was used by Westinghouse as their basis for design of waste packages in tuff. The time dependency was found to have an exponent of 0.47. From this data, they generated an equation for penetration,  $P = 200 t(y)^{0.47}$ , with P in μm.

The Westinghouse report also estimates the effect of temperature using a very limited data set for corrosion rate of cast steel and iron in brine and seawater. They found a value of Q/R of 2850. From a very sparse data set in a report by S. Pednekar, I determined a value of Q/R to be 2300. Thus the temperature effect from Westinghouse may represent conditions adequately for carbon steels in static waters. This report provides a combined penetration equation,  $P = 2,525,000 t(y)^{0.47} e^{-2850/T}$ . They estimated an error band of about +/- 25%. The penetration at 100°C would be 1.2, 3.6, 10.6, 31.2 and 92.0 mm for 1, 10, 100, 1000 and 10,000 years, respectively. The corrosion rate for these periods would then be 1.2, 0.36, 0.11, 0.03 and 0.01 mm/yr (or 48, 14.4, 4.4, 1.2 and 0.37 mils/yr). The calculated penetrations at 50°C would be 30% of those calculated at 100°C. The Westinghouse report also evaluates a pitting factor which is the ratio of pitting attack to general corrosion. The Gatun Lake data set yields a range from 2.6-3.4. (They then use a value of 4.0 for conservatism.) This is roughly consistent with values obtained for pitting factor by D. McCright of about 0.9-3.2. The pitting factor would be used as a multiple of the penetrations calculated using the above equation.

The recommended penetration equations can then be summarized as follows:

For high-temperature oxidation,  $P = 178,700 t(y)^{0.33} e^{-6870/T}$ .

For general corrosion,  $P = 2,525,000 t(y)^{0.47} e^{-2850/T}$ .

For general corrosion with a pitting factor,  $P = 10,100,000 t(y)^{0.47} e^{-2850/T}$ .

**APPENDIX F**

**WASTE PACKAGE CORROSION RATES**

**Alan Lamont**

*Preliminary, for discussion only.  
Not yet approved by all interested parties.*

June 23, 1993

**To:** YMIM Development File  
**From:** Alan Lamont  
**Subject:** Calibration of Corrosion Models in YMIM

## **Introduction**

The structure of the corrosion models in YMIM are described in the memo titled "Notes on Corrosion Models in YMIM". That memo provides the theory and the functional forms of the models and defines the parameters for them. This memo documents the process of deriving the required parameters which were calibrated based on judgements of corrosion experts at LLNL. The necessary data were elicited through an interview with Drs. D. McCright and D. Jones. The data were elicited as judgements about corrosion behavior in a format that was most natural for the experts. In several cases the form that was most natural for the experts was not the form directly required by YMIM. Some calculations were required to determine the values of the parameters actually used by the corrosion models in YMIM.

## **Dry Oxidation**

This is expected to be negligible. However, values from the "Degradation Mode Survey" can be used.

## **General Wet Oxidation**

As is described in the Memo "Description of Corrosion models in YMIM", the relationship between general wet oxidation rate and temperature is modeled as an inverted "U", with its maximum corrosion rate occurring at a temperature that is somewhat less than 100°C. In the current version of YMIM, this is modeled as a quadratic function which can be parameterized by: 1) the maximum corrosion rate, 2) the temperature corresponding to the maximum corrosion rate, 3) the corrosion rate at a lower temperature (i.e. near ambient), and 4) the value of the temperature corresponding to the lower corrosion rate.

*Preliminary, for discussion only.  
Not yet approved by all interested parties.*

Currently it is anticipated that the general wet oxidation mode will apply to the mild steel outer wall in a double wall container. Thus data were only obtained for mild steel. The values elicited for corrosion rates and temperatures were:

Maximum corrosion rate: 15 mils/yr (0.38 mm/yr) at 80°C

Lower corrosion rate: 5 mils/yr (0.12 mm/yr) at 20°C

As a means of checking the model one can calculate the corrosion rate at a temperature of 100°C. It was estimated that the corrosion rate at 100°C should be of the order of 8 mils/yr (0.2 mm/yr).

### **Probabilistic Pitting Model**

The probabilistic pitting model is calibrated by eliciting information about the distribution of annual pitting rates at two different temperatures. Using this information, the parameters required by the model are calculated.

In calibrating the pitting model two kinds of uncertainty, or variability are accounted for. First, the pitting model assumes that there will be variability in the actual pit depths that are measured across a container and between containers. Thus the pitting depths (or rates) that would exist during one period of a model run are represented as a probability distribution and not a point estimate.

In addition, there is uncertainty about the parameters of the distribution over pitting rates: the actual average pitting rate could be high or low. In conducting analyses of performance, this component of the uncertainty would be taken into account by making several runs, or through multiple realizations in simulation analysis.

Therefore, distributions were elicited for three conditions. The first represents a high condition—it is unlikely that the average pitting rate would be greater than the average of this distribution. The experts felt that there was only a chance of about 5% that the actual distribution would have a mean higher than this. The second represents a median condition—the mean of the actual distribution over pitting rates is roughly as likely to be smaller than this as it is to be larger. The third represents a low condition—it is unlikely that the actual mean pitting rate would be smaller than this. Again, the

*Preliminary, for discussion only.  
Not yet approved by all interested parties.*

experts felt that the chance that the actual mean would be smaller than this is in the order of 5%.

The values elicited from the experts are shown in Table 1. These elicitations were made in terms that were familiar to the experts. Additional calculations are needed to determine the corresponding parameters needed by the model. The discussion will illustrate the derivation of the model parameters using the median distribution at a temperature of 100°C. The parameters for the all the distributions are given in Table 2 at the end.

The basic data elicited for each condition and temperature were the mean and the 95th percentile of the growth rate. For the median distribution at 100°C it was judged that the mean pitting rate would be around 0.1 mm/yr. It was also judged that about 5% of the pits would grow at a rate about ten times the mean, or 1.0 mm/yr. The full set of judgements is presented in Table 1.

**Table 1: Summary of judgments used for estimating pitting model parameters**

Growth Condition	Temp = 70°C		Temp = 100°C	
	Mean growth, mm/yr	95th percentile, mm/yr	Mean growth, mm/yr	95th percentile, mm/yr
Low growth rate	0.0001	0.001	0.01	0.1
Median growth rate	0.001	0.01	0.1	1.0
High growth rate	0.01	0.1	1.0	10.0

To calibrate the parameters of the corrosion model we need to derive a mean and variance of the distribution using this data. The mean is given. As is discussed in the companion memo "Notes on Corrosion Models in YMIM", the underlying model of pit growth assumes that the pits grow randomly in increments and that the probability that a pit will grow by an increment is independent of its current depth. Consequently, it can be assumed that in the long

*Preliminary, for discussion only.  
Not yet approved by all interested parties.*

term, the pit depths will have a Normal probability distribution. Given the mean and the 95th percentile of the distribution, the variance can be calculated as follows: For the Normal distribution, the difference between the mean value and the 95th percentile value is equal to 1.645 times the standard deviation. Since in this case the difference is equal to  $(1.0 - 0.1)$  mm/yr, the standard deviation equals  $(0.9 / 1.645)$  or 0.547 mm. The variance of the annual growth equals 0.299 mm<sup>2</sup>.

From the memo "Notes on Corrosion Models in YMIM", the Poisson model of pit growth is parameterized by the expected rate of growth increments,  $\rho$ , and size of the increment of growth,  $g$ . To calibrate the parameters we have the relationships:

$$E(G) = g \rho t$$

and

$$\text{Var}(G) = g^2 \rho t$$

where

- G = total growth in a period of time,
- $\rho$  = expected number of growth increments per unit time,
- g = the incremental growth, when a pit grows, and
- t = the length of the period under consideration.

In this case, the time period is one year so  $t=1$ , since the data are given in terms of annual growth rates.

The above relationships lead to the following equations for  $g$  and  $\rho$ :

$$\rho = E^2(G)/\text{Var}(G)$$

$$g = E(G)/\rho$$

Given the values for the mean and variance of annual growth, the values of  $g$  and  $r$  for this case are:

$$\rho = 0.033$$

$$g = 2.994 \text{ mm}$$

*Preliminary, for discussion only.  
Not yet approved by all interested parties.*

The judgements used for estimating the parameters in all the cases are shown in Table 1 above. These values were used to calculate  $g$  and  $\rho$  using the procedure outlined above. Table 2 presents the resulting estimates.

**Table 2: Estimates of parameters of pitting model based on expert judgements**

Growth Condition	Temp = 70°C		Temp = 100°C	
	$g$ , mm	$\rho$	$g$ , mm	$\rho$
Low growth rate	0.003	0.033	0.299	0.033
Median growth rate	0.030	0.033	2.994	0.033
High growth rate	0.299	0.033	29.939	0.033

**APPENDIX G**

**SOLUBILITY DATA AND EXPERT ELICITATION RESULTS**

**Carl Bruch and Inez Triay**

10/10/93 10:00 AM  
A 10 10

Environmental  
Systems Inc.

101 Convention Center Drive, Suite 540  
Las Vegas, NV 89109  
702.794.1800

22 June 1993

Dear Ines,

I have completed an initial solubility data set for TSPA-II. It draws heavily on the expert elicitation that we attended at Sandia on 13 April and on the work of Nitsche et al. Due to the lack of consistent temperature-dependent data, we were able to incorporate the effects of temperature on solubility for many radionuclides. I have also enclosed some of my own comments and questions on it. Could you please review the data set and comments for accuracy and sensibility? I would appreciate any suggestions that you may have.

If you have any questions, please call me at (702) 794-1856. Thank you for your time.

Sincerely,



Table B.2.1: Proposed Solubilities for TSPA-II

RN	Solubility (g/m <sup>3</sup> )	Functional Form	Source
Ac	f(T)—Same as Am	Same as Am	Elicitation, Nitsche et al.
Am	f(T)	See Table B.2.1.a	Nitsche et al.
C	NA (gaseous)	NA (gaseous)	Golder
Cm	f(T)	T ≤ 55°C, [LT: 1.2e-6, 1.2e-5, 1.2e-4] T > 55°C, [LT: 1.5e-10, 1.5e-9, 1.5e-8]	Wilson
Cs	LT: 1.2, 3.9e+2, 2.1e+3	LT: 1.2, 3.9e+2, 2.1e+3	Golder, EPRI
I	NA (gaseous)	NA (gaseous)	Golder
Nb	LU: 9.3e-5, 9.3e-3	LU: 9.3e-5, 9.3e-3	Elicitation
Ni	LB: 5.9e-2, 5.9e+3, 105, 0.25	10**[2.0212*(0.25*DIST3+1)]	Elicitation
Np	f(T)	See Table B.2.1.b	Nitsche et al.
Pa	LU: 2.3e-5, 2.3	10**[5*DIST2-4.6383]	Elicitation
Pb	LB: 2.1e-3, 2.1, 6.6e-2, 0.08	10**[-1.1805*(0.08*DIST3+1)]	Elicitation
Pu	f(T)	See Table B.2.1.c	Nitsche et al.
Ra	LB: 2.3e-4, 2.3, 2.3e-2, 0.1	10**[-1.6383*(0.1*DIST1+1)]	Elicitation
Se	LT: 7.9e+2, 7.9e+3, 5.5e+5	LT: 7.9e+2, 7.9e+3, 5.5e+5	Golder, EPRI
Sm	f(T)—Same as Am	Same as Am	Elicitation, Nitsche et al.
Sn	U: 1.3e-6, 1.3e-2	0.013*DIST2+1.3e-6	Elicitation
Sr	LB: 9.0e-2, 90, 9.0, 0.12	10**[0.9542*(0.12*DIST1+1)]	Elicitation
Tc	LT: 3.5e-2, 1e+2, 9.9e+5	LT: 3.5e-2, 1e+2, 9.9e+5	Golder, EPRI
Th	LU: 2.3e-5, 2.3e-2	10**[3*DIST2-4.6383]	Elicitation
U	f(T)—Same as Np	Same as Np	Elicitation, Nitsche et al.
Zr	LU: 9.1e-8, 9.1e-3	10**[5*DIST2-7.0410]	Elicitation

All solubilities have units of g/m<sup>3</sup>.

DIST1=Normal distribution with  $\mu=0$  and  $\sigma=1$ ; for Ra and Sr.

DIST2=0 to 1; Uniform; for Pa, Sn, Th, Zr.

DIST3=Normal distribution with  $\mu=0$  and  $\sigma=1$ ; for Ni and Pb.

pH=6 to 9, uniform.

LB=log-beta distribution; min, max, expected value, coefficient of variation. These are approximated by a log-normal distribution.

LT: log-triangular distribution; min, expected value, max.

LU=log-uniform distribution; min, max.

N: normal distribution; mean, standard deviation.

U=uniform distribution; min, max.

Table B.2.1.a: Temperature- and pH-dependent solubilities for Am

pH	Solubility for the given temperature range		
	$T \leq 42.5^{\circ}\text{C}$	$42.5^{\circ}\text{C} < T < 75^{\circ}\text{C}$	$75^{\circ}\text{C} < T$
$\leq 6.5$	N: 4.4e-4, 1.5e-4	N: 6.1e-1, 1.7e-1	N: 4.1e-4, 4.1e-4
$6.5 < \text{pH} \leq 7.75$	N: 2.9e-4, 0.7e-4	N: 2.4e-3, 2.2e-3	N: 7.5e-5, 4.1e-5
$> 7.75$	N: 5.8e-4, 4.6e-4	N: 2.9e-3, 2.9e-3	N: 8.3e-5, 5.1e-5

Table B.2.1.b: Temperature- and pH-dependent solubilities for Np

pH	Solubility for the given temperature range		
	$T \leq 42.5^{\circ}\text{C}$	$42.5^{\circ}\text{C} < T < 75^{\circ}\text{C}$	$75^{\circ}\text{C} < T$
$\leq 6.5$	N: 1.3e+3, 0.07e+3	N: 1.5e+3, 0.09e+3	N: 2.8e+2, 0.2e+2
$6.5 < \text{pH} \leq 7.75$	N: 3.1e+1, 0.5e+1	N: 2.3e+2, 0.2e+2	N: 3.6e+1, 0.9e+1
$> 7.75$	N: 1.0e+1, 0.2e+1	N: 2.4e+1, 0.2e+1	N: 2.1e+1, 0.09e+1

Table B.2.1.c: Temperature- and pH-dependent solubilities for Pu

pH	Solubility for the given temperature range		
	$T \leq 42.5^{\circ}\text{C}$	$42.5^{\circ}\text{C} < T < 75^{\circ}\text{C}$	$75^{\circ}\text{C} < T$
$\leq 6.5$	N: 2.6e-1, 1.0e-1	N: 6.5e-3, 2.6e-3	N: 1.5e-3, 0.5e-3
$6.5 < \text{pH} \leq 7.75$	N: 5.5e-2, 3.4e-2	N: 8.9e-3, 2.2e-3	N: 2.1e-3, 0.2e-3
$> 7.75$	N: 7.0e-2, 1.9e-2	N: 2.9e-2, 0.2e-2	N: 1.8e-3, 0.1e-3

ALTERNATIVE SOLUBILITIES FOR AM, NP, AND PU

Following is the way that we would implement the linear dependence in semi-log space. The slopes and y-intercepts are derived from the work of Nitsche et al.

SOLAM = 10**(SOLA)	solubility of Am
SOLA = T: SMINA, SA, SMAXA	log of the solubility of Am
SA = MAM x TEMP + BAM	expected value of the log of the solubility of Am
SMINA = S - 1	minimum value of the log of the solubility of Am
SMAXA = S + 1	maximum value of the log of the solubility of Am
MAM	slope of the line in semi-log space (for Am)
BAM	y-intercept of the line in semi-log space (for Am)

MAM=IF(pH<=6.5, MAM1, (IF(pH<=7.75, MAM2, MAM3)))  
MAM1=IF(TEMP<=333, 0.08977, -0.1057)  
MAM2=IF(TEMP<=333, 0.02623, -0.05017)  
MAM3=IF(TEMP<=333, 0.01997, -0.05143)  
BAM=IF(pH<=6.5, BAM1, (IF(pH<=7.75, BAM2, BAM3)))  
BAM1=IF(TEMP<=333, -30.11, 34.98)  
BAM2=IF(TEMP<=333, -11.35, 14.09)  
BAM3=IF(TEMP<=333, -9.188, 14.59)

The values for the slope and y-intercept above were derived from work done by Nitsche et al. The table below summarizes the slopes and y-intercepts of the lines that join the logs of the solubilities.

Table B.2.1.a: Temperature- and pH-dependent solubilities for Am

pH	Slope and y-intercept of the line in semi-log space of the solubility for the given temperature range			
	T<=333K		T>333K	
	m	b	m	b
≤ 6.5	0.08977	-30.11	-0.1057	34.98
6.5<pH≤7.75	0.02623	-11.35	-0.05017	14.09
> 7.75	0.01997	-9.188	-0.05143	14.59

The dependencies for Np and Pu would be implemented in a similar manner with the values for the slope and y-intercept drawn from the following two tables.

Table B.2.1.b: Temperature- and pH-dependent solubilities for Np

pH	Slope and y-intercept of the line in semi-log space of the solubility for the given temperature range			
	T<=333K		T>333K	
	m	b	m	b
≤ 6.5	0.001771	2.586	-0.02430	11.27
6.5<pH≤7.75	0.02489	-5.926	-0.02687	11.31
> 7.75	0.01086	-2.236	-0.001993	2.024

Table B.2.1.c: Temperature- and pH-dependent solubilities for Pu

pH	Slope and y-intercept of the line in semi-log space of the solubility for the given temperature range			
	T ≤ 333K		T > 333K	
	m	b	m	b
≤ 6.5	-0.04577	13.05	-0.02123	4.882
6.5 < pH ≤ 7.75	-0.02260	5.475	-0.02090	4.909
> 7.75	-0.01094	2.105	0.04023	11.86

Date: 22 June 1993

Re: Comments on Proposed Solubilities for TSPA-II

1) For the radionuclides whose solubilities were assumed to behave similarly, we assumed that they were scaled precisely in the range of values given. Some "slop" should be incorporated eventually, but how much and in what manner?

As per the elicitation, the groups of radionuclides whose solubilities behave similarly were taken to be

- 1) Ra and Sr
- 2) Pa, Sn, Th, and Zr
- 3) Ni, Pb
- 4) Np, U
- 5) Ac, Am, and Sm.

For the first three groups, very little temperature-dependent data is available. Thus, the solubilities were assumed to be those elicited (which were valid for  $25^{\circ}\text{C} \leq T \leq 95^{\circ}\text{C}$ ,  $6 \leq \text{pH} \leq 9$ , and all groundwater compositions expected at the proposed repository). For the fourth and fifth groups, the most detailed and recent data (Nitsche et al., 1993) were for Np and Am, respectively. As per the elicitation, the solubilities of the other members of the groups were correlated directly to the solubilities of Np and Am.

As can be readily seen from Table B.1.2, the groundwater composition is very important in determining the temperature and pH dependence of the solubilities. In fact, even the trends are dependent on the composition. We tentatively chose to use the solubilities corresponding to J-13 water for four reasons: 1) The water from J-13 (tuff aquifer) is probably more representative of the water that will be found at the proposed repository than the water from UE-25p#1 (carbonate aquifer); 2) Most of the previous solubility work has assumed J-13 water, and this is consistent with PNL's TSPA-91 efforts; 3) More temperature-dependent data is available for J-13 in the work by Nitsche et al.; and 4) The solubilities of Np and Pu do not vary more than an order of magnitude between the two waters.

2) Invariably, there are only two or three temperatures for which solubilities are available. When incorporating the data into TSPA-II, we could assume step functions, linear dependence, quadratic dependence, or exponential dependence (probably on absolute temperature, rather than Celsius). We do not know how which form is most appropriate. The series of three step functions perhaps best represents our limited experimental data. This means that we are left with the task of choosing the temperatures at which the step functions occur. For simplicity, we have chosen the midpoints ( $42.5^{\circ}\text{C}$  and  $75^{\circ}\text{C}$ ) between the measured temperatures ( $25^{\circ}\text{C}$ ,  $60^{\circ}\text{C}$ , and  $90^{\circ}\text{C}$ ).

There is a problem associated with this sort of division of step functions. The consistent trend toward lower solubilities at  $90^{\circ}\text{C}$  is presumably because there is less oxygen dissolved in the water at high temperatures, but where should we draw the line? We have chosen the mid-point,  $75^{\circ}\text{C}$ , but  $80^{\circ}\text{C}$  or even  $85^{\circ}\text{C}$  might be more appropriate. Likewise, the lower division at  $42.5^{\circ}\text{C}$  might not be the best choice, but until we have more information this is the most reasonable one. By placing the transition at  $75^{\circ}\text{C}$ , we have set the solubility at its lowest value. From the thermal-hydrologic modeling exercises being undertaken, we believe that the repository could be in the  $75\text{-}97^{\circ}\text{C}$  range for thousands of years. Thus, the effect of underestimating the solubility on the total-system performance would be significant.

An alternative way of utilizing the work of Nitsche et al. is to assume a linear dependence on temperature in either linear or semi-log space. We have included the latter as a possible alternative: the log of the solubility is plotted versus the absolute temperature. Between data points, straight lines are drawn. To account for the effects of uncertainty and variability, the solubility is a triangular distribution centered about the line and extending up and down 1 unit. When the solubility is backed out, it is then a log-triangular distribution centered about the predicted temperature that extends on order of magnitude in either direction.

Given your general understanding of solubility kinetics and the state of site-specific data, do you have a preference for one implementation of the data over another? Are there general dependencies that would be good to follow?

3) Some of the solubilities that were elicited had log-beta distributions. These are hard to transform (when considering "linked" solubilities), so they were approximated using log-normal distributions. The differences are negligible for all, but perhaps Ni. For Ni, the log-normal distribution is broader, extends farther to the higher values, and has a slightly higher mean value. Thus, the log-normal distribution is nominally conservative with respect to the log-beta distribution.

To transform from a standard normal distribution  $Z$  ( $\mu_0=0$ ,  $\sigma_0=1$ ) to an arbitrary normal distribution  $X$  ( $\mu$ ,  $\sigma$ ), one uses

$$X = \sigma Z + \mu$$

The coefficient of variation,  $c_v$ , is defined as

$$c_v = s/x = \sigma/x,$$

where  $x$  is the mean value. Thus,

$$\sigma = xc_v = \mu c_v,$$

and

$$X = \mu[c_v Z + 1].$$

The transformation from a standard uniform distribution  $Y$  (from 0 to 1) to an arbitrary uniform distribution  $X$  (from  $C$  to  $D$ ) is much simpler:

$$X = LY + C,$$

where the length  $L$  of the interval is

$$L = D - C.$$

4) For Cm, I used Wilson's measured solubilities (using J-13 groundwater). He did not have any estimate of the error, so I used a log-triangular distribution that extended an order of magnitude in each direction. The temperature at which it switched was selected to be the mid-point, but I do not feel this is reasonable (does LANL have any suggestions?)

Table B.1.1: Nominal radionuclide solubilities.

	Solubilities for TSPAs (often generated using expert judgement)						Model-generated					Experimentally generated		
	Elicitation <sup>(1)</sup>	PNL <sup>(2)</sup>	SNL <sup>(3)</sup>	Goldler <sup>(4)</sup>	EPRJ <sup>(5)</sup>	Kerrisk <sup>(6)</sup>	Ogard and Kerrisk <sup>(7)</sup>	Kerrisk <sup>(8)</sup>	Pearson <sup>(9)</sup>	Wilson <sup>(10)</sup>	Nische et al. <sup>(11)</sup>	Nische and Edelstein <sup>(12)</sup>		
Ac	U: 2.3e-5, 2.3e-1	--	--	--	--	--	--	--	--	--	--	--		
Am	U: 2.4e-5, 2.4e-1, 1.2e-2	4.6e-3	LU: 2.9e-6, 9.2e-4, 1.6e-4	LT: 1.5e-7, 9.6e-2, 9.6e-1	LT: 1.5e-7, 9.6e-2, 9.6e-1	2.4e-3	1.7e-4 to 5.2e-3	2.4e-1	--	≤ 3e-4	2.9e-4 to 5.8e-4; 7.5e-2 to 7.5e-1	(2.7±0.5)e-1		
C	N/A: gaseous	high	--	NA	LT: 1, 1.4, 1.4e+2	large	--	large	--	≤ 1e-4	--	--		
Cm	--	--	--	LT: 2.4e-9, 9.6e-2, 9.1e-1	LT: 2.4e-9, 9.6e-2, 9.1e-1	--	--	2.5e-1	--	≤ 1.2e-5	--	--		
Cs	large	high	infinite	LT: 1.2, 3.9e2, 2.1e3	LT: 1.2, 3.9e2, 2.1e3	large	--	large	--	≤ 1.2	--	--		
I	large	high	infinite	NA	LT: 1, 3.9e+2, 1e+5	--	--	large	--	≤ 3e-3	--	--		
Nb	LU: 9.3e-5, 9.3e-3	--	--	LU: 1, 1e+5	LT: 1, 3.9e+2, 1e+5	--	--	--	--	--	--	--		
Ni	LN: 5.9e-2, 5.9e+3, 105, 0.25	--	--	LU: 5.9, 5.9e+4	--	--	--	5.9e+2	--	--	--	--		
Np	LN: 2.4e-3, 2.4e+3, 2.4, 2.25	9.5e-1	LU: 1.4e-5, 4.5e-3, 7.8e-4	LT: 4e-4, 3.6e+2, 7.1e+2	LT: 4e-4, 3.6e+2, 7.1e+2	7.1e+2	--	2.4e+2	3.3e-1	≤ 4e-4	1.0e+1 to 1.3e+3; 1.7 to 6.9e+2	(3.8±1.4)e+2; (1.7±0.2)e+2		
Pa	LU: 2.3e-5, 2.3	--	--	LU: 1, 1e+5	--	--	--	--	--	--	--	--		
Pb	LN: 2.1e-3, 2.1, 6.6e-2, 0.08	--	--	LU: 1, 1e+5	--	--	--	--	--	--	--	--		
Pd	--	--	--	LU: 1, 1e+5	--	--	--	--	--	--	--	--		

<b>Pu</b>	U: 2.4e-5, 2.4e-1, 1.2e-2	4.5e-6	LU: 3.8e-5, 1.2e-2, 2.1e-3	LT: 6e-5, 9.6e-4, 4.3e-1	LT: 6e-5, 9.6e-4, 4.3e-1	4.3e-1	7.4e-3 to 3.2	2.4	6e-2	≤ 5e-3	5.5e-2 to 2.6e-1; 1.1e-1 to 2.4e-1	0.33 to 12
<b>Ra</b>	LN: 2.3e-4, 2.3, 2.3e-2, 0.1	---	---	LU: 6.8e-4, 6.8	LT: 1e-5, 4e-4, 0.1	2.3e-2	2.1e-2 to 7.7e-2	6.8e-2	---	---	---	---
<b>Se</b>	large	high	infinite	LT: 7.9e+2, 7.9e+3, 5.5e+5	LT: 7.9e+2, 7.9e+3, 5.5e+5	---	---	---	---	---	---	---
<b>Sm</b>	like Am	---	---	LU: 3e-6, 3e-2	---	---	---	3.0e-4	---	---	---	---
<b>Sn</b>	U: 1.3e-6, 1.3e-2	high	LU: 1.3e-4, 4.0e-2, 6.9e-3	LT: 1.3e-4, 3.2e-3, 2.2e-2	LT: 1.3e-4, 3.2e-3, 2.2e-2	1.3e-4	---	1.3e-4	---	---	---	---
<b>Sr</b>	LN: 9.0e-2, 90, 9.0, 0.12	---	---	LU: 7e-1, 7e+3	---	8.5e+1	3.0e-1 to 4.7e+1	7.0e+1	---	≤ 3e-2	---	---
<b>Tc</b>	large	high	infinite	LT: 3.5e-2, 1e+2, 9.9e+5	LT: 3.5e-2, 1e+2, 9.9e+5	large	2.0e-7 to large	large	3.3e+1	≤ 3.5e-2	---	---
<b>Th</b>	LU: 2.3e-5, 2.3e-2	---	---	LU: 2.3e-6, 2.3e-2	---	---	---	2.3e-4	---	---	---	---
<b>U</b>	LN: 2.4e-3, 2.4e+3, 7.5, 2-25	8.6e+1	LU: 1.7e-5, 5.4e-3, 9.4e-4	LT: 5e-1, 2.4, 5e+1	LT: 5e-1, 2.4, 5e+1	4.9e+1	9.5e-3 to 4.1e+2	9.4e+2	5.5	≤ 5	---	---
<b>Zr</b>	LU: 9.1e-8, 9.1e-3, 9.1e-6	---	---	LU: 9.1e-8, 9.1e-4	---	---	---	9.1e-6	---	---	---	---

All solubilities are given in g/m<sup>3</sup>.

A preliminary evaluation by Tony Smith has concluded that the "important" elements (based on whole body dose due to the respective radionuclides) for TSPA-2 are Ac, Am, C, Cm, Cs, I, Nb, Ni, Np, Pa, Pb, Pu, Ra, Se, Tc, Th, and U. These elements are shown in bold in the left-hand column.

- [1] Solubility expert elicitation with LANL, held 13/4/93 at SNL. Although the distributions may incorporate experimental and modeling data, they are ultimately subjective estimates. The order of these entries is the shape of the distribution, the minimum value, the maximum value, the expected value or mean (optional), and the coefficient of variation (optional). The symbols for the distributions are U = uniform; LN = log-normal; and LU = log-uniform. At this workshop it was also stated that there were groups of radionuclides whose solubilities are highly correlated ("at least 80% rank correlation"). These were
- U, Np
  - Zr, Th, Pa, Sn
  - Am, Sm, Ac
  - Sr, Ra
  - Ni, Pb
- Furthermore, Pu has a medium correlation ("~60% rank correlation") with the group of radionuclides including Am, Sm, and Ac.
- [2] Eslinger, P.W., L.A. Doremus, D.W. Engel, T.B. Miley, M.T. Murphy, W.E. Nichols, M.D. White, D.W. Langford, and S.J. Ooderkirk, 1993. Preliminary Total-System Analysis of a Potential High-Level Nuclear Waste Repository at Yucca Mountain. PNL-8444, Pacific Northwest Laboratory, Richland, Washington. These solubilities were generated using EQ3/6 and are for oxidizing conditions, 44°C, and ??? water.
- [3] Barnard, R., M. Wilson, H. Dockery, J. Gauthier, P. Kaplan, R. Eaton, F. Bingham, and T. Robey. 1992. TSPA-1991: An Initial Total-System Performance Assessment for Yucca Mountain. SAND91-2795. Sandia National Laboratories, Albuquerque, New Mexico.
- [4] Golder Associates Inc., 1993. Application of RIP (Repository Integration Program) to the Proposed Repository at Yucca Mountain: Conceptual Model and Input Data Set. Golder Associates Inc., Seattle, Washington.
- [5] Risk Engineering, Inc., 1992. Demonstration of a Risk-Based Approach to High-Level Waste Repository Evaluation: Phase 2. EPRI TR-100384, Electric Power Research Institute, Pleasant Hill, California. These values consist of a review of the literature. The low, moderate, and high values are given.
- [6] Kerrisk, J. F., 1984. Solubility Limits on Radionuclide Dissolution At a Yucca Mountain Repository. LA-9995-MS, Los Alamos National Laboratory, Los Alamos, New Mexico. These solubilities were generated using EQ3/6 assuming J-13 water, oxidizing conditions (Eh of 700 mV), and pH 7. The solubilities for Ra, Sa, and Tc were estimated from reviews by Apps et al.<sup>[A1]</sup> and Allard.<sup>[A2]</sup>
- [7] Ogard, A. E., and J. F. Kerrisk, 1985. Groundwater Chemistry Along Flow Paths Between a Proposed Repository Site and the Accessible Environment. LA-10188-MS, Los Alamos National Laboratory, Los Alamos, New Mexico. Groundwaters from J-13, UE-25p#1, and H-3 are considered using EQ3. The composition of well USW H-3 is indicative of water below the proposed repository site. Water from well UE-25p#1 represents the carbonate aquifer underlying much of the area and is the most concentrated groundwater possible along the flow path. Well J-13 water is typical of wells surrounding Yucca Mountain; this well is capable of producing large volumes of water from a permeable zone at or near the static water level.
- [8] Kerrisk, J. F., 1985. An Assessment of the Important Radionuclides in Nuclear Waste. LA-10414-MS, Los Alamos National Laboratory, Los Alamos, New Mexico. In M. Wilson's SAND91-0155 report. These solubilities are a combination of computed (Kerrisk, 1984), measured (Nitsche and Edelstein, 1985), and estimated quantities.
- [9] Pearson, F. J., Jr., 1992. Solubility of Actinides and Technetium. Letter to R. E. Jackson, Intera, January 13, 1992. These solubilities were generated using EQ3NR and assume oxidizing conditions at 25°C, pH 7.5, and WN-1M model groundwater with Avonlea Bentonite pore solution.
- [10] These numbers are directly from "Submission of Data to the SEPDB", a LLNL letter from L. J. Jardine to SEPDB Administrator, SNL, on January 22, 1991. The data was abstracted from Wilson, C. N., 1990. "Results from NNWSI Series 3 Spent Fuel Dissolution Tests," PNL-7170, June 1990, and Wilson, C. N., "Results from Cycles 1 and 2 of NNWSI Series 2 Dissolution Tests," HEDL-TME85-22, May 1987. These solubilities are for 25°C.

The data from first report (Wilson, 1990) was used in "Waste-Package Release Rates for Site Suitability Studies," by W. W. -L. Lee, M. M. Sadeghi, P. L. Chambré, and T. H. Pigford, LBL-30707, April 1991. They concluded that the solubility of Np was  $3.0e-4$  g/m<sup>3</sup>, the solubility of Pu was  $9.5e-4$  g/m<sup>3</sup>, and the solubility of Am was  $3.8e-5$  g/m<sup>3</sup>.

- [11] These solubilities are from Nitsche, H., K. Roberts, T. Prussin, D. Keeny, S. A. Carpenter, K. Becraft, and R. C. Gatti, 1993. "Radionuclide Solubility and Speciation Studies for the Yucca Mountain Site Characterization Project," in High Level Radioactive Waste Management, Proceedings of the Fourth Annual International Conference, Las Vegas, Nevada, April 26-30, 1993, pp. 1490-1495. These solubilities assume 25°C and pH 6-8.5. The waters analyzed were J-13 (first range) and UE-2Sp#1 (second range), the former from the tuff aquifer and the latter from the carbonate aquifer. These waters are considered to bracket the compositions of the different groundwaters expected at the site.
- [12] Nitsche, H., and N. M. Edelstein, 1985. Determination of the Solubilities and Complexation of Waste Radionuclides Pertinent to Geologic Disposal at the Nevada Tuff Site. Topical Report "Solubilities and Speciation of Actinide Ions in Near-Neutral Solution," LBL-18900. These solubilities are for J-13 well water (pH =  $7.0 \pm 0.1$ ) at a temperature of  $25 \pm 1^\circ\text{C}$ . For Np, two solubilities are given. The first is for a solution with initially  $\text{NpO}_2^+$ , and the second is for groundwater initially containing  $\text{NpO}_2^{2+}$ .
- [A1] Apps, J. A., C. L. Carnahan, P. C. Lichtner, M. C. Michel, D. Perry, R. J. Silva et al., "Status of Geochemical Problems Relating to the Burial of High-Level Radioactive Waste, 1982," LBL-15103, March 1983.
- [A2] Allard, B., "Solubilities of Actinides in Neutral or Basic Solutions," in Actinides in Perspective, N. M. Edelstein, Ed., Proc. of the Actinides-1981 Conference, Pacific Grove, California, September 10-15, 1981 (Pergamon Press, New York, 1982).

Table B.1.2: Solubility as a function of temperature and pH [Nitsche et al., 1992a and 1992b].

	pH	J-13 Water			UE-25pH1 Water	
		Solubility at 25°C	Solubility at 60°C	Solubility at 90°C	Solubility at 25°C	Solubility at 60°C
Am	6	$(4.4 \pm 1.5) \times 10^{-4}$	$(6.1 \pm 1.7) \times 10^{-1}$	$(4.1 \pm 4.6) \times 10^{-4}$	$(7.5 \pm 2.7) \times 10^{-2}$	$(6.6 \pm 1.0) \times 10^{-4}$
	7	$(2.9 \pm 0.7) \times 10^{-4}$	$(2.4 \pm 2.2) \times 10^{-3}$	$(7.5 \pm 4.1) \times 10^{-3}$	$(7.8 \pm 3.9) \times 10^{-3}$	$(1.7 \pm 0.1) \times 10^{-4}$
	8.5	$(5.8 \pm 4.6) \times 10^{-4}$	$(2.9 \pm 3.2) \times 10^{-3}$	$(8.3 \pm 5.1) \times 10^{-3}$	$(7.5 \pm 1.9) \times 10^{-1}$	$(1.9 \pm 1.0) \times 10^{-3}$
Np	6	$(1.3 \pm 0.07) \times 10^{-3}$	$(1.5 \pm 0.09) \times 10^{-3}$	$(2.8 \pm 0.2) \times 10^{-2}$	$(6.9 \pm 1.4) \times 10^{-2}$	$(6.0 \pm 0.5) \times 10^{-3}$
	7	$(3.1 \pm 0.5) \times 10^{-1}$	$(2.3 \pm 0.2) \times 10^{-2}$	$(3.6 \pm 0.9) \times 10^{-1}$	$(1.1 \pm 0.3) \times 10^{-1}$	$(8.1 \pm 2.4) \times 10^0$
	8.5	$(1.0 \pm 0.2) \times 10^{-1}$	$(2.4 \pm 0.2) \times 10^{-1}$	$(2.1 \pm 0.09) \times 10^{-1}$	$(1.7 \pm 0.1) \times 10^0$	$(3.3 \pm 1.4) \times 10^0$
Pu	6	$(2.6 \pm 1.0) \times 10^{-1}$	$(6.5 \pm 2.6) \times 10^{-3}$	$(1.5 \pm 0.5) \times 10^{-3}$	$(2.0 \pm 0.1) \times 10^{-1}$	$(2.1 \pm 0.3) \times 10^{-3}$
	7	$(5.5 \pm 3.4) \times 10^{-3}$	$(8.9 \pm 2.2) \times 10^{-3}$	$(2.1 \pm 0.2) \times 10^{-3}$	$(1.1 \pm 0.1) \times 10^{-1}$	$(2.2 \pm 0.3) \times 10^{-2}$
	8.5	$(7.0 \pm 1.9) \times 10^{-3}$	$(2.9 \pm 0.2) \times 10^{-3}$	$(1.8 \pm 0.1) \times 10^{-3}$	$(2.4 \pm 0.2) \times 10^{-1}$	$(2.2 \pm 1.4) \times 10^{-1}$

Solubilities have units of g/m<sup>3</sup>.

Table B.1.7: Solubility as a function of temperature and oxygen fugacity [Wilson, 1990].

	Measured <sup>[1]</sup>		Predicted using EQ3/6 <sup>[2]</sup>				Phase
			Solubility at 25 °C		Solubility at 90 °C		
	Solubility at 25°C	Solubility at 85°C	$f_{O_2}=0.2$	$f_{O_2}=10^{-12}$	$f_{O_2}=0.2$	$f_{O_2}=10^{-12}$	
Am	3.9e-5	1.2e-7	1.2e-3	1.2e-3	---	---	Am(OH)CO <sub>3</sub>
			---	---	9.7e-4	9.7e-4	Am(OH) <sub>3</sub>
Cm	1.2e-5	1.5e-9	Cm not in thermodynamic database				
Np	3.0e-4	1.9e-4	1.5e-1	2.4e-4	1.5	2.4e-3	NpO <sub>2</sub>
Pu	9.5e-4	9.5e-6	9.5e-8	3.8e-9	3.0e-7	6.0e-10	PuO <sub>2</sub>
			1.2e+1	4.8e-1	1.5e+1	3.0e-2	Pu(OH) <sub>4</sub>
U	2.9e-1	1.5e-1	(1.5-2.3)e-2	(1.9-2.9)e-2	(3.7-5.9)e-4	(7.4-74)e-4	H
			(2.3-2.9)e-2	(2.9-3.7)e-2	5.9e-3	7.4e-3	H + S
			0.029-12	0.037-15	(0.59-23)e-2	(0.74-29)e-2	S
			1.2e+1	1.5e+1	2.3e-1	2.9e-1	S + Sch
			1.5e+1	1.9e+1	(2.3-3.7)e-1	(3.7-5.9)e-1	Sch

[1] Measured from Series 3 tests, 0.4 µm filtered. Used J-13 well water.

[2] Predicted for oxygen fugacities  $f_{O_2}=0.2$  (atmospheric) and  $f_{O_2}=10^{-12}$  with solubility control by precipitated secondary phases as listed: H = haiweeite; S = soddyite; Sch = schoepite. All phases are in the crystalline state, except Pu(OH)<sub>4</sub> which is amorphous.

Carl Brook  
TRW  
101 Convention Center Drive, Suite 540  
Las Vegas, NV 89109  
702-794-1800

Dear Carl:

In reply to the questions that you asked in your memo dated 22 June 1993 (questions 1 - 4 on the pages that I have numbered 6 and 7), I have the following observations. Regarding questions 1 and 2, the functional dependence of solubility with temperature can be expressed with thermodynamic rigor. However, using the functional dependence derived from thermodynamic considerations requires knowing the solubility products ( $K_{sp}$ ) of the dominating dissolution reactions. With regard to Nitsche's data reported in LA-12562-MS, it is important to make the following observations: (1) Nitsche only reports solubility data obtained from oversaturation, (2) the solid phases reported at 25°C and 60°C for Np do not match the solid phases found at 90°C, (3) information on the Pu solid phases formed is not available, and (4) it is not clear that equilibrium is obtained in the time scale of the experiments. These observations are important for the following reasons. (1) Deriving a  $K_{sp}$  from Nitsche's data requires writing a dissolution reaction; being able to describe that  $K_{sp}$  as a function of temperature requires that the same dissolution reaction takes place within the desired temperature range. It is not clear that this is the case for either Np or Pu. (2) If equilibrium is not attained during the solubility experiments, the variability of the solubility data with temperature could be a result of kinetic effects. In particular, the apparent solubility as measured by Nitsche could increase with temperature as a result of faster dissolution rates at higher temperatures. (3) In order to define a  $K_{sp}$ , equilibrium has to be attained from oversaturation and undersaturation. The same solubility for Am, Np, and Pu must be measured (regardless of whether Nitsche starts from an oversaturated solution or from an undersaturated solution using the solid phases formed during the oversaturation experiments). Data from undersaturation are not available in LA-12562-MS.

Nevertheless, I am including the thermodynamic treatment to obtain the functional dependence of an equilibrium constant (such as  $K_{sp}$ ) with temperature. I reiterate that this treatment is only valid when considering the same chemical reaction attaining equilibrium at different temperatures.

The symbols that are utilized in this derivation are defined as follows:

$K_{sp}$  = Solubility Product

G = Gibbs Free Energy

$\Delta G = \sum_{\text{products}} G_i - \sum_{\text{reactants}} G_i$

° refers to reactants and products in their standard state (1 atm)

H = Enthalpy

S = Entropy

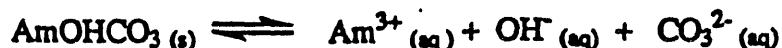
R = Gas Constant

T = Temperature

$C_p$  = Heat Capacity @ Constant Pressure

a, b, & c = constants

Assuming that the measured americium solubilities in J-13 are due the following reaction:



then,

$$K_{sp} = [\text{Am}^{3+}] [\text{OH}^-] [\text{CO}_3^{2-}]$$

Note that the reported crystalline form of  $\text{AmOHCO}_3$  is not always the same at different temperatures.

Equation 1 is a result of the Laws of Thermodynamics.

$$\Delta G = \Delta H - T\Delta S \quad @ \text{ Constant } T \quad (1)$$

Equation 2 describes the functional dependence of the heat capacity of a substance with temperature.

$$C_p = a + bT + cT^2 \quad (2)$$

Equation 3 describes the functional dependence of  $\Delta C_p$  with temperature; where  $\Delta C_p$  is the sum of the heat capacities of the products minus the corresponding sum for the reactants (it is the net change in heat capacity resulting from the reaction).

$$\Delta C_p = \Delta a + \Delta bT + \Delta cT^2 \quad (3)$$

Equation 4 is Kirchoff's formula.

$$\Delta C_p = \left[ \frac{\partial(\Delta H)}{\partial T} \right]_P \quad (4)$$

Substituting for  $\Delta C_p$  using equation 3 and integrating equation 4, yields equation 5, where  $\Delta H_i$  is an integration constant.

$$\Delta H = \Delta H_i + \Delta aT + \frac{1}{2} \Delta bT^2 - \Delta cT^3 \quad (5)$$

Equation 6 is a result of taking the partial derivative of equation 1 with respect to temperature at constant pressure.

$$\left[ \frac{\partial(\Delta G/T)}{\partial T} \right]_P = -\frac{\Delta H}{T^2} \quad \text{or} \quad \left[ \frac{\partial(\Delta G/T)}{\partial(1/T)} \right]_P = \Delta H \quad (6)$$

Substituting for  $\Delta H$  using equation 5 and integrating either form of equation 6, yields equation 7, where  $i$  is an integration constant.

$$\Delta G = \Delta H_i - \Delta a T \ln T - \frac{1}{2} \Delta bT^2 - \frac{1}{2} \Delta cT^3 + iT \quad (7)$$

Letting  $K$  equal  $K_{sp}$  and substituting for  $\Delta G^\circ$  in equation 8 (using equation 7), yields equation 9 after algebraic rearrangement.

$$\Delta G^\circ = -RT \ln K \quad (8)$$

$$-R \ln K = \frac{\Delta H_i}{T} - \Delta a \ln T - \frac{1}{2} \Delta bT - \frac{1}{2} \Delta cT^2 + i \quad (9)$$

Equation 9 describes the functional dependence of the solubility product with respect to temperature.

With respect to question 3 on page 7, I don't see anything wrong with approximating the solubilities using a log normal distribution.

With respect to question 4 on page 7, it seems reasonable to use Wilson's data for Cm (which I numbered pages 14 - 18). Temperature dependence of solubility in general has already been discussed. I don't have any specific information for Cm.

As you know Dave Morris is the PI for the solubility and speciation studies being conducted at LANL. I have asked Dave to review this write-up and correct any potential mistakes or provide you with additional information.

I am also enclosing the meeting report for the most recent meeting of the Radionuclide Solubility Working Group that Dave Morris sent to Ardyth Simmons. I call your attention to Table 1 on page 6 of SolWOG-2. This table summarizes the consensus solubility values for the actinides compiled during the Radionuclide Solubility Working Group Meeting.

Sincerely,



Inés R. Triay

cc: Dave Morris  
Tom Newton

**APPENDIX H**

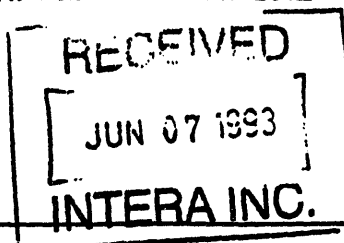
**DISTRIBUTION COEFFICIENT EXPERT ELICITATION RESULTS**

**Carl Bruch**

**Subject:**  $K_d$  Expert Elicitation with LANL and SNL

**Date:** 2 June 1993

**From:** Carl Bruch



**To:** Bob Andrews  
Sue Braumiller  
Tim Dale  
Jerry McNeish

---

On 1 June 1993, representatives from the two TSPA groups (SNL and INTERA) and Los Alamos National Laboratories (LANL) attended a meeting at Sandia. The objective was to generate the sorption distributions to be used in TSPA-II. This meeting was a follow-up to the 13 April expert elicitation on solubilities held at SNL. This memo summarizes the highlights of the meeting, the  $K_d$ s that were generated, and other information that I found interesting.

Attendees were: Rally Barnard (SNL), Jack Gauthier (SNL), Mike Wilson (SNL), Ines Triay (LANL), Arend Meijer (???), and myself. Paul Kaplan (SNL) and Tom Robey (SNL) were also there for some of the time.

Many factors influence the sorption of a particular element in a particular hydrogeologic unit. These include, but are not limited to, the groundwater chemistry, pH, and Eh, and temperature. The redox potential Eh of the system is particularly important as it determines oxidation state of the radionuclides, which in turn determines the solubility of the radionuclides. Oxidizing conditions for the site were assumed. The range of groundwaters included UE-25 p#1, J-13, and USW H-3. The pH range is from 6 to 9.

One of the major reasons that Yucca Mountain has been touted as a potential repository site is the presence of zeolites and their ability to retard radionuclides. The possibility of a hot repository has raised the question that the high temperatures may break down the zeolites. This has generated some concern on the project. Arend and Ines, however, affirmed that the zeolites are not destroyed by high temperatures. Experiments by Dave Bish, LANL indicate that the zeolites are dried out by the heat, but when the water is reintroduced, the zeolites return undamaged to their original state. Later, they said that when zeolites do alter, one would expect the sorptions to be similar to those for the devitrified and vitric tuffs. It may be that the alteration of zeolites is an extremely long-term process or one that only happens at sufficiently high temperatures, and Bish's research was unable to observe it.

It was also noted that although the zeolites sorb many radionuclides, including isotopes of Sr, Cs, and Ra, the actinides are not well sorbed by the zeolitic tuff. This is rather problematic as many of the "bad actors" in the TSPA inventories are actinides. However, it has been found that actinides sorb well to iron oxides. The iron oxide may be present in the nearfield (the waste package/EBS) and/or in the farfield (the tuffs). Thus, for the sorption of actinides, the container material and the quantity of iron oxide that will be available is important.

Iron oxide will be present in the nearfield as a consequence of the corrosion of the waste

package. The quantity of iron oxide depends on the chemical composition and thickness of the waste packages. Of the various designs under consideration, the 1" 825 with a 4" overpack of corrosion-allowance steel is probably the most suited for sorbing actinides. It is likely that the iron in the waste packages will corrode to a meta-stable state of  $\text{FeOOHnH}_2\text{O}$  that lasts thousands of years. The fact that actinides sorb well to this form of iron and its relative stability suggest that the presence of large quantities of iron in the repository area is would significantly retard the transport of radionuclides to the geosphere.

It is important to note that the degree of sorption on iron oxide is dependent on the pH of the water. For pH values below 8, cations generally will not sorb to iron oxide. On the other hand, at low pH, Np complexes as  $\text{NpO}_2$  which sorbs well to the tuff (actinides generally sorb well to iron oxide at low pH); at high pH, Np complexes as  $\text{Np}(\text{CO}_3)_2$  which does not sorb as well. Clearly, this is an area that needs more characterization as we incorporate more chemistry into our total-system models via groundwater pH and temperature.

In accounting for iron as a possible sorbing agent, it is important to be consistent and consider the possibility of colloid formation. It was mentioned that iron could form colloids and transport the radionuclides at lower temperatures where colloids are stable.

Zeolites sorb cations that are generally small and simple. Tc is an anion and is not expected to be sorbed by the zeolites.

The sorption of carbon was considered. There are different ways in which  $^{14}\text{C}$  can be retarded: exchange with  $\text{CO}_2$  in the water, calcite precipitation (at high temperatures), and sorption in the interfacial water layer. Aqueous sorption on iron oxide was provided. Ben Ross has considered retardation of gaseous carbon. His  $K_d$ s are dependent on temperature, but are approximately 40.

Tom Robey's stratigraphy was discussed. He divided the units by the degree of welding since that affects the flow the most in their geostatistical simulations. The units were then described by the type of tuff (devitrified, vitric, and zeolitic):

Tsw2	--	devitrified
Tsw3 (vitrophyre)	--	vitric
CHnv	--	vitric
CHnz	--	zeolitic
Prow Pass w	--	devitrified
Bullfrog n	--	zeolitic
Bullfrog w	--	devitrified

Although the vitrophyre has different permeabilities, it was assumed to have the sorptive properties of vitric tuff. The two tuffs are chemically similar, except that the vitrophyre has larger grains. There is also a practical reason: in the testing procedure, the vitrophyre samples are ground up so that they are like vitric tuff. It may be that assuming vitric properties for the vitrophyre is not conservative since the latter has less surface area on which the radionuclides can sorb. The impact of this nonconservative assumption is probably not significant, primarily because the vitrophyre is relatively thin in comparison to other layers (it overlies the vitric CHnv unit that is much thicker).

The elicitation did not distinguish between saturated-zone and unsaturated-zone  $K_d$ s. This was largely because there is no data for unsaturated sorption of radionuclides. Furthermore, it is unlikely that the quantity of water would significantly alter the  $K_d$ s. One possible effect was mentioned: in both the unsaturated and saturated zones, oxidizing conditions were assumed, but this might not be accurate since there is less oxygen available in the saturated zone. Thus, the saturated zone may be more reducing than the unsaturated zone.

In every case but one, as temperature increases, the sorption increases or stays constant. The exception (Np sorption on pure calcite) is confusing, and LANL has not been able to explain it yet. Nevertheless, assuming sorption coefficients for 25°C appears to be conservative.

The table that follows includes the  $K_d$  distributions (in ml/g) for the important elements/radionuclides in three basic types of tuff (D=devitrified, V=vitric, and Z=zeolitic) and for iron oxide (in the immediate vicinity of the waste package). In the table,  $E[x]$  is the mean, and  $CV[x]$  is the coefficient of variance that Paul Kaplan feeds into his beta distributions. The range of sorption values given are intended to be defensible: the maximum is conservative in that experiments have yielded  $K_d$ s with higher values than reported below. The values are for solute calculations only--they do not apply to colloidal transport or sorption.

Element	Rock	Min	Max	$E[x]$	$CV[x]$	Dist.	Comments
Am	D	100	2000			uniform	Ac, Cm, Nb, Sm, and Zr have the same distributions. Am sorption not sensitive to changes in pH.
	V	100	1000	-380	0.2	beta	
	Z	100	1000			uniform	
	Fe	1000	5000			uniform	
Cs	D	100	200			uniform	
	V	100	200			uniform	
	Z	500	3000			uniform	
	Fe			10		exponential	
Ni	D						Ask Malcolm Siegel for these numbers. Sorption will probably be like Cs, but reduced by a factor of -2.
	V						
	Z						
	Fe						Ni sorbs well to iron oxide. #s from Malcolm.
Pa	D			2		exponential	There is extremely limited data for these numbers.
	V			0.5		exponential	
	Z			4		exponential	
	Fe	500	1000			uniform	
Pb	D	100	500			uniform	Limited data available for Pb. Pb sorption is heavily influenced by organics in the groundwater (concentrations on the order of 1 ppm are significant).
	V	100	500			uniform	
	Z	100	500			uniform	

	Fe	100	1000			uniform	
Pu	D	50	200	100	0.25	beta	Pu sorption is dependent on many parameters, including the oxidation state and the groundwater pH, Eh, and composition.
	V	50	200	100	0.25	beta	
	Z	30	70	40	0.15	beta	
	Fe	1000	5000			uniform	
Ra	D	100	500			uniform	Ra sorption due to clays in the tuff.
	V	100	500			uniform	
	Z	1000	5000			uniform	
Sn	D	20	200			uniform	
	V	20	200			uniform	
	Z	100	300			uniform	
	Fe	0	5000			uniform	No data for Sn sorption on iron oxide.
	Fe			20		exponential	Ra very pH-dependent for Fe.
U	D	0	5			uniform	Use these numbers for the Se $K_d$ s to be conservative.
	V	0	4			uniform	
	Z	5	20	10	0.3	beta	
	Fe	100	1000			uniform	Academic work says that U should be retarded by Fe, but experience is otherwise (possibly due to organics).
C	DVZ			-40		???	Gaseous retardation from Ben Ross's work (some temperature dependence).
	Fe	100	300			uniform	These numbers are for sorption of aqueous radionuclides in the interfacial water layer.
Cl, I, Tc	All	0					

The group attending this meeting was about half the size of the one at the solubility elicitation and was more productive.

- We were able to obtain  $K_d$ s for all the radionuclides that we had been interested in. These were for three farfield environments (devitrified, vitric, and zeolitic tuffs) and one nearfield environment (iron oxide).
- Temperature was not considered explicitly (data is too sparse). It is conservative to assume the 25°C data for all times and temperatures.
- pH was not considered explicitly (data is too sparse). This is an important factor and should be considered in future analyses.
- We can consider the effect of different waste package designs on the sorption of radionuclides in the nearfield. To be consistent, though, we need to account for the possible formation of iron colloids and subsequent radionuclide transport.
- As for the numbers generated at the solubility expert elicitation, SNL will use these  $K_d$  distributions without modification for their portion of TSPA-II.

Sandia National Laboratories  
Albuquerque, New Mexico 87185

INFORMATION ONLY

date: June 4, 1993

to: My friend and colleague Jack

*Malcolm Siegel*

from: M. D. Siegel, 6115

subject: Kd distributions for Ni (ml/gm)

rock	min	max	distribution
dv tuff	0	500	normal
vitric tuff	0	500	normal
zeolitic	0	500	normal
iron oxyhydroxide	0	1000	skewed log normal

$\mu$   
250 }  
250 }  
250 }  
250 }  
min 8  
max 8  
ave 230 approx  
σ = 2.5 in log space

Carl -  
Here's what Malcolm gave me for Ni Kd distributions. Malcolm is on vacation for a month, so if you have any questions, give me a call and maybe we can figure it out together.

Jack Gauthier  
505-844-3330

P.S. Note the mean and std. dev. info to the right. →

**APPENDIX I**

**THERMALLY INDUCED RETARDED <sup>14</sup>C TRAVEL-TIME DISTRIBUTIONS**

**Benjamin Ross**

# Sandia National Laboratories

Albuquerque, New Mexico 87185

July 26, 1993

WBS: 1.2.5.4.1

QA: N/A

Carl E. Bruch  
M&O/INTERA  
101 Convention Center Dr., Suite P110  
Las Vegas, NV 89109

Subject: C-14 travel-time distributions from Ben Ross

Carl:

I learned recently that I was supposed to send you the information that we have regarding gas flow and  $^{14}\text{C}$  travel times. Enclosed with this letter is all the new information we have so far. Ben Ross and co-workers at Disposal Safety Inc. ran a new series of calculations for us with their computer models TGIF2 and PATHLINE2.

The problem setup, boundary conditions, etc., are mostly as described in their report *Numerical Studies of Rock-Gas Flow in Yucca Mountain* (SAND91-7034). There are two important differences. First, the new calculations were run with TGIF2 rather than TGIF. TGIF2 calculates gas flow coupled with heat flow, and provides a time-varying solution rather than being limited to steady-state solutions. The only documentation to date on TGIF2 is a very brief description of the governing equations in a conference proceeding ("Thermally Driven Gas Flow Beneath Yucca Mountain, Nevada," in *Multiphase Transport in Porous Media—1991*, edited by R. R. Eaton, M. Kaviany, M. P. Sharma, K. Vafai, and K. S. Udell, published by the American Society of Mechanical Engineers). The second difference is that a different repository layout was assumed. The assumed layout is enclosed. The computer model is 2-dimensional, so the actual calculations were made with three slices through the mountain. The same cross-sections were used as for their previous work (SAND91-7034), but only three cross-sections were used, rather than four, because of the reduced repository area assumed. Unfortunately, more recent information that we have received indicates that projected burnups are higher than we had assumed, and so the enclosed repository layout is not what we would use for the calculations if we were to do them today. Disposal Safety is going to re-run one of the cross-sections for us with the new information so that we can get an idea of the effect on the results.

The enclosures are the following:

- Ben Ross's cover letter to us, which gives a few details of the calculations.
- Eighteen <sup>14</sup>C-travel-time histograms, for starting times from 1000 years to 18,000 years.
- A floppy disk with eighteen <sup>14</sup>C-travel-time files on it.
- A drawing of the assumed repository layout.

The results that we have available cover only one repository thermal loading—57 kW/acre. Ben felt that the computer model needed additional modifications to be able to handle higher thermal loads, and there just wasn't time (the information enclosed took nearly a month of time on their computer). Ben would like to do a sensitivity study, varying the thermal load and other key parameters, but that will have to be put off till next year.

If you have questions about any of this, feel free to give me a call at (505) 844-9337. You may also want to talk to Ben; his phone number is (202) 293-3993.

Sincerely,

*Michael Wilson*

Michael L. Wilson  
YMP System Performance Assessments  
Department 6312

Copy w/o enclosures to:  
6312 H. A. Dockery  
6312 M. L. Wilson  
6352 10/12541/1.2/NQ

# Disposal Safety Incorporated

July 9, 1993

Sandia National Laboratories  
Attn.: Mike Wilson  
Division 6312  
P. O. Box 5800  
Albuquerque, NM 87185

Dear Mike:

Enclosed are the results of our carbon-14 travel time calculations for the TSPA-II exercise. The results are included both in machine-readable form and as histograms on paper.

There are 18 files and 18 histograms, each corresponding to a starting time for migration of carbon-14 particles. Starting times were each thousand years from 1000 to 18000 years after waste removal from the reactor. The number in the file name is the particle starting time.

Each file contains the travel times for 241 particles. One particle started from a randomly selected position in each 25-meter segment of three east-west cross-sections through the repository. The cross-sections were located on the N760000, N762500, and N765000 coordinates. At 1000 and 2000 years, portions of the repository had temperatures (averaged between rooms and pillars) above the boiling point. Travel times for particles in these areas were not calculated, which is reasonable because containers in regions where the rock is above the boiling point are unlikely to be breached. Consequently the files for these two starting times contain fewer than 241 travel times.

The calculations assumed a welded-tuff permeability of  $10^{-11}$  m<sup>2</sup>, a nonwelded-tuff permeability of  $10^{-12}$  m<sup>2</sup>, and a waste areal power density of 57 kW/acre with 30-year-old waste.

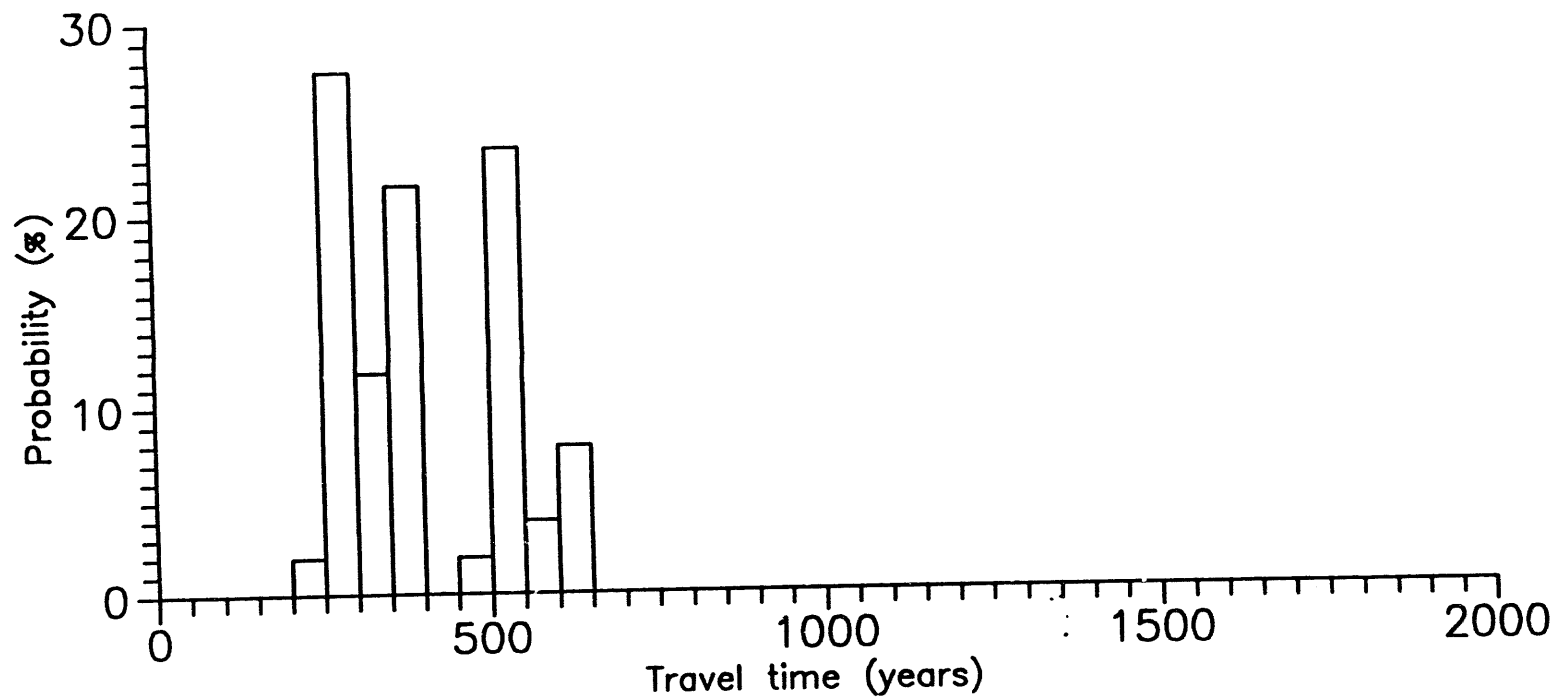
Please call me if you have any questions.

Sincerely,



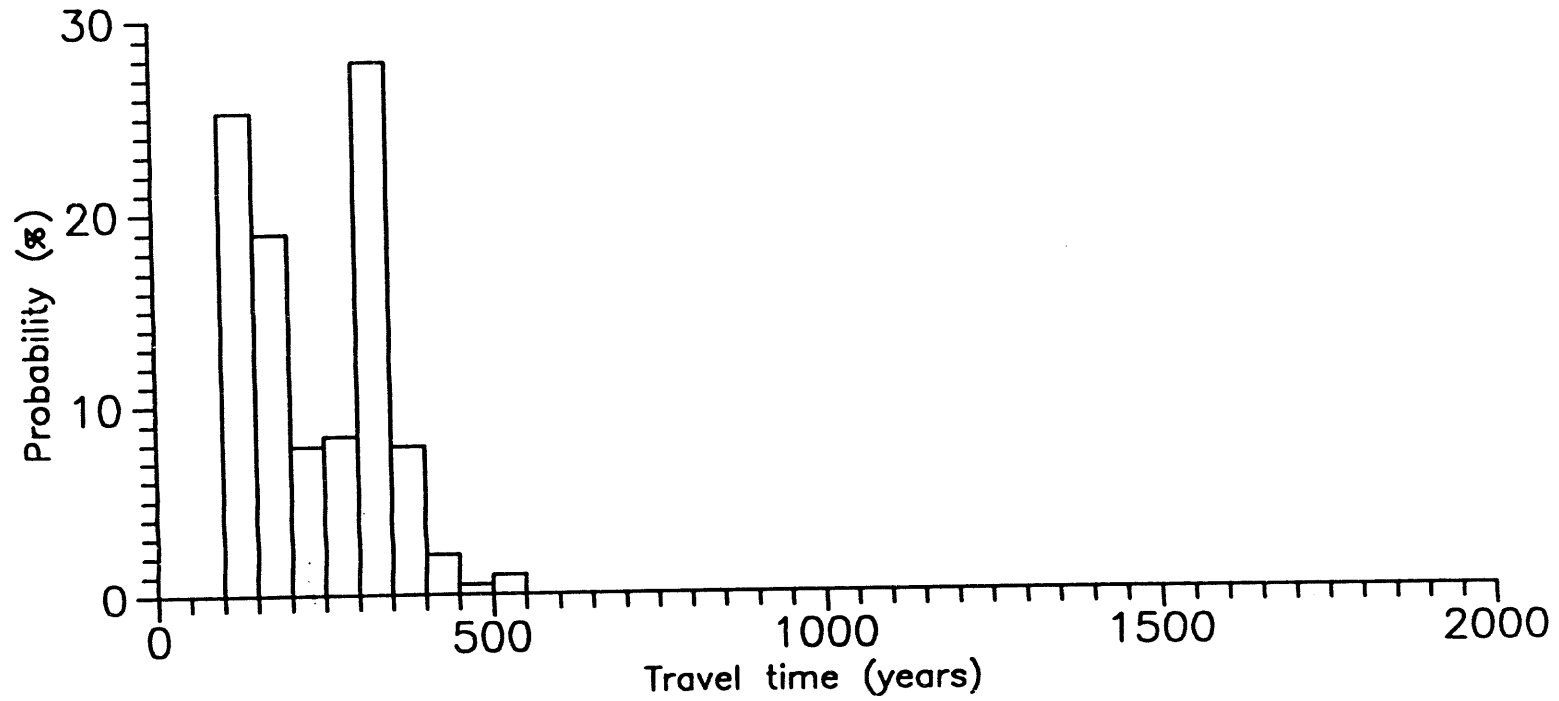
Benjamin Ross  
President

1660 L Street NW, Suite 314  
Washington, DC 20036  
(202) 293-3993

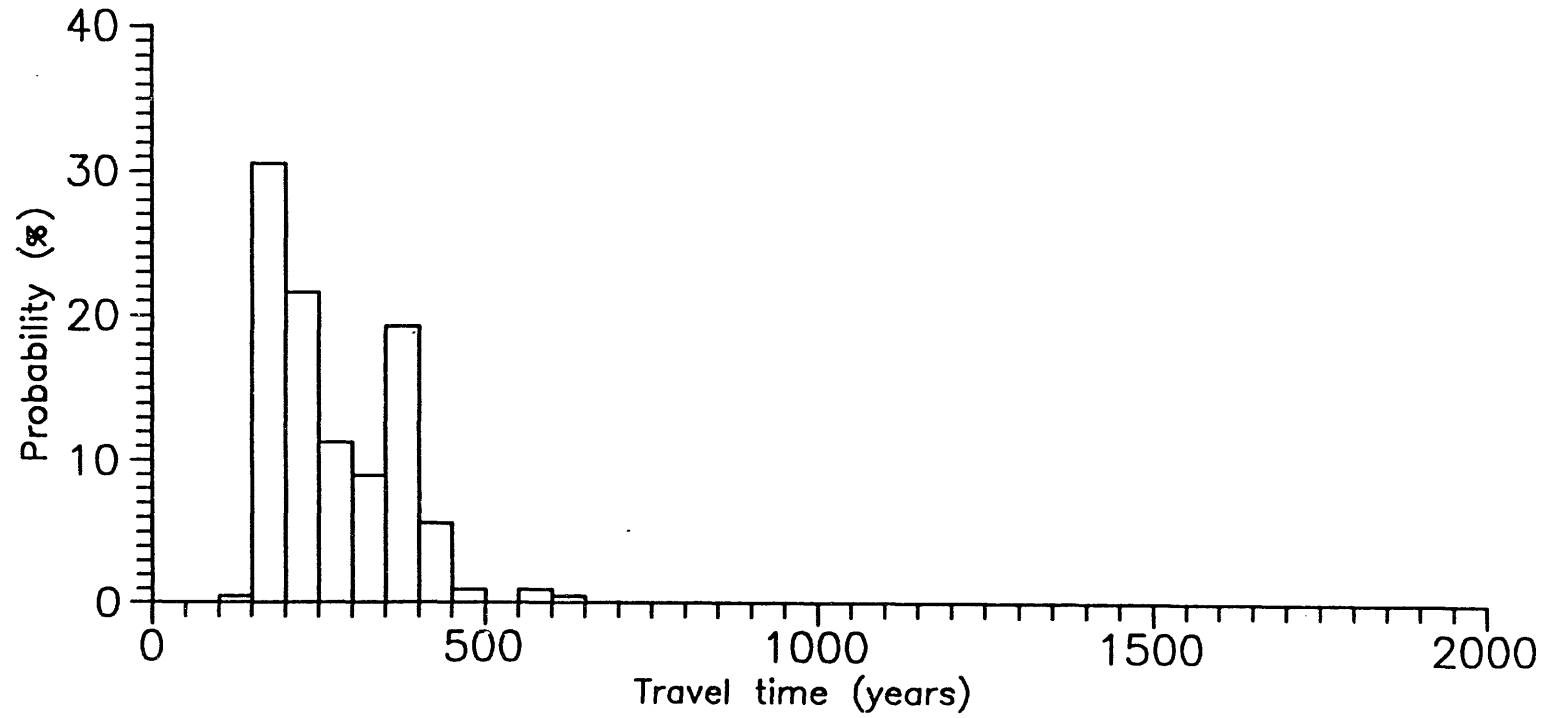


Retarded travel times of C-14 particles from the repository to the atmosphere with particles released at 1000 years

5-1

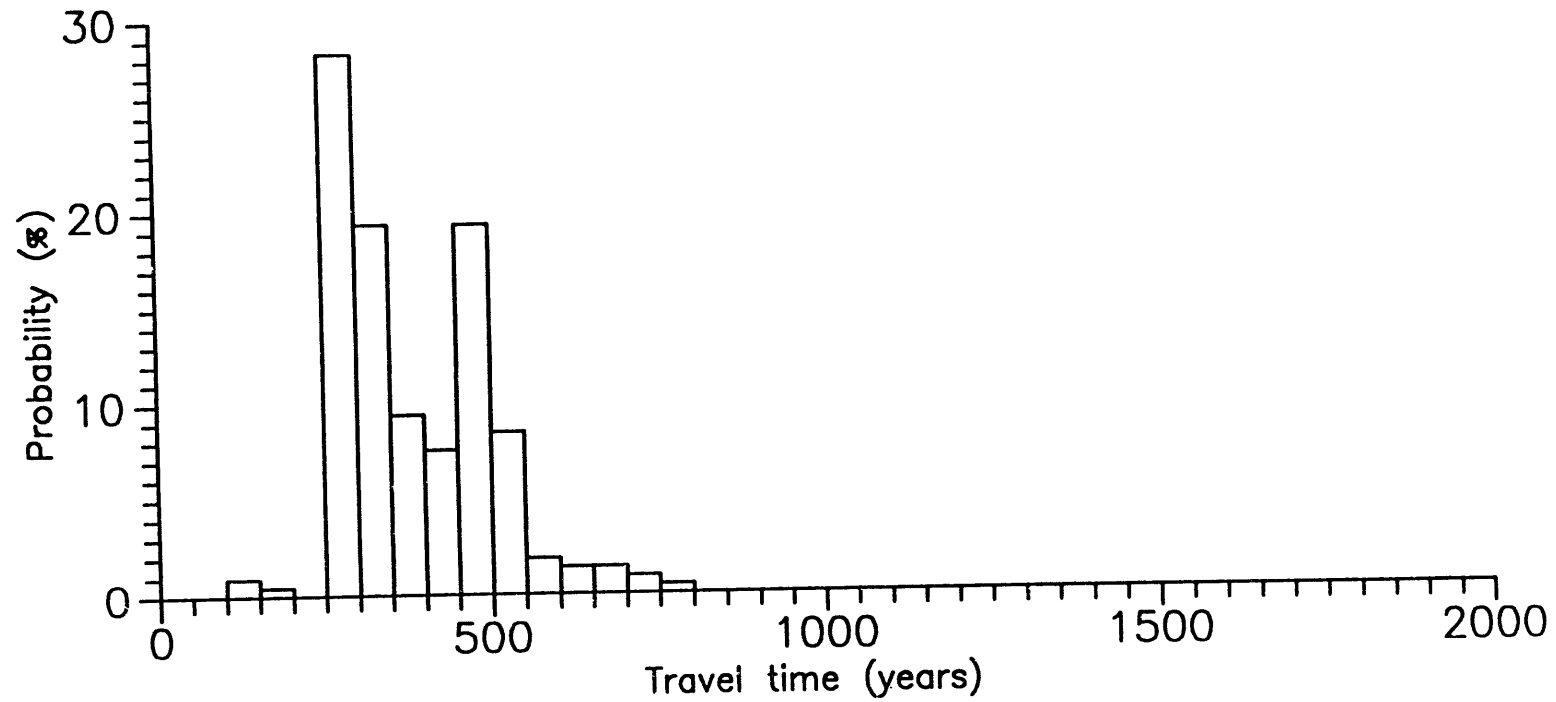


Retarded travel times of C-14 particles from the repository to the atmosphere with particles released at 2000 years

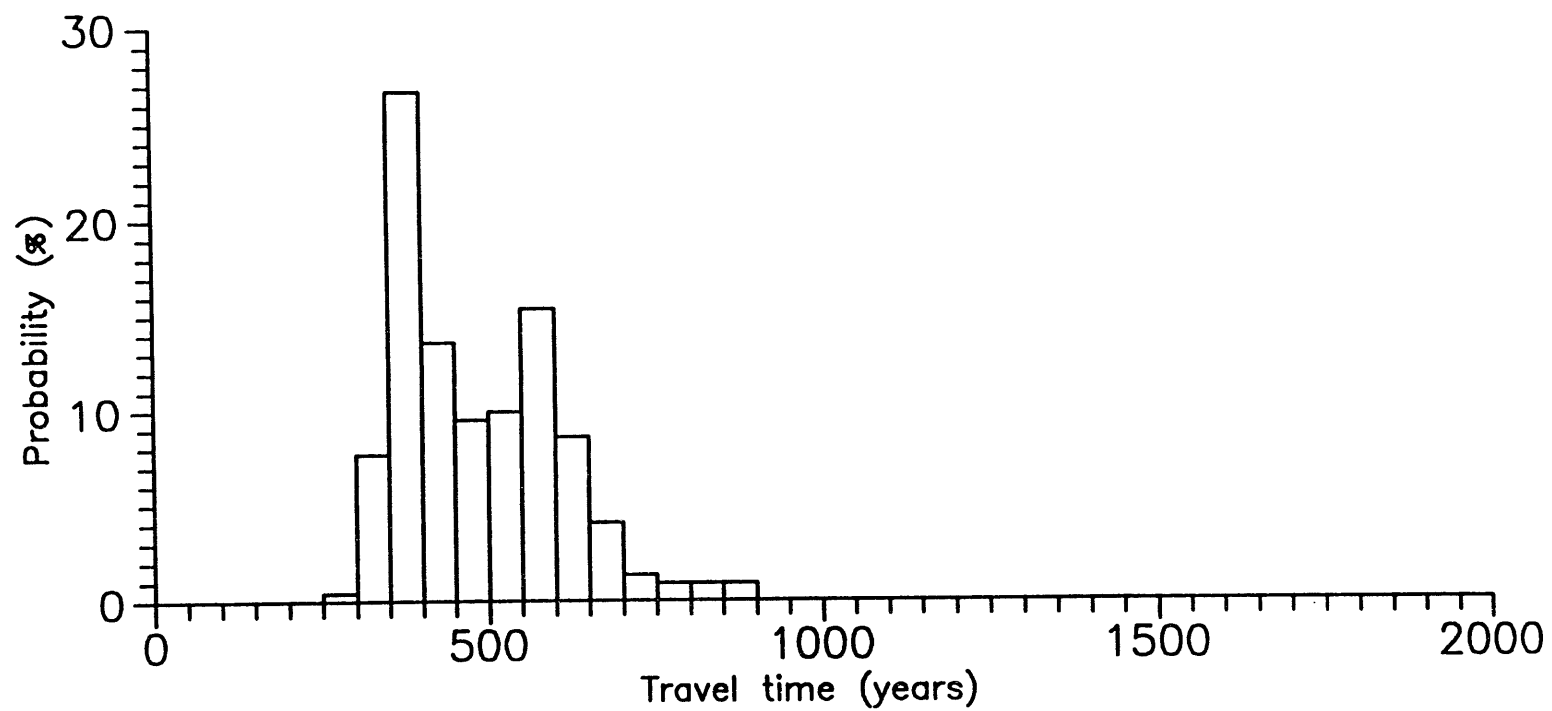


Retarded travel times of C-14 particles from the repository to the atmosphere with particles released at 3000 years

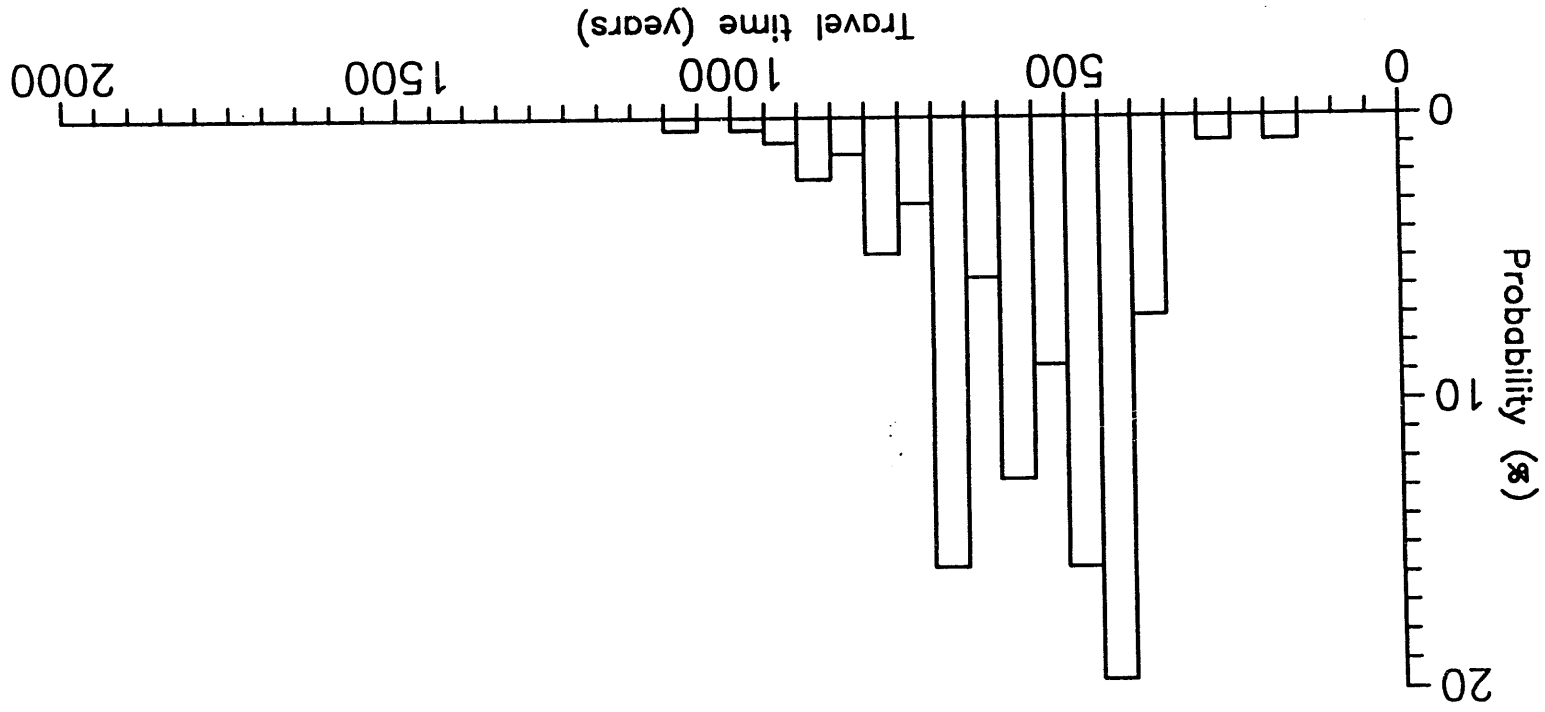
L-1



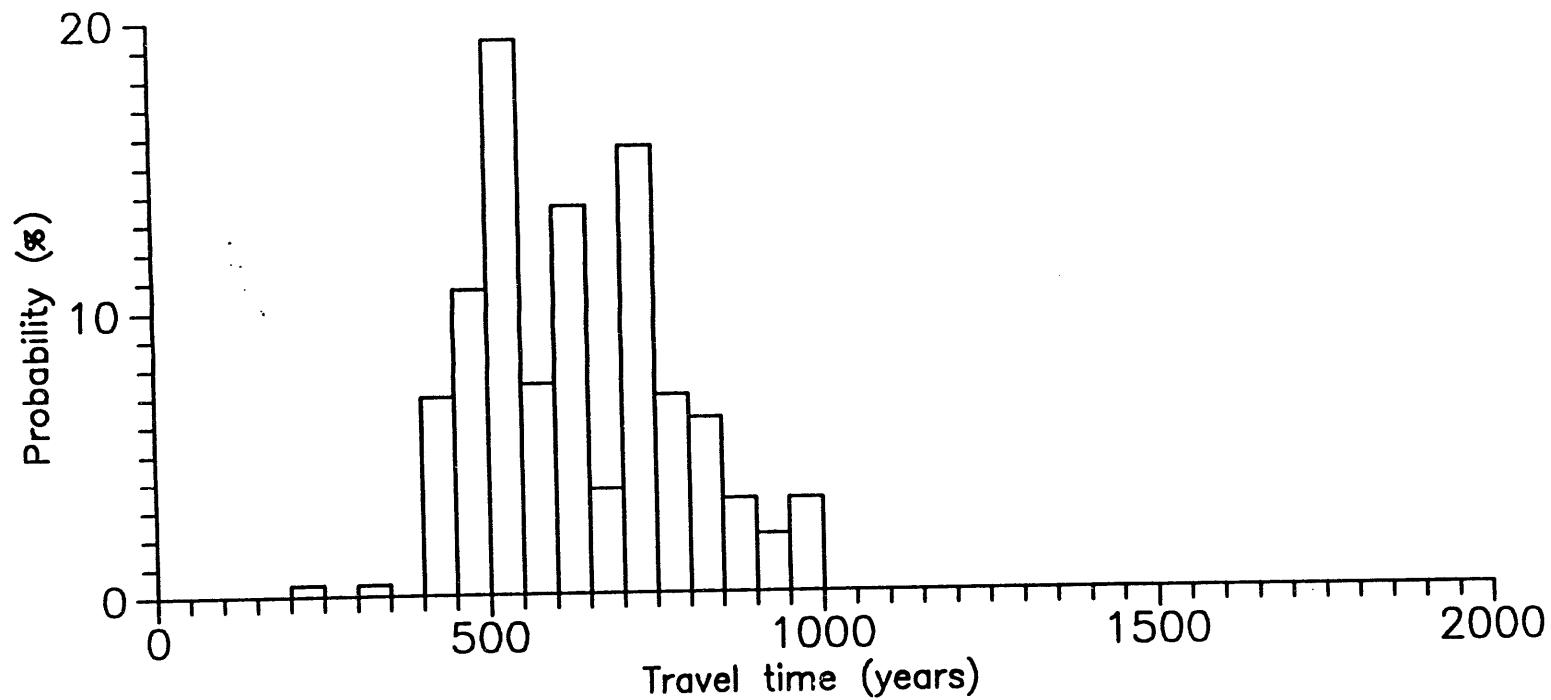
Retarded travel times of C-14 particles from the repository to the atmosphere with particles released at 4000 years



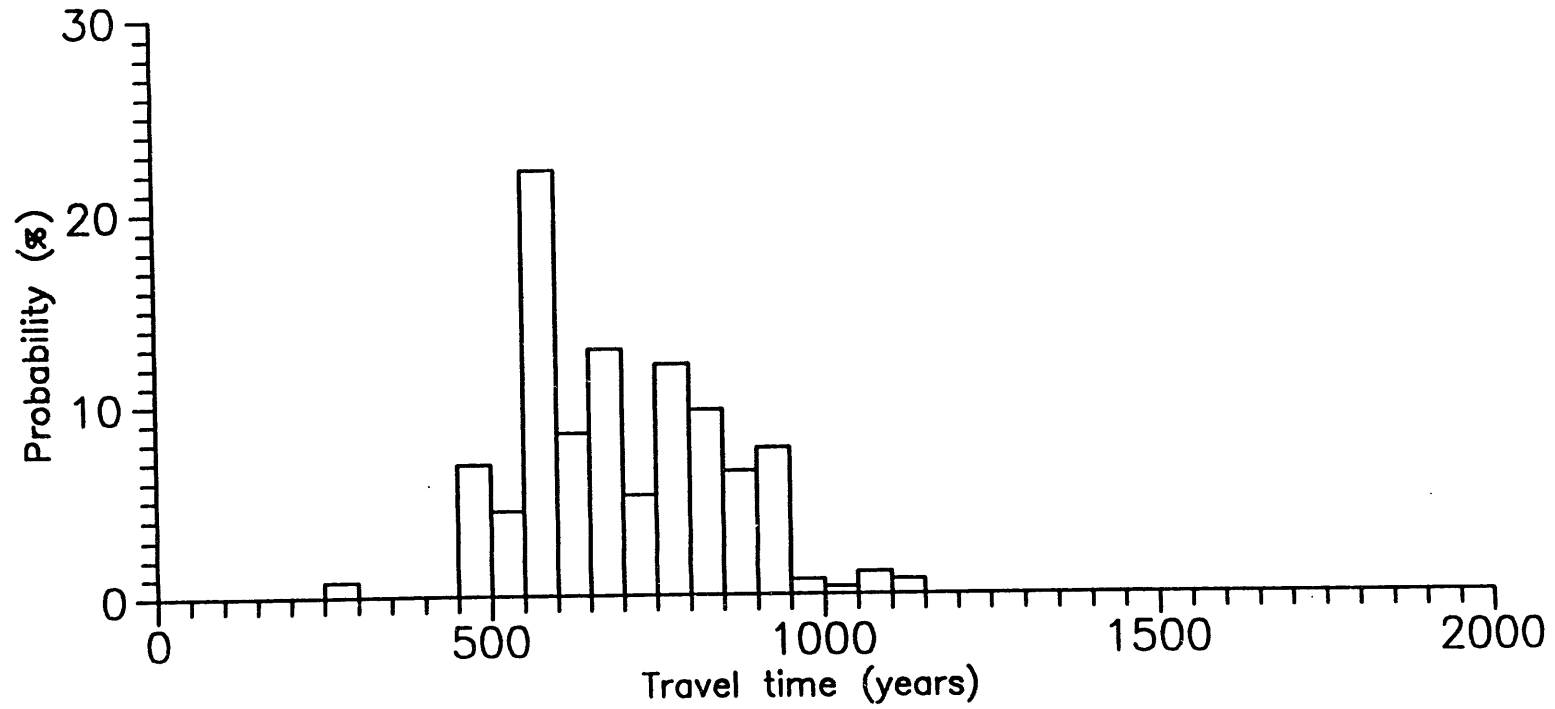
Retarded travel times of C-14 particles from the repository to the atmosphere with particles released at 5000 years



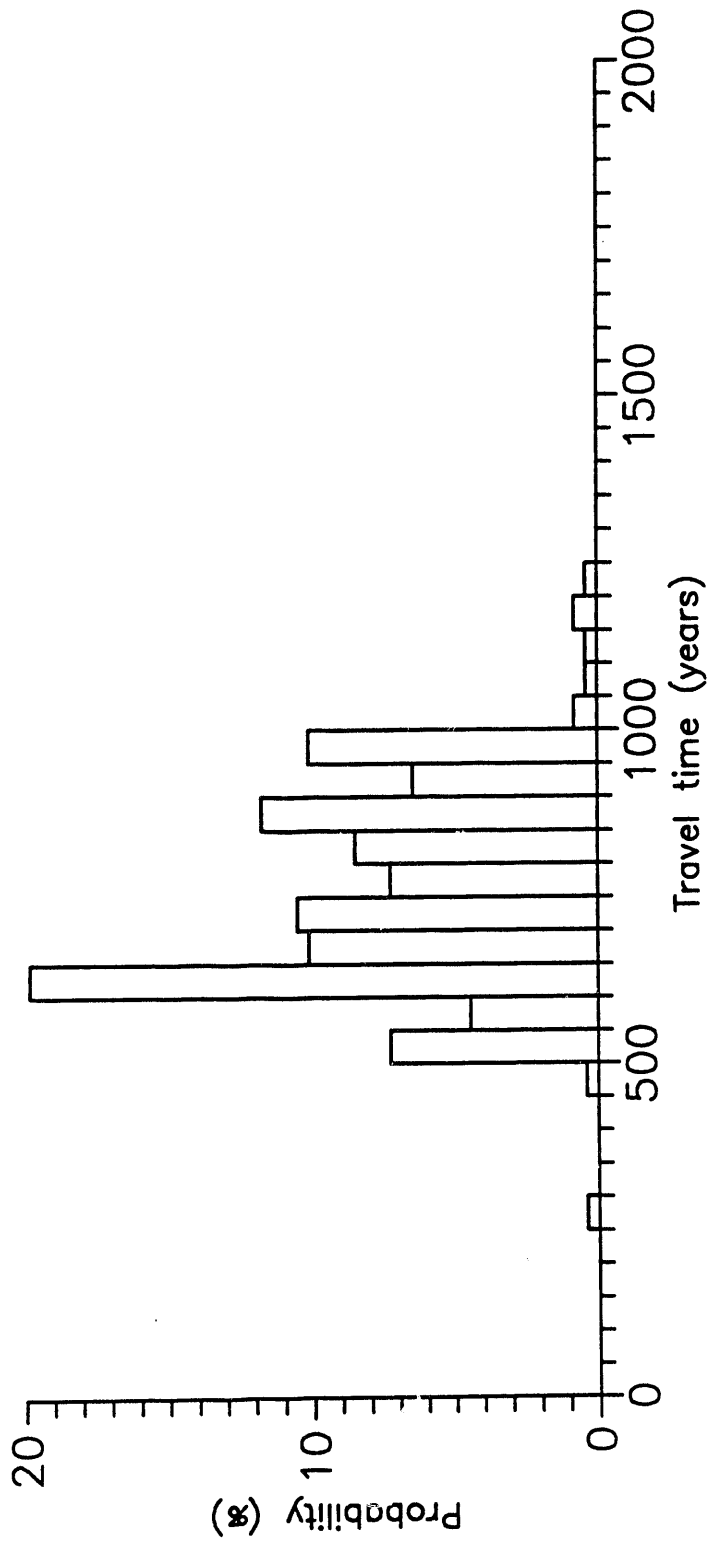
Retarded travel times of C-14 particles from the repository to the atmosphere with particles released at 6000 years



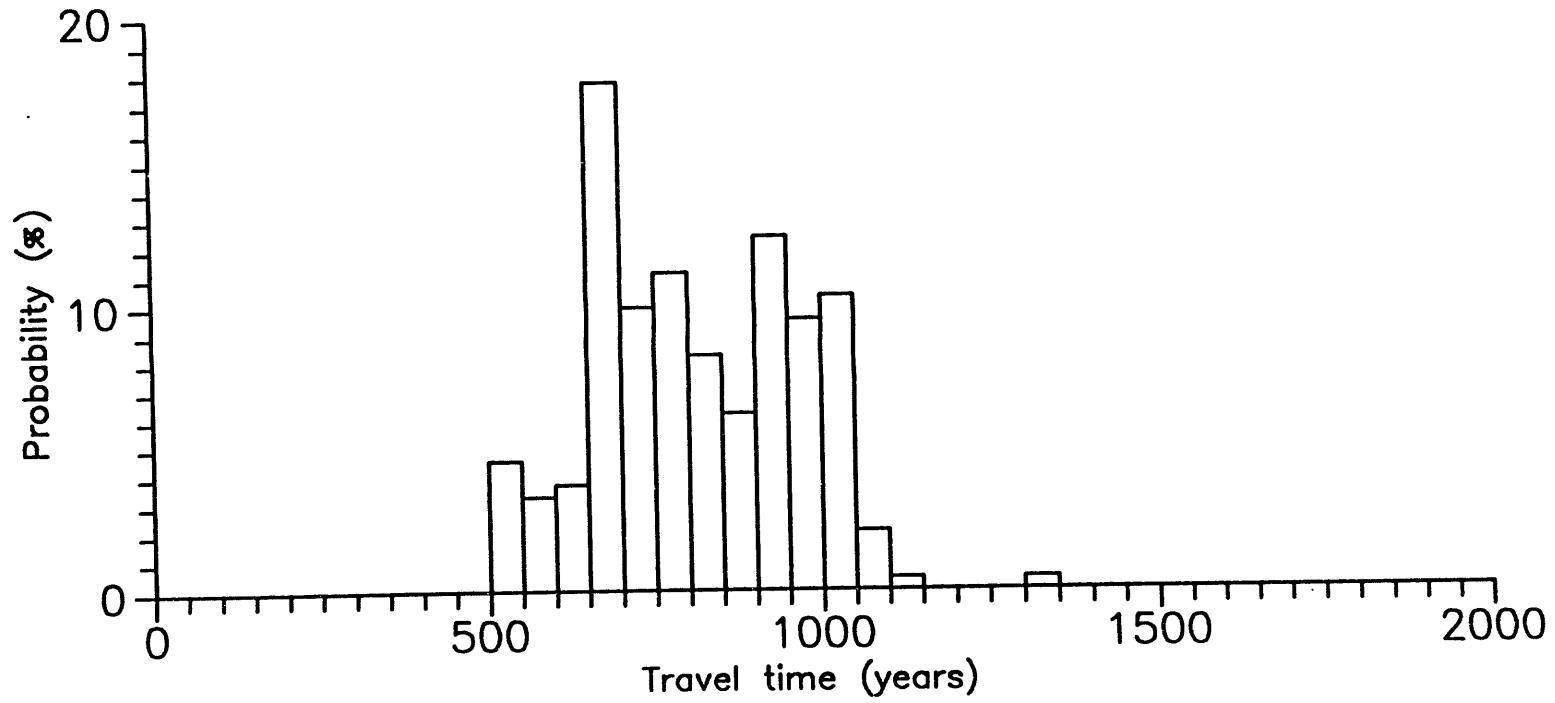
Retarded travel times of C-14 particles from the repository to the atmosphere with particles released at 7000 years



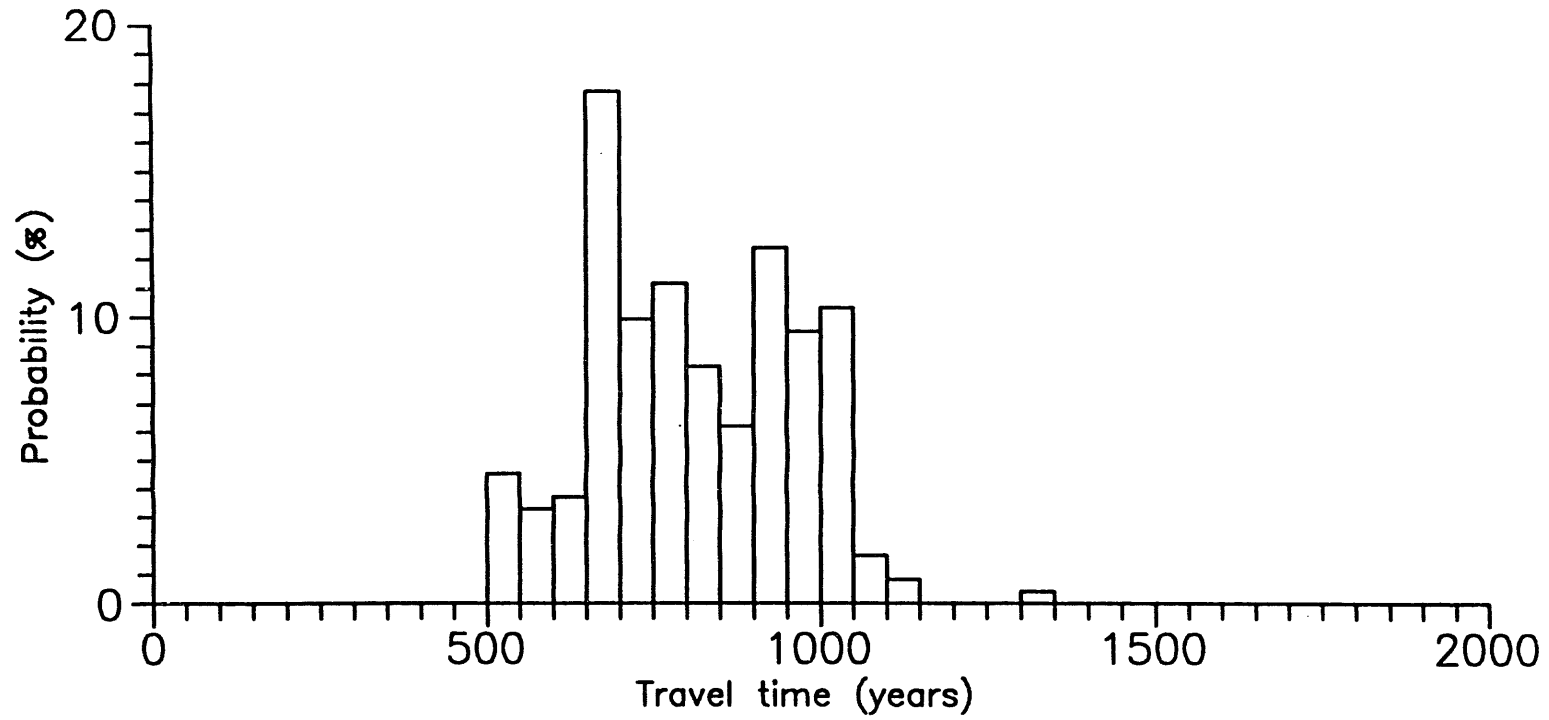
Retarded travel times of C-14 particles from the repository to the atmosphere with particles released at 8000 years



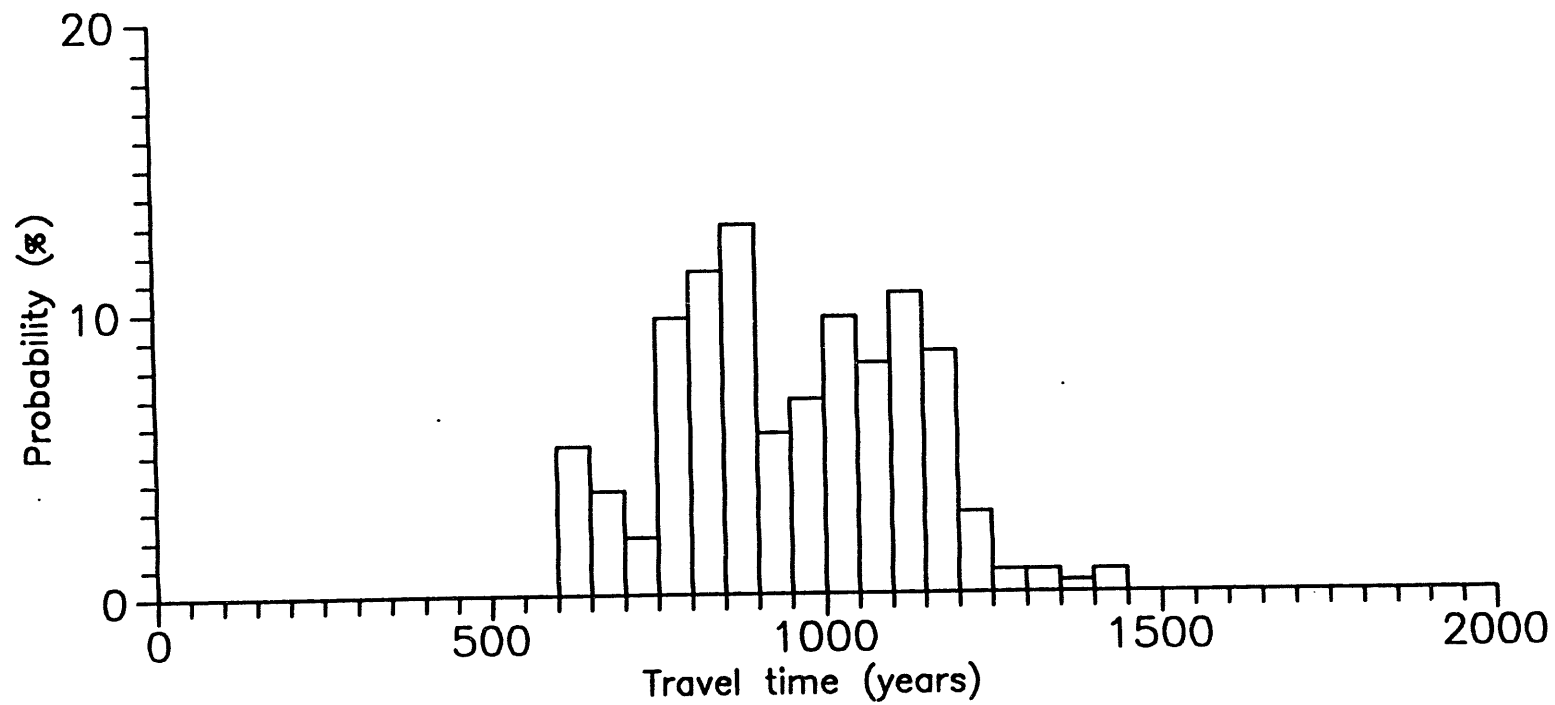
Retarded travel times of C-14 particles from the repository to the atmosphere with particles released at 9000 years



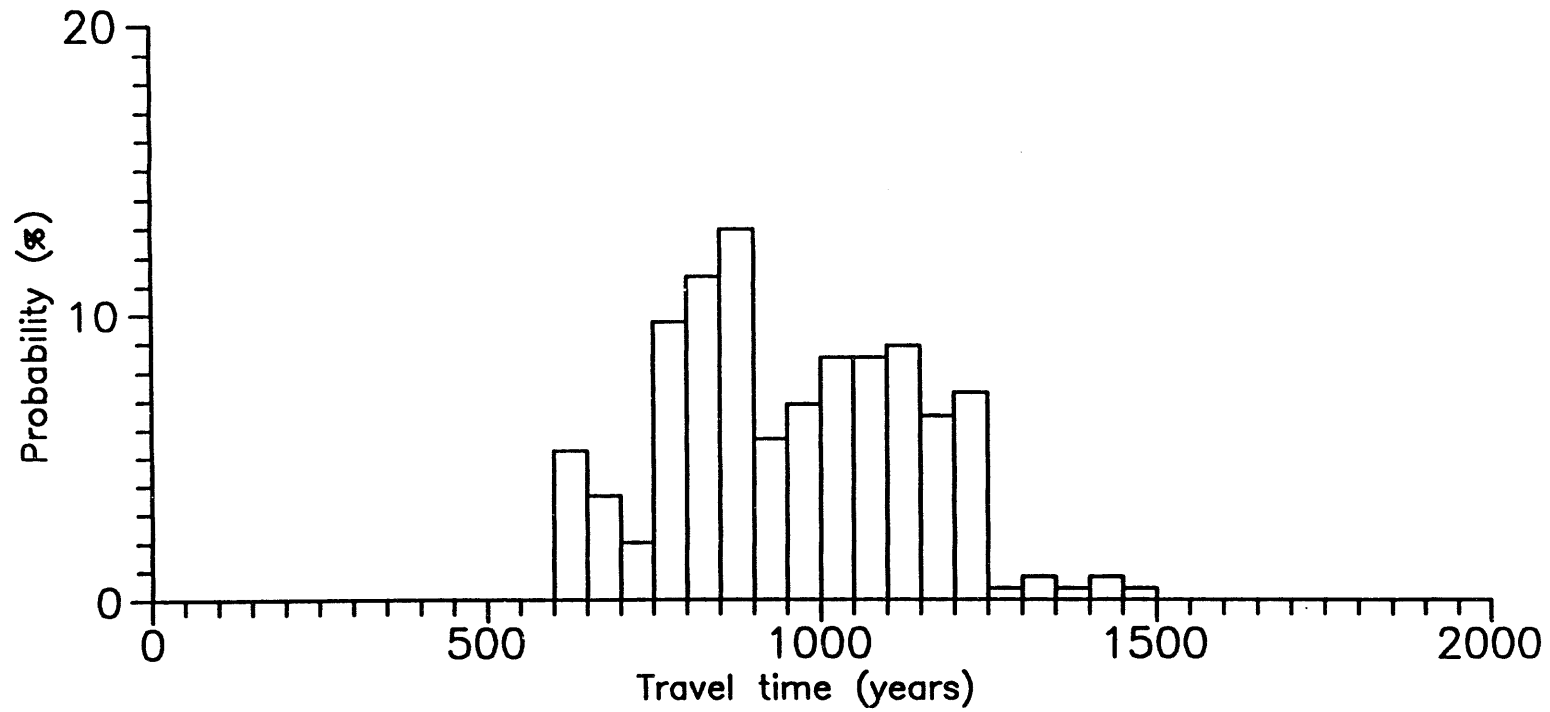
Retarded travel times of C-14 particles from the repository to the atmosphere with particles released at 10000 years



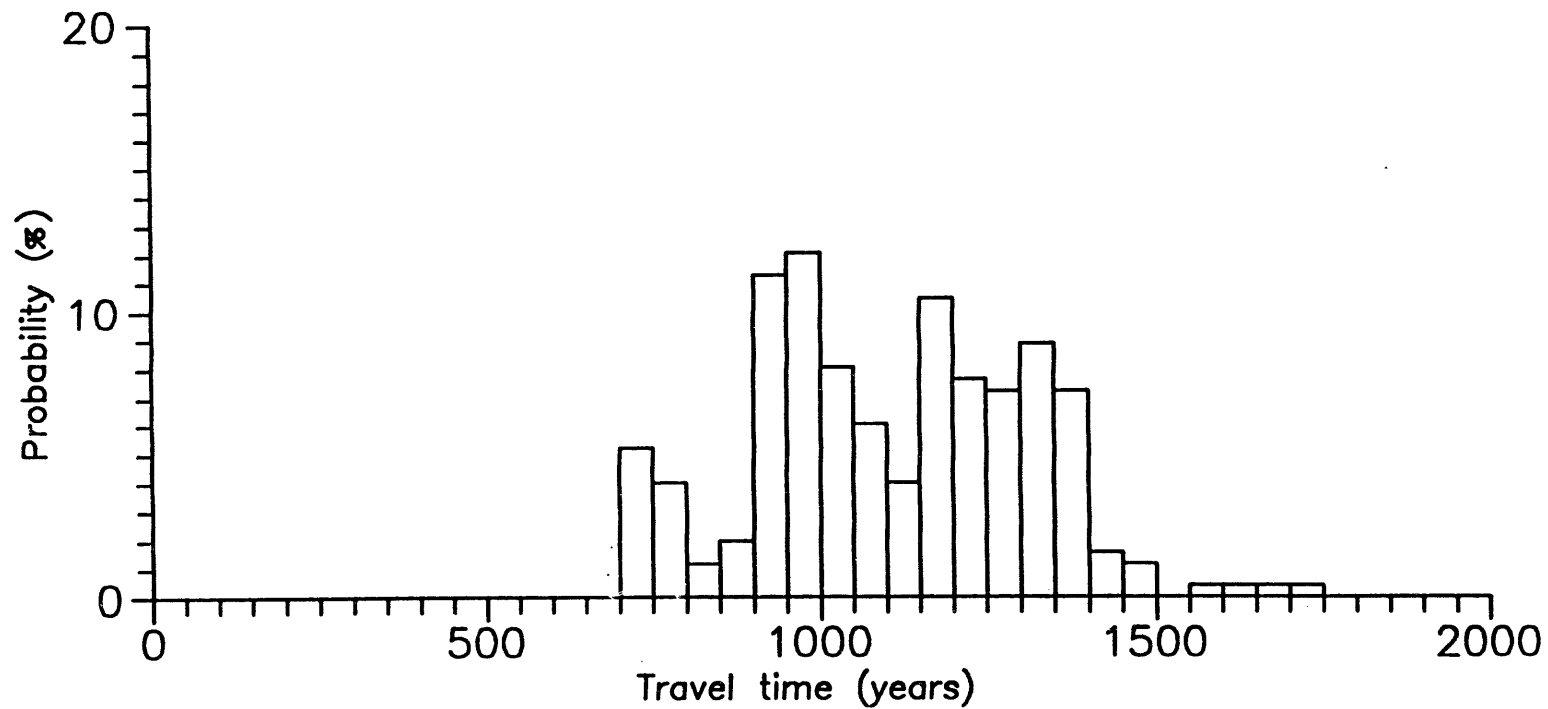
Retarded travel times of C-14 particles from the repository to the atmosphere with particles released at 11000 years



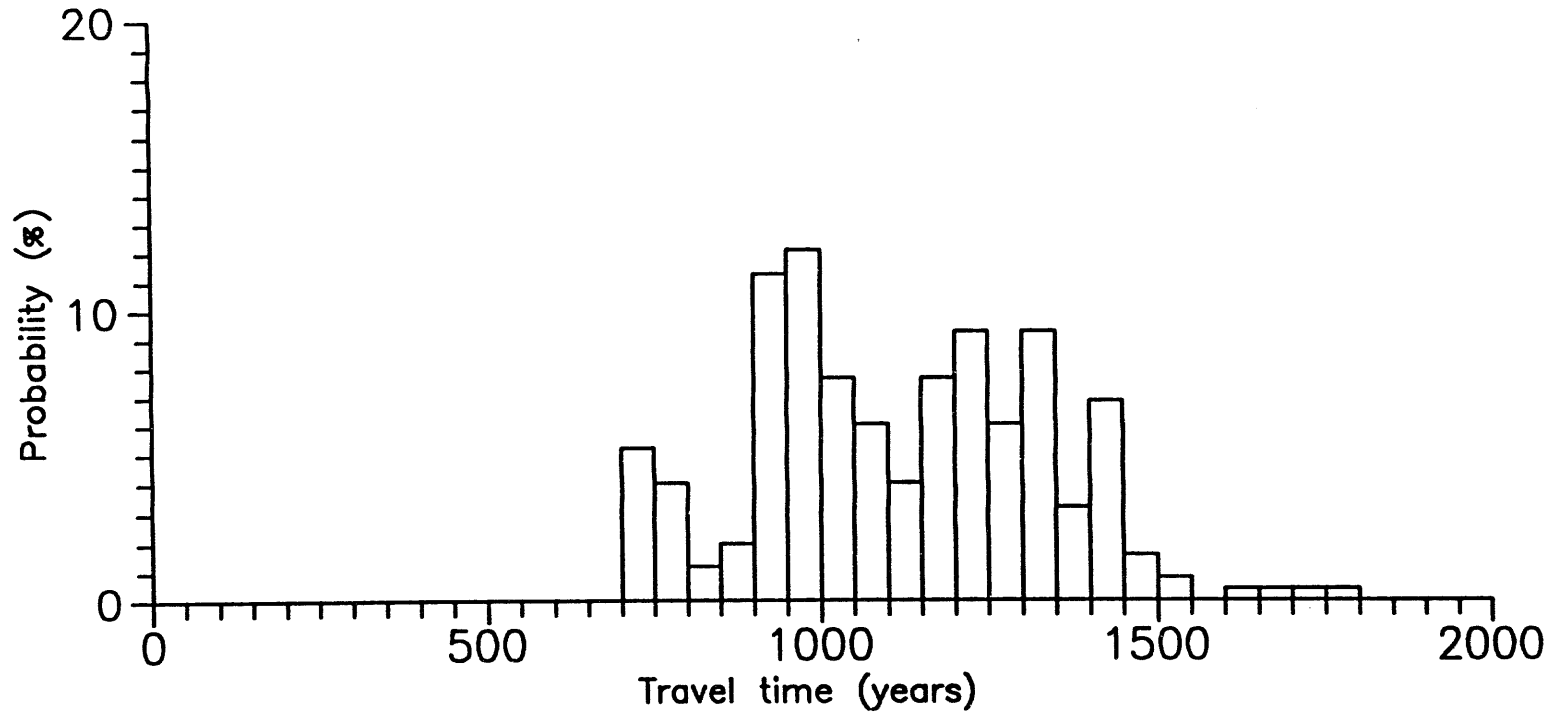
Retarded travel times of C-14 particles from the repository to the atmosphere with particles released at 12000 years



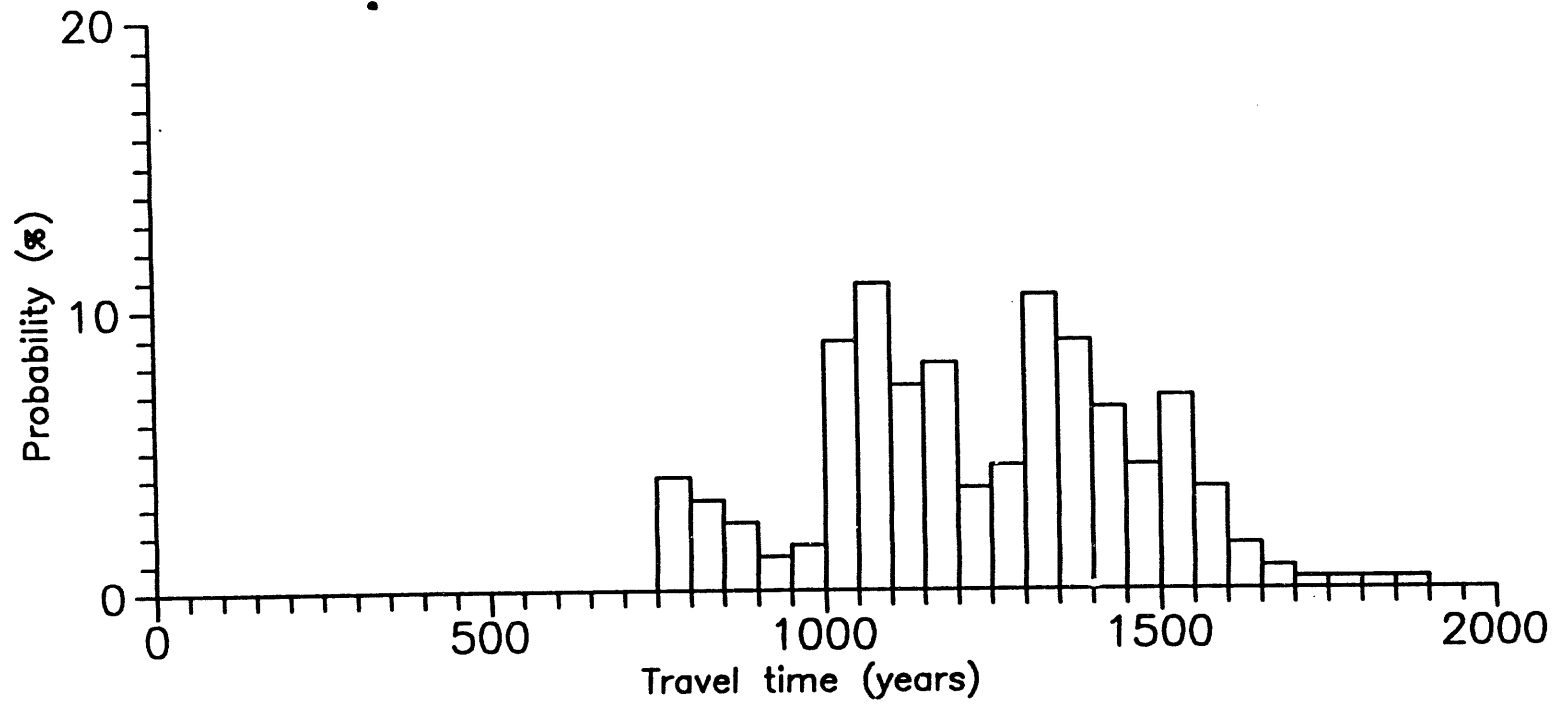
Retarded travel times of C-14 particles from the repository to the atmosphere with particles released at 13000 years



Retarded travel times of C-14 particles from the repository to the atmosphere with particles released at 14000 years



Retarded travel times of C-14 particles from the repository to the atmosphere with particles released at 15000 years



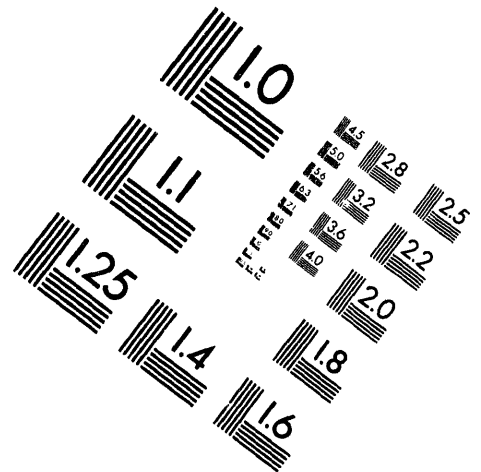
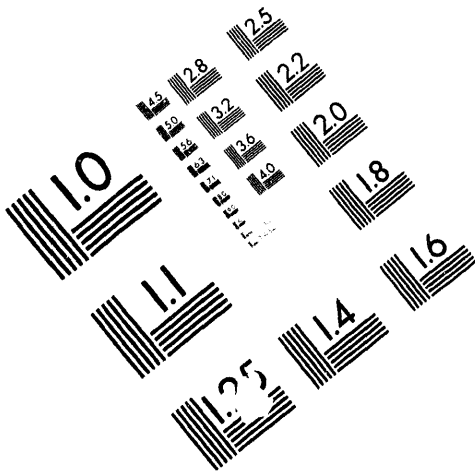
Retarded travel times of C-14 particles from the repository to the atmosphere with particles released at 16000 years



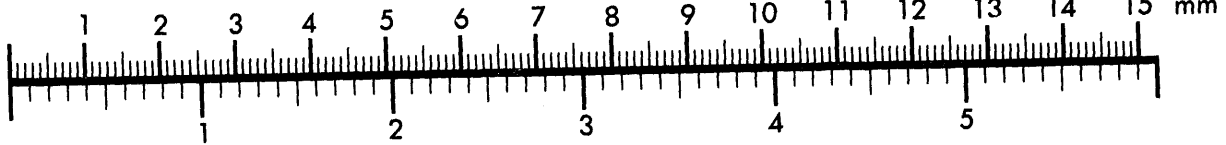
**AIM**

**Association for Information and Image Management**

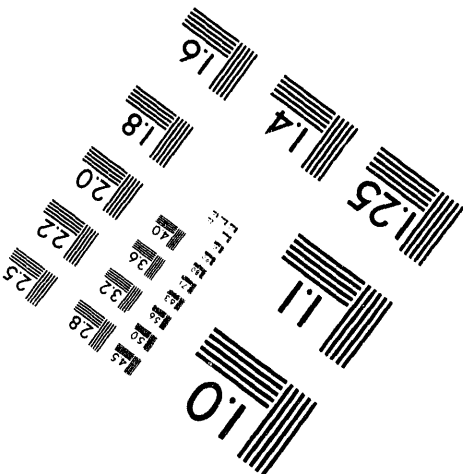
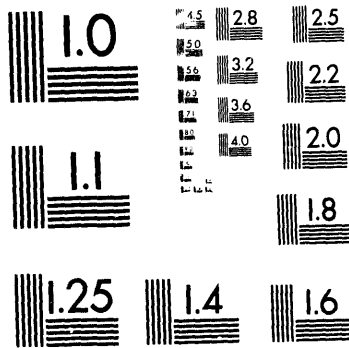
1100 Wayne Avenue, Suite 1100  
Silver Spring, Maryland 20910  
301/587-8202



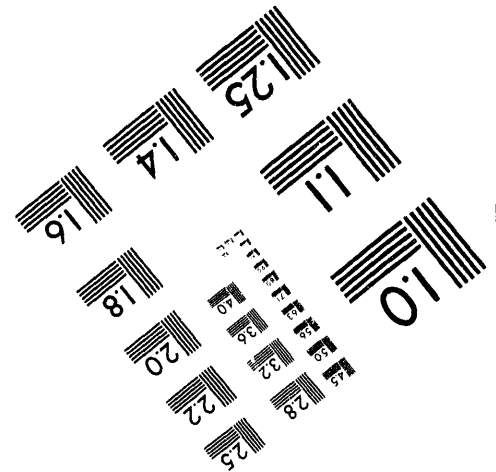
Centimeter



Inches

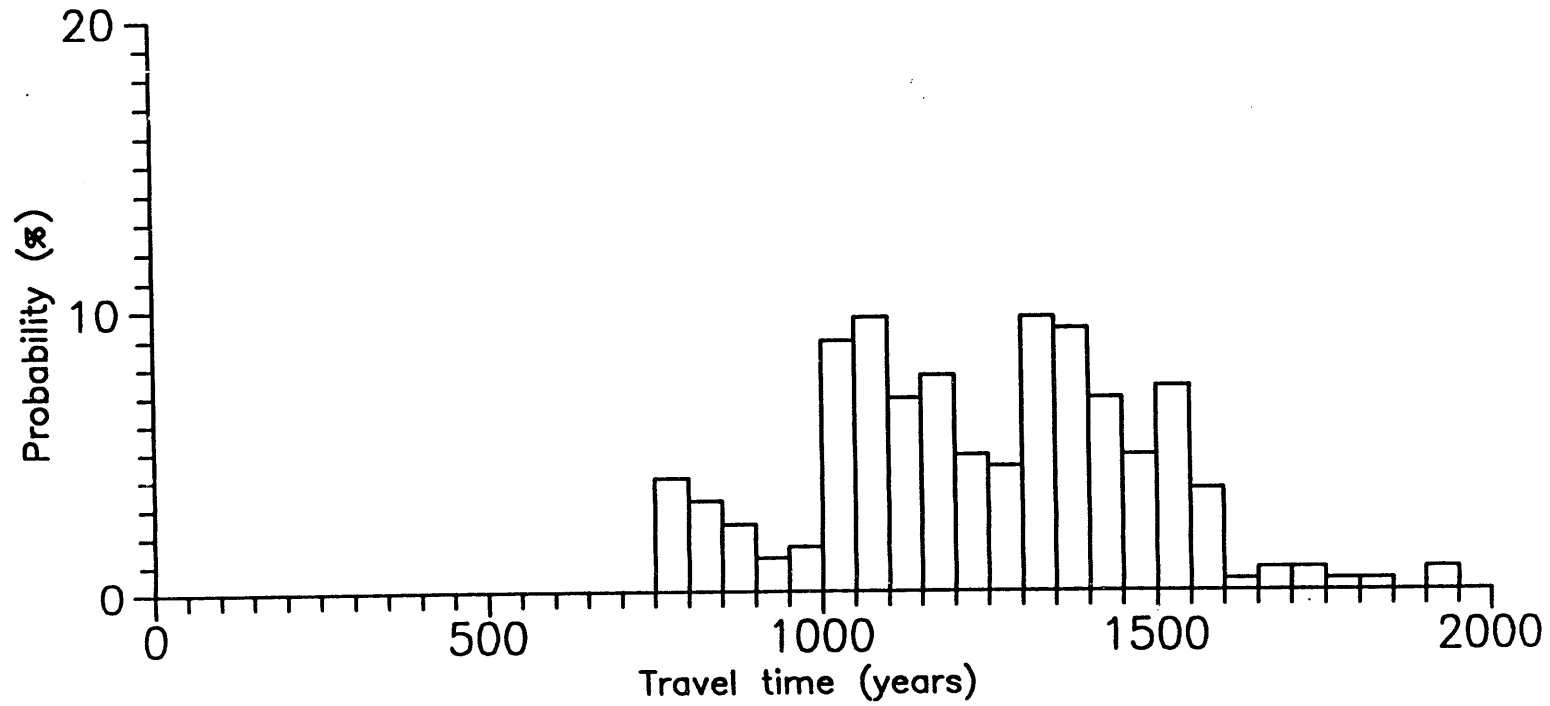


MANUFACTURED TO AIM STANDARDS  
BY APPLIED IMAGE, INC.

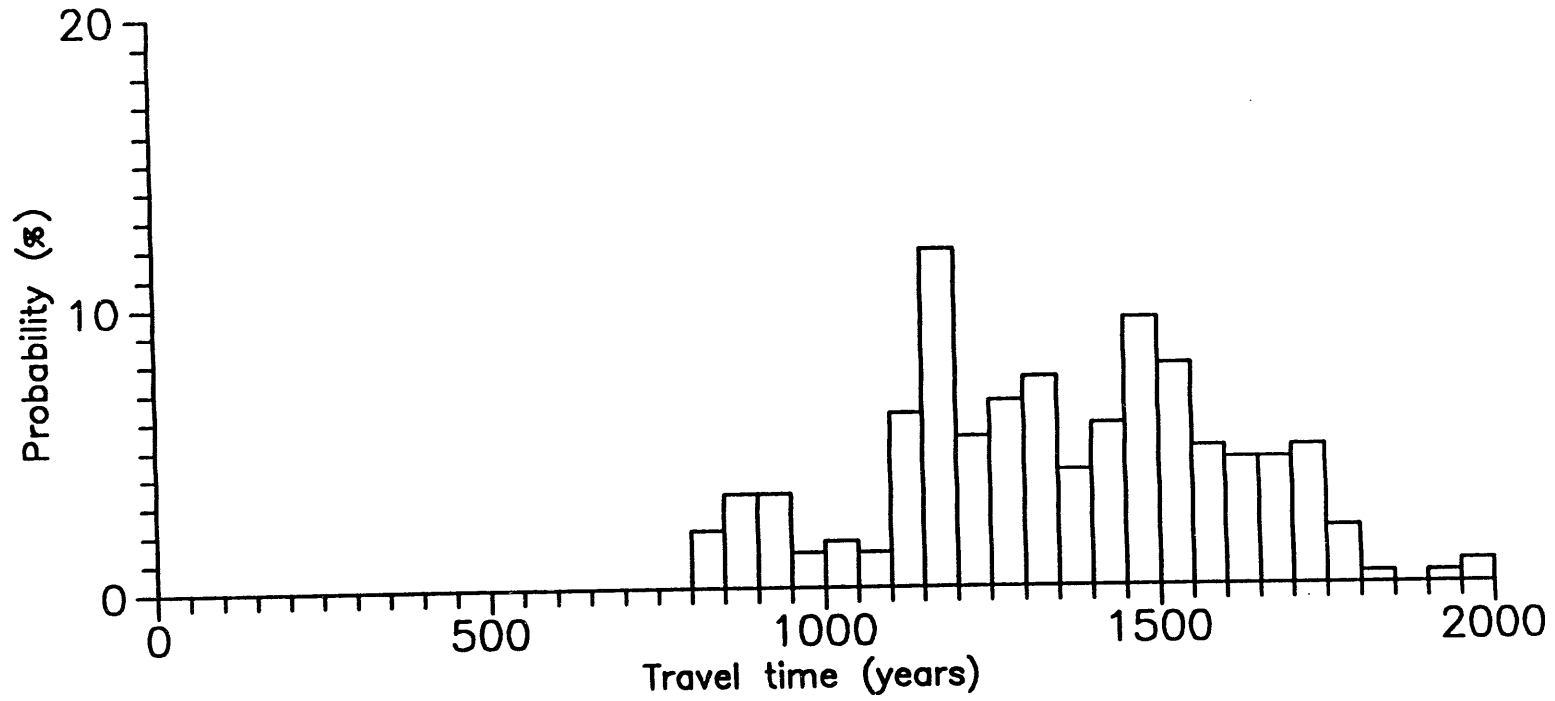


---

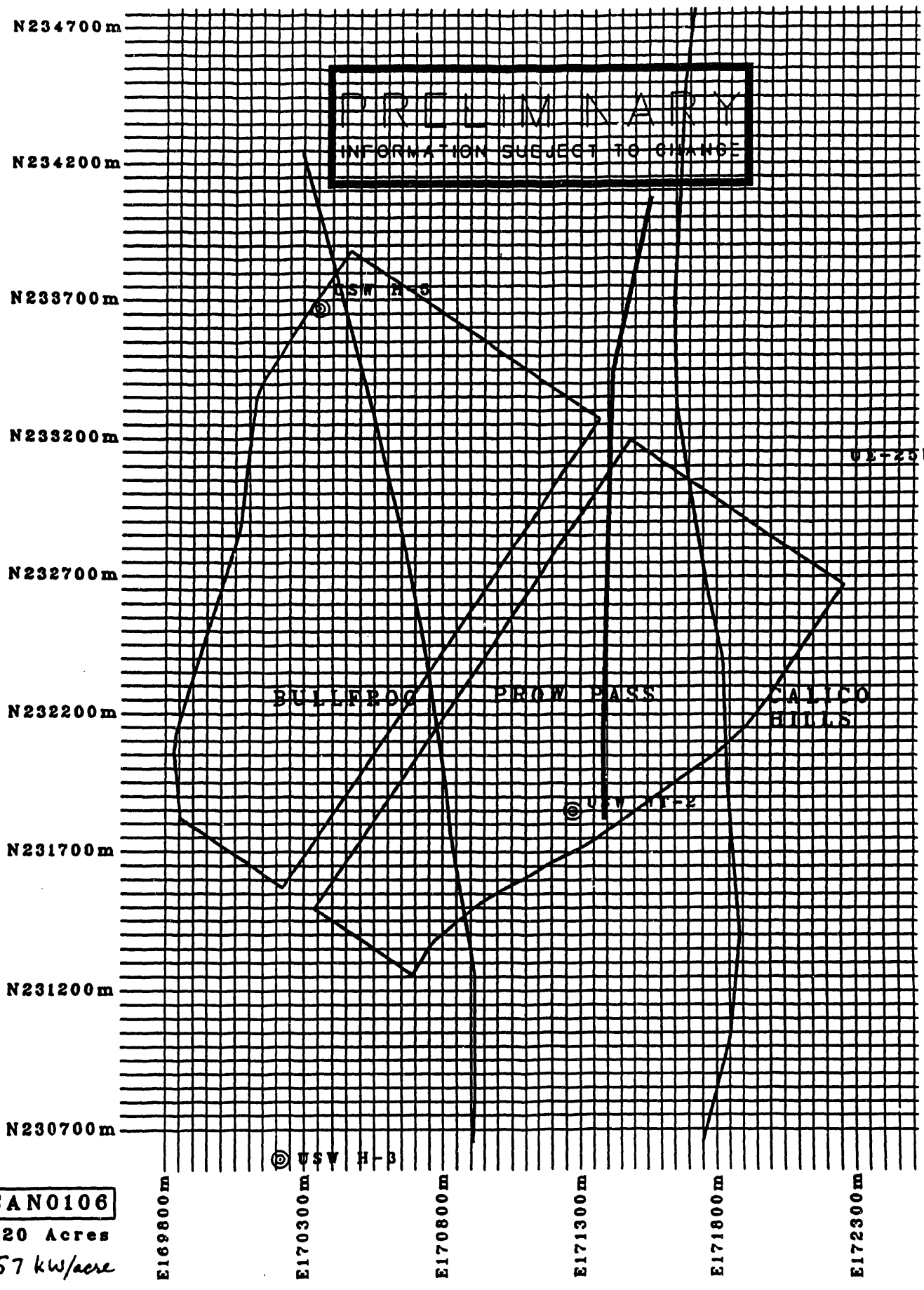
**5 of 5**



Retarded travel times of C-14 particles from the repository to the atmosphere with particles released at 17000 years



Retarded travel times of C-14 particles from the repository to the atmosphere with particles released at 18000 years



**SAN0106**  
 820 Acres  
 57 kw/acre

Yucca Mountain Site Characterization Project  
Publication Distribution List--March 18, 1994  
(Square-bracketed numbers following names  
indicate number of copies to be sent.)

1 of 28

- [1] D. A. Dreyfus (RW-1)  
Director  
Office of Civilian Radioactive Waste Management  
U.S. Department of Energy  
1000 Independence Avenue, S.W.  
Washington, DC 20585
  
- [1] L. H. Barrett (RW-2)  
Acting Deputy Director  
Office of Civilian Radioactive Waste Management  
U.S. Department of Energy  
1000 Independence Avenue, S.W.  
Washington, DC 20585
  
- [1] J. D. Saltzman (RW-4)  
Office of Strategic Planning & International Programs  
Office of Civilian Radioactive Waste Management  
U.S. Department of Energy  
1000 Independence Avenue, S.W.  
Washington, DC 20585
  
- [1] J. D. Saltzman (RW-5)  
Office of External Relations  
Office of Civilian Radioactive Waste Management  
U.S. Department of Energy  
1000 Independence Avenue, S.W.  
Washington, DC 20585
  
- [1] S. Rousso (RW-10)  
Office of Program and Resources Management  
Office of Civilian Radioactive Waste Management  
U.S. Department of Energy  
1000 Independence Avenue, S.W.  
Washington, DC 20585
  
- [1] J. C. Bresee (RW-10)  
Office of Civilian Radioactive Waste Management  
U.S. Department of Energy  
1000 Independence Avenue, S.W.  
Washington, DC 20585

Yucca Mountain Site Characterization Project  
Publication Distribution List--March 18, 1994  
(Square-bracketed numbers following names  
indicate number of copies to be sent.)

2 of 28

- [1] R. M. Nelson (RW-20)  
Office of Geologic Disposal  
Office of Civilian Radioactive Waste Management  
U.S. Department of Energy  
1000 Independence Avenue, S.W.  
Washington, DC 20585
  
- [1] S. J. Brocoum (RW-22)  
Analysis and Verification Division  
Office of Civilian Radioactive Waste Management  
U.S. Department of Energy  
1000 Independence Avenue, S.W.  
Washington, DC 20585
  
- [1] D. Shelor (RW-30)  
Office of Systems and Compliance  
Office of Civilian Radioactive Waste Management  
U.S. Department of Energy  
1000 Independence Avenue, S.W.  
Washington, DC 20585
  
- [1] J. Roberts (RW-33)  
Director, Regulatory Compliance Division  
Office of Civilian Radioactive Waste Management  
U.S. Department of Energy  
1000 Independence Avenue, S.W.  
Washington, DC 20585
  
- [1] G. J. Parker (RW-332)  
Regulatory Policy and Requirements Branch  
Office of Civilian Radioactive Waste Management  
U.S. Department of Energy  
1000 Independence Avenue, S.W.  
Washington, DC 20585
  
- [1] R. A. Milner (RW-40)  
Office of Storage and Transportation  
Office of Civilian Radioactive Waste Management  
U.S. Department of Energy  
1000 Independence Avenue, S.W.  
Washington, DC 20585

Yucca Mountain Site Characterization Project  
Publication Distribution List--March 18, 1994  
(Square-bracketed numbers following names  
indicate number of copies to be sent.)

3 of 28

- [1] S. Rousso (RW-50)  
Office of Contract Business Management  
Office of Civilian Radioactive Waste Management  
U.S. Department of Energy  
1000 Independence Avenue, S.W.  
Washington, DC 20585
- [1] T. Wood (RW-52)  
Director, M&O Management Division  
Office of Civilian Radioactive Waste Management  
U.S. Department of Energy  
1000 Independence Avenue, S.W.  
Washington, DC 20585
- [4] Victoria F. Reich  
Librarian  
Nuclear Waste Technical Review Board  
1100 Wilson Blvd., Suite 910  
Arlington, VA 22209
- [5] R. M. Nelson, Jr  
Acting Project Manager  
Yucca Mountain Site Characterization Project Office  
U.S. Department of Energy  
P. O. Box 98608--MS 523  
Las Vegas, NV 89193-8608
- [1] C. Kouts (RW-4)  
Office of Strategic Planning and International Programs  
Office of Civilian Radioactive Waste Management  
U.S. Department of Energy  
1000 Independence Avenue, S.W.  
Washington, DC 20585
- [1] A. Benson (RW-5)  
Office of External Relations  
Office of Civilian Radioactive Waste Management  
U.S. Department of Energy  
1000 Independence Avenue, S.W.  
Washington, DC 20585

Yucca Mountain Site Characterization Project  
Publication Distribution List--March 18, 1994  
(Square-bracketed numbers following names  
indicate number of copies to be sent.)

4 of 28

- [1] L. M. Smith (RW-20)  
Office of Geologic Disposal  
Office of Civilian Radioactive Waste Management  
U.S. Department of Energy  
1000 Independence Avenue, S.W.  
Washington, DC 20585
  
- [1] J. R. Dyer  
Director Regulatory Site Evaluation Division  
Yucca Mountain Site Characterization Project Office  
U.S. Department of Energy  
P.O. Box 98608--MS 523  
Las Vegas, NV 89193-8608
  
- [1] J. M. Boak  
Chief - Technical Analysis  
Yucca Mountain Site Characterization Project Office  
U.S. Department of Energy  
P.O. Box 98608--MS 523  
Las Vegas, NV 89193-8608
  
- [1] S. B. Jones  
Acting Director - Regulatory & Site Evaluation Division  
Yucca Mountain Site Characterization Project Office  
U.S. Department of Energy  
P.O. Box 98608--MS 523  
Las Vegas, NV 89193-8608
  
- [1] A. M. Simmons  
Technical Analysis Branch  
Yucca Mountain Site Characterization Project Office  
U.S. Department of Energy  
P.O. Box 98608--MS 523  
Las Vegas, NV 89193-8608
  
- [1] C. M. Newbury  
Technical Analysis Branch  
Yucca Mountain Site Characterization Project Office  
U.S. Department of Energy  
P.O. Box 98608--MS 523  
Las Vegas, NV 89193-8608

Yucca Mountain Site Characterization Project  
Publication Distribution List--March 18, 1994  
(Square-bracketed numbers following names  
indicate number of copies to be sent.)

5 of 28

- [1] E. T. Smistad  
Technical Analysis Branch  
Yucca Mountain Site Characterization Project Office  
U.S. Department of Energy  
P.O. Box 98608--MS 523  
Las Vegas, NV 89193-8608
  
- [1] C. L. West  
Director, Office of External Affairs  
DOE Nevada Operations Office, Nevada  
U.S. Department of Energy  
P.O. Box 98518  
Las Vegas, NV 89193-8518
  
- [8] Technical Information Officer  
DOE Nevada Operations Office  
U.S. Department of Energy  
P.O. Box 98518  
Las Vegas, NV 89193-8518
  
- [1] P. K. Fitzsimmons  
Technical Advisor  
Office of Assistant Manager for Environmental Safety and Health  
U.S. DOE/Nevada Operations Office  
P.O. Box 98518  
Las Vegas, NV 89193-8518
  
- [1] D. R. Elle  
Director  
Environmental Protection Division  
DOE Nevada Operations Office  
U.S. Department of Energy  
P.O. Box 98518  
Las Vegas, NV 89193-8518
  
- [1] Repository Licensing & Quality Assurance Project Directorate  
Division of Waste Management  
U.S. Nuclear Regulatory Commission  
Washington, DC 20555

**Yucca Mountain Site Characterization Project  
Publication Distribution List--March 18, 1994  
(Square-bracketed numbers following names  
indicate number of copies to be sent.)**

6 of 28

- [1] **Senior Project Manager for Yucca Mountain Repository Project Branch  
Division of Waste Management  
U.S. Nuclear Regulatory Commission  
Washington, DC 20555**
- [1] **NRC Document Control Desk  
Division of Waste Management  
U.S. Nuclear Regulatory Commission  
Washington, DC 20555**
- [1] **Philip S. Justus  
NRC Site Representative  
301 E. Stewart Ave., Room 203  
Las Vegas, NV 89101**
- [1] **E. P. Binnall  
Field Systems Group Leader  
Lawrence Berkeley Laboratory  
Building 50B/4235  
Berkeley, CA 94720**
- [1] **Center for Nuclear Waste Regulatory Analyses  
6220 Culebra Road  
Drawer 28510  
San Antonio, TX 78284**
- [3] **W. L. Clarke  
Technical Project Officer for YMP  
Lawrence Livermore National Laboratory  
Attn: YMP/LRC  
P.O. Box 5514  
Livermore, CA 94551**
- [1] **J. A. Blink  
Deputy Project Leader  
Lawrence Livermore National Laboratory  
101 Convention Center Drive, Suite 820, MS 527  
Las Vegas, NV 89109**

Yucca Mountain Site Characterization Project  
Publication Distribution List--March 18, 1994  
(Square-bracketed numbers following names  
indicate number of copies to be sent.)

7 of 28

- [1] T. A. Buscheck  
Lawrence Livermore National Laboratory  
Attn: YMP/LRC  
P.O. Box 5514  
Livermore, CA 94551
  
- [1] W. G. Halsey  
Lawrence Livermore National Laboratory  
Attn: YMP/LRC  
P.O. Box 5514  
Livermore, CA 94551
  
- [1] Alan Lamont  
Lawrence Livermore National Laboratory  
Attn: YMP/LRC  
P.O. Box 5514  
Livermore, CA 94551
  
- [4] J. A. Canepa  
Technical Project Officer for YMP  
Los Alamos National Laboratory  
EES-13, Mail Stop J521  
P.O. Box 1663  
Los Alamos, NM 87545
  
- [1] H. N. Kalia  
Project Leader for ESF Test Coordination  
Los Alamos National Laboratory  
101 Convention Center Drive, Suite 820, Mail Stop 527  
Las Vegas, NV 89101
  
- [1] N. Z. Elkins  
Deputy Technical Project Officer  
Los Alamos National Laboratory  
101 Convention Center Drive, Suite 820, Mail Stop 527  
Las Vegas, NV 89101

Yucca Mountain Site Characterization Project  
Publication Distribution List--March 18, 1994  
(Square-bracketed numbers following names  
indicate number of copies to be sent.)

8 of 28

- [1] Arend Meijer  
Los Alamos National Laboratory  
EES-13, Mail Stop J521  
P.O. Box 1663  
Los Alamos, NM 87545
  
- [1] I. R. Triay  
Los Alamos National Laboratory  
EES-13, Mail Stop J521  
P.O. Box 1663  
Los Alamos, NM 87545
  
- [2] L. E. Shephard  
Technical Project Officer for YMP  
Sandia National Laboratories  
Organization 6310  
P.O. Box 5800  
Albuquerque, NM 87185
  
- [1] R. W. Barnard  
Sandia National Laboratories  
Organization 6310  
P.O. Box 5800  
Albuquerque, NM 87185
  
- [1] H. A. Dockery  
Sandia National Laboratories  
Organization 6310  
P.O. Box 5800  
Albuquerque, NM 87185
  
- [1] J. H. Gauthier  
Sandia National Laboratories  
Organization 6310  
P.O. Box 5800  
Albuquerque, NM 87185

Yucca Mountain Site Characterization Project  
Publication Distribution List--March 18, 1994  
(Square-bracketed numbers following names  
indicate number of copies to be sent.)

9 of 28

- [1] Thomas Robey  
Sandia National Laboratories  
Organization 6310  
P.O. Box 5800  
Albuquerque, NM 87185
  
- [1] E. E. Ryder  
Sandia National Laboratories  
Organization 6310  
P.O. Box 5800  
Albuquerque, NM 87185
  
- [1] M. L. Wilson  
Sandia National Laboratories  
Organization 6310  
P.O. Box 5800  
Albuquerque, NM 87185
  
- [1] J. F. Devine  
Assistant Director for Engineering Geology  
U.S. Geological Survey  
106 National Center  
12201 Sunrise Valley Drive  
Reston, VA 22092
  
- [1] L. R. Hayes  
Technical Project Officer  
U.S. Geological Survey  
P.O. Box 25046  
Denver, CO 80225
  
- [1] V. R. Schneider  
Asst. Chief Hydrologist  
Office of Program Coordination & Technical Support  
U.S. Geological Survey  
12201 Sunrise Valley Drive--MS 414  
Reston, VA 22092

Yucca Mountain Site Characterization Project  
Publication Distribution List--March 18, 1994  
(Square-bracketed numbers following names  
indicate number of copies to be sent.)

10 of 28

- [1] J. S. Stuckless  
Geologic Division Coordinator  
Yucca Mountain Project  
U.S. Geological Survey  
P.O. Box 25046--MS 913  
Denver, CO 80225
  
- [1] D. H. Appel  
Chief  
Hydrologic Investigations Program  
U.S. Geological Survey  
P.O. Box 25046--MS 421  
Denver, CO 80225
  
- [1] E. J. Helley  
Branch of Western Regional Geology  
U.S. Geological Survey  
345 Middlefield Road--MS 427  
Menlo Park, CA 94025
  
- [1] R. W. Craig  
Chief  
Nevada Operations Office  
U.S. Geological Survey  
101 Convention Center Drive, Suite 860, MS 509  
Las Vegas, NV 89109
  
- [1] D. Zesiger  
U.S. Geological Survey  
101 Convention Center Drive, Suite 860, MS 509  
Las Vegas, NV 89109
  
- [1] G. L. Ducret  
Associate Chief  
Yucca Mountain Project Division  
U.S. Geological Survey  
P.O. Box 25046 - 421 Federal Center  
Denver, CO 80225

Yucca Mountain Site Characterization Project  
Publication Distribution List--March 18, 1994  
(Square-bracketed numbers following names  
indicate number of copies to be sent.)

11 of 28

- [1] A. L. Flint  
U.S. Geological Survey  
P.O. Box 327--MS 721  
Mercury, NV 89023
  
- [1] D. A. Beck  
Water Resources Division  
U.S. Geological Survey  
6770 So. Paradise Road  
Las Vegas, NV 89119
  
- [1] P. A. Glancy  
U.S. Geological Survey  
Federal Building, Room 224  
Carson City, NV 89701
  
- [1] Sherman S. C. Wu  
Branch of Astrogeology  
U.S. Geological Survey  
2255 N. Gemini Dr.  
Flagstaff, AZ 86001
  
- [1] J. H. Sass  
Branch of Tectonophysics  
U.S. Geological Survey  
2255 N. Gemini Dr.  
Flagstaff, AZ 86001
  
- [1] DeWayne Campbell  
Technical Project Officer for YMP  
U.S. Bureau of Reclamation  
Code D-3790  
P.O. Box 25007  
Denver, CO 80225
  
- [1] J. M. LaMonaca  
Records Specialist  
U.S. Geological Survey  
421 Federal Center  
P.O. Box 25046  
Denver, CO 80225

Yucca Mountain Site Characterization Project  
Publication Distribution List--March 18, 1994  
(Square-bracketed numbers following names  
indicate number of copies to be sent.)

12 of 28

- [1] W. R. Keefer  
U.S. Geological Survey  
913 Federal Center  
P.O. Box 25046  
Denver, CO 80225
  
- [1] M. D. Voegele  
Technical Project Officer for YMP  
Science Applications International Corp  
101 Convention Center Dr., Suite 407  
Las Vegas, NV 89109
  
- [2] L. D. Foust  
Nevada Site Manager  
TRW Environmental Safety Systems  
101 Convention Center Drive--MS 423  
Las Vegas, NV 89109
  
- [1] C. E. Ezra  
YMP Support Office Manager  
EG&G Energy Measurements, Inc  
MS V-02  
P.O. Box 1912  
Las Vegas, NV 89125
  
- [1] E. L. Snow  
Program Manager  
Roy F. Weston, Inc  
955 L'Enfant Plaza, S.W.  
Washington, DC 20024
  
- [1] Technical Information Center  
Roy F. Weston, Inc  
955 L'Enfant Plaza, S.W.  
Washington, DC 20024

Yucca Mountain Site Characterization Project  
Publication Distribution List--March 18, 1994  
(Square-bracketed numbers following names  
indicate number of copies to be sent.)

13 of 28

- [1] D. Hedges  
Vice President  
Quality Assurance  
Roy F. Weston, Inc  
4425 Spring Mountain Road, Suite 300  
Las Vegas, Nevada 89102
  
- [1] D. L. Fraser  
General Manager  
Reynolds Electrical & Engineering Co., Inc  
MS 555  
P.O. Box 98521  
Las Vegas, NV 89193-8521
  
- [1] R. F. Pritchett  
Technical Project Officer for YMP  
Reynolds Electrical & Engineering Co., Inc  
MS 408  
P.O. Box 98521  
Las Vegas, NV 89193-8521
  
- [1] B. W. Colston  
President/General Manager  
Las Vegas Branch  
Raytheon Services Nevada  
MS 416  
P.O. Box 95487  
Las Vegas, NV 89193-5487
  
- [1] R. L. Bullock  
Technical Project Officer for YMP  
Raytheon Services Nevada  
Suite P-250, MS 403  
101 Convention Center Dr.  
Las Vegas, NV 89109

Yucca Mountain Site Characterization Project  
Publication Distribution List--March 18, 1994  
(Square-bracketed numbers following names  
indicate number of copies to be sent.)

14 of 28

- [1] Paul Eslinger  
Manager  
PASS Program  
Pacific Northwest Laboratories  
P.O. Box 999  
Richland, WA 99352
  
- [1] A. T. Tamura  
Science and Technology Division  
Office of Scientific and Technical Information  
U.S. Department of Energy  
P.O. Box 62  
Oak Ridge, TN 37831
  
- [1] Carlos G. Bell, Jr.  
Professor of Civil Engineering  
Civil and Mechanical Engineering Dept  
University of Nevada, Las Vegas  
4505 So. Maryland Parkway  
Las Vegas, NV 89154
  
- [1] P. J. Weeden  
Acting Director  
Nuclear Radiation Assessment Division  
Environmental Monitoring Systems Laboratory  
U.S. Environmental Protection Agency  
P.O. Box 93478  
Las Vegas, NV 89193-3478
  
- [1] ONWI Library  
Office of Nuclear Waste Isolation  
Battelle Columbus Laboratory  
505 King Ave.  
Columbus, OH 43201
  
- [1] T. Hay  
Executive Assistant  
Office of the Governor  
State of Nevada  
Capitol Complex  
Carson City, NV 89710

Yucca Mountain Site Characterization Project  
Publication Distribution List--March 18, 1994  
(Square-bracketed numbers following names  
indicate number of copies to be sent.)

15 of 28

- [3] R. R. Loux  
Executive Director  
Agency for Nuclear Projects  
State of Nevada  
Evergreen Center, Suite 252  
1802 N. Carson St.  
Carson City, NV 89710
- [1] C. H. Johnson  
Technical Program Manager  
Agency for Nuclear Projects  
State of Nevada  
Evergreen Center, Suite 252  
1802 N. Carson St.  
Carson City, NV 89710
- [1] John Fordham  
Water Resources Center  
Desert Research Institute  
P.O. Box 60220  
Reno, NV 89506
- [1] David Rhode  
Desert Research Institute  
P.O. Box 60220  
Reno, NV 89506
- [1] Eric Anderson  
Mountain West Research-Southwest, Inc  
2901 N. Central Ave., #1000  
Phoenix, AZ 85012-2730
- [1] The Honorable Cyril Schank  
Chairman  
Churchill County Board of Commissioners  
190 W. First St.  
Fallon, NV 89406

**Yucca Mountain Site Characterization Project  
Publication Distribution List--March 18, 1994  
(Square-bracketed numbers following names  
indicate number of copies to be sent.)**

16 of 28

- [1] Dennis A Bechtel  
Coordinator  
Nuclear Waste Division  
Clark County Department of Comprehensive Planning  
301 E. Clark Ave., Suite 570  
Las Vegas, NV 89101
  
- [1] Juanita D. Hoffman  
Nuclear Waste Repository Oversight Program  
Esmeralda County  
P.O. Box 490  
Goldfield, NV 89013
  
- [1] Eureka County Board of Commissioners  
Yucca Mountain Information Office  
P.O. Box 714  
Eureka, NV 89316
  
- [1] Brad R Mettam  
Yucca Mountain Repository Assessment Office  
Inyo County  
P.O. Drawer L  
Independence, CA 93526
  
- [1] Lander County Board of Commissioners  
315 South Humboldt St.  
Battle Mountain, NV 89820
  
- [1] Jason Pitts  
Nuclear Waste Project Office  
Lincoln County  
P.O. Box 90  
Pioche, NV 89043
  
- [1] Judy Foremaster  
Nuclear Waste Project Office  
City of Caliente  
P.O. Box 158  
Caliente, NV 89008

Yucca Mountain Site Characterization Project  
Publication Distribution List--March 18, 1994  
(Square-bracketed numbers following names  
indicate number of copies to be sent.)

17 of 28

- [1] Vernon E. Poe  
Office of Nuclear Projects  
Mineral County  
P.O. Box 1600  
Hawthorne, NV 89415
- [1] Les W. Bradshaw  
Program Manager  
Nuclear Waste Repository Project Office  
Nye County  
P.O. Box 2389  
Pahrump, NV 89041
- [1] William Offutt  
Manager  
Nye County  
P.O. Box 153  
Tonopah, NV 89049
- [1] Phillip. A. Niedzielski-Eichner  
Nuclear Waste Repository Project Office  
Nye County  
P.O. Box 221274  
Chantilly, VA 22022-1274
- [1] Florindo Mariani  
Coordinator  
White Pine County  
P.O. Box 135  
Ely, NV 89301
- [1] Glenn Van Roekel  
Director of Community Development  
City of Caliente  
P.O. Box 158  
Caliente, NV 89008
- [1] Ray Williams, Jr.  
P.O. Box 10  
Austin, NV 89310

**Yucca Mountain Site Characterization Project  
Publication Distribution List--March 18, 1994  
(Square-bracketed numbers following names  
indicate number of copies to be sent.)**

18 of 28

- [1] **Charles Thistlethwaite, AICP  
Associate Planner  
Planning Department  
Inyo County  
Drawer L  
Independence, CA 93526**
  
- [1] **Nye County District Attorney  
P.O. Box 593  
Tonopah, NV 89049**
  
- [1] **Economic Development Department  
City of Las Vegas  
400 E. Stewart Ave.  
Las Vegas, NV 89101**
  
- [1] **Community Planning and Development  
City of North Las Vegas  
P.O. Box 4086  
North Las Vegas, NV 89030**
  
- [1] **Community Development and Planning  
City of Boulder City  
P.O. Box 61350  
Boulder City, NV 89006**
  
- [1] **Commission of the European Communities  
200 Rue de la Loi  
B-1049 Brussels  
BELGIUM**
  
- [2] **M.J. Dorsey  
Librarian  
YMP Research and Study Center  
Reynolds Electrical & Engineering Co., Inc  
P.O. Box 98521--MS 407  
Las Vegas, NV 89193-8521**

Yucca Mountain Site Characterization Project  
Publication Distribution List--March 18, 1994  
(Square-bracketed numbers following names  
indicate number of copies to be sent.)

19 of 28

- [1] Amy Anderson  
Argonne National Laboratory  
9700 So. Cass Ave.--Building 362  
Argonne, IL 60439
  
- [1] Steve Bradhurst  
P.O. Box 1510  
Reno, NV 89505
  
- [1] Michael L. Baughman  
35 Clark Road  
Fiskdale, MA 01518
  
- [1] Dr. Moses Karakouzian  
1751 E. Reno, #125  
Las Vegas, NV 89119
  
- [1] John F. Ahearne  
Sigma Xi  
The Scientific Research Society  
99 Alexander Drive, P.O. Box 13975  
Research Triangle Park, NC 27709
  
- [1] Jean M. Bahr  
Department of Geology and Geophysics  
University of Wisconsin-Madison  
1215 West Dayton Street--Weeks Hall  
Madison, WI 53706
  
- [1] R. Darryl Banks  
World Resources Institute  
1700 New York Avenue, N. W.  
Washington, DC 20006
  
- [1] Robert J. Budnitz  
Future Resources Associates  
2000 Center Street, Suite 418  
Berkeley, CA 94704

Yucca Mountain Site Characterization Project  
Publication Distribution List--March 18, 1994  
(Square-bracketed numbers following names  
indicate number of copies to be sent.)

20 of 28

- [1] Sol Burstein  
7475 North Crossway Road  
Milwaukee, WI 53217
- [1] Melvin W Carter  
4621 Ellisbury Drive  
Atlanta, GA 30338
- [1] Charles Fairhurst  
Department of Civil and Mineral Engineering  
University of Minnesota  
Minnneapolis, MN 55455
- [1] Charles McCombie  
NAGRA  
Hardstrasse 73, CH-5430  
Wettingen, Switzerland
- [1] P. Zuidema  
NAGRA  
Hardstrasse 73, CH-5430  
Wettingen, Switzerland
- [1] M. Thury  
NAGRA  
Hardstrasse 73, CH-5430  
Wettingen, Switzerland
- [1] S. Vomvoris  
NAGRA  
Hardstrasse 73, CH-5430  
Wettingen, Switzerland
- [1] Thomas H. Pigford  
College of Engineering  
Department of Nuclear Engineering  
University of California Berkeley  
Berkeley, CA 94720

**Yucca Mountain Site Characterization Project  
Publication Distribution List--March 18, 1994  
(Square-bracketed numbers following names  
indicate number of copies to be sent.)**

21 of 28

- [1] Arthur C. Uptoe  
1424 Seville Road  
Santa Fe, NM 87501
  
- [1] Chris Whipple  
ICF Kaiser Engineers  
Environment Group  
7th Floor  
1800 Harrison Street  
Oakland, CA 94612-3430
  
- [1] Gilbert F. White  
Institute of Behavioral Science  
University of Colorado  
Campus Box 482  
Boulder, CO 80309-0482
  
- [1] Susan D. Wiltshire  
J. K. Associates  
P.O. Box 2219  
Hamilton, MA 01982
  
- [1] Les W. Bradshaw  
Program Manager  
Nuclear Waste Repository Program  
Nye County  
P. O. Box 1767  
Tonopah, NV 89049
  
- [1] J. William Gunter  
Director  
Criteria & Standards Division  
Office of Radiation and Indoor Air  
U. S. Environmental Protection Agency  
401 M. Street, S. W.  
Washington, DC 20460

**Yucca Mountain Site Characterization Project  
Publication Distribution List--March 18, 1994  
(Square-bracketed numbers following names  
indicate number of copies to be sent.)**

22 of 28

- [1] **Margaret Federline  
Chief, Hydrology and Systems Performance Branch  
U. W. Nuclear Regulatory Commission  
High-Level Waste Management Division  
11555 Rockville Pike  
Rockville, MD 20552**
  
- [1] **D. Bullen  
Iowa State University  
Department of Mechanical Engineering  
107 Nuclear Engineering Lab  
Ames, Iowa 50011-2241**
  
- [1] **T. F. Dale  
Performance Assessment  
Civilian Radioactive Waste Management System  
Management and Operating Contractor  
6850 Austin Center Blvd  
Austin, TX 78731**
  
- [1] **J.A. McNeish  
Performance Assessment  
Civilian Radioactive Waste Management System  
Management and Operating Contractor  
14900 Landmark blvd., Suite 365  
Dallas, TX 75240**
  
- [1] **Suresh Pahwa  
Performance Assessment  
Civilian Radioactive Waste Management System  
Management and Operating Contractor  
6850 Austin Center Blvd  
Austin, TX 78731**
  
- [5] **R. W. Andrews  
Performance Assessment  
Civilian Radioactive Waste Management System  
Management and Operating Contractor  
2650 Park Tower Drive, Suite 800  
Vienna, VA 22180**

Yucca Mountain Site Characterization Project  
Publication Distribution List--March 18, 1994  
(Square-bracketed numbers following names  
indicate number of copies to be sent.)

23 of 28

- [1] T. A. Cotton  
Senior Staff  
Civilian Radioactive Waste Management System  
Management and Operating Contractor  
2650 Park Tower Drive, Suite 800  
Vienna, VA 22180
  
- [1] J. O. Cowles  
Chief Engineer  
Civilian Radioactive Waste Management System  
Management and Operating Contractor  
2650 Park Tower Drive, Suite 800  
Vienna, VA 22180
  
- [1] D. F. Fenster  
Requirements and Licensing  
Civilian Radioactive Waste Management System  
Management and Operating Contractor  
2650 Park Tower Drive, Suite 800  
Vienna, VA 22180
  
- [1] R. W. Godman  
Assistant General Manager, Operations  
Civilian Radioactive Waste Management System  
Management and Operating Contractor  
2650 Park Tower Drive, Suite 800  
Vienna, VA 22180
  
- [1] A. B. Greenberg  
Senior Staff  
Civilian Radioactive Waste Management System  
Management and Operating Contractor  
2650 Park Tower Drive, Suite 800  
Vienna, VA 22180
  
- [1] C. A. Heath  
Senior Staff  
Civilian Radioactive Waste Management System  
Management and Operating Contractor  
2650 Park Tower Drive, Suite 800  
Vienna, VA 22180

Yucca Mountain Site Characterization Project  
Publication Distribution List--March 18, 1994  
(Square-bracketed numbers following names  
indicate number of copies to be sent.)

24 of 28

- [1] A.S. Kubo  
Assistant General Manager, Systems  
Civilian Radioactive Waste Management System  
Management and Operating Contractor  
2650 Park Tower Drive, Suite 800  
Vienna, VA 22180
- [1] J. R. Levine  
Communications  
Civilian Radioactive Waste Management System  
Management and Operating Contractor  
2650 Park Tower Drive, Suite 800  
Vienna, VA 22180
- [1] J. J. Miller  
Systems Engineering  
Civilian Radioactive Waste Management System  
Management and Operating Contractor  
2650 Park Tower Drive, Suite 800  
Vienna, VA 22180
- [1] L. D. Rickertsen  
Senior Staff  
Civilian Radioactive Waste Management System  
Management and Operating Contractor  
2650 Park Tower Drive, Suite 800  
Vienna, VA 22180
- [1] Frank Ridolphi  
Strategic Planning  
Civilian Radioactive Waste Management System  
Management and Operating Contractor  
2650 Park Tower Drive, Suite 800  
Vienna, VA 22180
- [1] R. L. Robertson  
General Manager  
Civilian Radioactive Waste Management System  
Management and Operating Contractor  
2650 Park Tower Drive, Suite 800  
Vienna, VA 22180

**Yucca Mountain Site Characterization Project  
Publication Distribution List--March 18, 1994  
(Square-bracketed numbers following names  
indicate number of copies to be sent.)**

25 of 28

- [1] S. S. Sareen  
Senior Staff  
Civilian Radioactive Waste Management System  
Management and Operating Contractor  
2650 Park Tower Drive, Suite 800  
Vienna, VA 22180
  
- [1] E. C. Taylor  
Chief Scientist  
Civilian Radioactive Waste Management System  
Management and Operating Contractor  
2650 Park Tower Drive, Suite 800  
Vienna, VA 22180
  
- [1] Albin Brandstetter  
Performance Assessment  
Civilian Radioactive Waste Management System  
Management and Operating Contractor  
101 Convention Center Drive, Suite P110  
Las Vegas, Nevada 89109-2006
  
- [1] E. R. Brandstetter  
Performance Assessment  
Civilian Radioactive Waste Management System  
Management and Operating Contractor  
101 Convention Center Drive, Suite P110  
Las Vegas, Nevada 89109-2006
  
- [1] T. C. Geer  
Systems Engineering  
Civilian Radioactive Waste Management System  
Management and Operating Contractor  
101 Convention Center Drive, Suite P110  
Las Vegas, Nevada 89109-2006
  
- [1] Suresh Lingineni  
Performance Assessment  
Civilian Radioactive Waste Management System  
Management and Operating Contractor  
101 Convention Center Drive, Suite P110  
Las Vegas, Nevada 89109-2006

Yucca Mountain Site Characterization Project  
Publication Distribution List--March 18, 1994  
(Square-bracketed numbers following names  
indicate number of copies to be sent.)

26 of 28

- [1] M. A. Lugo  
Regulatory and Licensing  
Civilian Radioactive Waste Management System  
Management and Operating Contractor  
101 Convention Center Drive, Suite P110  
Las Vegas, Nevada 89109-2006
  
- [1] Richard Memory  
Systems Analysis  
Civilian Radioactive Waste Management System  
Management and Operating Contractor  
101 Convention Center Drive, Suite P110  
Las Vegas, Nevada 89109-2006
  
- [1] Srikanta Mishra  
Performance Assessment  
Civilian Radioactive Waste Management System  
Management and Operating Contractor  
101 Convention Center Drive, Suite P110  
Las Vegas, Nevada 89109-2006
  
- [1] S. P. Nesbit  
Regulatory and Licensing  
Civilian Radioactive Waste Management System  
Management and Operating Contractor  
101 Convention Center Drive, Suite P110  
Las Vegas, Nevada 89109-2006
  
- [1] M. W. Pendleton  
Technical Evaluation  
Civilian Radioactive Waste Management System  
Management and Operating Contractor  
101 Convention Center Drive, Suite P110  
Las Vegas, Nevada 89109-2006
  
- [1] L. D. Ramspott  
Senior Staff  
Civilian Radioactive Waste Management System  
Management and Operating Contractor  
101 Convention Center Drive, Suite P110  
Las Vegas, Nevada 89109-2006

Yucca Mountain Site Characterization Project  
Publication Distribution List--March 18, 1994  
(Square-bracketed numbers following names  
indicate number of copies to be sent.)

27 of 28

- [1] R. M. Sandifer  
Deputy for MGDS Operations  
Civilian Radioactive Waste Management System  
Management and Operating Contractor  
101 Convention Center Drive, Suite P110  
Las Vegas, Nevada 89109-2006
- [1] S. F. Saterlie  
Systems Analysis  
Civilian Radioactive Waste Management System  
Management and Operating Contractor  
101 Convention Center Drive, Suite P110  
Las Vegas, Nevada 89109-2006
- [1] Scott Sinnock  
Senior Staff  
Civilian Radioactive Waste Management System  
Management and Operating Contractor  
101 Convention Center Drive, Suite P110  
Las Vegas, Nevada 89109-2006
- [1] A. J. Smith  
Performance Assessment  
Civilian Radioactive Waste Management System  
Management and Operating Contractor  
101 Convention Center Drive, Suite P110  
Las Vegas, Nevada 89109-2006
- [1] R. K. St. Clair  
Regulatory Management and Integration  
Civilian Radioactive Waste Management System  
Management and Operating Contractor  
101 Convention Center Drive, Suite P110  
Las Vegas, Nevada 89109-2006
- [1] David Stahl  
Waste Package Design  
Civilian Radioactive Waste Management System  
Management and Operating Contractor  
101 Convention Center Drive, Suite P110  
Las Vegas, Nevada 89109-2006

Yucca Mountain Site Characterization Project  
Publication Distribution List--March 18, 1994  
(Square-bracketed numbers following names  
indicate number of copies to be sent.)

28 of 28

- [1] C. T. Statton  
Site Characterization  
Civilian Radioactive Waste Management System  
Management and Operating Contractor  
101 Convention Center Drive, Suite P110  
Las Vegas, Nevada 89109-2006
  
- [1] B. H. Thompson  
Systems Analysis  
Civilian Radioactive Waste Management System  
Management and Operating Contractor  
101 Convention Center Drive, Suite P110  
Las Vegas, Nevada 89109-2006
  
- [1] A. E. Van Luik  
Performance Assessment Management & Integration  
Civilian Radioactive Waste Management System  
Management and Operating Contractor  
101 Convention Center Drive, Suite P110  
Las Vegas, Nevada 89109-2006
  
- [1] R.G. Vawter  
Deputy for Management and Integration  
Civilian Radioactive Waste Management System  
Management and Operating Contractor  
101 Convention Center Drive, Suite P110  
Las Vegas, Nevada 89109-2006
  
- [1] E. M. Weaver  
Regulatory Management and Integration  
Civilian Radioactive Waste Management System  
Management and Operating Contractor  
101 Convention Center Drive, Suite P110  
Las Vegas, Nevada 89109-2006
  
- [1] J. L. Younker  
Regulatory and Technical Evaluation  
Civilian Radioactive Waste Management System  
Management and Operating Contractor  
101 Convention Center Drive, Suite P110  
Las Vegas, Nevada 89109-2006

**DATE**

**FILMED**

*9 / 8 / 94*

**END**

